

FTD-MT- 63-197

AD 603290

# TRANSLATION

TECHNICAL GAS DYNAMICS

By

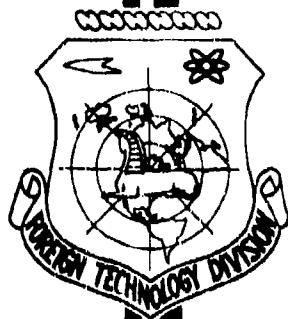
M. Ye. Deych

7764-71683

COPY	1	OF	3	myr
HARD COPY	\$ . 9.45			
MICROFICHE	\$ . 2.75			

648p

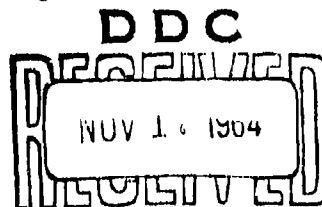
## FOREIGN TECHNOLOGY DIVISION



AIR FORCE SYSTEMS COMMAND

WRIGHT-PATTERSON AIR FORCE BASE

OHIO



DDC-IRA B

## FOREWORD

This document is a machine translation of Russian text which has been processed by the AN/GSQ-16(XW-2) Machine Translator, owned and operated by the United States Air Force. The machine output has been fully post-edited. Ambiguity of meaning, words missing from the machine's dictionary, and words out of the context of meaning have been corrected. The sentence word order has been rearranged for readability due to the fact that Russian sentence structure does not follow the English subject-verb-predicate sentence structure. The fact of translation does not guarantee editorial accuracy, nor does it indicate USAF approval or disapproval of the material translated.

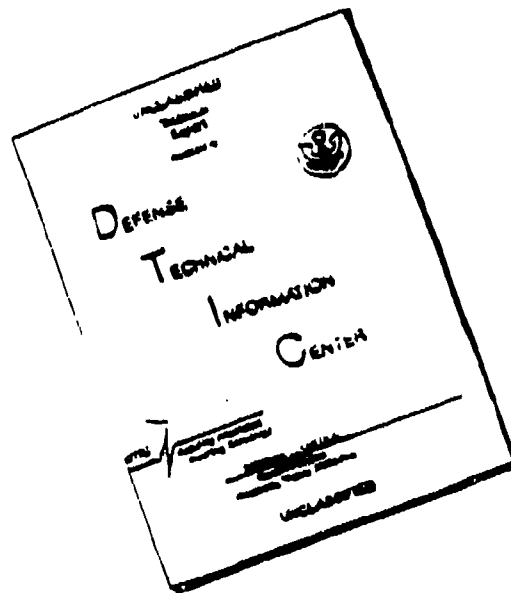
AD 608 090

TECHNICAL GAS DYNAMICS

M. Ye. Deych

Wright-Patterson Air Force Base, Ohio - AF Systems Command  
1961

# DISCLAIMER NOTICE



**THIS DOCUMENT IS BEST  
QUALITY AVAILABLE. THE COPY  
FURNISHED TO DTIC CONTAINED  
A SIGNIFICANT NUMBER OF  
PAGES WHICH DO NOT  
REPRODUCE LEGIBLY.**



# EDITED MACHINE TRANSLATION

TECHNICAL GAS DYNAMICS

BY: M. Ye. Deych

English Pages: 637

THIS TRANSLATION IS A RENDITION OF THE ORIGINAL FOREIGN TEXT WITHOUT ANY ANALYTICAL OR EDITORIAL COMMENT. STATEMENTS OR THEORIES ADVOCATED OR IMPLIED ARE THOSE OF THE SOURCE AND DO NOT NECESSARILY REFLECT THE POSITION OR OPINION OF THE FOREIGN TECHNOLOGY DIVISION.

PREPARED BY:

TRANSLATION DIVISION  
FOREIGN TECHNOLOGY DIVISION  
WP-APB, OHIO.

M. Ye. Deych

TEKHNIЧЕСКАЯ ГАЗОДИНАМИКА

Izdaniye Vtoroye Pererabotannoye

Gosudarstvennoye Energeticheskoye Izdatel'stvo

Moskva - 1961 - Leningrad

Pages 1-671

## TABLE OF CONTENTS

Preface to Second Edition.....	1
Chapter 1. Fundamental Concepts and Equations of Gas Dynamics;.....	4
1-1. Flow Parameters.....	4
1-2. Certain Fundamental Concepts of Aerohydrodynamics.....	7
1-3. Equation of Continuity.....	18
1-4. Equation of Momentum.....	23
1-5. Equation of Motion in a Hydrodynamical Form. I. S. Gromeko's Equations.....	27
Chapter 2. One-Dimensional Motion of Gas;.....	32
2-1. Fundamental Equations of a One-Dimensional Flow. Speed of Sound...	32
2-2. Different Forms of the Energy Equation.....	38
2-3. Flow Parameters in an Arbitrary Section of a Tube of Flow.....	41
2-4. Change in Speed Along a Tube of Flow. The Reduced Flow Rate of Gas.....	47
2-5. Certain Gas-Dynamic Functions of a One-Dimensional Adiabatic Flow.....	52
2-6. Peculiarities of Calculating a One-Dimensional Flow of a Real Gas.....	59
Chapter 3. Two-Dimensional Motion of Gas With Constant Entropy;.....	62
3-1. Potential Motion of Fluid.....	62
3-2. Pressure Coefficients. Critical Mach Number.....	69

3-3. Calculation of Influence of Compressibility by the Method of Small Disturbances.....	73
3-4. Theorem of N. Ye. Zhukovskiy.....	84
3-5. The Two-Dimensional Subsonic Potential Flow of Gas in Curvilinear Channels.....	87
3-6. Two-Dimensional Supersonic Flow.....	93
3-7. Diagram of Characteristics.....	104
3-8. The Intersection and Reflection of Waves of Rarefaction.....	110
Chapter 4. <sup>b</sup> Compression Shocks;.....	118
4-1. The Formation of Shock Waves.....	118
4-2. Equation of Oblique Shock.....	121
4-3. Shock Polar (Curve).....	132
4-4. Variation of Entropy in Shock.....	138
4-5. Compression Shock Losses. Constructing the Process on a Total Heat-Entropy (1-s) Diagram. Compression Shocks in a Real Gas.....	140
4-6. Intersection of Shocks.....	149
4-7. Stepwise Deceleration of Flow.....	155
4-8. The Reflection of Shocks.....	162
4-9. Interaction of Shock and Wave of Rarefaction.....	165
4-10. Conical Compression Shocks.....	167
4-11. Condensation Shocks (Thermal Shocks).....	174
Chapter 5. <sup>c</sup> Motion of Gas During Presence of Friction;..... <i>to p. iii</i>	186
5-1. Temperature of Stagnation in Viscous Fluid.....	186
5-2. Conditions of Gas-Dynamic Similarity.....	191
5-3. One-Dimensional Flow of Gas in the Presence of Friction. Basic Equations.....	197
5-4. Motion of Gas in a Cylindrical Tube.....	200
5-5. Frictional Losses in a Cylindrical Tube (Experimental Data).....	205
5-6. Boundary Layer. Fundamental Concepts and Equations.....	217
5-7. Arbitrary Thicknesses and the Integral Relationship for a Boundary Layer.....	223

5-8. A More General Expression for the Coefficient of Friction Drag in a Boundary Layer in the Presence of a Pressure Gradient.....	227
5-9. Calculation of Laminar Boundary Layer in the Presence of a Pressure Gradient.....	230
5-10. Transition of Laminar Boundary Layer into a Turbulent One.....	233
5-11. Calculation of Turbulent Boundary Layer.....	238
5-12. Boundary Layer During High Speeds. Experimental Data.....	246
5-13. Resistance of Bodies at Subsonic and Supersonic Speeds.....	260
5-14. Resistance of Poorly Streamlined Bodies in a Flow of Gas.....	269
5-15. Motion of Gas in Curvilinear Channels.....	279
5-16. Rotating Flows of a Viscous Gas.....	286
Chapter 6. <del>Outflow of Gas From Narrowing Nozzles and Apertures; The</del> Laval Nozzle;.....	294
6-1. Narrowing Nozzles.....	294
6-2. Narrowing Nozzle With Variable Mode of Flow.....	298
6-3. Outflow of Gas From Aperture With Sharp Edge. Second Critical Ratio of Pressures.....	311
6-4. Calculation of Supersonic Nozzle.....	320
6-5. Two-Dimensional Laval Nozzle Under Nonrated Conditions.....	328
6-6. Conical Laval Nozzles Under Nonrated Conditions. Reaction Force...	347
6-7. Supersonic Nozzle With Oblique Section.....	358
Chapter 7. Movement of Gas in Diffusers: <del>Stage of Ejector;</del> .....	362
7-1. Main Characteristics and Design of Diffusers.....	362
7-2. Subsonic Diffusers.....	371
7-3. Exhaust Ducts of Turbomachines.....	380
7-4. Supersonic Diffusers.....	388
7-5. The Ejector Stage.....	400
7-6. Ejector Stage at Variable Regimes; Limit Regime.....	408
7-7. Selection of Geometrical Parameters of the Ejector Stage.....	421
Chapter 8. <del>Flow of Gas Through Turbomachine Cascades;</del> <sup>to ch. iv</sup> .....	427

8-1. Geometric and Gas-Dynamics Parameters of Cascades. Peculiarities of the Flow in Cascades.....	427
8-2. Calculation of Potential Flow in Cascades According to Channel Theory.....	437
8-3. Forces Acting on Profile in Cascade. Theorem of N. Ye. Zhukovskiy for a Cascade.....	441
8-4. Classification of Losses and Fundamental Characteristics of Cascades.....	446
8-5. The Boundary Layer and Frictional Losses in Cascades.....	452
8-6. Edge Losses in Cascades.....	461
8-7. Certain Results of an Experimental Investigation of Two-Dimensional Cascades at Subsonic Speeds.....	471
8-8. Three-Dimensional Flow of Gas in Cascades. End Losses and Methods of Decreasing Them.....	479
8-9. Procedure for Calculating End Losses in Cascades.....	490
8-10. Structure of Flow and Losses in Reactive Cascades at Transonic and Supersonic Speeds.....	495
8-11. Calculation of Angle of Deflection of Flow in Nozzle Section and the Profiling of Reactive Cascades at Transonic and Supersonic Speeds.....	506
8-12. Structure of Flow in Impulse Cascades at Transonic and Supersonic Speeds.....	512
8-13. Reduced Flow Rate of Gas Through a Cascade. Peculiar Operating Conditions of Impulse Cascade in a Supersonic Flow.....	516
8-14. Profiling and Results of Experimental Investigation of Impulse Cascades During High Speeds.....	524
Chapter 9. <sup>to p. v</sup> Flow of Gas in a Turbomachine Stage;.....	532
9-1. Fundamental Equations.....	532
9-2. Parameters of Flow in Absolute and Relative Motions. One-Dimensional Flow Diagram.....	542
9-3. Equations for Calculating the Distribution of Flow Parameters Along a Radius Within the Scope of Flow Theory.....	553
9-4. Calculation of Flow in a Stage With Long Blades of Constant Profile.....	559
9-5. Certain Methods of Profiling Long Blades of Stages With an Axial Flow of Gas.....	564
9-6. Axial Stage With a Small Variation of the Reaction Along Radius...	571

Chapter 10. Methods of Experimental Investigation of Gas Flows and Blading of Turbomachines.....	579
10-1. Experimental Stands for Investigation of Bladings of Turbo- machines.....	579
10-2. Methods of Measurement of Parameters of the Working Fluid During the Investigation of Gas Flows.....	585
10-3. Optical Methods of Study of Gas Flows.....	599
10-4. Installations for Investigation of Cascades Under Static Conditions.....	607
10-5. Experimental Turbines.....	614
Appendix.....	620
Literature.....	628

In the second, revised edition of this book we consider the fundamental problems of high-speed gas motion. In the first part of the book, consisting of five chapters, we give the general theory of one-dimensional and plane flows. The material in subsequent chapters is applied. In them we examine, in sequence, the motion of gas in nozzles, diffusers, ejectors, lattices, and turbine stages.

This book is a training aid for the course on the fundamentals of gas dynamics for thermotechnical departments of power-engineering and polytechnical institutes.

The book can be useful for engineering and scientific workers in laboratories and design bureaus in factories.



## Preface to Second Edition

In the eight years that have elapsed from the time of first edition of this book, various branches of gas dynamics have developed very intensively. Significant successes were attained in solving a number of the most important gas-dynamic problems in the fields of rocket technology, aviation, interior and exterior ballistics, and industrial aerodynamics. The methods of gas dynamics have occupied a durable place in the thermoelectric power industry.

In connection with the need for increasing the efficiency of steam and gas turbines and compressors, vast developments have been achieved in the field of the gas dynamics of the flow section of turbomachines.

At the same time, during the past eight years there has been additional experience gained in teaching a number of classes in gas dynamics in power-engineering and polytechnical universities.

In these circumstances lies the basis for a substantial revision of the book. All chapters of the book, with the exception of Chapter 4, were subjected to methodical revision, their contents were revised substantially, and certain chapters have been entirely rewritten.

The theory of one-dimensional isentropic motion has been expanded into independent chapter (Chapter 2). Chapter 3 (theory of plane flow of an ideal compressible fluid), is expanded, with a more detailed account of approximation methods of calculating the influence of compressibility in subsonic flows. It includes a method

/

of calculating curvilinear channels.

Chapters 5-10 are virtually entirely rewritten.

In connection with the great practical importance of methods of calculating the losses to friction in different apparatuses, Chapter 5 gives a new account of the boundary layer theory during gradient flow, and the results of an experimental investigation of laminar and turbulent layers at high speeds. In this chapter the sections devoted to questions of gas-dynamic similarity, resistance of poorly streamlined bodies, and motion in tubes and curvilinear channels, are expanded.

Chapter 6 gives a presentation on calculating effuser flows in nozzles. Since we have published a specialized book, and also for the purpose of brevity, the theory of labyrinth seals is not expounded in this second edition. The methodology of designing nozzles in variable regimes is expanded and made more accurate.

The theory and methods of designing diffusers and ejectors comprises an independent chapter, Chapter 7. All sections of this chapter are based on the data of investigation made at the Moscow Institute of Power Engineering [MEI] and other institutes in recent years. In Chapter 7, special attention is devoted to the ducts of exhaust turbomachines.

Chapter 8 is written on the basis of results of theoretical and experimental investigations of lattices, obtained in 1954-1959. All experimental data in this chapter have been up-dated.

In Chapter 9 of the second edition, we discuss questions of gas motion in turbomachine stages. Here, new methods of calculating spatial flow of gas in the stages and certain results of experiments, obtained recently, are discussed. Questions of a variable system of stage regime, discussed in the special literature, are omitted in this edition.

In Chapter 10 are certain recent results, attained in the area of methods of experimental investigation of the flow sections of turbomachines. However, due to the limited size of this book, this chapter is presented in abridged form.

Unlike in the first edition, an attempt to analyze flows of real gas (Chapters 2-4), has been made.

In revising the book, we consider the remarks in published reviews of the book, and also those communicated to the author by persons using the first edition in their work. The entire book, intended as a training aid in the course of hydrogas-dynamics has been re-examined in accordance with changes in educational plans for heat-power engineering departments, and also by taking into account personal experience of teaching the course. The discussion of separate questions has been simplified and made more specific, misprints and errors in the first edition have been corrected.

The book, gives the results of investigations in the USSR and abroad. A significant part of the material consists of results of works conducted by collaborators in the Department of Steam and Gas Turbines, Moscow Institute of Power Engineering [MEI] and, in particular, the author.

During preparation of second edition the author strived to maintain general purpose of book, oriented for the study of fundamental problems in aerodynamics of flow section of turbomachines.

In work on the second edition, author was given much assistance by collaborators of Department of Steam and Gas Turbines [MEI]. Chapter 5 was written in collaboration with A. E. Zaryankin, Chapter 8 with the participation of A. V. Gubarev, and Chapter 10 in collaboration with F. V. Kazintsev.

Author was assisted by the following collaborators in the Department of Steam and Gas Turbines [MEI]: Engineers G. A. Filippov, A. V. Robozhev, and V. G. Filippova, and Doc. A. N. Sherstyuk.

In reviewing and editing the book valuable comments were made by the Doctor of Technical Sciences, S. G. Abramovich and Candidate of Technical Sciences, Doc. B. Ya. Shumyatskiy.

To the indicated persons, and also to the staff of the Department and Laboratory of Steam and Gas Turbines [MEI] the author expresses his deep gratitude.

MT-63-197

Technical Gas Dynamics. Second edition,  
revised. Moscow-Leningrad,  
Gosenergizdat, 1961.  
Pages: Cover - 671.

## CHAPTER 1

### FUNDAMENTAL CONCEPTS AND EQUATIONS OF GAS DYNAMICS

#### 1-1. Flow Parameters

The state of motionless gas, as is well-known, is characterized by the pressure, density, and temperature, i.e., parameters of the state. The relationship between parameters of the state is established in thermodynamics. For a perfect gas this relationship is expressed in simple form by equation of state:

$$\frac{p}{\rho} = gRT, \quad (1-1)$$

where  $g$  is the acceleration of the gravity force,  $m/sec^2$ ;

$R$  is a gas constant\*, having in engineering system of units the dimensionality  $kg \cdot m/kg \cdot deg$ .

For air the gas constant is

$$R = 29.27 \text{ kg} \cdot m/kg \cdot deg.$$

For superheated water vapor (approximately)

$$R = 47.1 \text{ kg} \cdot m/kg \cdot deg.$$

Instead of the density  $\rho$  in the equation of state there may appear the specific gravity or specific volume of gas.

-----  
\* In a number of cases, it is found convenient to combine the constant magnitudes in the equation of state (1-1) and to write it out as:

$$\frac{p}{\rho} = RT, \quad (1-1a)$$

where  $R = gR$  in engineering system of units has the dimensionality  $m^2/sec^2 \cdot deg$ . Here  $p$  in  $kg/m^2$ ,  $\rho$  in  $kg \cdot sec^2/m^4$  and  $T$  in  $K^\circ$ .

Between the density, specific gravity and specific volume there exists the evident relationship

$$\rho = \frac{\gamma}{g} = \frac{1}{gv}, \quad (1-1b)$$

where  $\gamma$  is the specific gravity;  $v$  is the specific volume.

In a gas motion the parameters of state are not only physical, but also dynamic characteristics of the flow. In general case, they vary in the transition from one point of space to another, and from one moment of time to another. Consequently  $p$ ,  $\rho$ , and  $T$  depend on position of point and on time and should be determined as point parameters.

At each point of a perfect gas in motion the parameters of states are associated with each other by the equation of state (1-1). In many practical important cases, the connection between parameters  $p$ , and  $T$  is expressed in more complex form. In an analysis of the physical properties of real gases sometimes it is impossible to disregard the natural volume of molecules and forces of interaction between them. These factors are reflected especially significantly, if the pressures of the gas are high and, consequently, concentration of molecules in a given volume is high.

Thus, in general case of a transient flow of gas the parameters of the state depend on the coordinates and time:

$$\left. \begin{aligned} p &= p(x, y, z, t); \\ \rho &= \rho(x, y, z, t); \\ T &= T(x, y, z, t). \end{aligned} \right\} \quad (1-2)$$

where  $x, y, z$  are coordinates of the point;  $t$  is the time.

For the solution of problem about flow of a compressible fluid, which in the final analysis reduces to establishment of an energy interaction between streamlined body and the fluid (external flow round) or--in case of internal flow (tubes [pipes] channels) - to establishment of an energy equilibrium of the flow, it is necessary to determine kinematic picture of flow, i.e., to find speed [velocity]\* field of flow. This means that equally with the relationships (1-2) there must be found the components of speed of a particle as a function of coordinates and time. The speed of a gas particle varies in the transition from point to point and with the passage of time.

---

\*Translation Editor's Note: The terms "speed" and "velocity" are not differentiated in this monograph.

Consequently, projections of the speed onto the coordinate axis can be represented by the equations:

$$\left. \begin{aligned} u &= u(x, y, z, t); \\ v &= v(x, y, z, t); \\ w &= w(x, y, z, t). \end{aligned} \right\} \quad (1-3)$$

where  $u$  -- projection of vector of speed  $\vec{c}$  onto the  $x$ -axis, and  $v$ ,  $w$  -- onto the  $y$ - and  $z$ -axes, respectively.

Parameters of flow of a real (viscous) fluid include also viscosity, which must be determined as a parameter at a point.

It is known that coefficient of viscosity is the ratio

$$\eta = \frac{\tau}{\frac{dc}{dn}} \quad (1-4)$$

where:  $\tau$  is the frictional force, pertaining to an isolated surface,  $\text{kg/m}^2$ ;

$\frac{dc}{dn}$  is the gradient of speed along normal to isolated surface of friction at a given point ( $\frac{1}{\text{sec}}$ ).

Coefficient of viscosity has dimensionality in engineering system of units  $\text{kg} \cdot \text{sec/m}^2$ .

In a general case, for real gas the coefficient of viscosity depends on the temperature and pressure. However, the dependence on pressure in wide range of the pressure changes is found to be very insignificant and can be ignored. Thus, coefficient of viscosity can be expressed in a dependence only on the temperature. Corresponding formulas for different gases are established experimentally.

We note that law of friction in gases, expressed by formula (1-4), belongs to Newton and is valid only for laminar flows. In turbulent modes of flow, coefficient of friction acquires completely new content in accordance with others, with a significantly more complex mechanism of the viscosity.

For solving the above-indicated fundamental problem it is necessary to determine  $u$ ,  $v$  and  $w$ , and also  $p$ ,  $\rho$  and  $T$  as functions of the coordinates and time. Henceforth there will be analyzed only steady flows of gas and the enumerated parameters of flow should be determined only in relation to the coordinates  $x$ ,  $y$  and  $z$ .

For this purpose, we shall set up six fundamental equations: equations of momentum in projections onto coordinate axis, equation of conservation of mass, equation of conservation of energy and the equation of state.

## 1-2. Certain Fundamental Concepts of Aerohydrodynamics\*

Before we proceed in deriving the fundamental equations of motion, we shall dwell on certain concepts of aerohydrodynamics, necessary for the discussions henceforth.

Let us assume in moving fluid a number of points, each of which lies in sense of the speed vector

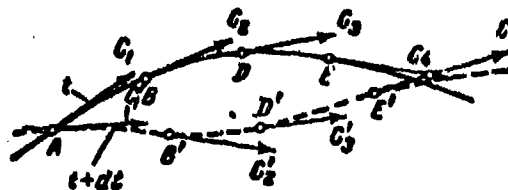


Fig. 1-1. Diagram for determining lines of flow.

of the preceding point. By decreasing the distance between neighboring points down to zero and drawing through these points a line, we obtain a line of flow. For each moment of time, the speed vectors will be tangent to this line. Consequently, motion of fluid particles at a given moment of time occurs along a line of flow.

If the motion is transient, than, obviously, the speed at point A at the following moment of time will differ from  $c_1$  in magnitude and direction (Fig. 1-1). As a result the line of flow will occupy a new position in space. It follows from this that in a transient motion the lines of flow change their shape and position in space.

---

\*In Sec. 1-2 very briefly there are discussed certain basic concepts of aerohydrodynamics, which are encountered in special chapters of the book.

For a steady motion the magnitude and sense of a vector of speed do not vary in time; in this case, the lines of flow maintain a constant shape and position in space.

On the line of flow  $s$  (Fig. 1-2) we isolate the elementary section  $ds$  and will project it onto the coordinate axis (sectors  $dx$ ,  $dy$ ,  $dz$ ). We shall find the angles between element  $ds$  and vector of speed  $\vec{c}$  with coordinate axes:

$$\cos(\widehat{xs}) = \frac{u}{c} = \frac{dx}{ds};$$

$$\cos(\widehat{ys}) = \frac{v}{c} = \frac{dy}{ds};$$

$$\cos(\widehat{zs}) = \frac{w}{c} = \frac{dz}{ds}.$$

Hence, we obtain:

$$\frac{dx}{u} = \frac{dy}{v} = \frac{dz}{w} = \frac{ds}{c}.$$

Consequently, differential equation of the lines of flow has the form:

$$\frac{dx}{u} = \frac{dy}{v} = \frac{dz}{w}. \quad (1-5)$$

We shall isolate in the moving fluid a certain infinitesimally small closed contour, through each point of which passes a line of flow (Fig. 1-3). The totality of all lines of flow will form a certain closed surface a tube of flow. The fluid, moving inside the tube of flow, is called an elementary flow.

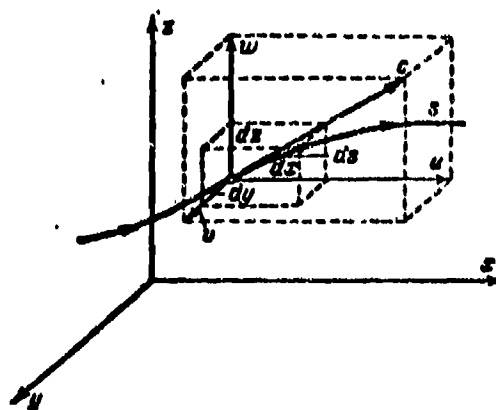


Fig. 1-2. Diagram for deriving differential equation of lines of flow.



In returning to the concept of a line of flow, we note that in a steady motion, it coincides with trajectory of particle. The trajectory is a line, expressing the path made in space by the particle for a certain time interval. The line of flow is an instantaneous line, along which at a given moment of time the aggregate of particles moves. It is obvious that only in a steady motion can these concepts conform, since in this case, the trajectories of all particles, passing through any one fixed point of space, will be identical

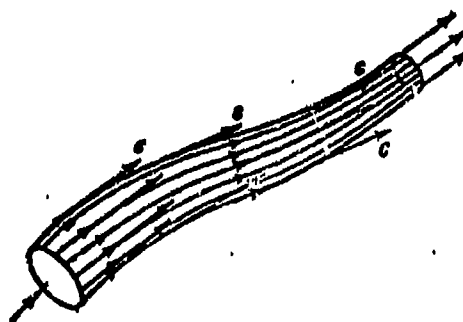


Fig. 1-3. Diagram for determining the tube of flow and elementary flow.

and, consequently, at each moment of time all particles, that lie on trajectory, will generate also a line of flow.

In the general case, the motion a fluid particle is complex. Equally with the translatory motion along certain trajectory the particle may rotate with respect to its own axis and in process of this motion is deformed.

Owing to the nonidentical speeds on different edges the particle experiences a linear deformation and shearing strain or shear. If at initial moment of motion the particle had the shape of a parallelepiped, then with the passage of time as the result of deformation, its shape changes. In case of a compressible fluid also the volume of particle changes.

In turning to Fig. 1-4, we shall analyze the rotation and deformation of one

of the edges of the parallelepiped shown in Fig. 1-2. If a point D (Fig. 1-4) projection of speed onto the x-axis will be  $u$ , then at point A it will be  $u + \frac{\partial u}{\partial y} dy$ . Under the effect of the difference of speeds at these points, equal to  $\frac{\partial u}{\partial y} dy$ , the edge

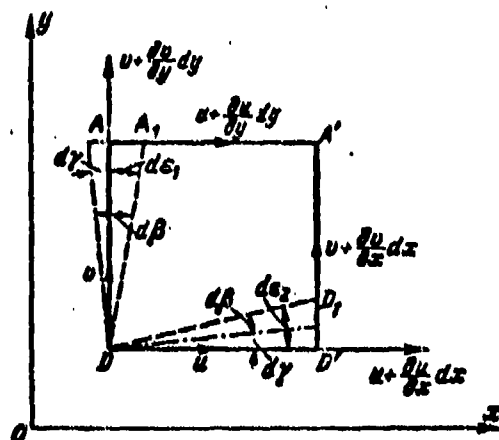


Fig. 1-4. Deformation of edges of particle of fluid in process of motion.

DA will be rotated by certain angle  $d\epsilon_1$ , after being transferred with respect to point D for an element of time  $dt$  to the position  $DA_1$ . The magnitude of the sector  $AA_1$  is determined by the formula

$$\overline{AA_1} = \frac{\partial u}{\partial y} dy dt.$$

During the considered element of time, point D' will be displaced along the y-axis by magnitude

$$\overline{DD_1} = \frac{\partial v}{\partial x} dx dt.$$

Here, the edges DA and DD' will be rotated by small angles  $d\epsilon_1$  and  $d\epsilon_2$ , which are determined by the evident equations:

$$d\epsilon_1 \approx \tan d\epsilon_1 = \frac{\overline{AA_1}}{dy} = \frac{\partial u}{\partial y} dt$$

and

$$d\epsilon_2 \approx \tan d\epsilon_2 = \frac{\overline{DD_1}}{dx} = \frac{\partial v}{\partial x} dt.$$

The considered displacements of the edges DA and DD' are caused by the rotation of the plane fluid element (edges of parallelepiped) and also by its deformation.

We note that if edge only was deformed, without rotation, then the edges DA and DD would be rotated by identical angle toward each other or in opposite directions. Conversely, if the edge completed only a rotary motion (as an absolutely solid body), then the edges DA and DD' would be rotated by an identical angle in one direction.

The motion of the element in the general case can be considered as the sum of deformational and rotational motions and thus there can be determined the angles  $d\epsilon_1$  and  $d\epsilon_2$ . By assuming that as a result of rotation (counter clockwise) the edges DA and DD' were rotated by an angle  $d\gamma$ , and as a result of deformation - complementarily by angle  $d\beta$ , we find:

$$d\epsilon_1 = d\beta - d\gamma;$$

$$d\epsilon_2 = d\beta + d\gamma.$$

From these two equations we obtain:

$$2d\gamma = d\epsilon_2 - d\epsilon_1.$$

The angular velocity of rotation of the edge will be equal to:

$$\frac{d\gamma}{dt} = \frac{1}{2} \left( \frac{d\epsilon_2}{dt} - \frac{d\epsilon_1}{dt} \right).$$

After substituting values of the derivatives  $\frac{d\epsilon_1}{dt}$  and  $\frac{d\epsilon_2}{dt}$ , we find the angular velocity of rotation of edge in such a form:

$$\omega_z = \frac{d\gamma}{dt} = \frac{1}{2} \left( \frac{\partial v}{\partial x} - \frac{\partial u}{\partial y} \right),$$

where  $\omega_z$  is the vector component of angular velocity of rotation, parallel to the z-axis (subscript z indicates direction of axis, relative to which the rotation takes place). We note that  $\omega_z$  is angular velocity of rotation of bisector of angle at point D. Analogous considerations result in the conclusion that the angular velocity of rotation of the two other edges, located in planes xoz and yoz, are expressed in terms of respective values of the partial derivatives  $\frac{\partial u}{\partial z}$ ,  $\frac{\partial w}{\partial x}$ ,  $\frac{\partial v}{\partial z}$ ,  $\frac{\partial w}{\partial y}$ , where the rotation of each edge of the parallelepiped is determined by two angular velocities.

Thus, equations for all three vector components of angular velocity of rotation

will have the form:

$$\left. \begin{aligned} \omega_x &= \frac{1}{2} \left( \frac{\partial w}{\partial y} - \frac{\partial v}{\partial z} \right); \\ \omega_y &= \frac{1}{2} \left( \frac{\partial u}{\partial z} - \frac{\partial w}{\partial x} \right); \\ \omega_z &= \frac{1}{2} \left( \frac{\partial v}{\partial x} - \frac{\partial u}{\partial y} \right). \end{aligned} \right\} \quad (1-6)$$

Equations (1-6) express vector components of angular velocity of rotation of a fluid particle  $\omega$ , magnitude of which is determined as the geometric sum of  $\omega_x$ ,  $\omega_y$  and  $\omega_z$ :

$$\omega = \sqrt{\omega_x^2 + \omega_y^2 + \omega_z^2}. \quad (1-7)$$

Formulas (1-6) determine in differential form the relationship between components of angular velocity of rotation and of speed of translational motion.

Rotation of particle around the axes, passing through the particle is called vortex motion. Experience shows that in all cases of motion of a real (viscous) fluid the entire field of flow or a portion of it is vortical. In those regions of the flow, where the vortex motion of the particles is absent, angular velocity of the rotation is equal to zero ( $\omega = 0$ ). In these regions, particles of the fluid may move along trajectories of any form, by being deformed in this connection but by not being rotated relative to their axes.

If in a particular case, at  $\omega = 0$  trajectories of the particles are closed curves, then such a motion will be a particular case of circulatory motion. It should be emphasized that in such a motion the particles realize a rotation around a certain axis, located outside the trajectory, but are not rotated with respect to their own axes.

Concepts of vortex and circulatory motions of a fluid play a major role in hydromechanics. In this connection, we shall dwell on one very important characteristic of the flow--the circulation of speed. Let us consider still another example of circulatory flow. In the flow around an asymmetric wing profile (Fig. 1-5) by a

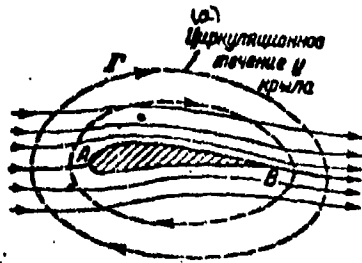


Fig. 1-5. Scheme of flow around wing profile.  
KEY: (a) Circulatory flow along wing.

two-dimensional parallel flow, the lines of flow in the region of flow along wing are distorted, since the wing disturbs the flow. The character of disturbance, introduced by wing in the flow, can be explained by determining speed at different points of field along the wing. In comparing local values of the speeds with speed of incident flow, it is readily established that the flow along the wing can be presented as the

sum of translational undisturbed flow and flow along the closed trajectories. Intensity of flow along the wing can be characterized by the magnitude of circulation of speed, which is determined by the equation

$$\Gamma = \oint c_{\perp} dl, \quad (1-8)$$

where  $c_{\perp}$  is the projection of vector of speed onto direction of element of contour  $l$ .

In a general case an arbitrarily selected contour  $l$  may not coincide with line of flow of circulatory flow.

Formula (1-8) can be written in such a form:

$$\Gamma = \oint c \cos(\widehat{c, l}) dl. \quad (1-9)$$

Thus, circulatory motion can be called that motion, at which the circulation of speed is different from zero. If  $\Gamma = 0$ , then the motion is called noncirculatory.\*

In calculating the circulation of speed by formula (1-9) it is necessary to agree on direction of the integration around the contour. A positive direction

---

\*In turning to formula (1-9), we see that expression for circulation of integral is reminiscent of the well-known equation of work of force vector. This external analogy makes it possible to understand the mechanical sense of circulation (product of speed by the length of trajectory) and gives the basis of arbitrarily calling the magnitude  $\Gamma$  the work of vector of the speed.

of the circulation, as a rule, is assumed that direction, at which the enclosed region of flow within contour remains to the right (Fig. 1-5).

The concept of circulation is very widely used in investigating vortex motions of a gas. In the theory of vortex motion there has been proven a number of fundamental theorems associating the circulation integral with fundamental characteristics of a vortex. We shall dwell first of all on the basic concepts of vortex motion: vortex line, vortex tube and vortex string.

These concepts closely agree with the presented above concepts of a line of flow, a tube of flow and an elementary flow.

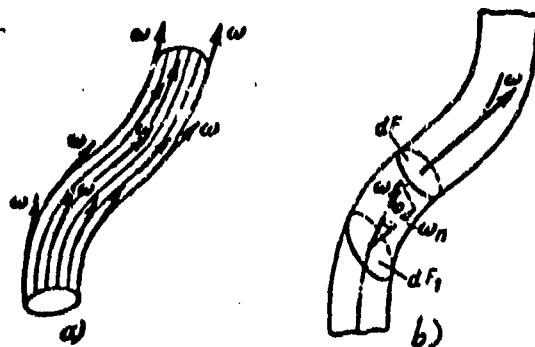


Fig. 1-6. Vortex tube and vortex filament.

Vortex line is that line in a flow, at each point of which the sense of the vector of the angular velocity coincides with the direction of tangent to this line. We remember that the vector of angular velocity is directed perpendicularly to the plane of rotation. Consequently, vortex line is the instantaneous axis of rotation of particles of a fluid, which are located on this line.

A vortex tube is a closed surface, consisting of vortex lines, constructed in an elementary contour (Fig. 1-6,a). The fluid, filling in the vortex tube, forms a vortex filament. If the vortex tube has a section of finite dimensions, then particles, filling it and being in rotation, will form vortex string.

Let us consider vortex filament (Fig. 1-6,b). We shall draw a section normal to the axis of the filament. The intensity or strength of the vortex filament is characterized by the doubled product of vector of angular velocity of rotation  $\omega$  by the

cross-section area of filament  $dF$ :

$$dJ = 2\omega_n dF.$$

In the general case considered section of filament may be drawn arbitrary at a certain angle to its axis (Fig. 1-6,b); then the intensity  $dJ$  is determined by the formula

$$dJ = 2\omega_n dF_1,$$

where  $\omega_n$  is the projection of vector of angular velocity onto direction of axis of vortex filament:

$$\omega_n = \omega \cos \varphi.$$

Thus, the strength of the vortex filament is determined as twice the product of area of an arbitrary section of the filament and the projection of vector  $\omega$  onto the direction of normal with respect to selected section.

In the theory of vortex motion it is proved that the circulation integral along a closed contour occupying the vortex filament is equal to the strength of vortex filament, i.e.

$$d\Gamma = dJ = 2\omega_n dF.$$

For a contour enveloping a vortex string of finite section, consisting of an infinite number of vortex filaments, circulation integral is determined by the line integral

$$\Gamma = 2 \oint \omega_n dF.$$

This expression, obtained by Stokes, makes it possible to formulate one of the basic theorems of the vortex motion: The circulation integral along any closed contour, made in a fluid is equal to the sum of the intensities of the vortices, enveloping the contour, if this contour by means of continuous deformation can contract to a point, by not going out beyond limits of the fluid. If the contour envelopes solid body (for example, profile of blade), then it is impossible to use the considered theorem in this case, since the contour can not contract to a point not going beyond the limits of the fluid.

However if the closed contour is drawn as is shown in Fig. 1-7 (contour ABCDA), then according to Stoke's equation we obtain:

$$\Gamma_{ABCD} = \Gamma_{AB} + \Gamma_{BC} + \Gamma_{CD} + \Gamma_{DA} = 2 \oint \omega_n dF,$$

since

$$\Gamma_{BC} = -\Gamma_{DA} \text{ and } \Gamma_{AB} = 2 \oint \omega_n dF + \Gamma_{CD}.$$

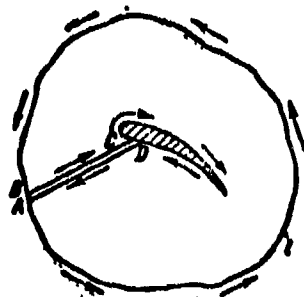


Fig. 1-7. Diagram for determining circulation integral along closed contour, enveloping the profile.

Stoke's formula leads to the conclusion that the core of a linear vortex of constant section is rotated, as a solid body, with a constant angular velocity. Actually, on the basis of the indicated theorem for a linear infinitely long vortex it is possible to write out that the circulation along the contour, enveloping the vortex,

$$\Gamma = 2\omega F = \text{const.}$$

At  $F = \text{const}$  at an arbitrary point of vortex core  $\omega = \text{const}$ . The linear speed in core will be:

$$c_n = \omega r,$$

where  $r$  is the radius of considered point.

Consequently, distribution of speeds in field of the vortex will be linear. On external surface of core speed has a maximum value:

$$c_{n \max} = \omega r_0$$

( $r_0$  is the radius of vortex).

In hydromechanics also the theorem of the invariability of circulation in time in an ideal inviscid fluid (theorem of Thompson) is proven.

According to Thompson's theorem for ideal fluid outside a vortex the circulation maintains a constant value along any contour, enveloping the vortex. The



circulatory flow around an infinitely long line vortex (outside vortex) has a hyperbolic field of speeds (Fig. 1-8), since

$$\Gamma = 2\pi\omega r^2 = 2\pi c_u r$$

and

$$c_u = \frac{c_{u \max} r_0}{r} = \frac{\Gamma}{2\pi r}.$$

It is readily seen that in accordance with Thompson's theorem in an ideal fluid a rotary vortex motion of the particles cannot appear or disappear. This also is physically intelligible,

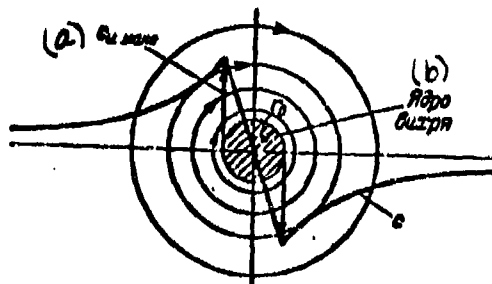


Fig. 1-8. Field of speeds in vortex core and in external flow.  
KEY: (a)  $C_u \max$ ; (b) Vortex core.

since in such liquid there is absent mechanism of transfer of rotation and stagnation.

By observing the flow of real viscous fluid, it is possible to point out a large number of examples of the generation and attenuation of vortices. In this connection condition of constancy of circulation, which is most important property of motion of an ideal fluid, is not maintained.

Differences in properties of ideal and real fluids can be traced with an analysis of the spectrum of asymmetric flow around the body. If trailing edge of body is made sharp (body of wing profile), then a continuous flow around such an edge by an ideal fluid must result in a tangential discontinuity beyond the profile (Fig. 1-9). In a real viscous fluid the presence of such a discontinuity results in the flow during descent from the trailing edge being whirled (Fig. 1-9,b).

Thus, the genesis of vortices, and consequently, also the circulation around a profile is explained by the influence of viscosity.



Fig. 1-9. Vortex formation during descent of flow from wing profile.

At the initial moment of time flow along the wing is without circulation. At the point descent by virtue of the property of viscosity there is generated an initial vortex (Fig. 1-9,b), which creates a circulation. Experience shows that with a not very large asymmetry this vortex generates along the trailing edge. The corresponding condition in the flow of an ideal fluid, according to which the point of descent should be on the trailing edge, is called the Zhukovskiy-Chaplygin postulate: in a continuous asymmetric flow round a profile by an ideal fluid around it there will form that circulation  $\Gamma$ , which assumes a descent of flow from the trailing edge.

This condition, formulated by N. Ye. Zhukovskiy and S. A. Chaplygin, makes it possible to calculate the circulation  $\Gamma$  and at the same time the wing lift.

### 1-3. Equation of Continuity

We shall isolate in a moving gas an elementary volume in the form of a parallelepiped (Fig. 1-10) and shall write out the condition of invariability of mass in time for this element. This condition will be expressed in the law of conservation of mass; it can be presented in the form:

$$\frac{d(\rho \Delta V)}{dt} = 0, \quad (1-10)$$

where  $\Delta V$  is the volume of element;

$\rho$  is the average density of the element.

We differentiate, by bearing in mind that  $\rho$  and  $\Delta V$  are variable values.

$$\Delta V \frac{d\rho}{dt} + \rho \frac{d\Delta V}{dt} = 0.$$

We shall divide this equation by  $\rho \Delta V$ . We obtain the equation of continuity in

the form:

$$\frac{1}{\rho} \frac{d\rho}{dt} + \frac{1}{\Delta V} \frac{d\Delta V'}{dt} = 0. \quad (1-10a)$$

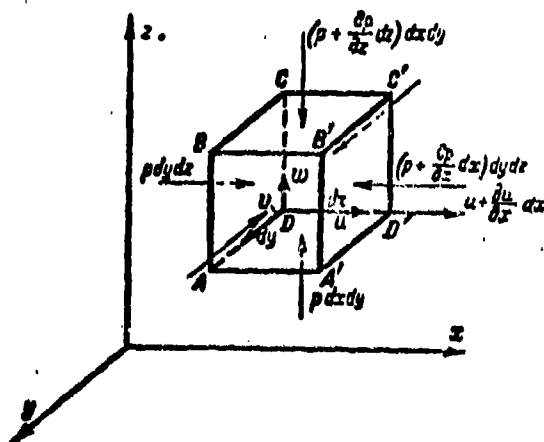


Fig. 1-10. Diagram for deriving Euler equation.

Here the derivative  $\frac{d\Delta V}{dt}$  expresses the rate of change of volume or, consequently, rate of volumetric deformation of fluid particle. The term  $\frac{1}{\Delta V} \frac{d\Delta V'}{dt}$  is the rate of the relative volumetric deformation.

In the particular case of an incompressible fluid, when  $\rho = \text{const}$  the latter equation acquires a very simple form:

$$\frac{d\Delta V}{dt} = 0,$$

which expresses the condition of constancy of volume of element: The rate of volumetric deformation of an element is equal to zero. It follows from this that a particle of an incompressible fluid is deformed in process of motion so that its volume is kept constant.

We shall determine the magnitude of rate of relative volumetric deformation of particle, expressing it in terms of its corresponding projections of speed  $u$ ,  $v$  and  $w$ .

We then calculate the linear deformation of particle in direction of the  $x$ -axis (Fig. 1-10). This deformation will occur in connection with the fact that rates of the edges  $ABCD$  and  $A'B'C'D'$  are not identical. If the rate of left edge is equal

to  $u$ , then the rate of the right will be  $u + \frac{\partial u}{\partial x} dx$ .

We assume that within the limits of each of the considered edges of parallelepiped, the speeds are constant. During element of time  $dt$  the left edge ABCD will be displaced by a distance  $u dt$  to the right. During the same time interval the edge A'B'C'D' will be displaced in the same direction by a distance  $(u + \frac{\partial u}{\partial x} dx) dt$ . Consequently, volume of element will change, since the speeds of these two edges are different. After calculating absolute change of volume of particle along the direction of x-axis, we obtain:

$$(u + \frac{\partial u}{\partial x} dx) dy dz dt - u dy dz dt = \frac{\partial u}{\partial x} dx dy dz dt.$$

In reasoning analogously, for other two pairs of edges there can be obtained the increments in volume of particle along the y- and z-axes in the following form:

$$\frac{\partial v}{\partial y} dx dy dz dt;$$

$$\frac{\partial w}{\partial z} dx dy dz dt.$$

The total change in volume of particle is determined as the sum of these increments.

Consequently, rate of relative volumetric deformation is determined very readily:

$$\frac{1}{\Delta V} \cdot \frac{d\Delta V}{dt} = \frac{\partial u}{\partial x} + \frac{\partial v}{\partial y} + \frac{\partial w}{\partial z}, \quad (1-11)$$

since volume of element  $\Delta V = dx dy dz$ .

After substituting (1-11) into the equation of continuity (1-10a), we obtain:

$$\frac{1}{\rho} \cdot \frac{d\rho}{dt} \left( \frac{\partial u}{\partial x} + \frac{\partial v}{\partial y} + \frac{\partial w}{\partial z} \right) = 0. \quad (1-10b)$$

We note here that entering into the equation (1-11) the direct partial derivatives  $\frac{\partial u}{\partial x}$ ,  $\frac{\partial v}{\partial y}$ ,  $\frac{\partial w}{\partial z}$  have a specific mechanical meaning. From preceding considerations it is obvious that these derivatives determine magnitude of rate of relative linear deformations of edges of the parallelepiped. Let us consider, for example, linear deformation of the edge DCC'D' in direction of x-axis. Since rate of edge CD is equal to  $u$ , and edge C'D' to  $u + \frac{\partial u}{\partial x} dx$ , then the elongation of edge along x

will be:

$$\left(u + \frac{\partial u}{\partial x} dx\right) dt - u dt = \frac{\partial u}{\partial x} dx dt.$$

The relative elongation amounts to  $\frac{\partial u}{\partial x} dt$ , and the rate of relative elongation  $\frac{\partial u}{\partial x}$ .

We now transform equation (1-10b). Since  $\rho = \rho(x, y, z, t)$  then the total derivative of density is equal to:

$$\frac{d\rho}{dt} = \frac{\partial \rho}{\partial x} \frac{dx}{dt} + \frac{\partial \rho}{\partial y} \frac{dy}{dt} + \frac{\partial \rho}{\partial z} \frac{dz}{dt} + \frac{\partial \rho}{\partial t}.$$

By bearing in mind that  $\frac{dx}{dt} = u$ ;  $\frac{dy}{dt} = v$ ;  $\frac{dz}{dt} = w$ , we obtain:

$$\frac{d\rho}{dt} = u \frac{\partial \rho}{\partial x} + v \frac{\partial \rho}{\partial y} + w \frac{\partial \rho}{\partial z} + \frac{\partial \rho}{\partial t}.$$

After substituting  $\frac{d\rho}{dt}$  into equation (1-10b) and transforming, we shall have:

$$\frac{\partial \rho}{\partial t} + \frac{\partial (\rho u)}{\partial x} + \frac{\partial (\rho v)}{\partial y} + \frac{\partial (\rho w)}{\partial z} = 0. \quad (1-12)$$

If the motion is steady, then  $\frac{\partial \rho}{\partial t} = 0$ .

For an incompressible fluid ( $\rho = \text{const}$ ) there is readily obtained from equation (1-12):

$$\frac{\partial u}{\partial x} + \frac{\partial v}{\partial y} + \frac{\partial w}{\partial z} = 0. \quad (1-13)$$

Equation (1-12) is equation of continuity of a gas flow in differential form. This equation was for the first time obtained by Euler in 1659. We see that it associates changes of the density with changes of components of the speed  $u$ ,  $v$  and  $w$ . By bearing in mind mechanical meaning of the partial derivatives  $\frac{\partial u}{\partial x}$ ,  $\frac{\partial v}{\partial y}$ , and  $\frac{\partial w}{\partial z}$ , expressing rates of relative linear deformation of fluid particle in the direction of the  $x$ ,  $y$ , and  $z$  axes, it is possible on the basis of the equation of continuity to conclude that the deformation of such a particle is subject to a definite law and cannot be arbitrary. For an incompressible fluid, equation (1-13) shows that a particle of an incompressible fluid in process of motion is deformed with the conservation of volume. For a compressible fluid a deformation of the particle takes place with a change in the volume. In this case equation of continuity associates the changes in volume and density of the particle.

Equation (1-12) is written out in a rectilinear system of coordinates. In many cases, especially in studying processes proceeding in turbomachine, it is convenient to use the cylindrical system of coordinates.

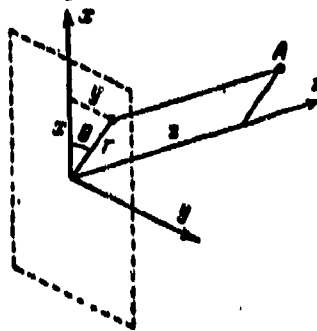


Fig. 1-11. Position of point in rectilinear and cylindrical coordinate systems.

The position of certain point A in cylindrical coordinates is determined by the radius vector  $r$ , polar angle  $\theta$ , and the  $z$ -axis (Fig. 1-11). By giving to the indicated coordinates infinitesimally small increments  $dr$ ,  $d\theta$  and  $dz$ , we shall isolate in the mass of the fluid the particle ABCDA'B'C'D' (Fig. 1-12).

The motion of the point in the considered coordinates is given, if components of the speed are known:

$c_r = \frac{dr}{dt}$  is the radial component;

$c_\theta = r \frac{d\theta}{dt}$  is the tangential component (normal to radius vector);

$w = \frac{dz}{dt}$  is the axial component of the speed.

We shall compose the equation of continuity in cylindrical coordinates. We shall calculate the rate of relative volumetric deformation of a moving fluid particle, shown in Fig. 1-12. The change in volume of this particle during an element of time  $dt$  in direction of radius vector can be expressed as:

$$\left[ \left( c_r + \frac{\partial c_r}{\partial r} dr \right) (r + dr) d\theta - c_r r d\theta \right] dz dt$$

or, by discarding first terms,

$$\left( \frac{c_r}{r} + \frac{\partial c_r}{\partial r} \right) r dr d\theta dz dt.$$

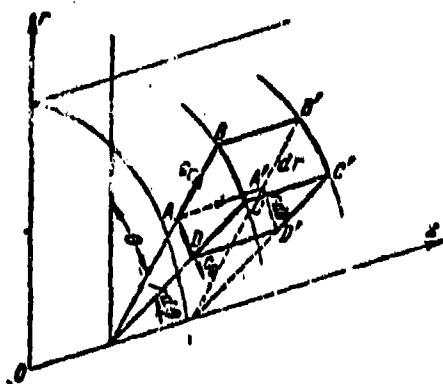


Fig. 1-12. Diagram for deriving Euler equations in the cylindrical system of coordinates.

The change of volume in a direction, normal to radius vector, will be:

$$\left[ \left( c_\theta + \frac{\partial c_\theta}{\partial \theta} d\theta \right) - c_\theta \right] dz dr dt = \frac{1}{r} \frac{\partial c_\theta}{\partial \theta} dz dr d\theta dt.$$

Along the z-axis the volume varies by the magnitude

$$\left[ \left( w + \frac{\partial w}{\partial z} dz \right) - w \right] r d\theta dr dt = \frac{\partial w}{\partial z} r dz dr d\theta dt.$$

Total change in volume for the considered time interval amounts to:

$$d\Delta V = \left( \frac{c_r}{r} + \frac{\partial c_r}{\partial r} + \frac{1}{r} \frac{\partial c_\theta}{\partial \theta} + \frac{\partial w}{\partial z} \right) r dz dr d\theta dt.$$

Then the rate of the relative volumetric deformation will be:

$$\frac{1}{\Delta V} \frac{d\Delta V}{dt} = \frac{c_r}{r} + \frac{\partial c_r}{\partial r} + \frac{1}{r} \frac{\partial c_\theta}{\partial \theta} + \frac{\partial w}{\partial z}.$$

After substituting this expression into the equation of continuity (1-10a) and expressing the total derivative of the density in cylindrical coordinates, after transformations finally we obtain:

$$\frac{\partial \rho}{\partial t} + \frac{\partial (\rho w)}{\partial z} + \frac{1}{r} \frac{\partial (\rho r c_r)}{\partial r} + \frac{1}{r} \frac{\partial (\rho c_\theta)}{\partial \theta} = 0. \quad (1-14)$$

#### 1-4. Equation of Momentum

Below there will be considered the motion of gas without an internal heat exchange in the absence of thermal conductivity and friction.

Such a motion, of course, is an idealized/<sup>model</sup> of a real motion, in which there are manifested frictional forces, there appear temperature gradients and there is

realized an internal heat exchange between neighboring particles.

The adopted simplified diagram of flow of a compressible fluid, however, plays a very important role in gas dynamics, since it serves as a well-known standard in the analysis of real processes of flow. Many practically important real cases of flow of gas are very close in their own properties to the considered idealized flow, the laws or regularities of which in these cases can be used for the calculations. With the indicated simplifications the obtainable relationships are widely used for an analysis of physical properties of flow, without an energy exchange with the environment.

We shall establish the basic principles to which such a schematized model of flow is subject.

We shall isolate in a fluid flow an elementary parallelepiped. Within the closed surface of the parallelepiped mass of fluid is confined. We shall apply to the considered element the theorem of momentum.

The change in momentum of a mass of gas, concentrated within the surface, occurs in a general case owing to the fact that each particle, by being displaced, occupies with the passage of time a new position and acquires a new speed, and also because at each point in space speed changes in time. In a steady motion the momentum varies only in connection with change in position of the particles.

In accordance with the well-known theorem of mechanics a change in momentum of the mass, enclosed in an isolated element, is equal to the momentum of external forces. We shall formulate the equation of momentum in projections onto coordinate axis (Fig. 1-10).

On the edge ABCD in direction of x-axis there acts the force of pressure  $p dy dz$ , the momentum of which will be:  $p dy dz dt$ .

The momentum of forces of pressure, acting on the edge A'B'C'D', is equal to:

$$-\left(p + \frac{\partial p}{\partial x} dx\right) dy dz dt.$$



We note that, in addition to the forces of pressure, on the element there may act the body forces (gravitational, magnetic and electrostatics). Of these most frequently it is necessary to consider gravitational force, that is gravity. For gases due to their relatively low density the gravity in comparison with the forces of pressure is found to be small and it usually can be ignored.

However, in certain problems the influence of body forces should be evaluated. We designate by  $X$ ,  $Y$  and  $Z$  the projections of unit of a body force (relating to a mass of fluid) on the coordinate axes  $x$ ,  $y$  and  $z$ . Then the projections of total body force on coordinate axes will be:

$$X\rho dx dy dz, Y\rho dx dy dz \text{ and } Z\rho dx dy dz.$$

We shall introduce the momentum of body forces in projection onto the  $x$ -axis, equal to  $X\rho dx dy dz dt$ . Then the total momentum is equal to the change in momentum:

$$X\rho dx dy dz dt = \frac{\partial p}{\partial x} dx dy dz dt = \rho dx dy dz du,$$

where  $\rho dx dy dz$  is the mass of element.

Consequently,

$$\frac{du}{dt} = X - \frac{1}{\rho} \cdot \frac{\partial p}{\partial x}. \quad (1-15a)$$

Analogous equations are obtained in the projection onto the  $y$ - and  $z$ -axes:

$$\frac{dv}{dt} = Y - \frac{1}{\rho} \cdot \frac{\partial p}{\partial y}. \quad (1-15b)$$

$$\frac{dw}{dt} = Z - \frac{1}{\rho} \cdot \frac{\partial p}{\partial z}. \quad (1-15c)$$

By bearing in mind that increments of the speed are equal to:

$$du = \frac{\partial u}{\partial x} dx + \frac{\partial u}{\partial y} dy + \frac{\partial u}{\partial z} dz + \frac{\partial u}{\partial t} dt;$$

$$dv = \frac{\partial v}{\partial x} dx + \frac{\partial v}{\partial y} dy + \frac{\partial v}{\partial z} dz + \frac{\partial v}{\partial t} dt;$$

$$dw = \frac{\partial w}{\partial x} dx + \frac{\partial w}{\partial y} dy + \frac{\partial w}{\partial z} dz + \frac{\partial w}{\partial t} dt,$$

for projections of the acceleration onto coordinate axes we shall obtain from

(1-15):

$$\left. \begin{aligned} \frac{du}{dt} &= \frac{\partial u}{\partial t} + u \frac{\partial u}{\partial x} + v \frac{\partial u}{\partial y} + w \frac{\partial u}{\partial z} = X - \frac{1}{\rho} \frac{\partial p}{\partial x}; \\ \frac{dv}{dt} &= \frac{\partial v}{\partial t} + u \frac{\partial v}{\partial x} + v \frac{\partial v}{\partial y} + w \frac{\partial v}{\partial z} = Y - \frac{1}{\rho} \frac{\partial p}{\partial y}; \\ \frac{dw}{dt} &= \frac{\partial w}{\partial t} + u \frac{\partial w}{\partial x} + v \frac{\partial w}{\partial y} + w \frac{\partial w}{\partial z} = Z - \frac{1}{\rho} \frac{\partial p}{\partial z}. \end{aligned} \right\} \quad (1-16)$$

The derivatives  $\frac{du}{dt}$ ,  $\frac{dv}{dt}$ , and  $\frac{dw}{dt}$  express projections of the total acceleration of a moving particle. Equations (1-16) show that the acceleration of a fluid element is caused by corresponding changes of pressure forces, acting on this element, and by the body forces. Equations (1-16) also were obtained by Euler.

We shall formulate now equations of momentum in cylindrical coordinates. For this purpose we shall find components of the acceleration in a new system of coordinates. The total acceleration along radius vector is expressed as sum of relative acceleration  $\frac{dc_r}{dt}$  and centripetal acceleration  $-\frac{c_\theta^2}{r}$ . Consequently, the radial acceleration is equal to:

$$\frac{dc_r}{dt} - \frac{c_\theta^2}{r}.$$

The total acceleration in a direction, normal to the radius vector, is composed of the tangential acceleration  $r \frac{d^2\theta}{dt^2}$  and the Coriolis acceleration  $2 \frac{dr}{dt} \frac{d\theta}{dt}$ , i.e.,

$$r \frac{d^2\theta}{dt^2} + 2 \frac{dr}{dt} \frac{d\theta}{dt} = \frac{1}{r} \frac{d(r c_\theta)}{dt} = \frac{dc_\theta}{dt} + \frac{c_r c_\theta}{r}.$$

Then the equation of momentum (1-15) can be written as:

$$\left. \begin{aligned} \frac{dc_r}{dt} - \frac{c_\theta^2}{r} &= R - \frac{1}{\rho} \frac{\partial p}{\partial r}; \\ \frac{dc_\theta}{dt} + \frac{c_r c_\theta}{r} &= \Theta - \frac{1}{\rho} \frac{\partial p}{r \partial \theta}; \\ \frac{dw}{dt} &= Z - \frac{1}{\rho} \frac{\partial p}{\partial z}, \end{aligned} \right\} \quad (1-17)$$

where  $R$ ,  $\Theta$  and  $Z$  are projections of the unit of body force onto the coordinate axes  $r$ ,  $\theta$  and  $z$ .

After substituting (1-17) values of the total derivatives  $\frac{dc_r}{dt}$ ,  $\frac{dc_\theta}{dt}$  and  $\frac{dw}{dt}$  in terms of partial derivatives finally we find:

$$\left. \begin{aligned} \frac{dc_r}{dt} + c_r \frac{\partial c_r}{\partial r} + \frac{c_\theta}{r} \frac{\partial c_r}{\partial \theta} + w \frac{\partial c_r}{\partial z} - \frac{c_\theta^2}{r} &= R - \frac{1}{\rho} \frac{\partial p}{\partial r}; \\ \frac{dc_\theta}{dt} + c_r \frac{\partial c_\theta}{\partial r} + \frac{c_\theta}{r} \frac{\partial c_\theta}{\partial \theta} + w \frac{\partial c_\theta}{\partial z} + \frac{c_r c_\theta}{r} &= \Theta - \frac{1}{\rho} \frac{\partial p}{r \partial \theta}; \\ \frac{dw}{dt} + c_r \frac{\partial w}{\partial r} + \frac{c_\theta}{r} \frac{\partial w}{\partial \theta} + w \frac{\partial w}{\partial z} &= Z - \frac{1}{\rho} \frac{\partial p}{\partial z}. \end{aligned} \right\} \quad (1-17a)$$

1.5. Equations of Motion in a Hydromechanical Form.  
I. S. Gromeko's Equations.

Equations of motion in form of Euler are general equations of mechanics. Peculiarities of the motion of a fluid medium may be reflected by introducing specific elements of the motion, this is, components of vortex, kinetic and potential energy, into equations of Euler.

Components of angular velocity of rotation  $w_x$ ,  $w_y$  and  $w_z$  can be directly introduced into the equations of motion (1-16) and (1-17a). If to left-hand side of the first of equations (1-16) we add, and then subtract  $v \frac{\partial v}{\partial x}$  and  $w \frac{\partial w}{\partial x}$ , then after simple transformation we obtain:

$$\frac{\partial u}{\partial t} + u \frac{\partial u}{\partial x} + v \frac{\partial v}{\partial x} + w \frac{\partial w}{\partial x} - v \left( \frac{\partial v}{\partial x} - \frac{\partial u}{\partial y} \right) + w \left( \frac{\partial u}{\partial z} - \frac{\partial w}{\partial x} \right) = X - \frac{1}{\rho} \frac{\partial p}{\partial x}.$$

By bearing in mind that

$$u \frac{\partial u}{\partial x} + v \frac{\partial v}{\partial x} + w \frac{\partial w}{\partial x} = \frac{\partial}{\partial x} \left( \frac{c^2}{2} \right),$$

and in considering formula (1-6), we present the first of the equations of motion

$$(1-16) \text{ in the form: } \frac{\partial u}{\partial t} + \frac{\partial}{\partial x} \left( \frac{c^2}{2} \right) - 2(vw_x - uw_y) = X - \frac{1}{\rho} \frac{\partial p}{\partial x}. \quad (1-18a)$$

Analogously it is possible to transform also the two other equations of motion.

As a result we obtain:

$$\frac{\partial v}{\partial t} + \frac{\partial}{\partial y} \left( \frac{c^2}{2} \right) - 2(wu_x - uv_z) = Y - \frac{1}{\rho} \frac{\partial p}{\partial y}; \quad (1-18b)$$

$$\frac{\partial w}{\partial t} + \frac{\partial}{\partial z} \left( \frac{c^2}{2} \right) - 2(uw_y - vw_x) = Z - \frac{1}{\rho} \frac{\partial p}{\partial z}. \quad (1-18c)$$

Analogously it is possible to transform equation (1-17a) in cylindrical system of coordinates. Components of angular velocity of rotation in this system of coordinates are expressed by the equations:

$$\left. \begin{aligned} w_r &= \frac{1}{2r} \left( \frac{\partial w}{\partial \theta} - \frac{\partial (c_\theta r)}{\partial z} \right); \\ w_\theta &= \frac{1}{2} \left( \frac{\partial c_r}{\partial z} - \frac{\partial w}{\partial r} \right); \\ w_z &= \frac{1}{2r} \left( \frac{\partial (c_\theta r)}{\partial r} - \frac{\partial c_r}{\partial \theta} \right). \end{aligned} \right\} \quad (1-19)$$

By using the known formulas for the conversion of rectilinear to cylindrical coordinates, there are readily expressed components of angular velocities  $\omega_r$ ,  $\omega_\theta$  and  $\omega_z$  through  $\omega_x$ ,  $\omega_y$  and  $\omega_z$ . The angular velocity of rotation  $\omega$  may be expressed in terms of the components  $\omega_x$ ,  $\omega_y$  and  $\omega_z$  on the basis of equation (1-19) since

$$\omega^2 = \omega_x^2 + \omega_y^2 + \omega_z^2 = \omega_r^2 + \omega_\theta^2 + \omega_z^2.$$

The sense of magnitudes  $\omega_r$ ,  $\omega_\theta$  and  $\omega_z$  is explained in Fig. 1-13. The component  $\omega_r$  determines that rotation of the particles, whose axis is the radius vector (radial vortex); component  $\omega_\theta$  characterizes the rotation of particles with respect to an axis, having the shape of a circle (annular vortex);  $\omega_z$  is the angular velocity of rotation about the z-axis.

We shall introduce on left side of the first equation (1-17a) the terms:  $\pm \omega \frac{\partial \omega}{\partial r}$ ,  $\pm c_\theta \frac{\partial \omega}{\partial r}$ ; then

$$\frac{\partial c_r}{\partial t} + \frac{\partial}{\partial r} \left( \frac{c^2}{2} \right) - 2(c_\theta \omega_z - \omega_\theta c_z) = R - \frac{1}{\rho} \frac{\partial p}{\partial r}; \quad (1-20)$$

analogously the second and third equations (1-17a) are transformed.

The advantages of equations of momentum (1-18)–(1-20) are evident. In distinction from equations of Euler they contain in explicit form magnitudes, characterizing peculiarities of the motion of a fluid – a readily deformable medium. These equations include components of angular velocity of rotation of the particles, i.e., terms, characterizing vortex motion of the fluid, the kinetic energy and potential energy of the pressure, and also potential energy of the body forces.

The introduction of these magnitudes considerably simplifies analysis of many complex forms of motion of fluid and, in particular, facilitates the investigation

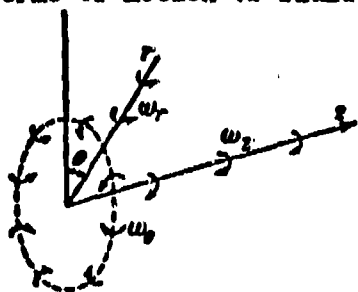


Fig. 1-13. Diagram for determining components of vortex in the cylindrical system of coordinates.

of certain properties of flow in the flow part of turbomachines.

In certain particular cases equations (1-18) or (1-20) are readily integrated.

For this purpose to the equations of motions there can be added an even simpler

and more graphic form, by introducing a certain function of the pressure

$$P = \int \frac{dp}{\rho}. \quad (1-21)$$

In addition, influence of body forces is evaluated by means of introducing the potential function  $U$ , whose partial derivatives by coordinates express projections of the acceleration of body forces onto the coordinate axes:

$$X = -\frac{\partial U}{\partial x}; \quad Y = -\frac{\partial U}{\partial y}; \quad Z = -\frac{\partial U}{\partial z}. \quad (1-22)$$

Then equations (1-18) acquire the form:

$$\left. \begin{aligned} \frac{\partial u}{\partial t} + \frac{\partial}{\partial x} \left( \frac{c^2}{2} + U + P \right) &= 2(v\omega_z - w\omega_y); \\ \frac{\partial v}{\partial t} + \frac{\partial}{\partial y} \left( \frac{c^2}{2} + U + P \right) &= 2(w\omega_x - u\omega_z); \\ \frac{\partial w}{\partial t} + \frac{\partial}{\partial z} \left( \frac{c^2}{2} + U + P \right) &= 2(u\omega_y - v\omega_x). \end{aligned} \right\} \quad (1-23)$$

Equations (1-23) were obtained by Kazan University Professor I. S. Gromeko in 1881.

For a steady motion  $\left( \frac{\partial u}{\partial t} = \frac{\partial v}{\partial t} = \frac{\partial w}{\partial t} = 0 \right)$

after multiplying both sides of equation (1-23) respectively by  $dx$ ,  $dy$  and  $dz$  and also summation we readily obtain

$$-d \left( \frac{c^2}{2} + U + P \right) = 2 \begin{vmatrix} dx & dy & dz \\ u & v & w \\ \omega_x & \omega_y & \omega_z \end{vmatrix}. \quad (1-24)$$

The determinant (1-24) is equal to zero in the following particular cases:

a) in the absence of vortices in a fluid, i.e., when

$$\omega_x = \omega_y = \omega_z = 0;$$

b) under the condition

$$\frac{dx}{u} = \frac{dy}{v} = \frac{dz}{w};$$

c) under the condition

$$\frac{dx}{\omega_x} = \frac{dy}{\omega_y} = \frac{dz}{\omega_z};$$

The conditions "b" and "c" are differential equations of the lines of flow and vortex lines, respectively [see equation (1-5)]; consequently, according

to conditions "b" and "c" the determinant (1-24) is equal to zero for the lines of flow and the vortex lines;

d) at

$$vw_x = wz_y; \quad wz_x = wv_y; \quad wv_x = vw_y,$$

or

$$\frac{u}{\omega_x} = \frac{v}{\omega_y} = \frac{w}{\omega_z}. \quad (1-25)$$

In all enumerated cases from (1-24) we obtain:

$$d\left(\frac{c^2}{2} + U + P\right) = 0,$$

or after integration

$$\frac{c^2}{2} + U + P = \text{const.} \quad (1-26)$$

Integral (1-26) is the equation of energy for a flow, i.e., it expresses energy balance of a fluid particle: the sum of kinetic and potential energy, i.e., total energy of particle : is a constant magnitude. It should be remembered that the function  $U$  expresses the potential energy of body forces, and  $P$  — the potential energy of forces of pressure. The first term in (1-26) gives the magnitude of the kinetic energy of a fluid particle. All the indicated components of the total energy relate to the mass of fluid flowing per second.

Despite the fact that the integral (1-26) has an identical form for all the considered cases, its meaning and region of application are different depending upon conditions for which the integral was obtained.

For the steady motion of a fluid without vortices (case "a") integral (1-26) is valid for all points of the flow.

In fulfilling conditions "b" or "c" the total energy of particle is kept constant only along a line of flow or vortex line respectively. In the transition from one line of flow to another or from one vortex line to a neighboring vortex line the magnitude of constant on the right side of (1-26) may change.

The condition "d" of the proportionality of linear and angular velocities (1-25) results in the integral (1-26), i.e., the constancy of the total energy of a fluid particle, valid for all points of the flow. Consequently, in the considered

particular case of vortex motion the total energy is kept constant for all vortex lines. A peculiarity of this type of motion is the circumstance that each particle revolves around the axis, along which it moves. Actually, condition (1-25) designates that the senses of the vectors of linear and angular velocities coincide, since proportionality of these vectors indicates that these vectors are oriented at identical angles to the axes of the coordinates. In the considered motion the lines of flow and vortex lines coincide. We note that in all cases under study during an adiabatic flow at points, associated between each other by the integral (1-26), the entropy remains constant.

Integral (1-26) may be transformed for the practically important case, when of the body forces only the force of gravity acts; in this connection

$$X=Y=0; \quad Z=-g$$

(the z-axis is directed vertically upward).

Consequently,

$$\frac{dU}{dz} = g \text{ and } U = gz.$$

After substituting these magnitudes equation (1-26) acquires the form:

$$\frac{c^2}{2} + gz + \int \frac{dp}{\rho} = \text{const.} \quad (1-27)$$

For an incompressible fluid ( $\rho = \text{const}$ ) we find:

$$\frac{c^2}{2g} + z + \frac{p}{\gamma} = \text{const.} \quad (1-28)$$

The last equation was obtained by D. Bernoulli. Magnitude  $z$  in this equation characterizes potential energy of location caused in the uniform field of the Earth's gravitation by the motion of a fluid particle, and is called the leveling height. Magnitude  $\frac{p}{\gamma}$  is the potential energy of pressure (piezometric height), and  $\frac{c^2}{2g}$  is the kinetic energy; all terms of equation (1-26) pertain to the weight per second of the flowing fluid.

## CHAPTER 2

### ONE-DIMENSIONAL MOTION OF GAS

A significant number of technical problems in gas dynamics can be solved by assuming the motion as one-dimensional, i.e., a motion, in which all parameters of flow vary only in one direction. To these conditions corresponds a flow of gas along slightly distorted streamlines or in tubes of flow.

As one-dimensional, it is possible to consider flow of gas in a tube with slightly varying cross-section and a small curvature of axis. In a number of cases, results of investigation of one-dimensional flow can be applied also to flows with nonuniform distribution of parameters by section.

#### 2-1. Fundamental Equations of a One-Dimensional Flow. Speed of Sound.

For obtaining fundamental equations of a one-dimensional motion let us consider the flow of gas in a tube of flow. The direction of axis is selected so that it coincides with the axis of tube (Fig. 2-1). We shall use first equation of system (1-16). By disregarding for a gas the influence of body forces, we assume

$$X = Y = Z = 0.$$

By bearing in mind that for considered one-dimensional flow  $u = c$ ,  $v = w = 0$  and by converting in equation (1-16) to a total derivative, we shall obtain:

$$c \frac{dc}{dx} + \frac{1}{\rho} \frac{dp}{dx} = 0, \quad (2-1)$$

or

$$c dc + \frac{dp}{\rho} = 0.$$



The equation for change in momentum (equation of momentum) (2-1) is valid only for those flows, in which there are absent frictional forces, i.e., for reversible flows. It is readily shown that in this case if the system is adiabatic, the change in parameters of state of a perfect gas is subject to the isentropic law:

$$\frac{P}{\rho^k} = \text{const.} \quad (2-2)$$

It should be noted that by formulating the arrangement of the process of flow, by considering that the flow is continuous, isolated energywise and frictionless we thereby determine its isentropicity, because in such a flow irreversible transformations of the mechanical energy into heat are lacking and, consequently, the entropy of flow does not change. Therefore, we can directly integrate equation (2-1), by assuming evident the connection (2-2).

Actually after integrating equation (2-1) and bearing in mind (2-2), we obtain:

$$\begin{aligned} \int c dc + \int \frac{dp}{\rho} &= \frac{c^2}{2} + \text{const } k \int \rho^{k-2} d\rho = \\ &= \frac{c^2}{2} + \frac{k}{k-1} \frac{P}{\rho} = \text{const.} \end{aligned} \quad (2-3)$$

This equation, known as Bernoulli's equation for a compressible fluid, expresses the principle of conservation of energy for an adiabatic flow. After a simple substitution

$$\frac{k}{k-1} \frac{P}{\rho} = \frac{k}{k-1} gRT = c_p T = i$$

it will be transformed to the form:

$$i + \frac{c^2}{2} = \text{const.} \quad (2-4)$$

Here the enthalpy of the gas  $i$  and heat capacity of gas at constant pressure  $c_p$  are related to a mass unit and are measured in mechanical units.\*

To the equation of energy (2-4) there can be given a simple gas kinetic interpretation. The term  $\frac{c^2}{2}$  in this equation expresses the energy of directed motion of particles and the enthalpy  $i$ , proportional to the temperature, determines the energy

---

\*In engineering thermodynamics the internal energy, enthalpy and heat capacity usually are expressed in thermal units. Here  $i(\text{kilocalorie/kg}) = \frac{A}{8} i(\text{m}^2/\text{sec}^2)$ , et cetera, where  $A$  is the heat equivalent of mechanical work.

of motion of molecules. Consequently, equation (2-4) expresses fact of mutual transformation of energy of the directed motion of particles and thermal energy.

Thus, we have established that with an isentropic flow of gas, the integral of equation of change in momentum coincides with equation of energy.\*

It should be noted that equations (2-3) and (2-4) can be directly obtained also from integral (1-26), written out for a compressible fluid (gas). By disregarding the influence of body forces, i.e., considering  $U = 0$ , from (1-26) there readily is obtained equation (2-3), by assuming a connection between  $p$  and  $\rho$  on basis of formula (2-2).\*\*

The equation of continuity for a one-dimensional steady flow can be obtained, by considering motion of gas in a tube of flow of variable section (Fig. 2-1). In assuming that across the section of the stream, the parameters of flow do not change, we consider the part of flow, included between sections 1-1 and 2-2. By definition a tube of flow is a closed surface, formed by streamlines.

-----

\*The equation of energy readily can be obtained from the first law of thermodynamics, written out for fluid a flow:

$$dQ = dI + d\left(\frac{c^2}{2g}\right) + dL_T,$$

where  $dQ$  is the specific quantity of heat, transmitted to a gas (or diverted from gas) in an elementary process;

$dL_T$  is the specific work, done by the gas.

For an energy-wise isolated flow ( $dQ = dL_T = 0$ ) after integration, we obtain (2-4).

\*\*Equation (2-4) is valid also for adiabatic flows (in presence of friction), accompanied by an increase in entropy. In this case energy balance of the particle must be supplemented by two terms: one which takes in consideration the work of resisting forces, and other, which expresses the increase of heat in gas flow. These two terms are identical in magnitude, but have opposite signs and therefore mutually cancel each other. This means that in such an isolated system, the work of forces of friction does not change the total energy of a particle; there varies only the relationship between energy of directed motion and thermal energy. The flow of gas is irreversible, a portion of the mechanical energy is irreversibly transformed into heat.

The gas particles do not penetrate through its lateral surface, since the vectors of the speed are tangent to this surface. For 1 sec through section 1-1 inside the considered part of tube there flows in a mass of gas, equal to  $\rho_1 c_1 F_1$ ; flowing out through section 2-2, is a mass of gas equal to  $\rho_2 c_2 F_2$ . Under the condition of continuity of flow these quantities should be identical, i.e.,

$$\rho_1 c_1 F_1 = \rho_2 c_2 F_2, \quad (2-5)$$

or 
$$m = \rho c F = \text{const}, \quad (2-5a)$$

where  $m$  is the mass of gas per second.

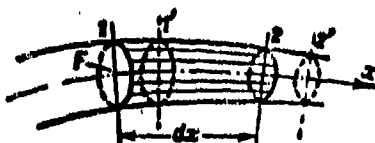


Fig. 2-1. Tube of flow (streamtube).

The equation of continuity can be obtained in differential form. After logarithmisation and differentiation under sign of logarithm formula (2-5a) acquires the form:

$$\frac{d\rho}{\rho} + \frac{dc}{c} + \frac{dF}{F} = 0. \quad (2-6)$$

We note that for stream of constant section, the equation of continuity (2-5) gives:

$$\rho c = \frac{m}{F} = \text{const}. \quad (2-7)$$

The product  $\rho c = \frac{m}{F}$  determines the specific flow rate of a mass of gas in a given section (flow rate of a mass through unit of area of section).

Expression (2-7) for specific flow rate can also be obtained directly from the differential equation of continuity (1-12) for a three-dimensional flow by assuming  $u = c$  and  $v = w = 0$ . Then, by assuming the motion steady and converting to a total derivative, we shall obtain:  $\frac{d(\rho c)}{dx} = 0$ .

Hence, by integrating, we obtain (2-7). It is obvious that by the sense of derivation the equation of continuity (1-12) in a transition to a one-dimensional flow, can give only the condition  $\rho c = \text{const.}$

For a one-dimensional flow of an incompressible fluid ( $\rho = \text{const}$ ) equation of continuity (2-5) takes the form:

$$\begin{aligned} c_1 F_1 &= c_2 F_2, \\ \text{or} \quad cF &= \text{const.} \end{aligned} \tag{2-8}$$

Formula (2-8) expresses condition of constancy of the volumetric flow rate of fluid per second, flowing through the sections of tube  $F_1$  and  $F_2$ . This formula is applicable to gas flows only in those cases, when in considered section of tube 1-2 the change in density can be disregarded. For gases this condition is fulfilled if the momentum is small in comparison with the speed of sound.

Speed of sound, as is known, is called the speed of propagation of small perturbations in a physical medium. The speed of sound is especially very important in analyzing processes of flow of a compressible fluid. Many properties of the flow, including also the character of variation of parameters of flow along a tube of given shape, under different conditions of interaction with the environment considerably depend on the circumstance, within what limits the ratios of the speed to the speed of sound lies.

Influence of compressibility in a gas flow becomes perceptible in that case, when, as a result of a change in pressure, the cubic deformation of particle and change in speed of the flows are commensurable.

We shall use the equation of continuity of a one-dimensional flow, after having written it in the form:

$$\frac{d\Delta V}{\Delta V} + \frac{dp}{p} = 0,$$

where  $\frac{d\Delta V'}{\Delta V'}$  is the relative change of volume of the element 1-2 (Fig. 2-1) transferred to a new position 1'-2'.

By multiplying this equality by  $dp$ , after transformations we obtain:

$$dp = -p \frac{dp}{p} \frac{d\Delta V'}{\Delta V'}.$$

From the equation of momentum (2-1) it follows:

$$dp = -\rho c dc.$$

By comparing the two last expressions, we obtain:

$$\frac{d\Delta V'}{\Delta V'} = \frac{c^2}{\left(\frac{dp}{p}\right)_s} \frac{dc}{c}.$$

(The subscript  $s$  attests to the isentropicity of the process).

We designate

$$\left(\frac{dp}{p}\right)_s = a^2; \quad (2-9)$$

then

$$\frac{d\Delta V'}{\Delta V'} = \frac{c^2}{a^2} \frac{dc}{c}.$$

Thus, we see that if  $c$  and  $a$  are magnitudes of one order, then the relative cubic deformation of the element will be of same order, as also the change of speed. At  $\frac{c}{a} \ll 1$  even significant changes in the speed do not result in large changes in the volume of the particles.

From courses in physics it is known that the magnitude  $a$ , determined by formula (2-9), is the speed of propagation of waves of small disturbance. A characteristic example of such waves is sound waves.

For a perfect gas the speed of sound is equal to:

$$a = \sqrt{k \frac{p}{\rho}} = \sqrt{k g R T}. \quad (2-9a)$$

For air ( $k = 1.4$ ) speed of the propagation of sound

$$a = 20.1 \sqrt{T}. \quad (2-9b)$$

Consequently, the speed of sound in a perfect gas depends only on the physical properties and the absolute temperature of the gas. This conclusion is in full agreement with gas kinetics concepts on the process of propagation of small

disturbances in a medium, consisting of moving molecules. The speed of propagation of a disturbance should depend on the speed of motion of molecules, which is determined by the temperature. It is well known that the average speed of the motion of molecules of a gas is close to the speed of sound.

In this connection, it is necessary to emphasize that ratio of squares of the speeds  $(\frac{c^2}{a^2})$  is a measure of the ratio of the average kinetic energy of directed motion to the average kinetic energy of random motion of the particles.

## 2-2. Different Forms of the Energy Equation.

The Bernoulli equation establishes the energy balance of an adiabatic flow of gas in a tube of flow. Above we become acquainted with two forms of this equation: (2-3) and (2-4).

The constant on the right side of the equation of energy can be expressed variously. By applying this equation to two sections of a tube of flow, in one of which the speed decreases to zero and, consequently, flow is stagnated, equations (2-3) and (2-4) can be written in the following form:

$$\frac{c^2}{2} + i = i_0; \quad (2-10)$$

$$\frac{c^2}{2} + \frac{k}{k-1} \frac{p}{\rho} = \frac{k}{k-1} \frac{p_0}{\rho_0} = \frac{k}{k-1} \bar{R} T_0 = c_p T_0, \quad (2-11)$$

where  $i_0 = c_p T_0$  is the enthalpy of the stagnated flow;

$p_0$ ,  $\rho_0$ ,  $T_0$  are parameters of stagnated flow or parameters of stagnation.

As a result of total stagnation of a flow all the kinetic energy of directed motion changes into heat energy. Let us note that with a total stagnation of the flow of a perfect gas, temperature of stagnation  $T_0$ , the same as the enthalpy, can have only one fully definite value, while the pressure of stagnation  $p_0$ , and the density  $\rho_0$  can assume any values where the ratio  $\frac{p_0}{\rho_0}$  remains constant.

Parameters of the stagnation are very important in analyzing both the theoretical and experimental problems of gas dynamics.

Thus, we see that the right-hand side of the equation of energy, expressing total energy of a particle, can be presented in terms of parameters of stagnation.

Suppose we consider other possible forms of the equation of energy.

We remember that

$$a^2 = k \frac{p}{\rho}.$$

Then, equation (2-11) acquires the form:

$$\frac{c^2}{2} + \frac{a^2}{k-1} = \frac{a_0^2}{k-1} = \text{const.} \quad (2-12)$$

where  $a_0$  is speed of propagation of sound in a completely stagnated medium.

If we apply the equation of energy to two sections of a tube of flow, in one of which the pressure  $p$  decreases to zero, then the speed of flow  $c$  will tend to a certain maximum magnitude  $c_{\text{max}}$ , which we call the maximum speed. In accordance with considered conditions this speed corresponds to outflow of gas in a vacuum ( $i = \infty$ ;  $p = 0$ ;  $T = 0$ ). Consequently, right-hand side of equation (2-12) can be expressed in terms of the maximum speed:

$$\frac{c^2}{2} + \frac{a^2}{k-1} = \frac{c_{\text{max}}^2}{2}. \quad (2-13)$$

With a maximum speed of the flow, equal to  $c_{\text{max}}$ , all the thermal energy of molecules will be converted into energy of the directed motion. A maximum speed of flow is virtually unattainable and is known as the theoretical limit for the speed of a gas.

One should bear in mind that with the approach of speed of flow to the maximum, the rarefaction of gas becomes very great, and therefore to the considered flow it is impossible to apply an equation of state of perfect gases and equation of energy in the form known to us (2-10) or (2-11).

From formula (2-12) there can be obtained still one expression for the constant on the right-hand side of the equation of energy.

According to (2-12) along axis of a tube of flow with an increase in the speed  $c$ , the speed of sound  $a$  falls. Completely obvious are the limits of the possible variations of  $c$  and  $a$ : speed of flow can change from zero to  $c_{\text{max}}$ , and the speed

of sound--from  $a_0$  to zero. In one of the sections of the tube of flow, the speed of the gas motion  $c$  may become equal to the local speed of sound, i.e.,

$$c = a = a_*$$

Here equation (2-12) will be written as:

$$\frac{a_*^2}{2} + \frac{a_*^2}{k-1} = \frac{k+1}{k-1} \frac{a^2}{2}$$

Consequently, the constant on the right-hand side of equation of energy can be expressed by the speed  $a$  and the equation of energy then acquires the form:

$$\frac{c^2}{2} + \frac{a^2}{k-1} = \frac{k+1}{k-1} \frac{a^2}{2} \quad (2-14)$$

A speed of flow, equal to local speed of sound  $a$  is called the critical speed.

From the equation of energy, written in different forms, it follows that between characteristic speeds and parameters of stagnation there exists a definite connection.

By equating the right-hand sides of equations (2-10)--(2-14), we can obtain such a relationship:

$$t_0 = \frac{k}{k-1} \frac{P_0}{\rho_0} = c_* T_0 = \frac{a_0^2}{k-1} = \frac{c_{max}^2}{2} = \frac{a^2}{2} \frac{k+1}{k-1} \quad (2-15)$$

Hence, we obtain an expression for the characteristic speeds of flow through parameters of stagnation.

Thus, the maximum speed will equal:

$$c_{max} = \sqrt{2t_0} = \sqrt{\frac{2k}{k-1} \frac{P_0}{\rho_0}} \quad (2-16)$$

Critical speed

$$a_* = \sqrt{\frac{2k}{k-1} RT_0} = \sqrt{\frac{2k}{k-1} \frac{P_0}{\rho_0}} \quad (2-17)$$

Besides,

$$c_{max} = a_* \sqrt{\frac{2}{k-1}} \quad (2-16a)$$

and

$$a_* = a_* \sqrt{\frac{2}{k+1}} \quad (2-17a)$$



From formulas (2-16) and (2-17) it follows:

$$\frac{c_{max}}{a_*} = \sqrt{\frac{k+1}{k-1}}. \quad (2-18)$$

Thus, we see that the maximum and critical speeds depend on physical properties of gas (coefficient of constant entropy  $k$ ) and the temperature of stagnation.

For air at  $k = 1.4$  and  $\bar{R} = 287.1 \text{ m}^2/\text{sec}^2 \cdot ^\circ\text{C}$

$$a_* = 18.3 \sqrt{T_*} \text{ m/sec.}$$

For superheated water vapor at  $k = 1.3$  and  $\bar{R} = 462.0 \text{ m}^2/\text{sec}^2 \cdot ^\circ\text{C}$

$$a_* \approx 22.8 \sqrt{T_*}.$$

By formula (2-18) we obtain:

$$\text{for air } \frac{c_{max}}{a_*} = 2.45;$$

$$\text{for superheated water vapor } \frac{c_{max}}{a_*} = 2.77.$$

### 2-3. Flow Parameters in an Arbitrary Section of a Tube of Flow (Streamtube\*)

By using equation of energy, we express parameters of flow in certain section of a tube of flow in terms of parameters of the stagnation and speed in this section.

For this purpose, after transforming formula (2-14), we obtain:

$$\frac{c^2}{2} + \frac{a^2}{k-1} = \frac{k+1}{k-1} \frac{a_*^2}{2} = \frac{c_{max}^2}{2}. \quad (2-14a)$$

By dividing all the terms by  $c^2$ , we obtain:

$$\frac{1}{2} + \frac{1}{k-1} \frac{a^2}{c^2} = \frac{k+1}{2(k-1)} \frac{a_*^2}{c^2} = \frac{1}{2} \frac{c_{max}^2}{c^2}. \quad (2-14b)$$

We introduce the following designations for the dimensionless speeds:

$$\left. \begin{aligned} M &= \frac{c}{a_*}; \\ \lambda &= \frac{c}{a_*}; \\ t &= \frac{c}{c_{max}}; \end{aligned} \right\} \quad (2-19)$$

\*TRANSLATION EDITOR'S NOTE: In this monograph it is assumed that the terms "tube of flow" and "streamtube" are interchangeable.

then equation (2-14b) will be have the form

$$\frac{1}{2} + \frac{1}{k-1} \cdot \frac{1}{M^2} = \frac{k+1}{2(k-1)} \cdot \frac{1}{\lambda^2} = \frac{1}{2} \cdot \frac{1}{\xi^2}. \quad (2-20)$$

Equation (2-20) establishes connection between dimensionless speeds. After simple transformations we obtain:

$$M^2 = \frac{2}{k+1} \cdot \frac{\lambda^2}{1 - \frac{k-1}{k+1} \lambda^2} = \frac{2}{k-1} \cdot \frac{\xi^2}{1 - \xi^2}. \quad (2-21)$$

We now use formula (2-10). We express the temperature of stagnation in such a form:

$$T_0 = T + \frac{c^2}{2c_p}. \quad (2-10a)$$

We divide left and right side by  $T_0$  and determine the ratio of temperatures:

$$\frac{T}{T_0} = \frac{a^2}{a_0^2} = 1 - \frac{c^2}{2c_p T_0};$$

since

$$c_p T_0 = \frac{k+1}{k-1} \cdot \frac{a^2}{2} = \frac{c_{max}^2}{2},$$

then

$$\frac{T}{T_0} = 1 - \frac{k-1}{k+1} \lambda^2 = 1 - \xi^2. \quad (2-22)$$

Besides, after determining from (2-10a) the ratio

$$\frac{T_0}{T} = 1 + \frac{c^2}{2c_p T}$$

and after having substituted on the right-hand side

$$T = \frac{a^2}{kR} = \frac{a^2}{c_p(k-1)},$$

we obtain:

$$\frac{T_0}{T} = 1 + \frac{k-1}{2} M^2. \quad (2-23)$$

For an isentropic flow

$$\frac{T}{T_0} = \left(\frac{p}{p_0}\right)^{\frac{k-1}{k}} = \left(\frac{\rho}{\rho_0}\right)^{k-1}. \quad (2-24)$$

In using formulas (2-22) and (2-23) it is possible to present the relative pressure and density of the gas in an arbitrary section of a tube of flow depending upon dimensionless speeds  $M$ ,  $\lambda$  and  $\xi$  (Table 2-1).

Thus, by knowing the parameters of the total stagnation of flow and one of dimensionless speeds, by equation (2-22) and (2-23) one can determine the temperature, and by formulas, presented in the Table 2-1,--the density and pressure of the

gas in the given section of tube of flow.

From the fundamental equations there is readily obtained a connection between parameters in two arbitrarily selected sections of a tube of flow.

From formulas (2-22) and (2-23) we express the temperature of stagnation in such a form:

$$T_0 = T \left( 1 + \frac{k-1}{2} M^2 \right) = \frac{T}{1 - \frac{k-1}{k+1} \lambda^2} = \frac{T}{1 - \xi^2}.$$

For two sections of an isentropic flow (1-1 and 2-2) we may write out the equation of energy for a perfect gas in such a form:

$$T_{01} = T_{02};$$

then

$$\frac{T_1}{T_2} = \frac{1 + \frac{k-1}{2} M_1^2}{1 + \frac{k-1}{2} M_2^2} = \frac{1 - \frac{k-1}{k+1} \lambda_2^2}{1 - \frac{k-1}{k+1} \lambda_1^2} = \frac{1 - \xi_2^2}{1 - \xi_1^2}. \quad (2-25)$$

In the concept of an isentropic flow, by using relationship (2-24), we obtain formulas for ratios of the pressures and densities (Table 2-1).

There also is readily obtained the ratio of the absolute speeds in these sections:

$$\frac{c_2}{c_1} = \frac{M_2 a_2}{M_1 a_1} = \frac{M_2}{M_1} \sqrt{\frac{T_2}{T_1}},$$

or after substitution  $T_2/T_1$  from (2-25):

$$\frac{c_2}{c_1} = \frac{M_2}{M_1} \sqrt{\frac{1 + \frac{k-1}{2} M_1^2}{1 + \frac{k-1}{2} M_2^2}}. \quad (2-26)$$

Since at  $T_0 = \text{const}$ , the speeds  $a_*$ ,  $a_0$  and  $c_{\text{max}}$  are constant, then

$$\frac{c_2}{c_1} = \frac{\lambda_2}{\lambda_1} = \frac{\xi_2}{\xi_1}.$$

We note that equations (2-22)–(2-26) and the formulas, presented in Table 2-1, are modifications of the equation of energy, obtained by means of transforming equation (2-10) and introducing dimensionless speeds.

In practical calculations of gas flows, there can be used any form of the equation of energy and parameters  $p$ ,  $\rho$  and  $T$  can be expressed in terms of any of the dimensionless speeds  $M$ ,  $\lambda$ ,  $\xi$ .

However, depending upon considered problem, it is found expedient to apply

Table 2-1

1) Ratio of densities;

2) Ratio of pressures.

$\frac{\rho}{\rho_0} = \left(1 + \frac{k-1}{2} M^2\right)^{\frac{1}{k-1}}$	$\frac{p}{p_0} = \left(1 + \frac{k-1}{2} M^2\right)^{\frac{k}{k-1}}$
$\frac{\rho}{\rho_0} = \left(1 - \frac{k-1}{k+1} \lambda^2\right)^{\frac{1}{k-1}}$	$\frac{p}{p_0} = \left(1 - \frac{k-1}{k+1} \lambda^2\right)^{\frac{k}{k-1}}$
$\frac{\rho}{\rho_0} = (1 - \xi^2)^{\frac{1}{k-1}}$	$\frac{p}{p_0} = (1 - \xi^2)^{\frac{k}{k-1}}$
$\frac{\rho_2}{\rho_1} = \left(\frac{1 + \frac{k-1}{2} M_1^2}{1 + \frac{k-1}{2} M_2^2}\right)^{\frac{1}{k-1}}$	$\frac{p_2}{p_1} = \left(\frac{1 + \frac{k-1}{2} M_1^2}{1 + \frac{k-1}{2} M_2^2}\right)^{\frac{k}{k-1}}$
$\frac{\rho_2}{\rho_1} = \left(\frac{1 - \frac{k-1}{k+1} \lambda_2^2}{1 - \frac{k-1}{k+1} \lambda_1^2}\right)^{\frac{1}{k-1}}$	$\frac{p_2}{p_1} = \left(\frac{1 - \frac{k-1}{k+1} \lambda_2^2}{1 - \frac{k-1}{k+1} \lambda_1^2}\right)^{\frac{k}{k-1}}$
$\frac{\rho_2}{\rho_1} = \left(\frac{1 - \xi_2^2}{1 - \xi_1^2}\right)^{\frac{1}{k-1}}$	$\frac{p_2}{p_1} = \left(\frac{1 - \xi_2^2}{1 - \xi_1^2}\right)^{\frac{k}{k-1}}$

a dimensionless speed, which assures a maximum simplicity of the final equations.

If in considered region, the speeds are less than the critical, i.e., if

$$0 < c < a_*,$$

then

$$0 < M < 1;$$

$$0 < \lambda < 1;$$

$$0 < \xi < \sqrt{\frac{k-1}{k+1}}.$$

If the speeds of flow are higher than the critical, i.e.,

$$a_* < c < c_{max},$$

then

$$1 < M < \infty;$$

$$1 < \lambda < \sqrt{\frac{k+1}{k-1}};$$

$$\sqrt{\frac{k-1}{k+1}} < \xi < 1.$$

In the first case, flow is called subsonic or subcritical, but in the second—supersonic or supercritical. Consequently, value of dimensionless speeds

$$M = \lambda = 1$$

divides region of flows with subsonic (subcritical) speeds and with supersonic (supercritical) speeds. It is possible to see that dimensionless speeds  $\lambda$  and  $\xi$  have finite limiting values, where the speed  $\lambda = 1$  at  $c = a_*$ . In certain cases is more convenient for use.

It must be emphasized that the dimensionless speeds have a specific physical meaning.

In Sec. 2-2 it was established that, depending upon relationships between  $c$  and  $a$ , to a greater or lesser degree there is manifested a compressibility of the flow and, consequently,  $M = \frac{c}{a}$  at each point of flow determines the degree of the influence of compressibility. Besides, physical value of the Mach number is ascertained in considering the magnitude

$$M^2 = \frac{c^2}{a^2} = \frac{2}{k-1} \cdot \frac{c^2}{T}$$

(since  $i = \frac{a^2}{k-1}$ ), whence it follows that the square of Mach number is proportional to the ratio of kinetic energy of flow to its potential energy at a given point.

By knowing that the square of the critical speed can be expressed by the enthalpy of stagnation:

$$a^2 = 2 \frac{k-1}{k+1} i_0.$$

it is possible to present  $\lambda^2$  in the following form:

$$\lambda^2 = \frac{k+1}{k-1} \cdot \frac{c^2}{i_0}.$$

Thus, the squares of dimensionless speed  $\lambda$ , and also  $\xi$  are proportional to the ratio of the kinetic energy of flow to its total energy  $i_0$ .

In flows of gas without an energy exchange with the environment, the total energy of the flow  $i_0$  is at each point a constant magnitude. Correspondingly, the constants are the speeds  $a_*$ ,  $a_0$  and  $c_{\max}$  depending only on  $i_0$  (at  $k = \text{const}$ ). In this case  $\lambda$  and  $\xi$  give us the speed of flow, related to different, but constant scales for the entire flow.

In energy nonisolated flow, when there takes place a heat exchange with the environment ( $dQ \neq 0$ ) or an exchange of mechanical work ( $dL_T \neq 0$ ), the total energy varies from point to point. In accordance with variations of  $i_0$  the speeds  $a_*$ ,  $a_0$ , and  $c_{\max}$  change.

It should be emphasized that formulas (2-23), (2-24), et al., associating the parameters of stagnation with the parameters of flow (Table 2-1), are valid also for flows with an energy exchange, but, however, in this case, connection between parameters of stagnation, the static parameters and dimensionless speeds, is local, i.e., it refers only to a given point or given section of tube of flow, where by  $p_0$  and  $\rho_0$  are understood the parameters of an isentropic stagnation at the given point. These equations cannot be applied to two different sections of the tube, since in the section between cross sections total energy of the flow varies. Consequently, formulas for static parameters, indicated in Table 2-1, and formulas (2-25) and (2-26) for such flows are inapplicable.

We note that the dimensionless speed  $M$  is one of the basic criteria in theory of similarity in analyzing processes of motion with high speeds\*, since the resistance coefficient basically depends on the ratio  $\frac{c}{a}$ .

#### 2-4. Change in Speed Along a Tube of Flow. The Reduced Flow Rate of Gas

We shall subject to a more detailed investigation the character of the change of speed along tube of flow. For this purpose, we shall use equations of a one-dimensional flow:

$$cdc + \frac{dp}{\rho} = 0;$$

$$\frac{dF}{F} + \frac{dp}{\rho} + \frac{dc}{c} = 0.$$

Simple transformations make it possible to obtain:

$$cdc - \frac{dp}{\rho} \left( \frac{dF}{F} + \frac{dc}{c} \right) = 0;$$

hence

$$(c^2 - a^2) \frac{dc}{c} = a^2 \frac{dF}{F}. \quad (2-27)$$

After dividing both sides of the equation by  $a^2 dx$  and expressing logarithmic derivative of the speed, we obtain:

$$\frac{1}{c} \cdot \frac{dc}{dx} = \frac{1}{F} \cdot \frac{dF}{dx}. \quad (2-28)$$

After expressing by means of (2-21)  $M^2$  in terms of  $\lambda^2$ , we obtain:

$$\frac{1}{\lambda} \frac{d\lambda}{dx} = \frac{1 - \frac{k-1}{k+1} \lambda^2}{\lambda^2 - 1} \frac{1}{F} \frac{dF}{dx}. \quad (2-29)$$

Equations (2-28) and (2-29) are differential equations of the distribution of speeds along axis of the tube of flow. They can be integrated, if there is known the form of the function  $F(x)$ . At the same time, these equations are very convenient for a qualitative analysis of the change of speed of flow in tubes of flow of different shape.

---

\*See Chap. 5

From equation (2-29) it follows that  $\frac{d\lambda}{dx} = 0$  at

$$\begin{aligned} \text{a) } \lambda &= 0; \\ \text{b) } \lambda &= \sqrt{\frac{k+1}{k-1}} = \lambda_{\max}; \\ \text{c) } \frac{dF}{dx} &= 0. \end{aligned} \quad (2-30)$$

The case "a" corresponds to a motionless gas and therefore it is of no interest. Case "b," which corresponds to the maximum speed of flow, is entirely obvious: at  $\lambda = \lambda_{\max}$  a further increase of the speed is impossible. Finally, the case "c" results in  $\frac{d\lambda}{dx} = 0$  only at  $\lambda \neq 1$ . It is readily seen that at the considered point  $x = x_*$ , the function  $F(x)$  has a maximum, a minimum or an inflection point. Consequently, in such sections of a tube of flow the speeds also have extreme values.

From equation (2-29) it may be concluded, that the derivative of the speed  $\frac{d\lambda}{dx} = \infty$  at  $\lambda = 1$  and  $\frac{dF}{dx} \neq 0$ . However, such a solution, signifying presence of a discontinuity of speed is physically impossible (we analyze continuously the varying motion of the gas).

Let us consider the qualitative picture of the flow of a gas in a tube of flow, having in  $x = x_*$  a maximum or minimum of the section (Fig. 2-2). Suppose the function  $F(x)$  has at this point a maximum (Fig. 2-2,a).

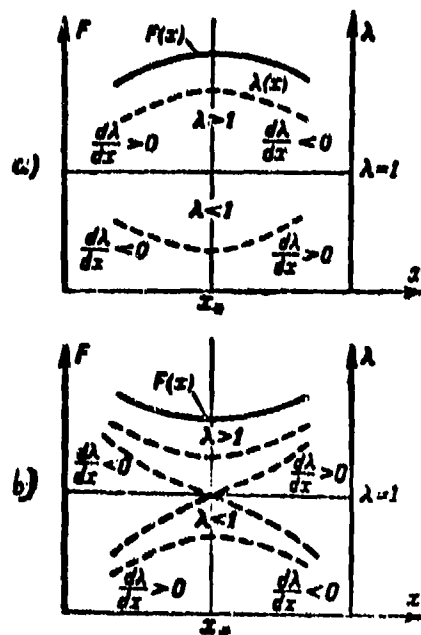


Fig. 2-2. Variation of speed along a tube of flow.



Let us assume that to the left of  $F(x) = F_{\max}$ , the speed  $\lambda < 1$ . Then, from (2-29) it follows that since  $\frac{dF}{dx} > 0$ , then  $\frac{d\lambda}{dx} < 0$ , i.e., speed in the tube of flow towards  $F_{\max}$  diminishes. To the right  $\frac{dF}{dx} < 0$  and  $\frac{d\lambda}{dx} > 0$  the speed of flow increases.

Analogously at  $\lambda > 1$  we shall have to the left  $\frac{d\lambda}{dx} > 0$  and to the right  $\frac{d\lambda}{dx} < 0$ .

If function  $F(x)$  has a minimum at the considered point, then to the left of  $F(x) = F_{\min}$  at  $\lambda < 1$  and  $\frac{dF}{dx} < 0$ , the speed will increase, since  $\frac{d\lambda}{dx} > 0$ , (Fig. 2-2b). At  $\lambda > 1$  there will be to the left  $\frac{d\lambda}{dx} < 0$ , to the right  $\frac{d\lambda}{dx} > 0$ .

Thus, we have shown that in a maximum section of a tube of flow the subsonic flow acquires a minimum speed, and the supersonic, a maximum. In an expanding part of tube of flow the speed of subsonic flow drops, but in narrowing--increases. The supersonic flow in the expanding part is accelerated, but in narrowing--is stagnated. At any values of  $\lambda$  at the entry the curve of speed in this case ( $F(x) = F_{\max}$ ) has an extreme. There follows from this a very important conclusion: the character of change of the speed along a tube of flow in principle is different for subsonic and supersonic flows. In the first case the flow of gas from the qualitative aspect will conduct itself the same as the flow of an incompressible fluid, and in the second case the curve of speed  $\lambda(x)$  has a character, analogous to the curve of the sections  $F(x)$ . It is obvious that in a tube of flow, having a maximum of section, a transition from the region of subsonic to the region of supersonic speeds and vice versa is impossible.

In a tube of flow with a minimum of section, speed of both the subsonic, and also of supersonic flow approaches the value  $\lambda = 1$  in the minimum section. If speed of flow in minimum section is  $\lambda = 1$  and  $d\lambda = 0$ , then a transition through the critical speed, obviously, is realized.

We consider now the change of pressure, temperature, and density of gas in a tube of flow. Directly from formula (2-13), et al., it follows that, there, where speed increases, temperature, density and pressure in an isentropic flow of gas, decrease, and vice versa.

Thus, in a narrowing stream in a subsonic flow, the temperature, pressure and density decreased, and in a supersonic flow, increase. In an expanding stream the picture will be reverse.

Parameters, corresponding to a section of tube of flow, in which  $\lambda = 1$ , we shall call critical parameters. They are readily determined by formula (2-22) and by formulas for  $\frac{P}{P_0}$  and  $\frac{\rho}{\rho_0}$ , presented in the Table 2-1, after substituting  $\lambda = 1$ :

$$T_c = \frac{2}{k+1} T_0; \quad (2-31)$$

$$P_c = \left( \frac{2}{k+1} \right)^{\frac{k}{k-1}} P_0; \quad (2-32)$$

$$\rho_c = \left( \frac{2}{k+1} \right)^{\frac{1}{k-1}} \rho_0. \quad (2-33)$$

We see that the critical parameters depend on the physical properties of gas (coefficient  $k$ ) and on parameters of complete stagnation.

In Table 2-2 there are presented values of the relative critical parameters (relating to corresponding parameters of stagnation) for different  $k$  coefficients.

Table 2-2. The Critical Ratios of Parameters for Different Gases

$k$	1,07	1,4	1,33	1,30	1,25	1,20	1,15	1,1
$\frac{T_c}{T_0}$	0,7491	0,8333	0,8584	0,8696	0,880	0,9091	0,9292	0,9524
$\frac{P_c}{P_0}$	0,6193	0,6330	0,6290	0,6270	0,624	0,6200	0,6173	0,6139
$\frac{\rho_c}{\rho_0}$	0,4867	0,5282	0,5404	0,5457	0,555	0,5645	0,5746	0,5847

The above-obtained fundamental laws, or regularities, determining the variation of parameters of flow in a tube of flow current, physically can be understood from a consideration of equation of constancy of the flow rate in a tube of flow [formula (2-7)]. By means of equation

$$\frac{P}{P_0} = \left( 1 - \frac{k-1}{k+1} \lambda^2 \right)^{\frac{1}{k-1}}$$

(Table 2-1) we define the specific flow rate of a gas:

$$\bar{m} = \frac{m}{F} = \rho c = \rho_0 a_* \lambda \left(1 - \frac{k-1}{k+1} \lambda^2\right)^{\frac{1}{k-1}}. \quad (2-34)$$

The mass flow rate per second  $m$  for each section of a tube of flow will be one and the same. Intensity of change of density  $\rho$  and the speed  $c$  will be different in subsonic and supersonic regions. In a subsonic region with an increase in  $c$ , the density decreases more gradually than the speed increases, therefore the tube of flow must be narrowed, section  $F$  must be diminished. At supersonic speeds, conversely, a decrease in the density will be more intense than the increase in speed, and the tube of flow will expand.

As can be seen from formula (2-34) function  $\bar{m}(\lambda) = 0$  at  $\lambda = 0$  and  $\lambda = \sqrt{\frac{k+1}{k-1}}$  and, consequently, at a certain  $\lambda$ , has an extreme value. For determination of this value of  $\lambda$ , we shall differentiate (2-34)

$$\frac{d\bar{m}}{d\lambda} = \frac{d(\rho c)}{d\lambda} = \rho_0 a_* \left(1 - \frac{k-1}{k+1} \lambda^2\right)^{\frac{2-k}{k-1}} (1 - \lambda^2).$$

It follows from this that maximum value of the specific flow rate corresponds to  $\lambda = 1$ , i.e., a critical value of speed, since  $\frac{d\bar{m}}{d\lambda}$  vanishes at  $\lambda = 1$ . Consequently,

$$\bar{m}_{max} = \rho_0 a_* \left(\frac{2}{k+1}\right)^{\frac{1}{k-1}} = \rho_* a_*. \quad (2-35)$$

The reduced flow rate is the name for the ratio

$$q = \frac{\bar{m}}{\bar{m}_{max}} = \frac{\rho c}{\rho_* a_*} = \left(\frac{k+1}{2}\right)^{\frac{1}{k-1}} \lambda \left(1 - \frac{k-1}{k+1} \lambda^2\right)^{\frac{1}{k-1}}. \quad (2-36)$$

In Fig. 2-3 dependencies of the parameters of flow  $\frac{p}{p_*}$ ;  $\frac{\rho}{\rho_*}$ ;  $\frac{T}{T_*}$  and the reduced flow rate  $q$  on the dimensionless speed (for different  $k$ ) are presented.

Here, there is given the corresponding scheme of the variations of sections of a tube of flow, along the axis of which the speed continuously increases. It is readily seen that with a maximum speed  $\lambda = \lambda_{max} = \sqrt{\frac{k+1}{k-1}}$ , the reduced flow rate  $q = \frac{F_*}{F} = 0$ , i.e.,  $F = \infty$ . Physically this is intelligible, since at  $\lambda = \lambda_{max}$   $p = 0$  (outflow into an absolute vacuum) and  $\rho = 0$ .

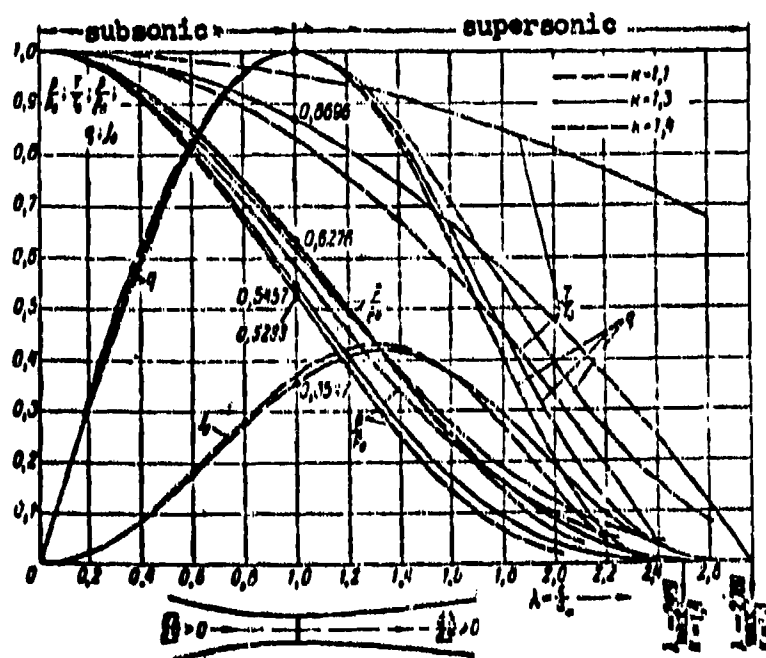


Fig. 2-3. Gas dynamic functions of a one-dimensional isentropic flow  $q, P/P_0, T/T_0, \rho/\rho_0, 1/\lambda$  ( $k = 1.1; 1.3; 1.4$ ).

Thus, we have established that in a tube of flow, having a minimum section, there may occur a transition through the critical speed. The necessary and sufficient conditions for such a transition are the conditions  $\lambda = 1$  and  $d\lambda/dx \neq 0$  in the minimum section. The reduced flow rate of the gas in this respect acquires a maximum value.

If the speed in minimum section will attain a critical value, and the second condition ( $d\lambda/dx \neq 0$ ) is not fulfilled, then a transition through the critical speed will not occur. This case corresponds to the manifestation of critical speeds in a tube of flow and is important both in the theory of the Laval nozzle and also in problems of external flow around bodies.

## 2-5. Certain Gas-Dynamic Functions of a One-dimensional Adiabatic Flow

Above (Sec. 2-3 and 2-4) we became acquainted with certain important

dimensionless characteristics of a one-dimensional flow of gas, which are expressed in the form of simple functions of dimensionless speeds  $M$ ,  $\lambda$ , or  $\xi$ . These gas-dynamic functions play an important role in realizing different gas-dynamic calculations, and also in processing the results of the experiment.

In addition to the already known, it is simple to obtain also gas-dynamic functions, which are encountered in transformations of equations of conservation of flow rate, momentum, and energy.

By means of the reduced flow rate  $q$  there is readily determined the total mass flow weight rate of a gas through a given section:

$$G = G_{Fpc} = G_{Fqa} \rho_a \quad (2-37)$$

or after substitution

$$\rho_a = \left(\frac{2}{k+1}\right)^{\frac{1}{k-1}} \rho_0 = \left(\frac{2}{k+1}\right)^{\frac{1}{k-1}} \frac{p_0}{R T_0} \text{ and } a_a = \sqrt{\frac{2kR}{k+1} T_0}$$

and transformations we find:

$$G = KF \frac{p_0 q}{\sqrt{T_0}} \quad (2-38)$$

where

$$K = \sqrt{\frac{kR}{2} \left(\frac{2}{k+1}\right)^{\frac{k+1}{k-1}}}$$

The flow rate can be expressed also in terms of the static pressure of the flow in a given section. For this purpose, we shall divide and multiply the right-hand side of formula (2-38) by  $p$ :

$$G = KF \frac{p_0 q}{p \sqrt{T_0}} = KF \frac{p}{\sqrt{T_0}} \sigma \quad (2-39)$$

where

$$\sigma = \frac{p q}{p} = \left(\frac{k+1}{2}\right)^{\frac{1}{k-1}} \lambda \left(1 - \frac{k-1}{k+1} \lambda^2\right)^{-1} \quad (2-40)$$

is a new function of dimensionless speed  $\lambda$ , depending also only on  $k$  and  $\lambda$ .

The equations of the rate flow in the form (2-38) and (2-39) can be used for calculating the adiabatic flow in an isolated system (without an energy exchange with the external medium) in the presence of friction. Actually, the condition for

the constancy of the flow rate (2-38) for two arbitrarily selected sections of the channel can be written in such a form:

$$F_1 \frac{p_{01} q_1}{\sqrt{T_{01}}} = F_2 \frac{p_{02} q_2}{\sqrt{T_{02}}}.$$

Since for an isolated system  $T_{01} = T_{02} = T_0$ , then

$$\frac{p_{02}}{p_{01}} = \frac{F_1}{F_2} \cdot \frac{q_1}{q_2}; \quad (2-41)$$

for channels of constant section

$$\frac{p_{02}}{p_{01}} = \frac{q_1}{q_2}. \quad (2-41a)$$

Formulas (2-41) and (2-41a) make it possible to find the variation of pressure of stagnation, stipulated by irreversible changes of state of the moving gas and, in particular, losses, caused by internal frictional forces.

Analogously by means of (2-39) there can be obtained ( $T_{01} = T_{02} = T_0$ ):

$$F_1 p_1 v_1 = F_2 p_2 v_2,$$

whence

$$\frac{p_2}{p_1} = \frac{F_1}{F_2} \cdot \frac{v_1}{v_2}, \quad (2-42)$$

or for cylindrical channel

$$\frac{p_2}{p_1} = \frac{v_1}{v_2}. \quad (2-42a)$$

Relationships (2-42) can be used for determining the static pressure in one of the sections of flow, if there are known the speeds in two sections ( $\lambda_1$  and  $\lambda_2$ ) and the static pressure in one of them.

We shall introduce still one function, that characterizes pulse of flow, equal to

$$J = \frac{G}{g} c + pF. \quad (2-43)$$

In considering that

$$F = \frac{G}{gpc},$$

we shall rewrite (2-43a) in the form of:

$$J = \frac{G}{g} \left( c + \frac{p}{\rho c} \right). \quad (2-43a)$$

From (2-17) and (2-22) we have:

$$\frac{p}{\rho} = gRT = gRT_0 \left(1 - \frac{k-1}{k+1} \lambda^2\right) = \frac{k+1}{2k} a_*^2 \left(1 - \frac{k-1}{k+1} \lambda^2\right)$$

and  $c = \lambda a_*$ ; then equation (2-43) can be written as:

$$J = \frac{G}{g} c + pF = \frac{k+1}{2k} \cdot \frac{G}{g} a_* \psi, \quad (2-44)$$

where

$$\psi = \lambda + \frac{1}{\lambda}, \quad (2-45)$$

a certain new function of the dimensionless speed  $\lambda$ .

Equation for the pulse of gas flow (2-44) was for the first time obtained by B. M. Kiselev. It is widely used in different problems and, in particular, for calculating energy nonisolated flows (calculation of flows with admission of removal of heat in the presence of frictional forces, calculation of sudden expanding of channel, the process of mixing, etc.).

The original equation of pulse (2-43a)

$$J = \frac{G}{g} a_* \left(\lambda + \frac{p}{\rho c a_*}\right)$$

is readily transformed to another form, by using new important function of the dimensionless static pressure

$$\pi = \frac{p}{\rho c a_*} = \frac{p}{\rho a_*^2} \lambda = \frac{p}{\rho a_*^2} \cdot \frac{1}{\lambda}. \quad (2-46)$$

After replacing here  $\frac{p}{\rho} = gRT$  and  $a_*^2$  by formula (2-17) we shall obtain\*.

$$\pi = \frac{k+1}{2k} \frac{1}{\lambda} \left(1 - \frac{k-1}{k+1} \lambda^2\right). \quad (2-46a)$$

Consequently, pulse of flow is expressed through function  $\pi$  by the formula

$$J = \frac{G}{g} a_* (\lambda + \pi), \quad (2-47)$$

and a connection between  $\psi$  and  $\pi$  is established by the relationship

$$\pi = \frac{k+1}{2k} \psi - \lambda. \quad (2-48)$$

\*Function  $\pi$  for the first time was proposed by A. F. Gandel'sman and used in works of A. A. Gukhman and A. F. Gandel'sman for the study of resistance of tubes during an adiabatic flow of gas.

We now use formulas (2-38) and (2-39) and replace the magnitude of the flow rate  $G$  in equations (2-44) and (2-47). After simple transformations we find:

$$J = k \epsilon F p_0 q (\lambda + \pi) = \bar{p}_* F p_0 q \psi \quad (2-49)$$

and

$$J = k \epsilon F p_0 (\lambda + \pi) = \bar{p}_* F p_0 \psi. \quad (2-50)$$

Here  $\epsilon_* = \left(\frac{2}{k+1}\right)^{\frac{k}{k-1}}$  is the critical ratio of the pressures;

$\bar{p}_* = \left(\frac{2}{k+1}\right)^{\frac{1}{k-1}}$  is the critical ratio of the density.

By means of formulas (2-40) and (2-50) there is readily established a connection between gas-dynamic functions  $q$ ,  $\sigma$ ,  $\psi$  and  $\pi$ .

In certain calculations it is convenient to introduce also the functions

$$\gamma = \bar{p}_* q \psi = k \epsilon_* q (\lambda + \pi) = (\lambda^2 + 1) \left(1 - \frac{k-1}{k+1} \lambda^2\right)^{\frac{1}{k-1}} \quad (2-51)$$

and

$$\Delta = \bar{p}_* \sigma \psi = k \epsilon_* \sigma (\lambda + \pi) = \frac{\lambda^2 + 1}{1 - \frac{k-1}{k+1} \lambda^2}. \quad (2-52)$$

Then

$$J = \gamma F p_0 = \Delta F p_0. \quad (2-53)$$

Function of a dimensionless static pressure  $\pi$  is encountered also in using the equation of energy. We shall express from (2-14) the speed of sound:

$$a^2 = \frac{k+1}{2} a_*^2 - \frac{k-1}{2} c^2.$$

After dividing this equation by  $a_*^2$ , we obtain:

$$\left(\frac{a}{a_*}\right)^2 = \frac{k+1}{2} \left(1 - \frac{k-1}{k+1} \lambda^2\right) = k \lambda \pi. \quad (2-54)$$

If we use the equation of energy in the form (2-11), it is simple to find ratio of the velocity head  $\frac{pc^2}{2}$  to the static pressure  $p$ :  $l = \frac{pc^2}{2p} = \frac{k}{k-1} \left(\frac{p_0}{p} \frac{p}{p_0} - 1\right).$

After substitution of the values  $\frac{p_0}{p}$  and  $\frac{p}{p_0}$  we shall obtain:

$$l = \frac{k}{k+1} \lambda^2 \left(1 - \frac{k-1}{k+1} \lambda^2\right)^{-1} = \frac{\lambda}{2\pi}. \quad (2-55)$$

The velocity head related to the pressure of stagnation, can be found by the formula

$$h = \frac{pc^2}{2p_0} = \frac{pc^2}{2p} \frac{p}{p_0} = \frac{\lambda}{2\pi} \frac{p}{p_0} = \frac{k}{k+1} \lambda^2 \left(1 - \frac{k-1}{k+1} \lambda^2\right)^{\frac{1}{k-1}}. \quad (2-56)$$



Thus, a number of characteristics of a one-dimensional gas flow is expressed in the form of functions of dimensionless speed  $\lambda$  and the coefficient of the isentropic process,  $k$ . The most important of the functions have been reduced to tables of gas-dynamic functions, constructed for different constant values  $k$  (Appendix 1). The use of such tables considerably simplifies gas-dynamic calculations, which accounts for the wide distribution of the tables.

At the same time an analysis of change of certain gas-dynamic functions makes it possible to make important conclusions about properties of gas flow. Thus, for example, in Fig. 2-4, supplementing Fig. 2-3, there are presented the functions  $\pi$ ,  $\sigma$ ,  $\Delta$ ,  $\gamma$  and  $j$  ( $k = 1.4$ ). The function  $j_0$  is shown in Fig. 2-4.

Function  $\pi$  monotonically diminishes with an increase of the speed  $\lambda$  and at  $\lambda = 1$  acquires a critical value, equal [formula (2-46a)] to:  $\pi_* = \frac{1}{k}$ .

In remembering the expression for critical ratio of the pressures, we readily find:

$$\frac{p_0}{p_*} = k \left( \frac{2}{k+1} \right)^{\frac{k}{k-1}}.$$

In turning to Fig. 2-4, it may be noted that the function  $\gamma$  varies slightly in the wide range of speeds  $0 \leq \lambda \leq 1.5$ . By bearing in mind meaning of this function [formula (2-51)], we readily come to the conclusion that with a constant pressure of stagnation the pulse of flow weakly depends on the dimensionless speed at  $\lambda \leq 1.5$ .

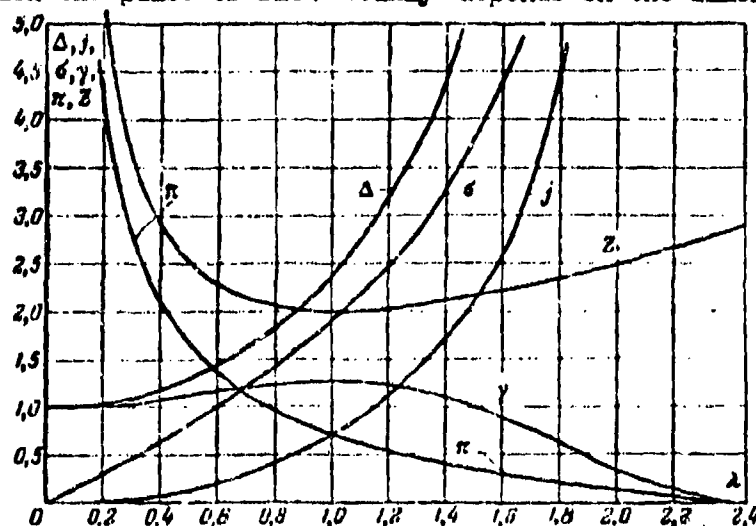


Fig. 2-4. Gas-dynamic functions  $\pi, \sigma, \Delta, j, \gamma$  of a one-dimensional flow of gas for  $k = 1.4$ .

With a constant static pressure, the pulse in the given section tensely increases with an increase of  $\lambda$ , since function  $\Delta$  sharply increases from unity at  $\lambda = 0$  to infinity at  $\lambda \rightarrow \lambda_{\max}$ .

The flow rate of a gas through a given section  $F$  varies very greatly with a variation of  $\lambda$ , if the static pressure is kept constant;

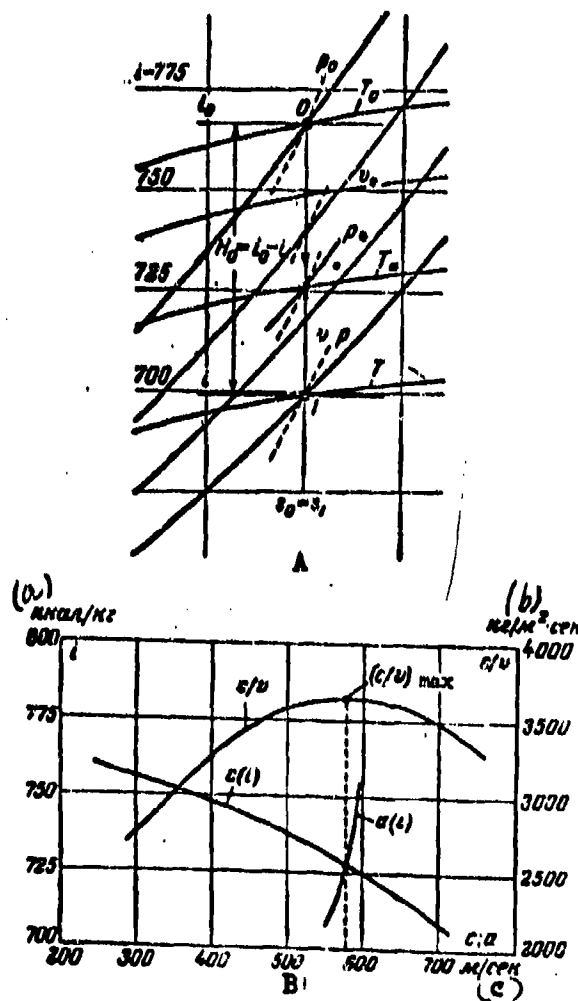


Fig. 2-5. Isentropic process of expansion (A) in a thermal diagram and (B) the determination of critical parameters for a real gas.  
KEY to b): (a) kcal/kg; (b)  $\text{kg/m}^2 \cdot \text{sec}$ ; (c) m/sec.

this is characterized by the behavior of function  $\sigma$  (Fig. 2-4).

In the above-presented formulas constants, depending only on  $k$ , appear. Values of certain constants are given in Table 2-3.

Table 2-3.

$k$	1.67	1.6	1.5	1.4	1.35	1.3	1.25	1.2	1.1
$\sqrt{k \left( \frac{2}{k+1} \right)^{\frac{k+1}{k-1}}}$	0.7218	0.7164	0.7011	0.683	0.670	0.667	0.653	0.6184	0.6235
$k \left( \frac{2}{k+1} \right)^{\frac{k}{k-1}}$	0.6128	0.7917	0.7089	0.7301	0.723	0.7093	0.6938	0.6803	0.6432

## 2-6. Peculiarities of Calculating a One-dimensional Flow of a Real Gas

The equation of energy (2-10) makes it possible to use extensively phase diagrams for calculating gasflows, which are especially important in investigating flows of real gases, change of state of which is not subordinated to equation (1-1), and the heat capacity is a function of the pressure and temperature.

In the practice of calculating heat engines (steam and gas turbines, compressors, et al.) most widely employed are thermal diagrams, in which along the axes of coordinates there are plotted the temperature and entropy, or enthalpy and entropy (T-s and i-s diagrams). Such diagrams constructed on the basis of experimental data make it possible with sufficient accuracy to calculate the different processes in change of state of gases, including in the region of moist vapor and near the line of saturation.

The T-s and i-s phase diagrams may be widely used in investigating gas flows.

Actually, we shall express from the equation of energy (2-10) the speed of the flow:

$$c = \sqrt{2(i_0 - i)}.$$

After substituting 1 (kilocalorie/kg) we shall obtain:

$$c = \sqrt{\frac{2H}{\lambda} (i_0 - i)}.$$

In substituting values of the constants  $g$  and  $\lambda$ , we find:

$$c = 91.53 \sqrt{(i_0 - i)}. \quad (2-10b)$$

Formula (2-10b) indicates that for determining the speed of flow it is necessary to know the difference between the enthalpies  $i_0 - i$ , which readily is determined by the  $i$ - $s$  diagram, if the parameters of complete stagnation of the gas ( $p_0$ ,  $T_0$ ) and static parameters of flow ( $p$ ,  $T$ ) are known.

In Fig. 2-5a, there is presented a portion of an  $i$ - $s$  diagram for water vapor. If we know any two parameters of the total stagnation ( $p_0$  and  $T_0$ ), then on the  $i$ - $s$  diagram there is found the point 0, which determines the state of a stagnated flow. This point can be found also by other parameters of state (for example,  $i_0$  and  $s_0$ ). By drawing a vertical line up to the intersection point with isobar of static pressure  $p$ , isotherm  $T$  or the isochore  $v$ , we determine the state of a moving gas (point 1) and first of all its enthalpy  $i$ ; then the speed of flow readily can be determined by equation (2-10b).

The difference of enthalpies  $H_0 = i_0 - i$  entering in this equation is called the isentropic differential of the enthalpies.

Thermal diagrams can be used also for calculating irreversible flows (see below). In this case, however, for determining the speed of flow three parameters of state are insufficient.

In considering the isentropic motion along a tube of flow of variable section on an  $i$ - $s$  diagram, there is readily found the specific flow rate of gas in different sections  $\frac{G}{F}$  and readily constructed this magnitude, and also other parameters depending on the speed  $c$  (Fig. 2-5, b). The maximum of specific flow rate corresponds to a critical section of the tube, determinate by the equation of flow rate:

$$\frac{F}{F_*} = \left( \frac{c}{c_*} \right)_{\max}.$$

Parameters in the critical section are found from the condition  $c = a$ . For this purpose it is possible to construct curves of variations of the speed of sound  $a(i)$  and of speed of flow  $c(i)$  depending upon the enthalpy; the intersection point of indicated curves gives the values  $a$  and  $i$  in the critical section. By transferring this point to an  $i$ - $s$  diagram there can be found also other parameters in this section (Fig. 2-5,b).

## CHAPTER 3

## TWO-DIMENSIONAL MOTION OF GAS WITH CONSTANT ENTROPY

3-1. Potential Motion of Fluid

A condition of irrotational motion can be obtained from equation (1-6). For a three-dimensional irrotational flow ( $\omega_x = \omega_y = \omega_z = 0$ ) from (1-6) it follows:

$$\left. \begin{aligned} \frac{\partial w}{\partial y} &= \frac{\partial v}{\partial z}; \\ \frac{\partial u}{\partial z} &= \frac{\partial w}{\partial x}; \\ \frac{\partial v}{\partial x} &= \frac{\partial u}{\partial y}. \end{aligned} \right\} \quad (3-1)$$

By bearing in mind the mechanical sense of the partial derivatives in equations (1-6), we may conclude that formulas (3-1) indeed express condition of an absence of the rotational motion of a fluid particle. On the other hand, equalities (3-1) mathematically express the fact that there exists a certain function of the coordinates  $\phi(x, y, z)$ , the partial derivatives of which for the coordinates are equal to projections of the speed onto corresponding axes of coordinates, i.e.,

$$\left. \begin{aligned} u &= \frac{\partial \phi}{\partial x}; \\ v &= \frac{\partial \phi}{\partial y}; \\ w &= \frac{\partial \phi}{\partial z}. \end{aligned} \right\} \quad (3-2)$$

Actually, a substitution of (3-2) into (3-1) results in an identities.

Function  $\phi(x, y, z)$  is called the potential of the speed.

The concept of the potential of speed in aerohydrodynamics is identical to the concept of the potential of forces in the mechanics of a solid body. From mechanics

it is known that derivative of the potential of forces in any direction gives a projection of potential force, acting in this direction. By analogy, intensity of change in potential of speed in direction of coordinate axes, determines projections of the speed onto the corresponding axes [formulas (3-2)].

The discussion above shows that the potential motion of a gas in an isolated system is isentropic, i.e., if the flow is irrotational and adiabatic, then the change in entropy in any direction in the flow is equal to zero and the flow of the gas is described by a certain function of the coordinates  $\phi(x, y, z)$ .

In being restricted in this chapter to a consideration of only two-dimensional potential flows of gas, we can obtain an equation of the potential of the speeds by means of Euler equations.

For a two-dimensional steady flow on the assumption  $X = Y = 0$ , equations (1-12) and (1-16) give:

$$\left. \begin{aligned} u \frac{\partial u}{\partial x} + v \frac{\partial u}{\partial y} &= -\frac{1}{\rho} \frac{\partial p}{\partial x}; \\ u \frac{\partial v}{\partial x} + v \frac{\partial v}{\partial y} &= -\frac{1}{\rho} \frac{\partial p}{\partial y}; \\ \frac{\partial(\rho u)}{\partial x} + \frac{\partial(\rho v)}{\partial y} &= 0. \end{aligned} \right\} \quad (3-3)$$

The pressure gradients  $\frac{\partial p}{\partial x}$  and  $\frac{\partial p}{\partial y}$  can be expressed in the following manner:

$$\left. \begin{aligned} \frac{\partial p}{\partial x} &= \left( \frac{\partial p}{\partial \rho} \right) \frac{\partial \rho}{\partial x} = a^2 \frac{\partial \rho}{\partial x}; \\ \frac{\partial p}{\partial y} &= \left( \frac{\partial p}{\partial \rho} \right) \frac{\partial \rho}{\partial y} = a^2 \frac{\partial \rho}{\partial y}. \end{aligned} \right\} \quad (3-4)$$

From the third equation (3-3) after differentiation we obtain:

$$u \frac{\partial \rho}{\partial x} + v \frac{\partial \rho}{\partial y} + \rho \left( \frac{\partial u}{\partial x} + \frac{\partial v}{\partial y} \right) = 0. \quad (3-5)$$

After substituting (3-4) into (3-3) we shall have:

$$\begin{aligned} \frac{\partial p}{\partial x} &= -\frac{\rho}{a^2} \left( u \frac{\partial u}{\partial x} + v \frac{\partial u}{\partial y} \right); \\ \frac{\partial p}{\partial y} &= -\frac{\rho}{a^2} \left( u \frac{\partial v}{\partial x} + v \frac{\partial v}{\partial y} \right). \end{aligned}$$

In substituting derivatives of the density in (3-5), we obtain:

$$\left( 1 - \frac{u^2}{a^2} \right) \frac{\partial u}{\partial x} + \left( 1 - \frac{v^2}{a^2} \right) \frac{\partial v}{\partial y} - \frac{uv}{a^2} \left( \frac{\partial u}{\partial y} + \frac{\partial v}{\partial x} \right) = 0. \quad (3-6)$$

By bearing in mind (3-2), we rewrite (3-6) in the form of:

$$\left( 1 - \frac{u^2}{a^2} \right) \frac{\partial^2 \phi}{\partial x^2} + \left( 1 - \frac{v^2}{a^2} \right) \frac{\partial^2 \phi}{\partial y^2} - \frac{2uv}{a^2} \frac{\partial^2 \phi}{\partial x \partial y} = 0. \quad (3-7)$$

Equation (3-7) is a nonlinear differential equation of the potential of speeds in partial derivatives of second order.

Introduction of potential of speed made it possible to reduce a system of three equations (3-3) to one (3-7), to decrease number of unknowns from six to five and to leave in the equation only the kinematic parameters.

If in investigated field of flow, there is known the potential of speed  $\Phi(x, y)$ , then under given boundary conditions there can be determined all parameters of the flow. The potential of speed makes it possible to determine the speed of flow ( $u, v$ ) by formulas (3-2). By means of the equation of energy jointly with equation of the isentropic process there are readily determined the pressure  $p$ , the density and temperature of gas  $T$ .

Thus, in investigating the potential motions of a gas, the chief problem reduces to a determination of the potential of speeds  $\Phi(x, y)$  for a given form of motion, i.e., to determining the solution of equation (3-7). If the potential function  $\Phi(x, y)$  is determined, then kinematic part of the problem is solved. Then, without special difficulties, there is solved also the dynamic part of problem. However, equation (3-7) in a general form, is not integrated.

Let us note that the potential function must satisfy specific initial and boundary conditions of a given concrete problem. As kinematic initial conditions there should be given distribution of parameters of flow in a definite — initial — region of flow, and also there should be known conditions on the boundary of streamlined body. In solving concrete problems of flow around bodies, most frequently there are given parameters of flow of a nondisturbed flow at an infinite distance from the body (initial conditions) and conditions of impenetrability — the normal component speed on surface of the body is equal to zero (boundary conditions).

Thus, for example, if a two-dimensional flow in infinity is parallel to the  $x$ -axis, the potential of the speed should correspond to the following conditions:



$$u_{\infty} = \left( \frac{\partial \Phi}{\partial x} \right)_{\infty} = c;$$

$$v_{\infty} = \left( \frac{\partial \Phi}{\partial y} \right)_{\infty} = 0.$$

Here also there must be known the remaining parameters:

$$\rho_{\infty}, p_{\infty}, T_{\infty}.$$

On boundary of the streamlined body, physical conditions of flow around dictate the distribution of speeds. By assuming a continuous flow around, we can write that the normal component of the speed on surface of streamlined body must be equal to zero and, consequently,

$$v_i = \left( \frac{\partial \Phi}{\partial y} \right)_i = 0.$$

In considering an ideal liquid (in absence of forces of viscosity), we must admit that particles of a fluid slip along the streamlined surface of a body and, consequently, tangential components of the speed

$$u_i = \left( \frac{\partial \Phi}{\partial x} \right)_i = c_i$$

(here, there is considered a mobile system of coordinates, located in such a way, that direction of the axis  $x$  at each point coincides with direction of the tangent to the surface of the body; the  $y$  axis is normal to the surface of the body and, consequently, to the streamlines).

A more detailed examination of equation (3-7), by which the potential function  $\Phi(x, y)$  is determined, however, shows that it possesses different properties depending upon relationship between components of the speed  $u$  and  $v$  and the speed of sound  $a$ . Actually, let us assume that magnitudes  $\frac{u}{a}$  and  $\frac{v}{a}$  are very small and they can be ignored, i.e., we assume that speed of gas flow is small in comparison with the speed of sound. Then, from (3-7) it follows:

$$\frac{\partial^2 \Phi}{\partial x^2} + \frac{\partial^2 \Phi}{\partial y^2} = 0. \quad (3-8)$$

Equation (3-8) characterizes the potential flow of an ideal incompressible fluid.

At high subsonic speeds, when the effect of compressibility cannot be ignored, the nonlinear differential equation (3-7) significantly is simplified in case this flow can be considered slightly disturbed (Sec 3-3).

A study of steady two-dimensional and certain axially symmetric flows of gas can also be simplified by introducing another function of coordinates — the stream function  $\Psi$ . In turning to third equation of system (3-3), we see that it is satisfied, if we assume

$$\rho u = \frac{\partial \Psi}{\partial y} \text{ and } \rho v = -\frac{\partial \Psi}{\partial x},$$

or

$$u = \frac{1}{\rho} \cdot \frac{\partial \Psi}{\partial y};$$

$$v = -\frac{1}{\rho} \cdot \frac{\partial \Psi}{\partial x}.$$

In order that the stream function and the potential of speed have identical dimensionality, the coefficient with derivatives is expediently reduced to a dimensionless form. Then, in the case of a potential flow equations for  $u$  and  $v$  will be written in the following form:

$$\left. \begin{aligned} u &= \frac{\rho_0}{\rho} \cdot \frac{\partial \Psi}{\partial y} = \frac{\partial \Phi}{\partial x}; \\ v &= -\frac{\rho_0}{\rho} \cdot \frac{\partial \Psi}{\partial x} = \frac{\partial \Phi}{\partial y}, \end{aligned} \right\} \quad (3-9)$$

where  $\Psi = \rho_0 \Phi$ .

In the simplest case of motion of an incompressible fluid in equations (3-9) the magnitude of relative density

$$\frac{\rho_0}{\rho} = \left(1 + \frac{k-1}{2} M^2\right)^{\frac{1}{k-1}} = 1 + \frac{1}{2} M^2 + \frac{2-k}{8} M^4 + \dots \quad (3-10)$$

may be assumed equal to unity,

Now equations (3-9) acquire the form:

$$\left. \begin{aligned} u &= \frac{\partial \Psi_n}{\partial y}; \\ v &= -\frac{\partial \Psi_n}{\partial x}. \end{aligned} \right\} \quad (3-11)$$

It is readily noted that in the case of an irrotational flow [condition (3-1)] function  $\Psi_n$  satisfies the equation

$$\frac{\partial^2 \Psi_n}{\partial x^2} = \frac{\partial^2 \Psi_n}{\partial y^2}.$$

If, in the entire region of flow of gas, the speeds vary insignificantly, it may be assumed  $\frac{\rho_0}{\rho} = \text{const}$ , then transition to equations (3-11) will be attained by a

substitution  $\Psi' = \frac{\rho_0}{\rho} \Psi$ . In such a substitution the speed of gas is simply equal to speed of an incompressible fluid:

$$u = u_n; \quad v = v_n.$$

Thus, the indicated simplest case of a transition from subsonic flows of gas to flows of incompressible fluid are in essence, simply a disregard of the influence of compressibility. Possibilities of such a disregard, stipulated by dependence of the density on the Mach number, are very limited. In reality, if it were required that magnitude  $\frac{\rho_0}{\rho}$  differ from unity by not more than 2%, then in accordance with (3-10) Mach number should be not larger than 0.20.

The physical importance of the stream function  $\Psi$  is explained in determining the flow rate of a gas through an elementary open profile in a two-dimensional flow. It is possible to show that stream function numerically is equal to the volumetric flow rate of gas through such an elementary profile. It follows from this that the stream function conserves the constant value along streamlines of a two-dimensional flow.

Actually, we shall draw in plane of flow a certain profile  $LL_1$  (Fig. 3-1) and shall calculate the volumetric flow rate  $V$  through this profile. In accordance

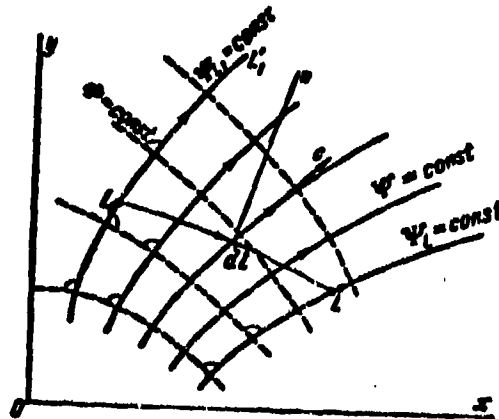


Fig. 3-1. Diagram for deriving a condition of irrotational motion.

with designations in Fig. 3-1 we obtain\*:

$$V = \int_L c_n dl = \int_L [u \cos(x, n) + v \cos(y, n)] dl = \int_L (udy - vdx),$$

since

$$u dl \cos(x, n) = u dy$$

and

$$v dl \cos(y, n) = v dx.$$

But

$$u dy - v dx = d\psi;$$

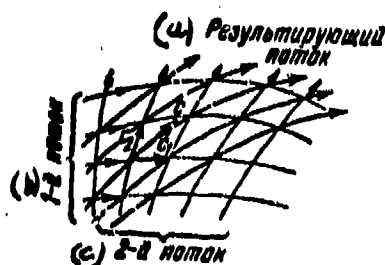
then

$$V = \int_L d\psi = \int_L \left( \frac{\partial \psi}{\partial y} dy + \frac{\partial \psi}{\partial x} dx \right) = \psi_{L_1} - \psi_{L_2}.$$

Region of flow, limited by the streamlines  $\psi_{L_1} = \text{const}$  and  $\psi_{L_2} = \text{const}$ , is the tube of flow. Consequently, difference between values of stream function

$\psi_{L_1} - \psi_{L_2}$  is equal to the volumetric flow rate of fluid through the section of tube of flow, limited by streamlines, passing through points  $L$  and  $L_1$ .

From equations (3-11) it follows that for an incompressible fluid



$$\left. \begin{aligned} \frac{\partial \Phi_n}{\partial x} &= -\frac{\partial \psi_n}{\partial y}; \\ \frac{\partial \Phi_n}{\partial y} &= \frac{\partial \psi_n}{\partial x}. \end{aligned} \right\} \quad (3-12)$$

Fig. 3-2. The Composition of two-dimensional progressive flows.

KEY: (a) Resultant flow; (b) 1st flow; (c) 2nd flow.

By adding to function  $\Phi$  different constant values, we shall obtain a family of isopotential lines. By using conditions (3-12), it is possible to show that the streamlines (lines  $\psi_n = \text{const}$ ) and isopotential lines (lines  $\Phi_n = \text{const}$ ) are mutually orthogonal, i.e., they intersect at a right angle (Fig. 3-1).

\*The dimension of profile in a direction, normal to plane of figure, is assumed equal to unity.

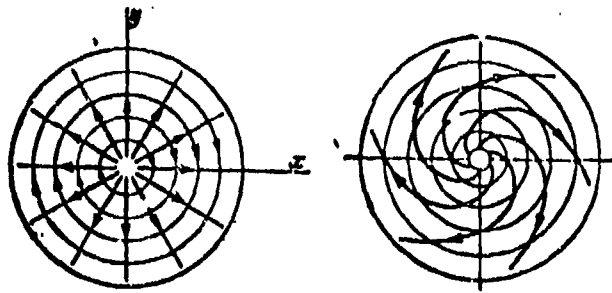


Fig. 3-3. Vortex source (Vortex Sink).

The equation of potential of speeds of a two-dimensional flow of an incompressible fluid (3-8) makes it possible to develop the widely used method of superposing the potential flows. From theory of differential equations of an elliptic type, it is known that if function  $\Phi_{n1}, \Phi_{n2}, \dots, \Phi_{nn}$  are solutions of such an equation, then the sum  $\Phi_n = \Phi_{n1} + \Phi_{n2} + \dots + \Phi_{nn}$  is also a solution of this equation. It follows from this that, by composing potentials of the speed  $\Phi$  and of stream function  $\psi$  of the simplest flows, there can be obtained the characteristic of a more composite motion. Here the potentials of speeds and of the stream function are composed algebraically, and vectors of speeds — geometrically.

Method of superposition of potential flows under certain conditions can be used also for constructing composite flows of compressible fluid.

In Fig. 3-2 there is presented the simplest case of composing two two-dimensional progressive flows, intelligible without explanations.

Another example of the composition of potential flows is shown in Fig. 3-3. The composition of a two-dimensional source (sink) and circulatory flow gives a more composite motion, called a vortex source (vortex sink), the streamlines of which have a spiral shape.

### 3-2. Pressure Coefficients. Critical Mach Number

We shall dwell on certain simple concepts, very essential in concrete theoretical and experimental problems of gas dynamics and which we shall use in the future.

Suppose we place in the gas flow of subsonic speed, a certain curvilinear

airfoil and then we examine the variation of the parameters of an elementary stream, encompassing such an airfoil (Fig. 3-4).

The disturbance of the flow at subsonic speeds created by airfoil will be propagated in all directions, including that against the flow. Under the effect of  $K$  these disturbances the elementary streams, moving towards the airfoil, will be deformed. At the tip of airfoil, central stream expands; speed of flow here drops and at the point of branching,  $A$ , vanishes. At this point the parameters will be equal to parameters of the total stagnation of the flow. On the forward portion of airfoil section of stream decreases, as a consequence of which speed increases, and the pressure drops. On upper and lower surfaces of airfoil there continues a contraction of stream with corresponding increase in speed. At a certain point the section of the stream is at a minimum. At this place the speed will be maximum. Further, on the rear surfaces of airfoil the stream again expands, its speed drops, and the pressure increases.

Thus, as a result of the deformation of small streams, the nature of which is determined by the shape of the streamlined body, along surface of airfoil the pressure decreases. The distribution of pressures causes the generation of aerodynamic forces, acting on the airfoil: The force of lift, caused by difference of pressures

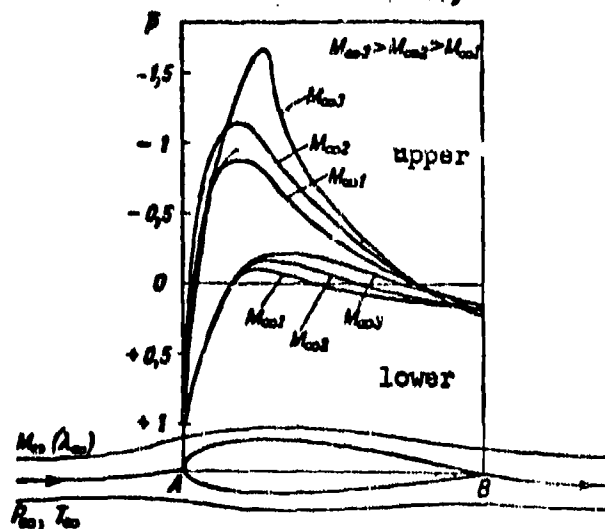


Fig. 3-4. Distribution of pressure coefficients along airfoil.

on upper and lower surfaces of an airfoil, and force of drag, caused by the difference of pressures on the forward and rear part of airfoil and by frictional forces\*.

The distribution of pressures along streamlined surface is characterized by dimensionless magnitude--the pressure coefficient, which is determined as the ratio of difference between pressures at the given point on surface and of a static, infinity to the velocity head, undisturbed flow:

$$\bar{p} = \frac{p - p_{\infty}}{\frac{\rho_{\infty} c_{\infty}^2}{2}}. \quad (3-13)$$

The velocity head can be expressed in terms of the dimensionless speed  $M_{\infty}$  or  $\lambda_{\infty}$ , by using formulas (2-21) and (2-55).

Then

$$\bar{p} = \frac{2}{k} \frac{1}{M_{\infty}^2} \left( \frac{p}{p_{\infty}} - 1 \right) = \frac{k+1}{k \lambda_{\infty}^2} \left( \frac{p}{p_{\infty}} - 1 \right) \left( 1 - \frac{k-1}{k+1} \lambda_{\infty}^2 \right). \quad (3-14)$$

In certain cases the distribution of pressures along surface is characterized by the dimensionless pressure  $\tilde{p}$ , which is the ratio of the pressure at a given point to pressure of stagnation of an undisturbed flow:

$$\tilde{p} = \frac{p}{p_0}.$$

It is obvious that connection between pressure coefficient  $\bar{p}$  and the relative pressure  $\tilde{p}$  is expressed by formula

$$\tilde{p} = \frac{p_{\infty}}{p_0} \left( 1 + \frac{k}{2} M_{\infty}^2 \bar{p} \right) = \frac{1 + \frac{k}{2} \bar{p} M_{\infty}^2}{\left( 1 + \frac{k-1}{2} M_{\infty}^2 \right)^{\frac{k}{k-1}}}. \quad (3-15)$$

At low speeds of incident flow, it is more convenient for calculating the pressure coefficient to use formula (3-13).

In Fig. 3-4 there is shown the approximate distribution of  $\bar{p}$  along surface of airfoil. As long as speed  $c_{\infty}$  is significantly less than the speed of sound, character of deformation of small streams, and at the same time, also the picture of distribution of pressure coefficients along the airfoil with a change in speed

---

\*If we disregard influence of viscosity and consider subsonic and nondetached flow around an airfoil, as is done in the present chapter, then the force of drag will be absent.

of undisturbed flow are kept virtually constant. However, by the degree of increase in  $M_\infty$  the influence of compressibility becomes all more perceptible; distribution  $\bar{p}$  along airfoil starts to vary especially greatly there, where the local speeds in the stream (on surface of airfoil) are higher. In minimum section of the stream the speed is the maximum. We shall find the dependence between dimensionless speed  $M_\infty$  and speed at certain point on the airfoil  $M_1$ .

For this purpose we use formula (3-14), after replacing in it the ratio of the pressures by corresponding M numbers:

$$\frac{p}{p_\infty} = \frac{\frac{p}{p_1}}{\frac{p_\infty}{p_1}} = \left( \frac{1 + \frac{k-1}{2} M_\infty^2}{1 + \frac{k-1}{2} M_1^2} \right)^{\frac{k}{k-1}};$$

we obtain

$$\bar{p} = \frac{2}{k M_\infty^2} \left[ \left( \frac{1 + \frac{k-1}{2} M_\infty^2}{1 + \frac{k-1}{2} M_1^2} \right)^{\frac{k}{k-1}} - 1 \right]. \quad (3-16)$$

At a certain value  $M_\infty = M_*$  in the minimum section of the tube of flow there is established a critical speed  $M_1 = 1$ . Corresponding magnitude of pressure coefficient will be:

$$\bar{p}_* = \frac{2}{k M_*^2} \left[ \left( \frac{2}{k+1} \right)^{\frac{k}{k-1}} \left( 1 + \frac{k-1}{2} M_*^2 \right)^{\frac{k}{k-1}} - 1 \right]. \quad (3-17)$$

The magnitude  $M$  is called the critical M number of incident flow; it determines that value of dimensionless speed of incident flow, with which maximum local speed on airfoil of a body becomes equal to local speed of sound. From a determination of the critical M number, it follows that this magnitude differentiates subsonic regimes of flow round a body into two groups. The first group of subcritical regimes ( $M_\infty < M_*$ ) is characterized by the fact that at all points of the field of flow, the local speeds are subsonic ( $M_1 < 1$ ). To second group ( $M_\infty > M_*$ ) belong regimes of flow around with local supersonic speeds.

In the investigation of two-dimensional motions of a compressible fluid, referring both to the first, and also especially to the second group of regimes, it is necessary to consider influence of compressibility. This problem is solved in



works of a number of Soviet scientists. Even in 1902, S. A. Chaplygin in his work "On Gas Jets" published a method of calculating the compressibility for a two-dimensional flow. This work has been very valuable at present and has been the beginning for majority of contemporary researches on determining the effect of compressibility in the flow around bodies by flow of gas. The Soviet scientists S. A. Khristianovich, L. I. Sedov, et al., by fruitfully developing the idea of S. A. Chaplygin worked out reliable methods of calculating the effect of compressibility. These methods are widely used also in solving problems associated with the flow of gas in the flow part of turbomachines.

Together with relatively complex methods of calculating the influence of compressibility by a number of authors there have been proposed approximate methods, making it possible by the value of these or other assumptions to simplify the problem and by means of comparatively simple calculations to evaluate the influence of compressibility on the flow around a body. These include methods by L. Prandtl, S. G. Nuzhin, G. F. Burago, A. N. Sherstyuk, and others.

### 3-3. Calculation of Influence of Compressibility by the Method of Small Disturbances

The considered below simplest method of evaluating the influence of compressibility in two-dimensional subsonic flow will be used in those cases when the disturbance of the flow can be assumed weak.

We shall select a system of coordinate axes so that the x-axis is directed by the speed of undisturbed flow, and the y-axis is normal to the speed.

After designating by  $c'$  and correspondingly  $u'$  and  $v'$  the additional speeds, caused by any other disturbance of flow (thus, for example, influence of streamlined body), we shall present the speed at certain point of a disturbed flow in such a form:

$$c = c_{\infty} + c', \text{ or } u = u_{\infty} + u'; v = v'.$$

Here we assume that  $v_{\infty} = 0$ , since the flow at infinity is parallel to x-axis ( $c_{\infty} = u_{\infty}$ ). By assuming further that  $u'$  and  $v'$  are small magnitudes of order  $\Delta$

we come to the conclusion that the derivatives

$$\frac{\partial u}{\partial x} = \frac{\partial u'}{\partial x}; \quad \frac{\partial u}{\partial y} = \frac{\partial u'}{\partial y}; \quad \frac{\partial v}{\partial x} = \frac{\partial v'}{\partial x}; \quad \frac{\partial v}{\partial y} = \frac{\partial v'}{\partial y}$$

have the same order  $\Delta$ . After having evaluated terms appearing in equation (3-6),

we shall find:  $1 - \frac{u^2}{a^2} = 1 - \frac{u_{\infty}^2}{a^2} + \bar{\Delta} + \bar{\Delta}^2$ ;  $1 - \frac{v^2}{a^2} = 1 - \bar{\Delta}^2$ ;  $\frac{uv}{a^2} = \bar{\Delta}$ ,

where  $\bar{\Delta}$  and  $\bar{\Delta}^2$  are small magnitudes, having an order  $\Delta$  or  $\Delta^2$ .

An evaluation of the terms, appearing in equation (3-6), makes it possible to simplify this equation, if we disregard terms, whose order of smallness is higher than  $\Delta$ . After the indicated simplifications we obtain:

$$(1 - M_{\infty}^2) \frac{\partial u}{\partial x} + \frac{\partial v}{\partial y} = 0, \quad (3-18)$$

or for a potential flow

$$(1 - M_{\infty}^2) \frac{\partial^2 \Phi}{\partial x^2} + \frac{\partial^2 \Phi}{\partial y^2} = 0. \quad (3-19)$$

Thus, the discussed method, proposed by L. Prandtl, is founded on the assumption that the deviation of speed of disturbed flow from the speed of the undisturbed flow  $c_{\infty} = u_{\infty}$  is so small that the degrees of the indicated deviation higher than the first can be ignored. The equation for potential of speed (3-19) in distinction from (3-7) is a linear differential equation, therefore the method of small perturbations is brought about by the method of linearization. The considered method may give satisfactory results in calculating the flow around thin slightly curved airfoils located at small angles to direction of speed of undisturbed flow, and also in investigating flow in channels with a small curvature of the confining walls. We note that near the branching points of flow (critical points on surface of streamlined body) the basic assumption of method is not valid, since in these regions, flow is stagnated and magnitude in change of speed is commensurable with the speed at infinity.

Equation (3-19) at subsonic speeds can be reduced <sup>to</sup>/equation (3-8), which determines the potential of speed of flow of an incompressible fluid. Actually, we shall compare the considered subsonic flow of gas with flow of an incompressible fluid, by assuming that the speed and density of both flows at infinity will be

identical. Let us assume that the potentials of the speeds of flows being compared are associated by the relationship

$$\Phi = \sigma \Phi_H. \quad (3-20)$$

We shall designate coordinates of points of flow of an incompressible fluid  $x_H$  and  $y_H$ . We shall assume further that between coordinates  $x$ ,  $y$  and  $x_H$ ,  $y_H$  there exists a dependence of following form:  $\frac{y_H}{y} = \theta \frac{x_H}{x}$ .

For simplification it is possible to assume  $x = x_H$ , then

$$y_H = \theta y. \quad (3-21)$$

We now substitute relationships (3-20) and (3-21) into equation (3-19):

$$(1 - M_\infty^2) \frac{\partial^2 \Phi_H}{\partial x_H^2} \sigma + \theta^2 \frac{\partial^2 \Phi_H}{\partial y_H^2} \sigma = 0.$$

It follows from this that if we take

$$\frac{y_H}{y} = \theta = \sqrt{1 - M_\infty^2}, \quad (3-22)$$

then equation (3-19) will be transformed to the form:

$$\frac{\partial^2 \Phi_H}{\partial x_H^2} + \frac{\partial^2 \Phi_H}{\partial y_H^2} = 0. \quad (3-8a)$$

Equation (3-8a) in the new variables coincides with equation (3-8). By using the obtained relationships, there readily is found a connection between parameters of the two flows being compared.

Let us consider the flow around one and the same body by a flow of an incompressible fluid and a flow of gas. We shall designate with  $\alpha$  and  $\alpha_H$  the angles of slope of small sections of streamlines (Fig. 3-5). By bearing in mind that in accordance with basic assumption of method, these angles are small, we shall find:

$$\tan \alpha \approx \alpha \approx \frac{dy}{dx}; \quad \tan \alpha_H \approx \alpha_H \approx \frac{dy_H}{dx_H}. \quad (3-23)$$

In an ideal fluid one of the streamlines coincides with the contour of body.

At the boundary line of flow there must be fulfilled the condition

$$\tan \alpha = \tan \alpha_H,$$

or according to (3-23)

$$\frac{dy}{dx} = \frac{dy_H}{dx_H}.$$

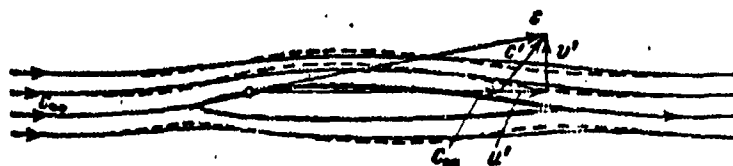


Fig. 3-5. Stream lines in a flow around an airfoil by flow of gas (dotted line) and an incompressible fluid.

In considering that the speeds at infinity are identical, we find that the indicated condition is observed, if  $v = v_H$  or  $\frac{\partial \Phi}{\partial y} = \frac{\partial \Phi_H}{\partial y_H}$ ; on the basis of relationships (3-20) and (3-22) we establish that in considered case  $\sigma = 1$ , or

$$\sigma = \frac{1}{\beta} = \frac{1}{\sqrt{1 - M_\infty^2}}.$$

The ratio of the longitudinal components of the speed in the two flows being compared is equal to:

$$\frac{u}{u_H} = \frac{\partial \Phi}{\partial x} \cdot \frac{\partial x}{\partial \Phi_H} = \sigma = \frac{1}{\sqrt{1 - M_\infty^2}}. \quad (3-24)$$

For comparison of distribution of pressures, it is sufficient to compare pressure gradients in both flows, since earlier, it was assumed that  $x = x_H$  and, consequently, ratio of the finite differences of pressures is equal to the ratio of the gradients

$$\frac{dp}{dx} \frac{dx}{dp_H} = \frac{\Delta p}{\Delta p_H}.$$

On the basis of the equation of momentum (2-1) the pressure gradients in compressible and incompressible fluid will be:

$$\frac{dp_H}{dx} = -\rho_H c_H \frac{dc_H}{dx}; \quad \frac{dp}{dx} = -\rho c \frac{dc}{dx};$$

then

$$\frac{\Delta p}{\Delta p_H} = \frac{\rho c}{\rho_H c_H} \frac{dc}{dc_H}.$$

or with a consideration of formula (3-14)

$$\frac{p}{p_H} = \frac{c}{c_H} \frac{dc}{dc_H} = \frac{c_\infty + c'}{c_\infty + c'_H} \frac{d(c_\infty + c')}{d(c_\infty + c'_H)},$$

where  $c'$ ,  $c'_H$ , as previously, are additional speeds (small magnitudes), caused by disturbance introduced by streamlined body.

After corresponding transformations finally we obtain:

$$\frac{p}{p_H} = \sigma = \frac{1}{\sqrt{1 - M_\infty^2}}. \quad (3-25)$$

From formulas (3-24) and (3-25) it follows that in the flow around one and

the same body by a gas the speed and difference between pressures is greater than in the case of a flow around by incompressible fluid.

This difference between flows of gas and an incompressible fluid can be explained by the dependence of the density of gas on the speed (Sec. 2-4). In Fig. 3-5 there are shown streamlines during flow around a body by a compressible and incompressible fluid with identical parameters and speed  $c_\infty$  of the nonperturbed flow.

Another simplification of the original equations, based also on the assumption on weak disturbance of a flow, was given by A. N. Sherstyuk, who had developed a simplified, but more accurate method of calculating the influence of compressibility.

For evaluating the influence of compressibility in a weakly disturbed two-dimensional flow with subcritical speeds ( $M_\infty < M_1$ ) we shall use the equation of continuity (1-12), after writing it out for a two-dimensional steady motion of a gas:

$$\frac{\partial}{\partial x} \left( \frac{\rho}{\rho_0} u \right) + \frac{\partial}{\partial y} \left( \frac{\rho}{\rho_0} v \right) = 0, \quad (3-26)$$

and also we use the condition of absence of vortices (3-1) for a two-dimensional flow.

In this case from formulas (1-6) we obtain:

$$\omega_z = \frac{1}{2} \left( \frac{\partial u}{\partial y} - \frac{\partial v}{\partial x} \right) = 0. \quad (3-1a)$$

We now consider the flow around a wing profile, shown in Fig. 3-5, by a two-dimensional gas flow.

By following A. N. Sherstyuk, we convert in the equations (3-26) and (3-1a) from speeds  $u, v$  of a flow of compressible fluid to speeds in the flow of an incompressible fluid  $u_H, v_H$  after assuming

$$c_H = c \left( \frac{\rho}{\rho_\infty} \right)^\theta. \quad (3-27)$$

Here the exponent  $\theta$  is determined on the basis of simplified associations corresponding to the assumption on a small disturbance of the flow;  $\rho$  is the density at a given point;  $\rho_\infty$  is the density of an undisturbed flow.

As has already been noted above, in accordance with method of small disturbances it is possible to assume:

$$u = c_\infty + u'; \quad \frac{u'}{c_\infty} \ll 1; \quad (3-28)$$

$$v = v'; \quad \frac{v'}{c_\infty} \ll 1. \quad (3-28a)$$

For an incompressible fluid, analogous simplifications are valid:

$$u_n = c_{\infty n} + u'_n; \frac{u'_n}{c_{\infty n}} \ll 1 \quad (3-29)$$

and

$$v_n = v'_n; \frac{v'_n}{c_{\infty n}} \ll 1.$$

In using these relationships, by substituting (3-28) into equations (3-27) and (3-5a) and by discarding terms of second order of smallness, there readily is obtained:

$$\left. \begin{aligned} \frac{1-M_{\infty}^2}{1-\theta M_{\infty}^2} \frac{\partial u_n}{\partial x} + \frac{\partial v_n}{\partial y} &= 0; \\ \frac{1}{1-\theta M_{\infty}^2} \frac{\partial u_n}{\partial y} - \frac{\partial v_n}{\partial x} &= 0. \end{aligned} \right\} \quad (3-30)$$

In order that equations (3-30) are reduced to equations of continuity and a lack of vortices for an incompressible fluid, it is sufficient to assume, as previously, a connection between coordinates in a compressible and an incompressible fluid (3-22):

$$x = x_n; \quad \frac{y_n}{y} = \sqrt{1-M_{\infty}^2}$$

and, besides, to assume:

$$\theta = \frac{1 - \sqrt{1-M_{\infty}^2}}{M_{\infty}^2}. \quad (3-31)$$

Actually, after substituting (3-22) and (3-31) into equations (3-30) we find:

$$\frac{\partial u_n}{\partial x} + \frac{\partial v_n}{\partial y_n} = 0; \quad \frac{\partial u_n}{\partial y_n} - \frac{\partial v_n}{\partial x} = 0. \quad (3-32)$$

It follows from this that the speeds  $u_H$  and  $v_H$  actually are local speeds in the flow of an incompressible fluid during flow around the same body at same angle of attack.

For determining speeds during flow around a body by a compressible fluid it is necessary at first to calculate field of speeds in the flow of the incompressible fluid with the same magnitude and in the same direction of speed of the undisturbed flow ( $c_{H\infty} = c_{\infty}$ ). Here, the local dimensionless speed  $\lambda$  at an arbitrary point of flow will be:

$$\lambda = \lambda_n \left( \frac{p_{\infty}}{p} \right)^{\frac{1}{k}} = \lambda_n \left[ \frac{1 - \frac{k-1}{k+1} \lambda_n^2}{1 - \frac{k-1}{k+1} \lambda_{\infty}^2} \right]^{-\frac{1}{k-1}}. \quad (3-27a)$$

The dependence  $\theta = f(\lambda_\infty)$  is presented in Fig. 3-6. From this graph it follows that coefficient  $\theta$  can be considered approximately constant at numbers  $\lambda_\infty < 0.7$  to 0.8. The sharp increase in  $\theta$  at large  $\lambda_\infty$  stipulates the nonvalidity of the considered method in this region.

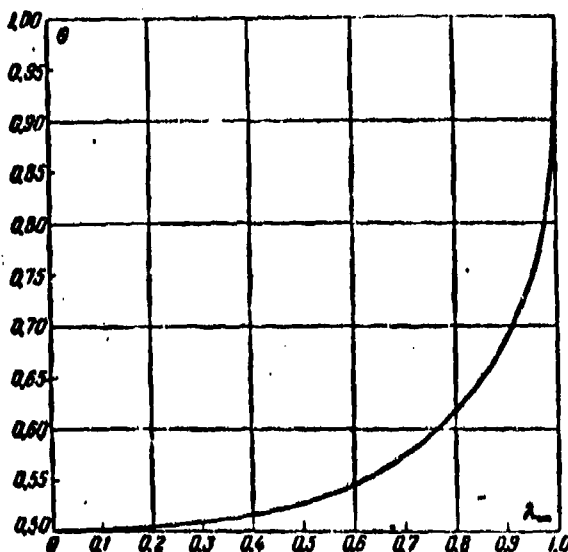


Fig. 3-6. The dependence of the exponent on the dimensionless speed  $\lambda_\infty$ .

The connection between speeds in a compressible and incompressible fluids by formula (3-27a) for different speeds of incident flow is shown in Fig. 3-7. With an increase in  $\lambda_\infty$ , the speed in the flow of a compressible fluid at a given point of a streamlined body intensively increases in comparison with the speed in an incompressible fluid.

We shall establish now a connection between pressure coefficients in incompressible and compressible fluids:

From the Bernoulli equation for an incompressible fluid

$$p_\infty + \rho \frac{c_\infty^2}{2} = \bar{p}_n + \rho \frac{c_n^2}{2}$$

we find the pressure coefficient in the following form:

$$\bar{p}_n = \frac{2(p_\infty - p_n)}{\rho c_\infty^2} = 1 - \left( \frac{c_n}{c_\infty} \right)^2 = 1 - \left( \frac{\lambda_n}{\lambda_\infty} \right)^2. \quad (3-33)$$

For a compressible fluid the pressure coefficient is determined by formula (3-16). In expressing  $\bar{p}$  in terms of the dimensionless speeds  $\lambda$  and  $\lambda_\infty$ , we find

(Table 2-1):

$$\bar{p} = \frac{k+1}{k\lambda_\infty^2} \left( 1 - \frac{k-1}{k+1} \lambda_\infty^2 \right) \left[ \left( \frac{1 - \frac{k-1}{k+1} \lambda_\infty^2}{1 - \frac{k-1}{k+1} \lambda_\infty^2} \right)^{\frac{k}{k-1}} - 1 \right]. \quad (3-34)$$

By using formulas (3-27a), (3-33) and (3-34), there can be obtained a connection between pressure coefficients in compressible and incompressible fluids  $\bar{p}$  and  $\bar{p}_H$ . This connection is presented in Fig. 3-8 and 3-9. Here, there is shown the dependence between  $\bar{p}$  and  $\bar{p}_H$  for different values of  $\lambda_\infty$ . Curves in Fig. 3-8

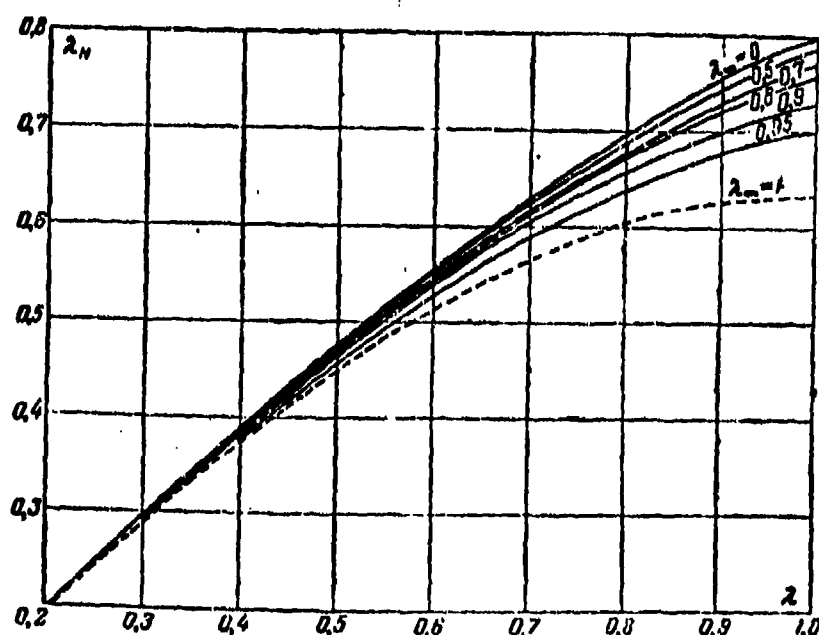


Fig. 3-7. The relationship between dimensionless speeds in compressible and incompressible fluids according to A. N. Sherstyuk.

are useful for converting positive values of  $\bar{p}_H$ . In this case the pressure at the considered points on surface of the body is higher than the pressure of the incident flow. The graph in Fig. 3-9 is used for converting negative values of  $\bar{p}_H$ . The dotted line, limiting the diagram  $p = f(\bar{p}_H)$  from above, corresponds to values  $\bar{p}$ , at which  $\lambda = 1$ . In other words, this line determines the critical values of dimensionless



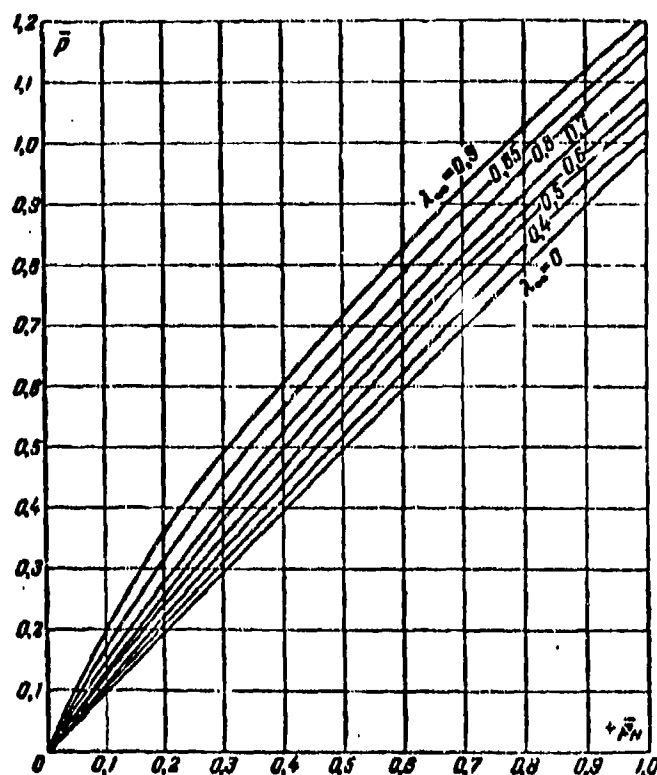


Fig. 3-8. Relationship between positive pressure coefficients in a compressible ( $\bar{p}$ ) and incompressible ( $\bar{p}_H$ ) fluid at different  $\lambda_\infty$ .

speed of incident flow  $M_\infty = M$  depending on  $\bar{p}$  or on  $\bar{p}_H$  and thereby limits that region of magnitudes  $M_\infty \leq M_* = f(\bar{p}_H)$  for that which there may be made a calculation of influence of compressibility by considered method.

In Fig. 3-10 there is presented a curve on the basis of data of a well-developed theory, establishing the dependence between minimum pressure coefficient at point of enclosing the body during flow around it by an incompressible fluid  $\bar{p}_{H \min}$  and the critical number  $\lambda$  of incident flow. The curve in Fig. 3-10 in coordinates  $(\bar{p}_{H \min}, \lambda)$  reproduces the boundary line  $\lambda = 1$  in Fig. 3-10.

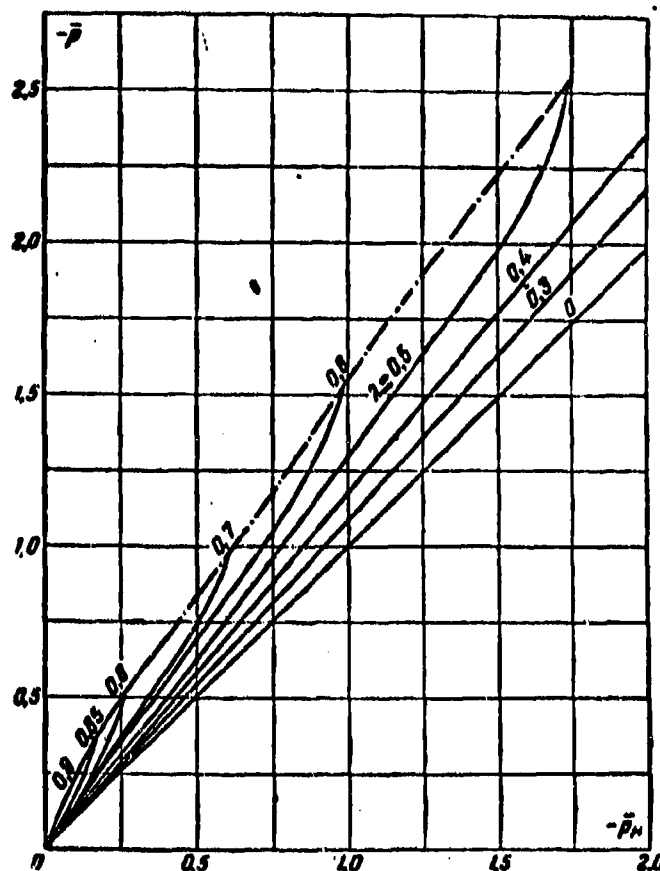


Fig. 3-9. Relationship between negative pressure coefficients for compressible  $\bar{p}$  and incompressible  $\bar{p}_H$  fluids at different  $\lambda_\infty$ .

The formula for calculating this curve can be obtained from (3-33) by means of (3-27a). Actually, from these relationships we have:

$$\bar{p}_n = 1 - \left( \frac{\lambda_n}{\lambda_\infty} \right)^2 = 1 - \left( \frac{\lambda}{\lambda_\infty} \right)^2 \left( \frac{p_\infty}{p} \right)^{\frac{2k}{k-1}}. \quad (3-35)$$

After replacing the ratio  $\frac{p_\infty}{p}$  (Table 2-1), we obtain:

$$\bar{p}_n = 1 - \left( \frac{\lambda}{\lambda_\infty} \right)^2 \left( \frac{1 + \frac{k-1}{k+1} \lambda_\infty^2}{1 - \frac{k-1}{k+1} \lambda^2} \right)^{\frac{2k}{k-1}}.$$

After assuming  $\lambda = 1$  and  $\lambda_\infty = \lambda_k$ , we find:

$$\bar{p}_{n, \lambda_k} = 1 - \frac{1}{\lambda_k^2} \left( \frac{\frac{2k}{k+1}}{1 - \frac{k-1}{k+1} \lambda_k^2} \right)^{\frac{2k}{k-1}}. \quad (3-36)$$

Thus, if there is known the distribution of pressures along contour of body at low speeds, when the influence of compressibility can be disregarded (distribution  $\bar{p}_H$ ), then, by using curves in Fig. 3-8 and 3-9, there readily can be found the

distribution of pressures at high subsonic speeds with a consideration of the compressibility. As can be seen from graphs, the influence of compressibility is seen in the fact that in the region of positive values  $\bar{p}$ , the pressure coefficients for compressible fluid will be larger, and in the region of negative values—lower, than for an incompressible fluid.

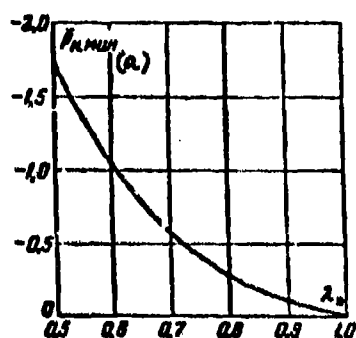


Fig. 3-10. The dependence between pressure coefficients  $\bar{p}_{H \min}$  and the dimensionless critical speed  $\lambda_*$ .  
KEY: (a)  $\bar{p}_{H \min}$ .

Consequently, owing to the compressibility, the absolute values of pressure coefficient increase. Here the regions of minimum pressures becomes steeper and they are extended (Fig. 3-4)\*. From a consideration of Fig. 3-4 it is evident that with an increase in  $M$  the area, included between the curves of pressures for upper and lower surfaces of the airfoil increase. Here,

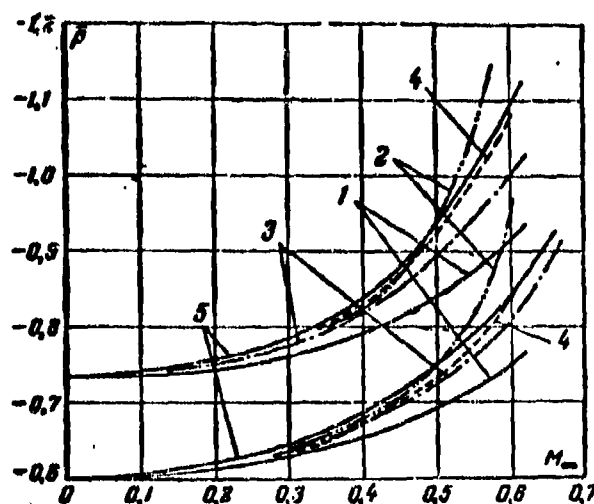


Fig. 3-11. Comparison of experimental and calculated pressure coefficients. 1--after Prandtl; 2--after S. A. Khristianovich; 3--according to formula of Karman-Tsien (3-37); 4--after A. N. Sherstyuk; 5--experiment

\*The corresponding graphs of change of pressure coefficients along airfoil and blade are presented in Chapters 5 and 8.

obviously, the lifting force, with an increase in  $M_\infty$ , increases.

All conclusions of the considered method are well verified by experimental data.

A comparison of experimental and calculated values of  $\bar{p}$  at point of upper surface of wing profile, located in flow at a small angle of incidence, is shown in Fig. 3-11. The airfoil has a relatively larger thickness and curvature.

For comparison in Fig. 3-11 there are presented also the computed curves, corresponding to formula (3-25) by L. Prandtl and on basis of more accurate formula of Karman-Tsien:

$$\bar{p} = \frac{\bar{p}_n}{\sqrt{1-M_\infty^2} + \frac{\bar{p}_n M_\infty^2}{2(1+\sqrt{1-M_\infty^2})}} \quad (3-37)$$

The coincidence of calculation by formulas (3-27a)---(3-34) and by formula (3-37) with the experiment is entirely satisfactory. Significantly poorer are the results obtained with the use of formula (3-25).

#### 3-4. Theorem of N. Ye. Zhukovskiy

The theory of the force effect of flow of an ideal fluid on streamlined bodies is based on the well-known theorem by N. Ye. Zhukovskiy. N. Ye. Zhukovskiy established the vortex origin of the force of interaction and found a simple connection between this force and the intensity of circulatory flow, generating during flow around a body. This problem was solved by N. Ye. Zhukovskiy in 1906.

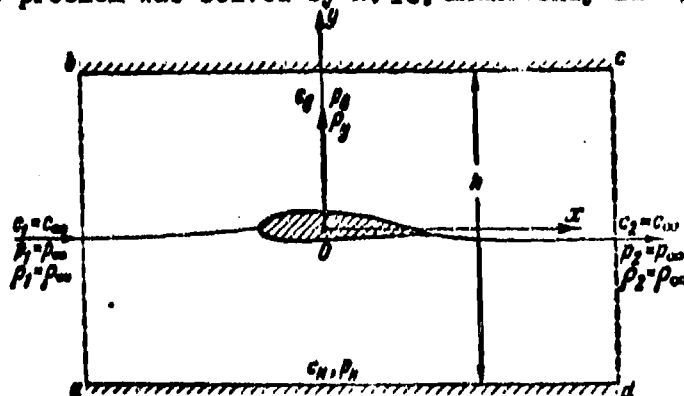


Fig. 3-12. Diagram for proof of theorem by N. Ye. Zhukovskiy.

For proof\* of theorem by Zhukovskiy we shall use the diagram, shown in Fig. 3-12. We shall place the wing airfoil in a two-dimensional flow between two impermeable flat control surfaces, oriented along flow and separated from each other at a distance  $h$ . The system of coordinates  $xOy$  will be placed so that the direction of  $x$ -axis coincides with the sense of the vector of speed of undisturbed flow  $c_\infty$ . At an infinite distance from the airfoil we shall draw sections  $ab$  and  $cd$ , normal to the direction of flow.

In assuming that the airfoil is flowed around continuously, and by applying theorem of the variation of momentum to the mass of fluid, included within volume  $abcd$ , we shall find that the force, directed against the flow and the so-called drag of profile, is determined by the formula \*\*

$$P_x = \int_{(h)} (p_1 - p_2) dy - \int_{(h)} \rho_1 c_1 (c_1 - c_2) dy.$$

Since the speeds and pressures in the sections  $ab$  and  $cd$  are identical, then

$$P_x = 0.$$

The presented result was obtained for the first time by L. Euler in 1745 and independently of him in a more general form by d'Alembert. It may seem paradoxical, since it contradicts experience. However, one should bear in mind that this result is obtained on the assumption of the absence of viscosity and separation of flow from the surface of a streamlined contour. In reality always to a certain degree, both of these factors take place.

In a practical respect there can be made the conclusion that one should make an effort to obtain those shapes of a contour, with which there would be assured a continuous flow around and the minimum effect of the forces of viscosity; in this

---

\*The below presented proof of the theorem of N. Ye. Zhukovskiy was proposed by G. F. Burago.

\*\*The considered forces we refer to a unit of length of wing.

case, obviously, resisting force will be the minimum.

We shall find now the magnitude of force  $P_y$ , normal to vector of speed  $c_\infty$ . This force is called the lifting force. After designating in terms of  $p_H$  pressure on the lower control surface and in terms of  $p_B$  the pressure on upper control surface, we obtain:

$$-P_y + \int_{-\infty}^{\infty} (p_H - p_B) dx = 0,$$

since the projection of the speeds along the impenetrable control surfaces onto the x-axis is equal to zero. Consequently,

$$P_y = \int_{-\infty}^{+\infty} (p_H - p_B) dx. \quad (3-38)$$

By increasing the distance  $h$  between the walls in a limiting case (at  $h \rightarrow \infty$ ) we will receive a flow around a body by infinite flow. Here the flow along the walls will be slightly perturbed. Speeds of such a flow, as is known, can be presented in the form of [formulas(3-28)]:

$$\left. \begin{aligned} c_H &= c_\infty + c'_H; \\ c_B &= c_\infty + c'_B. \end{aligned} \right\} \quad (3-28b)$$

where  $c'_H$ ,  $c'_B$ , are small additional speeds along the walls, caused by influence of streamlined body.

Pressure at an arbitrary point of a perturbed flow is associated with pressure at infinity by Bernoulli's equation:

$$\frac{P}{\rho} = \frac{P_\infty}{\rho_\infty} + \frac{k-1}{2k} (c_\infty^2 - c^2),$$

which under the usual assumption (a slightly disturbed flow) on the basis of (3-28b)

will be transformed to the form:  $\frac{P}{\rho} = \frac{P_\infty}{\rho_\infty} - \frac{k-1}{k} c_\infty c'$ .

Hence, by bearing in mind that  $\frac{P}{\rho^k} = \frac{P_\infty}{\rho_\infty^k}$  and  $\frac{\rho_\infty}{\rho} = \frac{k}{a_\infty^2}$ , after simple transformations we find:

$$\frac{P}{P_\infty} \approx 1 - k M_\infty^2 \frac{c'}{c_\infty}, \quad (3-39)$$

or

$$P = P_\infty - \rho_\infty c_\infty c'. \quad (3-39a)$$

Equation (3-39) or (3-39a) is valid for a linearized flow and is called the Bernoulli linearized equation. Equation (3-39a) can be written out for sections

on the upper and lower control surfaces:

$$p_u = p_\infty - \rho_\infty c_\infty c'_u$$

and

$$p_s = p_\infty - \rho_\infty c_\infty c'_s$$

By substituting  $p_H$  and  $p_B$  into equation (3-38), we find:

$$P_y = \rho_\infty c_\infty \int_{-\infty}^{+\infty} (c'_s - c'_u) dx.$$

It is readily seen that the integral  $\int_{-\infty}^{+\infty} (c'_s - c'_u) dx$  it is possible to express in terms of circulation of speed over the closed contour (Fig. 3-12).

Actually,  $\Gamma_{abed} = \Gamma_{ab} + \Gamma_{bc} + \Gamma_{cd} + \Gamma_{da};$

since  $\Gamma_{bc} = \int_{-\infty}^{+\infty} (c_\infty + c'_u) dx; \Gamma_{da} = - \int_{-\infty}^{+\infty} (c_\infty + c'_s) dx; \Gamma_{ab} = - \Gamma_{cd},$

then

$$\Gamma_{abed} = \int_{-\infty}^{+\infty} (c'_s - c'_u) dx.$$

Consequently,

$$P_y = \rho_\infty \Gamma c_\infty.$$

(3-40)

Formula (3-40) expresses the theorem of N. Ye. Zhukovskiy, which is a fundamental theorem in aerodynamics. Theorem of Zhukovskiy can be formulated as: during flow around a body by a planar-parallel infinite flow of an ideal compressible fluid onto a body of unit span there acts a force, equal to the product of the circulation of speed  $\Gamma$  by the speed  $c_\infty$  and by the density  $\rho_\infty$  of the undisturbed flow. The direction of this force is normal to the direction of the speed of undisturbed flow  $c_\infty$ . Here as it follows from the conclusion, if the circulation integral calculated clockwise along the outline, proves to be positive, then also  $P_y$  will be positive. The lifting power  $P_y$  frequent is called the Zhukovskiy force. For determining  $P_y$  it is necessary to know magnitude of circulation integral, which is calculated on the basis of the Zhukovskiy-Chaplygin (Sec. 1-2) postulate.

### 3-5. The Two-Dimensional Subsonic Potential Flow of a Gas in Curvilinear Channels

In considering a two-dimensional or axially symmetric potential motion of a

gas along curvilinear trajectories, we shall select as the independent variables, the distance along the streamlines (S) and along equipotential lines (n) (Fig. 3-13).

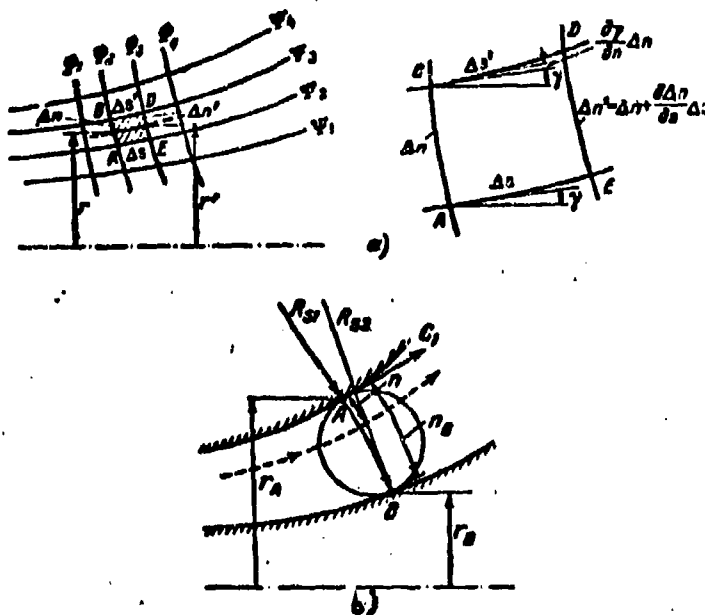


Fig. 3-13. Diagram for deriving equations of motion in a curvilinear channel.

We shall transform the equations of continuity (1-14) and of lack of vortices [third equation of system (3-1)] in the new coordinates. For an elementary volume, limited in plane of the figure by sectors of the streamlines  $\Delta S$  and  $\Delta S'$  and the equipotential lines  $\Delta n$  and  $\Delta n'$ , the condition of continuity will be written in such a form:

$$\frac{\partial}{\partial S} (\rho c r \Delta n) = 0,$$

or

$$\frac{\partial \ln(\rho c r)}{\partial S} + \frac{1}{\Delta n} \cdot \frac{\partial \Delta n}{\partial S} = 0,$$

where  $r$  is the radius of center of gravity of section  $\Delta n$  (Fig. 3-13,a). Further,

since

$$\frac{\partial \Delta n}{\partial S} = \frac{\partial \gamma}{\partial n} \Delta n,$$

( $\gamma$  is angle of the streamline's slope), we shall present the equation of continuity in such a form:

$$\frac{\partial \ln(\rho c r)}{\partial S} + \frac{\partial \gamma}{\partial n} = 0.$$

(3-41)



The condition of absence of vortices will be (Fig. 3-13):

$$\frac{\partial}{\partial n}(c\Delta S) = 0.$$

After differentiation we shall obtain:

$$\frac{\partial \ln c}{\partial n} + \frac{1}{\Delta S} \frac{\partial \Delta S}{\partial n} = 0.$$

Since (Fig. 3-13,a)

$$\frac{\partial \Delta S}{\partial n} = -\frac{\partial \gamma}{\partial S} \Delta S,$$

then finally we obtain:

$$\frac{\partial \ln c}{\partial n} - \frac{\partial \gamma}{\partial S} = 0. \quad (3-42)$$

Equations (3-41) and (3-42) are valid for axisymmetrical flows of a compressible fluid. For two-dimensional problems these equations are simplified and are reduced to the following form:

$$\left. \begin{aligned} \frac{\partial \ln(\rho c)}{\partial S} + \frac{\partial \gamma}{\partial n} &= 0; \\ \frac{\partial \ln c}{\partial n} - \frac{\partial \gamma}{\partial S} &= 0. \end{aligned} \right\} \quad (3-41a)$$

The obtained equations make it possible by the most simple methods to calculate flow of gas in a two-dimensional or axially symmetric curvilinear channels\*. For this purpose it is necessary to find the distribution of the speeds along equipotential lines in the channel.

For an approximate determination of the length of equipotential lines in channel there are inscribed circles (Fig. 3-13,b), tangent to walls at points A and B. Through points of tangency there is drawn an arc of the circle, normal to walls of channel, which approximately gives the length of an equipotential line.

Such a method of determining the lines  $\phi = \text{const}$  is valid only when their curvature is small.

The equations of continuity (3-41) and (3-41a) show character of variation of angle of slope of speed vector in cross-section of channel, and the equation for the absence of vortices makes it possible to formulate the condition, which the diagram of speeds must satisfy on any streamline, including also on walls of channel:

$$\frac{1}{c} \cdot \frac{\partial c}{\partial n} = \frac{\partial \gamma}{\partial S} = K.$$

\*The calculation under discussion of flow in channels was worked out by S. Samoylovich and A. N. Sherstyuk.

For finding of the distribution of speeds along the lines  $\Phi = \text{const}$  we shall use equation (3-42), after replacing

$$\frac{\partial \gamma}{\partial S} = -\frac{1}{R_s}.$$

where  $\frac{1}{R_s}$  is the curvature of streamline.

Then

$$\frac{\partial c}{\partial n} = -\frac{c}{R_s}.$$

We multiply both sides of this expression by the trinomial  $R_{s1} + n + Kn^2$  and then add to it the magnitude  $c \frac{\partial}{\partial n} (R_{s1} + n + Kn^2)$ .

After simple transformations we find:

$$\frac{\partial}{\partial n} [c(R_{s1} + n + Kn^2)] = -c \left( \frac{R_{s1} + n + Kn^2}{R_s} - 1 - 2Kn \right).$$

The left-hand side of this expression vanishes at  $n = 0$ ; the constant  $k$  can be selected in such a manner that the derivative  $\frac{\partial}{\partial n} [c(R_{s1} + n + Kn^2)]$  is equal to zero also at  $R_{s1} = R_{s2}$  (Fig. 3-13,b). In this case it differs little from zero and at all points of the lines  $\Phi = \text{const}$ . This condition means that law of variation of speeds along line  $\Phi = \text{const}$  will be:

$$c(R_{s1} + n + Kn^2) = \text{const},$$

or

$$\frac{c}{c_1} = \frac{1}{1 + \bar{n} - K_1 \bar{n}^2}, \quad (3-43)$$

where

$$K_1 = \frac{x-1}{2\bar{R}_{s2} - \bar{n}_B}; \quad \bar{n} = \frac{n}{R_{s1}}; \quad \bar{R}_{s2} = \frac{R_{s2}}{R_{s1}}; \quad x = \frac{\bar{R}_{s2} - 1}{\bar{n}_B}.$$

The variation of speeds along boundaries of channel is established by means of formula (3-43), valid also for a compressible fluid. The condition of constancy of flow through the channel serves as the original condition.

At small numbers  $M < 0.4$ , when the influence of compressibility can be ignored, volumetric flow of fluid through a plane channel will be:

$$Q = \int_{-n_B}^{n_B} c dn.$$

STOP HERE

STOP HERE

By means of formula (3-43), after integration we obtain:

$$\delta = \frac{Q}{c_1 \bar{n}_B} = \frac{c_m}{c_1} = \frac{1}{\bar{n}_B} \frac{1}{\sqrt{1+4K_1}} \ln \frac{1-2K_1 \bar{n}_B / (1-\sqrt{1+4K_1})}{1-2K_1 \bar{n}_B / (1+\sqrt{1+4K_1})} \quad (3-44)$$

Here  $c_m$  is the average speed in section of channel;  $c_1$  is the speed at a point on a convex wall.

For convenience in calculating in Fig. 3-14 there is presented a graph of the relationship  $\delta = f(\bar{n}_B, x)$ , expressed by formula (3-44).

In the case of an axially symmetric channel the volumetric flow of a fluid is determined by the formula  $Q = 2\pi \int_0^{\bar{n}_B} R_s c dn$ .

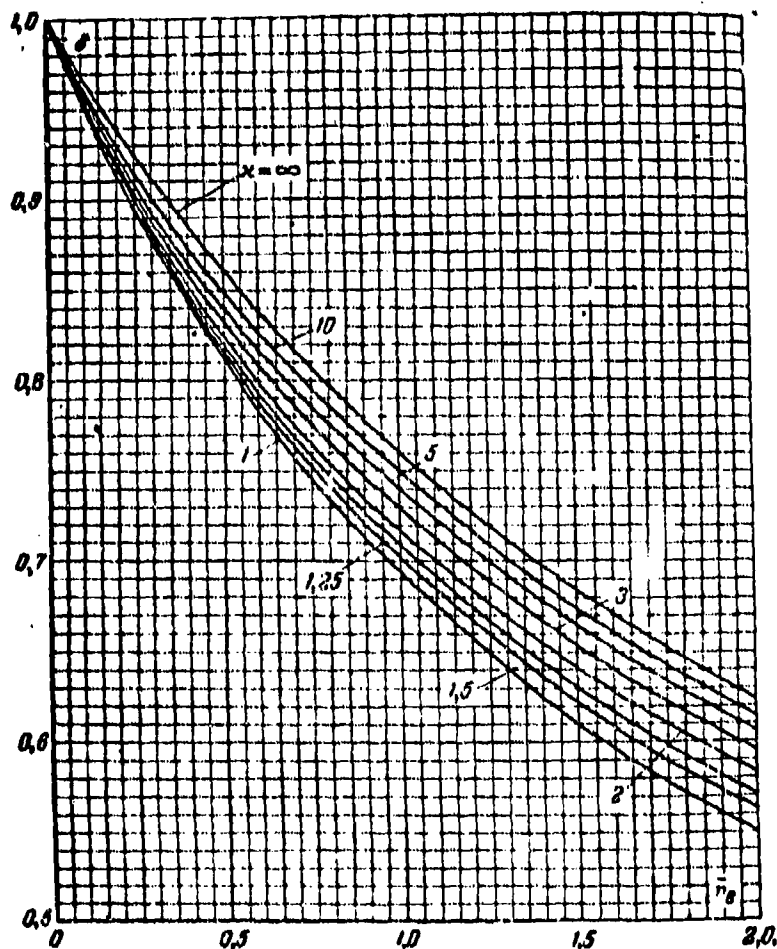


Fig. 3-14. Graph of dependence  $\delta$  on  $\bar{n}_B$  and  $x$ .

In simplifying the solution of problem, it is possible to assume a linear connection between  $R_s$  and  $\bar{n}$ :  $R_s \approx R_{s1} + \frac{n}{n_B}(R_{s2} - R_{s1})$ .

By analogy with formula (3-44) there can be obtained\*:

$$\begin{aligned} \delta_s &= \frac{Q}{2\pi R_{s1} c n_B} = \delta - K_s Z. \\ K_s &= 1 - \frac{R_{s2}}{R_{s1}}; Z = \frac{1}{2K_s n_B} \left( \bar{n} - \frac{1}{n_B} \ln \frac{c_1}{c_s} \right). \end{aligned} \quad (3-45)$$

The calculation of axially symmetric channels is considerably simplified by using the graphs, presented in Fig. 3-15.

The above-presented formulas (3-44) and (3-45) are valid for small M numbers (incompressible fluid). However, law of distribution of speeds, expressed by formula (3-43), can also be assumed for a compressible liquid in the same form:

$$\frac{\lambda}{\lambda_1} = \frac{1}{1 + \bar{n} - K_s \bar{n}^2}. \quad (3-43a)$$

The weak influence of compressibility on the diagram of speeds in cross-section is explained by the fact that the condition of irrotational motion, used for obtaining (3-43), does not contain density.

A marked change of curvature of streamlines and of the distribution law of speeds in a cross-section is noted only at high dimensionless speeds and significant gradients of speeds along the channel.

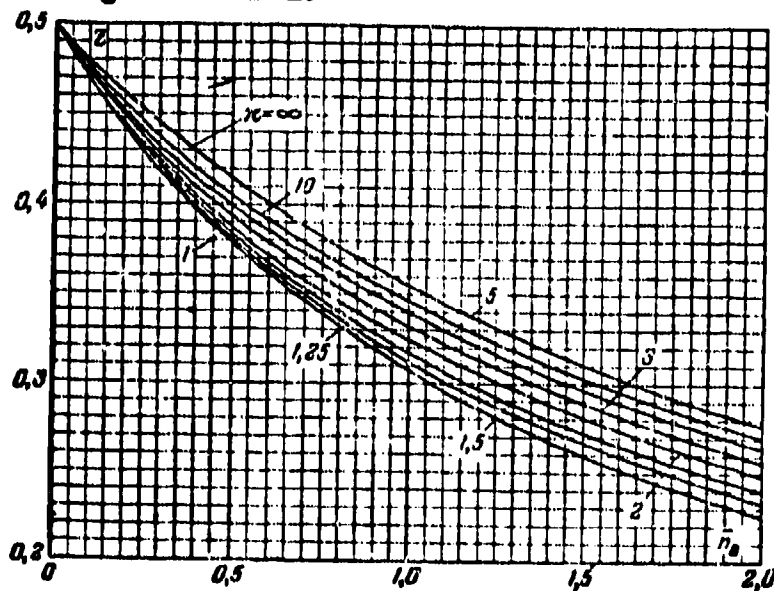


Fig. 3-15. Graph of dependence  $\bar{z}$  on  $\bar{n}_B$  and  $x$ .

\* Formulas (3-44) and (3-45) are valid if the internal and external walls of a channel have a curvature of one sign.

In a wide range of subsonic speeds ( $M \leq M_*$ ) the calculation of the channel with a consideration of the compressibility can be made by means of introducing the average density in the given section. On the basis of method of small disturbances by A. N. Sherstyuk it has been shown that the average reduced flow rate in a section, is equal to:

$$q_m = \frac{G}{G_*}$$

where  $G$  is the mass flow rate and  $G_*$  the critical flow rate of a gas through a given section, associated with the average speed and density by the relationship

$$q_m = \frac{\rho_m}{\rho_*} \lambda_m$$

( $\rho_m, \lambda_m$  are the average density and dimensionless speed for the section). The average density  $\rho_m = q_m \rho_* \frac{1}{\lambda_m}$  readily can be determined by  $q_m$  by means of tables of gas-dynamic functions. Speeds with a consideration of the compressibility can be determined by the simple formula:  $\frac{\lambda}{\lambda_m} = \frac{c}{c_m}$  ( $c$  and  $c_m$  are speeds, determined without a calculation of the compressibility).

The above-shown method is useful for calculating different channels, for example, channels of turbomachine cascades.\*

### 3-6. Two-Dimensional Supersonic Flow

Let us turn to the study of basic properties of a two-dimensional supersonic flow. For this purpose let us consider simplest case of a steady uniform supersonic flow moving with a constant speed along the wall BA (Fig. 3-16). Let us assume that along the normal to the wall BA the speeds also do not change. At point A of this wall there appears disturbance of the flow, caused by a change in direction of wall by a small angle. Owing to smallness of the angle  $d\delta$  disturbance of point A, expressed in the variation of parameters of flow (the pressure and temperature decrease, the speed increases), may be considered weak.

It is readily seen that in a supersonic flow the disturbance can be propagated

---

\*See Sec. 8-2.

only in the direction of flow, since the speed of the motion of particles of gas is higher than the speed of propagation of weak disturbances ( $c_1 > a_1$ ). The disturbance, appearing at the point A, is carried along the flow, where a certain line Am serves as the boundary between two different regions of flow: to the left of line Am there is located the undisturbed region of flow, but to the right of this line the flow is disturbed by a change in direction at point A. Thus, the line Am is the boundary, separating undisturbed part of flow from disturbed. Since in considered case it is a matter of a weak disturbance, then this line is called boundary of weak or sonic disturbances, a weak wave, a characteristic or a Mach line. Here we have in mind that any weak disturbances of the flow are propagated with the speed of sound (Chapter 2).

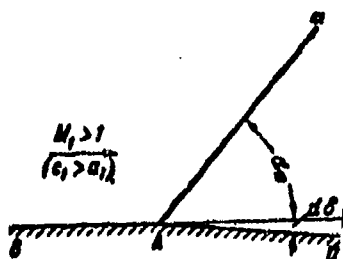


Fig. 3-16. Flow round corner point by supersonic flow.

Mechanism of the propagation of weak disturbances can be analyzed more specifically, by considering another continuous effective source of the disturbance in a two-dimensional infinite supersonic flow.

Such a source of weak disturbances might be a fine-pointed body of infinite span

with very small aperture angle of front wedge (Fig. 3-17). The small variations of parameters of flow created by the body are propagated with the speed of sound  $a_1$ , while the speed of flow incident to body is  $c_1 > a_1$ .

The waves of disturbance are circular infinite cylinders, whose radius is readily determined as  $a_1 \Delta t$ , where  $\Delta t$  is the time interval, calculated from moment of onset of considered wave at point A. During the same time interval the particles traverse a path, equal to  $c_1 \Delta t$ . Consequently, the center of observed wave is transferred to a new position  $A_1$ . With a continuous flow around body at point A in succession there will form an infinite number of waves, moving in the direction of flow. Since the speed of the flow is  $c_1 > a_1$ , then the later-formed waves will

lag from the preceding, where the entire family of waves has two common tangents.  $Am$  and  $Am_1$ , proceeding from point  $A$ .

This is readily verified by finding the relationship between radii of wave, and the displacement of its center:  $\frac{r_1}{AA_1} = \frac{r_2}{AA_2} = \dots = \frac{a_1 \Delta t}{c_1 \Delta t} = \frac{1}{M} = \sin \alpha_m$ ,

where  $\alpha_m$  is the angle of slope of the tangent to sense of speed vector  $c_1$ .

The appearance of lines  $Am$ ,  $Am_1$  can be assumed as the result of the continuous weak (sonic) disturbances of the flow; they stationarily are associated with source of disturbances (tip of body).

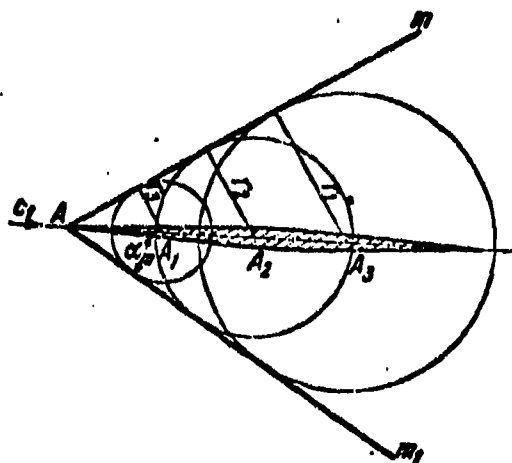


Fig. 3-17. Flow around of thin-pointed body by supersonic flow.

With the intersection of such a wave, the particle of gas experiences, a change of all parameters: pressure, density, temperature and speed. However, in connection with the smallness of the disturbance these changes are infinitesimally small. In the considered case of flow around a sharp tip of body there occurs an insignificant compression of the flow and the pressure behind the waves  $Am$ ,  $Am_1$  increases by a small magnitude  $dp$ , and the speed correspondingly decreases by  $dc$ . Therefore, the waves  $Am$ ,  $Am_1$  are called weak compression waves.

In those cases, when transition through wave is accompanied by an expansion of the flow and, consequently, by a decrease in pressure by  $dp$ , the wave is called a weak wave of rarefaction. Sonic waves of rarefaction develop, for example,

during flow around an external obtuse angle (Fig. 3-16) by a supersonic flow.

From a consideration of flow around a thin wedge, it may be concluded, that in a supersonic flow, there will be formed characteristics of two families, located at an angle  $\pm \alpha_m$  to the vector of speed at the given point.

From the formula 
$$\alpha_m = \pm \arcsin \frac{1}{M}$$

it follows that in accelerated supersonic flow angles of the characteristics in direction of flow decrease, but in diffuser flow they grow. Hence, it is possible

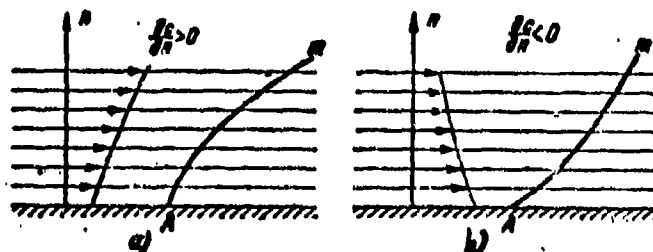


Fig. 3-18. Weak waves in two-dimensional flow with a nonuniform field of speed.

also to conclude that with a change of speeds in transverse direction to the flow the characteristics acquire a curvilinear form.

Thus, if along the normal to streamlines the speeds increase the characteristic by convexity is turned towards undisturbed region of the flow (Fig. 3-18). If, conversely, the speeds in the direction, normal to wall, decrease, then characteristic by convexity is turned toward the disturbed region of flow. With a complex nonuniform distribution of the speeds in flow the characteristics may acquire also a more complex form.

Let us turn now to the study of finite disturbances of a supersonic flow. Here we shall consider at first only those disturbances which cause a continuous variation of the parameters of flow.

Let us assume that along the wall BA a uniform supersonic flow moves (Fig. 3-19). Beyond point A gas enters into a region of lower pressure ( $p_2 < p_1$ ). Here, the flow is deflected from the direction of wall BA, by being turned at a certain angle with respect to point A towards the lower pressure. The disturbance, created by point A, is propagated in supersonic flow along the characteristics



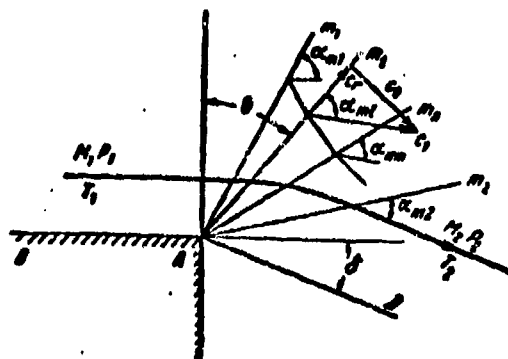


Fig. 3-19. Diagram for forming a wave of rarefaction during flow around angle by supersonic flow.

$Am_1, Am_2, \dots, Am_n$ , forming a stationary wave of rarefaction  $m_1 Am_2$ . The disturbance of the supersonic flow begins in characteristic  $Am_1$ ; slope angle of wave  $Am_1$  to direction of undisturbed flow is determined by the formula  $\alpha_{m_1} = \arcsin \frac{1}{M_1}$ . The disturbance is concluded on line  $Am_2$ ; position of this characteristic can be determined if the speed of disturbed flow is known:

$$\alpha_{m_2} = \arcsin \frac{1}{M_2}.$$

Between the characteristics  $Am_1$  and  $Am_2$  there occurs an expansion of the gas from  $p_1$  to  $p_2$ . With the intersection of the wave of rarefaction, the streamlines correspondingly are distorted, since during a flow around point A the flow expands. The speed of flow increases, and temperature and density decrease. The characteristics  $Am_1, Am_2, \dots, Am_n$ , et cetera, correspond to intermediate points of the streamline within the limits of the wave of rarefaction; along each characteristic the parameters of flow remain constant. The angles between characteristics and tangents to streamlines in the direction of flow decrease:

$$\alpha_{m_1} > \alpha_{m_2} > \alpha_{m_n}.$$

In considering the gradual transition to parameters of the disturbed flow  $M_2$  and  $p_2$  with infinitesimally small intervals  $\Delta M$  and  $\Delta p$  within the limits between  $Am_1$  and  $Am_2$ , it is possible to construct an infinite number of characteristics, comprising a stationary wave of rarefaction of finite intensity. Intensity of wave  $m_1 Am_2$  varies with a change in pressure  $p_2$ . Here, if the parameters of an

undisturbed flow remain constant, characteristic  $Am_1$  maintains its former position, and the characteristic  $Am_2$  is transferred depending on the change in  $p_2$ . With an increase of  $p_2$ , the characteristic  $Am_2$  approaches  $Am_1$  and at  $p_2 = p_1$  both characteristics coincide (weak disturbance of flow).

We shall establish the dependence between parameters of flow at the boundaries of wave of rarefaction. For this purpose we shall use fundamental equations — of a two-dimensional flow — Euler equations. By bearing in mind that parameters of flow along characteristics do not change, the indicated equations are used in cylindrical coordinates.

For a two-dimensional steady motion of gas, equations (1-17a) and (1-14) in coordinates  $(r, \theta)$  acquire the form\*: 
$$\left. \begin{aligned} c_r \frac{\partial c_r}{\partial r} + \frac{c_\theta}{r} \frac{\partial c_r}{\partial \theta} - \frac{c_\theta^2}{r} &= -\frac{1}{\rho} \frac{\partial p}{\partial r}; \\ c_r \frac{\partial c_\theta}{\partial r} + \frac{c_\theta}{r} \frac{\partial c_\theta}{\partial \theta} + \frac{c_r c_\theta}{r} &= -\frac{1}{\rho} \frac{\partial p}{r \partial \theta}; \\ \frac{\partial(\rho c_r)}{\partial r} + \frac{\partial(\rho c_\theta)}{\partial \theta} &= 0. \end{aligned} \right\} \quad (3-46)$$

In considering the simplest case, when the undisturbed flow before the wave of rarefaction has a uniform field of speeds and characteristics, which form the wave of rarefaction, are rectilinear, it is possible to assume that the parameters of flow maintain constant values along any radius within limits of a wave.

Mathematically this condition can be written out as:

$$\frac{\partial p}{\partial r} = \frac{\partial c}{\partial r} = \frac{\partial \rho}{\partial r} = 0.$$

Then, in the equations (3-46) it is possible to convert to a total derivative.

After simplifications we obtain:

$$c_\theta = \frac{dc_r}{d\theta}; \quad (3-46a)$$

$$c_\theta \left( c_r + \frac{dc_\theta}{d\theta} \right) = -\frac{1}{\rho} \cdot \frac{dp}{d\theta}; \quad (3-46b)$$

$$\rho \left( c_r + \frac{dc_\theta}{d\theta} \right) + c_\theta \frac{d\rho}{d\theta} = 0. \quad (3-46c)$$

Equation (3-46c) expresses in polar coordinates the condition of a two-dimensional irrotational flow.

Actually, from the third equation (1-19), in assuming  $\omega_z = 0$ , there readily

\* The influence of body forces is ignored.

is obtained formula (3-46c)

Hence, we arrive at the conclusion that during a flow around the angle point A the flow remains potential and irrotational, and consequently, also the entropy of flow, intersecting the wave of rarefaction, is kept constant.

The common solution of equations (3-46b) and (3-46c) makes it possible to establish still one important property of supersonic flow.

We shall substitute in (3-46b) the derivative of the density:

$$\frac{d\rho}{d\theta} = \left(\frac{d\rho}{dp}\right) \frac{dp}{d\theta} = 1/a^2 \frac{dp}{d\theta}.$$

By discarding from (3-46b) and (3-46c)  $\frac{dp}{d\theta}$ , we obtain:

$$c_\theta = a.$$

The latter means that the deflection of flow in a wave of rarefaction occurs in such a manner that the component of speed, normal to radius vector, is equal to the speed of sound at the given point.

This conclusion may be obtained also from an analysis of picture of propagation of weak disturbances in a supersonic flow (Fig. 3-19). It follows from this that the usual assumption about constancy of parameters of flow along a radius makes it possible to consider the generation of a wave of rarefaction of finite intensity as a result of a progressive expansion of flow in the system of an infinite set of weak (sonic) waves of rarefaction.

We shall establish now how the speed and pressure along streamline intersecting a wave of rarefaction vary. For this purpose we shall use the equation of energy:

$$a^2 = \frac{k+1}{2} a_0^2 - \frac{k-1}{2} c^2;$$

by bearing in mind that

$$c^2 = c_r^2 + c_\theta^2; \quad c_\theta = a,$$

we obtain:

$$\frac{k+1}{2} c_0^2 = \frac{k+1}{2} a_0^2 - \frac{k-1}{2} c_r^2.$$

We substitute in this equation  $c_0 = \frac{dc_r}{d\theta}$ ; then we shall obtain a differential equation for determining radial component  $c_r$ :

$$\frac{dc_r}{\sqrt{\frac{k+1}{k-1}a^2 - c^2}} = \sqrt{\frac{k-1}{k+1}} d\theta.$$

By integrating the last expression, we arrive at the equation

$$\arcsin m \frac{c_r}{a_0} = m(\theta + K),$$

where

$$m = \sqrt{\frac{k-1}{k+1}}.$$

The constant of integration  $K$  is determined from the boundary condition.

We assume that at  $\theta = 0$  radial component of the speed  $c_r = 0$ ; this means that we examine the expansion of an undisturbed flow, having a speed, equal to the speed of sound ( $\lambda_1 = 1$ ); hence  $K = 0$ .

Finally, we obtain:

$$\lambda_r = \frac{c_r}{a_0} = \frac{1}{m} \sin(m\theta).$$

The component of speed  $c_\theta$  is determined by the equation

$$\lambda_\theta = \frac{c_\theta}{a_0} = \frac{d\lambda_r}{d\theta} = \cos(m\theta).$$

The dimensionless speed  $\lambda$  at an arbitrary point of wave of rarefaction

$$\lambda^2 = \lambda_r^2 + \lambda_\theta^2 = \frac{1}{m^2} \sin^2(m\theta) + \cos^2(m\theta),$$

or

$$\lambda^2 = 1 + \frac{2}{k-1} \sin^2(m\theta).$$

(3-47)

For determining the pressure at the same point, we shall use the equation

$$\lambda^2 = \frac{1}{m^2} \left[ 1 - \left( \frac{p}{p_0} \right)^{\frac{k-1}{k}} \right].$$

Hence, after substituting  $\lambda$  from (3-47) we obtain:

$$\frac{p}{p_0} = \left[ \frac{1 + \cos(2m\theta)}{k+1} \right]^{\frac{k}{k-1}}. \quad (3-48)$$

In using formula (3-47) or (3-48) and by bearing in mind, that in a wave of rarefaction the process is isentropic, it is possible also to calculate the change in density and temperature in a wave of rarefaction:  $\frac{\rho}{\rho_0}$  and  $\frac{T}{T_0}$ .

Formula (3-47) shows that the limiting value of angle  $\theta$ :

$$\sin^2(m\theta_{\max}) = 1,$$

or

$$\theta_{\max} = \frac{\pi}{2} \sqrt{\frac{k+1}{k-1}} = \frac{\pi}{2} \frac{1}{m}. \quad (3-49)$$

corresponds to the maximum speed  $\lambda_{\max} = \sqrt{\frac{k+1}{k-1}} = \frac{1}{m}$ .

In this case during the flow around an angle, the flow acquires a pressure  $P_2 = 0$  (escape into vacuum). We note that in such a regime, the direction of boundary characteristic  $A_m$  coincides with direction of streamline of the deflected flow, since

$$\alpha_m = \arcsin \frac{1}{\lambda_1} = \arcsin \frac{a_1}{c_1} = 0.$$

It must be emphasized that the considered regime of flow ( $\lambda = \lambda_{m \pm A}$ ) is a theoretical, limiting regime.

The second limiting regime of flow round the angle point corresponds to the value of speed  $\lambda = 1$ . Here  $\theta = 0$  (sonic flow with infinitesimal change of pressure at point A).

Equations (3-47) and (3-48) are applicable also for other supersonic values of the speed before a wave of rarefaction, larger than unity, but here initial angle of reading is determined by the formula

$$\theta_1 = \frac{1}{m} \arcsin \sqrt{\frac{k-1}{2} (\lambda_1^2 - 1)}$$

and line of reading is placed not perpendicularly to the direction of undisturbed flow, but at an angle  $\theta_1 + \alpha_m$  to it.

Of great practical interest is the possibility of determining the shape of streamline within the limits of a wave of rarefaction. For the solution of this problem it is possible to use the differential equation of streamlines of a two-dimensional flow in polar coordinates

$$\frac{dr}{c_r} = \frac{r d\theta}{c_\theta}.$$

In using formula for  $\lambda$ , and  $\lambda_1$ , we obtain:

$$d \ln r = \frac{1}{m} \tan \alpha(m\theta) d\theta.$$

After integration we obtain the expression

$$r = r_0 [\cos(m\theta)]^{-\sqrt{\frac{k-1}{k+1}}}. \quad (3-50)$$

where  $r_0$  is the radius vector of streamline at  $\theta = 0$ .

From equation (3-50) it follows that all the streamlines within the limits of the wave of rarefaction are a system of similar curves; the distance between neighboring streamlines in accordance with basic properties of supersonic flow increases in the direction of the flow.

As has already been indicated, the flow around an angle point by a supersonic flow is potential. Components of the speed  $c_r$ ,  $c_\theta$ , can be expressed in terms of the potential of speed:

$$c_r = \frac{\partial \Phi}{\partial r}; \quad c_\theta = \frac{\partial \Phi}{r \partial \theta}.$$

Hence after substituting  $c_r$  or  $c_\theta$  and integrating we obtain:

$$\Phi = a_m \frac{1}{m} r \sin(m\theta). \quad (3-51)$$

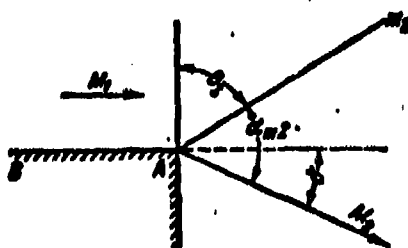


Fig. 3-20. Diagram for determining angle of deflection in wave of rarefaction.

We shall dwell in the conclusion on the method of calculating the angle of deflection of a flow  $\delta$ . From Fig. 3-20 it follows that with a known position of boundary characteristic  $Am_2$  the angular deflection is determined by the formula

$$\delta = \theta_1 + \alpha_{m_2} - \frac{\pi}{2}. \quad (3-52)$$

By bearing in mind that

$$\alpha_{m_2} = \arcsin \left( \frac{1}{\lambda_2} \sqrt{\frac{(k+1) - (k-1)\lambda_2^2}{2}} \right),$$

and according to (3-47)

$$\theta_1 = \sqrt{\frac{k+1}{k-1}} \arcsin \left( \sqrt{\frac{(k-1)\lambda_1^2 - (k-1)}{2}} \right)$$

we obtain:

$$\delta = \sqrt{\frac{k+1}{k-1}} \arcsin \left( \sqrt{\frac{(k-1)\lambda_1^2 - (k-1)}{2}} \right) + \arcsin \left( \frac{1}{\lambda_2} \sqrt{\frac{(k+1) - (k-1)\lambda_2^2}{2}} \right) - \frac{\pi}{2}. \quad (3-53)$$

By applying known trigonometric transformation, from (3-53) we find:

$$\delta = \sqrt{\frac{k+1}{k-1}} \arcsin[k - (k-1)\lambda_2^2] + \arccos\left[k - (k+1)\frac{1}{\lambda_2^2}\right] - \frac{\pi}{2}. \quad (3-53a)$$

The magnitude  $\delta$  can be presented in relation to  $M_2$  or  $p_2/p_0$ . Corresponding values of  $\delta$  for three different indices  $k = 1.135$ ; 1.3 and 1.4 are shown in Fig. 3-21 and in the table of functions of isentropic flow (See Appendix).

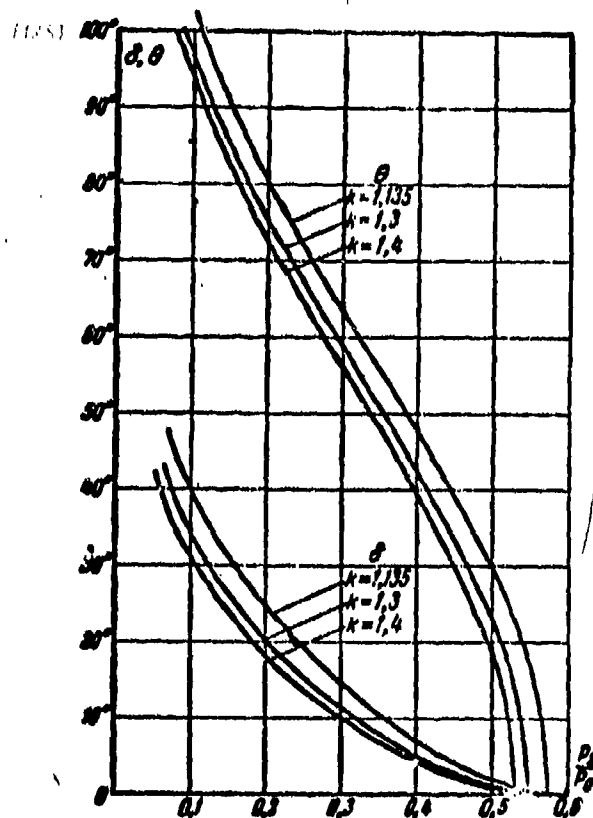


Fig. 3-21. Change of angles  $\delta$  and  $\theta$  in relation to ratio of the pressures.

A maximum angle of deflection  $\delta_{\max}$  corresponds to a maximum speed of flow  $\lambda_{\max}$  (or  $p_2/p_0 = 0$ ). In this case, as was already pointed out,  $a_{m2} = 0$  and, consequently,

$$\delta_{\max} = \theta_{\max} - \frac{\pi}{2}.$$

or by taking into account (3-49) we obtain:

$$\delta_{\max} = \frac{\pi}{2} \left( \sqrt{\frac{k+1}{k-1}} - 1 \right). \quad (3-54)$$

### 3-7. Diagram of Characteristics

By using equation (3-53), we now consider the change in speed along a certain streamline EFH (Fig. 3-22). Let us assume that the speed of undisturbed flow before angle point A  $\lambda_1 = 1$ . Beyond the angle point the pressure is  $p_2 = 0$ . Thus, along the streamline EFH there occurs a continuous expansion of the flow from  $p_1 = p_*$  to  $p_2 = 0$ ;

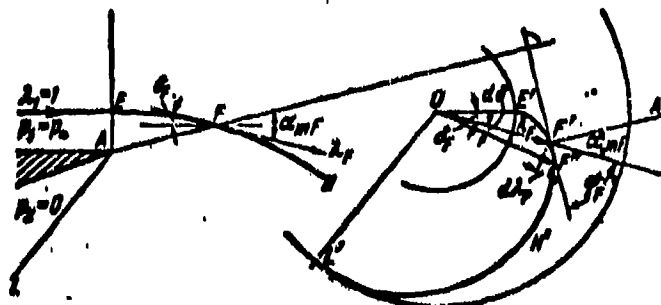


Fig. 3-22. Hodograph of speed vector in flow around an angle by supersonic flow.

here the speed of flow increases from  $\lambda_1 = 1$  to  $\lambda_2 = \lambda_{\max}$ . At each point of streamline one can determine the magnitude and sense of the speed vector  $\lambda$ . We shall plot these vectors from a certain center O. Then the ends of vectors will describe curve--hodograph of the speed for a given streamline.

We note that points of the hodograph of speed E'F'H' correspond to points of the EFH streamline. It follows from this that the sector  $OE' = 1$ , and the sector  $OL = \sqrt{\frac{k+1}{k-1}}$ . Equation (3-53), expressing the function  $\delta(\lambda)$ , is the equation of hodograph of speed in polar coordinates. According to (3-53) hodograph of speed is an epicycloid.

We shall dwell more specifically on certain properties of a hodograph of speed.



We shall draw in the plane of flow the characteristic AF, intersecting the streamline EFH at point F (Fig. 3-22), and we shall find in plane of hodograph the point F' corresponding to it. This can be done, by drawing from point O the line of speed vector  $\lambda_F$  at an angle  $\delta_F$  to direction of flow OE'. The sense of the vector

$\lambda_F$  coincides with the direction of tangent to streamline at point F. In displacement to an infinitely closely located point F', the speed of the flow varies by  $d\lambda_F$  (angular deflection changed by  $d\delta$ ). Angle between tangent to hodograph at point F and speed vector can be found by the equation

$$\tan \varphi_F = \frac{\lambda_F d\delta}{d\lambda_F}.$$

The magnitude  $\frac{d\lambda_F}{\lambda_F}$  is determined by differentiation of the equation (3-53); we obtain:

$$d\delta = \sqrt{\frac{\lambda^2 - 1}{1 - \frac{k-1}{k+1}\lambda^2}} \cdot \frac{d\lambda}{\lambda}.$$

Consequently,

$$\frac{d\lambda_F}{\lambda_F} = \frac{d\delta}{\sqrt{M_F^2 - 1}}.$$

It is obvious that

$$\tan \varphi_F = \sqrt{M_F^2 - 1}.$$

The angle between the normal to the hodograph F'A' and the direction of the undisturbed flow OF' is equal to:  $\tan \alpha_{mF} = \frac{1}{\tan \varphi_F} = \frac{1}{\sqrt{M_F^2 - 1}},$

or

$$\sin \alpha_{mF} = \frac{1}{M_F}.$$

Consequently, the normal to hodograph of speed F'A' is characteristic in the plane of flow, since angle of this normal with the sense of the speed vector is equal to angle of slope of characteristic  $\alpha_{mF}$ . From this follows the obvious conclusion of the mutual orthogonality of characteristics and tangents to hodograph of speed (Fig. 3-22). Line of hodograph of speed E'F'H'L' is called the characteristic of flow in the plane of hodograph (plane u, v). It should be emphasized that all streamlines have a common hodograph of speed, i.e., form of characteristic in plane of hodograph does not depend on character of flow and is identical for all two-dimensional supersonic flows of gas with given physical properties.

Just as in field of flow, in plane of hodograph it is possible to construct two characteristics, symmetrical with respect to the axis, which refer to two

different families. For the solution of a number of practical problems it is convenient to use grid of characteristics of first and second family. Totality of characteristics of two families in the plane of the hodograph is called the diagram of characteristics. The diagram of characteristics can be constructed by equation (3-53) or graphically.

Graphic method is based on the following consideration. We establish the character of the relationship between the speed vector and angle of slope of characteristic  $\alpha_m$ . We note that in the plane of hodograph the supersonic region is included in annular region between the two circles (Fig. 3-23). The radius of internal circle is equal to  $\lambda = 1$ . External circle has a radius, equal to  $\sqrt{\frac{k+1}{k-1}}$ . As has already been indicated, with a change of speed from  $\lambda = 1$  up to  $\lambda = \sqrt{\frac{k+1}{k-1}}$ , angle of slope of characteristic varies within limits from  $\alpha_m = \frac{\pi}{2}$  to  $\alpha_m = 0$ .

In considering that

$$\sin^2 \alpha_m = \frac{(k+1) - (k-1)\lambda^2}{2\lambda^2}$$

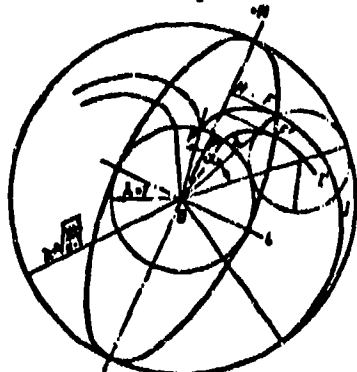
and  $\lambda^2 = \lambda_x^2 + \lambda_y^2$  where  $\lambda_y = \lambda \sin \alpha_m$ , we arrive at the equation

$$\frac{k-1}{k+1} \lambda_y^2 + \lambda_x^2 = 1.$$

Thus, dependence  $\alpha_m(\lambda)$  in polar coordinates  $(\lambda, \alpha_m)$  is expressed by the ellipse equation. Length of minor semiaxis of ellipse is equal to unity, length of major semiaxis is equal to  $\sqrt{\frac{k+1}{k-1}}$ .

We shall place the ellipse in plane of hodograph (Fig. 3-23).

The sector, connecting the center  $O$  with a certain point on arc of ellipse  $P$ , determines the speed vector  $\lambda$  on scale of the construction. The angle between



vector  $\lambda$  and major semiaxis of ellipse is equal to  $\alpha_m$ .

It is obvious that the major semi-axis  $ON$  gives the direction of the characteristic in field of flow, and the minor semiaxis  $OL$  the direction of characteristic in plane

Fig. 3-23. Diagram for constructing characteristics in hodograph plane.

of hodograph. Consequently, sector FG, parallel to OL, is tangent to the characteristic in plane of hodograph at the point F.

By drawing at several points of the ellipse sectors, parallel to the minor axis, and by rotating ellipse around the center O, we can construct a group of characteristics of the first family in the plane of hodograph PFJ, P'F'J', et cetera.

Since in the rotation the ellipse passes over each point of annular region twice, then there readily is drawn another group of epicycloids, composing the second family of characteristics (dotted curves in Fig. 3-23). Characteristics of the second family are the mirror image of characteristics of first family.

The hodograph of speed can also be obtained by means of rolling without slipping of circle with radius  $\frac{1}{2} \left( \sqrt{\frac{k+1}{k-1}} - 1 \right)$  along inner circle of annular region (dashed-dotted circle in Fig. 3-23).

The diagram of characteristics in plane of hodograph is used for approximate calculations of two-dimensional supersonic flows. For this purpose in the plane of hodograph there are drawn sectors of the characteristics of two families at an identical and fairly small distance from each other. For practical use, the portion of annular region, located in sector with a  $70^\circ$  angle is sufficient. Each epicycloid is appropriated a specific number.

We note that any circle in plane of the hodograph is a line of constant modulus of speed, and any radial line, proceeding from the center of O, determines the sense of a speed vector at a given point (Fig. 3-24). The internal circle is subdivided into degrees; reading of angle will be made from the horizontal axis of plane of hodograph (positive angles are plotted upwards, and negative - downwards).

Every epicycloid is appropriated a number, showing angle of radial line, as whose extension the epicycloid under consideration (Fig. 3-24) serves. Epicycloids of first family, proceeding upwards, have the subscript 1 ( $10_1, 20_1, 30_1$  etc.); proceeding downwards, they are designated correspondingly by the subscript 2 ( $10_2, 20_2, 30_2$ , etc.).

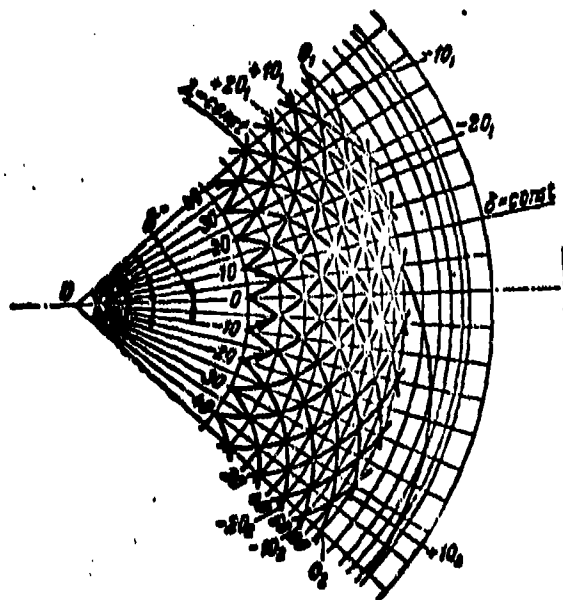


Fig. 3-24. Designation of characteristics and circles (lines  $\lambda = \text{const}$ ) in diagram of characteristics.

The circles (lines  $\lambda = \text{const}$ ) also are designated by a specific number.

With an acceleration from  $\lambda = 1$  up to a given value  $\lambda$  the flow is deflected at a certain angle  $\delta$ , which can be found by superposing the two radial lines intersecting the characteristic in the circle of radius  $\lambda = 1$  and in circle of radius

$\lambda$  (Fig. 3-24). Along the circle the angle of deflection  $\delta$  maintains a constant value; it is equal to the halfsum of numbers of the epicycloids of the two families, intersecting on the given circle. If the number epicycloids of both families decreases or increases by one and the same magnitude, then the point corresponding to it in the plane of hodograph is displaced along the circle.

Each circle in the diagram of characteristics is designated by a number, showing the sum of numbers of the epicycloids [having a different sign (+)] or difference between numbers of the epicycloids [having an identical sign (+ or -)], intersecting on a given circle, and equal to twice the angle of deflection of

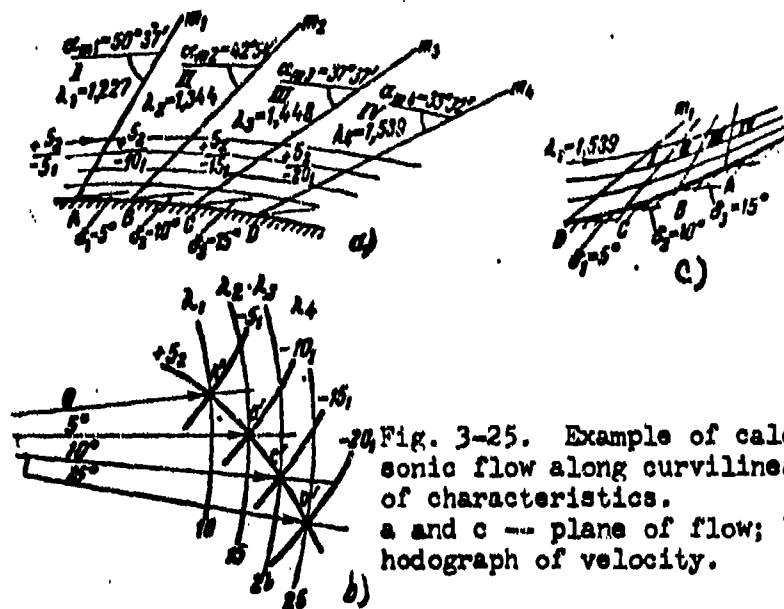


Fig. 3-25. Example of calculation of supersonic flow along curvilinear wall by method of characteristics.  
a and c -- plane of flow; b -- plane of hodograph of velocity.

flow in the expansion from  $\lambda = 1$  to  $\lambda$ , corresponding to the considered circle.

Below there are presented examples, illustrating the methodology of using the diagram of characteristics.

Thus, in Fig. 3-25a there is illustrated the flow around a convex curvilinear wall by a two-dimensional supersonic flow. For an approximate calculation of the flow we shall replace the smooth line of wall ABCD by a broken line; each sector of this line (AB, BC, CD) is rotated by an identical angle, equal, for example, to  $5^\circ$ . Before the characteristic  $Am_1$  there are known speed of flow  $\lambda_1 = 1.227$  and the corresponding angle  $\alpha_{m_1} = 50^\circ 37'$ . In the plane of hodograph (Fig. 3-25,b) to this characteristic corresponds point  $A'$ , which in the diagram of characteristics can be selected arbitrarily in circle 10, corresponding to a speed  $\lambda_1 = 1.227$ .

We shall take this point at the intersection of the characteristics  $\frac{+52}{-51}$ .

In the transition to region II the flow is deflected by an angle of  $5''$ .

STOP HERE

STOP HERE

By following along the characteristic  $+5_2$  in plane of hodograph, we find the circle passing through point B' (number of circle is equal to 15, the sum of 5 and 10), the corresponding speed in region II,  $\lambda_2 = 1.344$  and angle  $\alpha_m = 42^\circ 54'$ . By proceeding to region III and further to region IV, successively we find in diagram of characteristics the points C' and D' and the corresponding speeds of flow  $\lambda_3$  and  $\lambda_4$ , and also  $\alpha_m$  and  $\alpha_m$ .

Completely analogously there can be made a calculation of flow around a concave wall (Fig. 3-25,c). If speed before  $Dm_1$  is equal to  $\lambda_1 = 1.539$ , and the angle of rotation of sectors DC, CB, BA are identical and, as in the case "a," are taken equal to  $5^\circ$ , then the variation of speed and direction of flow in regions I, II, III and IV are found by the diagram of characteristics, by crossing along epicycloids  $+5_2$  from the point D' to the point A'.

### 3-8. The Intersection and Reflection of Waves of Rarefaction

In Fig. 3-26 there is presented diagram of the intersection of two waves of rarefaction, forming as the result of changes in the directions of the channel walls at angles of  $\delta_1$ , and  $\delta_2$ , respectively.

Since the angle  $\delta_2 < \delta_1$ , then the wave BCD has smaller intensity in comparison with wave ACE. If we assume that at all points of region I, the speeds are identical, then the first characteristics AC and BC have an identical angle of slope to streamlines of undisturbed flow. In region II there is established a pressure, that can be determined by formulas in Sec. 3-6. To the right of characteristic AE the pressure  $p_3$  will be less than  $p_2$ , since flow traverses a more intense wave of rarefaction ACE. In zones II and III, the streamlines acquire a direction, parallel to the walls  $AA_1$  and  $BB_1$ . Following this, the streamlines once again intersect sectors of the waves of rarefaction DIKF and EFGH, which are a continuation of waves ACE and BCD. Here the pressure of flow lowers to  $p_4$ , and the speed correspondingly increases ( $\lambda_{IV} > \lambda_{III} > \lambda_{II} > \lambda_I$ ).

At the intersection of the waves DIKF and EFGH the streamlines are deflected in opposite directions; here the streamline  $a - a$  is rotated at a larger angle, than the streamline  $b - b$ . To the right of KFG the streamlines have an identical direction and are deflected at an angle  $\Delta \delta = \delta_1 - \delta_2$  from initial direction, since the intersecting waves have a different intensity. The resultant deflection

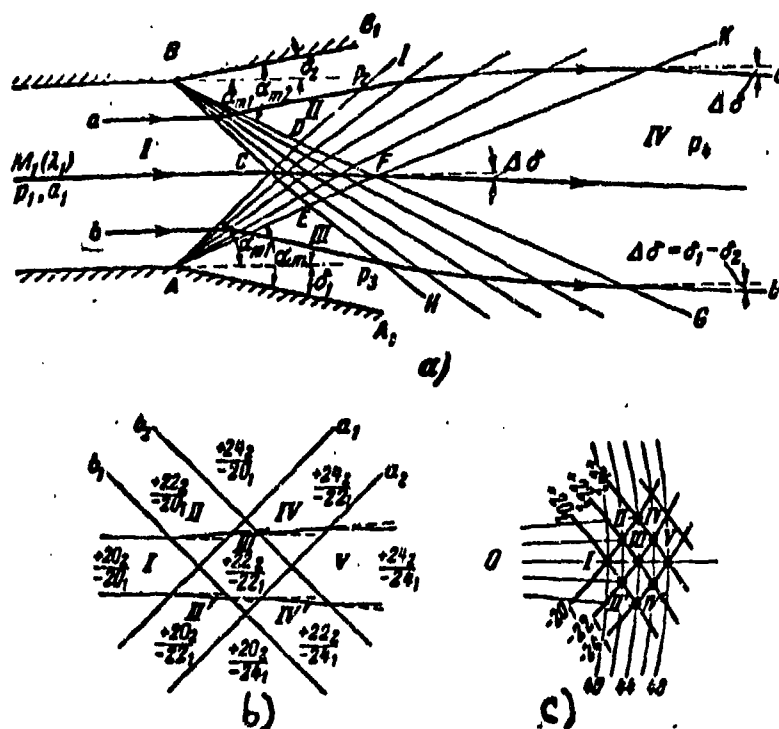


Fig. 3-26. The reaction between two waves of rarefaction.

of flow occurs in that direction, which is dictated by the more powerful wave, in the given case by wave AJKA.

Parameters of the flow beyond the system of intersecting waves (region IV) can be determined by formulas, presented in preceding paragraphs. The construction of spectrum of flow and determination of parameters in zone of intersecting waves can be realized by means of the diagram of characteristics.

We now consider the intersection of two pairs of characteristics (Fig. 3-26,b), where the parameters and direction of flow in region I will be considered given. The magnitude and direction of speed in this region are determined at that point in plane of hodograph, at which the epicycloids of the two families intersect. Suppose for the considered example, the number  $\lambda$  in region I is equal to 1.522, and corresponding epicycloids have the numbers  $+20_2$  and  $20_1 \left( \frac{+20_2}{-20_1} \right)$  (number of circle 40). The direction of the flow in region I coincides with direction of the radial line 0 (See diagram of characteristics). In the transition to region II, the flow intersects the characteristic  $b_1$ , where we assume that in the transition through this characteristic the angle of deflection of flow amounts to  $1^\circ$ . Then, in being displaced along epicycloid  $20$ , we find in the plane of the hodograph the point corresponding to the state of flow in region II  $\left( \frac{+22_2}{-20_1} \right)$ . Analogously we find the magnitude and direction of speed in zone III after the intersection of the characteristic  $a_1$ . The corresponding epicycloids have the numbers  $+22_2$  and  $21_1 \left( \frac{+22_2}{-21_1} \right)$ . In the transition into region IV, the deflection of the flow occurs in opposite direction by the same magnitude ( $1^\circ$ ). In this case, in being displaced along the epicycloids  $-22_1$ , we find the magnitude of the speed in zone IV, which is determined by the sum of numbers of the epicycloids  $+24_2$  and  $-22_1$ . The transition to region V from region IV is associated with a turn of the flow by an angle of  $1^\circ$  in the opposite direction. Simultaneously, there occurs a subsequent expansion of the flow and the sum of the numbers of epicycloids increases. To this zone correspond epicycloids  $\frac{+24_2}{-24_1}$ . The speed of flow here amounts to  $\lambda_V = 1.558$ . The successive transition through characteristics of rarefaction in the diagram of characteristics is shown in Fig. 3-26,c. Here the points I', II', III', etc., correspond to regions I, II, III...in Fig. 3-26,b. The considered method of constructing the flow in the zone of intersecting sound waves is approximate. At the base of the method there is posed the assumption that at the intersection of each characteristic the flow is turned and expanded by identical magnitudes, i.e., all waves have an



identical intensity. Within the limits between neighboring characteristics, the parameters of the flow are considered constant.

By the indicated method it is possible to calculate the flow in the quadrangle CDFE (Fig. 3-26,a), within the limits of which an intense expansion of gas and a deformation of the streamlines occur. In this region, the characteristics are curvilinear. If both interacting waves of rarefaction possess an identical intensity, then the quadrangle CDFE is symmetric, and a deflection of neutral streamline in zone IV does not occur.

Thus, we see that as a result of interaction between waves of rarefaction an expansion and acceleration of the flow occur.

Of practical interest is the case of reflection of waves of rarefaction from wall or free boundary of the stream. The first case is shown in Fig. 3-27,a.

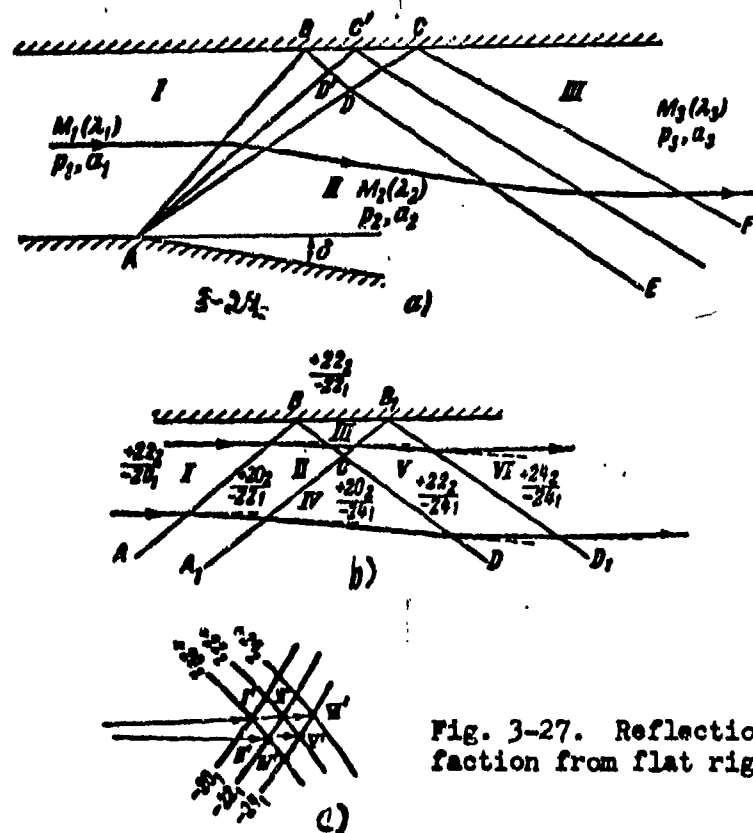


Fig. 3-27. Reflection of wave of rarefaction from flat rigid wall.

At the intersection of primary wave of rarefaction ABC, the streamlines, in being deformed, turn at an angle  $\delta$ . The first characteristic AB is reflected from the wall, where the element of reflected wave ED intersects the primary wave of rarefaction. Consequently, along ED, the pressure must drop, and the speed — increase. To such conclusion we arrive, in considering the behavior of streamlines immediately along wall: here during continuous flow around the streamlines are parallel to the wall and, consequently, turned at angle  $\delta$  to the streamlines, located beyond the characteristic AD. Such a deflection denotes a rarefaction of supersonic flow. Hence, we conclude that the wave of rarefaction is reflected from flat wall in form of wave of rarefaction, i.e., maintains the sign of influence on flow.

It is readily seen that the reflected characteristics comprise with the direction of wall, an angle, less than the angle of corresponding primary characteristics, since the speed beyond the point of drop increases.

With distance from the wall angle of reflected characteristic decreases in connection with the fact that characteristic intersects the region of rarefaction (in sector ED), and along the characteristic the speed increases. It follows from this that sectors of characteristics, lying within the limits of the primary wave of rarefaction, will be curvilinear. Only beyond the last characteristic DC do the reflected characteristics become rectilinear. An analogous conclusion can be made also for sections of primary characteristics AD', et al.

In the transition through primary and reflected waves of rarefaction the flow expands: the pressure drops, and the speed correspondingly increases. Parameters of flow in zone II are determined by known values  $\lambda_1, p_1, a_1, \delta$ . Parameters of zone III can be found, by considering that angle of rotation of flow in reflected wave EBCF is equal to  $\delta$ . Then, after determining  $\lambda_2, p_2, a_2$  by the same formula we find  $\lambda_3, p_3, a_3$ .

The construction of the reflected wave can be made by using the method of characteristics. Thus, for example, let us assume that in the transition through

characteristic AB, falling on wall at point B (fig. 3-27,b), the direction of speed changes by  $1^\circ$ . If speed before AB amounts to  $\lambda_1 = 1.522$  (epicycloids  $\frac{+20}{-20_1}$ ), then in the zone ABCA the numbers of corresponding characteristics in plane of hodograph are equal to  $\frac{+20_2}{-22_1}$  ( $\lambda_{11} = 1.535$ ). At the intersection of reflected wave BC, flow is reverted to initial direction and, consequently, in this region magnitude and direction of speed are determined at the point of diagram of characteristics  $\frac{+22}{-22_1}$  ( $\lambda_{111} = 1.558$ ).

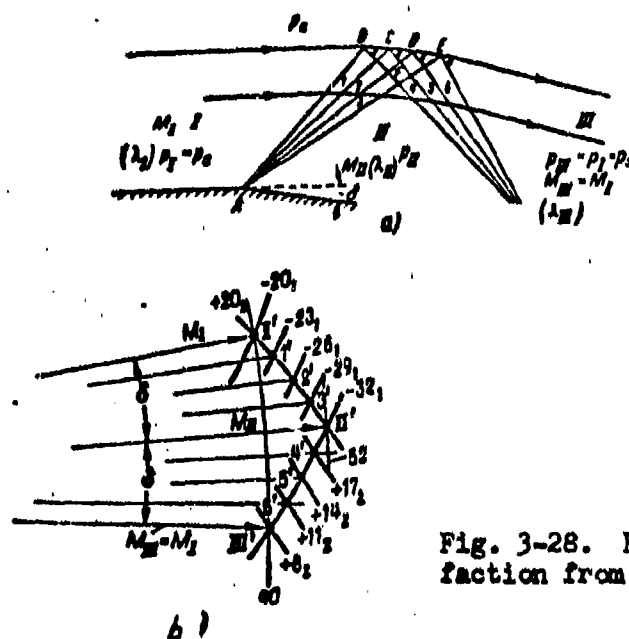


Fig. 3-28. Reflection of wave of rarefaction from a free edge of the stream.

The transition from zone II to zone IV results in a new change of magnitude and direction of speed, corresponding to the characteristics  $\frac{+20_2}{-24_1}$  ( $\lambda = 1.558$ ).

As a result of intersection of reflected wave BD the flow is deflected in an opposite direction (wave of rarefaction) and its characteristics will be  $\frac{+22_2}{-24_1}$  ( $\lambda_v = 1.575$ ). Finally, beyond the second reflected wave  $B_1 D_1$ , the magnitude and direction of speed correspond to the characteristics  $\frac{+24_2}{-24_1}$  ( $\lambda_{v1} = 1.595$ ). The position of the corresponding points in the diagram of characteristics can be seen in Fig. 3-27,c.

Analogously it is possible to consider the reflection from the free boundary of stream of wave of rarefaction ABE, forming during flow around the exterior angle (Fig. 3-28). Characteristics, by not penetrating into external medium, are reflected

from the edge, where the streamlines and edge of stream are distorted. Along the wave AB, pressure is equal to pressure of external medium  $p_a$ ; after last wave  $p_{11} < p_a$ . However, directly on edge of stream on external side the pressure, temperature and speed do not change. Consequently, if along the sector of characteristic BF the pressure drops, then along FE it increases. But the sector FE intersects the reflected wave. This means that in the transition through the reflected wave, the pressure increases up to the value  $p_a$ .

Hence we conclude that wave of rarefaction from the free edge of stream is reflected, as a compressional wave. Characteristics of the reflected wave converge. This is obvious, since the angle between reflected characteristics and the edge remain identical (at points B, C, D, E - the pressure, speed and temperature are identical).

In reflected wave, the compression of the gas occurs gradually (without discontinuity), and change of state is isentropic.

The construction of the process in waves of rarefaction and compression in the diagram of characteristics is shown in Fig. 3-28, b. The points I', 1', 2', etc., make it possible to determine the magnitude and direction of the speed in the regions of flow I, 1, 2, etc., (Fig. 3-28, a). By intersecting both waves, flow turns at an angle, equal to  $2\delta$ .

Thus, we see that the reflection of waves of rarefaction from a free edge occurs with a change in sign of the influence on flow. As a result of the interaction of wave of rarefaction with the edge there occurs a deflection of the stream.

Principal distinction between properties of reflected waves from wall and a free edge is explained finally by the fact that along streamlined wall distribution of the parameters of flow is dictated by the flow itself, while on free edge it is given by external medium.

The considered examples of interaction of waves by no means exhaust range of problems in this region, with which one must encounter in the practice of

an experiment and in theoretical investigations. However, these examples can be assumed as the basis of a study of other, more complex cases.

FIGURE 1

5  
4  
3  
2  
1  
0

STOP HERE

5  
4  
3  
2  
1  
0

STOP HERE

## CHAPTER 4

### COMPRESSION SHOCKS

#### 4-1. The Formation of Shock Waves

In the preceding chapters, we considered properties of an isentropic gas flow. In this connection we studied the mechanism of propagation in flow of such disturbances, which do not cause a change in its entropy. We turn now to a study of finite disturbances, the propagation of which is accompanied by an increase of entropy of the gas flow.

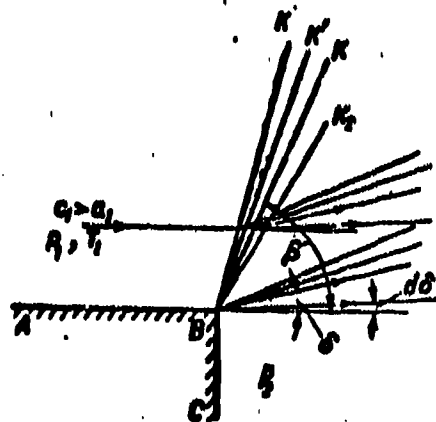


Fig. 4-1. Supersonic flow of gas into a region of higher pressure.

For this purpose let us consider the motion of a supersonic flow along a flat wall AB, flowing into medium with higher pressure (Fig. 4-1). To the left of point B the speed will be  $c_1$ , pressure  $p_1$  and temperature  $T_1$ . To the right of point B (after line BC) there is maintained a pressure  $p_2$ , higher than  $p_1$ . If the difference between pressures  $p_2 - p_1$  is small, then at the point B, a weak compressional wave  $BK_1$  develops.

STOP HERE

STOP HERE

If change in pressure at point B becomes finite, then, as the experiment shows, the wave will be transferred to the position BK and will possess not an infinitesimally small but a finite intensity. According to the degree of increase in pressure  $p_2$ , the line BK will be deflected to the left with respect to point B ( $BK'$ ,  $BK''$  etc.). In the transition through wave BK, the gas is compressed and flow is deflected at a certain angle  $\delta$  upwards from direction of the undisturbed flow AB. With a rise of  $p_2$ , the compression of the gas in wave BK and the angle of deflection  $\delta$  increase.

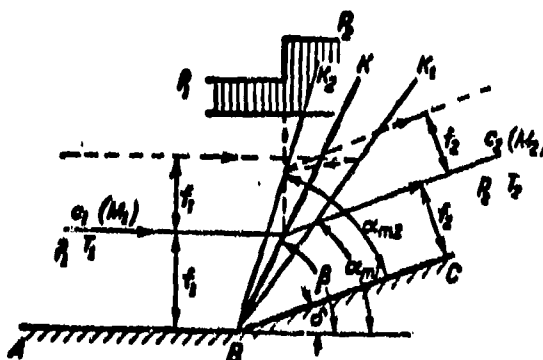


Fig. 4-2. Flow around an internal angle by a supersonic flow.

The wave BK is called a plane oblique compression shock or a plane shock wave. In the transition through such shock wave the flow experiences intermittent changes in pressure, speed, and other parameters. The position of the shock is determined by the angle  $\beta$  between plane of shock BK and the initial direction of flow AB (Fig. 4-1).

The formation of oblique shock waves can be traced also in the simplest example of flow around the wall ABC, deflected at point B at a certain finite angle  $\beta$  towards the flow (Fig. 4-2)

Owing to such a change in direction of wall, the section of stream decreases and the stream contracts. In a supersonic flow this results in an increase of pressure ( $p_2 > p_1$ ). Here, the increase in pressure occurs intermittently in the transition through the surface BK, which is the surface of shock. It is possible to show that during a flow around the considered wall, a continuous transition from parameters in region ABK to parameters in region KBC is physically impossible.

Actually, boundary of disturbance for the region ABK<sub>1</sub> must be the sound wave

$BK_1$ , whose angle of slope to the vector of speed  $c_1$  will be  $\alpha_{m1} = \arcsin \frac{a_1}{c_1}$ . The second boundary of disturbance  $BK_2$  has angle of slope  $\alpha_{m2} = \arcsin \frac{a_2}{c_2}$ . Since  $c_2 < c_1$  and  $a_2 > a_1$ , then  $\alpha_{m2} > \alpha_{m1}$ . The characteristic  $BK_2$  is found to be in the undisturbed region  $ABK_1$  and the lines of flow must have the shape, shown by dotted line which physically is absolutely unrealistic.

It is possible to assume that an oblique shock occupies a mean position between waves  $BK_1$  and  $BK_2$ ; then the angle of an oblique shock  $\beta$  is associated by a simple approximate relationship with the angles  $\alpha_{m1}$ ,  $\alpha_{m2}$  and  $\delta$ :

$$\beta \approx \frac{1}{2} (\alpha_{m1} + \alpha_{m2} + \delta).$$

We considered stationary case of the formation of an oblique shock wave, motionless relative to the focus of the disturbance.

Such a case corresponds to the incidence of a two-dimensional supersonic flow of constant speed onto an infinite wedge or the motion of flat wedge in a medium with a constant supersonic speed. In a non-stationary motion the compression shocks may develop also at subsonic speeds of the motion. In the general case of a non-stationary motion the shock wave, which is the result of a finite compression or rarefaction of the flow, can be displaced relative to a solid body, which caused the shock wave.

We shall analyze conditions of the formation of such moving shock waves. Suppose in a tube of constant section there is a piston (Fig. 4-3). The thrust of the piston causes to the left a weak wave of rarefaction  $m' - n'$ , and to the right, a weak compressional wave  $m - n$ . By continuing to increase the rate of piston thrusts, we shall create a series of weak waves of disturbances ( $m'_1 - n'_1$ ,  $m_1 - n_1$ , etc.), being displaced in the flow of gas in opposite directions from the piston, each with its own speed corresponding to the speed of sound in a given region.

It is readily seen that to the right each thrust raises the pressure of the gas by a small magnitude, and to the left — lowers it. Consequently, in region III the pressure and temperature will be higher than in regions II and I, and consequently,



speed of sound  $a_{III} > a_{II} > a_I$ . Conversely, in regions II', III' the speeds of sound will be less than in region I' ( $a'_{III} < a'_{II} < a'_I$ ). Consequently, to the right of the piston, the weak waves of compression overtake one another; to the left the waves of rarefaction will lag behind each other.

After a certain interval of time, waves to the right coalesce into single wave, the front of which will be boundary between the undisturbed and disturbed regions.

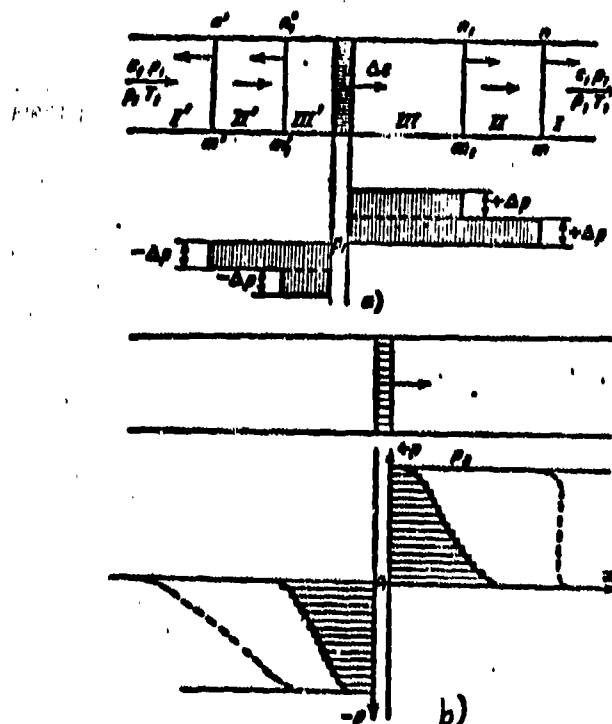


Fig. 4-3. Propagation of weak disturbances in a tube.

#### 4-2. Equation of Oblique Shock

As also previously, we shall consider a flow of gas which has been established without a heat exchange with the environment and without friction. We assume that at certain point in the supersonic flow there appeared an oblique shock wave (Fig. 4-4). Gas parameters before the shock are designated by the subscript 1, and after the shock by the subscript 2.

Let us consider the motion of a gas along lines of flow ABC, intersecting the plane of oblique shock at point B. As has been pointed out, in the transition

through an oblique shock the line of flow is deformed, as it is deflected by a certain angle  $\delta$ . The speed prior to and after oblique shock can be presented as components normal to plane of shock ( $c_{n1}$  and  $c_{n2}$ ) and tangent to it ( $c_{t1}$  and  $c_{t2}$ ) and thus triangles of the speeds prior to and after the shock can be constructed.

It is obvious that

$$c_1^2 = c_{n1}^2 + c_{t1}^2$$

and

$$c_2^2 = c_{n2}^2 + c_{t2}^2.$$

For solving the basic problem on oblique shock, which reduces to establishment of a connection between parameters prior to and after the shock and to determining the losses arising in the transition through the shock, we use the fundamental laws of mechanics.

Law of the conservation of mass — equation of continuity — for two sections of a tube of flow prior to and after the shock can be written out in the following form:

$$\rho_1 c_{n1} = \rho_2 c_{n2}. \quad (4-1)$$

The law of conservation of momentum — equation of variation of momentum — in a projection onto the normal to the plane of oblique shock gives:

$$p_1 - p_2 = \rho_1 c_{n1} (c_{n2} - c_{n1}),$$

$$\text{or} \quad p_1 + \rho_1 c_{n1}^2 = p_2 + \rho_2 c_{n2}^2.$$

(4-2)

Fig. 4-4. Diagram for deriving basic equations of an oblique shock.

In projection onto plane of shock we obtain:

$$\rho_1 c_{n1} (c_{t2} - c_{t1}) = 0,$$

since the pressure along all surfaces parallel to surface of shock remains constant. Consequently,

$$c_{t1} = c_{t2} = c_t.$$

(4-3)

STOP HERE

STOP HERE

Thus, the tangential components of the speeds prior to and after a plane oblique shock wave are identical.

The law of the conservation of energy -- Bernoulli's equation -- can be used in any form known to us. The considered flow occurs without a heat exchange with the environment and, consequently, total energy of the flow is kept constant:

$$\begin{aligned} \frac{c_1^2}{2} + \frac{k}{k-1} \frac{p_1}{\rho_1} &= \frac{c_2^2}{2} + \frac{k}{k-1} \frac{p_2}{\rho_2} = \frac{a^2}{2} \frac{k+1}{k-1}, \\ \text{or} \quad \frac{c_{n1}^2}{2} + \frac{k}{k-1} \frac{p_1}{\rho_1} &= \frac{c_{n2}^2}{2} + \frac{k}{k-1} \frac{p_2}{\rho_2} = \\ &= \frac{a^2}{2} \frac{k+1}{k-1} - \frac{c_t^2}{2}. \end{aligned} \quad (4-4)$$

We shall find a connection between the speeds prior to and after the shock.

We shall transform equation (4-2); by taking into account formula (4-1) we obtain:

$$\frac{p_1}{\rho_1} + c_{n1}^2 = \frac{c_{n1}}{c_{n2}} \left( \frac{p_2}{\rho_2} + c_{n2}^2 \right). \quad (4-2a)$$

From the equation of energy (4-4) we shall express ratio of the pressure to density:

$$\frac{p_1}{\rho_1} = \frac{k-1}{2k} \left( a^2 \frac{k+1}{k-1} - c_{n1}^2 - c_t^2 \right) \quad (4-4a)$$

and

$$\frac{p_2}{\rho_2} = \frac{k-1}{2k} \left( a^2 \frac{k+1}{k-1} - c_{n2}^2 - c_t^2 \right). \quad (4-4b)$$

After substituting (4-4a) and (4-4b) into the equation (4-2a), we obtain:

$$a^2 + c_{n1}^2 - \frac{k-1}{k+1} c_t^2 = (a^2 + c_{n2}^2) \frac{c_{n1}}{c_{n2}} = \frac{k-1}{k+1} \frac{c_{n1}}{c_{n2}} c_t^2.$$

After simple transformations we arrive at equation

$$c_{n1} c_{n2} = a^2 - \frac{k-1}{k+1} c_t^2. \quad (4-5)$$

Formula (4-5) establishes a connection between normal components of speeds during transition through an oblique shock and is the original for obtaining dependences between other parameters of the flow prior to and after the shock.

We shall replace in formula (4-5)  $a^2$  according to the equation

$$\begin{aligned} a^2 &= \frac{k-1}{k+1} (c_{n1}^2 + c_t^2) + \frac{2}{k+1} a_1^2 = \\ &= \frac{k-1}{k+1} (c_{n2}^2 + c_t^2) + \frac{2}{k+1} a_2^2; \\ \text{then} \quad c_{n1} c_{n2} &= \frac{k-1}{k+1} \left( \frac{c_{n1}^2}{a_1^2} + \frac{2}{k-1} \right) a_1^2; \end{aligned} \quad (4-6)$$

$$c_{n1} c_{n2} = \frac{k-1}{k+1} \left( \frac{c_{n2}^2}{a_2^2} + \frac{2}{k-1} \right) a_2^2. \quad (4-6a)$$

STOP HERE

or, by expressing the speed of sound in terms of the pressure and density  $a^2 = k \frac{p}{\rho}$ ,

we shall obtain:

$$\frac{p_1}{\rho_1} \left( \frac{c_{n1}^2}{a_1^2} + \frac{2}{k-1} \right) = \frac{p_2}{\rho_2} \left( \frac{c_{n2}^2}{a_2^2} + \frac{2}{k-1} \right). \quad (4-7)$$

We shall use the equation of continuity (4-1); by squaring both sides of this equation:

$$\rho_1^2 c_{n1}^2 = \rho_2^2 c_{n2}^2$$

and by substituting

$$\rho_1 = k \frac{p_1}{a_1^2} \text{ and } \rho_2 = k \frac{p_2}{a_2^2},$$

we obtain:

$$p_1 p_1 \frac{c_{n1}^2}{a_1^2} = p_2 p_2 \frac{c_{n2}^2}{a_2^2}. \quad (4-8)$$

By eliminating successively from equation (4-7) by means of equation (4-8)  $\rho_1$  and  $\rho_2$  or  $p_1$  and  $p_2$ , we arrive at the expressions

$$\left( \frac{c_{n1}^2}{a_1^2} + \frac{2}{k-1} \right) \frac{c_{n1}^2}{a_1^2} p_1^2 = \left( \frac{c_{n2}^2}{a_2^2} + \frac{2}{k-1} \right) \frac{c_{n2}^2}{a_2^2} p_2^2 \quad (4-9)$$

and

$$\left( 1 + \frac{2}{k-1} \frac{a_1^2}{c_{n1}^2} \right) \frac{1}{p_1} = \left( 1 + \frac{2}{k-1} \frac{a_2^2}{c_{n2}^2} \right) \frac{1}{p_2}. \quad (4-10)$$

From equation (4-6) and (4-6a) there can be obtained:

$$\frac{c_{n2}^2}{a_2^2} = \frac{\frac{c_{n1}^2}{a_1^2} + \frac{2}{k-1}}{\frac{2k}{k-1} \frac{c_{n1}^2}{a_1^2} - 1}. \quad (4-11)$$

From the triangles of speeds in the shock the obvious relationships ensue:

$$\left. \begin{aligned} c_{n1} &= c_1 \sin \beta; \\ c_{n2} &= c_2 \sin \gamma; \\ c_1 &= c_1 \cos \beta = c_2 \cos \gamma. \end{aligned} \right\} \quad (4-12)$$

where

$$\gamma = \beta - \delta.$$

Then from equation (4-11) together with formulas (4-12) there can be obtained:

$$M_2^2 = \frac{M_1^2 + \frac{2}{k-1}}{\frac{2k}{k-1} M_1^2 \sin^2 \beta - 1} + \frac{M_1^2 \cos^2 \beta}{\frac{k-1}{2} M_1^2 \sin^2 \beta + 1}. \quad (4-11a)$$

or

$$\lambda_2^2 = \lambda_1^2 \cos^2 \beta \frac{1 - \frac{k-1}{k+1} \lambda_1^2 \cos^2 \beta}{\lambda_1^2 \sin^2 \beta} \quad (4-11b)$$

Equations (4-9) and (4-10) together with equations (4-11) and (4-12) after simple transformations give the sought relationships:

$$\begin{aligned} \frac{p_2}{p_1} &= \frac{k-1}{k+1} \left( \frac{2k}{k-1} M_1^2 \sin^2 \beta - 1 \right) = \\ &= \frac{2k}{k+1} \left( \frac{2}{k+1} \frac{\lambda_1^2 \sin^2 \beta}{1 - \frac{k-1}{k+1} \lambda_1^2} - \frac{k-1}{2k} \right) \end{aligned} \quad (4-13)$$

FIRST

$$\frac{p_2}{p_1} = \frac{\frac{k+1}{k-1}}{\frac{2}{k-1} \frac{1}{M_1^2 \sin^2 \beta} + 1} = \frac{\lambda_1^2 \sin^2 \beta}{1 - \frac{k-1}{k+1} \lambda_1^2 \cos^2 \beta} \quad (4-14)$$

From equation of state there readily is found the ratio of the absolute temperatures prior to and after the shock:  $\frac{T_2}{T_1} = \frac{p_2 p_1}{p_1 p_2}$

After substituting  $\frac{p_2}{p_1}$  and  $\frac{p_1}{p_2}$  we obtain:

$$\frac{T_2}{T_1} = \left( \frac{k-1}{k+1} \right)^2 \left( \frac{2k}{k-1} M_1^2 \sin^2 \beta - 1 \right) \left( \frac{2}{k-1} \frac{1}{M_1^2 \sin^2 \beta} + 1 \right) \quad (4-15)$$

Formulas (4-5), (4-11) - (4-15) express variations of the parameters of gas during the transition through an oblique shock wave depending on the coefficient  $k$ , the speed of flow prior to shock  $M_1$ , and angle of oblique shock  $\beta$ . These formulas at the same time reveal fundamental physical properties of an oblique shock. Thus, from formula (4-13) it may be concluded, the normal component of the speed prior to the shock is larger than the critical speed. Actually, since  $\frac{p_2}{p_1} > 1$  and  $M_1^2 \sin^2 \beta = \frac{c_{a1}^2}{a_1^2}$ , we conclude that  $\frac{2k}{k+1} \left( \frac{c_{a1}^2}{a_1^2} - \frac{k-1}{2k} \right) > 1$

and consequently,

$$\frac{c_{a1}^2}{a_1^2} > 1.$$

The normal component of the speed after the shock is lower than the critical speed:

$$c_{a2} < a_2.$$

STOP HERE

STOP HERE

From formula (4-13) it follows, in addition, that the angle of the oblique shock is larger than the angle of the characteristic  $a_{m1}$ .

At

$$\beta = a_{m1} = \arcsin \frac{1}{M_1}$$

$$\frac{p_2}{p_1} = \frac{T_2}{T_1} = 1.$$

In this case, an oblique shock degenerates into weak (sonic) compression wave (weak shock) and the angle of deflection of flow tends to zero.

The connection between the angles  $\beta$  and  $\delta$  is established by equation (4-6), which can be transformed to the form:  $\frac{c_{n2}}{c_{n1}} = \frac{k-1}{k+1} \left( 1 + \frac{2}{k-1} \frac{a_1^2}{c_{n1}^2} \right).$

But on the basis of formulas (4-12)

$$\frac{c_{n2}}{c_{n1}} = \frac{c_{n2}}{c_1} \cdot \frac{c_1}{c_{n1}} = \frac{T_{2N}}{T_{2N1}} = \frac{\tan(\beta - \delta)}{\tan \beta}. \quad (4-16)$$

Consequently,

$$\frac{\tan(\beta - \delta)}{\tan \beta} = \frac{k-1}{k+1} \left( 1 + \frac{2}{k-1} \frac{1}{M_1^2 \sin^2 \beta} \right).$$

In remembering that

$$\tan(\beta - \delta) = \frac{\tan \beta - \tan \delta}{1 + \tan \beta \tan \delta},$$

we obtain:

$$\tan \delta = \frac{M_1^2 \sin^2 \beta - 1}{\left[ M_1^2 \left( \frac{k+1}{2} - \sin^2 \beta \right) + 1 \right] \tan \beta}. \quad (4-17)$$

In Fig. 4-5 there are presented graphs of  $\delta(\beta)$  at different values of  $\lambda_1$  for  $k = 1.3$ . We note that with an increase in speed of the undisturbed flow, the maximum angle of deflection of flow  $\delta_m$  increases. It should be emphasized that in accordance with double solution of equation (4-17) for the single value of the angle  $\delta$  of deflection of flow there correspond two different  $\beta$  values. Experience shows that only a smaller value of  $\beta$  corresponds to a plane oblique shock.

Above, on the assumption that a shock occupies an intermediate position between characteristics of undisturbed and disturbed flows, there was given the formula

$$\beta \approx \frac{1}{2} (a_{m1} + a_{m2} + \delta). \quad (4-17a)$$

STOP HERE

STOP HERE

A comparison of this formula with the accurate expression (4-17) for several values of  $\lambda_1$  is given also in Fig. 4-5. The curves show that with an increase in speed before the shock  $\lambda_1$  the divergence between results of the calculation by accurate and approximate formulas increase.

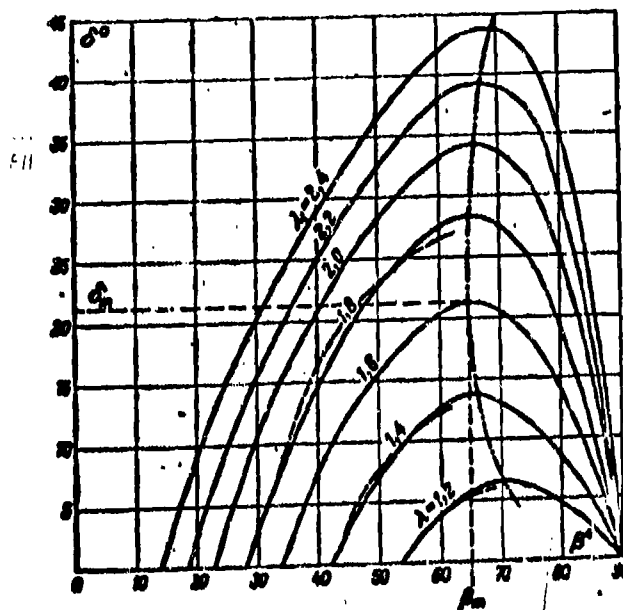


Fig. 4-5. Relationship between the angle of deflection of flow and angle of shock at different speeds in undisturbed flow (for  $k = 1.3$ ).  
 ———— accurate formula (4-17);  
 - - - - - approximate formula (4-17a).

The magnitude of the error depends also on  $\delta$ .

From equation (4-17) it follows that  $\delta = 0$  at  $\beta = \alpha_{m1}$  and at  $\beta = \frac{\pi}{2}$ . Thus, the curve  $\delta = \delta(\beta)$  has a maximum, the location of which is determined by the ordinary method. After differentiating equation (4-17) and equating the derivative to zero, after transformation we obtain:

$$\sin^2 \beta_m = \frac{1}{k M_1^2} \left[ \frac{k+1}{4} M_1^2 - 1 + \sqrt{(k+1) \left( 1 + \frac{k-1}{2} M_1^2 + \frac{k+1}{16} M_1^4 \right)} \right] \quad (4-18)$$

where  $\beta_m$  is the angle of oblique shock, corresponding to maximum angle of

deflection of flow  $\delta_m$ .

It follows from this that at  $M_1 = 1$ , the angle  $\beta_m = \frac{\pi}{2}$ , and at  $M_1 = \infty$ , the angle  $\beta_m = \arcsin \left( \sqrt{\frac{k+1}{2k}} \right)$ . For intermediate values the angle  $\beta_m$  with an increase in  $M_1$  at first decreases, and later increases somewhat.

Equation (4-11a) makes it possible to trace the change of speed of flow after the oblique shock,  $M_2$ , depending on  $M_1$  and  $\beta$ . With an increase in  $\beta$  (with a constant  $M_1$ ),  $M_2$  decreases; the drop of speeds in the shock increases.

At a certain value  $\beta = \beta_*$  speed after the shock becomes sonic ( $M_2 = 1$ ). With a subsequent increase in  $\beta$  the flow after the shock will be subsonic.

The magnitude  $\beta_*$  can be determined by equation (4-11a), by substituting  $M_2 = 1$ . Then, after transformations we obtain:

$$\sin^2 \beta_* = \frac{1}{kM_1^2} \left[ \frac{k+1}{4} M_1^2 - \frac{3-k}{4} + \sqrt{(k+1) \left( \frac{9+k}{16} - \frac{3-k}{8} M_1^2 + \frac{k+1}{16} M_1^4 \right)} \right]. \quad (4-19)$$

We note that at  $M_1 = 1$ , the angle  $\beta_* = \beta_m = \frac{\pi}{2}$ ; at  $M_1 = \infty$  the angle  $\beta_* = \beta_m = \arcsin \left( \sqrt{\frac{k+1}{2k}} \right)$ .

To the last value of  $\beta_*$  there corresponds the maximum angle  $\delta_m$ , determined from (4-17):

$$\delta_m = \arctan \left( \frac{1}{\sqrt{k^2 - 1}} \right).$$

For the values  $M_1 < \infty$ , the angle  $\beta_m > \beta_*$  and, consequently,  $M_{2m} < 1$ . This means that at the maximum angle of deflection of flow, the speed after the shock will be subsonic. Since, however, for all  $M_1$  the angles  $\beta_m$  and  $\beta_*$  are very close, then as a first approximation it is possible to assume that the maximum angle of deflection for each value of the speed of an undisturbed flow will be attained at a sonic speed after the shock ( $M_2 \approx 1$ ).

We established that the parameters of flow after an oblique shock depend on angle of the oblique shock  $\beta$ . With an increase of  $\beta$ , the pressure, temperature, and density of the gas after the shock increase (parameters of flow prior to shock are assumed constant), and the dimensionless speed decreases. The angle of deflection of flow, as has been indicated, at first increases (at  $\beta < \beta_m$ ), and then it decreases



(at  $\beta > \beta_m$ ).

In the particular case  $\beta = \frac{\pi}{2}$ , variations of the parameters in the shock are found to be maximum, and the angle of deflection  $\delta = 0$ . Such a shock is located normal to the direction of the speed of undisturbed flow and is called a normal shock.

A normal shock is a particular case of an oblique shock; the fundamental equations of a normal shock are obtained from formulas (4-11) — (4-15) after substituting  $\beta = \frac{\pi}{2}$ .

Variations in pressure and density in a normal shock are found from formulas (4-13) and (4-14):

$$\frac{p_2}{p_1} = \frac{k+1}{k-1} \left( \frac{2k}{k-1} M_1^2 - 1 \right) = \frac{\lambda_1^2 - \frac{k-1}{k+1}}{1 - \frac{k-1}{k+1} \lambda_1^2}; \quad (4-20)$$

$$\frac{\rho_2}{\rho_1} = \frac{\frac{k+1}{2} M_1^2}{1 + \frac{k-1}{2} M_1^2} = \lambda_1^2; \quad (4-21)$$

The ratio of the temperatures — from formula (4-15):

$$\frac{T_2}{T_1} = \left( \frac{k+1}{k-1} \right)^2 \left( \frac{2k}{k-1} M_1^2 - 1 \right) \left( \frac{2}{k-1} \frac{1}{M_1^2} + 1 \right). \quad (4-22)$$

The dimensionless speed after a normal shock can be obtained by formula (4-11a):

$$M_2^2 = \frac{M_1^2 + \frac{2}{k-1}}{\frac{2k}{k-1} M_1^2 - 1} \quad (4-23)$$

or by formula (4-11b)

$$\lambda_1 \lambda_2 = 1, \quad (4-24)$$

i.e.

$$c_1 c_2 = a_*^2. \quad (4-24a)$$

We see that the product of speeds prior to and after a normal shock is equal to the square of the critical speed. Hence, first of all, it follows that speed of a gas after a normal shock is always smaller than the critical speed ( $c_2 < a_*$ ).

Formulas (4-20) — (4-23) show that the intensity of a normal shock increases with an increase in speed of the undisturbed flow  $M_1$  (or  $\lambda_1$ ). The ratio of the densities at the maximum speed tends to a finite limit;

STOP HERE

STOP HERE

$$\lim_{\lambda_1^2 \rightarrow \frac{k+1}{k-1}} \frac{p_2}{p_1} = \frac{k+1}{k-1},$$

and the ratios of the pressures and temperatures increase infinitely.

It is necessary to bear in mind, however, that at high supersonic speeds, when as a result of shocks the temperature and pressure of gas increase very intensively, the obtained formulas are approximate, since they do not consider the developing dependence of the heat capacity on the temperature, the dissociation of the molecules, and deviation of properties of real gases from properties of a perfect gas, the state of which is described by equation (1-1).

Formulas of an oblique shock can be transformed to a form convenient for an analysis of the influence of physical properties of a gas (coefficient  $k$ ). For this purpose we shall introduce the dimensionless speed  $\xi = \frac{c}{c_{\max}}$  and will express the coefficient of the isentropic process in terms of the maximum speed  $\lambda_{\max}^2 = \frac{k+1}{k-1}$ .

$$k = \frac{\lambda_{\max}^2 + 1}{\lambda_{\max}^2 - 1}.$$

After replacing  $k$  in equations (4-13) and (4-14) by its value, we obtain:

$$\frac{p_2}{p_1} = \frac{\lambda_{\max}^2 - 1}{\lambda_{\max}^2} \cdot \frac{\sin^2 \beta}{\xi_1^2 - 1} - \frac{1}{\lambda_{\max}^2} \quad (4-13a)$$

and

$$\frac{p_2}{p_1} = \frac{\lambda_{\max}^2}{1 - \xi_1^2} \cdot \frac{1}{1 + \frac{\xi_1^2 \sin^2 \beta}{\xi_1^2 - 1}} \quad (4-14a)$$

The speed after the shock is expressed by the equation [formula (4-11b)]

$$\frac{\lambda_2^2}{\lambda_1^2} = \frac{\xi_2^2}{\xi_1^2} = \cos^2 \beta + f(\xi_1, \beta). \quad (4-11b)$$

where

$$f(\xi_1, \beta) = \frac{\frac{1}{\xi_1^2} - \cos^2 \beta}{\sin^2 \beta} \cdot \frac{1}{\lambda_1^2}.$$

As is evident, each of the presented formulas contains two cofactors, one of which depends only on  $\xi_1$  and  $\beta$  and does not depend on  $k$ , and the second is a function of only  $k$ .

Such structure of formulas of a shock makes it possible to evaluate approximately

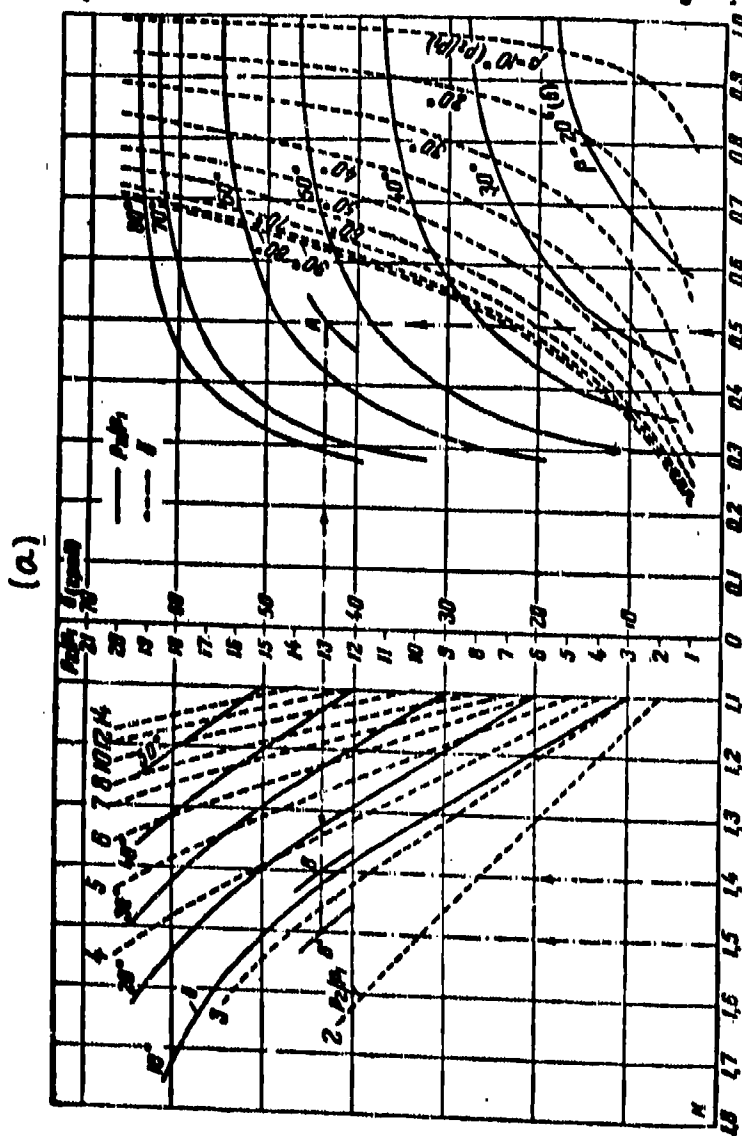


Fig. 4-6. Influence of coefficient  $k$  on intensity of an oblique shock.  
[KEY  $\alpha =$  (degrees).]

5  
4  
3  
2  
1  
0

STOP HERE

STOP HERE

the influence of change of physical properties of a gas and to make a calculation of the parameters of an oblique shock with different constant values of  $k^*$ .

For determining other parameters of the shock it is possible to use obvious relationships. Ratio of the temperatures

$$\frac{T_2}{T_1} = \frac{1 - \epsilon_1^2}{1 - \epsilon_2^2}$$

Angle of shock

$$\tau_{sh} = \left( 1 + \frac{1 - \epsilon_1^2}{\epsilon_1^2} \cdot \frac{1}{\sin^2 \theta} \right) \tau_{sh} - \epsilon_2 \frac{1}{\lambda_{max}}$$

For calculating shocks at different  $k$ , there can be constructed  $p_2/p_1$  graphs depending on  $\epsilon_1$ ,  $\beta$  (or  $\delta$ ) and  $k$  (Fig. 4-6). The influence of  $k$  can be evaluated with identical  $\beta$  or  $\delta$ . A comparison with identical  $\beta$  shows that with a decrease in  $k$  the intensity of the shock increases.

#### 4-3. Shock Polar (Curve)

The relationship between parameters in a shock can be presented graphically in a very convenient form. For this purpose let us consider the triangles of speeds in a shock (Fig. 4-7).

We shall locate the vector of speed prior to shock  $c_1$  along the x axis (sector OD). The sectors OF and FD are, respectively, the tangential  $c_t$  and the normal  $c_{n1}$  components of speed prior to shock. By knowing the angle of deflection of flow  $\delta$ , we draw the line of the

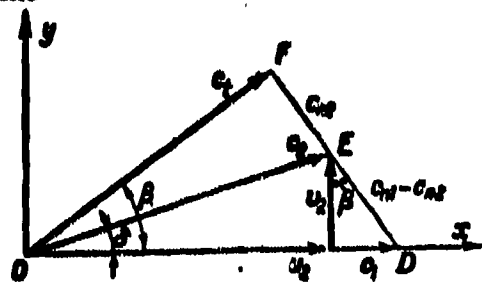


Fig. 4-7. Triangles of speeds on shock.

speed vector after the shock  $c_2$  up to the intersection with section FD. The

\*The formulas are given by M. V. Polikovskiy.

STOP HERE

STOP HERE

Intersection point (point E) determines value of vector  $c_2$ , and the sector EF expresses normal component of the speed after the shock.

The speed vector  $c_2$  can be presented by two other components:  $u_2$  and  $v_2$ . The components  $u_2$  and  $v_2$  are projections of  $c_2$  onto the direction of speed of flow before the shock and onto the normal to this direction.

We shall find the equation of the curve described by the end of speed vector after shock  $c_2$  with a constant value of the speed vector before the shock  $c_1$  and variable values of angle of change in direction of flow after shock  $\beta$ .

In expressing this equation in form of a relationship between  $u_2$  and  $v_2$ , we shall obtain a curve of speed after shock in the plane of hodograph of speed.

For obtaining the sought relationship we use the fundamental equation of an oblique shock (4-5). After substituting in this equation the values  $c_{n1}$  and  $c_t$  from formulas (4-12), we obtain:

$$c_1 \sin \beta \left( c_1 \sin \beta - \frac{v_2}{\cos \beta} \right) = a_1^2 - \frac{k-1}{k+1} c_1^2 \cos^2 \beta, \quad (4-25)$$

since (Fig. 4-5)

$$c_{n2} = c_{n1} - \frac{v_2}{\cos \beta}.$$

We transform equation (4-25) to the following form:

$$c_1^2 \cos^2 \beta \tan^2 \beta - c_1 v_2 \tan \beta = a_1^2 - \frac{k-1}{k+1} c_1^2 \cos^2 \beta.$$

Hence, bearing in mind that

$$\cos^2 \beta = \frac{1}{1 + \tan^2 \beta} \text{ and } \tan \beta = \frac{c_1 - u_2}{v_2},$$

we obtain:

$$\begin{aligned} c_1^2 (c_1 - u_2)^2 - c_1 (c_1 - u_2) [v_2^2 + (c_1 - u_2)^2] &= \\ &= a_1^2 [v_2^2 + (c_1 - u_2)^2] - \frac{k-1}{k+1} c_1^2 v_2^2. \end{aligned}$$

Finally,

$$v_2^2 = (c_1 - u_2)^2 \frac{a_1^2 - \frac{c_1^2}{2}}{\frac{a_1^2}{2} + \frac{k-1}{k+1} c_1^2 - a_1^2}. \quad (4-26)$$

Curve, corresponding to equation (4-26), presented in Fig. 4-8, is called a shock polar. The curve belongs to a class of hypocissoids. Shock polar can be widely used for calculating oblique shocks by the graphoanalytical method and for ascertaining certain peculiarities of such shocks.

We shall turn first of all to the limiting values  $v_2$ , being given by equation

STOP HERE

STOP HERE

(4-26).

It is readily seen that  $v_2 = 0$  at

$$u_2 = c_1$$

and

$$u_2 c_1 = a_*^2.$$

The first case ( $u_2 = c_1$ ) corresponds to a shockless process; an oblique shock wave transforms into a wave of weak disturbance (characteristic). Tangents to hypocissoid at the point D are located at an angle  $\alpha_{ml} = \arcsin \frac{1}{M_1}$  to the vector  $c_1$ .

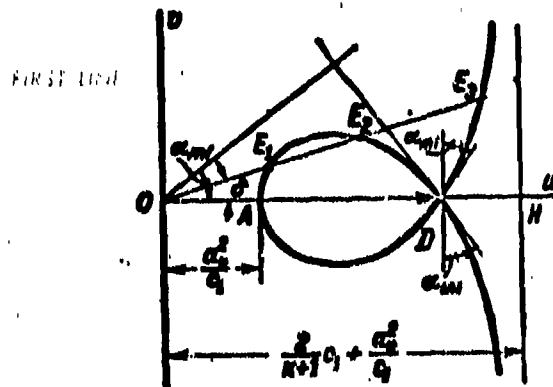


Fig. 4-8. Shock polar in plane of hodograph.

We note that this point is simultaneously a point of the diagram of characteristics and the shock polar here transforms into an epicycloid.

Second case ( $u_2 c_1 = a_*^2$ ) characterizes the transition of an oblique shock into a normal shock, the angle of which  $\beta = \frac{\pi}{2}$ . Point A corresponds to this case in the hypocissoid.

From equation (4-26) it follows that  $v_2$  can be reverted to infinity at

$$u_2 = \frac{2}{k+1} c_1 + \frac{a_*^2}{c_1}.$$

It is obvious that branches of the hypocissoid asymptotically approach the straight line drawn parallel to the  $y$  axis at a distance  $OH = \frac{a_*^2}{c_1} + \frac{2}{k+1} c_1$  from the origin of the coordinates. These branches have no physical meaning, since they give values of the speed after the shock (point  $E_3$  in Fig. 4-8) larger than prior to shock. A shock of rarefaction would correspond to such conditions, but shocks of rarefaction cannot exist. By discarding the outer branches of hypocissoid as physically unreal (see below), we note that the shock polar within the limits

between extreme points A and D gives two values for speed vector after the shock.  
FIRST LINE C.T. ILST

Usually plane shocks are realized at values of the speed vector of flow after a shock corresponding to the points  $E_2$  (Fig. 4-9,a). The second value of speed  $c_2$ , corresponding to the points  $E_1$ , in a plane shock may be realized only under special conditions.

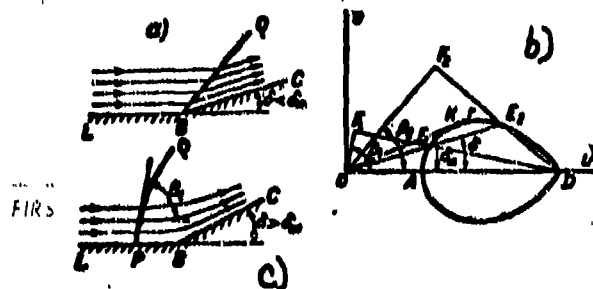


Fig. 4-9. Separation and distortion of compression shock.

We now consider a supersonic flow of gas along the wall LBC (Fig. 4-9a) gradually increasing the angle of deflection of flow  $\delta$  (angle of change in direction of wall at point B). At small values of  $\delta$ , close to zero, the disturbance of the flow is small and speed after the shock ( $c_2$ ) is close to the speed prior to shock ( $c_1$ ). According to the degree of increase of  $\delta$ , point  $E_2$  (Fig. 4-9,b) is displaced along the shock polar from D to  $E_2$ , where the point  $E_2$  gives a speed after the shock  $M_2 = 1$ . A subsequent very small increase in  $\delta$  brings the flow after the shock to a state determined by point K. Here the flow after the shock already is subsonic ( $M_2 < 1$ ) and  $\delta$  will attain the maximum value  $\delta_m$ .

In Fig. 4-10 there is presented flow around a wedge by a supersonic flow. If the half-aperture angle of wedge  $\delta$  is less than  $\delta_m$  for a given speed  $M_1$ , then on the tip of wedge there will occur two rectilinear oblique shocks: AB and AB<sub>1</sub>, forming the so-called head shock wave of wedge.

With a subsequent increase of the angle  $\delta > \delta_m$  the shock emerges from forward point and it is distorted (Fig. 4-9,c). This is explained by the fact that the speeds of the propagation of the disturbances become higher than the speed of flow. Actually, by increasing the angle of change in direction of wall  $\delta$ , we thereby

STOP HERE

STOP HERE

increase the compression of flow, i.e. its pressure, density and temperature. At the same time also the speed of propagation of disturbances, equal to speed of sound of disturbed flow  $a_2 = \sqrt{kgRT_2}$ , increases. At  $\delta > \delta_m$  this speed becomes higher than the speed of the flow and therefore the disturbances penetrate forward along the flow. However, with distance from the wall BC (Fig. 4-9,c) the pressure, density and temperature decrease at the same time, the speed of propagation of

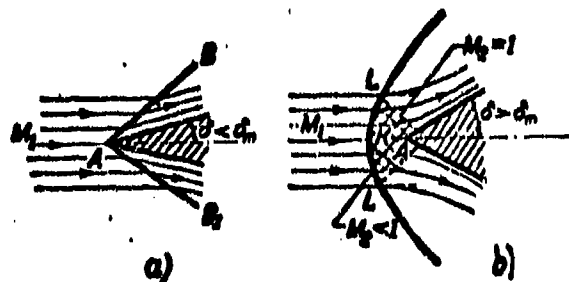


Fig. 4-10. Flow around wedge by a supersonic flow.

disturbances will decrease. At a certain distance from the wall there will occur the locus of points PQ (Fig. 4-9,c), in which the speed of propagation of disturbances decreases to the speed of the flow. Obviously, beyond the limits of this surface, the disturbances caused by wall cannot penetrate, since they will be moved forward by the flow. The surface PQ separates the zone of undisturbed flow from zone of disturbed flow and it is the receding shock wave.

Consequently, if  $\delta > \delta_m$ , then the plane oblique shock alternates with a curved shock (4-10), that is located not at the tip of wedge but at a certain distance before it. This distance depends on speed of undisturbed flow  $M_1$  and  $\delta$ . With an increase in  $M_1$ , the shock approaches the tip of body. With an increase of angle of deflection at  $\delta > \delta_m$  the shock withdraws from the body.

The flow around rounded tip of body by a supersonic flow always will occur with the formation of a curved bow wave, detached from the tip, and the distance between wave and tip for central line of flow will depend on the speed  $M_1$  and on the shape of the tip.

We note that at  $\delta = \delta_m$  the flow after the shock is subsonic and  $M_2$  is somewhat



less than unity (point K in Fig. 4-9,b). Since for a neutral line of flow branching at point A (Fig. 4-10),  $\beta = \frac{\pi}{2}$  and  $\delta = 0$ , then element of the shock intersecting this line must be a straight line. The speed of flow after element of direct shock will be determined by point A on shock polar (Fig. 4-9b). The flow after the shock on this line of flow is always subsonic.

All sectors of the shock, except the central, are located at different angles to the vector of speed of undisturbed flow  $\beta_1 < \frac{\pi}{2}$ .

In considering such a distorted bow wave, consisting of large number of small rectilinear elements, one may be convinced that as the distance from the central line of flow increases, the angle of slope of elements of shock  $\beta_1$  increases. Here it is possible to use a shock polar for calculating the flow after the shock for each streamline individually. To the sector of bow wave KL there correspond points of the shock polar from A to  $\underline{r}$ , in which speed  $M_2 = 1$ . In this sector the flow after the curved shock will be subsonic. Consequently, if the bow wave is detached from body, then in a certain region adjacent to tip of body the flow will be subsonic (this region in Fig. 4-10,b is hachured), and the lines of flow here will have a different curvature. At various points after the shock the pressures will be different.

With increasing distance from the point  $\underline{K}$ , there decreases the slope of shock elements and, at the same time, the shock intensity decreases. At a certain point L the speeds after the shock become sonic. Above this point, the state after the shock is determined by the sector of shock polar from  $\underline{r}$  to D. At an infinite distance from the body, a curved shock degenerates into a weak wave of compression to which the point D on shock polar corresponds.

Thus, if there occurs a distortion and separation of shock from tip of body, then each point of shock polar characterizes the state after the shock only for one line of flow, and not for entire region of flow, as takes place in the case of a plane shock. Consequently, not one point of the hypocissoid, but its entire branch

AD, corresponds to a curvilinear shock.

In the Table 4-1  $\theta_m$  values for two values of  $k = 1.4$  and  $1.3$  are presented. The  $\theta_m$  values depend on  $M_1$  ( $\lambda_1$ ) number and the physical properties of the gas ( $k$ ) and they may be determined by equation (4-17) under the condition of substituting in it  $\beta = \beta_m$  from equation (4-18).

TABLE 4-1

Values of Maximum Angles of Deflection of Flow in a Plane Oblique Compression Shock.

$\lambda_1$	$k = 1.4$	$k = 1.3$	$\lambda_1$	$k = 1.4$	$k = 1.3$
	$\theta_m$	$\theta_m$		$\theta_m$	$\theta_m$
1	0	0	1.7	25°13'	24°42'
1.2	5°25'	5°14'	1.8	28°55'	28°18'
1.3	9°41'	9°30'	1.9	32°00'	31°30'
1.4	13°55'	13°24'	2.0	35°00'	34°18'
1.5	18°00'	17°30'	2.2	40°15'	39°40'
1.6	21°41'	21°15'	2.4	45°00'	43°50'

#### 4-4. Variation of Entropy in Shock.

As it is known from thermodynamics, for an elementary process without heat exchange with the environment, taking place in a perfect gas, the change of entropy is determined by the equation  $ds = c_p \frac{dT}{T} - R \frac{dp}{p}$ ;

since

$$\frac{dT}{T} = \frac{dp}{p} - \frac{dp}{\rho},$$

then

$$ds = (c_p - R) \frac{dp}{p} - c_p \frac{dp}{\rho} = \frac{R}{k-1} \left( \frac{dp}{p} - k \frac{dp}{\rho} \right).$$

By integrating this equation, we obtain

$$\Delta s = \frac{R}{k-1} \left( \ln \frac{p_2}{p_1} + k \ln \frac{\rho_1}{\rho_2} \right),$$

or

$$\Delta s = \frac{R}{k-1} \ln \frac{p_2}{p_1} \left( \frac{\rho_1}{\rho_2} \right)^k. \quad (4-27)$$

STOP HERE

STOP HERE

For a reversible (isentropic) process  $\Delta s = 0$  and

$$\frac{P_2}{P_1} \left( \frac{\rho_1}{\rho_2} \right)^k = 1.$$

We shall examine how the entropy varies during a transition through a shock wave. After eliminating from equations (4-13) and (4-14)  $M_1^2 \sin^2 \beta$ , we obtain:

$$\frac{P_2}{P_1} = \frac{1 - \frac{k+1}{k-1} \frac{P_2}{P_1}}{\frac{P_2}{P_1} - \frac{k+1}{k-1}} \quad (4-28)$$

By making a calculation, it is readily verified that for a compression shock for which  $\frac{P_2}{P_1} > 1$ , always

$$\frac{P_2}{P_1} > \left( \frac{\rho_2}{\rho_1} \right)^k$$

and, consequently, according to (4-27) in the transition through a shock the entropy of the gas increases.

An increase of entropy during transition through a shock is explained by the irreversible character in the change of state of gas in the shock, by the "shock" character of the process. As a result of such a process, part of the kinetic energy of gas irreversibly changes into heat; if there is no energy exchange with the environment the internal energy of the flow irreversibly increases. The curve characterizing the process, proceeding according to equation (4-28), is called the shock adiabat.

For expansion shock  $\frac{P_2}{P_1} < 1$  and  $\frac{P_2}{P_1} \left( \frac{\rho_1}{\rho_2} \right)^k < 1$  we obtain  $\Delta s < 0$ , which is impossible if there is no energy exchange with the environment, since it contradicts the second law of thermodynamics. It follows from this that an expansion shock cannot appear in a flow without energy exchange with environment, since this would contradict second law of thermodynamics. It follows from this that an expansion in a Chapter 3, in a supersonic flow the wave of rarefaction with continuous drop in pressure is an absolutely stable phenomenon; entropy in the transition through such wave is kept constant.

The change of entropy in a compression wave can be expressed in terms of the parameters  $M_1$  and  $\beta$  by substituting in equation (4-27)  $\frac{P_2}{P_1}$  and  $\frac{\rho_2}{\rho_1}$  per formulas (4-13) and (4-14); then

STOP HERE

STOP HERE

$$\Delta s = \frac{R}{k-1} \ln \left[ \left( \frac{k-1}{k+1} \right)^{k+1} \left( \frac{2k}{k-1} M_1^2 \sin^2 \beta - 1 \right) \times \right. \\ \left. \times \left( \frac{2}{k-1} \frac{1}{M_1^2 \sin^2 \beta} - 1 \right)^k \right]. \quad (4-29)$$

Equation (4-29) makes it possible to conclude that a change in entropy in an oblique shock depends on speed of the undisturbed flow  $M_1$  and angle of the oblique shock  $\beta$ . With a constant speed  $M_1$  the entropy in the transition through shock varies in accordance with the change of angle  $\beta$ . If the shock is rectilinear and, consequently, along the shock  $\beta$  maintains a constant value, then for all lines of flow crossing the shock the change in entropy will be identical. If, however, the shock is curved, then the increase in entropy for each line of flow will be different, since along the shock the angle  $\beta$  varies. This means that after curved shock the flow will be vortical; after a normal shock the flow remains potential.

By using equation (4-28), it is possible to consider the change of state of gas during transition through a weak shock. By assuming  $p_1 = p$ ,  $\rho_1 = \rho$  and that the pressure and density in the shock change by an infinitesimally small value, i.e.,

$$p_2 = p + dp; \quad \rho_2 = \rho + d\rho;$$

from (4-28) we obtain:

$$\frac{p + dp}{p} = \frac{\rho^{\frac{k+1}{k-1}} (\rho + d\rho)}{(\rho + d\rho)^{\frac{k+1}{k-1}} \rho}.$$

Hence, by disregarding infinitesimally small terms of second order, we arrive at the equation of the isentropic process:  $\frac{dp}{p} = k \frac{d\rho}{\rho}.$

Thus, the change of state in a shock of infinitesimally small intensity (weak shock) is isentropic.

#### 4-5. Compression Shock Losses. Constructing the Process on a Total Heat-Entropy (i-s) Diagram. Compression Shocks in a Real Gas.

We now consider in greater detail the energy transformations in shocks. In

assuming a flow without an energy exchange with the environment, we conclude that the total energy of flow during transition through the shock does not change. This means that

$$\frac{c_1^2}{2} + \frac{k}{k-1} \frac{p_1}{\rho_1} = \frac{c_2^2}{2} + \frac{k}{k-1} \frac{p_2}{\rho_2},$$

or by using parameters of total stagnation,

$$\frac{p_{01}}{\rho_{01}} = \frac{p_{02}}{\rho_{02}}. \quad (4-30)$$

Condition (4-30) can be replaced by an equivalent condition of constancy of enthalpy of stagnation during transition through a shock:

FIRST LINE OF THIS

$$i_{01} = i_{02} = i_0. \quad (4-30a)$$

or at

$$\left. \begin{aligned} c_p &= \text{const}; \\ T_{01} &= T_{02} = T_0. \end{aligned} \right\} \quad (4-30b)$$

By bearing in mind these conditions, let us consider the process of a shock in an  $i$ - $s$  diagram (Fig. 4-11). By knowing pressure of stagnation prior to shock and the enthalpy of stagnation  $i_0$ , we shall find in the  $i$ - $s$  diagram the point  $O_1$ , characterizing state of an isentropically stagnated gas prior to shock. By the known speed of flow prior to shock  $c_1$  or the pressure  $p_1$  we find the point D, which determines the state of moving gas ahead of the shock. In a shock the static pressure of the flow increases to  $p_2$ . If there is known the angle of deflection of flow and, consequently,  $\beta$ , then the state of the gas behind the shock is defined (point  $E_2$  in Fig. 4-11), since by formula (4-29) there can be found the increment of entropy  $\Delta s^*$ . We note that the line connecting points D and  $E_2$  in Fig. 4-11 does not characterize the change of state of gas in a shock, since in a total heat-entropy diagram the nonquasistatic processes can be presented only by the initial and terminal points of the process.

If the flow behind the shock is isentropically stagnated, then the state of

\*A perfect gas is considered.

STOP HERE

STOP HERE

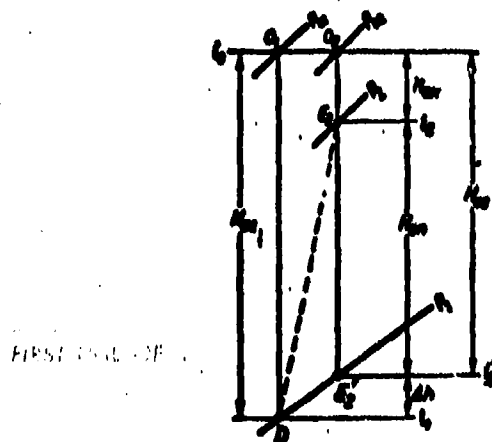


Fig. 4-11. Compression shock in a thermal diagram.

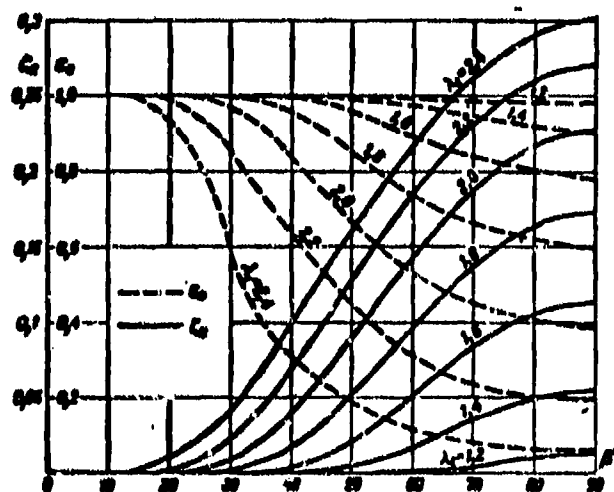


Fig. 4-12. Loss factors and the relation of stagnation pressures in a shock, depending on the angle  $\beta$  and the speed of undisturbed flow.

STOP HERE

STOP HERE

total stagnation is characterized by the point  $O_2$ , at which there readily is found the value  $p_{O2}$ . If we now grant the flow the possibility of being isentropically expanded down to pressure before the shock, then its state will be determined by point  $E'_2$ . The speed of gas here can be calculated by the equation of energy:

$$\frac{Ac_2^2}{2g} = i_0 - i'_2 = H_{02} \text{ Kcal/Kg}$$

where  $H_{02}$  is the isentropic drop of the enthalpies behind the shock.

The magnitude  $H_{02}$  can be considered as the sum

$$H_{02} = H_{0k} + H_{0n}$$

where  $H_{0k}$  is the kinetic energy of flow behind shock:

$$H_{0k} = \frac{Ac_2^2}{2g};$$

$H_{0n}$  is the change of potential energy of flow in the shock:

$$H_{0n} = \frac{A(c_1^2 - c_2^2)}{2g}.$$

It is obvious that

$$H_{0k} < H_{0n}$$

where  $H_{01} = \frac{Ac_1^2}{2g}$  is the isentropic drop of enthalpies before shock.

The losses of kinetic energy in the shock will be:

$$\Delta h = H_{01} - H_{02} = \frac{A}{2g} (c_1^2 - c_2^2),$$

where  $\Delta h$  readily is determined by an total heat-entropy (i-s) diagram as the difference of the enthalpies  $i'_2 - i_1$ .

The loss of energy is readily associated with the main parameters of the shock.

We shall express

$$H_{01} = \frac{Ak}{k-1} \frac{p_{01}}{\gamma_{01}} \left[ 1 - \left( \frac{p_1}{p_{01}} \right)^{\frac{k-1}{k}} \right] = i_0 - i_1$$

and

$$H_{02} = \frac{Ak}{k-1} \frac{p_{02}}{\gamma_{02}} \left[ 1 - \left( \frac{p_2}{p_{02}} \right)^{\frac{k-1}{k}} \right] = i_0 - i'_2.$$

Consequently,

$$\Delta h = \frac{Ak}{k-1} \frac{p_{01}}{\gamma_{01}} \left[ \left( \frac{p_1}{p_{01}} \right)^{\frac{k-1}{k}} - \left( \frac{p_2}{p_{02}} \right)^{\frac{k-1}{k}} \right] = i'_2 - i_1, \quad (4-31)$$

since

$$\frac{p_{01}}{\gamma_{01}} = \frac{p_{02}}{\gamma_{02}}.$$

We shall introduce the concept of loss factor of energy in a shock:

$$\zeta = \frac{\Delta h}{H_{01}} = 1 - \frac{H_{02}}{H_{01}}; \quad (4-32)$$

then after substituting  $H_{01}$  and  $H_{02}$  we obtain:

$$\zeta = \frac{2}{k-1} \frac{1}{M_1^2} \left[ \left( \frac{p_2}{p_{01}} \right)^{\frac{k-1}{k}} - 1 \right], \quad (4-33)$$

STOP HERE

or by means of (2-21)

$$\zeta_0 = \left[ \frac{k+1}{k-1} \frac{1}{\lambda_1^2} - 1 \right] \left[ \left( \frac{P_{01}}{P_{02}} \right)^{\frac{k}{k-1}} - 1 \right]. \quad (4-33a)*$$

The ratio  $\frac{P_{01}}{P_{02}} = \pi_0$  characterizes the change of pressure of total stagnation in a shock. This magnitude can be presented as a function of the parameters of a shock  $M_1$  and  $\beta$ .

Since 
$$\frac{P_{01}}{P_1} = \frac{P_1}{P_2} \frac{P_{02}}{P_2},$$

then from (4-13) and Table 2-1 we obtain:

$$\frac{P_{01}}{P_1} = \frac{k-1}{k+1} \left( \frac{2k}{k-1} M_1^2 \sin^2 \beta - 1 \right) \left( 1 + \frac{k-1}{2} M_1^2 \right)^{\frac{k}{k-1}}. \quad (4-34)$$

Hence by means of (4-11a) we obtain:

$$\pi_0 = \frac{\left( \frac{k+1}{k-1} \right)^{\frac{k}{k-1}} (M_1^2 \sin^2 \beta)^{\frac{k}{k-1}}}{\left( M_1^2 \sin^2 \beta + \frac{2}{k-1} \right)^{\frac{k}{k-1}} \left( \frac{2k}{k-1} M_1^2 \sin^2 \beta - 1 \right)^{\frac{1}{k-1}}}. \quad (4-35)$$

We present, depending on the same parameters of the shock, the loss factor in the shock  $\zeta_0$ , by using formulas (4-33) and (4-35):

$$\zeta_0 = \frac{2}{k-1} \frac{1}{M_1^2} \left[ \left( \frac{k-1}{k+1} \right)^{\frac{k}{k-1}} \left( \frac{2k}{k-1} M_1^2 \sin^2 \beta - 1 \right)^{\frac{1}{k-1}} \times \right. \\ \left. \times \left( 1 + \frac{2}{k-1} \frac{1}{M_1^2 \sin^2 \beta} \right) - 1 \right]. \quad (4-36)$$

After replacing the number  $M_1$  by  $\lambda_1$  in formula (2-21), we shall obtain a relationship in the form of:  $\zeta_0 = \varphi(\lambda_1, \beta)$ .

In Fig. 4-12 there is presented a graph of  $\pi_0$  and  $\zeta_0$  in an oblique shock, depending on the angle  $\beta$  and dimensionless speed of undisturbed flow  $\lambda_1$  for  $k = 1.3$ . From the graph it is clear that the loss factor intensively increases with an increase in the angle of oblique shock and with an increase of speed  $\lambda_1$ , attaining a maximum at  $\beta = \frac{\pi}{2}$  (normal shock).

\*From formula (4-33a) it follows that the loss factor  $\zeta_0 = 0$  at  $\lambda_1 = 1$ . If  $\lambda_1 = \lambda_{1\max} = \sqrt{\frac{k+1}{k-1}}$ , then formula (4-33a) gives an indetermination which readily is expanded.

STOP HERE

STOP HERE



During flow around a body by a supersonic flow, before body there appears a shock wave (compression shock); during transition through this wave, the entropy of gas increases, and the speed decreases.

Thus, in a supersonic flow of an ideal fluid there appears a special form of resistance — wave drag, depending on the losses in shocks and consequently on the form and intensity of the shocks. As we have seen, the form of the shock and its intensity depend on the shape of the body and speed of the streamline flow. In considering that with a decrease in the angle of deflection  $\alpha$  (and, consequently,  $\beta$ ) losses in the shock decrease, it may be concluded, that cusped bodies in a supersonic flow should possess a smaller resistance than round bodies.

The change of losses in shocks depending on their intensity can be traced in a thermal diagram. The construction of a "shock polar" in a thermal diagram is conveniently made in the following manner.\*

According to the parameters before shock  $p_1$  and  $T_1$  we find the point D (Fig. 4-13) and at a known speed  $c_1$ , the point  $O_1$ . We are given a number of values of  $\beta$  from  $\beta = \alpha_{m1} = \arcsin \frac{1}{M}$  to  $\beta = \frac{\pi}{2}$ . For each value of  $\beta$  we determine  $\frac{p_2}{p_1}$  and  $\frac{T_2}{T_1}$ , and plot on the total heat-entropy (i-s) diagram the points  $E'_2, E''_2$ , etc., up to point A, which corresponds to a normal shock. The locus of these points gives the state of gas in total heat-entropy coordinates, corresponding to a shock polar. We note that the obtained curve should be tangent to line of isentropic change of state  $O_1D$ , since during infinitesimally small disturbances of the flow the entropy of the gas remains constant.

For each point of curve (for example,  $E''_1$ ) there readily are determined: the kinetic energy behind shock  $H_{02} = \frac{\rho_2 c_2^2}{2g}$ , the change of potential energy in shock  $H_{01}$  and the losses of kinetic energy  $\Delta h$ . At the same time here one can determine

\*The corresponding curve in the total-heat entropy (i-s) diagram can be called a "shock polar" only conditionally, since it is not a vector curve. The presented construction is valid for an ideal gas.



Such diagrams make it easy to determine characteristics of a shock on the basis of two given parameters. In the supplement there are given diagrams of oblique shocks for  $k = 1.3$  and  $k = 1.4$ .\*

The method of using a diagram of oblique shocks is explained in Fig. 4-14. In upper right quadrant of diagrams there are plotted the graphs  $\delta = \delta(\beta)$  and  $\frac{p_2}{p_1} = \bar{p}(\beta)$ , corresponding to different but constant values of speed before shock  $\lambda_1$ . On each curve there is inscribed the value  $\lambda_1$ , in parentheses there is indicated the magnitude expressed by the given curve. In left upper quadrant there are presented graphs  $\delta = \delta(\lambda_1)$  and  $\frac{p_2}{p_1} = \bar{p}(\lambda_1)$  for different but constant values of  $\lambda_1$ . In lower left quadrant there is given the dependence of ratio of temperatures in shock on speed behind shock  $\frac{T_2}{T_1} = \bar{T}(\lambda_1)$ . In the lower right quadrant there are drawn curves of loss factors of energy in shock  $\zeta_e = \zeta_e(\beta)$  and the recovery factors of the pressures  $\epsilon_r = \epsilon_r(\beta)$ . Thus, as a parameter for all curves of the diagram there was selected the speed of flow before the shock  $\lambda_1$ .

We shall explain in an example the method of using the diagram. We assume that we know the angle of deflection  $\delta$  of a line of flow and speed of flow before the shock  $\lambda_1$ . On the curve  $\delta = \delta(\beta)$  we find the point A corresponding to the given value of  $\lambda_1$ . By projecting this point onto the horizontal axis, we shall find at point  $A_1$  the angle of the oblique shock  $\beta_1$ . On curve  $\frac{p_2}{p_1} = \bar{p}(\beta)$ , corresponding to the same value  $\lambda_1$ , we obtain the point  $A_2$ , which determines the ratio of the densities  $\rho_2/\rho_1$ . Knowing  $\lambda_1$  and  $\delta$ , on curve  $\delta = \delta(\lambda_1)$  in the left quadrant we find the point  $B_1$ , which determines dimensionless speed behind the shock  $\lambda_2$ . Proceeding with the same value of  $\lambda_1$  to the curve  $\frac{p_2}{p_1} = \bar{p}(\lambda_1)$ , we obtain at point  $B_2$  the ratio of pressures in the shock  $\frac{p_2}{p_1}$ . At point C on the curve  $\frac{T_2}{T_1} = \bar{T}(\lambda_1)$  we determine the ratio of the temperatures  $\frac{T_2}{T_1}$ . By projecting the point  $A_1$  onto the lines  $\zeta_e = \zeta_e(\beta)$  and  $\epsilon_r = \epsilon_r(\beta)$  at points  $D_1$  and  $D_2$ , we shall find the values of the coefficient

\*A. Ye. Zaryankin calculated the shock diagrams.

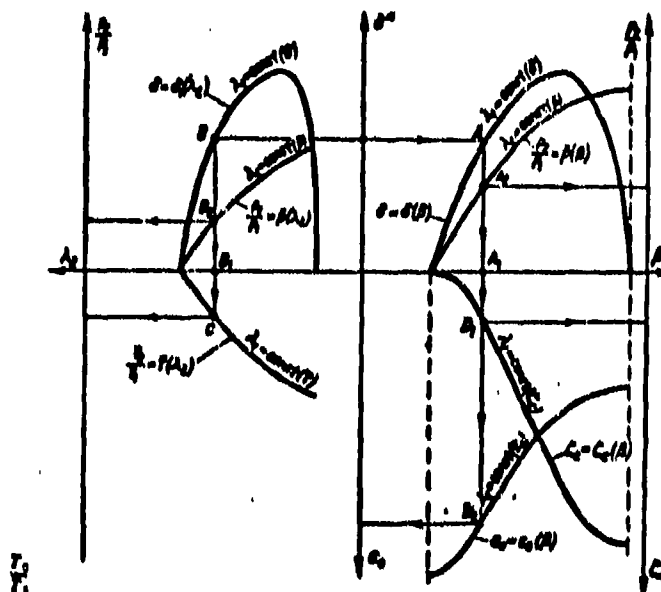


Fig. 4-14. Method of using diagram of oblique shocks.

of energy losses and the pressure recovery factor. The considered diagram makes it possible to calculate the shock by any two parameters. Thus, for example, the given parameters may be  $\lambda_1$  and  $\beta_1$ ,  $\frac{p_2}{p_1}$  and  $\beta_1$ , and  $\beta_1$  and  $\beta_2$ , et cetera.

The thermal diagram is convenient for calculating a compression shock in a real gas and, in particular, in moist vapor and dissociating air. Parameters of the flow before the shock and the angle of deflection in a shock usually are known. Being given a number of values of the shock angle, it is simple to find the corresponding values of normal components of the speed:

$$c_{n1} = c_1 \sin \beta_1; \quad c_{n2} = \frac{c_1 \cos \beta_1}{\sqrt{\gamma(\beta_1 - \beta_2)}}.$$

By the fundamental equations (4-1)---(4-4) there are determined parameters behind the shock  $i_{21}$ ,  $p_{21}$  and specific volume  $v_{21}$ , corresponding to the current value  $\beta_1$ . The sought solution can be found on a total-heat-entropy ( $i-s$ ) diagram at the point of intersection of two curves, one of which is constructed on the basis of the parameters  $i_{21}$ ,  $p_{21}$ , and the second by  $i_{21}$ ,  $v_{21}$  (Fig. 4-13,a). From the diagram are taken the values of  $i_2$ ,  $p_2$ ,  $v_2$ ; real slope angle of the shock is determined by

the formula

$$\tan \beta = \frac{\bar{v}-1}{2 \tan \delta} \pm \sqrt{\left(\frac{\bar{v}-1}{2 \tan \delta}\right)^2 - \bar{v}}$$

where  $\bar{v} = \frac{v_1}{v_2}$ .

This problem is solved by means of an auxiliary graph, on which there will be plotted the curves  $v'_{21}(\beta_1)$  and  $v_{21}(\beta_1)$  (Fig. 4-13b). For constructing the second curve, it is necessary on a total-heat-entropy ( $i-s$ ) diagram to convert from values  $p_2$  and  $i_2$  to values  $v'_2$ . The solution is obtained at the point intersection of these curves, where there are determined  $v_2$  and  $\beta$  and correspondingly all the remaining parameters behind the shock. In particular, the speed behind the shock

$$c_2 = \frac{c_1}{v} \frac{\sin \beta}{\sin(\beta - \delta)}.$$

#### 4-6. Intersection of Shocks.

We now consider certain practically important cases of the interaction shocks.

Two consecutive changes in direction of wall ABCD (Fig. 4-15,a) at angle  $\delta$  result in the formation of the two oblique shocks: BK and CK. The angle of the second shock  $\beta_2 > \beta_1$ , since after the first shock the flow has a speed  $\lambda_2 < \lambda_1$ . As a result, the shocks intersect at point K. After the intersection point both shocks merge into one shock KF. The streamline intersecting a system of two shocks is deformed as it turns at points  $b$  and  $d$  at an angle  $\delta$ ; at the intersection of the shocks the speeds of the flow decrease and the pressure increases intermittently.

Considering the streamline KH and assuming that penetration of particles of gas from region 4 into region 3' and, conversely, from region 3' into region 4 does not occur, it may be concluded that in the indicated regions the pressures and directions of the speeds should be identical (a transverse pressure gradient is absent). But if it is assumed the direction of the streamline behind shock KF is the same as behind the second shock CK, i.e., that the total deflection of the streamline amounts to  $2\delta$ , then pressure in regions 3 and 3' will be different, since the streamline  $bd$  has passed through two shocks and the streamline KH only

through one shock. Consequently, the loss in the first case will be less than in

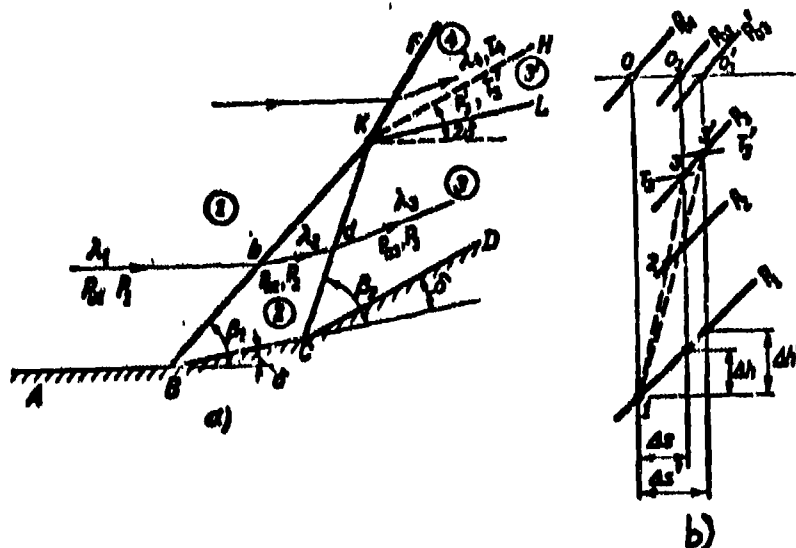


Fig. 4-15. Interaction of two successively distributed oblique shocks.

the second (during compression with an infinite number of shocks of infinitesimally small intensity the process will be isentropic—without losses), where  $p_2$  may be smaller or larger than  $p'_3$ . Hence, it may be concluded that regions of flow 3 and 3' are divided by a weak wave of rarefaction or a weak shock wave KL, at the intersection of which the flow acquires a pressure  $p_4 = p'_3$ . The intensity of the wave KL on this assumption readily is determined. Actually, knowing the angle  $\delta$  and  $\lambda_1$ , we find the pressure  $p_4$  behind the shock KF. We know the pressure  $p_3$  as a result of calculating the shocks BK and CK. The ratio  $\frac{p_4}{p_3}$  gives the intensity of the reflected wave KL.

In a general case the angle of deflection of flow at points B and C may be non-identical. Depending on the relationship between angles  $\delta_1$  and  $\delta_2$  ( $\delta_1$  —deflection in the first shock BK and  $\delta_2$ , the deflection in the second shock CK) and total angle of deflection  $\delta_1 + \delta_2$ , the intensity of reflected wave KL and also total losses in considered system of shocks vary. Calculations indicate that the intensity of reflected wave KL, as a rule, is small; and therefore a change in direction of the flow in this wave is negligibly small. This makes valid the assumption about

the change in direction of flow in wave KF by an angle  $\delta_1 + \delta_2$ .

Depending on the speed of undisturbed flow and total angle of deflection  $\delta_1 + \delta_2$ , also the sign of wave KL changes.

It is characteristic that the speed behind the shock KF is always smaller than speed behind the shock CK ( $\lambda_4 < \lambda_3$ ); it follows from this that the line KH is line of tangential discontinuity of the speed. In a viscous fluid along KH there is developed a vortex motion.

The change of state of gas along a streamline during transition through the considered system of shocks can be presented in a thermal diagram (Fig. 4-15,b). At point 2 there is determined the state of gas behind the first shock, and at point 3--after the second shock, since the angles  $\beta_1$  and  $\beta_2$  are known. There readily are determined also all the parameters behind the shocks:  $p_3$ ,  $T_3$ ,  $\lambda_3$ , and the parameters of the stagnation  $p_{03}$ ,  $p'_{03}$ .

Point 3' on the isobar  $p_3$  gives the state of gas behind the shock KF\*. At point 0'\_3 we find pressure of stagnation behind the shock KF,  $p'_{03} < p_{03}$ . The losses of energy in the shock KF are higher than the total losses in the shocks BK and CK, i.e.,  $\Delta s' > \Delta s$ . Thus, with given limits of changes in pressures, the stagnation of flow by one shock causes a larger loss of energy than in case of successive stagnation by two successive shocks.

A limiting case is the stagnation of flow along a smooth concave wall, at each point of which flow experiences a deflection at a small angle  $d\delta$  (Fig. 4-16). Here along the wall there will be formed a compression wave consisting of infinite set of characteristics of compression. The motion of a gas through such a compression wave is accomplished with a constant entropy. However, a smooth isentropic stagnation here can occur only in layer of gas adjacent to wall. As a

---

\*In constructing the process on a total-heat-entropy ( $i-s$ ) diagram we assume  $p_2 \approx p'_2$ .



7

1



waves can be either compression waves or waves of rarefaction.

Different from the considered case is the case of the intersection two oblique shocks shown in Fig. 4-17. The oblique shocks appear as a result of a change in direction of the two opposite walls of channel at different angles  $\delta_1$  and  $\delta_2$ . The directions of the flow in zones II and III will be nonidentical: in zone III, the deflection will be larger by an angle  $\delta_1 - \delta_2$ . The parameters of the flow after oblique shocks AB and A<sub>1</sub>B readily may be determined by known parameters before the shocks  $\lambda_1$ ,  $p_1$ ,  $T_1$  and the angles  $\delta_1$  and  $\delta_2$ , if these angles are smaller than the corresponding maximum value  $\delta_{m1}$  for the given vector of the speed  $\lambda_1$ .

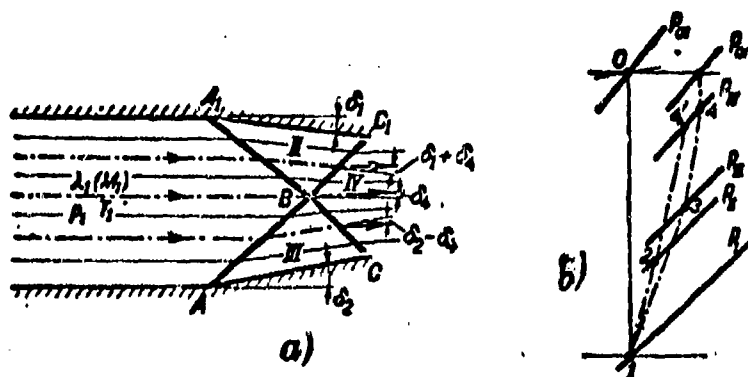


Fig. 4-17. Diagram of the intersection of two oblique shocks.  
a--normal intersection; b--process in shocks in a thermal diagram.

Parameters of flow in region IV can be found by proceeding from boundary conditions for a line of flow passing through the point B. We assume that the directions of speeds and pressures at all points of region IV will be identical. Hence, there is determined the angle between vector of speed in zone IV and the vector  $\lambda_1$ . Actually, if the resultant deflection of flow in zone IV is designated  $\delta_4$ , then from a consideration of Fig. 4-17 it is readily established that the deflection of flow at the intersection of shock BC<sub>1</sub> is equal to  $\delta_1 + \delta_2$ , and at the intersection of BC it is  $\delta_1 - \delta_2$ . Being given different values of the

pressure in zone IV ( $p_{IV}$ ) by formulas (4-13) and (4-17) or by diagrams of oblique shocks, we find the slope angles of shocks, BC and  $BC_1$  and angle of deflection of flow  $\delta_1 + \delta_4$  and  $\delta_2 - \delta_4$ . The value  $p_{IV}$ , at which magnitudes of  $\delta_4$  determined by parameters of zones II and III will be identical, can be found after constructing the dependence of  $\Delta BC_1$  and  $\delta_{\Delta BC}$  on  $p_{IV}$ . The intersection point of these curves will give the sought value  $\delta_4$ . Knowing the magnitude  $\delta_4$ , we find angles of the oblique shocks  $\beta_{BC_1}$  and  $\beta_{BC}$ .

A change in the state of the gas along two streamlines crossing zones II and III in thermal diagram is shown in Fig. 4-17,b. The total increment of entropy for these lines of flow will be identical only in those cases when  $\delta_1 = \delta_2$ . If intensity of the shocks AB and  $A_1B$  is different, then the increment of the entropy along considered line of flow will be different (point 4 and 4' in Fig. 4-17,b). If at all points of zone IV the pressures are identical, the speeds, temperatures and densities behind the shocks  $BC_1$  and BC will be different. Along the line of flow passing through the point B there will be formed tangential discontinuity of the speeds, as a result of which in a viscous gas there appears a vortex.

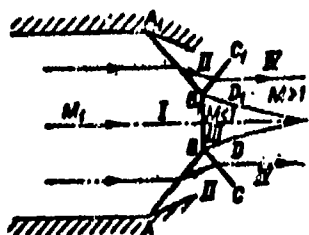


Fig. 4-18. A Bridge-like Shock.

The stable existence of a system two intersecting oblique shocks is not possible under all conditions. If angles of the second shocks  $\beta_{BC}$  and  $\beta_{BC_1}$  are larger than corresponding values of  $\beta_m$ , the character of the flow changes. Near the neutral line of flow passing through point B

there will form a curved shock. A system

of intersecting normal oblique shocks transforms into a bridge-like shock (Fig. 4-18). Here losses of energy in the flow increase.

#### 4-7. Stepwise Deceleration of Flow

FIRST SHOCK

Stepwise deceleration of flow can be obtained by applying different systems of oblique shocks. In the preceding section it was shown that if within given limits of the changes of static pressure the number of oblique shocks is increased by means of increasing successive changes in direction of wall, then, the deceleration of flow will be smoother, and the total relative losses will decrease. Usually after the last oblique shock there is a normal shock in which there occurs a transition to a subsonic speed.

Deceleration of flow in different systems of shocks was investigated in detail by G. I. Petrov and Ye. P. Ukhov. By following the basic conclusion of this work, we shall examine the particular case of stagnation of flow in two shocks -- oblique and normal.

The considered problem is formulated thus: to determine the angle of slope of first--an oblique--shock, with which the transition from a given supersonic speed to subsonic occurs with minimum losses (Fig. 4-19). The calculation of such a system can be realized in sequence by applying diagram of oblique shocks (See Appendix). With a given speed of the undisturbed flow  $\lambda_1$  and a selected value of angle  $\delta$  (or  $\beta_1$ ) there readily are determined the speed  $\lambda_2$  and pressure  $p_2$  after an oblique shock. The corresponding loss of energy  $\zeta_e$  or change in pressure of the total stagnation  $\epsilon_{\Sigma}$  also is determined by diagram of oblique shocks (or by formulas in Sec. 4-5).

Analogously there can be found the speed and static pressure after a normal shock ( $\lambda_2$  and  $p_2$ ) and coefficient of loss of energy  $\zeta_e$  (or  $\epsilon_{\Sigma}$ ).

As example, in Fig. 4-19 there is shown the change of speed of flow and the loss factors in a system of oblique and normal shocks, depending on the angle  $\beta_1$ , for  $\lambda_1 = 2.0$  ( $k = 1.3$ ). The curves indicate that for a given speed  $\lambda_1$  there is a most advantageous combination of oblique and normal shocks with which the total losses will be the minimum.

Actually, with an increase in angle of an oblique shock  $\beta_1$  the loss factor  $\zeta_{c1}$  increases in an oblique shock and the speed after an oblique shock  $\lambda_1$  decreases. It is obvious that at  $\delta = 0$  and  $\beta_1 = \alpha_{m1} = 22^\circ 45'$  (for  $\lambda_1 = 2.0$ ), an oblique shock transfers to the characteristic. In this case  $\zeta_{c1} = 0$ . The limiting value of the angle  $\beta_1$ , with which there still is possible the existence of a plane oblique shock, amounts to  $\beta_1 = \beta_{m1} = 65^\circ 40'$ . At this value of  $\beta_1$  the flow after an oblique shock has a subsonic speed. In the indicated limits of the changes of the angle  $\beta_1$  ( $22^\circ 45' - 65^\circ 40'$ ) after an oblique shock there may exist a normal shock. At  $\beta_1 = 22^\circ 45'$  there exists only a normal shock, and at  $\beta_1 = 65^\circ 40'$ —only an oblique shock.

By varying within these limits the angle of an oblique shock and by calculating  $\lambda_1$  and  $p_2$  (parameters before a normal shock), there can be found parameters of a gas after a normal shock. The speed after a normal shock  $\lambda_2 = \frac{1}{\lambda_1}$  increases with an increase in  $\beta_1$  from  $\lambda_2 = 0.5$  at  $\beta_1 = 22^\circ 45'$  to  $\lambda_2 = \lambda_1 = 1$  at  $\beta_1 = 65^\circ 40'$ .

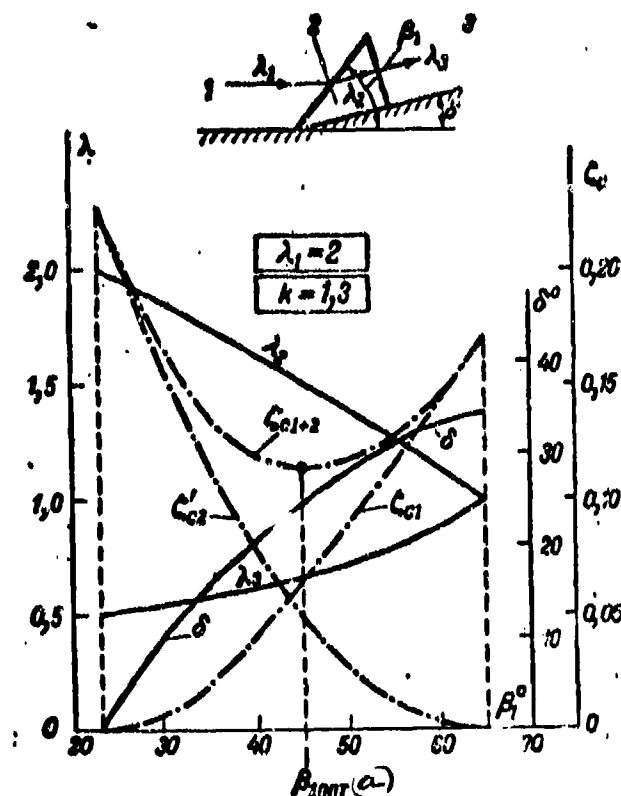


Fig. 4-19. Change of speeds and losses in a system of two shocks (oblique + normal) depending on angle of oblique shock  $\beta_1$  at  $\lambda_1 = 2.0$ ;  $k = 1.3$ . KEY: (a) opt.

In determining the loss factors in a normal shock it is necessary to relate the magnitude of the losses to the kinetic energy of the undisturbed flow, i.e., to calculate

$$\zeta'_{s2} = \zeta_{s2} \left( \frac{\lambda_1}{\lambda_2} \right)^2,$$

where  $\zeta_{s2}$  is determined by the diagram of oblique shocks for  $\lambda_2$ . In Fig. 4-19 there are plotted the values  $\zeta'_{s2}$ . It may be seen that  $\zeta'_{s2}$  decreases with an increase of  $\beta_1$ . At  $\beta_1 = 22^\circ 45'$   $\zeta'_{s2} = \zeta_{s2} = 0.227$ , and at  $\beta_1 = 65^\circ 40'$ ,  $\zeta'_{s2} = 0$ .

Coefficient of total losses in the system of two shocks, obviously, will be equal to:

$$\zeta_{s1+2} = \zeta_{s1} + \zeta'_{s2}.$$

The curve of total losses in the system of two shocks has a minimum at  $\beta_1 = 45^\circ$ . It is obvious that the value  $\beta_1$  is optimum with respect to losses of energy in the system of shocks.

Analogous calculations can be made for different speeds  $\lambda_1$  by determining the most advantageous value of  $\beta_1$ . Results of such calculations are given in Fig. 4-20, where total loss factor  $\zeta_s$  is presented depending on  $\beta_1$  for different values of  $\lambda_1$ . With heavy lines there are drawn  $\zeta_s$  curves in a range of angles  $\beta_1$  with which there is possible the existence of a system of oblique and normal shocks. The dotted line ABCD connects points corresponding to  $\beta_1 = \alpha_{m1}$ . For these points an oblique shock has an infinitesimally small intensity and, consequently, flow deceleration is realized only in one normal shock. The points FGHJ correspond to the angle  $\beta_1 = \beta_{1*}$  with which the flow after a plane shock has a sonic speed. For  $\beta_1 > \beta_{1*}$  the  $\zeta_s$  curves are drawn with thin lines. In this case the calculation can be presented under the assumption of the existence of a shock after which speed is subsonic. At  $\beta_1 = 90^\circ$  it becomes normal. It is readily seen that at  $\beta_1 = \alpha_{m1}$  and  $\beta_1 = 90^\circ$  the loss factor  $\zeta_s$  has an identical value.

A comparison of curves in Fig. 4-20 shows that optimum values  $\beta_{1\text{opt}}$  depend on the speed of the undisturbed flow  $\lambda_1$ . With an increase of  $\lambda_1$  up to certain limits, the  $\beta_{1\text{opt}}$  values decrease. For  $\lambda_1 = 1.6$  loss factor at the optimum value

$\beta_{opt} = 52^\circ$  amounts to  $\zeta_2 = 0.035$ . In this case, one normal shock gives (point A in Fig. 4-20)  $\zeta_{22} = 0.113$ , and one oblique shock with a speed after the shock equal to the speed of sound (point J in Fig. 4-20),  $\zeta_{e1} = 0.073$ . Consequently, the transition from one shock to a system of two shocks (oblique + normal) makes it

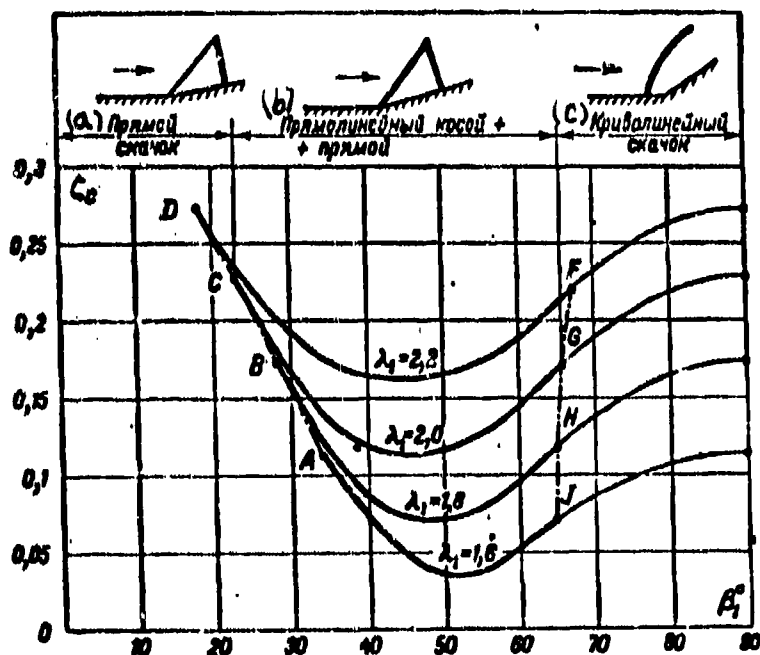


Fig. 4-20. Curves of loss factors in a system of two shocks (oblique + normal) as a function of the angle of oblique shock  $\beta_1$  and the speed  $\lambda_1$ ;  $k = 1.3$   
KEY: (a) normal shock; (b) rectilinear oblique + normal; (c) curved shock.

possible to decrease the loss factor more than twofold. At large values of  $\lambda_1$ , a two-step deceleration is even more effective.

One should note that with an increase in  $\lambda_1$ , the minimum of the curves  $\zeta_2$  becomes more gentle. This circumstance makes it possible to select optimum values of  $\beta_1$  in such a manner that also the static pressure after the second normal shock is the maximum. The ratio of the static pressure after a system of shocks  $p_3$  to the total pressure before the shock  $p_{01}$  can be presented in the following form:

$$\frac{p_3}{p_{01}} = \frac{p_2}{p_1} \frac{p_1}{p_0} \frac{p_0}{p_{01}};$$

here  $\frac{P_2}{P_1}$  characterizes the increase of static pressure in an oblique and  $\frac{P_2}{P_1}$ , in a normal shock.

The change of these magnitudes, and also  $\zeta_{01} = \frac{P_{02}}{P_{01}}$  and  $\zeta_{02} = \frac{P_{03}}{P_{02}}$ , depending on angle of oblique shock  $\beta_1$  for  $\lambda_1 = 2.0$  is presented in Fig. 4-21. With an increase of  $\beta_1$  the ratio of pressures in an oblique shock  $\frac{P_2}{P_1}$  increases, and in a normal  $\frac{P_2}{P_1}$  decreases. The graph shows that relative static pressure after the system of shocks for  $\lambda_1 = 2.0$  has a maximum at  $\beta_1 = 40^\circ$ , while minimum value of  $\zeta_0$  was obtained at  $\beta_1 = 45^\circ$ .

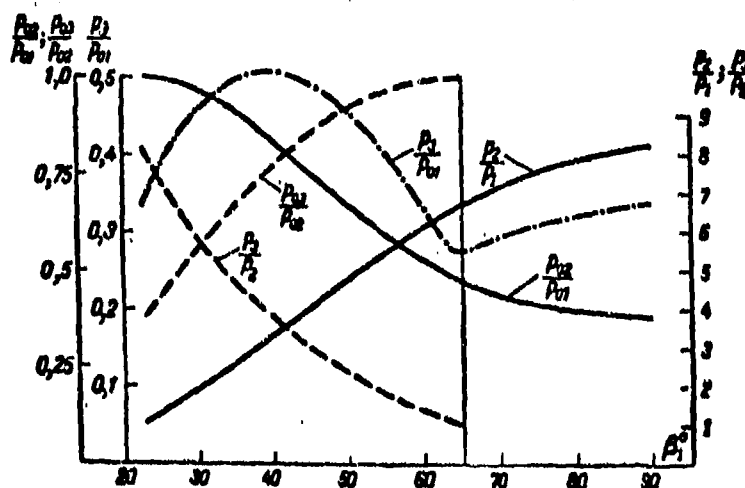
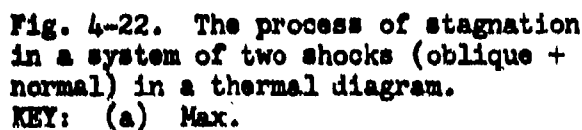


Fig. 4-21. Change of static pressure and stagnation pressure in a system of two shocks (oblique + normal) depending on the angle of oblique shock  $\beta_1$  for  $\lambda_1 = 2.0$ ;  $k = 1-3$ .

In considering that curves  $\zeta_0$  in the vicinity of the minimum are mildly sloping, the optimum values of  $\beta_1$  may be selected by the data of the calculation for the recovery of static pressure in the system of shocks, i.e., one can select of  $\beta_{1,opt}$  somewhat smaller than is dictated by the curves  $\zeta_0$ .

Such a solution is expedient in that case when the basic problem reduces to maximum recovery of the static pressure in the system of shocks, as, for example, takes place for supersonic diffusers.

The stepwise deceleration of the flow in a system of shocks can be graphically presented in a thermal diagram. In Fig. 4-22 this process is shown for two shocks.



160



angle  $\beta_{1, \text{opt}}$  losses of energy in the system of shocks are found to be minimal (point  $B_3$ ). With another, close value of angle  $\beta_1$ , the losses are somewhat higher ( $\Delta h'_{a+n} > \Delta h_{a+n}$ ), but the static pressure will attain a maximum possible value  $p_{3\text{max}}$  (point  $B_2$ ). Line of the limiting states can be built by means of successive calculations of the system of shocks.

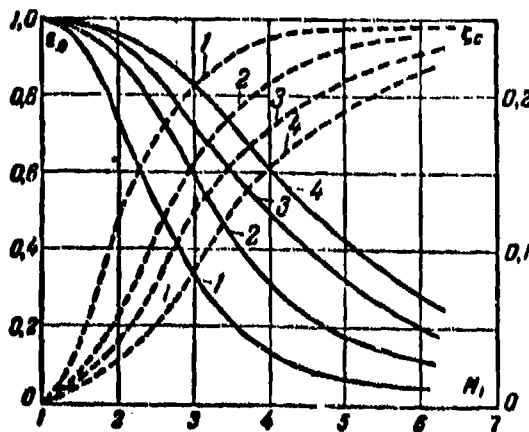


Fig. 4-23. Change of losses in shocks in a step-by-step deceleration (Fig. 4-22 indicates the number of shocks).

For a perfect gas there can be obtained equation of this line in form of a relationship between the change in entropy and change of enthalpy in a system of shocks.

At high supersonic speeds, for the transition to subsonic speeds it is expedient to apply more complex systems of shocks, consisting of several oblique shocks and one final normal shock. With an increase in the number of oblique shocks the energy losses will decrease. For each speed of the flow  $M_1$ , with a given number of oblique shocks, there exists an optimal scheme of arrangement of shocks which can be found by a step-by-step calculation.

The graphs given in Fig. 4-23 clearly show the advantage of the more complex systems of shocks at large supersonic speeds. The curves  $\zeta_c = \zeta(M_1)$  make it possible to select the most rational scheme of stepwise deceleration for a given speed.

#### 4-8. The Reflection of Shocks

##### a) Reflection from a Rigid Wall

We shall consider the reflection of an oblique shock from a straight rigid wall, parallel to the direction of speed of an undisturbed flow (Fig. 4-24). A shock will form at point A, where the change in direction of wall is at an angle  $\delta$ .

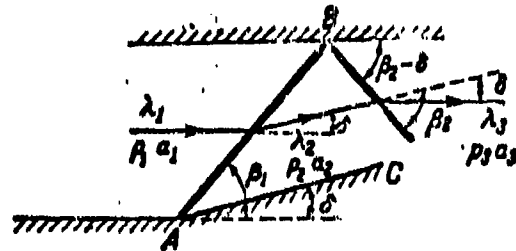


Fig. 4-24. Diagram of a normal reflection of a plane oblique shock from a rigid wall.

During the transition through the primary shock AB, the line of flow is deflected to the straight wall by the angle  $\delta$ . It is obvious that at point B this change in direction is unrealizable and the boundary line of flow maintains the direction of the wall. This means that at point B the wall forcibly deflects the line of flow in the opposite direction by the angle  $\delta$ . As a result there appears a reflected oblique shock BC. We note that the angles of the incident and reflected shocks are not identical, since before the shock BC the dimensionless speed  $\lambda_2 < \lambda_1$  at the same angle of deflection  $\delta$ . From the graph  $\beta = f(\delta, \lambda_1)$  (Fig. 4-5) it is clear that the angle  $\beta_2 > \beta_1$ .

The calculation of reflected shock encounters no difficulties. By knowing parameters of the undisturbed flow  $\lambda_1$ ,  $p_1$  and the angle of deflection  $\delta$ , by means of the diagram of shocks there are readily determined parameters of the flow after a primary shock:  $\lambda_2$ ,  $p_2$  and  $\beta_1$ . With the same value  $\delta$  we find the state of gas after a reflected shock:  $\lambda_3$ ,  $p_3$  and  $\beta_2$ . By the above-discussed method we find the losses of energy in primary and reflected shocks. One should bear in mind that such a reflection of an oblique shock is not always possible. If the angle of deflection  $\delta$  is larger than maximum value for the speed  $\lambda_1$ , then picture of

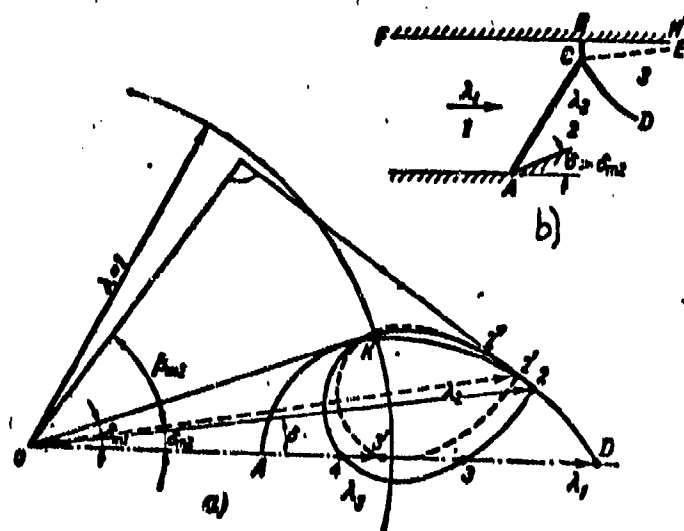


Fig. 4-25. Analysis of reflection of a shock in a diagram of shock polars.  
 a—determination of angles and speeds in an irregular reflection; b— $\lambda$ -shaped shock during reflection.

reflection varies. Let us assume that in diagram of shock polars (Fig. 4-25, a) the sector  $OD$  depicts the speed of flow up to the shock,  $\lambda_1$ . If the angle of deflection of wall  $\delta < \delta_{m2}$ , then the hypocissoid corresponding to the speed after the shock  $\lambda_2$  (sector  $O2$ ) intersects the line of vector  $\lambda_1$  (points 3 and 4).

At  $\delta = \delta_{m2}$  the line  $OD$  is tangential to the shock polar  $\lambda_2$  (point 3'). The picture of the flow here remains as previously (Fig. 4-24). Vector of speed after second shock  $O3'$  ( $\lambda_2$ ) will be less than unity (the speed is subsonic).

If  $\delta > \delta_{m2}$ , then a shock polar constructed for the speed  $\lambda_2$  does not have common points with the vector  $OD$  and the reflected shock cannot assure an equalizing of the flow. Part of flow directly adjacent to wall becomes subsonic. The reflected shock  $CD$  is distorted and is displaced against the flow. Here also the primary shock  $AB$  is deformed. The element  $CB$  of this shock becomes normal to the wall. The system of shocks acquires an  $\lambda$ -shaped form. After the normal shock sector the flow is subsonic. After the curved portion of reflected shock the flow

may be supersonic. As a result there will form a line of tangential discontinuity CE, on both sides of which the pressures are identical and the temperature and densities are different, since change of entropy in the transition through BC and AC—CD will be different. In region 3 after the  $\lambda$ -shaped shock the flow is vortical.

The reflection of shock shown in Fig. 4-25,b can appear at large angles of deflection  $\delta$  and small supersonic speeds  $M_1$ . We shall emphasize that the mechanism of the genesis of the  $\lambda$ -shaped and bridge-like shocks is identical.

#### b) Reflection from the Free Edge of Stream

Such a reflection is considered in Fig. 4-26. At all points on the edge FBE the pressure is identical and equal to the pressure of the environment  $p_a$ . In the stream the same pressure takes place only before the shock AB. In the transition through the shock AB, the pressure changes from  $p_1 = p_a$  to  $p_2 > p_a$ . Consequently, at point B two pressures are characteristically simultaneous:  $p_a$  from the direction of medium and  $p_2$  from direction of stream. Such a point is the focus of the disturbance of a supersonic flow, creating a stationary wave of rarefaction. In the flow around the point B, the pressure of the flow must drop from  $p_2$  to  $p_a$ , which also results at supersonic speeds in the formation of the wave BCD.

The first characteristic BD comprises with the direction of vector  $M_2$  the angle  $\alpha_{m2} = \arcsin \frac{1}{M_2}$ , where  $M_2$  is the speed of flow after the shock AB ( $M_2 < M_1$ ). The angle of the latter characteristic is  $\alpha_{m3} = \arcsin \frac{1}{M_3}$ . Here, the speed after reflected wave of rarefaction  $M_3$  is determined by the ratio  $\frac{p_a}{p_{02}}$ , where  $p_{02}$  is the pressure of stagnation after an oblique shock.

The reflection of a shock results in the deformation of edge of stream, which at point B is deflected at an angle  $\delta_2 > \delta_1$ . This deflection is caused by an expansion of the stream. Thus, with a reflection from the free edge of the stream, along which the pressure is kept constant or drops, the shock wave will transform

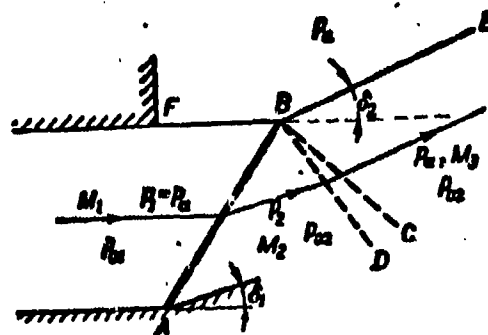


Fig. 4-26. Reflection of oblique shock from free edge of stream.

into a wave of rarefaction. If the pressure along the edge increases, then, depending upon intensity of change of pressure, reflection can be extinguished or it occurs with maintenance of sign (as also from a rigid wall).

#### 4-9. Interaction of Shock and Wave of Rarefaction

During flow around bodies of finite dimensions by a supersonic flow of a perfect gas, the intensity of the shocks at various distances from the body will be different. Owing to interaction with waves of rarefaction, the intensity of the shocks decreases with distance and at an infinite distance becomes infinitesimally small.

Let us consider as an example flow around a pointed plate (Fig. 4-27). On the forward sharp ( $\beta < \beta_m$ ) tip of plate there appears a plane oblique shock AB. During flow around the point D there will form a stationary wave of rarefaction, where the characteristic at which deflection of flow begins is located at the angle

$$\alpha_{rd} = \arcsin \frac{1}{M_2},$$

where  $M_2$  is the speed after the shock.

Since

$$\alpha_{rd} + \beta > \beta_1,$$

then characteristic will intersect shock wave at a certain point B. The second boundary of the wave of rarefaction is the characteristic located at an angle

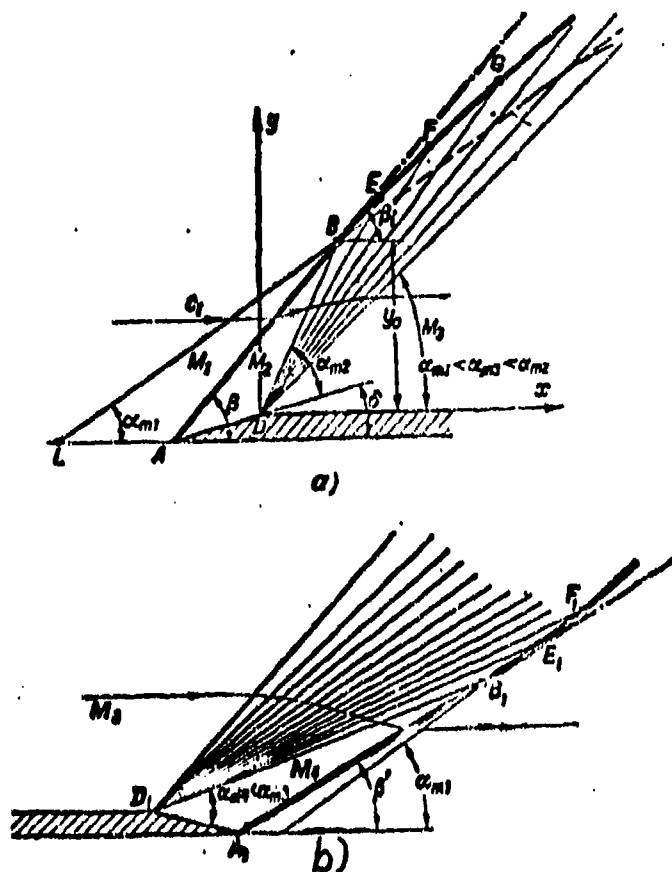


Fig. 4-27. Diagram of interaction between shock and wave of rarefaction.

$$\alpha_{m3} = \arcsin \frac{1}{M_3} \quad .$$

In the sector to the right of point B, the wave of rarefaction interacts with the oblique shock. In the region AED, the speed is constant and equal to  $M_2$ ; the streamlines are parallel to the generatrix of the wedge AD. We shall draw through the point B the characteristic of undisturbed flow at an angle  $\alpha_{m1} = \arcsin \frac{1}{M_1}$ , to the direction of velocity vector  $c_1$ . Since the oblique shock is located at an angle

$\beta_1 \approx \frac{1}{2}(\alpha_{m1} + \alpha_{m2} + \delta)$ , and the angle of the wave DE closest to DB is smaller than  $\alpha_{m2}$ , then in the sector BE the oblique shock is deflected by a small angle so that  $\beta_1 < \beta$ ; with a decrease in slope of angle of the shock  $\beta_1$ , also the angle of deflection of flow  $\delta_1$  decreases. Corresponding deflections of the shock and changes in angle of turn of flow  $\delta_1$  take place also in the sectors EF, FG, et cetera.

Consequently, the shock in starting from point B is distorted and is deflected in the direction of flow; the angle of the shock decreases as it approaches  $\alpha_{mi}$ .

In accordance with the basic formulas of a shock it may be concluded that in the interaction with a wave of rarefaction the intensity of the shock decreases and, consequently, losses in the shock decrease. The change in entropy, as analysis shows, becomes equal to zero at infinity.

Analogous results are obtained if the wave of rarefaction is located before the shock (Fig. 4-27,b). At point  $D_1$  there appears a wave of rarefaction and at point  $A_1$  a shock wave. In interacting with the wave of rarefaction the shock is distorted. Since after the intersection with the last characteristic of the wave of rarefaction  $D_1B_1$  the shock  $A_1B_1$  occurs in a zone of lower speeds, the angle of it,  $\beta_1$ , increases.

We note that in real (viscous) fluid also the viscosity contributes to the attenuation of the shocks.

#### 4-10. Conical Compression Shocks

In the preceding section of this chapter there have been considered compression shocks in a two-dimensional flow. During flow round axially symmetric bodies, surfaces of discontinuity have an axially symmetric form. Let us consider peculiarities of an axially symmetric shock in an example of flow around of circular cone (Fig. 4-28). Before the cone there will form a conical shock, the apex of which coincides with apex of cone if aperture angle of cone is less than maximum value for given speed of the incident flow.

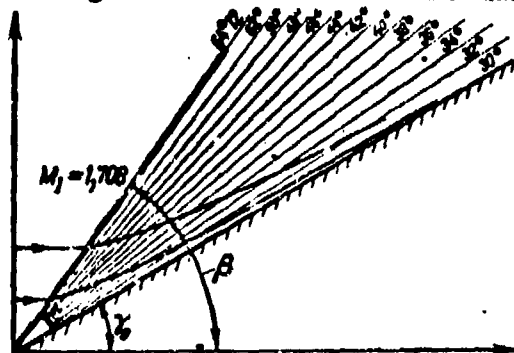


Fig. 4-28. Shape of lines of flow in the disturbed region after a conical shock during flow around a cone

The basic relationships during the transition through the surface of a conical shock, as is readily seen, will be the same as that for a two-dimensional shock. [equations (4-13), (4-14), etc.]. With identical apex angles of the wedge and cone, shock on cone will have a smaller angle of slope than on wedge, since the cone causes a smaller constraint of flow than wedge of infinite span of the same aperture angle. During transition through a conical shock the lines of flow, just as in case of a two-dimensional shock, undergo discontinuity. However, since a shock in a cone is weaker than in a wedge, immediately after the shock the lines of flow will be oblique to the vector of speed of undisturbed flow at an angle smaller than aperture angle of cone  $\gamma$ . Calculations show that in the disturbed region the lines of flow are not straight, as in a flow around a wedge, but are curved; here their curvature is different and depends on the distance from surface of cone. The curvature of the lines of flow nearest to surface of cone is very small.

From Fig. 4-28 it follows that with distance from the shock the angle of slope of the lines of flow to axis of cone increases and the lines of flow asymptotically approach direction given by generatrix of cone. Here it is possible to see that annular tube of flow formed by two adjacent lines of flow has a smoothly narrowing form. The lines of flow are turned convexly to the surface of cone.

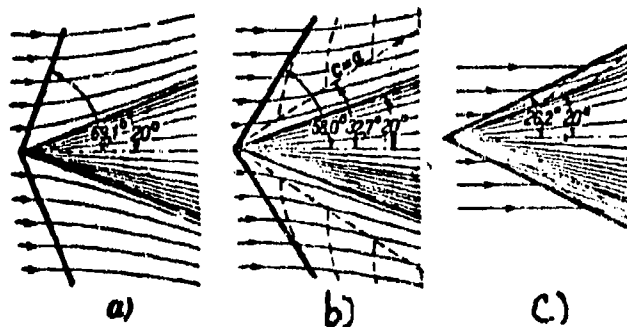


Fig. 4-29. Diagram of spectra of flow round a cone at different speeds of undisturbed flow.



During supersonic speeds such form signifies a decrease in speeds and an increase of pressures along the lines of flow, i.e., deceleration of the flow. It follows from this that after a conical shock the compression of the gas is prolonged. However, if within the limits of shock an increase in pressures is accompanied by an increase in entropy, then the compression of gas in disturbed region after shock occurs isentropically without losses. On this basis it may be concluded that with an identical ratio of the pressures  $\frac{p_2}{p_1}$  ( $p_2$  is the pressure on the surface of stream-lined wedge or cone) the compression of the gas during flow around cone occurs with smaller losses than during flow around a wedge, since for a cone the total increase in pressure is the sum of the isentropic compression and the compression along shock adiabatic line.

In supersonic part of disturbed region, owing to curvature of the lines of flow, the characteristics are curved.

In Fig. 4-29 there are illustrated three possible cases: (a) the speeds at all points of disturbed region are less than the speed of sound, (b) case of mixed flow, when speed directly after shock is supersonic, and then becomes subsonic, (c) and, finally, when flow after the shock is completely supersonic. The character of flow after the shock with a constant magnitude  $\gamma$ , depends on speed of incident flow.

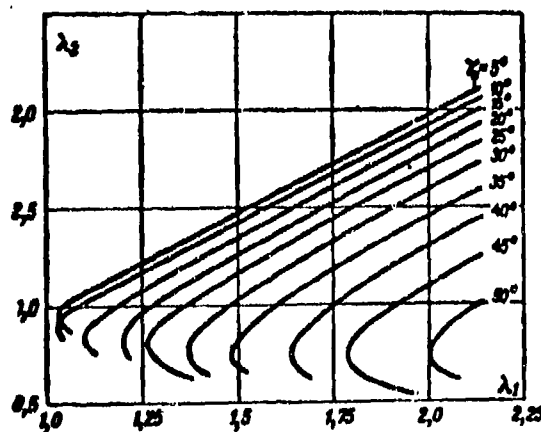


Fig. 4-30. The dependence of speeds on surface of cone on speed of undisturbed flow and angle of cone.

Speeds and pressures on the surface of the cone vary with the change of speed of undisturbed flow and half-angle of cone  $\gamma_0$ .

In Fig. 4-30 there are presented graphs of change in dimensionless speed on surface of cone  $\lambda_1$  depending upon angle  $\gamma_0$  and  $\lambda_1$ . One should note that during a given mode of flow around, at all points of conical surface the speeds and pressures have constant values. For a cone, the same as for a wedge, the theoretical solution of the problem gives during one and the same mode two possible values of slope of angle of shock and of parameters on surface of cone (lower branches of curves in Fig. 4-30). However, practically, as a rule, there are realized smaller values of the shock angles (upper branches of curves in Fig. 4-30). Therefore, there can be made the conclusion that with an increase in  $\gamma_0$  the speeds on surface of cone decrease and the pressures increase. The increase in speed of undisturbed flow leads to opposite results.

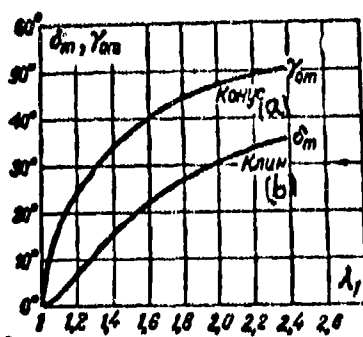


Fig. 4-31. Dependence of maximum angles of wedge and cone on velocity of undisturbed flow ( $k = 1.4$ )  
KEY: (a) Cone; (b) Wedge.

Such a character of variation of parameters of flow on surface of a cone takes place as long as angle of the cone does not attain a limiting value, with which there occurs a withdrawal and deformation of shock, the same as in the case of a wedge.

A conical shock will transform into an axially symmetric surface of discontinuity with a curvilinear generatrix. However,

the maximum half-angle of the cone  $\gamma_{0m}$ , with which for a given  $\lambda_1$  there occurs a transformation of a conical shock into an axially symmetric with a curvilinear generatrix, will be larger than the corresponding values  $\delta_m$  for a wedge. In Fig. 4-31 there are presented dependence of maximum angles of deflection  $\delta_m$  and  $\gamma_{0m}$  on the number  $\lambda_1$  for a wedge and a cone.

For a conical shock it is possible to construct in plane of hodograph  $u, v$  and

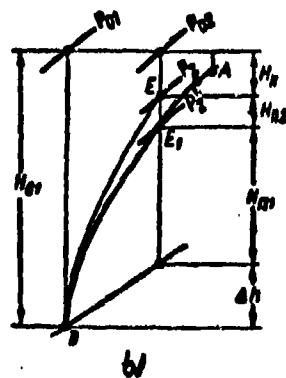
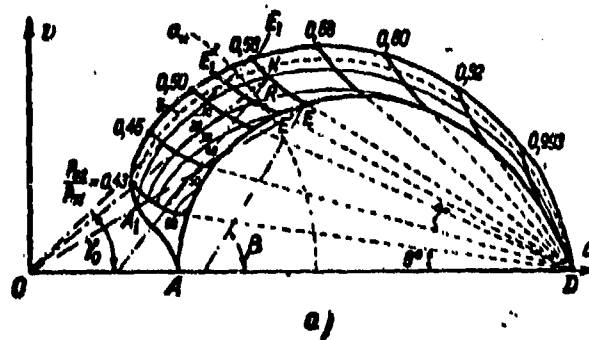


Fig. 4-32. Shock polar for conical shock in plane of hodograph and in thermal diagram for  $k = 1.4$  (apple-shaped curves).

in the thermal diagram a shock polar (Fig. 4-32).

In the plane of the hodograph the change of speed directly in a conical shock is expressed by line DEA, where the vector of speed after shock is determined by the sector OE (speed of undisturbed flow OD). The angle of shock  $\mu$  can be found by drawing a normal at the point E to the sector DE. The change in speed in disturbed region after the shock is described by the curve  $EE_1$ . This line corresponds to the isentropic change of speed (compression) after the shock.

The apple-shaped curve  $DE_1A$  defines the hodograph of speed on surface of cone; it is possible to call it a shock polar of the cone. Slope of the sector  $OE_1$  determines halfangle of cone  $\gamma$ . The region included between the curves DEA and  $DE_1A$  characterizes the flow in the disturbed region. At any point N the sector ON determines the magnitude and direction of the speed. The normal drawn to the hodograph of speed at point N gives the halfangle of conical surface passing through this point in plane of flow.

Each intermediate curve  $DNA_1$  corresponds to a constant value in of difference of angles  $\delta - \gamma$ . Since in the disturbed region the pressure of total stagnation does not change, then the constant value  $\frac{P_{02}}{P_{01}}$  corresponds to the hodograph of speed  $EE_1$ . By plotting these values for different points E, it is possible with the use of the shock polar to determine the change in pressure of stagnation. In the plane of the hodograph it is possible to draw an arc of a circle with a radius  $a_*$ , which will differentiate the group of modes of flow around a cone with subsonic speeds after shock. Here there are readily established points of the disturbed flow in which the speed of flow is equal to the critical. For a given shock angle  $\mu$  these points are obtained by the intersection of arc  $a_*$  and the hodograph of speed  $E'E'_1$  (point R).

In a thermal diagram, the shock polar is constructed by an already known method (Fig. 4-32,b). Line  $DE_1A$  corresponds to a change of state of gas after a conical shock with a change in  $\lambda$  from  $\lambda_0 = \infty$  (point D) to  $\lambda_0 = \frac{\pi}{2}$  (normal shock). At a definite value  $\gamma$ , and correspondingly  $\lambda$ , the state of the flow immediately after

shock is characterized by the point  $E_1$ , determining change of entropy (loss  $\Delta h$ ) and change of potential energy of gas in the shock ( $H_{s1}$ ). The sector  $E_1E$  corresponds to the isentropic compression after the shock, and at point E there can be found parameters of the gas on the surface of cone. Corresponding change in the potential energy is equal to  $H_{s2}$ . At identical angles of a two-dimensional and a conical shock ( $\beta = \theta$ ) variations of parameters happen to be close, since the isentropic compression in the disturbed region is significantly less intense than shock compression in a shock.

In a system of conical shocks it is possible to realize stepwise deceleration of a supersonic flow, the same as in a system of plane shocks.

In conclusion it is necessary to make the following remarks.

Up to the present we have assumed that any shock is a geometric line (or surface).

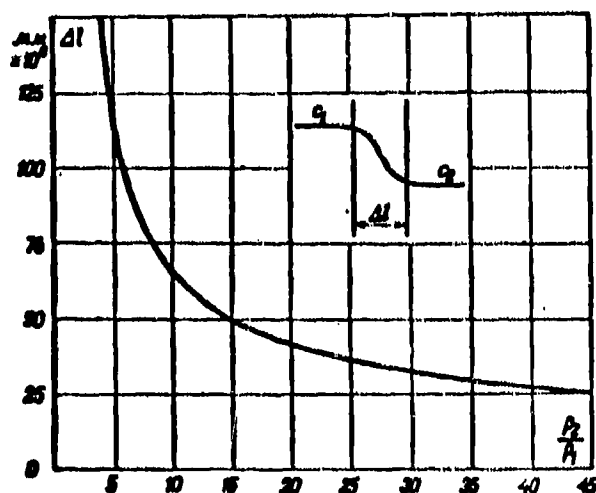


Fig. 4-33. Thickness of shock depending on its intensity.

This means that the transition from parameters of an undisturbed flow to parameters after a shock is realized in an infinitely thin layer. The existence of two adjacent regions of flow with different temperatures and speeds in a real-viscous-gas is possible only in a certain transitional layer of finite thickness, within the limits of which there also occurs a very intense, but continuously gradual change of the parameters.

By including methods of the kinetic theory of gases and the fundamental equation of gas dynamics with a consideration of the thermal conductivity viscosity, it is possible to obtain an approximate evaluation of thickness of a normal shock.

Calculations show that the thickness of a shock has the order of twice the length of free path of molecule and therefore decreases with an increase in its intensity. A corresponding graph of the change of thickness of shock depending on  $\frac{P_2}{P_1}$  with the pressures not too low is presented in Fig. 4-33. We see that the thickness of the shock under ordinary conditions is very small. Experiments confirm that the above-adopted simplified diagram of an infinitely thin shock and the derived formulas in this assumption under ordinary conditions very accurately reflect the actual picture. One should bear in mind that in rarefied gases with great lengths of free path the thickness of transitional region may be found to appear very substantial; obviously, in this case the obtained relationships for a shock may give appreciable errors.

#### 4-11. Condensation Shocks (Thermal Shocks)

Shocks may generate not only in adiabatic flows, but also in those cases, when in a small length of the flow there occurs an intense admission or withdrawal of energy (for example, heat). Here there will form shocks, called thermal. Of maximum interest are two types of thermal shocks: propagation of detonation and combustion and condensation shocks, associated with the motion of two-phase fluid and, in particular, of moist vapor or air.

The first type of thermal shocks has been studied in detail and discussed in special literature. The second type--condensation shocks, which are widely encountered in aerodynamic experiments, in Laval, nozzles in the flow parts of turbomachines--have been studied in less detail.

An analysis of properties of condensation shocks is based on certain assumptions:

a) condensation occurs instantaneously, so that there will be formed sharp boundary,

separating gas with noncondensed water vapors from gas containing the condensate; b) effect of condensation reduces to release of the latent heat of vaporization; c) this process is accompanied by change of physical properties of the gas component and by a decrease of its weight portion in the mixture; a change of physical properties of the gas and its parameters occurs only within the limits of the shock; d) influence of viscosity, thermal conductivity, and diffusion can be ignored; e) the gas phase is satisfied by the equation of state  $\frac{p}{\rho} = RT$ , and  $k$  varies only during the transition through a shock; f) after a shock the liquid phase has the same speed as the gaseous.

The fundamental equations of a condensation shock\* are general equations, derived in Sec. 4-2.

Taking into account the designations adopted in Fig. 4-34, equation of continuity is written in the following form:

$$\rho_1 c_{n1} = \rho_2 (1 + l) c_{n2} = \rho_2 (1 + l) (u_2 \sin \beta_k - v_2 \cos \beta_k), \quad (4-37)$$

where  $\beta_k$  is the angle of oblique condensation shock;

$l = \frac{\rho_n \lambda}{\rho_2 (1 - \gamma)}$  is the ratio of mass of liquid to mass of gas after shock;

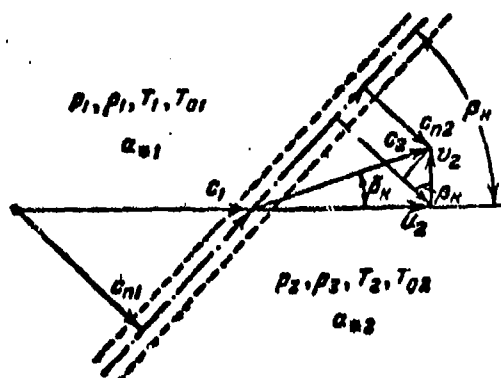


Fig. 4-34. Diagram for deriving equation of an oblique condensation shock.

\*See list of references. A theoretical investigation of condensation shocks for the first time was made by S. Z. Belen'kiy. In the work by R. German there is given the solution for a normal condensation shock. In the work by V. A. Andreyev and S. Z. Belen'kiy there is considered the more general case of an oblique shock. F. Ross solved the problem of an oblique condensation shock by taking into account the changes in the physical properties of the gas.

$\lambda$  is the degree of humidity after shock;

$\rho_n$  is the density of the liquid;  $c_{n2} = u_n \sin \beta_n - v_n \cos \beta_n$ .

Equation of momentum in projections onto the normal to shock and onto the shock plane will be

$$p_2 - p_1 = \rho_1 c_{n1}^2 - \rho_2 (1 + \lambda) (u_n \sin \beta_n - v_n \cos \beta_n)^2; \quad (4-38)$$

$$\begin{aligned} \rho_1 c_{n1} c_t &= \rho_2 (1 + \lambda) c_{n2} c_t = \\ &= \rho_2 (1 + \lambda) (u_n \sin \beta_n - v_n \cos \beta_n) (u_n \cos \beta_n + v_n \sin \beta_n) = 0, \end{aligned}$$

where

$$c_t = c_n \cos \beta_n = u_n \cos \beta_n + v_n \sin \beta_n. \quad (4-39)$$

Equation of energy will be written as follows:

$$\frac{c_1^2}{2} + i_1 = \frac{c_2^2}{2} + i_2 - \Delta i_0, \quad (4-40)$$

where  $\Delta i_0 = i_{02} - i_{01}$  is the change of enthalpy of stagnation due to liberation of heat during condensation.

Since the enthalpy of stagnation at the intersection of shock varies, then the critical speed up to and after shock will be nonidentical:

$$a_{c1} = \sqrt{2 \frac{k_1 - 1}{k_1 + 1} i_{01}}; \quad a_{c2} = \sqrt{2 \frac{k_2 - 1}{k_2 + 1} i_{02}}.$$

Here  $k_1, k_2$  are coefficients of the isentropic process up to and after the condensation shock.

The relationship between critical speeds is expressed by formula

$$\frac{a_{c1}^2}{a_{c2}^2} = \frac{i_{01}}{i_{02}} = \frac{K}{1 + \Delta i_0}. \quad (4-41)$$

where

$$\Delta i_0 = \frac{i_{02}}{i_{01}}; \quad K = \frac{k_1 - 1}{k_1 + 1} \cdot \frac{k_2 + 1}{k_2 - 1}.$$

The left-hand side of the equation of energy (4-40) can be presented in the following form

$$\frac{c_1^2}{2} + \frac{k_1}{k_1 - 1} \frac{p_1}{\rho_1} = \frac{k_1 + 1}{2(k_1 - 1)} a_{c1}^2, \quad (4-40a)$$

and the right-hand side

$$\frac{c_2^2 + v_2^2}{2} + \frac{k_2}{k_2 - 1} \frac{p_2}{\rho_2 (1 + \lambda)} = \frac{k_2 + 1}{2(k_2 - 1)} a_{c2}^2 = i_{02} (1 + \Delta i_0) \quad (4-40b)$$

Considering that

$$\tau_{2n} \lambda_n = \frac{c_2 - u_2}{v_2} \quad \text{and} \quad \tau_{2n} \lambda_n = \frac{v_2}{u_2}. \quad (4-42)$$

\* $i_1$  is the enthalpy of gas phase without a calculation of the heat of condensation.



where  $\beta_x$  is the angle of deflection of line of flow at the intersection of condensation shock, by means of expressions (4-37), (4-38), (4-40), (4-41) and (4-42) we obtain an equation of the shock polar for a condensation shock in the form:

$$\bar{v}_2^2 = (\lambda_1 - \bar{u}_2)^2 \frac{\frac{\lambda_1}{\lambda_1 - \bar{u}_2} \left[ \frac{\bar{u}_2 \lambda_1 - \bar{u}_2}{2} - \frac{\bar{u}_2^2}{k_1 + 1} \lambda_1^2 - \lambda_1 \bar{u}_2 + \right.}{\frac{(k_1 - 1) \bar{u}_2^2 - (k_1 + 1)(1 + \bar{\Delta} \bar{I}_0)}{(k_1 - \bar{k})(k_1^2 - 1)}} - 1 - \frac{\bar{\Delta} \bar{I}_0 - \bar{k}}{(k_1 - \bar{k})(k_1^2 - 1)} \left. \right] - 1 + \bar{k} \frac{\lambda_1 (\lambda_1 - \bar{u}_2)}{(k_1 - \bar{k})(k_1 + 1)} + 1 \quad (4-43)$$

Here the following designations have been adopted:

$$\lambda_1 = \frac{c_1}{a_{1,1}}; \quad \bar{u}_2 = \frac{u_2}{a_{1,1}}; \quad \bar{v}_2 = \frac{v_2}{a_{1,1}}; \quad \bar{k} = k_1 - k_2.$$

Equation (4-43) at  $\bar{\Delta} \bar{I}_0 - \bar{k} = 0$  transforms into formula (4-26) for an adiabatic shock.

By means of (4-43) on basis of formulas (4-42) there are determined the angle of oblique condensation shock  $\beta_x$  and the angle of deflection of flow  $\beta_x$ .

From the equation of energy (4-40b) there may be obtained a formula for determining the number  $M_2$  after shock:

$$M_2 = \sqrt{\frac{c_2 p_2}{p_2 k_2} (1 + I)} = \left[ (1 + \bar{k})(k_1 - 1 - \bar{k}) \left( \frac{k_1 + 1}{2(k_1 - 1)} \cdot \frac{1 + \bar{\Delta} \bar{I}_0}{\bar{u}_2^2 + \bar{v}_2^2} - \frac{1}{2} \right) \right]^{-\frac{1}{2}} \quad (4-44)$$

The ratio of the pressures in the shock we find by the formula

$$\frac{p_2}{p_1} = \frac{1 + k_1 M_1^2 \sin^2 \beta_x}{1 + \frac{(k_1 - \bar{k})(1 + \beta_1 M_1^2)}{\bar{u}_2^2 + \bar{v}_2^2} (\bar{u}_2 \sin \beta_x - \bar{v}_2 \cos \beta_x)^2} \quad (4-45)$$

Analogously to procedure in deriving formula (4-35), we obtain a formula for the ratio of the stagnation pressures in a condensation shock:

$$\frac{p_{02} - p_2}{p_{01} - p_1} = \frac{\left[ 1 + (k_1 - 1 - \bar{k}) \frac{M_2^2}{2} \right]^{\frac{k_1 - \bar{k}}{k_1 - 1 - \bar{k}}}}{\left[ 1 + (k_1 - 1) \frac{M_1^2}{2} \right]^{\frac{k_1}{k_1 - 1}}}. \quad (4-46)$$

The ratio of the densities in the shock

$$\frac{\rho_2}{\rho_1} = \frac{p_2}{p_1} \left( \frac{M_2}{M_1} \right)^2 \frac{\lambda_1^2}{u_2^2 + v_2^2}. \quad (4-47)$$

The obtained system of six equations (4-42) — (4-47) makes it possible to find parameters after the shock  $v_2$ ,  $u_2$ ,  $M_2$ ,  $p_{02}$ ,  $p_2$  and  $\tan \beta_k$  with the given parameters before shock  $c_1$ ,  $p_1$ ,  $\rho_1$ ,  $a_{*1}$  and of the knowns  $\Delta \bar{I}_0$ ,  $j$ ,  $\bar{k}$ .

By means of general relationships individual particular cases are readily examined.

In many practically important cases it is possible to consider that physical properties of gas are kept constant ( $k_1 = k_2$ ;  $\bar{k} = 0$ ) and that the mass of condensed phase after shock is negligible in comparison with the gaseous ( $j = 0$ ). In this case equation (4-43) will be simplified and acquires the form:

$$\bar{v}_2^2 = (\lambda_1 - \bar{u}_2)^2 \frac{\lambda_1 \left( \bar{u}_2 - \frac{\Delta \bar{I}_0}{\lambda_1 - \bar{u}_2} \right) - 1}{\frac{2}{k+1} \lambda_1^2 - \lambda_1 \bar{u}_2 + 1}. \quad (4-48)$$

The common solution of the original equations after corresponding simplifications makes it possible to obtain a connection between normal components of speed in a condensation shock in the following form:

$$\bar{c}_{n2} = b_0 \frac{\bar{c}_{n1}^2 + 1}{2\bar{c}_{n1}} \pm \sqrt{b_0^2 \left( \frac{\bar{c}_{n1}^2 + 1}{2\bar{c}_{n1}} \right)^2 - 1}, \quad (4-49)$$

where

$$\bar{c}_{n1} = \frac{c_{n1}}{b_{01}}; \quad \bar{c}_{n2} = \frac{c_{n2}}{b_{02}}; \quad b_{01} = \sqrt{a_{*1}^2 - \frac{k-1}{k+1} c_1^2 \cos^2 \beta_{n1}};$$

$$b_2 = \sqrt{a_2^2 - \frac{k-1}{k+1} c_1^2 \cos^2 \beta_k}$$

and

$$\frac{b_1^2}{b_2^2} = \frac{1 - \frac{k-1}{k+1} \lambda_1^2 \cos^2 \beta_k}{\frac{1}{a_2^2} - \frac{k-1}{k+1} \lambda_1^2 \cos^2 \beta_k} \quad (4-50)$$

The quantity  $\bar{a}_*$  is determined by formula (4-41). For the ratio of the pressures in shock we find:

$$\frac{P_2}{P_1} = \frac{2k}{k-1} \left( \frac{k-1}{2} M_1^2 \sin^2 \beta_k + 1 \right) \left( \frac{1}{b_*} \cdot \frac{c_{a1}}{c_{a2}} - 1 \right) + 1.$$

This equation changes to formula (4-13) at  $\bar{b}_* = 1$  (adiabatic shock) after substituting  $\frac{c_{a1}}{c_{a2}}$  from equations (4-5) and (4-11).

From equation (4-48) it follows that vertical component of the speed after the shock vanishes at three values of the vector  $u_2$ . The first corresponds to the degeneration of the shock into a weak wave  $[u_2 = \lambda_1(a_* - \bar{a}\lambda_1)]$ . The second and third values are obtained from the condition

$$\lambda_1 \left( \bar{u}_2 - \frac{\bar{\Delta I}_0}{\lambda_1 - \bar{u}_2} \right) - 1 = 0,$$

or

$$\bar{u}_2^2 - \left( \lambda_1 + \frac{1}{\lambda_1} \right) \bar{u}_2 + \frac{1}{a_*^2} = 0.$$

The two roots of this equation will be:

$$(\bar{u}_2)_{1,2} = \frac{\lambda_1^2 + 1}{2\lambda_1} \pm \sqrt{\left( \frac{\lambda_1^2 + 1}{2\lambda_1} \right)^2 - \frac{1}{a_*^2}},$$

i.e.,

$$(\bar{a}_2)_{1,2} = \left( \frac{c_2}{a_2} \right)_{1,2} = \frac{1}{2} \frac{\bar{a}_0(\lambda_1^2 + 1)}{\lambda_1} \pm \sqrt{\frac{\bar{a}_0^2(\lambda_1^2 + 1)^2}{4\lambda_1^2} - 1}. \quad (4-51)$$

The obtained relationship expresses a connection between speeds for a normal condensation shock. Here it is readily verified, by having set into equation (4-49) conditions of a normal shock:  $\beta_k = \frac{\pi}{2}$  and  $\bar{b}_* = \bar{a}_*$ . From equation (4-51) it follows that the speed after a normal shock depends on  $\lambda_1$  and  $\bar{\Delta I}_0$  — the heat liberated during condensation, which in turn is determined by quantity of the condensing gas.

From equations (4-49) and (4-50) it follows that the quantities  $\bar{b}_*$  and  $\bar{a}_*$  cannot be less than a certain limiting value for a given  $\bar{c}_{n1}$  or  $\lambda_1$ , since otherwise  $\bar{c}_{n2}$  and  $\lambda_2$  will be imaginary quantities. From (4-51) for a normal shock

$$\bar{a}_{*min} = \frac{2\lambda_1}{\lambda_1^2 + 1}.$$

In accordance with formula (4-41) at  $k_1 = k_2$ , the maximum change of enthalpy of stagnation in the shock corresponds to the minimum value of  $\bar{a}_*$ :

$$\bar{\Delta h}_{0max} = \left( \frac{\lambda_1^2 - 1}{2\lambda_1} \right)^2. \quad (4-52)$$

In a general case for an oblique shock, from equation (4-49) we shall obtain:

$$\bar{b}_{*min} = \frac{2\bar{c}_{n1}}{\bar{c}_{n1}^2 + 1};$$

correspondingly from (4-50) we shall have:

$$\bar{a}_{*min} = \frac{2(k+1)}{\sqrt{\frac{[k+1+\lambda_1^2(2k\sin^2\beta_k+1-k)]^2}{\lambda_1^2\sin^2\beta_k} + 4(k-1)\lambda_1^2\cos^2\beta_k}}. \quad (4-53)$$

and

$$\bar{\Delta h}_{0max} = \frac{1 - \bar{a}_{*min}^2}{\bar{a}_{*min}^2}.$$

As it was pointed out, the relative change of enthalpy of stagnation in a condensation shock  $\bar{\Delta h}_0$  characterizes the quantity of condensing liquid. The obtained relationships show that condensation shocks can appear only with definite quantities of condensing liquid. The limit of condensation in a shock depends on speed before the shock and on the angle of shock.

In returning to an analysis of the equation of shock polar (4-48), let us note that  $\bar{v}_2 = \infty$  at

$$\bar{a}_2 = \frac{1}{\lambda_2} \left( \frac{2}{k+1} \lambda_1^2 + 1 \right) \quad \text{or} \quad \frac{a_2}{a_{*2}} = \frac{\bar{a}_2}{\lambda_2} \left( \frac{2}{k+1} \lambda_1^2 + 1 \right).$$

The dependence (4-48) graphically is presented in Fig. 4-35 for different values of  $\bar{a}_*$ . For a plane oblique condensation shock with a given  $\bar{a}_*(\bar{\Delta h}_0)$

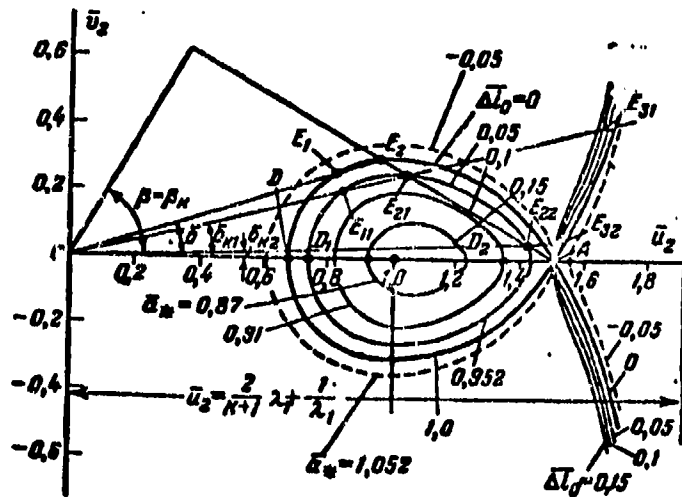


Fig. 4-35. Shock polars of condensation shocks for different values of  $\Delta I_0$  (different relative humidity);  $\lambda_1 = 1.5$ ;  $k = 1.4$ .

in the shock polar we find two points:  $E_{21}$  and  $E_{22}$ , corresponding to two different angles of the shock. Here point  $E_{21}$  corresponds to a curved condensation shock. The points  $E_3$  correspond to an expansion shock.

The value  $\bar{a}_* = 1$  corresponds to a shock polar of an adiabatic shock. As  $\bar{a}_*$  decreases (as  $\Delta I_0$  increases) the angle condensation shock at a given  $\delta_*$  increases. In accordance with formula (4-51), two values of the vector  $\bar{u}_2$  (points  $D_1$  and  $D_2$ ) correspond to a normal condensation shock. The negative sign before the root in (4-51) gives the point  $D_1$ , and the positive —  $D_2$ .

Thus, equations (4-43) and (4-48) and the shock polar in Fig. 4-35 show that there is theoretically possible the existence of four types of normal and oblique condensation shocks, corresponding to different speeds before the shock and to the quantities  $\bar{a}(\Delta I_0)$ .

The corresponding classification is shown in Table 4-2.

However, if we consider certain subsidiary conditions, then there are found possible at most two types: 1) supersonic shocks, in which  $c_{n1} > a_1$ ,  $c_{n2} < a_2$  and the condensation is accompanied by the compression of gas ( $p_2 > p_1$ ); 2) subsonic

TABLE 4-2

## Possible Types of Condensation Shocks

(a) Нормальная составляющая скорости перед скачком	(b) Отношение критических скоростей	(c) Нормальная составляющая скорости за скачком	Тип (d) скачка
$c_{n1} < a_1$	$1 > \bar{a}_* > \bar{a}_{* \text{ min}}$	1. $c_{n2} > a_1$	(e) Скачок разрежения
		2. $c_{n2} < a_1$	
$c_{n1} > a_1$	$1 > \bar{a}_* > \bar{a}_{* \text{ min}}$	3. $c_{n2} > a_1$	(f) Скачок уплотнения
		4. $c_{n2} < a_1$	

KEY: (a) Normal component of speed before shock; (b) ratio of critical speeds; (c) Normal component of speed after shock; (d) type of shock; (e) expansion shock; (f) shock wave.

shocks, corresponding to conditions  $c_{n1} < a_1$ ;  $c_{n2} < a_2$  and in which the condensation is accompanied by rarefaction of gas ( $p_2 < p_1$ ). Shocks corresponding to the relationships  $c_{n1} > a_1$  and  $c_{n2} > a_2$  cannot be actually realized, since such a shock would be displaced relative to the gas which is ahead of it with a supersonic speed and its genesis could not be reflected in the state of this gas.

Condensation shocks in a subsonic flow cannot transfer gas into a region of supersonic speeds ( $c_{n1} < a_1$ ;  $c_{n2} < a_2$ ), since in this case it is necessary to divert from the gas heat, which does not correspond conditions of condensation.

We shall determine the change of entropy in condensation shocks.

In particular case  $\bar{k} = 0$ , we shall obtain:

$$\Delta s = R \ln \left[ \left( 1 + \bar{\Delta} \bar{f}_* \right)^{\frac{\bar{k}}{\bar{k}-1}} \frac{p_{21}}{p_{*1}} \right]. \quad (4-54)$$

Formula (4-54) contains the ratio  $\frac{p_{21}}{p_{*1}}$ , which can be found by equation (4-46) by substituting  $\bar{k} = 0$ ; here  $M_2$  and  $\frac{p_2}{p_1}$  are determined by formulas (4-44) and (4-45).

Studying equation (4-54), it is possible to be assured that for shocks of the first three types (Table 4-2)  $\Delta s > 0$ . However, by drawing upon the subsidiary

condition (thermodynamic state before shock must correspond to the beginning of a rapid condensation) and considering the effect of the heat exchange, it is possible to show that the shock of first type, as well as fourth, is impossible.

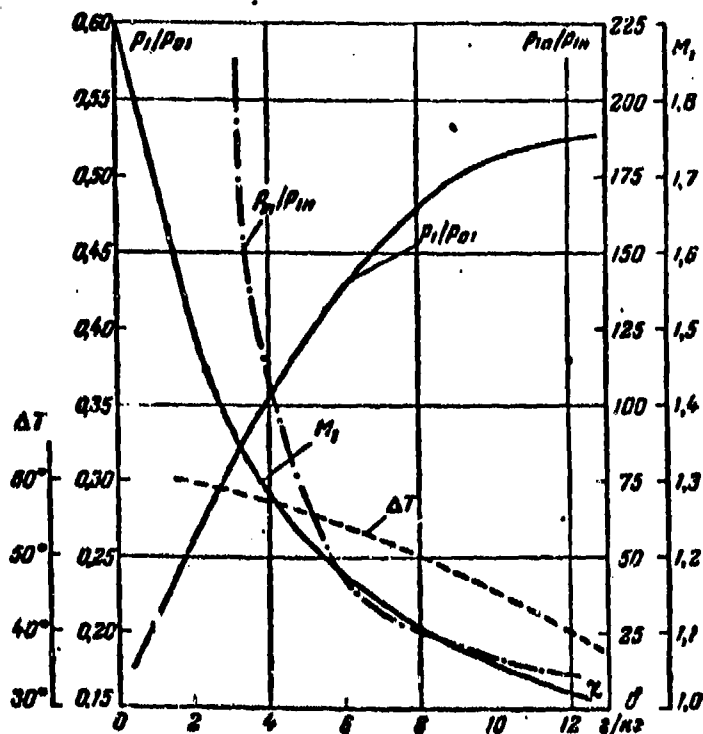


Fig. 4-36. Dependence of the relative pressure and  $M_1$  number on absolute humidity  $x$  in Laval nozzles.

Experience confirms the possibility of the formation of shocks of second and third types.

The air humidity and speed of flow exert a decisive influence on the position of shock, its shape, and intensity. In Fig. 4-36 there are presented curves of relative pressure and  $M_1$  number before condensation shock of depending upon absolute humidity of air  $x$  by experiments of A. A. Stepchikov, made in Laval nozzles. With an increase in humidity the condensation shock is transferred into region of lower  $M_1$  numbers.

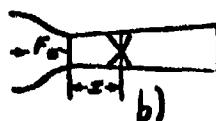
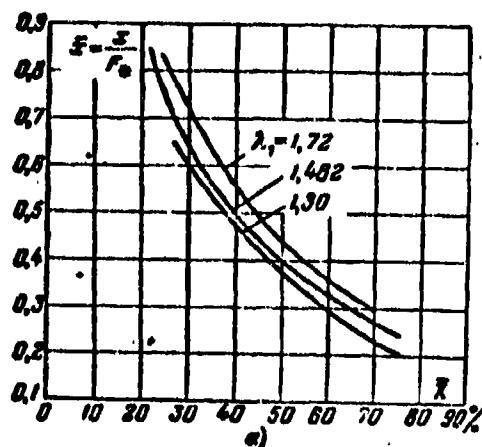


Fig. 4-37.

a — change in position of condensation shocks in Laval nozzle depending upon the speed  $\lambda_1$  and relative humidity  $\bar{x}$ ; b — diagram of shock in nozzle.

With an increase of humidity the supersaturation of flow of air by water vapor, determined by the ratio of the partial vapor pressures to pressure of saturation  $\frac{P_{1n}}{P_{1n}}$ , and also the supercooling  $\Delta T = T_{H1} - T_1$  (Fig. 4-36), where  $T_{H1}$  is the temperature of saturation, and  $T_1$  — temperature before shock, decrease. As the humidity increases the magnitudes of the supersaturation and supercooling decrease.

The displacement of the condensation shock depending upon humidity is explained, apparently, by the fact that with a decrease in the amount of water vapor, its condensation occurs at a lower temperature, corresponding to a high  $M_1$  number.

In the displacement also the shape of the shock changes: with a high humidity the shock becomes bridge-like and approaches a normal shock; with a decrease in the humidity there is observed, as a rule, a system of two intersection shocks.



In conclusion let us note that the discussed theory of condensation shocks ignores questions on the mechanism of condensation--the genesis and development of nuclei of condensation.

## CHAPTER 5

### MOTION OF GAS DURING PRESENCE OF FRICTION

#### 5-1. Temperature of Stagnation in Viscous Fluid

In analysing the motion of a real (viscous) fluid it is necessary to consider dissipation of energy, caused by internal friction and thermal conduction, i.e., thermodynamic irreversibility of process.

The motion of viscous fluid is described by the system of equations of conservation: flow, momentum and energy. Equation of continuity (1-12), as has already been indicated, is valid also for viscous fluid. Equation of momentum in form of Euler (1-16) should be augmented by terms, which take into consideration the influence of viscosity.

It should be emphasized that for irreversible processes of motion, integrals of equation of motion and energy do not conform. In deriving the equation of energy for a flow (Sec. 2-1) it was indicated that it was valid also for adiabatic (irreversible) flows. However, this remark is fully valid only in particular case, when the work of forces of friction completely will be converted into heat. Such a process corresponds to simplest scheme of a one-dimensional flow or motion of gas with a uniform field of speeds.

In analysing the motion of a viscous fluid with a nonuniform distribution of speeds in the flow, the condition of equivalence of frictional heat and work of friction is not fulfilled. In such a flow only part of work of friction is

transformed into heat, but the other part causes a purely mechanical effect: rebuilding of the field of speeds, in process of which there occurs a redistribution of kinetic energy between particles of the fluid. It follows from this that different particles obtain a varying quantity of frictional heat and have a varying reserve of total energy. Consequently, the condition  $i_0 = \text{const}$ , in the general case is not an integral of equation of energy for entire mass of fluid, since in the flow there will be formed a local redistribution of the energy.

As example, let us consider motion of a viscous compressible fluid between two flat walls (Fig. 5-1). The upper wall is moved in direction of the x-axis with

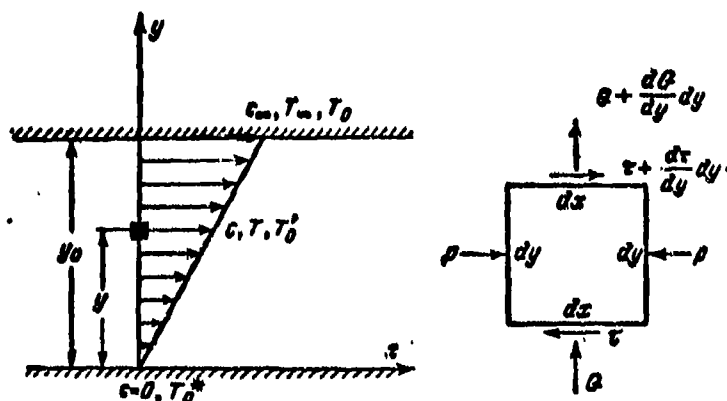


Fig. 5-1. For deriving equation of energy for flow of compressible viscous fluid between two flat walls (flow without gradient)

a constant speed, equal to speed of gas  $c_\infty$ . On the lower wall speed is equal to zero, since this wall is motionless.\* We assume that the pressure is kept constant along the x- and y- axes, i.e.,  $\frac{\partial p}{\partial x} = \frac{\partial p}{\partial y} = 0$ .

If the speed of motion of upper wall is small, for a adiabatic flow it is possible to assume that temperature is constant and identical for all points of the flow. If, however, magnitude  $c_\infty$  is fairly high, then it is necessary to consider that temperature  $T$  is a function of  $y$ . In such a flow the effect of compressibility

\*The considered particular case of motion of gas is call Couette flow.

is developed only in connection with a change in temperature of gas; density of gas varies in accordance with the formula (for an ideal gas)

$$\rho(y) = \frac{p}{RT(y)} = \frac{\text{const}}{T(y)}.$$

Since in considered problem the speeds along the x-axis do not change, and the pressure is kept constant both along the y- and x-axes then the law of conservation of energy is formulated very simply: quantity of heat, admitted to the element, plus the work of forces of frictions is equal to zero.

We shall designate:  $Q$  as quantity of heat, transmitted to element in unit of time from neighboring particles;  $\tau$  is the stress of friction. The quantity of heat, received by the element, is determined as a difference (Fig. 5-1):

$$Qdx - \left( Q + \frac{dQ}{dy} dy \right) dx = - \frac{dQ}{dy} dy dx^*.$$

The difference between the works due to frictional forces per second we find by equation

$$\left[ \left( \tau + \frac{d\tau}{dy} dy \right) \left( c + \frac{dc}{dy} dy \right) - \tau c \right] dx = \frac{d}{dy} (\tau c) dy dx.$$

Then equation of energy will be:

$$\frac{d}{dy} (-Q + \tau c) = 0,$$

or

$$-Q + \tau c = \text{const.}$$

The constant on the right-hand side of equation of energy is determined from boundary conditions. Thus, at  $y = 0$ ,  $c = 0$  and  $Q = Q_0$ , where  $Q_0$  is the specific quantity of heat, transmitted to flow of gas from an external source.

Consequently,

$$-Q + \tau c = -Q_0.$$

For a laminar flow  $\tau$  is determined by formula (1-4)

We remember that

$$Q = -\lambda \frac{dT}{dy}.$$

---

\*The dimension of an element in the direction of x-axis is adopted for the unit.

where  $\lambda$  is the coefficient of thermal conductivity.

After simple transformations we obtain:

$$\lambda \frac{dT}{dy} + \rho c \frac{dc}{dy} = \mu \frac{d}{dy} \left( \frac{c_p T}{Pr} + \frac{c^2}{2} \right) = -Q_0.$$

The magnitude

$$Pr = \frac{\mu c_p}{\lambda}$$

is called the Prandtl number. Let us note that the thermal conductivity and viscosity coefficients appearing in the expression for  $Pr$  depend on the temperature:

$$\lambda = \lambda(T), \mu = \mu(T).$$

The integral of equation of energy for the case  $\mu = \text{const}$  makes it possible to associate the static enthalpy in the flow with enthalpy along a fixed wall in following manner:

$$i - i_0 + Pr \frac{c^2}{2} = -Pr Q_0 \int_0^y \frac{dy}{\mu}.$$

where in a linear distribution of the speed  $\int_0^y \frac{dy}{\mu} = \int_0^y \frac{du}{\tau_0} = \frac{u}{\tau_0}$ ;

$\tau_0$  is the stress of friction on wall,  $i_0 = c_p T_0$  is the enthalpy of stagnation on wall.

Consequently,

$$i - i_0 + Pr \frac{c^2}{2} = -Pr \frac{Q_0}{\tau_0} c. \quad (5-1)$$

For the upper wall, moving together with flow with a speed  $c_\infty$ , there is readily obtained:

$$i_\infty - i_0 + Pr \frac{c_\infty^2}{2} = -Pr \frac{Q_0}{\tau_0} c_\infty. \quad (5-1a)$$

By means of (5-1) and (5-1a) after simple transformations we find:

$$i + Pr \left( \frac{c^2}{2} + \frac{Q_0}{\tau_0} c \right) = i_\infty + Pr \left( \frac{c_\infty^2}{2} + \frac{Q_0}{\tau_0} c_\infty \right). \quad (5-1b)$$

or

$$\begin{aligned} \frac{i}{i_\infty} - \frac{T}{T_\infty} &= 1 + Pr \frac{k-1}{2} \left( 1 - \frac{c^2}{c_\infty^2} \right) M_\infty^2 + \\ &+ Pr \frac{Q_0}{\tau_0 c_\infty} (k-1) \left( 1 - \frac{c}{c_\infty} \right) M_\infty^2. \end{aligned} \quad (5-1c)$$

We find for the case of an adiabatic flow ( $Q_0 = 0$ ) a relation between temperatures of stagnation on moving wall and in an arbitrary section of flow (at a distance  $y$ ), by taking into consideration that the temperature of stagnation and

thermodynamic temperature are associated by the relationship

$$T'_0 = T + \frac{c^2}{2c_p} \quad (5-1d)$$

By bearing in mind that there is considered the case  $c_p = \text{const}$ , consequently  $i = c_p T$ , and for an adiabatic flow and  $Q_0 = 0$ , from (5-1) and (5-1d) we obtain:

$$T'_0 = T'_0 + (1 - \text{Pr}) \frac{c^2}{2c_p} \dots$$

For a moving wall by means of equations (5-1a) and (5-1d) we will have:

$$T_0 = T'_0 + (1 - \text{Pr}) \frac{c_\infty^2}{2c_p}$$

Consequently,

$$\frac{T'_0}{T_0} = 1 - (1 - \text{Pr}) \frac{c_\infty^2 - c^2}{2c_p T_0} = 1 - (1 - \text{Pr}) (\xi_\infty^2 - \xi^2), \quad (5-2)$$

where

$$\xi_\infty = \frac{c_\infty}{\sqrt{2T_0}}; \xi = \frac{c}{\sqrt{2T_0}}$$

Formula (5-2) indicates that for  $\text{Pr} \neq 1$  in a viscous gas temperature of stagnation, i.e., total energy is not kept constant through the section. At  $\text{Pr} = 1$  the temperature of stagnation  $T'_0 = T_0 = \text{const}$ . for all points of flow.

The Pr number characterizes the relationship between heat, liberated due to friction, and heat, eliminated from element by thermal conductivity. At  $\text{Pr} < 1$ , which takes place for all gases, the heat dissipation is accomplished more intensively than its liberation. In this case  $T'_0 < T_0$ . At  $\text{Pr} > 1$  the liberation of frictional heat occurs more intensively than its elimination, and  $T'_0 > T_0$ .

For a perfect gas the Pr number is a physical constant, independent of the state of gas.

For the more general case of a two-dimensional flow of gas, when the speeds depend on x and y differential equations of energy can be presented in such a form\*:

$$\frac{\rho u}{\text{Pr}} \left( \frac{\partial T \left( 1 + \text{Pr} \frac{k-1}{2} M^2 \right)}{\partial x} + \frac{\partial T \left( 1 + \text{Pr} \frac{k-1}{2} M^2 \right)}{\partial y} \right) = -u \frac{\partial T \left( 1 + \frac{k-1}{2} M^2 \right)}{\partial x} + v \frac{\partial T \left( 1 + \frac{k-1}{2} M^2 \right)}{\partial y} \quad (5-3)$$

\*The derivation of differential equations of energy and momentum can be found in the book by L. G. Loytsyanskiy et al. (See list of references).

The equations of momentum with the addition of terms, considering influence of viscosity (equation of Navier-Stokes), are written in the following form:

$$\begin{aligned} \frac{\partial u}{\partial t} + u \frac{\partial u}{\partial x} + v \frac{\partial u}{\partial y} &= X - \frac{1}{\rho} \cdot \frac{\partial p}{\partial x} + \nu \left[ \left( \frac{\partial^2 u}{\partial x^2} + \frac{\partial^2 u}{\partial y^2} \right) + \right. \\ &\quad \left. + \frac{1}{3} \cdot \frac{\partial}{\partial x} \left( \frac{\partial u}{\partial x} + \frac{\partial v}{\partial y} \right) \right]; \\ \frac{\partial v}{\partial t} + u \frac{\partial v}{\partial x} + v \frac{\partial v}{\partial y} &= Y - \frac{1}{\rho} \cdot \frac{\partial p}{\partial y} + \\ &\quad + \nu \left[ \left( \frac{\partial^2 v}{\partial x^2} + \frac{\partial^2 v}{\partial y^2} \right) + \frac{1}{3} \cdot \frac{\partial}{\partial y} \left( \frac{\partial u}{\partial x} + \frac{\partial v}{\partial y} \right) \right]. \end{aligned} \quad (5-4)$$

These equations are supplemented by the equation of continuity (1-12) for a two-dimensional flow:

$$\frac{\partial \rho}{\partial t} + \frac{\partial (\rho u)}{\partial x} + \frac{\partial (\rho v)}{\partial y} = 0; \quad (5-4a)$$

equation of state (1-1) and equation of friction, for example, for a laminar flow by Newton's law (1-4).

During investigation of motion of gas in pipes and channels by taking into account the viscosity, and also in studying the flow around bodies by a gas flow, the problem reduces to determination of the losses of energy and aerodynamic forces, acting on a streamlined surface. For this purpose it is necessary to solve together the closed system of six equations (5-3), (5-4), (5-4a), (1-1), (1-4), by determining the unknown functions of the coordinates:  $p$ ,  $\rho$ ,  $u$ ,  $v$ ,  $T$  and  $\tau$  (for a steady flow).

## 5-2. Conditions of Gas-Dynamic Similarity

In connection with very great difficulties of solving the system of equations of motion in the general case (such solutions are obtained successfully only for simplest particular cases) in practice the drag coefficients and loss factors of energy frequently are determined experimentally by means of testing models under laboratory conditions. At same time it is necessary to observe such conditions in testing models, which assure the reliability of obtained results and allow us to extend these results to natural objects.



Fig. 5-2. Schematic Diagram of Similar flows.

The widely applied method of similarity in mechanics allows us to formulate the indicated conditions of model tests and it establishes a procedure of transferring results of laboratory investigations to objects in nature.

The aerodynamic forces, acting on a streamlined body or on wall of a channel (including also forces of resistances) are expressed in terms of dimensionless coefficients. We shall establish, on what kind of parameters, in general case the drag coefficients depend.

For this purpose let us consider the flow around two geometrically similar bodies by a fluid (Fig. 5-2).

In the case of the kinematic and dynamic similarity of two considered phenomena, the fields of speeds and forces in the two flows should be reciprocally proportional. Then, by introducing scales of the lengths  $L$ , time  $T$ , and mass  $M$ , it is possible to present an association between the lengths times and masses of two similar flows in following manner:  $\underline{L}' = L\underline{L}$ ;  $\underline{t}' = T\underline{t}$ ;  $\underline{m}' = M\underline{m}$ .

The scales of all other magnitudes, appearing in equations (5-4), readily are expressed by means of the indicated scales.

Let us assume that equations (5-4) express a connection between flow parameters of the first flow. By bearing in mind dimensionality of magnitudes, appearing in these equations, reflected in units of measurement: length of  $x, y$  [m], speed  $u, v$  [m/sec], density  $\rho$  [kg  $\cdot$  sec<sup>2</sup>/m<sup>4</sup>], kinematic viscosity  $\nu$  [m<sup>2</sup>/sec], mass  $m$  [kg  $\cdot$  sec<sup>2</sup>/m] and pressure  $p$  [kg/m<sup>2</sup>], it is easy to associate parameters of first and



second flows by means of scalar coefficients.

$$\begin{aligned}\frac{x}{x'} &= \frac{y}{y'} = L; \quad k_c = \frac{c}{c'} = \frac{n}{n'} = \frac{v}{v'} = \frac{L}{T}; \\ k_l &= \frac{l}{l'} = \frac{M}{L^3}; \quad k_v = \frac{v}{v'} = \frac{L^2}{T}; \\ k_p &= \frac{p}{p'} = \frac{M}{T^2 L^2}.\end{aligned}\quad (5-5)$$

Here, and above the prime designates flow parameters of the second flow. Relationships between parameters (5-5) are an evident result of the proportionality of the linear dimensions, times and masses of the two similar flows.

By arranging axis of the coordinates in both flows identically, by means of substitution of relationships (5-5) into the first equation (5-4) it is possible to write for the second flow:

$$\begin{aligned}\frac{k_c}{T} \frac{\partial u}{\partial t} + \frac{k_c^2}{L} \left( u' \frac{\partial u}{\partial x} + v' \frac{\partial u}{\partial y} \right) &= M X - \frac{k_p}{k_l L} \frac{1}{\rho} \frac{\partial p}{\partial x} + \\ &+ \frac{k_l k_c}{L^3} v' \left[ \left( \frac{\partial^2 u}{\partial x^2} + \frac{\partial^2 u}{\partial y^2} \right) + \frac{1}{3} \frac{\partial}{\partial x} \left( \frac{\partial u}{\partial x} + \frac{\partial v}{\partial y} \right) \right].\end{aligned}\quad (5-6)$$

Equation (5-6) expresses equation of momentum in a differential form for the second flow, written out in terms of parameters of the first flow.

All terms of equations (5-4) and (5-6) have, naturally an identical dimensionality,  $\frac{L}{T^2}$  [m/sec<sup>2</sup>], of which one is readily convinced by means of relationships (5-5). In order that the flows are dynamically similar, it is necessary that they satisfy one and the same differential equations of motion. It follows from this that complex factors in front of terms of equation (5-6) are identical, i.e.,

$$\frac{k_c^2}{L} = \frac{k_c}{T} = M = \frac{k_p}{k_l L} = \frac{k_l k_c}{L^3},$$

or

$$\frac{L}{k_c T} = 1; \quad \frac{ML}{k_c^2} = 1; \quad \frac{k_p}{k_l k_c^2} = 1; \quad \frac{k_l}{L k_c} = 1.$$

By replacing here the scalar coefficients from (5-5), finally we obtain by taking into account the equation of energy (5-3) the following conditions of similarity:

$$\frac{lc}{\nu} = \frac{\nu c'}{\nu'}; \quad \frac{cl}{l} = \frac{c'l'}{l'}; \quad \frac{gl}{c^3} = \frac{g'l'}{c'^3};$$

$$\frac{\rho}{\rho'} = \frac{\rho' c'}{\rho c}; \quad \frac{\rho c}{\lambda} = \frac{\rho' c'}{\lambda'}.$$

(5-7)

Thus, the two flows are dynamically similar, if there are fulfilled relationships (5-7) between parameters of these flows. Relationships (5-7) are called criteria of similarity (dimensionless numbers). The first relationship (5-7) establishes an equality of the Reynolds numbers in the two flows:

$$Re = \frac{lc}{\nu} = Re'.$$

The Reynolds' number expresses the relationship between forces of viscosity and forces of inertia in the flow.

The second condition is unique, where there appear similar time intervals  $t$  and  $t'$ , and it is obtained as a result of the similarity of terms, containing the local accelerations ( $\frac{\partial u}{\partial t}$  and  $\frac{\partial v}{\partial t}$ ) in the equations of motion. The local accelerations characterize only transient, including also periodic, processes of motion of a gas. Consequently, second equality is condition of similarity for transient flows.

The relation

$$Sh = \frac{cl}{l} Sh'$$

is called the Strouhal number; for a periodic motion.

$$Sh = \frac{c}{n l},$$

where  $n = \frac{1}{t}$  is the frequency of periodically non-stationary process.

The third equation gives an equality of a dimensionless number which takes into consideration the influence of body forces in the flow. If the acceleration in field of Earth's attraction can be assumed to be constant ( $g = g'$ ), then, this criterium, called the Froude number, is readily presented in such a form:

$$Fr = \frac{l}{c^2} = Fr'.$$

In gas flows the influence of body forces, as a rule, is small and therefore the Fr number during the simulating of gas flows is not taken into account.

Fourth equation (5-5) expresses connection between static pressures and velocity heads at similar points of similar flows. The magnitude

$$\bar{p} = \frac{2p}{\rho c^2} = \bar{p}'$$

can be considered as a characteristic, which takes into consideration the influence of compressibility. Here it is easy to check, by replacing p in terms of speed of sound.

$$p = \frac{\rho c^2}{k}.$$

Then, for the two flows we obtain:

$$k \frac{c^2}{a^2} = k' \frac{c'^2}{a'^2}.$$

or

$$kM^2 = k'M'^2.$$

Consequently, identity of the  $\bar{p}$  numbers has as its own consequence an equality of kM numbers at similar points of flows. It follows from this that the M number, known by us from the preceding, emerges, as the dimensionless numbers, which reflect the property of compressibility. To the same degree also index of isentropy k in a perfect gas should be considered as a dimensionless number.

In considering differential equation of energy (5-3) for compressible viscous fluid, can be obtained additional, already familiar from the preceding, Prandtl dimensionless number:

$$Pr = \frac{\mu c_p}{\lambda}.$$

From this equation there ensues also identity of criteria k and M for the gas flows.

In a turbulent flow there is introduced the important characteristic--the degree of turbulence:

$$E = \frac{\bar{\epsilon}}{\epsilon_m},$$

where  $\overline{c^2} = \frac{1}{\Delta t} \int_{t_1}^{t_2} (c - c_m)^2 dt$  is the mean square rate of the pulsation;  $c$  is instantaneous value of speed;  $c_m$  is average speed of turbulent flow:

$$c_m = \frac{1}{\Delta t} \int_{t_1}^{t_2} c dt.$$

In summarizing, let us note that necessary conditions of similarity of two flows reduce to an equality of the determining criteria at similar points in nature and models and of the identity of initial and boundary conditions.

An analysis of equations of motion and the dimensionality of magnitudes, determining the resistance of streamlined body or loss of energy in flow of gas, showed that the corresponding dimensionless characteristics of the drag are functions of the fundamental dimensionless numbers:\*

$$\begin{aligned} c_x &= c_x(\text{Re}, M, \text{Pr}, \text{Sh}, E); \\ \zeta &= \zeta(\text{Re}, M, \text{Pr}, \text{Sh}, E), \end{aligned} \quad (5-7a)$$

where  $c_x$  — is the drag coefficient (see Sec. 5-13);

$\zeta$  — is the loss factor of energy (see Sec. 4-5; 5-14; 8-5 et al.)

In an investigation of different phenomena not all the criteria have an identical physical value. Depending upon the specific problem one or several criteria may have predominant value, while another group of criteria does not exert a marked effect on characteristics of the motion.

Thus, for example, for a steady-motion of incompressible fluid, the  $M$  and  $\text{Sh}$  numbers lose their meaning and the dependence (5-7a) is simplified.

With a consideration of the compressibility in a steady motion for gases with identical physical properties  $c_x = c_x(\text{Re}, M)$ .

The equality of all dimensionless numbers can be assured only in an experiment involving natural phenomena; this, however is associated with major difficulties.

---

\* In the relationship (5-7a) criterion  $k$  does not appear, since according to molecular-kinetic theory of gases, the condition  $\text{Pr} = \text{Pr}'$  is equivalent to condition  $k = k'$ .

Usually there is made an approximate similarity (partial modeling) on the basis of one or two of the most important criteria. Results of experiment are simply corrected also for other criteria, if there are known the values of these criteria in the experiment and dependence of studied characteristics on these criteria.

In an investigation of flows, in which there are two or three determining criteria (for example,  $Re$ , and  $M$  or  $Re$ ,  $M$  and  $Sh$ ), it is necessary to put principles of individual modeling into practice, i.e., to assure possibility of independent change of each of the criteria in a specific range of its values.

In conclusion, let us note that the above-considered method of dimensional analysis may prove to be very effective, if there are known the physical parameters, determining investigated process, but it does not succeed in solving or even in writing out a system of differential equation of the problem.

In these cases the method of dimensionality in combination with experimental data makes it possible to obtain a solution for a whole class of mechanically similar phenomena.

### 5-3. One-dimensional Flow of Gas in the Presence of Friction. Basic Equations.

Basic equations of a steady adiabatic motion of a viscous gas are the well-known equations of continuity, momentum, and energy.

The equation of momentum of a one-dimensional steady flow without an exchange of energy from the environment in the presence friction can be written in such a form:

$$\rho c dc + \frac{dp}{\rho} + dX_{tp} = 0, \quad (5-8)$$

where  $dX_{tp}$  is the unit impulse of the frictional force.

The magnitude  $dX_{tp}$  can be expressed by the hydraulic formula:

$$dX_{tp} = \zeta \frac{c^2}{2} \cdot \frac{dx}{D}, \quad (5-9)$$

where  $\zeta$  is the drag coefficient;  $D$  is the inner diameter of pipe.

By solving commonly the equations (5-8), (5-9), (2-14) and (2-6) there can be obtained a differential equation of distribution of speeds along a tube of variable cross-section by taking into consideration the influence of viscosity. It is obvious that this equation is analogous to (2-29), but it should contain still another term which takes into consideration the influence of viscosity. Simple computations result in such an expression:

$$(2^2 - 1) \frac{d\lambda}{\lambda} = \left(1 - \frac{k-1}{k+1} \lambda^2\right) \frac{dF}{F} - \zeta \frac{k}{k+1} \lambda^2 d\bar{x}, \quad (5-10)$$

where  $\bar{x} = \frac{x}{D}$ .

A formula, determining change of pressure of flow along a tube of variable cross-section, by following the already known method, discussed in Chapter 2, can be obtained in the following form:

$$\frac{dp}{p} = -\frac{2k}{k+1} \frac{\lambda^2}{\lambda^2 - 1} \left( \frac{dF}{F} - \frac{\frac{k}{k+1} \lambda^2}{1 - \frac{k-1}{k+1} \lambda^2} \zeta d\bar{x} \right). \quad (5-11)$$

From equations (5-10) and (5-11) it may be concluded, that the variation of parameters of flow in a tube of variable cross-section takes place under the influence of two factors: deformation of flow (change in tube section) and forces of friction. Equations show that influence of friction always is unilateral. Thus, for example, at subsonic speeds ( $\lambda < 1$ ) in a narrowing tube ( $dF > 0$ ) friction promotes the acceleration of flow ( $d\lambda > 0$  and  $dp < 0$ ). At supersonic speeds in the same tube ( $dF < 0$ ) friction results in a more gradual drop in the speed and correspondingly to more gradual increase in pressure in comparison with an ideal process without losses.

From equations (5-10) and (5-11) it follows that in simplest case of tube of nonvarying cross-section ( $dF = 0$ ) at  $\lambda < 1$ , we have  $\frac{d\lambda}{\lambda} > 0$  and  $\frac{dp}{p} < 0$  and, consequently, flow is accelerated. It is simple to see that in this case at a supersonic speed ( $\lambda > 1$ )  $\frac{d\lambda}{\lambda} < 0$ : the flow is decelerated.

In comparing the influence of a change of section of tube (deformations of tube of flow [stream tube]) and influence of friction, it may be concluded, that in

subsonic and supersonic flows, friction qualitatively results in the same change in speed of flow, as a decrease in the section of tube.

Consequently, influence of forces of friction in a flow can be replaced by an equivalent deformation of the stream—i.e., by a decrease of its section in the direction of the motion.

The competence of such a replacement results from the following considerations. The motion of a gas in a tube without an energy exchange, but in the presence of forces of friction is an irreversible adiabatic process. Such a process, as we have already known, is accompanied by an increase in entropy. The increase in entropy can be expressed by equation (4-27).

For a system without an exchange of energy (by bearing in mind, that  $T_{01} = T_{02}$  and that the equation of state gives  $\frac{p_{02}}{p_{01}} = \frac{\rho_{02}}{\rho_{01}}$ ) we obtain:

$$\Delta s = R \ln \frac{p_{02}}{p_{01}} = R \ln \frac{1}{c_0}. \quad (5-12)$$

Since the entropy increases in direction of flow, the pressure of stagnation  $p_{02}$  should decrease.

On basis of equation of continuity (2-41) for two sections of the tube, let us note that in both cases at identical magnitudes  $F_1$ ,  $\lambda_1$  and  $\lambda_2$ , the section  $F_2$  subject to frictional forces must be larger than for an isentropic flow.

The magnitude  $\lambda$  can be considered as active section of the stream. For a tube of constant section ( $F = \text{const}$ ) it is obvious that an active section  $\lambda$  in presence of friction decreases, since the magnitude  $c_0$  decreases.

Equation (5-10) may be used for certain conclusions about the location of section, corresponding to extreme values of speed. We express from equation (5-10) logarithmic derivative of the section:

$$\frac{dF}{F} = \frac{(\lambda^2 - 1) \frac{d\lambda}{\lambda} + \frac{k}{k+1} \lambda^2 d\lambda}{1 - \frac{k-1}{k+1} \lambda^2};$$

it follows from this that at  $d\lambda = 0$  and  $\lambda \neq 1$

$$\frac{dF}{F} = \frac{\frac{k}{k+1} \lambda^2 d\lambda}{1 - \frac{k-1}{k+1} \lambda^2} > 0. \quad (5-13)$$

Consequently, a section, corresponding to a maximum speed at  $\lambda < 1$  and to minimum speed at  $\lambda > 1$ , does not coincide with the minimum section, but is displaced towards the expanding portion of the tube. Correspondingly, the section in the diverging portion of tube also corresponds to the critical conditions ( $\lambda = 1$ ). This means that the minimum and critical section of tube in the presence of friction do not coincide. In this case, by assuming in (5-10)  $\lambda = 1$ , we obtain:

$$\frac{dF}{F} = \frac{k}{2} d\bar{x} > 0.$$

#### 5-4. Motion of Gas in a Cylindrical Tube

From equation (5-10) for a cylindrical tube  $\frac{dF}{F} = 0$  we obtain:

$$\left(\frac{1}{\lambda^2} - 1\right) \frac{d\lambda}{\lambda} = \frac{k}{k+1} d\bar{x}. \quad (5-14)$$

From preceding considerations and also directly from an analysis of equation (5-14) it is easy to reach the conclusion that the critical speed of flow can occur only in exit section of cylindrical tube. Actually, according to equation (5-14) at  $\lambda < 1$  and  $d\lambda > 0$  the flow in pipe is accelerated, and at  $\lambda > 1$  and  $d\lambda < 0$  it is decelerated. The case  $\lambda = 1$  in intermediate section of tube contradicts equation (5-14) and is physically unrealistic.

Let us assume that drag coefficient is a constant value.\* Then, equation (5-14) can be integrated.

The integral of equation (5-14) we write as:

$$\frac{1}{\lambda^2} - \frac{1}{\lambda_1^2} - \ln \frac{\lambda^2}{\lambda_1^2} = \frac{2k}{k+1} \bar{x}, \quad (5-14a)$$

where  $\lambda_1$  is the dimensionless speed in initial section of tube;

$\lambda$  is dimensionless speed in certain section at a distance of  $\bar{x}$  from the initial section.

\*Such assumption is justified only as a first approximation. In reality it depends on the Re and M numbers.



We introduce a dimensionless coordinate, which is called the reduced length of tube:

$$\chi = \frac{2k}{k+1} \zeta \bar{x}.$$

Then, equation (5-14a) may be written out as:

$$\chi = \frac{1}{\lambda_1^2} - \frac{1}{\lambda^2} - \ln \frac{\lambda^2}{\lambda_1^2}. \quad (5-15)$$

The relationship between  $\lambda$  and  $\chi$  with a constant value of  $\lambda_1$  is shown in Fig. 5-3. Magnitude  $\chi$  has a maximum at  $\lambda = \lambda_1 = 1$ .

Maximum value of reduced length of tube is expressed by the formula

$$\chi_{\max} = \frac{1}{\lambda_1^2} - 1 + \ln \lambda_1^2. \quad (5-16)$$

The curves  $\chi(\lambda)$  consist of two branches, corresponding to subsonic ( $\lambda < 1$ ) and supersonic ( $\lambda > 1$ ) flows in a pipe of constant section (Fig. 5-3).

The curves graphically illustrate the impossibility of a transition of speeds in a cylindrical tube from one region to another. In such a tube as was shown

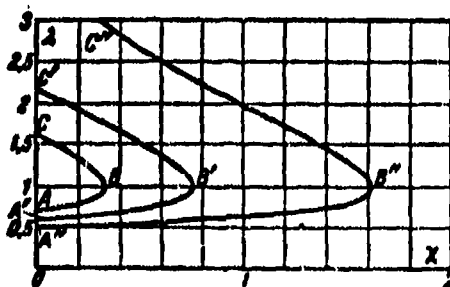


Fig. 5-3. Dependence of dimensionless speed at exit of tube on speed at entry and the reduced length of tube.

above, with a definite speed at entry  $\lambda_1$  and corresponding length at exit, there will be attained a critical speed ( $\lambda_1 = 1$ ).

The section of curve AB (Fig. 5-3) corresponds to subsonic flows at entry into tube ( $\lambda_1 < 1$ ) while the section CB corresponds to supersonic ( $\lambda_1 > 1$ ). Point B determines the maximum magnitude of the function  $\chi$  for a given value of  $\lambda_1$ .

From formula (5-16) it follows that when  $\lambda_1 = 1$   $\gamma = 0$ .

Graphically, the dependence (5-16) is presented in Fig. 5-4. The curve also has two branches. The lower branch corresponds to subsonic speeds at tube entry --- and the upper to supersonic speeds.

Thus, equation (5-16) shows that for cylindrical tube of given dimensions  $\underline{l}$

and  $D$  at a speed at tube exit  $\lambda_2 = 1$  and

for definite values  $k$  and  $\zeta$ , the dimensionless speed at tube entry is  $\lambda_1$ , and at

the same time the reduced gas flow  $q_1$  has

strictly specific values.

At a subsonic speed at entry to a

cylindrical tube of length  $\underline{l}$ , characterized

by a drag coefficient  $\zeta$ , in a steady

motion there can pass through a maximum amount of gas, if  $\lambda_2 = 1$ .

The absolute flow of gas through a tube of maximum length will be equal to:

$$G_{max} = gF(\rho_1 c_1)_{max} = gF q_{1, max} \rho_{01} a_{01} = \\ = gF \left( \frac{k+1}{2} \right)^{\frac{1}{k-1}} \cdot \lambda_{1, max} \left( 1 - \frac{k-1}{k+1} \lambda_{1, max}^2 \right)^{\frac{1}{k-1}} \rho_{01} d.$$

By remembering that

$$\rho_{01} a_{01} = \rho_{01} \left( \frac{2}{k+1} \right)^{\frac{1}{k-1}} \sqrt{\frac{2k}{k+1} R T_{01}} = \\ = \left( \frac{2}{k+1} \right)^{\frac{1}{k-1}} \sqrt{\frac{2k}{(k+1)R}} \cdot \frac{\rho_{01}}{\sqrt{T_{01}}},$$

we obtain:

$$G_{max} = F \sqrt{\frac{2gk}{(k+1)R}} \lambda_{1, max} \left( 1 - \frac{k-1}{k+1} \lambda_{1, max}^2 \right)^{\frac{1}{k-1}} \frac{\rho_{01}}{\sqrt{T_{01}}}. \quad (5-17)$$

Thus, for increasing the absolute flow of gas through cylindrical tube of specific dimensions it is necessary to increase pressure of total stagnation at

tube entry or with constant value  $p_{01}$  -- to decrease the temperature of stagnation  $T_0$ . At the same time at exit section of tube there will be as before, a critical speed, the absolute value of which decreases as the stagnation temperature lowers. However, the flow will increase owing to the increase in density.

At supersonic speeds at tube entry as the experiment shows there are detected certain new properties of the flow, which are not described by equation (5-15). Let us note that according to equation (5-15) at  $\lambda_1 > 1$  speed in tube must continuously fall towards exit section according to curve CB in Fig. 5-3, and the pressure -- correspondingly continuously increases. However, in reality the change in speeds and pressures in tube in a number of cases occurs intermittently.

Prior to a more detailed discussion of this case of motion of gas, we shall find dependencies, determining variation of parameters of flow between two arbitrary sections.

Since in an isolated tube  $i_0 = \text{const}$ , then for any two sections there can be written  $T_{01} = T_{02} = \text{const}$ . From this condition we obtain equation for  $T/T_0$  in the form of equation (2-22).

For ratios of the pressures it is possible to use formulas (2-41a) and (2-42). After simple transformations we obtain an association between the static and total pressures in the following form:

$$\frac{p}{p_0} = \left( \frac{2}{k+1} \right)^{\frac{1}{k-1}} q_1 \frac{1 - \frac{k-1}{k+1} \lambda^2}{\lambda} \quad (5-18)$$

Hence, at  $\lambda = \lambda_c = 1$ , there is determined the critical ratio of pressures:

$$q_c' = \left( \frac{2}{k+1} \right)^{\frac{k}{k-1}} q_1 = q_c q_1 \quad (5-19)$$

Formula (5-19) shows that the critical ratio of pressures  $\frac{p}{p_{01}}$  for irreversible flows will be less than for isentropic flows for which

$$q_c = \left( \frac{2}{k+1} \right)^{\frac{k}{k-1}}$$

Equations (5-18) and (5-15) make it possible to construct graphs of the change in pressures along a tube for given values of  $q_1$  and  $\lambda$ .

A similar graph is shown in Fig. 5-5 for the case of supersonic speed at tube entry  $\lambda_1 = 1.76$  and  $q_1 = 0.453$ . Here, the curve AB characterizes increase in pressure in tube to a critical value at point B, equal to:

$$s'_1 = 0.528 \cdot 0.453 = 0.239.$$

If there is known the distribution of speeds along the tube and it readily is calculated by equation (5-14a) then it is possible by formulas (4-20) and (4-24) to determine speeds and pressures after a normal shock wave in each given section (line CB).

After a normal shock the flow is subsonic and, consequently, the pressure in it under the forces of friction should fall. Thus, if a normal shock occurs directly in the entry section, then a subsequent change in pressure proceeds according to curve CD.

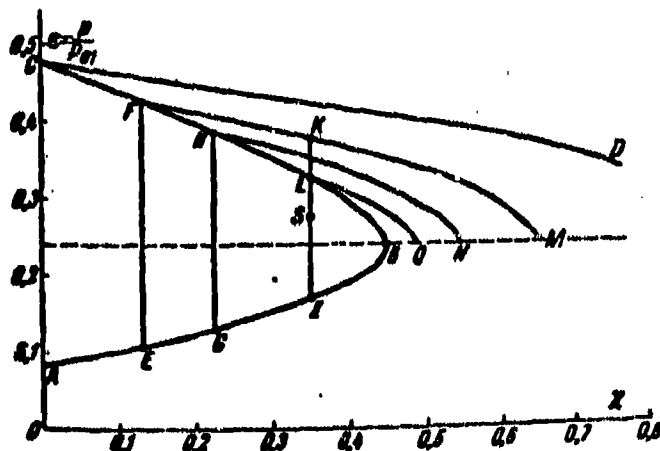


Fig. 5-5. Distribution of pressures along a tube of constant section.

The character of the change in pressures in the subsonic section of tube at different intermediate positions of the shock are presented respectively by the curves FM, HN etc. A diagram of pressures makes it possible to analyze the different modes of flow in the tube.

At the indicated speed at entry  $\lambda_1$  and the reduced flow of gas  $q_1$ , modes in a tube without shocks are possible in those cases, when  $\chi < \chi_{\max}$ , where the maximum value of reduced length corresponds to point B. Under the condition  $\chi < \chi_{\max}$  shocks in tube occur only while pressure at tube exit is greater than corresponding

pressure, indicated by curve AB.

Let us assume that the tube has a length, determined by point I ( $\lambda = 0.35$ ) and pressure for exit section is given by point L, which lies on the curve CB. In this case, the normal shock is located in exit section of tube IL. If pressure of medium, where gas flows from the tube, is determined by point K, then the normal shock is transferred into the tube and is located in section EF, in which section FK corresponds to a lowering of the pressure in the subsonic section of the tube. A subsequent increase of pressure in the medium results in a subsequent displacement of the shock into the tube (toward entry section).

If pressure of the medium is determined by the point S, then in the tube shocks do not occur while in the flow issuing from the tube, there will form a cone shock (or system of plane oblique shocks, if the tube is of a rectilinear section). With a decrease in pressure to magnitude of pressure of point I, the intensity of the cone shock decreases. At point I, the cone shock degenerates into weak conical wave, at the intersection of which entropy does not change.\*

If, finally, the pressure of medium is less than pressure at point I, then behind the exit section there will form a conical stationary wave of rarefaction and the flow of gas is extended beyond the confines of the tube.

Curves of pressures in tube (Fig. 5-5) show that with a constant length  $\lambda$  and outlet pressure  $p_2$  with an increase of speed at entry  $\lambda$ , a normal shock is displaced towards the exit section. With an increase in resistance of tube (by means of, for example, connection of an additional section of tube) the displacement of shock occurs in the opposite direction (toward tube entry).

#### 5-5. Frictional Losses in a Cylindrical Tube (Experimental Data)

Above there was considered motion of viscous gas in a tube under the assumption

\*Different systems of shocks forming in flow at tube exit are considered in detail in Chapter 6.

that the drag coefficient  $\zeta$  is constant.

In reality, drag coefficient depends on the Reynolds number and--in a general case--on the dimensionless speed  $M$ . Such a dependence has been established experimentally.

The Reynolds number for a arbitrary section of a cylindrical tube is determined by the formula

$$Re = \frac{\rho c D}{\mu}$$

For a cylindrical tube

$$\rho c = \rho_1 c_1 = q_1 \rho_{01} a_1 = q_1 \left( \frac{2}{k+1} \right)^{\frac{1}{k-1}} \sqrt{\frac{2k}{k+1} p_{01} \rho_{01}};$$

consequently,

$$Re = \left( \frac{2}{k+1} \right)^{\frac{1}{k-1}} \sqrt{\frac{2k}{k+1} p_{01} \rho_{01}} \frac{q_1 D}{\mu} \quad (5-20)$$

From formula (5-20) it is evident that the  $Re$  number varies along tube only as a result of a change in the coefficient of viscosity  $\mu$ , which depends on the temperature. It is possible to show, however, that in heat-insulated tube the changes in temperatures are small. Thus, with a change in speed of the water vapor in a tube from  $\lambda_1 = 0.2$  to  $\lambda_2 = 1$  temperature varies by 11%, while the pressure decreases by 4.5 times and the density by 5 times.

The change in coefficient of viscosity of air depending upon temperature can be evaluated by the approximate formula

$$\mu = \mu_0 \left( \frac{T}{273} \right)^a \quad (5-21)$$

where  $a$  is a constant value;  $\mu_0$  is a coefficient of viscosity at the temperature  $T = 273^\circ$ .

On basis of experimental data for air

$$a = 0.76; \mu_0 = 1.76 \cdot 10^{-4}$$

A more simple dependence for  $\mu$  is expressed by the formula

$$\mu \cdot 10^4 = 1.757 + 0.00483 T^\circ C$$

The basic problem of experimental investigation of adiabatic flows of gas in tubes, reduces to a determination of the drag coefficients  $\zeta$  and, consequently,

to determining the losses of energy. The procedure of experimentally determining the local values of drag coefficients in different sections of tube is based on equation (5-8), which after dividing all terms by  $a_*^2$  acquires the form:

$$d\lambda + \frac{dp}{\rho \lambda a_*^2} + \zeta \frac{\lambda}{2} d\bar{x} = 0. \quad (5-22)$$

By noting that for a cylindrical tube the product

$$\rho \lambda a_*^2 = q \rho_* a_*^2 = q_* k p_*$$

is a constant value by bearing in mind (2-46), we write equation (5-22) out in the form:

$$d\lambda + d\pi + \zeta \frac{\lambda}{2} d\bar{x} = 0.$$

FIGURE 2.11

Here, the function  $\pi$  depends only on  $\lambda$  according to formula (2-46a).

After substitution of this function we obtain:

$$d\lambda + \frac{k+1}{2k} d \left[ \frac{1}{\lambda} \left( 1 - \frac{k-1}{k+1} \lambda^2 \right) \right] + \zeta \frac{\lambda}{2} d\bar{x} = 0.$$

Hence, it is possible to express the drag coefficient:

$$\zeta = \frac{k+1}{k} \left( \frac{1}{\lambda^2} - \frac{1}{\lambda} \right) \frac{d\lambda}{d\bar{x}}. \quad (5-23)$$

Equation (5-23) is the original for experimental determination of local values of  $\zeta$ . By proceeding in this equation to finite differences, we will have:

$$\zeta = \frac{k+1}{k} \left( \frac{1}{\lambda^2} - \frac{1}{\lambda} \right) \frac{\Delta \lambda}{\Delta \bar{x}}. \quad (5-24)$$

If there are known, the flow of gas  $G$ , the stagnation temperature,  $T_0$ , and the distribution of pressures along the tube [ $p = p(x)$ ], then, according to formula (5-24) there can be found an average drag coefficient for a certain small sector of tube of length  $\Delta \bar{x}$ . If the sectors  $\Delta \bar{x}$  are chosen small, then the value of  $\zeta$  determined in such a way does not differ greatly from its local value.

For finding the connection between  $p$  and  $\lambda$  it is possible to use formula (5-18).

After having substituted the value  $q$ , here from the equation of continuity, we obtain:

$$\frac{p}{p_*} = \frac{k+1}{2k} \frac{G a_*}{q F \lambda p_*} \left( 1 - \frac{k-1}{k+1} \lambda^2 \right). \quad (5-25)$$

Let us consider at first certain results of an experimental investigation of flows at low speeds in cylindrical tubes.

In Fig. 5-6 there is shown the change of velocity profile in tube depending upon the Re number for a turbulent mode. Here is drawn diagram of speeds for a laminar flow in a tube. A comparison of the curves shows that velocity profile in a turbulent mode is significantly more "filled in", than in a laminar flow, and besides with an increase in the Re number the filling-in of profile increases.

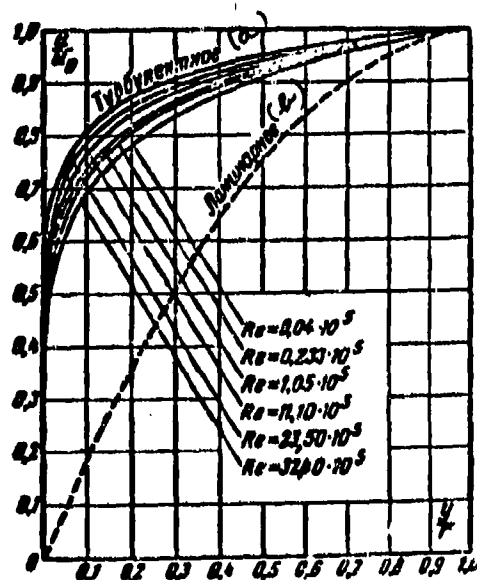


Fig. 5-6. Distribution of speeds in laminar and turbulent modes in a tube.  
KEY: (a) Turbulent; (b) Laminar.

As is known, during a turbulent motion, occurring in tubes at  $Re > 3000$ , displacements of the macroparticles\* in a transverse direction take place. Here, particles of the external flow, possessing great kinetic energy in being transferred to the surface, increase the kinetic energy of the particles along the wall moving at low speeds, and conversely, the particles, which have moved from the wall to

\*By macroparticles are understood particles of a fluid (gas), containing a fairly large number of molecules-microparticles,—for possibility of applying laws of statistics to them.



core of flow, retard here the motion of fluid.

In accordance with change of profile of speed depending upon the Re number, the drag coefficient of the tube must also vary as a function of this parameter.

For an evaluation of the drag coefficient of cylindrical tubes at low speeds it is possible to use curves of the All-Union Thermotechnical Institute; these curves were constructed by G. A. Murin (Fig. 5-7). Here the  $\zeta$  coefficient is presented in relation to the Re number and the value inversely proportional to the relative roughness  $D/k_s$ , where  $k_s$  is the average height of protuberances of the roughness. Let us note that at large values of  $D/k_s$  (small roughness) values of  $\zeta$  according to curves of the All-Union Thermotechnical Institute satisfactorily agree with the Nikuradse formula:

$$\frac{1}{\sqrt{\zeta}} = -0.8 + 2 \log(\text{Re} \sqrt{\zeta}). \quad (5-26)$$

The All-Union Thermotechnical Institute (VTI) curves and formula (5-26) clearly show that the influence of the Reynolds number on drag coefficient in a smooth tube extends to very large values  $\text{Re} \geq 10^6$ . As the roughness increases the influence of Re (at  $\text{Re} > 2 \cdot 10^6$ ) on the increase of roughness lessens. In Fig. 5-7 the dotted line connects points, corresponding to those Re values, above which the influence of this parameter is virtually unobserved. To the right of this line is located region, which conventionally is called self-modelling.\*

Let us turn now to a consideration of influence of second basic dimensionless number, the M number on the drag coefficient in tubes. Corresponding experimental data were obtained at Central Scientific Research Institute for Boilers and Turbines (MOTSRTI)\*\* and at Moscow Institute of Power Engineering (MEI)\*\*\* and several other organizations.

\*Region in which drag coefficient is independent of the Reynolds number.

\*\*A. A. Gukhman, N. V. Ilyukhin, A. F. Gandelsman, and L. N. Maurits, Journal of Technical Physics, No. 12, 1954.

\*\*\*B. S. Petukhov, A. S. Sukomel, and V. S. Protopopov. Investigation of friction drag and coefficient of Temperature Recovery of Wall in Motion of Gas in round Tube with a high subsonic speed. Heat-power Engineering, 1957, No. 3.

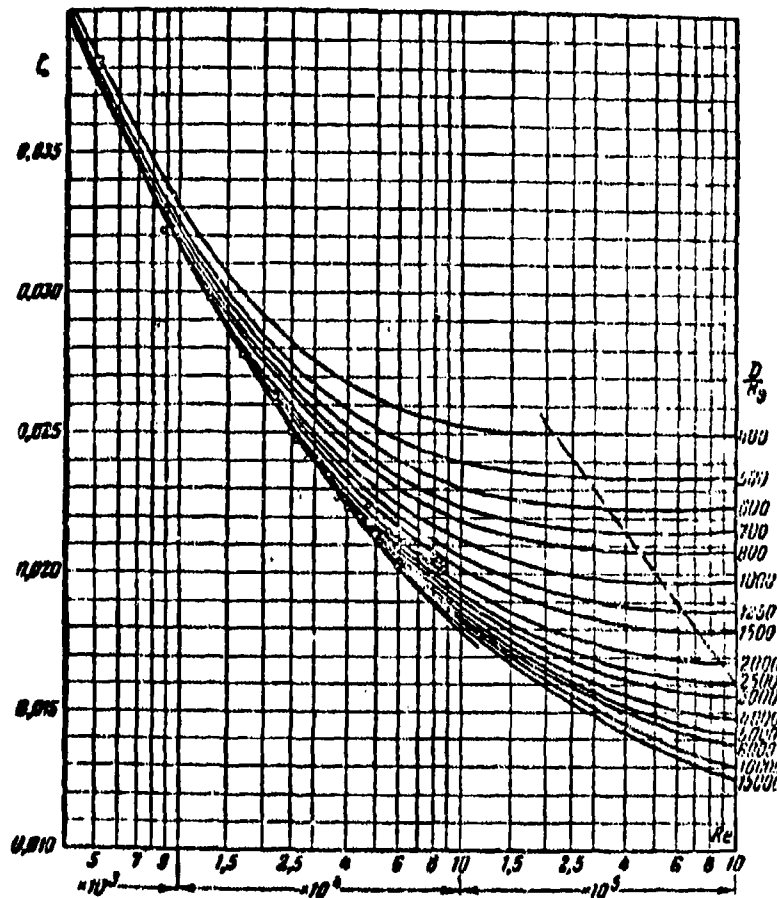


Fig. 5-7. Dependence of drag coefficient  $\zeta$  of steel tube on Re number and relative roughness on basis of All-Union Electro technical Institute data.

In Fig. 5-8 there is shown the distribution of static pressures along length of smooth tube at subsonic speeds, corresponding to different  $Re_1$  and  $M_1$  numbers at tube entry. In accordance with methodology of conducting experiments, curves in Fig. 5-8 show a cumulative influence of  $Re_1$  number and ratios of the pressures ( $M_1$  number), since a separate modeling with respect to Re and M was not realized. As  $\epsilon$  decreases ( $Re_1$  increases) the character of the pressure curves varies and especially intensively in exit section ( $\bar{x} > 60$  to 70). The transition to large Re and  $M_1$  values is accompanied by an increase in the pressure gradient: slope of

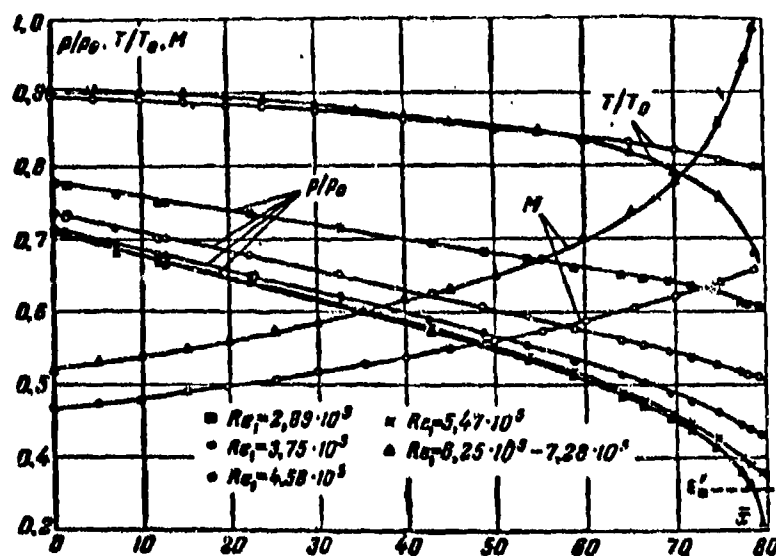


Fig. 5-8. Distribution of pressures, temperatures and speeds along length of tube for subsonic speeds.

lines  $p$  increases. For the group of modes, corresponding to supercritical differential of pressures in the tube, the static pressure in exit section exceeds pressure of the environment but it is shown to be lower than the magnitude  $s'$ , which corresponds to critical outflow. The value  $s'$  can be found by formulas (5-19) or (5-25), after substituting  $\lambda = 1$ .

The magnitude  $s'$  is marked in Fig. 5-8 by a dotted line. It follows from this that the critical section which does not coincide with exit section of tube is located inside at a certain small distance from the exit section. With increase in fall of pressures critical section is displaced towards the flow.

Special investigations of exit sector behind critical section show that in this region the flow possesses supersonic speeds. Results of investigation of field of speeds and pressures in exit section are shown in Fig. 5-9. Here there is clearly evident the nonuniformity in the distribution of static pressures along diameter of tube, where the pressure on the axis in all sections behind the critical is higher than along the wall.

Diagrams of speeds (Fig. 5-9) make it possible to conclude that thickness of

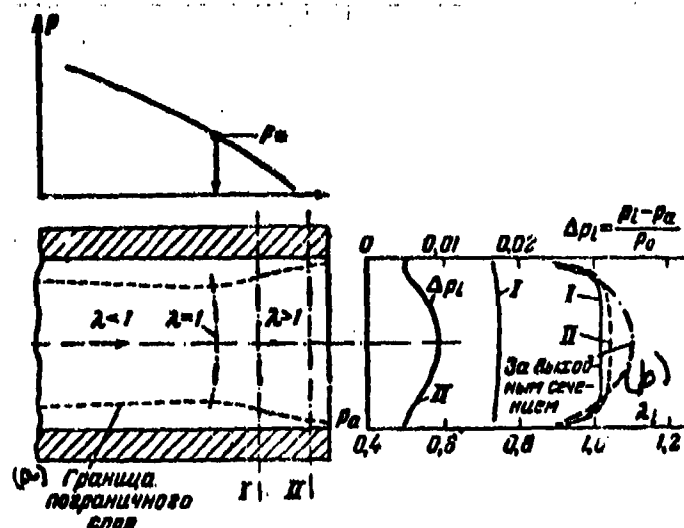


Fig. 5-9. Change of static pressures and speeds along diameter of tube near exit section.  
KEY: (a) Limit of boundary layer; (b) Behind exit section

the subsonic next-to-wall layer in exit section decreases in the direction of flow. It is possible to assume that such a structure of flow is explained by interaction of flowing steam with environment. Owing to the intense suction from the next-to-wall layer, in the environment, there occurs its thinning in exit section (Fig. 5-9). In this connection at core of flow there are created conditions, necessary for a transition to supersonic speeds: section of flow core increases downstream. The pressure of the environment "penetrates" through subsonic part of next-to-wall layer inside exit section, and pressure on wall is found to be lower than the pressure on the axis.

One should emphasize that a reconstruction of the flow in exit section of pipe is accompanied by sharp change in profile of speed in the next-to-wall layer.

In Fig. 5-10 there are plotted the values of  $\bar{\zeta} = \frac{\zeta}{\zeta_0}$  depending on  $M$ , on basis of data from Central Scientific Research Institute for Boilers and Turbines (MO TsKTI) and Moscow Institute of Power Engineering (MEI). The dependence of  $\bar{\zeta}$  on  $Re$  at large subsonic speeds according to experimental data is maintained practically the same as for an incompressible fluid. Consequently, the relation  $\bar{\zeta}$ , taken at identical values of  $Re$ , reflects influence of only the  $M$  number.

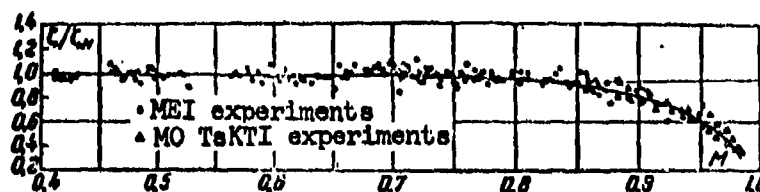


Fig. 5-10. Dependence of drag coefficient on M number at subsonic speeds on basis of data of Central Scientific Research Institute for Boilers and Turbines (MO Ts KTI) and the Moscow Institute of Power Engineering (MEI)

The graph in Fig. 5-10 shows that at  $M < 0.70$  to  $0.75$  drag coefficient is independent of  $M$  and is very close to  $\zeta_0$ . For this region the calculation of  $\zeta$  can be made by any empirical formula [for example, (5-26)] or by the All-Union Technical Institute (VTI) curves.\*

In the range of  $M$  numbers  $0.0$  to  $0.8$  and  $Re = 3 \cdot 10^3$  to  $3 \cdot 10^5$  the formula, obtained at the Moscow Institute of Power Engineering (MEI) agrees satisfactorily with the experiment:

$$\zeta = 0.0334 Re_x^{-0.2}, \quad (5-27)$$

where  $Re_x = Re \bar{x}$  is  $Re$  number, related to length of tube.

At  $M > 0.7$  to  $0.75$  drag coefficient of tube decreases with an increase of  $M$ ; an especially intensive lowering of  $\zeta$  is observed at speeds  $M > 0.85$ .

Let us remember that the change of pressure in an elementary section of pipe  $dx$  is expressed by the well-known hydraulic formula:

$$dp = \zeta \frac{\rho c^2}{2} d\bar{x}.$$

The difference in forces of pressure, acting on separated element of liquid, during uniform motion in pipe is equal frictional force on wall of pipe, i.e.,

$$\frac{\pi D^2}{4} dp = \tau_w D dx = \frac{\pi D^2}{4} \zeta \frac{\rho c^2}{2D} dx.$$

Hence, there can be obtained a formula, associating frictional stress on wall and  $\zeta$ :

$$\zeta = \frac{8\tau_w}{\rho c^2}. \quad (5-28)$$

\*In the latter case it is necessary to verify that for rough pipes the influence of compressibility on  $\zeta$  at  $M < 0.7$  to  $0.8$  also will be small. This assumption is required as an experimental verification.

In accordance with formula (5-28) results of above-discussed experimental investigation can be expressed as: influence of compressibility, noticeably manifesting itself at  $M > 0.75$ , results in a certain decrease of frictional force, related to kinetic energy of flow in a given section.

Physically this result is explained by the fact that with an increase in the  $M$  number, the pressure gradients increase in tube (Fig. 5-8). An increase of the pressure gradients in a nozzle flow causes deformation of profile of speed along the wall; the filling in of the profile of speed increases. Besides, the next-to-wall layer at same time is made thinner.

Transonic flow is especially sensitive to a change of section which is seen from equation (5-8). Therefore, in the terminal section of pipe, where  $M > 0.9$ , there are observed very large negative pressure gradients and a correspondingly sharp lowering of  $\zeta$ .

A sharp decrease in  $\zeta$  at  $M > 0.9$  is associated also with the fact that range of speeds  $M = 0.9$  to  $1.0$  is found near the end section of pipe, where next-to-wall layer is destroyed. In a calculation by formula (5-28) a significant deformation of speed profile in exit section of pipe is not taken into consideration.

By evaluating the influence of compressibility on the drag coefficient of pipe at supersonic speeds, it is necessary to distinguish three basic modes of flow in tube. The first mode corresponds to a shockless motion of flow, the speeds of which in each section of pipe are supersonic. As was already shown, such a mode is possible, if the length of cylindrical tube is less than limiting value ( $X < X_{\max}$ ). If, however, in pipe there is a corresponding source of disturbance, then at  $X < X_{\max}^{\text{super-}}$  sonic flow can be saturated with shock waves. Disturbance of flow in tube can be caused by an angular change in direction of wall, which will be formed in section of joint of Laval nozzle with tube. In simplest case, diverging section of nozzle is made conical with different aperture angles. The larger is the aperture angle of nozzle, the larger is the angular displacement of flow at tube entry and the more

intense is the shock, formed at point of change in direction of wall. Such modes of flow with a conical shock, when the flow up to exit section remains supersonic, constitute the second group of modes. Finally, if  $X > X_{\max}$ , then inside the pipe there occurs a complicated system of shocks, after which the flow will be subsonic; this is the third group of modes of flow. The distribution of parameters of flow along length of tube in those indicated cases proves to be considerably different.

For the third group of modes, when as a result of shocks the flow becomes subsonic, the character of distribution of pressure on basis of data of Neumann and Lustwerk is shown in Fig. 5-11 (for  $\lambda_1 = 2.2$ ). According to extent of increase in pressure in exit section of tube, system of shocks is transferred to the nozzle. The intensity of shocks at the same time increases. Let us note that extent of system of shocks proves to be significant. For the system of shocks the flow is subsonic, and pressure along the tube drops.

In accordance with different character of distribution of pressures along a cylindrical tube at supersonic speeds also the drag coefficients will be different. In a uniform supersonic flow in tube (without shocks) the drag coefficient has a minimum value.

In Fig. 5-12 are plotted values of drag coefficient depending on  $M$  on basis of data of Central Scientific Research Institute for Boilers and Turbines for the interval of numbers  $M = 0.0$  to  $1.65$ . Here, there are reproduced experimental points for subsonic speeds, partially presented in Fig. 5-8, and there are added results of later investigations for  $M > 1$ . Characteristic for range of small supersonic speeds should be assumedly the marked increase of  $\zeta$ ; here, the drag coefficient varies from  $0.007$  to  $0.018$ .

It is possible to assume that in this section there occurs a "turbulization" of the next-to-wall layer in tube, i.e., transition of it from laminar to a turbulent mode.\* In the preceding range  $M = 0.95$  to  $1.03$ , where pressure gradients will

\*The analogous character of change of  $\zeta$  is noted in initial section of tube, where there occurs a transition of the laminar mode to the turbulent.

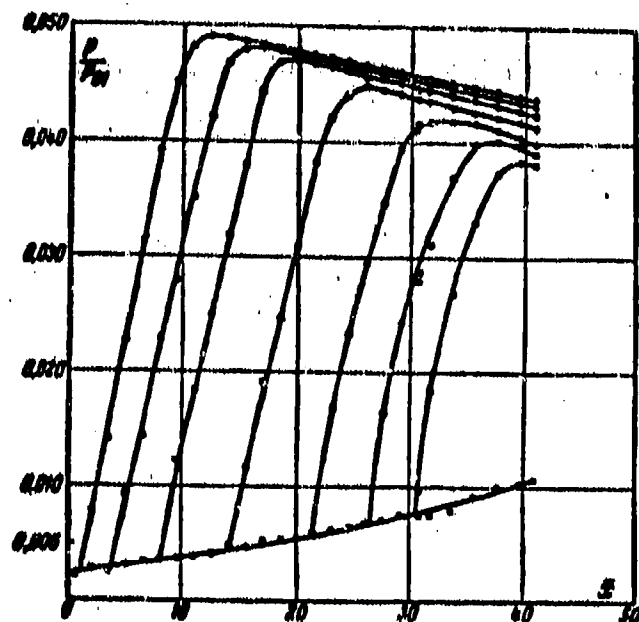


Fig. 5-11. Distribution of pressures along length of tube at supersonic speeds at entry;  $\lambda_1 = 2.2$  (air).

attain maximum values, apparently, there occurs a "laminarization" of the next-to-wall layer, since with large negative pressure gradients intensity of turbulent pulsations diminishes.

In the sector  $M = 1.25$  to  $1.6$ ,  $\zeta$  lowers and at  $M = 1.65$  will attain a minimum value  $\zeta \approx 0.01$ . This lowering is explained by the filling in of profile of speed in the region of a supersonic flow with negative pressure gradients.

At  $M > 1.3$ , the influence of Reynolds number on  $\zeta$  is small.

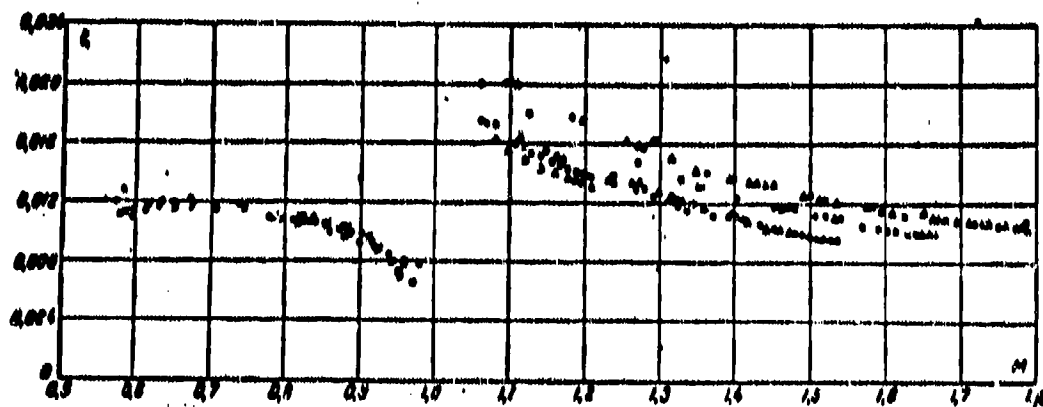


Fig. 5-12. Dependence of coefficient  $\zeta$  on Mach number for cylindrical tube on basis of Central Scientific Research Institute for Boilers and Turbines data.



### 5-6. Boundary Layer. Fundamental Concepts and Equations\*

Contemporary ideas about the mechanism of resistance of bodies, flowed around by a gas, and methods of calculating the resistance are based on the boundary layer theory.\*\*

As experience shows at large Re numbers influence of viscosity is concentrated

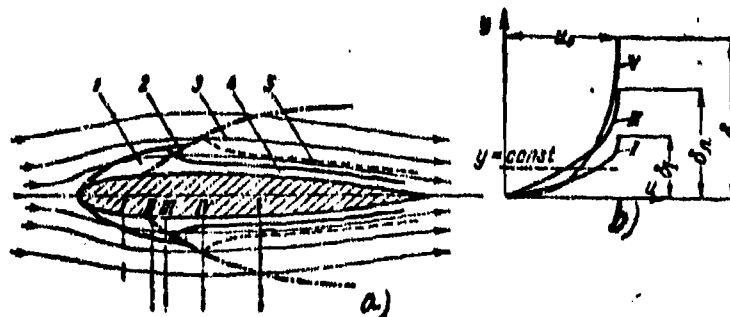


Fig. 5-13. Diagram of formation of boundary layer on surface of wing profile.

a--change in thickness and structure of layer along surface: 1--laminar section of layer; 2--transitional region; 3--turbulent section of layer; 4--laminar sublayer; 5--transitional layer; 6--distribution of speeds in different sections of layer.

\* Sections 5-6 to 5-12 were written jointly with A. Ye. Zaryankin.

\*\* Theory and methods of calculating boundary layer are given in detail in the monograph by L. G. Loytsyanskiy (See list of references).

in the region of flow, directly adjacent to surface of body. This region has a small extent in comparison with length in direction of a normal to surface of body and it is called the boundary layer. Outside the boundary layer the flow has a negligibly small vorticity and on this basis it is considered potential. In the boundary layer the speeds vary from zero on surface of body to speed of potential flow at outer limit. Since the thickness of layer is small, then gradients of speeds in this region will attain large values and, consequently, flow here possesses great vorticity.

The character of distribution of speeds in the boundary layer on flat wall is shown in Fig. 5-13. Directly on the wall the fluid adheres to surface ( $\lambda_1 = 0$ ). In a thin boundary layer with increasing distance from surface of body the speeds vary greatly and at a small distance from surface will attain the speed of external flow.

The resistance of streamlined bodies depends considerably on the mode of flow in the boundary layer. The motion of a fluid in a boundary layer may be laminar or turbulent.

Laws of change in speed along normals to surface for laminar and turbulent modes must be different.

Since speeds in the boundary layer vary from zero on wall, then it is natural to assume that certain section of boundary layer, adjacent to wall, always is in a laminar mode. This assumption is confirmed by distribution of speeds along wall in a boundary layer.

We now consider more specifically the condition of the formation of a boundary layer on surface of a wing profile (Fig. 5-13).

In direction of flow along surface, the thickness of boundary layer  $\delta$  increases. We note that concept of an outer limit and thickness of boundary layer are not determinate, since a change in longitudinal speeds during transition from boundary layer to the external flow occurs smoothly. Approximately the outer limit of layer is determined at those points, where longitudinal speed differs from the

speed of external flow by a small magnitude of an order of one percent (1%).

Outer limit of boundary layer does not coincide with the lines of flow, since particles of external flow continuously penetrate into the boundary layer (Fig. 5-13).

Fore section of layer, located near the tip of profile, usually is laminar. At a small distance from tip (section II in Fig. 5-13, a and b) is found a laminar velocity profile. In a certain section III, there begins a transition from a laminar orderly motion to a turbulent motion which bears an oscillating character.

In the transitional zone, the flow in boundary layer is mixed: significant part of layer, nearest to surface, is in a laminar mode.

Beyond the transitional region there is developed a steady turbulent layer. Here region of the laminar sublayer is so small that experimentally it is difficult to detect. As can be seen from Fig. 5-13b, turbulent layer has a fuller velocity profile.

The diagram of the formation of a boundary layer in Fig. 5-13 is expressed not on an identical scale along the x - and y - axes. The thickness of the layer  $\delta$  is very small in comparison with dimensions of the body and amounts to hundredths and thousandths of the chord of profile.

Calculation of a laminar boundary layer is based on differential equations of energy (5-3) and the motion of a viscous fluid (5-4). By using cited above physical peculiarities of motion in layer, equation (5-4) can be considerably simplified.

For this purpose we now turn in the equations (5-4) to dimensionless magnitudes. For simplicity let us consider steady motion of an incompressible fluid. As scales of longitudinal speeds and coordinates we select a certain characteristic speed  $u_0$  and characteristic linear dimension  $L_0$ . Scales of transverse speeds and coordinates are designated respectively by  $v_0$  and  $\delta$ . We designate scales for pressure and density  $p_0$  and  $\rho_0$ . Then after transformations, analogous to transformations in Section 5-2, we obtain following system of equations:

$$\left. \begin{aligned} u \frac{\partial u}{\partial x} + \frac{L_0 v_0}{u_0} v \frac{\partial u}{\partial y} &= - \frac{\rho_0 p_0}{\rho u_0^2} \frac{\partial p}{\partial x} + \frac{v}{L_0 u_0} \frac{\partial^2 u}{\partial x^2} + \frac{v L_0}{\delta^2 u_0} \frac{\partial^2 u}{\partial y^2}; \\ u \frac{\partial v}{\partial x} + \frac{L_0 v_0}{u_0} v \frac{\partial v}{\partial y} &= - \frac{\rho_0 p_0 L_0}{\rho u_0 v_0} \frac{\partial p}{\partial y} + \frac{v}{L_0 u_0} \frac{\partial^2 v}{\partial x^2} + \frac{v L_0}{\delta u_0} \frac{\partial^2 v}{\partial y^2}; \\ \frac{\partial u}{\partial x} + \frac{L_0 v_0}{u_0} \frac{\partial v}{\partial y} &= 0. \end{aligned} \right\} \quad (5-29)$$

Scales of magnitudes, appearing in the system of equations (5-29), can be selected on the basis of following considerations. If the scales  $u_0$  and  $L_0$  express the characteristic speed and linear dimension of the streamlined body, then, the magnitudes  $v_0$ ,  $\delta$ ,  $\rho_0$  and  $p_0$  for the present remain indefinite. By using this arbitrary rule, equations (5-29) are readily reduced to a canonical form.

Indeed, by assuming  $p_0 = \rho_0 u_0^2$ ,  $\rho_0 = 1$  we obtain  $\frac{p_0 p_0}{\rho_0 u_0^2} = 1$ , and the transverse scales  $v_0$  and  $\delta$  will be selected in such a way that the coefficients  $\frac{L_0 v_0}{\delta u_0}$  and  $\frac{\delta L_0}{\delta^2 u_0}$  are constant and independent of the Re number.

Let us assume  $\frac{L_0 v_0}{\delta u_0} = 1$  and  $\frac{\delta L_0}{\delta^2 u_0} = 1$ .

In principle these complexes can be equated to any constant, but in the given case expressions for transverse scales are obtained most readily.

In solving written system relative to  $v_0$  and  $\delta$  for scales of transverse speeds and linear dimensions, we obtain the following values

$$\delta = \frac{L_0}{\sqrt{\text{Re}}}; v_0 = \frac{u_0}{\sqrt{\text{Re}}}. \quad (5-30)$$

Here, equations (5-29) will acquire the form:

$$\left. \begin{aligned} u \frac{\partial u}{\partial x} + v \frac{\partial u}{\partial y} &= -\frac{\partial p}{\partial x} + \frac{1}{\text{Re}} \left( \frac{\partial^2 u}{\partial x^2} + \frac{\partial^2 u}{\partial y^2} \right); \\ \frac{1}{\text{Re}} \left( u \frac{\partial v}{\partial x} + v \frac{\partial v}{\partial y} \right) &= -\frac{\partial p}{\partial y} + \frac{1}{\text{Re}} \left( \frac{\partial^2 v}{\partial x^2} + \frac{\partial^2 v}{\partial y^2} \right); \\ \frac{\partial u}{\partial x} + \frac{\partial v}{\partial y} &= 0. \end{aligned} \right\} \quad (5-31)$$

If we admit that the unknown magnitudes  $u$ ,  $v$ ,  $p$  and their derivatives with increase in Reynolds number tend to definite limits at fixed points, then at large Re in the equations (5-31) it is possible to discard all terms, having the factors  $\frac{1}{\text{Re}}$  and  $\frac{1}{\text{Re}^2}$ , as small magnitudes in comparison to other terms.

As a result of converting again to dimensional magnitudes we obtain differential equations of the laminar boundary layer in L. Prandtl's form

$$\left. \begin{aligned} u \frac{\partial u}{\partial x} + v \frac{\partial u}{\partial y} &= -\frac{1}{\rho} \frac{\partial p}{\partial x} + \nu \frac{\partial^2 u}{\partial y^2}; \\ \frac{\partial p}{\partial y} &= 0; \\ \frac{\partial u}{\partial x} + \frac{\partial v}{\partial y} &= 0. \end{aligned} \right\} \quad (5-32)$$

System (5-32) must be solved under the following boundary conditions:

$$y=0; u=0; v=0;$$

$$y \rightarrow \infty; u \rightarrow u(x).$$

The latter condition means that speed in boundary layer transforms asymptotically to the speed of external flow. In reality this transition, as has already been mentioned, occurs at value of  $y$ , commensurable with transverse scale  $\delta$ .

The obtained condition of  $\frac{\partial p}{\partial y} = 0$  means that distribution of pressures at outer limit of layer and on surface of streamlined body coincides. It follows from this that at all points of cross section of layer, the pressures are identical, i.e., pressure of external flow is transmitted through boundary layer to surface of body without change.

The condition  $\frac{\partial p}{\partial y} = 0$  made it possible to explain the very important phenomenon of separation of boundary layer. Let us consider the flow around a certain curvilinear surface AB (Fig. 5-14), by assuming that pressure of external flow along this surface at first decreases, will attain a minimum value at the point M and then increases. The section of external flow, in which pressure gradient is negative ( $\frac{\partial p}{\partial x} < 0$ ), is called the nozzle or convergent sector. Region of flow after point M, characterized by positive pressure gradients ( $\frac{\partial p}{\partial x} > 0$ ), is called the diffuser sector. In the nozzle sector, the external flow is accelerated, and in the diffuser sector is decelerated. By considering that in boundary layer  $\frac{\partial p}{\partial y} = 0$ , we conclude that a completely analogous distribution of pressures takes place also along the surface AB at any distance  $y < \delta$  in the boundary layer.

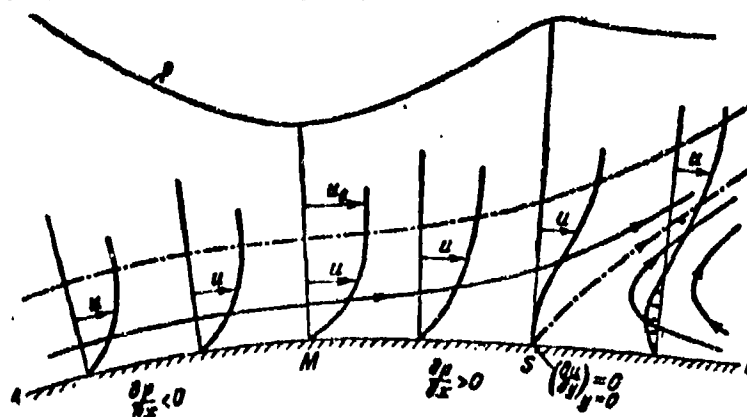


Fig. 5-14. Diagram of formation of separation of boundary layer.

Within the limits of the boundary layer speeds before point M increase, and after it decrease (see diagrams of speeds in Fig. 5-14). Particles of the fluid near wall possess small kinetic energy, in which in diffuser region along surface AB reserve of kinetic particle energy decreases. As a result in a certain section S, particles along wall cannot surmount the stagnation influence of external flow and they remain behind. The diagram of speeds acquires characteristic peaked form. On the wall, curve of speeds satisfies condition

$$\left(\frac{\partial u}{\partial y}\right)_{y=0} = 0. \quad (5-32a)$$

Further beyond point S under influence of a differential of pressures, directed against flow, a return motion of particles along wall begins. In encountering the main flow the returning particles are pushed from wall which also results in a separation of the boundary layer and in sharp increase in its thickness. Beyond the point of the separation S, diagram of speeds has also the very characteristic loop-shaped form, in which directly along the wall

$$\left(\frac{\partial u}{\partial y}\right)_{y=0} < 0.$$

The discussion shows that the separation of the boundary layer during flow around a smooth wall can occur only in the diffuser region.

In using equations (5-32), it is readily shown that the position of point of separation of a laminar boundary layer is independent of the Re number. Actually, the solution of system (5-32), gives:

$$u = f(x, y), \quad (5-32b)$$

where  $\underline{x}$  and  $\underline{y}$  are dimensionless coordinates.

Then, by having differentiated with respect to  $\underline{y}$  and by using at the point of separating the condition (5-32a), we obtain:

$$f(x_s, 0) = 0.$$

Inasmuch as the scale along x-axis does not depend on the Re number we reach the conclusion that the coordinate of point of separation of a laminar layer also is independent of the Reynolds number.

### 5-7. Arbitrary Thicknesses and the Integral Relationship for a Boundary Layer

Above it was indicated that concept of thickness of boundary layer does not have an accurate quantitative definition. Indeed, the speed in boundary layer  $u$  with an increase of  $y$  asymptotically approaches the value of speed of external flow  $u_0$ . The magnitude  $\delta$  depends on where there is selected the point, arbitrarily indicating the limit of the layer.

Therefore, in calculations of the boundary layer there are introduced other integral thicknesses, depending on  $\delta$ : thickness of displacement  $\delta^*$ , momentum thickness  $\delta^{**}$  and energy thickness  $\delta^{***}$ .

For ascertaining physical meaning of indicated thicknesses we shall compare flow of an ideal and viscous fluid near a rigid wall (Fig. 5-15).

In the absence of friction for a unit of time through cross section of flow with a height  $dy$  and width, equal to unity, mass  $\rho_0 u_0 dy$  will flow. In the boundary layer during the same time through section  $dy$  mass  $\rho u dy$  will flow.

The difference between these quantities will amount to:

$$\begin{aligned} & \rho_0 u_0 \int_0^{\delta} \left(1 - \frac{u}{u_0}\right) dy = \\ & = \rho_0 u_0 \int_0^{\delta} \left(1 - \frac{u}{u_0}\right) dy + \rho_0 u_0 \int_{\delta}^{\infty} \left(1 - \frac{u}{u_0}\right) dy. \end{aligned}$$

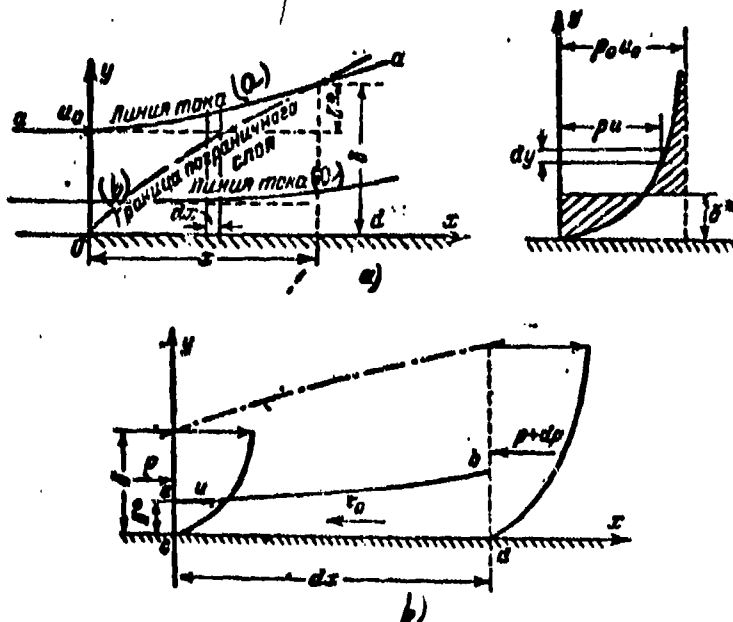


Fig. 5-15. Diagram for determining arbitrary thicknesses of boundary layer (a) For deriving equations of momentum for a boundary (b).  
KEY: (a) Line of flow; (b) Boundary layer limit.

The second integral on right side is small in comparison with the first. Therefore an integration made only within the limits of physical thickness of layer  $\delta$ , suffices.

After having divided the determined excess of mass by  $\rho_0 u_0$ , we obtain:

$$\delta^* = \int_0^\delta \left(1 - \frac{u}{u_0}\right) dy. \quad (5-33)$$

The magnitude  $\delta^*$  indicates displacement of the line of flow in direction of external normal to contour of streamlined body.

At the same time  $\delta^*$  characterizes decrease in the flow of fluid through the section of layer, "normal" to wall, caused by "displacement" of liquid by boundary layer, and therefore, is called the thickness of displacement.

The momentum thickness  $\delta^{**}$  is equal to that thickness of the layer of fluid, moving with speed  $u_0$  outside of boundary layer, whose momentum is equal to the impulse of friction forces in the boundary layer. This momentum, "lost" in boundary layer, will be equal to:

$$\int_0^\delta \rho u (u_0 - u) dy = \int_0^\delta \rho u u_0 \left(1 - \frac{u}{u_0}\right) dy.$$

We divide the obtained expression by  $\rho_0 u_0^2$ . Then we obtain:

$$\delta^{**} = \int_0^\delta \frac{u}{u_0} \left(1 - \frac{u}{u_0}\right) dy. \quad (5-34)$$

The mass of fluid  $\rho u dy$  loses kinetic energy in boundary layer, equal to  $\rho u (u_0^2 - u^2) dy$ . For the entire layer this loss will amount to:

$$\int_0^\delta \rho u u_0^2 \left(1 - \frac{u^2}{u_0^2}\right) dy.$$

Then the energy thickness

$$\delta^{***} = \int_0^\delta \frac{u^2}{u_0^2} \left(1 - \frac{u^2}{u_0^2}\right) dy \quad (5-35)$$

is the thickness of fluid moving outside of layer and possessing the kinetic energy, lost in the boundary layer.

For solution of problems on the flow of compressible fluid in a number of cases, it is expedient to have an identical structure of formulas, determining the integral thicknesses. Therefore, together with formula (5-33) thickness of displacement  $\delta^*$  frequently is calculated by the formula

$$\delta^* = \int_0^\delta \frac{\rho}{\rho_0} \left(1 - \frac{u}{u_0}\right) dy. \quad (5-36)$$



In this connection, naturally the previous physical meaning of thickness of displacement is destroyed. For an incompressible fluid equations (5-33) and (5-36) are found to be identical.

The solution of the problem on the resistance of a body in the flow of a viscous fluid with a continuous flow around reduces to the establishment of distribution of forces of friction along streamlined surfaces of body, and consequently, to a calculation of the boundary layer.

The widely used method of approximation in calculations is based on evaluating the change in momentum in boundary layer. We shall make such an evaluation.

For a determination of the thickness of displacement, it follows that entire mass of fluid, flowing into boundary layer, can be arbitrarily replaced by a mass, located between the line ab and wall cd (Fig. 5-15), speed of which is equal to zero ("displaced" mass), and mass, flowing above ab with a speed  $u_0$ .

From the side of wall frictional forces will act on the displaced mass and in the direction of flow forces of pressure will be applied. Speeds above the line of displacement ab are equal to  $u_0 = u_0(x)$  also within limits of considered volume, on the basis of differential equations of a boundary layer (5-32)  $\frac{\partial p}{\partial y} = 0$ . In applying the equation of momentum there can be found the magnitude of loss of momentum in the section dx:

$$dI = r_0 dx + dp_0^*, \quad (5-37)$$

where  $r_0 dx$  and  $dp_0^*$  are the impulses of frictional and pressure forces acting on the displaced mass of the fluid.

The momentum I, on the basis of equation (5-34) can be expressed in terms of the loss of momentum:

$$I = \rho_0 u_0^2 \delta^{**}.$$

Inasmuch as at the external limit of boundary layer the flow is considered

---

\*The derivation of the integral relationship presented below is given by A. P. Melnikov.

potential, longitudinal pressure gradient  $\frac{dp}{dx}$  readily is expressed on the basis of the Bernoulli equation by the speed  $u_0$  and density  $\rho_0$ :

$$\frac{dp}{dx} = -\rho_0 u_0 \frac{du_0}{dx} = -\rho_0 u_0 u_0'.$$

In substituting this magnitude in (5-37), we find:

$$u_0^2 \delta^{**} \frac{d\rho_0}{dx} + \rho_0 \delta^{**2} 2u_0 u_0' + \rho_0 u_0^2 \frac{d\delta^{**}}{dx} = \tau_0 - \rho_0 u_0 u_0' \delta^{**}. \quad (5-37a)$$

We substitute further

$$\frac{d\rho_0}{dx} = \frac{d\rho_0}{dp} \cdot \frac{dp}{dx} = -\frac{1}{a_0^2} \rho_0 u_0 u_0'$$

and then divide (5-37a) by  $\rho_0 u_0^2$ . As a result, we obtain for a compressible fluid the following equation:

$$\frac{d\delta^{**}}{dx} + \frac{u_0' \delta^{**}}{u_0} (2 + H - M_0) = \frac{\tau_0}{\rho_0 u_0^2}. \quad (5-38)$$

Here

$$H = \frac{\delta^{**}}{\delta^*} 2 \frac{dM_0}{dM_0} = \frac{u_0}{a_0}.$$

Equation (5-38) is called the integral relationship, since magnitudes  $\delta^{**}$  and  $\delta^*$  are expressed by the integrals (5-33) and (5-34).

Integral relationship (5-38) for a boundary layer can be obtained by not resorting to concept of thickness of displacement. For this purpose the equation of momentum is applied to a volume of fluid, enclosed between two infinitely close cross sections of boundary layer (Fig. 5-15b). By substituting in (5-38) expressions for the arbitrary thicknesses  $\delta^*$ ,  $\delta^{**}$  and by replacing  $u_0'$  by  $\frac{dp}{dx}$ , after transformations we find:

$$\frac{d}{dx} \int_0^{\delta^*} \rho u^2 dy - u_0 \frac{d}{dx} \int_0^{\delta^*} \rho u dy = -\tau_0 - \delta \frac{dp}{dx}. \quad (5-39)$$

For an incompressible fluid, we obtain:

$$\frac{d}{dx} \int_0^{\delta^*} u^2 dy - u_0 \frac{d}{dx} \int_0^{\delta^*} u dy = -\frac{\tau_0}{\rho} - \frac{\delta}{\rho} \cdot \frac{dp}{dx}. \quad (5-39a)$$

The integral relationship for a boundary layer is useful for calculating both laminar and also turbulent boundary layers, since in its derivation no assumptions were made with respect to the tangential stress  $\tau_0$ . This magnitude is determined differently depending on mode of flow of fluid in boundary layer which also is a reflection of the different nature of friction in laminar and turbulent motions.

In the generation of separation the equation of momentum can serve for determining the location of point of separation at which  $\tau_0 = \rho \left( \frac{\partial u}{\partial y} \right)_{y=0} = 0$ .

5-8. A More General Expression for the Coefficient of Friction Drag in a Boundary Layer in the Presence of a Pressure Gradient.

In the equation of momentum, there remain two sought variables: thickness of layer  $\delta$  (or the mutually associated arbitrary thicknesses  $\delta^*$  and  $\delta^{**}$ ) and frictional stress on wall  $\tau_0$ .

In the general case  $\tau_0$  is determined by speed at external limit of boundary layer, its derivatives  $u'_0, u''_0, u'''_0$  et cetera by speed at external limit of boundary example, the momentum thickness  $\delta^{**}$ , density  $\rho$ , temperature  $T$ , and coefficient of kinematic viscosity  $\nu$ .

Consequently,

$$\tau_0 = \varphi(u_0; u'_0; u''_0; \dots; T; \rho; \delta^{**}; \nu). \quad (5-40)$$

By using basic assumptions of the theory of dimensionality from the functional dependence (5-40) it is simple to obtain a structural formula for the drag coefficient.

We adopt as the basic dimensionalities the speeds  $u_0$ , the densities  $\rho$ , lengths  $\delta^{**}$  and the temperatures  $T$ . By a simple verification we are readily convinced that, by combining the indicated magnitudes, there can be obtained a dimensionality of all remaining parameters. Actually,  $\tau_0$  has the dimensionality of  $\text{kg}/\text{m}^2$ . The same dimensionality will apply to the complex  $\rho u_0^2$ :  $[\text{kg} \cdot \text{sec}^2 / \text{m}^4 \cdot \text{m}^2/\text{sec}^2]$ . Consequently, the ratio  $\tau_0/\rho u_0^2$ , which is a local coefficient of friction  $c_f$ , is found to be dimensionless. By converting in expression (5-40) from dimensional magnitudes to dimensionless, we obtain

$$c_f = \frac{\tau_0}{\rho u_0^2} = \varphi\left(\text{Re}^{**}; M; \frac{u'_0 \delta^{**}}{u_0}; \frac{u''_0 \delta^{**2}}{u_0}; \dots\right). \quad (5-41)$$

Here  $\text{Re}^{**} = \frac{u_0 \delta^{**}}{\nu}$  is the Reynolds number, calculated on the basis of the momentum thickness.

The number of dimensionless parameters in expression (5-41) can be reduced, if we assume that the frictional stress is determined just as in case of laminar flow by only the first derivative of the speed  $u'_0$ .

This assumption is confirmed for disturbed flows and flows with small positive pressure gradients. Near point of separation the role of leading (highest) derivative increases, and here the maintaining of only the first derivative already is insufficient.

Further, it is possible to show that in relating the physical constant  $\nu$  and  $\rho$  to temperature conditions on wall M number is excluded from the dependence (5-41). Thus, by taking into account the adopted assumptions

$$c_f = \frac{\tau_w}{\rho_w u_0^2} = \varphi \left( Re_w^{**}; \frac{u_0'^{***}}{u_0} \right), \quad (5-42)$$

where  $Re_w^{**} = \frac{u_0 \delta^{**}}{\nu_w}$ ,  $\nu_w$  — is the kinematic viscosity, calculated on the basis of temperature of wall.

We expand (5-42) into a series with respect to the parameter  $\frac{u_0'^{***}}{u_0}$ :

$$c_f = \frac{\tau_w}{\rho_w u_0^2} = \psi_0(Re_w^{**}) + \psi_1(Re_w^{**}) \frac{u_0'^{***}}{u_0} + \psi_2(Re_w^{**}) \left( \frac{u_0'^{***}}{u_0} \right)^2 + \dots \quad (5-43)$$

Here  $c_f$  is a local coefficient of friction, calculated on basis of density along wall  $\rho_w$ .

Expression (5-43) is general both for a laminar, as well as for turbulent modes of flow in a boundary layer. Depending upon the mode of flow, the coefficients  $\psi_0$ ,  $\psi_1$ ,  $\psi_2$  etc. will acquire different values.

We find a concrete form of expression (5-43) for laminar flow. For this purpose, we write (5-43) in such a form:

$$c_f = \frac{\tau_w}{\rho_w u_0^2} = \psi_0 \left[ 1 + \frac{\psi_1}{\psi_0} \cdot \frac{u_0'^{***}}{u_0} + \frac{\psi_2}{\psi_0} \cdot \frac{u_0'^{***2}}{u_0^2} + \dots \right]. \quad (5-44)$$

At  $u_0' = 0$  formula (5-44) should conform with corresponding formula for drag coefficient of flat plate during a gradientless flow around it.

In this case, problem is solved fairly accurately by means of numerical integration of the system (5-32) and independently of method of solution for a flow without gradient, the drag coefficient  $c_{f0}$  is expressed by the formula

$$c_{f0} = \psi_0 = \frac{c_{f0}}{Re_w^{**}}.$$

where  $a_0$  is a constant value.

Consequently,

$$c_f = \frac{a_0}{Re_w^{1/2}} \left[ 1 + \frac{\psi_1}{a_0} \frac{u_0'^{3/2}}{v} + \frac{\psi_2}{a_0} \frac{u_0'^{5/2}}{v^2} + \dots \right].$$

At the point of separation  $\tau_s = 0$ ; in this case the expression in square brackets should vanish. In taking into consideration that position of point of separation does not depend on  $Re^{**}$  number, we obtain:  $\psi_1 = \text{const}$ ;  $\psi_2 = \text{const}$ ;  $\psi_3 = \text{const}$  etc. Hence

$$c_f = \frac{1}{Re_w^{1/2}} \left[ a_0 + a_1 \frac{u_0'^{3/2}}{v} + a_2 \frac{u_0'^{5/2}}{v^2} + \dots \right]. \quad (5-45)$$

The coefficients  $a_0$ ,  $a_1$ ,  $a_2$  etc. in the general case, are determined experimentally. However, for a laminar boundary layer they can be determined also theoretically. Thus, for example, A. M. Basin obtained  $a_0 = 0.22$ ;  $a_1 = 1.85$ ;  $a_2 = -7.35$ .

We designate

$$\frac{u_0'^{3/2}}{v} = f \quad (5-46)$$

and

$$\zeta(f) = [a_0 + a_1 f + a_2 f^2 + \dots]; \quad (5-47)$$

then

$$c_f = \frac{1}{Re_w^{1/2}} \zeta(f). \quad (5-48)$$

The parameter  $f$  frequently is called the shape parameter; as will be pointed out below, it determines the shape of profile of speed in the laminar boundary layer. One should note that structure of the shape parameter, containing the derivative  $\frac{du_0'}{dx}$ , reflects influence of longitudinal pressure gradient of the external flow.

For a turbulent layer, numerous experimental data give at  $u_0' = 0$ :

$$c_{f0} = \phi_0 = \zeta Re_w^{-m}, \quad (5-49)$$

and for drag coefficient, there is obtained from (5-44) the following formula:

$$c_f = Re_w^{-m} [\zeta + a_1 f + \dots]. \quad (5-50)$$

Here

$$\Gamma = \frac{u_0'^{3/2}}{u_0} Re_w^{-m}. \quad (5-51)$$

The parameter  $f$  (The "Bari" parameter), just as the shape parameter  $f$ , reflects the influence of longitudinal pressure gradient and Reynolds number on the velocity profile in a turbulent layer.

By knowing the dependence for  $c_f$  and the law of change of magnitude  $H = \frac{\delta^*}{\delta}$ , depending upon longitudinal pressure gradient, it is simple to obtain from the integral relationship (5-38) a differential equation for determining the thicknesses of a boundary layer.

We shall consider separately the solution of equation (5-38) for laminar and turbulent layers.

#### 5-9. Calculation of Laminar Boundary Layer in the Presence of a Pressure Gradient.

The calculation of a boundary layer reduces to the solution of the integral relationship (5-38) [or (5-39)], which contains three unknown magnitudes: the momentum thickness  $\delta^*$ , the drag coefficient  $c_f = \frac{\tau_w}{\rho u_0^2}$  and magnitude  $H = H\left(M; \frac{dP}{dx}\right)$ .

Consequently, for the solution of problem it is necessary to have still two additional relationships, associating the indicated magnitudes. By using the more general expression (5-48) for drag coefficient and by considering for simplicity the case of an incompressible fluid, we obtain an equation with two unknowns:  $\delta^*$  and  $H$ , the association between which is simple to obtain, if the profile of speed in boundary layer is known.

In the general case, the speed in cross section of layer depends on local pressure gradient and distance from the wall  $y$ . The influence of pressure gradient is taken into consideration by the shape parameter  $f$ . Consequently, the relative velocity at point of layer can be presented in such a form:

Then,

$$\frac{u}{u_0} = \varphi\left(\frac{y}{\delta^*}, f\right).$$

$$\begin{aligned} \delta^* &= \int_0^{\delta^*} \left(1 - \frac{u}{u_0}\right) dy = \int_0^{\delta^*} \left[1 - \varphi\left(\frac{y}{\delta^*}, f\right)\right] dy \\ &= \delta^* \int_0^1 \left[1 - \varphi\left(\eta, f\right)\right] d\left(\frac{y}{\delta^*}\right). \end{aligned}$$

After integrating obtained expression within the indicated limits, we find:

$$\delta^* = \delta^{**} H(f),$$

or

$$\frac{\delta^*}{\delta^{**}} = H\left(\frac{u^{\prime 2}}{u_0^2}\right). \quad (5-52)$$

Further, after substituting into the equation (5-38) the relationships (5-48) and (5-52), we obtain after simple transformations a first order differential equation relative to the shape parameter  $f$ :

$$\frac{df}{dx} = \frac{u_0''}{u_0^2} f + \frac{u_0'}{u_0} F. \quad (5-53)$$

Here

$$F = 2 \{ \zeta(f) - 2 / [2 + H(f)] \}.$$

The specific type of function  $F(f)$  depends on the shape of speed profile in boundary layer. Calculations show that  $F(f)$  differs little from a linear function, i.e.,

$$F(f) = a - bf.$$

In this respect, equation (5-53) transforms to a linear equation relative to the parameter

$$\frac{df}{dx} = a \frac{u_0'}{u_0} + \left( \frac{u_0''}{u_0^2} - b \frac{u_0'}{u_0} \right) f,$$

integral of which has the form:

$$f = \frac{au_0'}{u_0^2} \int u_0'^{-1} dx + c \frac{u_0'}{u_0}.$$

If at  $x = 0$   $u_0 = 0$ , then from condition of finiteness of  $f$  a constant of integration  $c = 0$ , should be assumed.

In practice it is more convenient to make calculations by using dimensionless magnitudes.

After assuming  $\bar{u}_0 = \frac{u_0}{u_\infty}$  and  $\bar{x} = \frac{x}{L}$ , where  $u_\infty$  is the speed of incident flow, and  $L$  is length of streamlined surface, we obtain:

$$f(\bar{x}) = \frac{a\bar{u}_0'}{\bar{u}_0^2} \int \bar{u}_0'^{-1}(\bar{x}) d\bar{x}. \quad (5-54)$$

The constants  $\underline{a}$  and  $\underline{b}$  can be assumed equal to 0.45 and 5.35 respectively.

For the momentum thickness we obtain:

$$\bar{\delta}^{**} = \frac{\delta^{**}}{L} = \sqrt{\frac{1}{Re_L} \frac{a}{u^2} \int \bar{u}_0'^{-1} d\bar{x}}. \quad (5-55)$$

Further, by formula (5-48) it is simple to determine the local drag coefficient

$c_f$ , also by the expression  $\delta^* = H(f)\delta^{**}$  —that is the displacement thickness.

Values of functions  $\zeta(f)$  and  $H(f)$  are shown in Fig. 5-16.

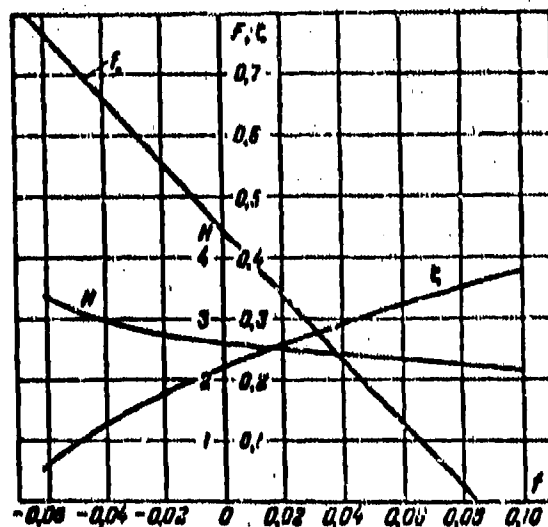


Fig. 5-16. Dependence of magnitudes  $\zeta$ ,  $F$  and  $H$  on the parameter  $f$ .

The considered method of calculation can be extended also to the case of flow of compressible fluid, if we convert to a new variable, proposed by A. A. Dorodnitsyn

$$\xi = \int \frac{\rho}{\rho_0} dx \text{ and } \eta = \int \frac{\rho}{\rho_0} dy.$$

Then for a compressible fluid we obtain:

$$f(\bar{x}) = \frac{0.45\lambda_0'}{\lambda_0'^{2.25} \left(1 - \frac{k-1}{k+1} \lambda_0'^2\right)^{2.25}} \int_0^{\bar{x}} \lambda_0'^{4.25} \left(1 - \frac{k-1}{k+1} \lambda_0'^2\right)^{2.25} d\bar{x}. \quad (5-56)$$

The calculation by formulas (5-48), (5-54), (5-55) and (5-56) are found to be relatively simple and assure an entirely satisfactory accuracy.

For example, we now calculate the laminar boundary layer over a flat plate.

Here  $u_0 = \text{const}$ ;  $u_0' = 0$ ;  $f = 0$  and  $m = 1$ .



Then, from (5-55), (5-47) and (5-48) we obtain:

$$\begin{aligned} \delta^{**} &= \bar{\delta}^{**} L = L \sqrt{\frac{0.45 \nu}{u_0 L}}; \zeta(\eta) = 0.22; \\ c_f &= 0.22 \frac{1}{\frac{u_0 \delta^{**}}{\nu}} = \frac{0.22 \nu}{u_0 \sqrt{\frac{0.45 \nu L}{u_0}}} = 0.332 \sqrt{\frac{\nu}{u_0 L}}; \\ \tau_0 &= c_f \mu_0 u_0^2 = 0.332 \sqrt{\frac{\mu_0^3}{L}}. \end{aligned} \quad (5-57)$$

#### 5-10. Transition of Laminar Boundary Layer Into a Turbulent One

Under certain conditions a laminar boundary layer loses stability and transforms into a turbulent. The tentative limit of loss of stability of a laminar flow can be established by the critical Reynolds number  $Re_{cr}$ . By using analogy between phenomena of transition from a laminar to a turbulent mode in a cylindrical tube and in a boundary layer, it is possible, as has already been indicated, to introduce the characteristic Reynolds numbers for the layer, relative to the thicknesses\*  $\delta$ ,  $\delta^*$  and  $\delta^{**}$ :

$$Re_\delta = \frac{u_0 \delta}{\nu}; Re^* = \frac{u_0 \delta^*}{\nu}; Re^{**} = \frac{u_0 \delta^{**}}{\nu}.$$

Experimental data indicate that the critical values of  $Re_\delta$ , number of the boundary layer have the same order as that for tubes, but they can fluctuate within wider limits ( $Re_{cr} = 2,000$  to  $5,000$ ). According to numerous investigations, the critical  $Re_{cr}$  number depends basically on the state of surface of streamlined body, degree of turbulence (perturbation) of external flow and gradient of speed, i.e., parameter  $\beta$ .

Theoretical and experimental investigations of the stability of laminar boundary layer have indicated that "loss of stability" occurs either as a result of superposition of the disturbances, caused by protuberances in the roughness on the surface of streamlined body, or as result of finite disturbances, introduced into boundary

\*The magnitude  $Re^{**}$  was introduced earlier in deriving equation (5-41) et al.

layer by the external flow. The first cause is found to be significant only with a minor turbulence of the incident flow (order 0.1%) and high degree of roughness.

In using general assumptions in the theory of dimensionality and experimental data, it is simple to obtain an appropriate relationship in explicit form. In omitting its derivation, we now write the formula for determining  $Re_{cr}$ , obtained by A. P. Melnikov:

$$Re_{cr}'' = \frac{0.055}{E_0^{5/3}} \left(1 - \frac{l}{l_s}\right)^{2/3} + 225, \quad (5-58)$$

where  $E_0$  is the initial degree of turbulence;

$l$  is the shape parameter;

$l_s$  is the value of the shape parameter at point of separation; for a laminar layer it is possible to assume  $l_s = -0.085$ .

Thus, for determining the point of loss of stability a laminar boundary layer it is necessary to find by equation (5-55) the change in the momentum thickness along surface of body under consideration and to construct the curves  $Re_{cr}'' = \varphi(\bar{x})$  [equation (5-58)] and  $Re'' = \varphi_1(\bar{x}) = \frac{u_\tau^2}{\nu}$ .

Intersection point of indicated curves will be the sought coordinate of  $\bar{x}_{cr}$ .

Results of the experimental investigation indicate that transition of laminar boundary layer to a turbulent occurs in a certain region, whose dimensions depend on the local pressure gradient, the  $M$  and  $Re$  numbers, the degree of turbulence and certain other factors.

The determination of the position and extent of transitional zone, and also character of change of  $\delta''$  in this zone comprises an important part of the problem in calculating mixed layer and, in particular, subsequent turbulent sector.\*

The transitional region can be determined experimentally by means of measurement of profiles of speed in different sections along length of surface. Character of change of profile of speed in transitional region can be traced in Fig. 5-17, a. At a distance  $x = 35$  mm from leading edge of plate, the layer is laminar; all points will form a curve, corresponding to equation  $\frac{u}{u_\tau} = 2\frac{y}{\delta} - 2\left(\frac{y}{\delta}\right)^3 + \left(\frac{y}{\delta}\right)^4$ . In

\*L. M. Zysina-Molozhen's works and others are devoted to an investigation of the transitional region.

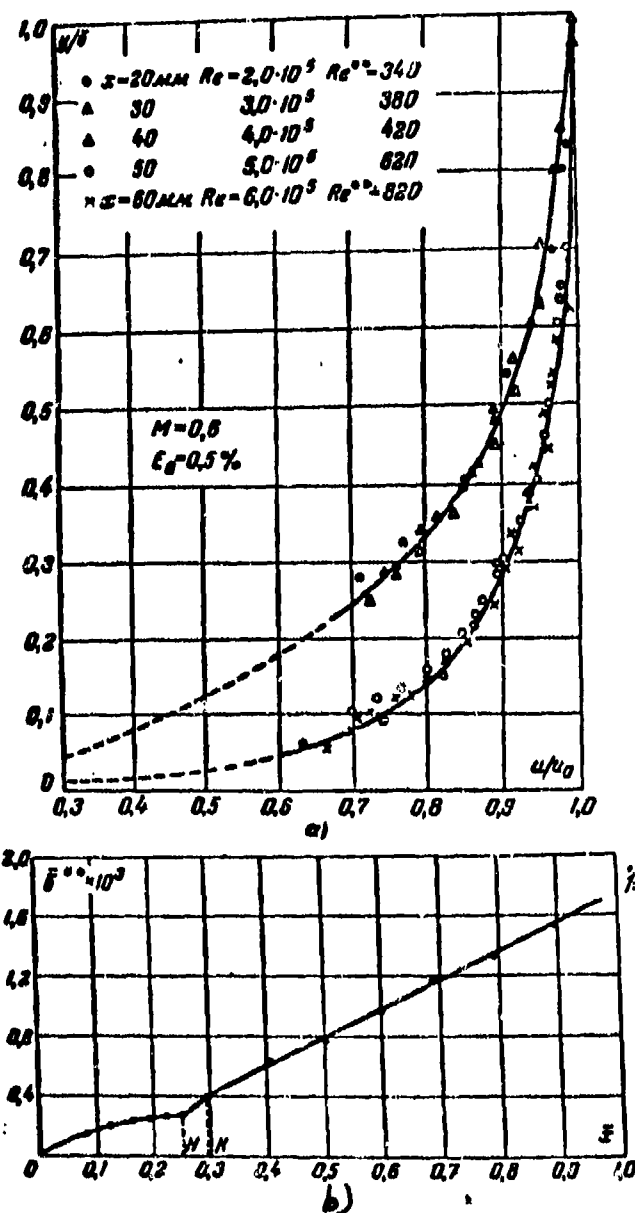


Fig. 5-17. a—change of profile of speed in boundary layer along flat wall; b—change of momentum thickness along a flat wall.

the transition in the sector  $x > 50$  mm, profiles of speed abruptly are deformed and acquire a form, typical for a turbulent boundary layer.

Profiles of the speed in boundary layer make it possible to calculate the momentum thickness  $\delta''(x)$  and on basis of character of change of this magnitude to fix the extent of transitional zone (Fig. 5-17, b).

The length of the transitional region is assumedly is determined in fractions of the total length of streamlined surface.

Changes of  $r^{**}$  in this region are characterized by the magnitude

$$r^{**} = \frac{Re_H^{**}}{Re_H^{**}},$$

where  $Re_H^{**}$ ,  $\delta_H^{**}$  are the Re number and the momentum thickness at the end and  $Re_H^{**} = \frac{u_H \delta_H^{**}}{\nu}$  is the Re number and  $\delta_H^{**}$  at the beginning of the transitional region. In a flow without gradient, the magnitude  $r^{**} = \frac{\delta_H^{**}}{\delta_H^{**}}$ .

In the general case,  $r^{**}$  depends on profile of speed at the beginning of transitional zone, Re and M numbers, and the degree of turbulence. With an increase of Re and M numbers magnitude  $r^{**}$  somewhat increases (Fig. 5-18). On basis of experiments at the Moscow Institute of Power Engineering a change in  $E_0$  within the limits 0.5--1.5% does not result in noticeable changes of the magnitude of  $r^{**}$ . A further increase of  $E_0$  causes a sharp decrease in  $r^{**}$ .

For characteristics of the speed profile's influence in Fig. 5-19 is shown graph  $r^{**} = \varphi_1(f_0)$ , where  $f_0$  is the shape parameter at the beginning of the transitional zone. As is evident from curve, with an increase of shape parameter  $r^{**}$  increases. Analogously depending on the shape parameter  $f_0$  also the extent of transitional zone  $s$  (Fig. 5-19) changes. Such a behavior of the curves  $r^{**} = \varphi_1(f_0)$  and  $s = \varphi_2(f_0)$  can be explained in the following manner. In the transitional zone,

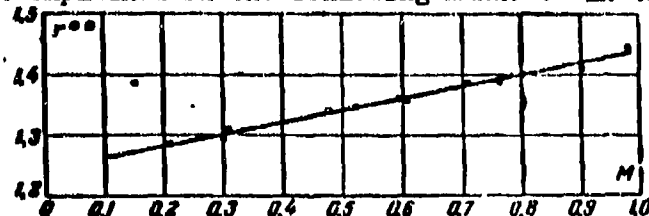


Fig. 5-18. Dependence of magnitude  $r^{**}$  on M number.

as result of a transverse displacement of the particles, the thickness of boundary layer increases, and profile of speed becomes fuller. If, as a result of increase of the thickness of  $\delta$  there occurs an increase of  $\delta^{**}$ , then, an increase in fullness of profile of speed causes a decrease in the integral thickness of  $\delta^{**}$ . In the nozzle region, of basic importance is the increase in thickness of the boundary layer  $\delta$ , since here profile of speed is fairly full and as a result of the transition its fullness changes insignificantly.\* Conversely, in diffuser region as a result of transition of laminar flow to turbulent, there occurs a significant deformation of profile of speed, in which the greater this deformation proves to be, the larger is the positive pressure gradient in the place where the transition occurs.

At a certain value of parameter  $f_0$  in diffuser region both factors, affecting the magnitude  $\delta^{**}$ , mutually are compensated and magnitude  $r^{**}$  is found to be equal to unity. The extent of the transitional zone at same time also proves to be significant. On basis of experiments at Moscow Institute of Power Engineering (MEI),  $r^{**} = 1$  at  $f_0 = -0.06$  to  $0.07$ .

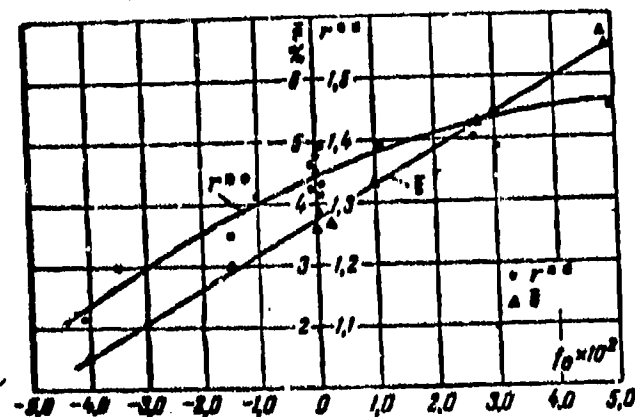


Fig. 5-19. Dependence of magnitude  $r^{**}$  and  $\delta^{**}$  on the shape parameter  $f_0$ .

\* It must be noted that in the nozzle region with large pressure gradients a transition of turbulent layer into a laminar (page 215) is possible. Such a transition is very probable at  $M \approx 1$ .

If, however, for any reason the transition begins at  $f < -0.07$ , then, apparently, the process of turbulization of the layer and reconstruction of profile of speed will occur against the flow, while profile of a laminar layer will not be found to be sufficiently stable.

Hence, incidentally it follows that the separation of boundary layer can occur only in the region either of laminar, or turbulent motion, since transition of a laminar layer to turbulent in the diffuser region occurs at a value of parameter  $f$ , smaller than its value at the point of separation.

On the basis of processing experimental data for calculation, the transitional regions are obtained by following empirical formulas:

$$\bar{s} = \left(\frac{10^6}{Re}\right)^{0.15} (3.7 + 5.5 f_0) / \epsilon; \quad (5-59)$$

$$r^{**} = (7 + 100 f_0)^{0.12} \frac{f_0}{2} + 0.12 M. \quad (5-60)$$

In knowing the magnitudes  $\bar{s}$  and  $r^{**}$ , there are readily found the coordinates of the sector, from which one should make a calculation of the turbulent layer, and the value of its momentum thickness.

#### 5-11. Calculation of Turbulent Boundary Layer

The calculation of turbulent boundary layer is constructed on the basis of experimental data, which makes it possible to express approximately the friction stress in the layer.

In many cases it is convenient to use an approximate power distribution law of speeds in the layer, expressed by the formula

$$\frac{u}{u_\epsilon} = \left(\frac{y}{\delta}\right)^n. \quad (5-61)$$

Formula (5-61) is constructed on the basis of a comparison of profiles of speed in turbulent layer and in a cylindrical tube. As was pointed out, the velocity profile in pipe varies with a change of Re number (Fig. 5-6). Consequently,

the exponent  $n$  in formula (5-61) is function of the Reynolds number. Thus, the basis of experiments of N. Nikuradze an exponent of  $n$  power varies within the limits of  $\frac{1}{6}$  to  $\frac{1}{10}$  during change of  $Re$  from  $4 \cdot 10^3$  to  $3 \cdot 10^6$ . However, as a first approximation, the exponent of  $n$  power can be assumed as constant in a definite range of Reynolds numbers. In the calculations frequently it is assumed  $n = \frac{1}{7}$  and the profile of speed is given by the formula

$$\frac{u}{u_0} = \left(\frac{y}{\delta}\right)^{\frac{1}{7}}. \quad (5-62)$$

The friction stress on wall during turbulent motion can be represented also by a simplified empirical dependence

$$\tau_0 = \zeta \rho u_0^2 \left(\frac{u_0 \delta^{**}}{\nu}\right)^m. \quad (5-63)$$

By substituting the empirical coefficients  $\zeta = 0.00655$ , and  $m = -0.166$  into formula (5-63) and by considering the particular case of a flow without gradient from equation (5-38) we find:

$$c_{f_0} = \frac{d\delta^{**}}{dx} = 0.00655 Re^{*-0.166}. \quad (5-64)$$

We introduce in this equation  $Re_x = \frac{u_0 x}{\nu}$ . Let us note that

$$\frac{d\delta^{**}}{dx} = \frac{d\left(\frac{\delta^{**} u_0}{\nu}\right)}{d\left(\frac{x u_0}{\nu}\right)} = \frac{d Re^{**}}{d Re_x}. \quad (5-65)$$

Then differential equation for the momentum thickness will be written as:

$$\frac{d Re^{**}}{d Re_x} = 0.00655 Re^{*-0.166}. \quad (5-66)$$

In assuming that on wall there will be formed only a turbulent layer, we integrate equation (5-66). Then, we obtain:

$$Re^{**} = 0.0153 Re_x^{\frac{6}{7}}.$$

Hence, by replacing  $Re^{**}$  and  $Re_x$ , we find an equation for the momentum thickness:

$$\delta^{**} = 0.0153 \left(\frac{\nu}{u_0}\right)^{\frac{1}{7}} x^{\frac{6}{7}}. \quad (5-67)$$

or after expressing  $\delta^{**}$  as a function of  $Re_x$ , we find:

$$\delta^{**} = 0.0153 x Re_x^{-\frac{1}{7}}. \quad (5-68)$$

The obtained simple solution for the momentum thickness in a turbulent layer does not take into consideration the influence of compressibility and of longitudinal pressure gradient. It is valid at  $M \leq 0.5$  and  $\frac{dp}{dx} = 0$ .

As has already been mentioned, the equation of momentum (5-38) associates three unknown magnitudes:  $\delta^*$ ,  $\delta^{**}$  and  $\tau_0$ . Additional associations, necessary

for solution of problem, are established experimentally.

In Fig. 5-20, empirical dependence  $H_0 = H(M)$  for a flat plate with zero pressure gradient is given. The magnitude  $H_0$  depends greatly on  $M$  number; this dependence can be approximately represented by following formula:

$$H_0 = H_{\infty}(1 + aM^2) = H_{\infty}(1 + 0.3M^2), \quad (5-69)$$

where for an incompressible fluid with a zero pressure gradient it is possible to assume  $H_{\infty} = 1.3$  to  $1.4$ , in which a smaller value of  $H_{\infty}$  corresponds to large  $Re$  numbers. With an increase in the  $M$  number the relative momentum thickness decreases somewhat (Fig. 5-26).

The influence of pressure gradient on the parameter  $\bar{H}$  can be seen in Fig. 5-21, where the dependence  $\bar{H} = H/H_0$  on the Buri parameter  $\Gamma$  is given.

It follows from this that in some of moderate values of parameter  $\Gamma$  ( $-0.015 < \Gamma < 0.02$ )  $\bar{H}$  varies by 7%. Therefore, in constructing the solution in the mentioned range only the variation of  $H_0 = H(M)$  will be considered.

For a drag coefficient in a turbulent layer for the general case, formula (5-50) was obtained. If we relate  $\tau_0$  to the density at outer limit of boundary layer  $\rho_1$ , then, formula (5-50) can be presented in the form:

$$\begin{aligned} \frac{\tau_0}{\rho_1 u_0^2} &= \frac{\rho_0}{\rho_1} Re_0^{n-m} (\zeta + a\Gamma) = \\ &= (\zeta + a\Gamma) Re_0^{n-m} \left(1 + \frac{k-1}{2} M_0^2\right)^{-1}. \end{aligned} \quad (5-70)$$



Fig. 5-20. Influence of  $M$  number on the parameter,  $H_0$ .

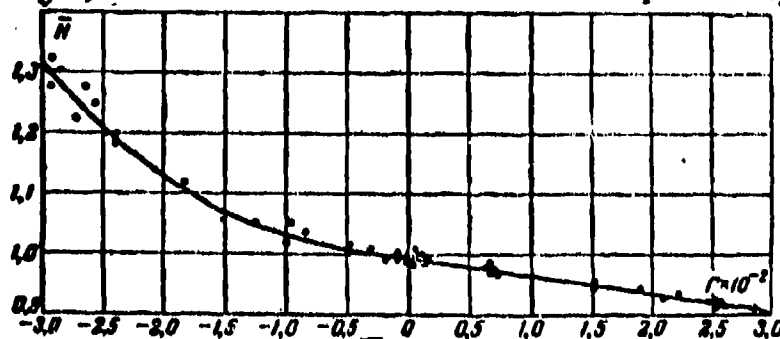


Fig. 5-21. Variation of magnitude  $\bar{H}$  depending on the Buri parameter  $\Gamma$ .



We set up (5-69) and (5-70) into a integral relationship (5-38). After simple, but laborious transformations there can be obtained a differential equation relative to concerning parameter  $\Gamma$  in the following form::

$$\Gamma' + p(\bar{x})\Gamma + Q(\bar{x}) = 0, \quad (5-71)$$

where  $\bar{x}$  is the dimensionless length of streamlined surface.

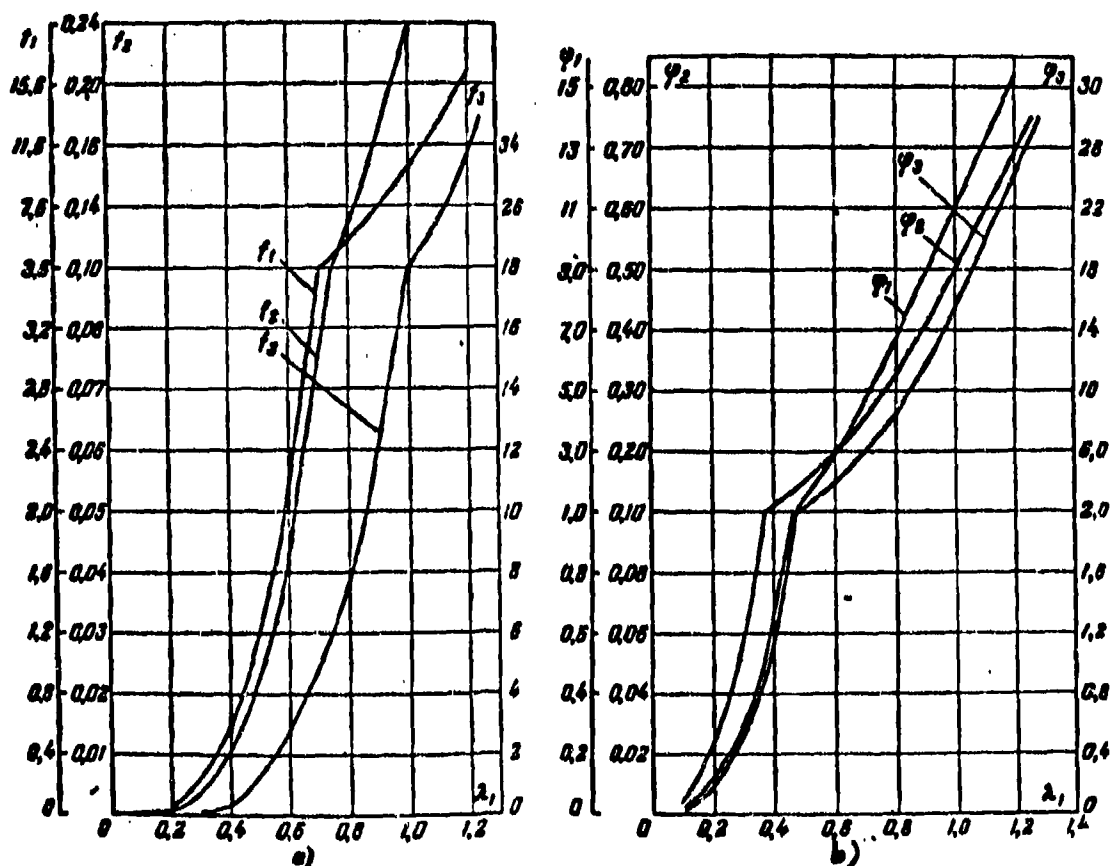


Fig. 5-22. a—dependence of functions  $\psi_1, \psi_2$  and  $\psi_3$  on  $\bar{x}$ ; b—dependence of functions  $f_1, f_2$  and  $f_3$  on  $\bar{x}$ .

Equation (5-71) pertains to type of linear and can be reduced to quadratures and solved relative to the parameter  $\Gamma$ . It serves for determining the parameter  $\Gamma$ , by eliminating the region, near the point of separation.

With the equality to zero of constant  $a$  and tending of  $\lambda$  towards zero, the solution transforms to formula (5-67).

By introducing a number of simplifications, we obtain during small pressure

gradients ( $\Gamma > -0.02$ ) for the momentum thickness of the expression

$$\bar{\delta}^{**} = \frac{1}{\lambda_0^{1.35} \text{Re}_*^{0.2} (6 - \lambda_0^2)^{1.45}} \left[ \delta_0^{**1.25} \lambda_0^{4.17} \text{Re}_*^{0.25} (6 - \lambda_0^2)^{1.81} + \right. \\ \left. + 0.0026 \int_{\lambda_0}^{\lambda} \lambda_0^{3.92} (6 - \lambda_0^2)^{2.81} d\lambda \right]^{0.8}. \quad (5-72)$$

Here  $\bar{\delta}_0^{**}$  and  $\lambda_0$  are values of the momentum thickness and dimensionless speed at the beginning of turbulent sector;  $\text{Re}_* = \frac{aL}{\nu_w}$  is the Reynolds number, determined by the critical speed  $a$  and the kinematic viscosity on the wall.

In introducing the designations:

$$f_1 = \lambda_0^{2.35} (6 - \lambda_0^2)^{1.45}; \\ f_2 = 0.0026 \lambda_0^{3.92} (6 - \lambda_0^2)^{2.81}; \\ f_3 = \lambda_0^{4.17} (6 - \lambda_0^2)^{1.81}, \quad (5-73)$$

we transform (5-72) to the form:

$$\bar{\delta}^{**} = \frac{1}{f_1 \text{Re}_*^{0.2}} \left[ \delta_0^{**1.25} \text{Re}_*^{0.25} f_1 + \int_{\lambda_0}^{\lambda} f_2 d\lambda \right]^{0.8}. \quad (5-74)$$

The functions  $f_1$ ,  $f_2$ , and  $f_3$  on  $\lambda$ , are presented in Fig. 5-22, a.

The calculation by formula (5-74) with use of calculating graphs is found to be relatively simple and is in good agreement with experimental data.

With large pressure gradients for momentum thickness we obtain:

$$\bar{\delta}^{**} = \frac{1}{\varphi_1 \text{Re}_*^{0.2}} \left[ \delta_0^{**1.25} \text{Re}_*^{0.25} \varphi_1 + \int_{\lambda_0}^{\lambda} \varphi_2 d\lambda \right]^{0.8}. \quad (5-75)$$

Here,

$$\left. \begin{aligned} \varphi_1 &= \lambda_0^{2.35} (6 - \lambda_0^2)^{1.3} e^{0.103 \lambda_0^2}; \\ \varphi_2 &= 0.0078 \lambda_0^{2.69} (6 - \lambda_0^2)^{2.62} e^{0.31 \lambda_0^2}; \\ \varphi_3 &= \lambda_0^{2.94} (6 - \lambda_0^2)^{1.62} e^{0.131 \lambda_0^2}. \end{aligned} \right\} \quad (5-76)$$

The corresponding values  $\varphi_1$ ,  $\varphi_2$  and  $\varphi_3$  are shown in Fig. 5-22, b.

In conclusion we shall dwell on essential difference between properties of laminar and turbulent layers. For the purpose, in the Table 5-1 are presented the basic calculating formulas for simplest case of flow around a flat wall (flow with gradient) by an incompressible fluid.

Table 5-1

a) Основные харак- теристики погра- ничного слоя	b) Режим пограничного слоя	
	с) ламинарный	д) турбулентный
е) Закон распре- деления скоростей по сечению слоя	$\frac{u}{u_0} = \left[ 2 \frac{y}{\delta} - \right. \\ \left. - 2 \left( \frac{y}{\delta} \right)^3 + \left( \frac{y}{\delta} \right)^4 \right]$	$\frac{u}{u_0} = \left( \frac{y}{\delta} \right)^{1/7}$
ф) Толщина слоя	$\delta \approx 5,83 \left( \frac{\nu x}{u_0} \right)^{1/2} = \\ = 5,83 x Re_x^{-1/2}$	$\delta \approx 0,211 \left( \frac{\nu x}{u_0} \right)^{1/4} x^{3/4} \approx \\ \approx 0,211 x Re_x^{-1/4}$
г) Толщина вытес- нения	$\delta^* \approx 1,72 x Re_x^{-1/2} \approx 0,38$	$\delta^* \approx 0,02 x Re_x^{-1/4} \approx 0,0958$
h) Толщина поте- ри импульса	$\delta^{**} \approx 0,664 x Re_x^{-1/2} \approx \\ \approx 0,11758$	$\delta^{**} \approx 0,015 x Re_x^{-1/4} \approx \\ \approx 0,0718$
и) Напряжение трения	$\tau_0 = 0,332 \mu_0^2 Re_x^{-1/2}$	$\tau_0 = 0,0132 \mu_0^2 Re_x^{-1/4}$
ж) Местный коэф- фициент трения	$c_f = 0,664 Re_x^{-1/2}$	$c_f = 0,0263 Re_x^{-1/4}$
к) Коэффициент сопротивления трения	$C_f = 1,328 Re_x^{-1/2}$	$C_f = 0,0507 Re_x^{-1/4}$

KEY: a) Basic characteristics of boundary layer; b) Mode (Regime) of boundary layer; c) Laminar d) Turbulent; e) Distribution law of speeds along a section of layer; f) Thickness of layer; g) Thickness of displacement; h) Momentum thickness; i) friction stress; j) Local coefficient of friction; k) Drag coefficient of friction.

A comparison shows: 1) speed profile in turbulent layer is more filled in than in the laminar; 2) thickness of turbulent layer increases along wall significantly more rapidly than that of laminar, since in the first case  $\delta$  increases proportionately to  $x^{6/7}$  and in the second--proportionally to  $x^{1/2}$ ; 3) a comparison of local drag coefficients of friction shows that with identical  $Re_x$  values resistance of friction in turbulent boundary layer is significantly higher than in the laminar.

This very important conclusion is well corroborated by experimental data. In Fig. 5-23 are given experimental and calculation relationships of the

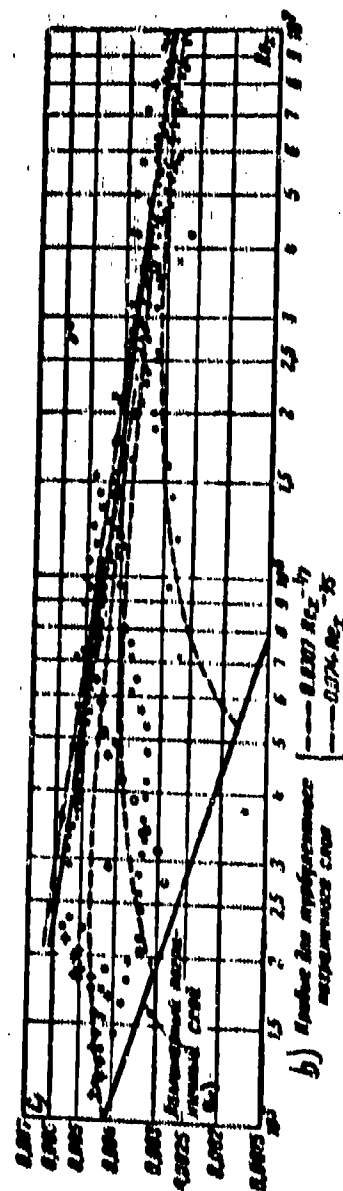


Fig. 5-23. Comparison of friction coefficients of plate on basis of experimental and calculated data depending on  $Re$ .  
KEY: a) Laminar boundary layer; b) Curves for a turbulent layer

coefficients  $c_f$ , obtained for a turbulent mode by means of different semi-empirical formulas. The curves show a fairly high accuracy of the formula, given in Table 5-1.

A comparison of  $c_f$  for laminar and turbulent layers shows that with an identical value  $Re_x = 4 \cdot 10^4$ , coefficient  $c_{fturb}$  doubly exceeds  $c_{flam}$  ( $c_{fturb} = 0.0054$ ;  $c_{flam} = 0.0022$ ). With an increase in  $Re_x$  the difference  $c_{fturb} - c_{flam}$  sharply increases.

It follows from this that in the continuous flow around a body, it is necessary to strive to tightening of laminar section of layer, i.e., to displacement of region of transition in direction of the flow.

The detected difference in resistances to friction during laminar and turbulent modes is explained by different mechanism of friction in any one case. If in a laminar mode, the resistance is caused by skin friction between layers of liquid (mixing of macroparticles—molecules), then in a turbulent mode there take place intense transverse dislocations of microparticles. It is obvious that mixing of these particles is associated with the loss of large amount of momentum, i.e., with manifestation of substantial forces of friction in the flow.

Numerous experiments in accordance with conclusions of the semiempirical theory indicate still one essential difference in properties of laminar and turbulent boundary layers. The point of separation of laminar layer at large  $Re$  numbers occupies a fixed position on a streamlined surface. The point of separation of turbulent layer with an identical distribution of parameters of external flow is situated beyond the point of separation in a laminar layer. In other words, turbulent layer is detached later than the laminar. This becomes understood from a consideration of profiles of speed during any one mode of the layer: the kinetic energy of the particles moving near wall during turbulent mode is significantly greater than during a laminar mode.

In those cases, when on streamlined surface there exists a mixed boundary layer, it is necessary to summarize the resistance in laminar and turbulent sectors.

The above discussed procedure of calculation does not consider the influence of initial turbulence of flow. For small degrees of turbulence, the equation of momentum of boundary layer for incompressible fluid was obtained by V. A. Vrublivskaya in such a form:

$$(1 + AE_0^2) \frac{d\delta^{**}}{dx} + \frac{\bar{u}_0^2 \delta^{**}}{u_0^2} (2 + \delta^{**}) = \frac{\gamma_0}{\rho u_0^2} + E_0^2. \quad (5-77)$$

Here  $A = \frac{2}{\delta^{**}} \cdot \bar{u}_0$  is the averaged value of speed of external flow;  $\delta^{**}$  is the momentum thickness of loss calculated on the basis of averaged speeds.

The graphical solution of equation (5-77) for a flow without gradient is shown in logarithmic coordinates in Fig. 5-24. Here there are plotted the experimental points, relating to the experiment on flat wall conducted at Moscow Institute of Power Engineering (MEI). Graphs in Fig. 5-24 clearly show the influence  $E_0$  on losses in boundary layer; thus at  $Re_x = 2 \cdot 10^6$  the increase in  $E_0$  from 0 to 5% increases the  $Re^{**}$  number and consequently, the magnitude of frictional losses in the layer by 70%.

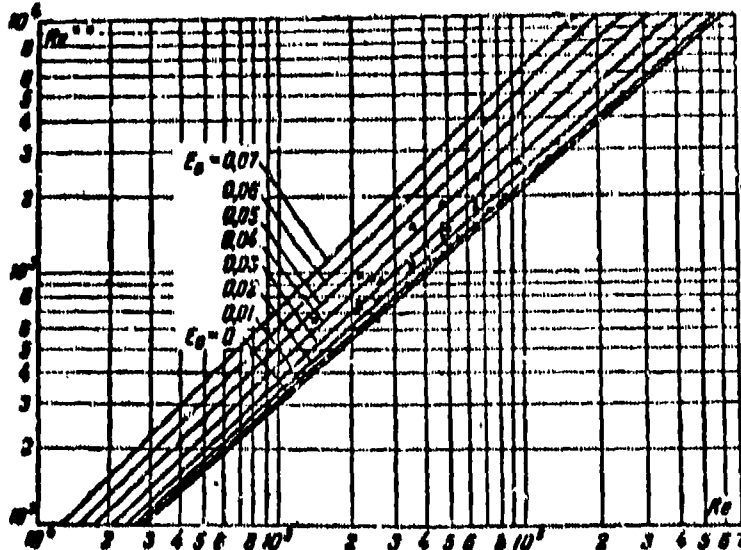


Fig. 5-24. Influence of degree of turbulence on the momentum thickness in the turbulent boundary layer.

#### 5-12. Boundary Layer During High Speeds. Experimental Data

We shall analyze certain results of an experimental investigation of a turbulent boundary layer during high subsonic speeds in a flow without gradient and sub-critical speeds ( $M < M$ ).

In Fig. 5-25 are given six profiles of speeds, obtained with a constant Re number equal to  $2.5 \cdot 10^6$ , and a variable M number. All the experimental points in the interval  $M = 0.31$  to  $0.98$  will form one curve, which can be presented by a dependence of the form:

$$\frac{\lambda}{\lambda_0} = f\left(\frac{M}{M_0}\right). \quad (5-78)$$

Consequently, with a zero pressure gradient with a variation in M number the profiles of speed in coordinates  $y, z$  vary similarly. In addition, in the indicated ranges of changes in M number the thickness of the boundary layer at constant Re number changes insignificantly; therefore, it is possible to speak not only about the similarity, but also about identity of profiles of speed. Hence, it may be concluded, that the influence of compressibility at  $M < 1$  directly on profile of speed in boundary layer is reflected insignificantly. Thus, as a first approximation profile of speed at  $M > 0$  it can be presented by the ordinary power formula (5-62).

Formula (5-62), of course, is not the only one. Any dependence, satisfactorily approximating the profile of speed in boundary layer of an incompressible fluid, can be extended to the flow of a compressible fluid. Limits of such extrapolation are not confined, apparently, by sonic speed and can be extended to supersonic speeds.

A subsequent processing of profiles of speed gives possibility of calculating the value of integral thicknesses  $\delta^*$ ,  $\delta^{**}$  and to construct curves of their change depending upon M number (Fig. 5-26). The dispersion of experimental points in the range of transonic speeds is explained by generation of a nozzle flow. Curves for transonic speeds were drawn through points, obtained with a minimum pressure gradient; therefore, in the range of sonic and supersonic speeds, main mass of points is located under the curves. The scattering points, detected in the area of subsonic speeds, is explained by the fact that here there have been plotted points, relating to different Re numbers.

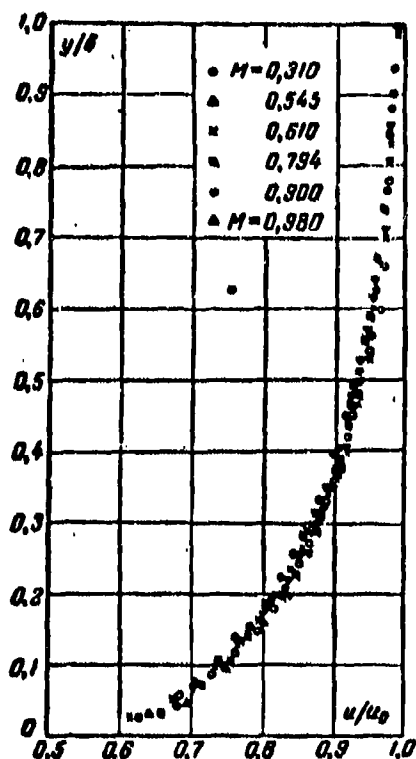


Fig. 5-25. Influence of M number on profile of speed in turbulent boundary layer.

pressure gradient is given. In approaching a sonic speed, the decrease in momentum thickness amounts to about 15%.

The independence of profile of speed on M number gives the basis for considering Re number as basic parameter, determining profile of speed in absence of pressure gradient, and to extend the results of numerous experiments in determining its influence in an incompressible fluid to the flow of a compressible fluid.

In Fig. 5-27 there are given six profiles of speeds, obtained with variation of Re number and a constant M number. An increase in Re number from  $0.61 \cdot 10^6$  to  $1.08 \cdot 10^6$  results in a characteristic change of profile of speed. A subsequent increase in Re number does not cause a marked change in profile of speed. In other

The obtained picture is in full agreement with theoretical results. An increase in M number results in a drop in the momentum thickness and to an increase in thickness of displacement  $\delta^*$ . Such behavior to the curves with identical profiles of speed is caused by change in density across boundary layer, in which an opposite influence of this change on the thicknesses  $\delta'$  and  $\delta''$  is explained by the fact that subintegral functions by which thicknesses  $\delta'$ ,  $\delta''$ , are expressed, react differently on a change of density.

For approximate quantitative evaluation of the influence of compressibility on the momentum, thickness  $\delta''$  in Fig.

5-26, the change of relative thickness

$$\frac{\delta''_0}{\delta''_\infty} = \bar{\delta}_0'' \text{ depending upon M with zero}$$



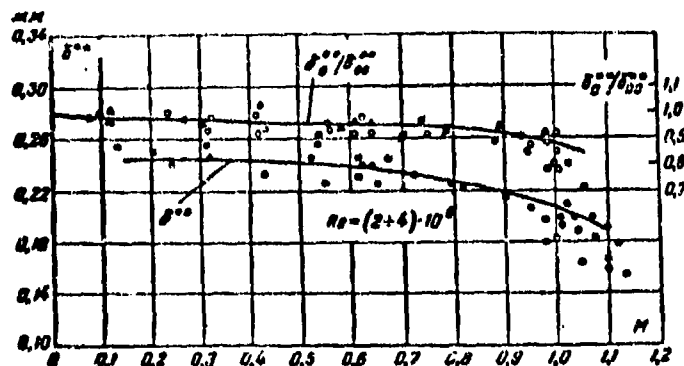


Fig. 5-26. Influence of M number on the momentum thickness.

words, starting from magnitude  $Re \approx 10^6$ , profiles of speed can be expressed by a general relationship.

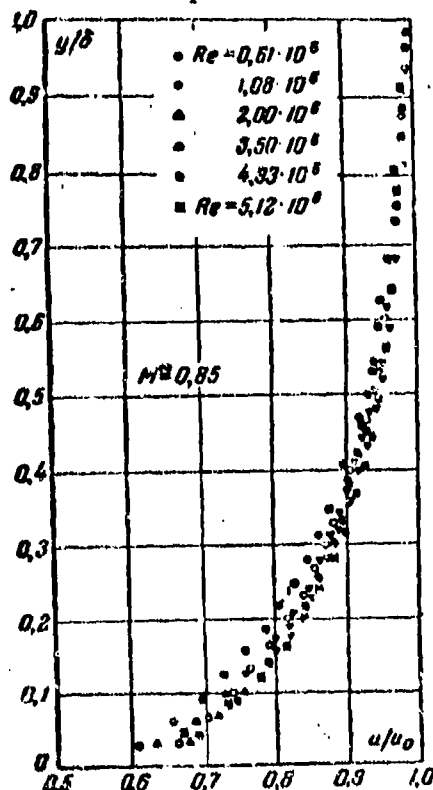


Fig. 5-27. Influence of Re number on profile of speed in turbulent boundary layer.

Investigation of influence of Re number on integral thicknesses  $\delta'$  and  $\delta''$  showed that with an increase in Re, as well as in case of an incompressible fluid, these magnitudes decrease. In the range of small Re values the change in  $\delta''$  is found to be fairly marked. With an increase in Re number a decrease of thickness  $\delta''$  occurs less intensively. Analogously also the displacement thicknesses vary.

Thus, the influence of Re number at high speeds on turbulent boundary layer from the qualitative side proves to be of the same order as in the flows of an incompressible fluid.

For investigation of question on influence of M number in the presence of a pressure gradient profiles of speed in diffuser region (Fig. 5-28,a) and in the nozzle flow (Fig. 5-28b) were plotted. As can be seen from given curves, all experimental points independently of M number will form practically one curve. This

fact once again confirms the earlier made conclusion about the fact that at subsonic speeds change in M number does not result in marked changes of profiles of speed. Consequently, main factor, determining flow in boundary layer of compressible fluid, is the longitudinal pressure gradient.

Results of investigation show that the influence of compressibility on the structure of turbulent boundary layer is indirect. With a change of M number the distribution of pressures along streamlined surface varies. With an increase of M number the absolute values of pressure gradient increases. In accordance with this

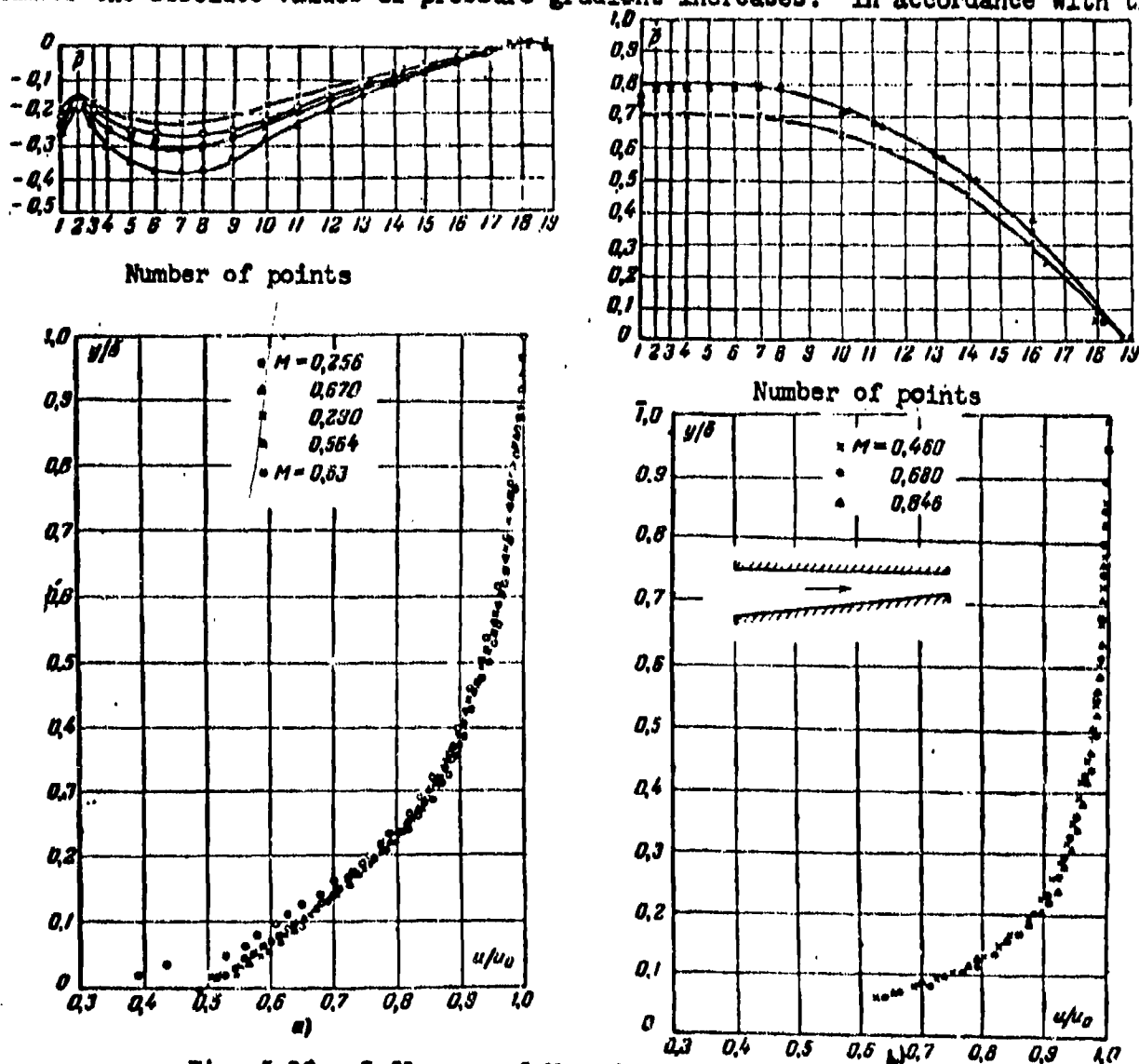


Fig. 5-28. Influence of M number on profile of speed in a turbulent boundary layer.  
a—profile of speed in diffuser region,  $Re = 1.5 \cdot 10^5$ ;  
b—profile of speed in nozzle region,  $Re = 2 \cdot 10^5$ .

main characteristics of layer vary. In a nozzle flow  $\delta''$  decreases, but in diffuser--increases.

The change in longitudinal pressure gradient from a positive to a negative value results in a substantial deformation of profiles of speed. This is very evident in Fig. 5-29, where there are illustrated speed profiles, obtained in diffuser channel with different pressure gradients.

In Fig. 5-30 the curve of the change of the momentum thickness, as a function of parameter  $\Gamma$ , obtained from an experiment is given. In order to exclude influence of compressibility, the thickness  $\delta''$  was related to a corresponding thickness  $\delta_0''$  for a flow without gradient with the same speed of external flow. All

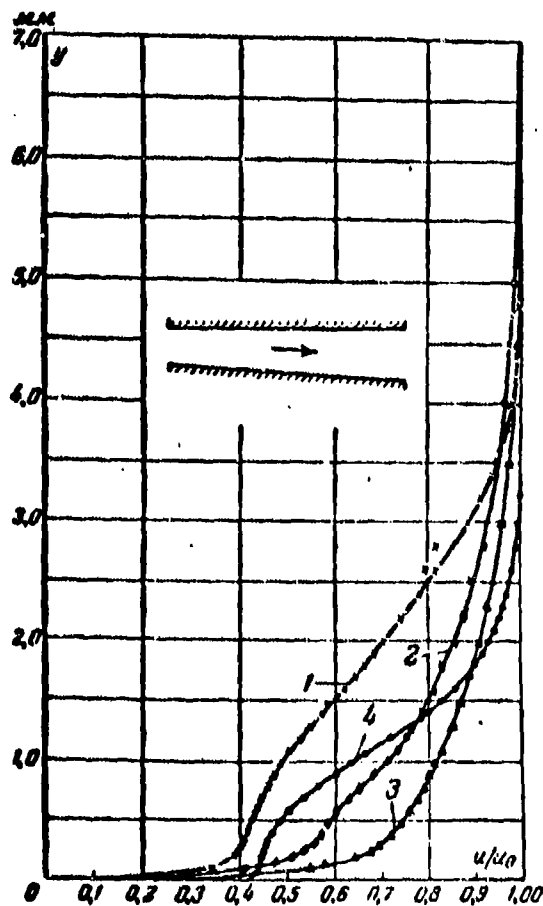


Fig. 5-29. Profiles of speed in diffuser with different pressure gradients.

- 1—  $\delta'' = 0.61$  mm;  $\delta' = 1.095$  mm;  $M = 0.960$ ;  $H = 2.4$ ;  $H_0 = 1.65$ ;
- 2—  $\delta'' = 0.552$  mm;  $\delta' = 0.765$  mm;  $M = 0.548$ ;  $H = 1.57$ ;  $H_0 = 1.4$ ;
- 3—  $\delta'' = 0.384$  mm;  $\delta' = 0.52$  mm;  $M = 0.54$ ;  $H = 1.52$ ;  $H_0 = 1.4$ ;
- 4—  $\delta'' = 0.37$  mm;  $\delta' = 0.638$  mm;  $M = 0.985$ ;  $H = 2.2$ ;  $H_0 = 1.7$

points are grouped around one curve.

From the curve it follows that in the given case  $\delta^{**}$  is a function of the one parameter  $\Gamma$ . Consequently, when distribution of speed at outer limit of boundary layer is nearly linear, calculation on basis of one-parameter method is physically well-based. The lack of experimental data, referring to other values of second derivative, makes it impossible to make more general conclusions.

Experimental data, characterizing the influence of initial turbulence on the structure of boundary layer are shown in Fig. 5-31. With an increase in  $E_0$ , fullness of profile of speed increases. However, filling in of the profile depends considerably on sign and magnitude of gradient of speed of external flow. The maximum influence  $E_0$  is shown to be in diffuser flow which the graphs of change  $\bar{\delta}^{**}$  along flat wall with different pressure gradients (Fig. 5-32) corroborate. Least sensitive to a change in  $E_0$  is the nozzle flow ( $\frac{dp}{dx} < 0$ ).

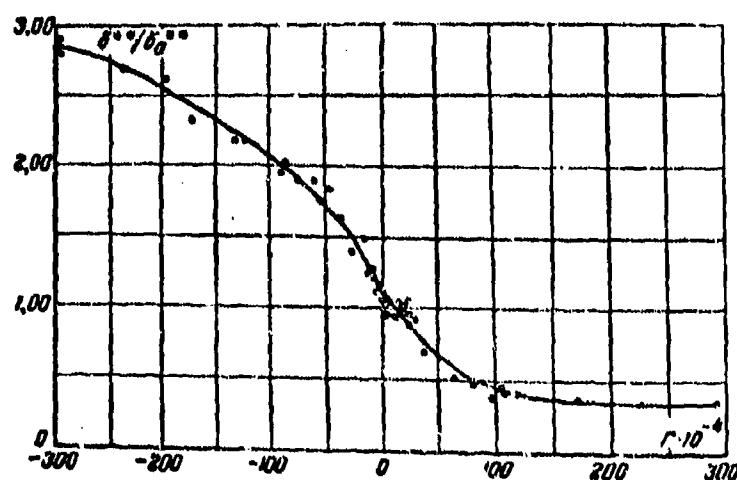


Fig. 5-30. Dependence of relative momentum thickness on the parameter  $\Gamma$ .

With an increase of Reynolds number, the influence of  $E_0$  decreases (Fig. 5-32). An analogous result is obtained also with different  $M$  numbers; with an increase in  $M$  the divergence of curves decreases, especially at  $M$ , close to unity.

We note that in connection with increasing filling-in of profile of speed in the layer, the parameter  $H = \frac{\delta^*}{\delta^{**}}$  markedly lowers with an increase in the degree of

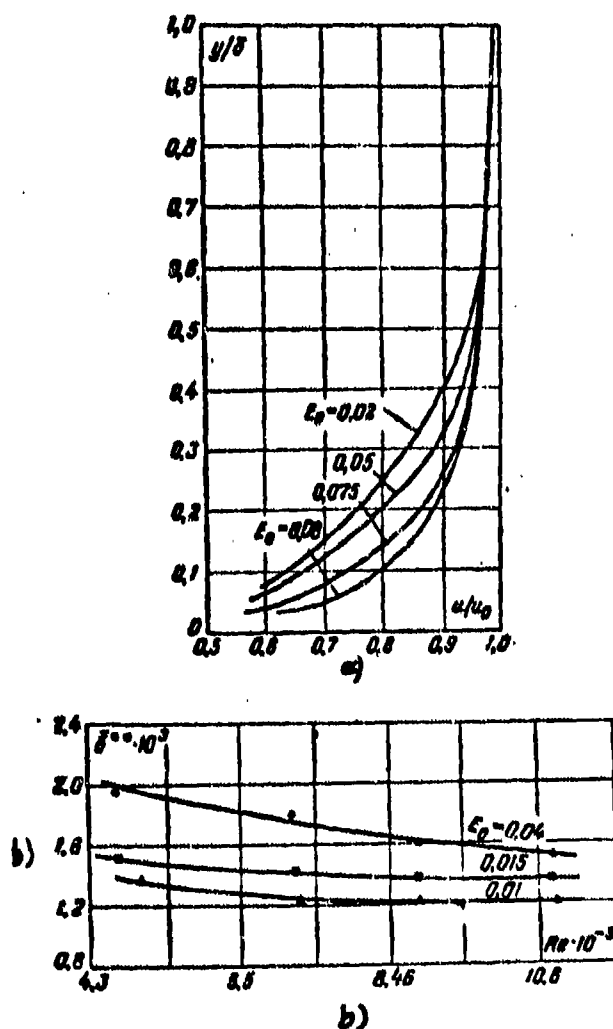


Fig. 5-31. Influence of initial turbulence  
a—on profiles of speed in a turbulent bound-  
ary layer; b—on the momentum thickness with  
different pressure gradients.

turbulence; depending upon sign of longitudinal pressure gradient, this lowering amounts to 15-20%.

Especially great is the influence of initial turbulence with a detached flow around a surface. In this case the increase in  $E_0$  results in a sharp displacement of point of separation along flow and to an improvement of flow around a surface.

The given data indicates that in calculation of the turbulent boundary layer,

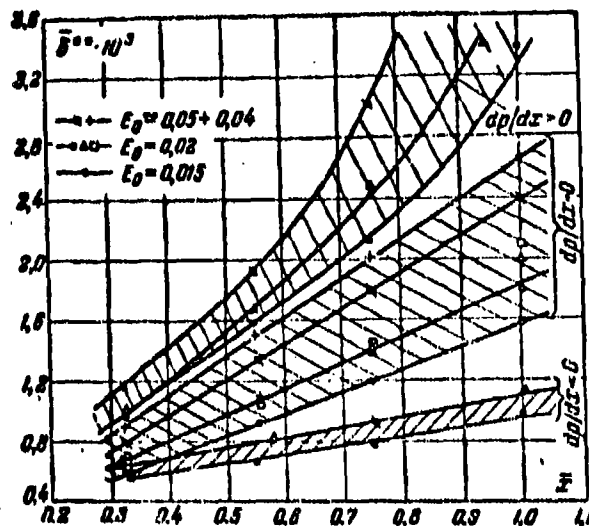


Fig. 5-32. Influence of initial turbulence on the momentum thickness with a gradient flow.

it is necessary to consider the influence of initial turbulence. The marked divergences between experimental and calculated [by formula (5-70)] values of  $\delta^{**}$  are marked at  $E_0 > 3\%$ .

Let us analyze certain properties of boundary layer at transonic speeds.\*

If speed of oncoming flow,  $M_\infty$ , is greater than the critical value  $M_{*}$ , then along surface of streamlined body there will be formed range of supersonic speeds.

The range of supersonic speeds has a limited extent in direction, normal to the streamlined surface. In the direction of flow (along streamlined surface) the region of supersonic speeds also is limited. This conclusion is readily reached by remembering that at a certain distance after the body speed should be subsonic, since speed of an undisturbed flow (before body) is subsonic.

Thus, the zones of supersonic speeds, occurring at  $M_\infty > M_{*}$ , have a local character. In the local supersonic range, the flow of gas at first is accelerated, but later is stagnated. However, stagnation of supersonic flow, as a rule, occurs with the formation of a shock. Owing to the large accelerations in zone of supersonic

\*The considered questions here of flow around bodies at transonic speeds is partially discussed in Chapter 3.

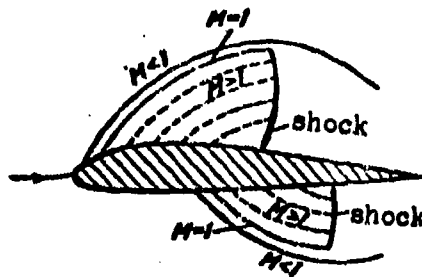


Fig. 5-33. Schematic diagram the formation of shock wave in a local supersonic zone.

speeds the gas is found to be greatly overexpanded, that is, its pressure falls significantly below pressure of external medium. This overexpansion of supersonic flow is extinguished by a shock wave.

As already indicated above, speeds at a distance from body vary in magnitude and direction (disturbance of flow in direction from body decreases). Owing to this, the forming shock waves will be curved with varying intensity along line of shock: behind the shock the flow becomes vortical. The forming shock waves enclose the region of supersonic speeds. Its fore limit is line of the transition (line  $M_1=1$ ). For an ideal fluid, surface of streamlined body (Fig. 5-33) serves as the enclosing surface.

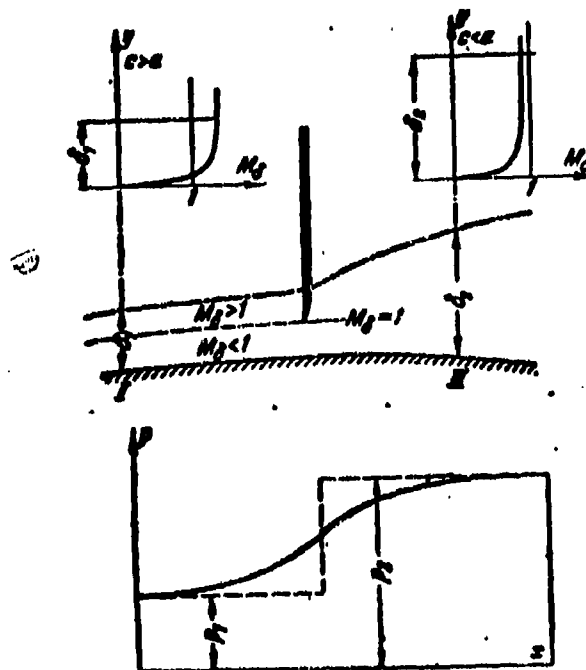


Fig. 5-34. Diagram of interaction between a normal shock and the boundary layer.

In the real case of a viscous gas, the location and extent of local supersonic zone, and also structure of the shock change. The mechanism of interaction of shocks with boundary layer constitutes an important part of problem of resistance of bodies at transonic speeds.

Shock waves in a local supersonic zone create large pressure gradients which are propagated into the region of boundary layer. The disturbances, appearing in boundary layer, are propagated against the flow and also along the flow; they also exert an influence on field of flow along the streamlined surface.

We now consider at first simplest case, when in supersonic zone there will be formed one normal shock\* (Fig. 5-34). In boundary layer the speeds vary from zero at wall to a supersonic value in external flow. Consequently, within the limits of layer there is located a line of transition ( $M = 1$ ), which divides region of boundary layer into subsonic and supersonic parts. We note that in a turbulent boundary layer the subsonic part has a relatively smaller thickness, than in a laminar boundary layer. It is obvious that an increase of pressure is propagated through subsonic part of layer to meet the flow.

An increase of pressures in zone of shock may result in the generation of a separation. During a turbulent mode the intensity of shock, causing a separation, must be higher, since, as it was pointed out above, a turbulent layer always is detached later. We note that since in subsonic part of layer an increase in pressure is propagated against the flow, then point of separation, as a rule, is located ahead of the shock.

Since the intensity of shock in direction from wall varies (in accordance with change of speeds), then in the boundary layer there will form a transverse pressure gradient and basic condition, assumed in calculating the layer ( $\frac{\partial p}{\partial y} = 0$ ), in the region of shock is not observed. The disturbance propagating in subsonic part of

---

\*As was shown in Chapter 4, in a nonuniform supersonic flow, the shock is curved. Therefore, the scheme under analysis is only a first approximation.



layer, results in the disturbance of this condition also ahead of the shock.

Hence, we conclude that the mode of flow in a boundary layer must exert a great influence on the location of a shock in a local supersonic zone, and on the structure and intensity of a shock. This influence is explained by difference in velocity profile of laminar and turbulent layers. One should, however, consider that distribution of speeds in boundary layer depends not only on the mode of flow, but also on character of change of speed of external flow, and consequently, on curvature of streamlined surface.

Experimental investigations confirm the generation of structurally different shocks in laminar and turbulent boundary layers (Fig. 5-35).

In a laminar layer, local shocks have, as a rule, a  $\lambda$ -shaped form; such a shock consists of an oblique curved shock, merging with a more powerful and more extensive shock of small curvature, enclosing the supersonic zone. The occurrence of a curved shock can be explained as follows. The increase in pressure, by being propagated to the subsonic parts of layer, causes a marked increase in its thickness before the shock. The lines of flow in the boundary layer are deflected from surface of body; as a result, there appears a system of weak waves of compression, which also will form an oblique shock. With an increase in Re number (at  $M_1 = \text{const}$ ) on basis of degree of equalizing field of speeds in boundary layer, the curvature of the lines of flow before shock decreases and in a developed turbulent velocity profile the first shock disappears; there remains one, but a more powerful shock of small curvature.

The separation of flow in a local supersonic zone does not occur in all cases. Sometimes depending upon distribution of speed in external flow, the separation has a local character and at a certain distance behind the shocks there is restored a normal flow around the surface by the subsonic flow. In the diffuser flow after the shocks the separation usually develops and proceeds to the root region after the body.

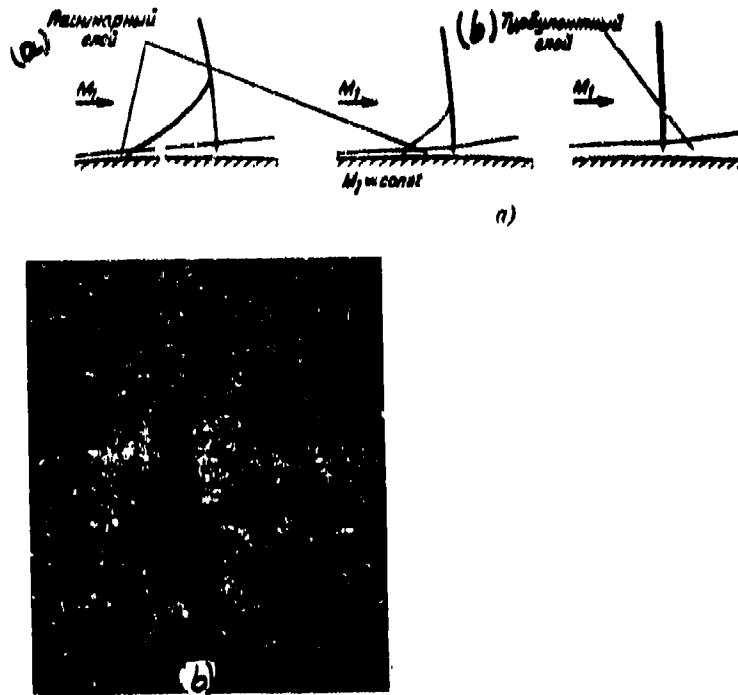


Fig. 5-35. Diagrams of shocks (a) and spectrum of flow (b) in a local supersonic zone in laminar and turbulent modes of a boundary layer.  
KEY: (a) Laminar layer; (b) Turbulent layer

In Fig. 5-36 there is presented a diagram showing the formation of separation in a supersonic region. Point of transition from a laminar layer to turbulent (point T), as a rule, is located close to the point of separation s.

We now turn to a brief consideration of the diagram of interaction between boundary layer during supersonic speeds and waves of rarefaction and shock waves. Since in a real supersonic flow there always will form shock waves and waves of rarefaction, then one of important problems in the theory of boundary layer at  $M_\infty > 1$  is the study of interaction of shocks and waves with the boundary layer. Experimental data make it possible to conclude that conditions of interaction of shock with boundary layer can be different depending upon intensity of shock, the distribution of speeds of external flow and mode of flow in layer.

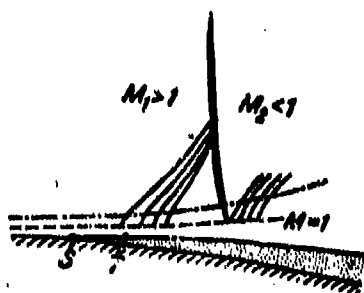


Fig. 5-36. Schematic diagram of separation of boundary layer before shock wave.

Diagrams illustrating principles of the interaction of shocks and waves of rarefaction with boundary layer are shown in Fig. 5-37. With a low intensity of shock (Fig. 5-37,a) before it close to point of its fall, there occurs a "swelling" of the layer.

As a result, before the shock there will form a system of weak waves of compression, creating the reflected shock CD.

The flow around the thickened subsonic part of layer is accompanied by the formation of a weak wave of rarefaction and a second reflected shock FE. With a significant intensity of the lowering shock (Fig. 5-37,b) the increase of pressures before shock near point of lowering may result in a separation of the flow.

In the fall of a wave of rarefaction, to the wall, the thickness of the boundary layer before the wave may diminish.

Thus, we see that actual diagram of the reflection of shocks and waves of rarefaction from a wall, by a streamlined viscous fluid, differs considerably from the diagrams, considered in Chapters 3 and 4, for an ideal fluid. The main distinction consists in the fact that the shocks (waves of rarefaction) through subsonic part of layer, change the field of flow before point of fall, and the simultaneously deformed boundary layer creates new wave formations. However, main property of a rigid wall, reflecting the shock (waves) with the same sign, is maintained also in a viscous flow.

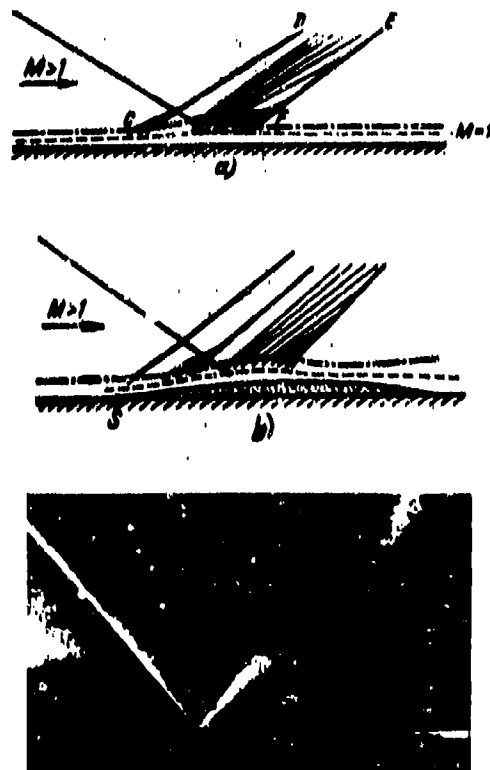


Fig. 5-37. Diagrams illustrating interaction of shocks with boundary layer at supersonic speeds.

### 5-13. Resistance of Bodies at Subsonic and Supersonic Speeds

Pressure and tangential frictional forces act on streamlined body flowed around by a gas. The resultant of these forces is the total aerodynamic force. In studying a two-dimensional flow around conventionally the aerodynamic force is represented by two components:  $P_x$  and  $P_y$  (Fig. 5-38). As is known\*, the component  $P_x$ , whose direction coincides with direction of speed of incident flow is called the force of drag, and the component  $P_y$ , normal to vector of speed of incident flow arbitrarily is called the lifting force or the Zhukovskiy force.

In bearing in mind origin of force  $P_x$ , drag is subdivided into frictional resistance and resistance of pressure. Such a division, in spite of a certain

\*See Chapters 3 and 5.

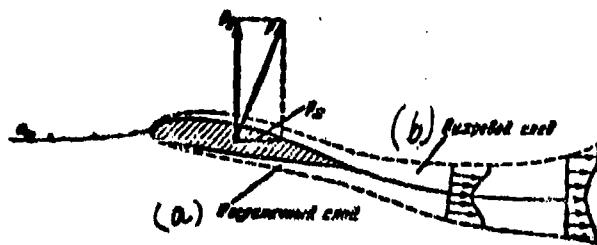


Fig. 5-38. Forces, acting on streamlined body.  
KEY: (a) Boundary layer; (b) Vortex trace

conventionality, is practically very convenient in calculating the resistance.

A body, placed in a flow, creates a disturbance, as a result of which in the region, adjacent to body parameters of the flow vary. The distribution of the pressures along the surface of the body depends on its shape and orientation in the flow and also on the speed of the undisturbed flow. The distribution of frictional forces along the body surface also depends on these factors.

The distribution of pressures along surface of body is characterized by the pressure coefficient. We now consider the distribution of pressures along wing profiles of different shape at different small angles of attack (Fig. 5-39) for low speeds.\* On upper and lower surfaces near top of profile there occurs an intense acceleration of flow with a corresponding lowering of pressure. These sectors of the profile are the nozzle sectors. The lowering of pressure on upper surface of profile occurs more intensively than on the lower. Behind points of minimum on lower and upper surfaces flow is decelerated. This region of flow along wing is the diffuser sector. We note that the diffuser sector on upper surface is characterized by higher values of the pressure gradient. On trailing edge of profile where there

\*Usually the distribution of pressures is conventionally constructed on basis of the profile chord in which the negative values of pressure coefficient (rarefaction) are plotted upwards, and the positive--downwards.

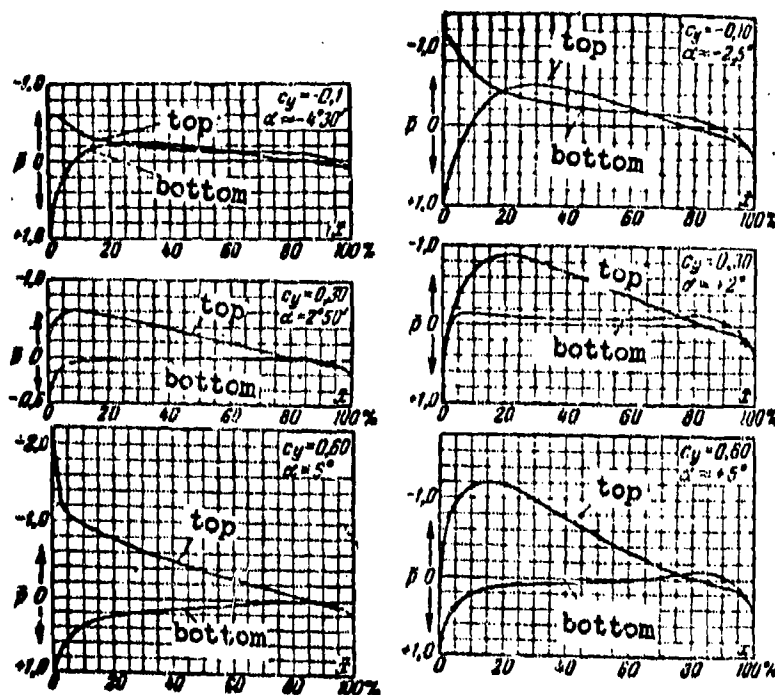


Fig. 5-39. Distribution of pressures along two profiles of varying thickness at different angles of attack for low subsonic speeds.  $\alpha$ —angle of attack;  $c_y$ —coefficient of lifting force.

occurs a merging of the flows, streaming off from upper and lower surfaces of profile, total pressure is not restored, since in boundary layer irreversible losses take place (Fig. 5-38).

At angle of incidence the picture of pressures in the profile varies considerably. Significant diffuser sectors appear on lower surface along that tip.

As we have seen, during descent from trailing edge of profile there will be formed a vortex wake, saturated with vortices, generating in the boundary layer. The structure of a vortex wake varies with distance from the profile. Vortices, generating in the boundary layer, are developed in the separation from profile and then at a significant distance after the body die out as a result of the interaction with external flow. At the same time the energy of vortices will be transformed into heat. Vortex formation results in a lowering of pressure in the region of trailing edge and beyond the profile in trace.

With a known distribution of pressure along contour of wing there can be

found the projection of forces of pressure onto the sense of a vector of speed

$c_{\infty}$ .

It is readily seen that

$$P'_x = \int_i P_i \cos(x_i, n) ds,$$

where  $ds$  is an element of profile surface.

The force  $P'_x$ , caused by difference of pressures at points of streamlined body and directed against its motion, is the resistance force of the pressures. In addition to the force  $P'_x$  the resultant of tangential forces of friction  $P''_x$  acts on the profile.

Thus, the total drag of body in a plane flow is sum of resistance of pressure and resistance of friction:

$$P_x = P'_x + P''_x.$$

It must be especially emphasized that the resistance of pressure and resistance of friction have one and the same cause viz.--the viscosity of the fluid. The profile drag is defined as the resistance of a cylindrical wing during its continuous flow around by an infinite two-dimensional flow.

For evaluating the force of interaction between the flow and streamlined body there are introduced dimensionless coefficients of forces, which are called aerodynamic coefficients.

Thus, resistance of body is characterized by the drag coefficient

$$c_x = \frac{2P_x}{\rho_{\infty} c_{\infty}^2 F} = \frac{2P_x}{\kappa M_{\infty}^2 \rho_{\infty} F},$$

where  $F$  is the characteristic area\* of the body;

$\rho_{\infty}$  is the static pressure of undisturbed flow.

The coefficient of the lifting force by analogy is the magnitude

$$c_y = \frac{2P_y}{\rho_{\infty} c_{\infty}^2 F} = \frac{2P_y}{\kappa M_{\infty}^2 \rho_{\infty} F}.$$

---

\*In formulas for  $c_x$  and  $c_y$  of wing profiles there is introduced the wing area, equal to the product of chord of profile and the length of wing.

As has already been indicated, the forces, acting on streamlined body, and consequently, and aerodynamic coefficients  $c_x$  and  $c_y$  depend on the shape of the body, the mode of its flow around and orientation of body in the flow. During low speeds, when compressibility is virtually inevident, the shape of the body, angle of incidence and Re number exert the chief influences on the drag coefficient. The existence of such dependence, corroborated by numerous experiments ensues from the physical nature of resistance of pressure and resistance of friction.

Actually, depending upon shape of body the character of the disturbance, created by body in the flow varies. In this connection, the distribution of parameters of the flow along the contour of the body and, consequently, both components of the force  $P_x$  vary. The resistance of friction varies in connection with change of structure of boundary layer and mode of flow in it.

An analogous reconstruction of spectrum of flow around occurs with a change of orientation of body in the flow. In this case in exactly the same way—the total resistance of the body and its component vary. Hence, also it follows that in a complete equilibrium of resistances of body, the specific effect of the resistance of pressure and resistance of friction may vary depending upon the indicated parameters. Thus, profiles of a well streamlined shape at low speeds have a comparatively small profile drag, in which resistance of friction is fundamental. With an increase of the relative thickness of profile and angle of attack, the role of resistance of pressure increases. The resistance of friction at first varies little, but later diminishes. Just like the total force of drag so can the coefficient of resistance be presented in the form of two components:

$$c_x = c_{xA} + c_{xTP},$$

where  $c_{xA}$  is the drag coefficient of pressure;

$c_{xTP}$  is the drag coefficient of friction.

With an increase of thickness of profile the positive pressure gradients in the root portion of profile increase and point of separation is displaced against



flow. For this reason resistance of pressure increases. Since in this connection the magnitude of surface of friction is reduced, then  $c_{xrp}$  diminishes.

With an increase in  $Re_\infty$  number for a well streamlined profile,  $c_{xa}$  insignificantly diminishes, since the thickness of the boundary layer and zone of separation decrease. At the same time, with an increase of  $Re_\infty$  also the coefficient of friction decreases (See preceding paragraphs). In evaluating the influence of the shape of body and  $Re_\infty$  number sometimes it must be assumed that boundary layer exerts an influence on the external flow: The lines of flow in the external flow are displaced by the boundary layer. A detailed investigation make it possible to establish that distribution of pressures along contour of profile in the flow of a viscous fluid coincides with distribution of pressures along contour around a certain fictitious body (obtained from profile by means of thickening it by the magnitude of thickness of displacement  $\delta^*$ ), flowed around by an ideal fluid. It follows from this that the structure of boundary layer is determined by the external flow, but on the other hand, boundary layer can exert an opposite effect on the external flow. We note the opposite effect of the layer is found to be especially great along the trailing edge of profile, where the thickness of layer has a maximum value. The thickness and distribution of speeds in boundary layer along trailing edge to a significant degree exert an influence on the profile drag.

The  $Re_\infty$  number exerts an influence on the separation of the flow, which may manifest itself with large angles of attack, when positive pressure gradients in diffuser regions attain large values. An increase in the  $Re_\infty$  number, which results in the turbulization of the layer, may sharply decrease the coefficient of profile resistance at a large angle of attack, since the separation is displaced towards trailing edge of profile and the resistance of pressure lowers. An increase in  $Re_\infty$  number during a mixed continuous flow around displaces the region of transition against flow and may result in an increase in the frictional resistance.

At large  $M_\infty$  values of the incident flow, compressibility exerts an influence

on profile resistance. During continuous flow around slender bodies of a well streamlined shape the point of transition is displaced along the flow and the drag coefficient decreases somewhat. With the occurrence of a separation along contour of body an increase in  $M_\infty$  displaces the point of separation against the flow, by which the streamlining of body deteriorates. It should be noted that, besides this, with an increase of  $M_\infty$  the intensity of the vortex motion in the wake of the body increases.

A marked increase of drag coefficient is detected at transonic speeds. In this case, drag coefficient as a function of  $M$  number sharply increases and depending on the shape of body can by several times exceed the value of  $c_x$  at  $M_\infty < M_*$ . Previously it was shown that shocks frequently result in a separation of the flow which causes even a sharper increase in the resistance.

The character of distribution of pressures about the profile at transonic speeds can be seen in Fig. 5-40,a (zone of supersonic speeds is shaded). Here there are clearly noted the places of location of shocks and increase of pressures in the shocks. In Fig. 5-40,b the curve of coefficients of profile resistance in this zone of speeds for a wing profile is presented.

The above mentioned peculiarity of flow around bodies at transonic speeds characterize specific effect of compressibility. The discussion above shows that an increase of the coefficient of profile resistance at  $M_\infty > M_*$  is explained by an increase in the resistance of pressure. In a well-developed system of shocks on the profile and in separation of flow, the contribution of resistance of friction is small and its change cannot be explained by such a significant increase in  $c_x$ . We note that at  $M_\infty > M_*$  there can occur a sharp decrease in coefficient of lifting force  $c_y$ ; a change in  $c_y$  also is stipulated by the redistribution of pressures along the profile and proceeds usually at larger  $M_\infty$  numbers than those, at which an increase in  $c_x$  is noted.

The manifestation of sonic speeds at points of the profile can be established

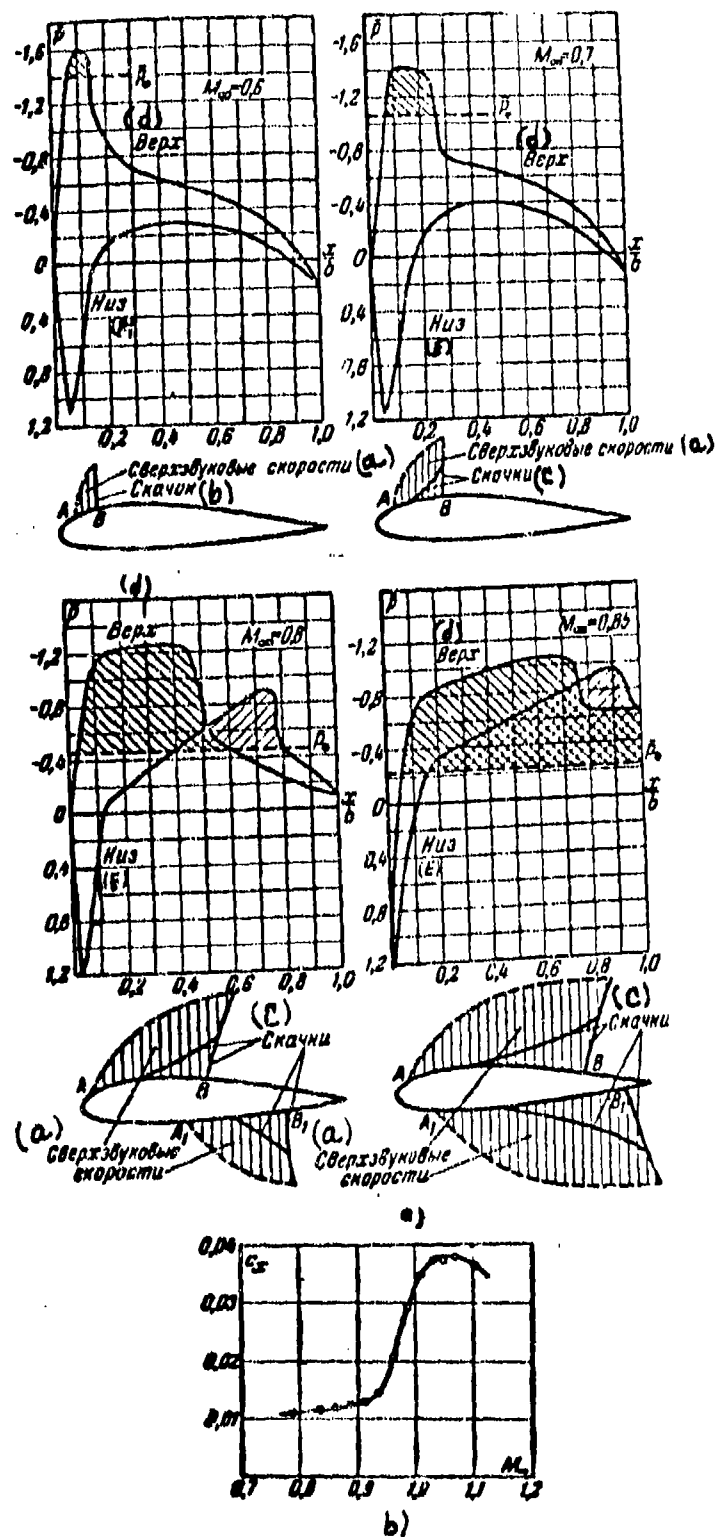


Fig. 5-40. Distribution of pressures along profile at transonic speeds a) and drag coefficients of profile depending upon  $M_\infty$  number b).  
KEY: (a) Supersonic speeds; (b) Shock; (c) Shocks; (d) Upper; (e) Lower.

by the picture of distribution of pressures. The pressure coefficient at these points acquires a value, which is determined by formula (3-17).

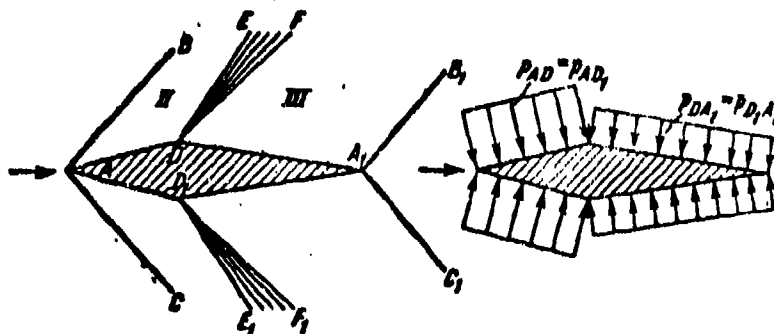
From the preceding it follows that the  $M_c$  value depends not only on shape of the body, but also on the orientation of body in the flow, i.e., on angle of attack.

At supersonic speeds of incident flow resistance of pressure basically is determined by the wave resistance. The location and intensity of shocks and waves of rarefaction depend on the shape of the streamlined body, location of body in flow and the  $M_\infty$  number.

We now consider the flow around a diamond-shaped profile at  $M_\infty > 1$ . (Fig. 5-41). By knowing the geometric dimensions of profile, by using formulas, given in Chapters 3 and 4, it is possible by a calculation method to construct a picture of flow around such a profile: to find the angles and intensity of the forward and tail shocks ABC and  $A_1B_1C_1$  and waves of rarefaction DEF and  $D_1E_1F_1$ . Then, we will determine pressure in regions II and III. By finding projection of resultant force on direction of nonperturbed flow, we are certain of the existence of a resistance force caused by the change of pressures in shocks and waves of rarefaction. We note that in distinction from subsonic speeds this portion of resistance of pressure at transonic and supersonic speeds (wave resistance) is separated into an independent category. Coefficient of profile resistance is presented in such a form:

$$c_x = c_{x, \text{viscous}} + c_{x, \text{wave}}$$

where  $c_{wv}$  is the coefficient of wave resistance of the body.



**Fig. 5-41. Spectrum of flow around a diamond-shaped profile by a flow of supersonic speeds.**

#### 5-14. Resistance of Poorly Streamlined Bodies In a Flow of Gas

Bodies which in any position are flowed around with a separation of flow are called poorly streamlined. For poorly streamlined bodies even at low speeds, a significant part of total resistance is the resistance of pressure.

Specific peculiarities of spectrum of a separation flow around can be traced in the example of a sphere or a cylinder.

In Fig. 5-42 distribution curves of pressures along the sphere contour at  $M=0$  (incompressible fluid) for different Reynolds numbers are presented. In sector from the forward point up to point M, pressure along contour of sphere sharply diminishes (nozzle region), and then after frontal section is observed an increase in pressure (diffuser region). At a certain point S there occurs a separation of the layer; beyond line of separation the pressure varies slightly.

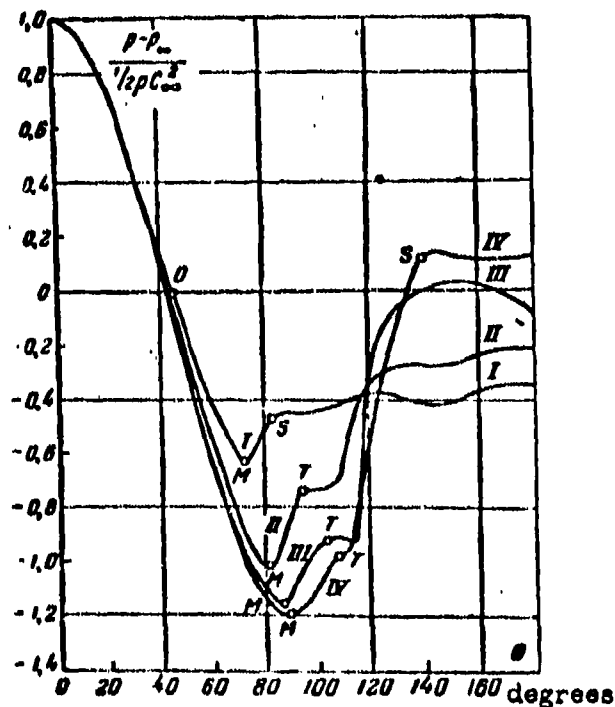


Fig. 5-42. Distribution of pressures along contour of sphere at different Reynolds numbers.  
I-- $Re = 157,200$ ;  $c_x = 0.471$ ; II-- $Re = 251,300$ ;  $c_x = 0.313$ ; III-- $Re = 298,500$ ;  $c_x = 0.151$ ; IV-- $Re = 424,500$ ;  $c_x = 0.143$ .

At considered speeds ( $M_\infty \approx 0$ ) a significant influence on distribution of

pressures is exerted by the Reynolds number. It is possible to note that with an increase of  $Re_\infty$  pressure at point M decreases, but at point S--increases. Characteristic also is the displacement of points M and S along the flow.

Numerous experiments confirm the existence of dependence of drag coefficient of sphere (cylinder) on  $Re_\infty$  number. In Fig. 5-43 corresponding graphs are given. Here, there can be noted five characteristic regions of the variation of  $c_x$ . At  $Re_\infty < 2 \cdot 10^3$  to  $3 \cdot 10^3$   $c_x$  decreases\* with an increase of  $Re_\infty$  and especially intensively in zone of small  $Re_\infty < 100$ . In the sector  $Re_\infty = 2 \cdot 10^3$  to  $2 \cdot 10^4$ , drag coefficient increases somewhat (region III), but then in the interval  $Re_\infty = 2 \cdot 10^4$  to  $2 \cdot 10^5$   $c_x$  is maintained constant (region IV). After this in a narrow range of variations of  $Re_\infty = 2 \cdot 10^5$  to  $4 \cdot 10^5$  ( $4.5 \cdot 10^5$ )  $c_x$  it decreases in the form of a depression (region V). At  $Re_\infty > 4.5 \cdot 10^5$  there is noted a certain increase of  $c_x$ , after which  $c_x$  acquires virtually a constant value.

Experiments show that the transition from one region to another is accompanied by change in spectrum of flow around sphere (Fig. 5-43). At small  $Re_\infty < 100$  the chief role is played by resistance of friction, in which a sharp decrease in  $c_x$  with an increase of the Reynolds number in this region corroborates the lack of a quadratic dependence between resistance force and the speed  $c_\infty$ . The formation of separation in the afterbody causes further gradual drop in  $c_x$  with an increase of  $Re_\infty$ . Region III is characterized by a slight increase of  $c_x$ , which is explained by intensification of vortex motion in afterbody. In this region resistance of friction in boundary layer is small. The resistance of pressure plays major role.

Here, as well as in the region IV, on line of separation, the layer is laminar. As is known, the position of point of separation of laminar layer does not depend on the Reynolds number. Consequently, at a certain value  $Re_\infty \approx 10^5$  to  $2 \cdot 10^4$ , line of separation occupies a fixed position on surface of sphere (cylinder) and a further

---

\*Upper limit  $Re < 3 \cdot 10^3$  corresponds to a sphere, and the lower  $Re < 2 \cdot 10^3$  to a cylinder.

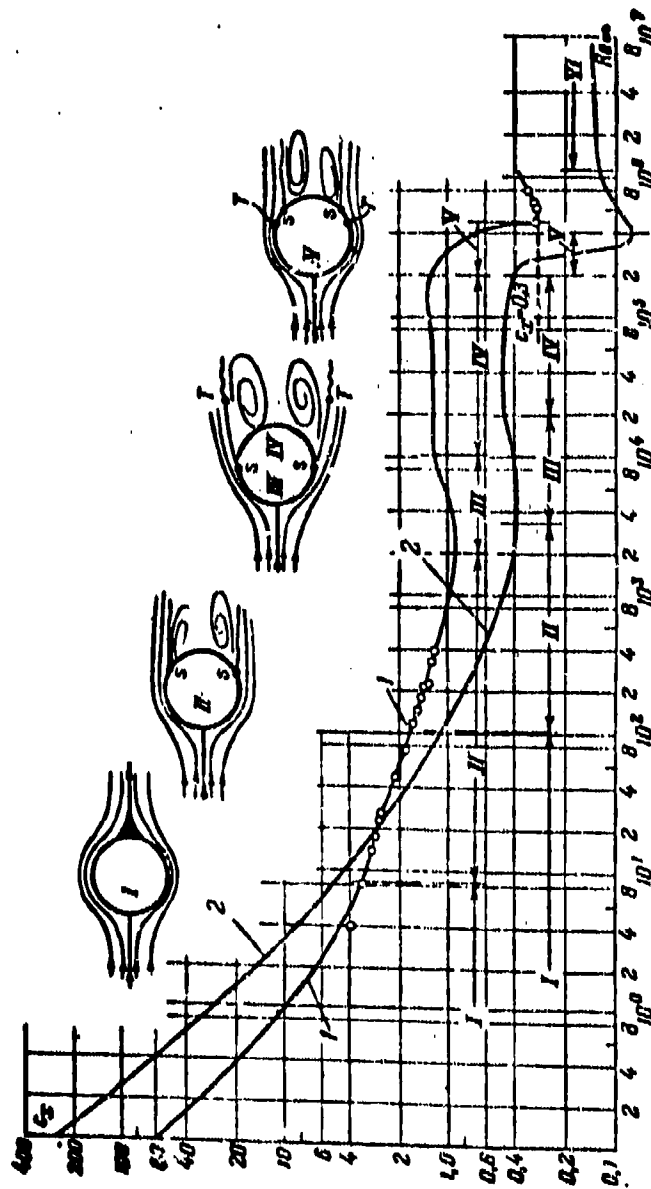


Fig. 5-43. Diagrams of flow around and drag coefficients of sphere and cylinder depending on the Reynolds number.  
1—for cylinder; 2—for sphere.

increase in  $Re_\infty$  does not result in a change in position of the line S.

Region IV, the corresponding constant value of  $c_x$  is called the region of auto-modelling on basis of Reynolds number. However, also in this interval of variations of  $Re_\infty$  there occurs a reconstruction of spectrum of flow around sphere. The laminar layer separating at point S is made turbulent at a certain point T on the boundary of zone of separation. With an increase in  $Re_\infty$  number line of transition T is displaced towards line of separation S, since in this connection the turbulence in afterbody vortex region is increased.

In attaining a certain critical Reynolds number  $Re_{cr} \approx 3 \cdot 10^5$  to  $4 \cdot 10^5$ , point of transition coincides with point of separation. Consequently, at point of separation the layer is turbulent, and possesses great resistivity to separation.

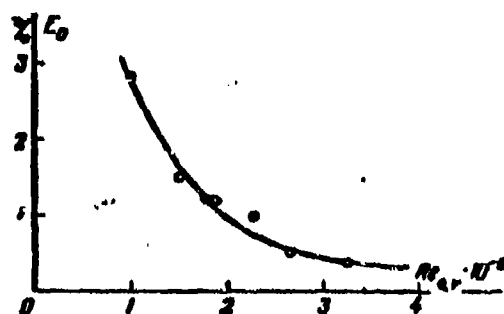


Fig. 5-44. Change of critical Reynolds number  $Re_{cr}$  depending upon degree of turbulence  $E_0$  for  $M \approx 0$ .

As a result of change of mode in motion in layer near separation, the point S abruptly is displaced along flow and the flow around sphere is improved critically: the drag coefficient decreases by 2 to 4 times (region V in Fig. 5-43). The decrease in  $c_x$  occurs owing to lowering of resistance of pressure, since resistance of friction in turbulent layer is greater than in laminar. This phenomenon is called the critical region of Reynolds number of poorly streamlined bodies.

The position of line of transition T at  $Re_\infty < Re_{cr}$  depends on degree of turbulence of incident flow. Therefore, also critical  $Re_{cr}$  number varies considerably



depending upon  $E_0$ . The corresponding experimental curve is shown in Fig. 5-44. With an increase of turbulence to  $E_0 \approx 3\%$  critical number  $Re_{cr}$  decreases almost 3.5 times.

Curve in Fig. 5-44 can be used for determining degree of turbulence of incident flow on basis of critical  $Re_{cr}$  number. In this respect, the value  $Re_{cr}$  corresponding to drag coefficient of sphere  $c_x = 0.3$  (Fig. 5-43) is considered as the critical  $Re_{cr}$  number.

One should note that at  $Re > Re_{cr}$  (region VI in Fig. 5-43) drag coefficient at first increases somewhat and later virtually is independent of  $Re$ : this zone is second region of auto-modeling, corresponding to the fixed position of point of separation of turbulent layer.

Thus, on surface of sphere there are three characteristic points: minimum of pressure (M), separation (S) and transition (T), in which turbulization of layer occurs. Mutual location of points M, S and T exerts a decisive influence on mechanism of flow around and resistance of sphere at low speeds.

A study of influence of compressibility on the position of indicated points makes it possible to evaluate change of spectrum of flow around and resistance of sphere during transition to large  $M_\infty$  numbers.

Experiments show that as the  $M_\infty$  number increases the picture of distribution of pressures along contour of sphere varies (Fig. 5-45). Important is the fact that at  $M_\infty > M_{cr} > 0.3$  with an increase in  $M_\infty$  pressure in afterbody behind sphere lowers.

At  $M_\infty > M_{cr}$  on surface of sphere there will form annular zones of supersonic speeds, which are enclosed by shock waves. The corresponding spectra of flow around are shown in Fig. 5-46. Influence of  $Re_\infty$  number on these modes lowers, however, it remains significant. Only at  $M_\infty > 0.8$ , influence of  $Re_\infty$  virtually is not observed. In the  $M_\infty > M_{cr}$  the pressure in afterbody continues to lower and will attain minimum values at  $1.1 > M_\infty > 0.8$  (Fig. 5-45).

For high subsonic speeds, characteristic are the sharp reduction of diffuser region and the decrease pressure gradients in it. At these speeds, the separation occurs in the zone of location of local shock waves (Fig. 5-46) independently of the mode of flow in boundary layer—laminar or turbulent.

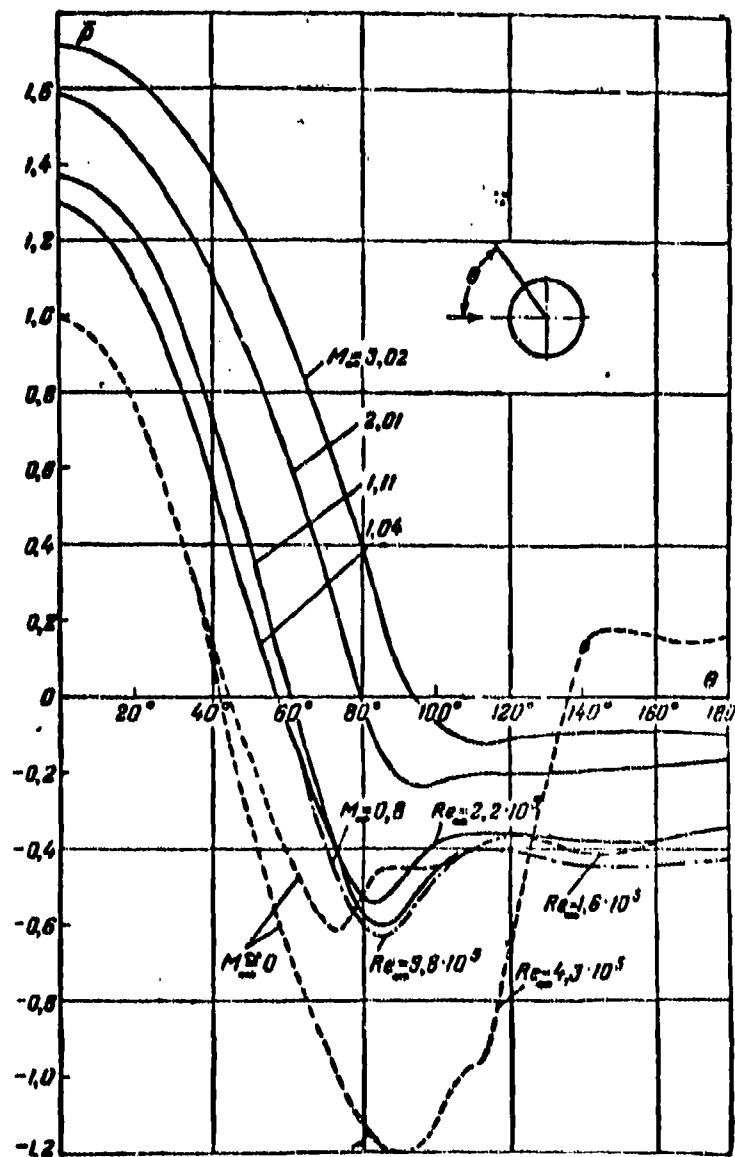


Fig. 5-45. Distribution of pressures along contour of sphere at different  $M_\infty$  numbers.

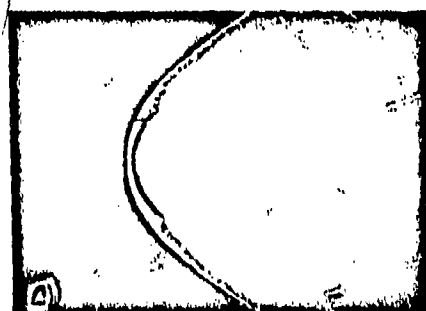
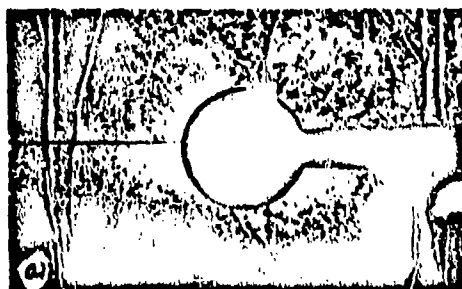


Fig. 5-46. Spectra of flow around a sphere at transonic and supersonic speeds.  
 a--  $M_\infty = 1.1$ ; b--  $M_\infty = 1.8$ ; c--  $M_\infty = 3.0$ .

At high supersonic speeds ( $M_\infty > 1.5$ ) pressure curves have a different character: the pressure at minimum points continues to increase and the diffuser sector is displaced along flow. The pressure in afterbody of sphere increases with an increase of speed.

Graphs of the pressures can be used for an approximate determination of characteristic lines of the surface of the sphere. Corresponding curves  $\theta_M$

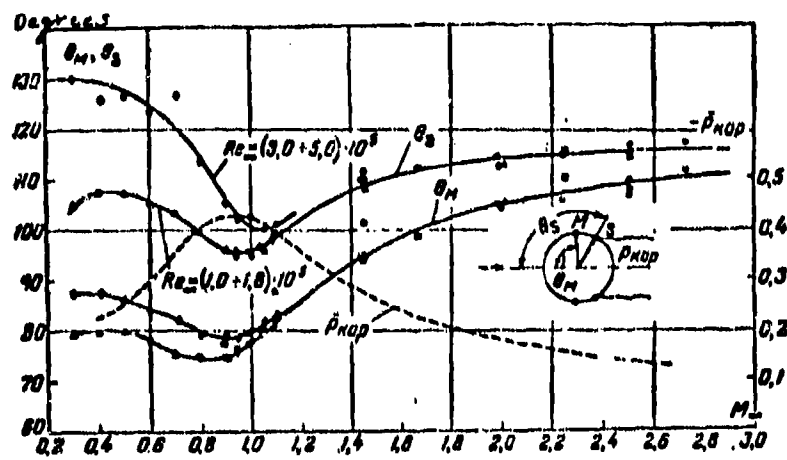


Fig. 5-47. Change of position of lines of pressure minimum and separation depending on  $M_\infty$  number for a sphere. Change of pressure in afterbody of sphere depending on  $M_\infty$  (experiment of author).

and  $\theta_S$  are shown in Fig. 5-47. Here it is possible to see that in the speed range  $M_\infty = 0.3$  to  $1.1$  there takes place a significant dislocation of line of separation, and besides independently of character of flow around sphere at  $M_\infty = 0.2$  the values  $\theta_M$  and  $\theta_S$  decrease, i.e., line of separation is displaced against the flow and flow around the sphere deteriorates.

Consequently, both for  $Re_\infty < Re_{cr}$ , and also for  $Re_\infty > Re_{cr}$ , the influence of compressibility at  $M_\infty < 1$  is found to be qualitatively identical. With an increase in  $M_\infty$ , the flow around a sphere approaches those conditions, which correspond to a separation of a laminar layer. In the region of supersonic speeds, angle of separation  $\theta_S$  increases with an increase of  $M_\infty$  number and the flow around of sphere improves (Fig. 5-47). Intensity of displacement of line of separation lowers at

$M_\infty > 2$ . In such flow modes before sphere there will form a curved shock wave (Fig. 5-46); at points of separation weak conical shocks generate.

Thus, in the subsonic region with an increase of  $M_\infty$  number, line of separation is displaced towards fore critical point and at  $M_\infty = 0.95$  to 1.0 it occupies a position nearest to it, but at supersonic speeds the separation is displaced in direction towards afterbody. Hence, it may be concluded, that at subsonic speeds with an increase of  $M_\infty$  the streamlining of sphere deteriorates and at supersonic speeds—improves.

The discussion above shows that at speeds of  $M_\infty \geq M_*$  the position of lines of separation on sphere depends considerably on mode of flow in boundary layer and, consequently, on  $Re$ . Influence of compressibility here is reflected in the fact that with an increase of  $M_\infty$  critical  $Re_{cr}$  number increases (Fig. 5-47). This means that turbulization of layer at point of separation occurs at large  $Re$  numbers and line of transition  $T$ , approaches line of separation  $S$ , more gradually. In other words, the compressibility delays the transition of a laminar into a turbulent mode of flow.

At  $1 > M_\infty > M_*$  in investigated range of  $Re_\infty$  numbers the critical change of picture of flow around, associated with turbulization of layer, in general, is not detected and beyond dependence of  $Re_\infty$ , streamlining of sphere sharply deteriorates. Hence, it may be concluded, that at transonic speeds shocks result in a separation of the laminar layer approximately in one and the same section.

Influence of number  $M_\infty$  on drag coefficient of sphere  $c_x$  can be evaluated by curves in Fig. 5-48. With an increase  $M_\infty < M_*$ ,  $c_x$  increases, in which in a pre-drag stall flow around ( $Re_\infty < Re_{cr}$ , curve 1) drag coefficients increase less intensively, than in a post-drag stall flow around ( $Re_\infty > Re_{cr}$ , curve 2). At  $M_\infty > M_*$  influence of  $Re_\infty$  on  $c_x$  weakens and for  $M > 0.8$  curves of  $c_x$  for different  $Re_\infty$  virtually coincide.

The total drag coefficient of sphere can be presented in the form:

$$c_x = c_{xT} + c_{x\text{exp}},$$

where  $c_{xr}$  is the coefficient of the head drag;

$c_{x\text{ kop}}$  is the coefficient of afterbody effect.

In Fig. 5-48 in addition there are presented the curves  $c_{x\text{ kop}} = c_x(M_\infty)$ .

A comparison of curves  $c_x$  and  $c_{x\text{ kop}}$  shows that coefficient of the head of sphere

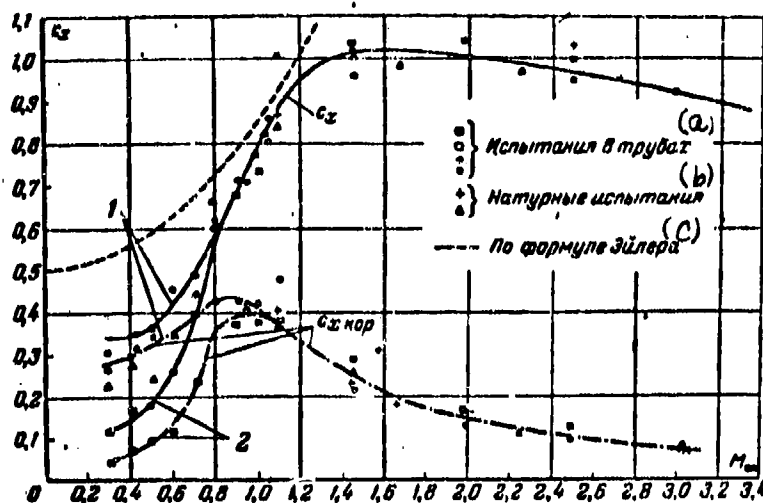


Fig. 5-48. Drag coefficients of sphere depending on  $M_\infty$  number on basis of data of tests in wind tunnel and under field conditions.

KEY: (a) Tests in tubes; (b) Field tests; (c) By Euler formula

$c_{xr} = c_x - c_{x\text{ kop}}$  at subsonic speeds increases insignificantly. Consequently, the "compressibility stall" of sphere resistance in zone of transonic speeds, which is expressed in very sharp increase of  $c_x$  (from 0.15—0.35 to 0.9—0.95) occurs mainly as the result of increase of afterbody resistance.

At supersonic speeds,  $c_x$  continues to increase and will attain a maximum value at  $M_\infty \approx 1.6$ . Maximum [portion] of curve  $c_x$  this zone is very gentle. At  $M_\infty > c_{x\text{ kop}}$  intensively decreases.

In Fig. 5-48 also results of other investigations are given. It is characteristic that at transonic and supersonic speeds all experimental data agree very well.\*

\*In Fig. 5-48, there is plotted also the curve  $c_x$ , constructed by the Euler formula:

$$c_x = 0.5 \left( 1 + \frac{1}{2} M_\infty^2 \right).$$

It is curious to note that the Euler formula, derived about 200 years ago, gives results close to experimental values of  $c_x$  at  $M_\infty < 1$ .

At  $M_\infty > 1$  the resistance of a poorly streamlined body is practically independent of  $Re$ .

#### 5-15. Motion of Gas in Curvilinear Channels.

In the motion of gas in curvilinear channels specific phenomena develop. Actually, let us consider the flow of gas along a channel of constant cross-section, in which the flow makes a  $90^\circ$  turn (Fig. 5-49). Momentum in channel is small in comparison to speed of sound, so that influence of compressibility can be disregarded. In connection with the fact that the particles of gas moved along curvilinear trajectories, the pressure at external (bend) and internal (convex) walls of channel is found to be different and varies differently in direction of motion. Since the particles in the core of flow under action of centrifugal forces are pushed to external wall, then pressure along AB increases in comparison to pressure of incoming flow  $p_1$ , and along  $A_1B_1$ —decreases (Fig. 5-49,a). After the turn the pressure on concave wall lowers, but on convex increases; at a significant distance after the turn the pressures are equalized.

Thus, in sections of curvilinear channel there is established nonuniform distribution of speeds and pressures; here a transverse pressure gradient develops. Particles of fluids, moving in a boundary layer along flat walls, are under the influence of difference in pressure and in possessing small speed in direction of main motion, will overflow towards internal wall, in undergoing a greater deflection, than particles, more distant from the walls. According to conditions of continuity in the core of flow, there should develop compensating flows, directed towards external wall. As a result in the channel there will form a secondary vortex motion, superposed onto main flow. The streamlines of secondary flow are enclosed within cross section of channel (Fig. 5-49,b).

The secondary flow consists of two flows, which near the flat walls are directed towards convex surface, and in center of channel—to concave surface of

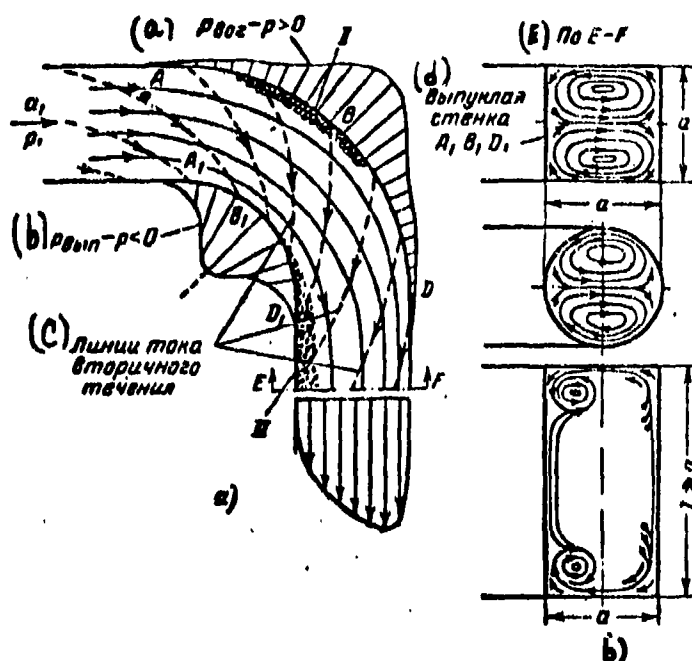


Fig. 5-49. Diagram of flow in curvilinear channels with varying shape of cross section.

KEY: a) P concave -  $p > 0$ ; b) P convex -  $p < 0$ ;  
 c) Streamlines of secondary flow; d) Convex wall  $A_1, B_1, D_1$ ; e) Along E-F

channel. Secondary flows have symmetrically-helical character. The streamlines of secondary flow on flat walls are indicated by dotted line (Fig. 5-49,a).

Along section of concave wall AB and along section of convex wall  $B_1D_1$  is the diffuser flow. Depending upon the shape of curvilinear channel here there can appear separations (zone I and II in Fig. 5-49,a). The separation on concave wall AB can be localized by subsequent nozzle flow in the sector BD. The separation in sector  $B_1D_1$  has a larger extent along the flow.

Structure of secondary flow in curvilinear channel and additional loss of energy caused by it considerably depend on geometric shape of channel and mode of flow (Re and M number).

Experiments show that structure of secondary flows varies with a change of shape of cross-section of channel (Fig. 5-49,b). The greatest differences in the above-considered diagram are detected in channels with a rectilinear shape of cross-section ( $l \gg a$  and  $l \leq a$ ). In the case,  $l \gg a$ , secondary motion of gas along



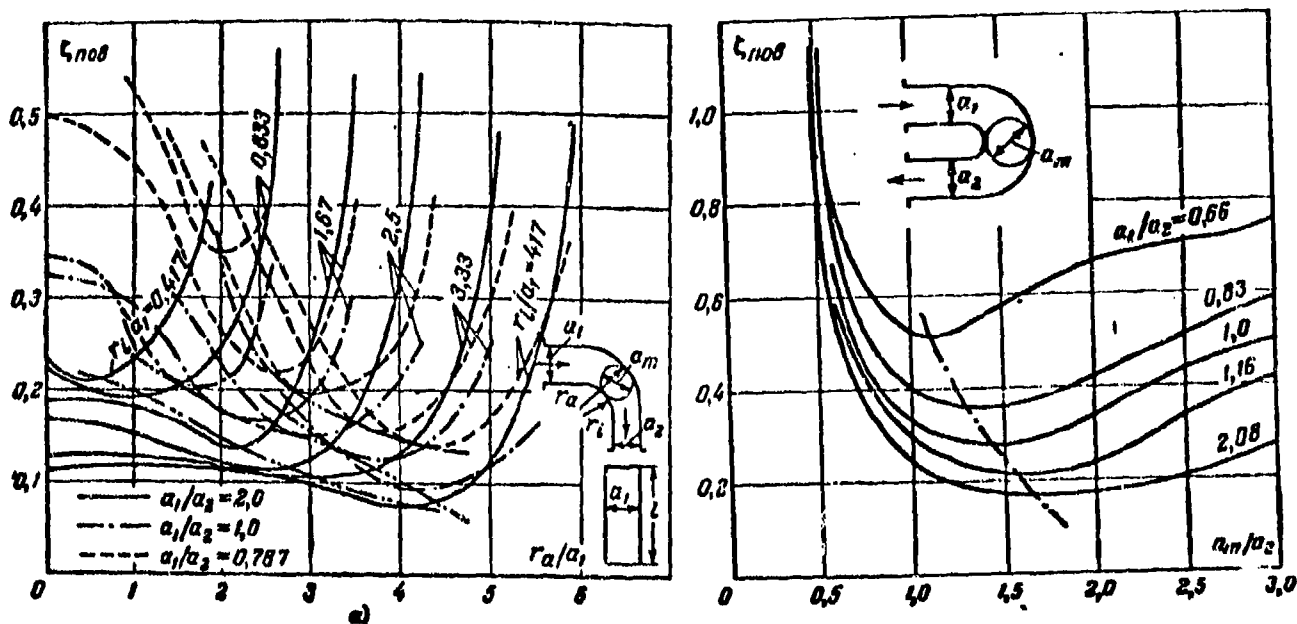


Fig. 5-50. Influence of radius of curvature of concave and convex walls of curvilinear channel with angle of rotation  $90^\circ$  (a) and the influence of ratios of cross-sections of channel with angle of rotation  $180^\circ$  on losses according to Kh. Nippert's data ( $1/a_1=4$ ).

concave and convex walls is hampered, since particles must make a long path, during the period of which friction is reflected. Such an overflowing is found possible only in the boundary layer along flat walls; it begins on concave surface (along flat walls) and continues on flat walls towards convex surface, where boundary layer, participating in peripheral motion, coalesces with boundary layer of main flow and intensively swells. At the same time owing to motion in boundary layer from concave surface to convex in core of flow along flat walls there will form compensating flows, directed to concave wall. These flows jointly with boundary layer, moving along flat walls in opposite direction, will form closed vortex regions, embracing not the entire section of walls, but only a portion of it close to the convex and flat walls. In the channel of rectilinear cross-section under consideration the secondary flow degenerates into a pair of vortices, revolving in opposite directions.

In the formation of the secondary flow a part of kinetic energy of flow is

expanded. The loss of energies, caused by curvature of channel can be considered as the sum: a) of additional losses to friction due to secondary motion; b) of vortex losses in zones of separation; c) losses, caused by vortex compensating flows. The largest portion of losses consists of vortex losses resulting from separation.

In Fig. 5-50,a there are presented Kh. Wippert's data characterizing the influence of certain geometric characteristics of channel on losses. Here coefficient  $\zeta_{\text{nos}}$  is defined as the difference between total energies at entry and at exit, related to the kinetic energy heat at the entry into channel.

As can be seen from Fig. 5-50,a  $\zeta_{\text{nos}}$  considerably depends on internal  $r_1$  and external  $r_2$  radii of curvature and geometric nozzle condition of channel, determined by the relation  $\bar{a} = \frac{a_1}{a_2}$ . If  $\bar{a} > 1$ , then the channel is a nozzle type and if  $\bar{a} < 1$ , then the channel is a diffuser type. With a given ratio of  $\bar{a}$ , the change in  $r_1$  or  $r_2$  results in a change of the ratio  $\bar{a}_m = \frac{a_m}{a_1}$  and, consequently, of the cross-section area along axis of flow. Points of minimum of curves  $\zeta_{\text{nos}}$  correspond to different  $\bar{r}_2 = \frac{r_2}{a_1}$  depending on  $\bar{r}_1 = \frac{r_1}{a_1}$ . Optimum values of  $\bar{r}_1$  are somewhat less than  $\bar{r}_2$ . With a given  $\bar{r}_1$ , an increase in  $\bar{r}_2 > r_{\text{aopt}}$  results in an especially sharp increase of losses. In this case, curvilinear channel acquires an alternately narrowing-expanding shape; speeds of flow at the turn and the losses increase.

Curves in Fig. 5-50,a also reflect influence of parameter  $\bar{a}$ . In diffuser channel ( $\bar{a} < 1$ ) losses are greater than in channels of constant cross-section ( $\bar{a} = 1$ ) and of nozzle ( $\bar{a} > 1$ ) sections.

In the entire range of values of  $\bar{r}_1$  and  $\bar{r}_2$  the envelope of curves  $\zeta_{\text{nos}}(\bar{r}_1, \bar{r}_2)$  lies higher for diffuser channel ( $\bar{a} = 0.787$ ). The channel of constant section ( $\bar{a} = 1$ ) occupies an intermediate position.

An analogous influence of geometric parameter  $\bar{a}$  is detected also for a channel with angle of rotation  $180^\circ$  (Fig. 5-50,b). The minimum of losses in such channels corresponds to values  $\bar{a}_m > 1$ , in which optimum compression in exit part of channel decreases with a transition to diffuser channels ( $\bar{a} < 1$ ).

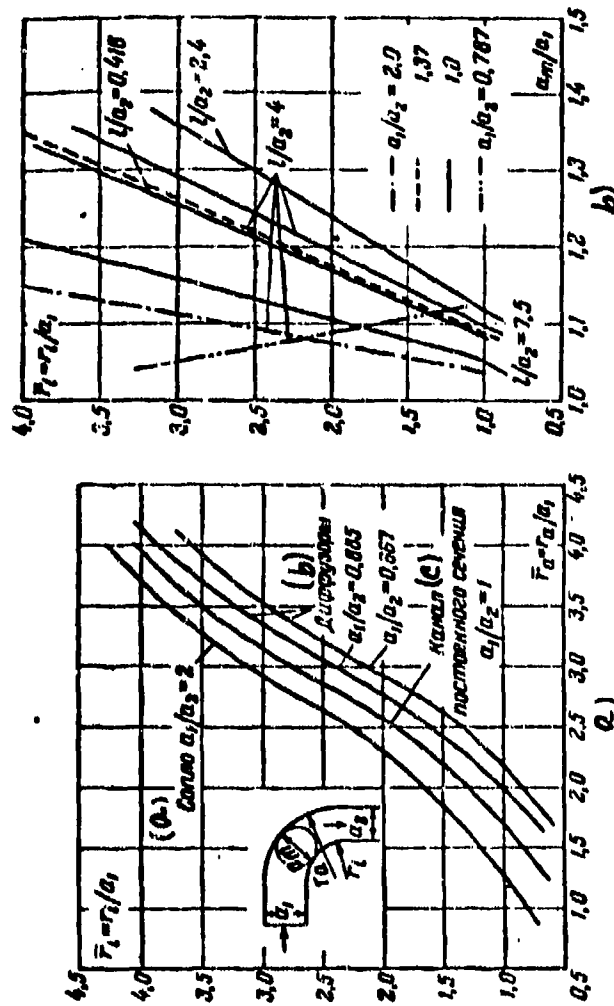


Fig. 5-51. Optimum relationships of geometric parameters of curvilinear channel with angle of rotation 90°, assuring minimum losses from secondary flows, after Kh. Nippert.  
 KEY: (a) Nozzle  $a_1/a_2 = 2$ ; (b)  $a_1/a_2 = 0.885$ ,  $a_1/a_2 = 0.667$ , Diffusers; (c) Channel of constant cross-section  $a_1/a_2 = 1$ .

In Fig. 5-51 there are given values of radii of curvature and relationship of characteristic sections of channel, assuring minimum intensity of secondary flows in a curvilinear channel. From the graphs it follows that in diffuser and slightly nozzleed channels it is expedient to make average cross-section of channel  $a_m$  larger ( $\bar{a}_m > 1$ ), and then to assure a nozzle flow by a corresponding compression ( $\frac{a_m}{a_1} > 1$ ). In this case difference of pressures decreases between concave and convex surfaces in sections, where curvature of channel is a maximum, and, consequently, the intensity of the secondary lowers. Besides, the compression of exit part of channel reduces region of separation on convex wall  $A_1B_1$  (Fig. 5-49,a), and in certain cases also prevents a separation. Experiments of Kh. Nippert showed that depending upon angle of rotation, and radii of curvature of concave and convex walls, the optimum relationships of magnitude  $a_m$  and  $a_1$  vary.

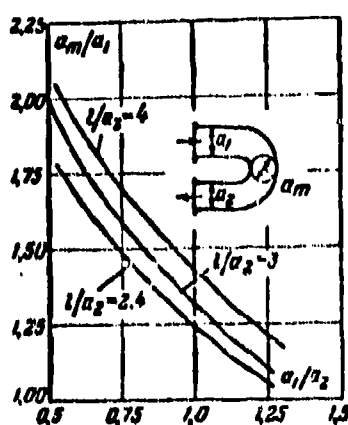


Fig. 5-52. Optimum values of  $\bar{a}_m$  depending on geometric nozzle-state of curved channel.  $\bar{a}_1$  on basis of data of Kh. Nippert. Angle of rotation  $180^\circ$ .

These relationships depend also on geometric nozzle state of channel, i.e., on  $\bar{a}$ . Experiments show that with an increase of radii of curvature of back and concave surface losses from secondary flows decrease. At the same time (Fig. 5-51,a) with increase of radius of curvature,  $\bar{r}_1$  optimum value of  $\bar{a}_m$  increases at a given angle of turn of flow and degree of channel convergence ( $\bar{a}$ ). The dependence of  $\bar{a}_m$  on  $\bar{a}$ , corresponding to minimum losses in

curvilinear channel with angle of rotation  $180^\circ$  is shown in Fig. 5-52.

One must also note the influence of relative height of channel  $\frac{1}{a_2}$  on the optimum value of parameter  $\bar{a}_m$ . As can be seen from Fig. 5-51,b, the relationship  $\bar{a}_m = f(\frac{1}{a_1})$  has a maximum, the position of which is determined by the overall channel construction  $\bar{a}$ .

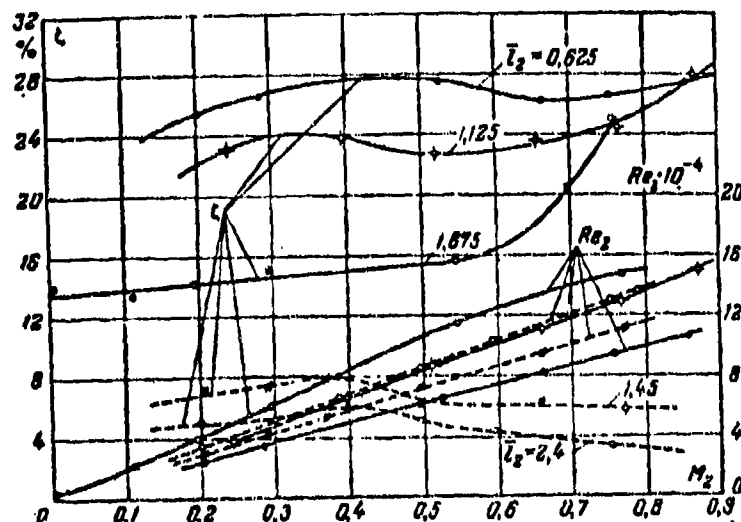


Fig. 5-53. Change of loss factors in curvilinear channels depending on  $M_2$  number at exit (experiments of V. I. Nikitin)<sup>2</sup>

The influence of the two most important mode parameters—the  $Re$  and  $M$  numbers—on the loss and structure of flow in curved channels can be evaluated on the basis of curves in Fig. 5-53. With an increase in  $Re$ , the losses in channel decrease and turbulization of layer near separation results in the displacement of line of separation along flow which also causes a sharp lowering of the losses.

Influence of compressibility at pre-stall speeds is reflected in the fact that intensity of secondary flows lowers. Analysis of distribution curves of pressures (Fig. 5-54) shows that with an increase in  $M$ , transverse pressure gradients in channel decrease, since pressure coefficients increase more intensely on convex surface, than on the concave. At  $M > M_1$ , on concave wall there appear local zones of supersonic speeds and the shocks enclosing them. The separation of flow, caused by shocks, results in an increase of loss factors (Fig. 5-53). At supersonic speeds there is noted a lowering of losses from secondary flows.

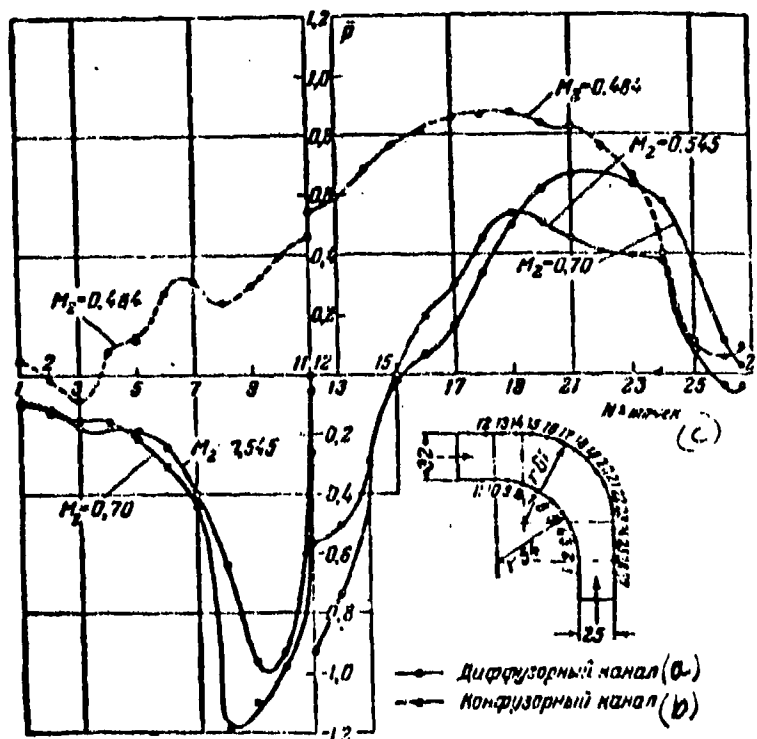


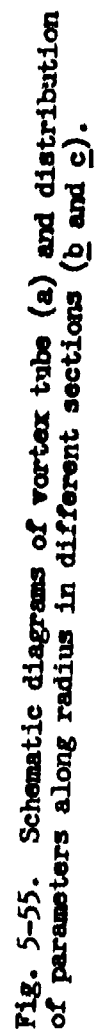
Fig. 5-54 Distribution of pressures along contour of curvilinear channel—nozzle channel,  $l_2=2.4$ ; — diffuser channel  $l_2=1.875$ .  
(a) Diffuser channel (b) Nozzle channel; (c) No. of points.

#### 5-16. Rotating Flows of a Viscous Gas

In Sec. 5-1 it was noted that the enthalpy of stagnation in the flow of a viscous gas with nonuniform distribution of speeds is a variable quantity and the condition  $i_0 = \text{const}$  cannot serve as a characteristic of the flow and as an integral of the equation of energy of adiabatic flow.

Most clearly this effect is detected in rotating flows of gas and, in particular, in a Ranque vortex tube (Fig. 5-55).

Gas is fed into vortex tube by nozzles tangentially under pressure (section OO in Fig. 5-55, a) and will form within tube a rotating flow. From one side, (in section AA) flow leaves through aperture located on axis of tube. On opposite end of tube exit aperture is made in the form of annular slot, located along periphery (Section BB). As the experiment shows the gas, flowing through central



aperture (in section AA), has a significantly lower temperature of stagnation, than on periphery in section BB (Fig. 5-55,b). Thus, for example, on basis of I. Hartnett and B. Ekkert's data the maximum difference of stagnation temperatures corresponds to section I—I and will attain a magnitude  $T_{a_0} - T_0 = 75$  to  $80^\circ \text{C}$ . According to the degree of distance from section OO, profile of stagnation temperatures levels off and in section III, the indicated difference will attain only  $40^\circ \text{C}$ . It is characteristic that stagnation temperature on periphery  $T$  varies along tube less intensely, than temperature on axis of tube, which sharply increases towards section BB. The lowest stagnation temperature on axis corresponds to section I · I. Consequently, in such a tube there occurs temperature separation of gas flow, in which through central aperture strongly cooled gas flows out.

Velocity profiles in different sections show (Fig. 5-55,b) that in tube there occurs an intense rebuilding of flow: speed towards periphery intensely decreases towards section III—III, and in core on axis somewhat increase.

The nonuniform distribution of speeds along radius explains intense dissipation of mechanical energy, internal liberation of heat and nonuniform distribution of stagnation temperature. About the very intense dissipation of energy it is possible to judge on the basis of experimental graphs of the distribution of stagnation pressure and static pressure (Fig. 5-55,c).

An approximate theoretical solution of considered problem can be obtained for simplest case of one-dimensional circular motion of a gas. Let us assume that the field of axial components of speed in tube are uniform. Surfaces of the flow of such rotational motion of gas will be cylindrical: radial components of speed and their derivatives vanish. By ignoring the influence of body forces and by assuming the motion steady, it is possible to use equation of conservation of energy (5-3) in the cylindrical system of coordinates:

$$\frac{d}{dr} \left\{ \mu r \left[ \frac{d}{dr} \left( \frac{t}{Pr} + \frac{c_0^2}{2} \right) - \frac{c_0^2}{r} \right] \right\} = 0. \quad (5-79)$$



Here  $c_\theta$  is the circumferential (tangential) component of speed.

In assuming in addition,  $\mu = \text{const}$ , equation (5-79) can be integrated. The total integral (5-79) for considered case was obtained by L. A. Vulis in such a form:

$$i + \text{Pr} \frac{c_\theta^2}{2} = \text{Pr} \int c_\theta^2 \frac{dr}{r} + \text{const.} \quad (5-80)$$

For obtaining of the sought relationship in finite form it is necessary to know law of variation of  $c_\theta(r)$ . It is expedient to consider two limiting cases: a) in assumption of circulatory (quasipotential) flow, distribution of speeds in which is subject to the condition  $c_\theta r = \text{const}$ , (Sec. 1-2), and b) for a linear distribution of speeds  $c_{\theta,r} = \text{const}$ , corresponding to vortex core (quasi solid flow) (Sec. 1-2).

In the first case after substituting in (5-80)

$$c_\theta^2 = \frac{c_{\theta 0}^2}{r^2},$$

where  $c_{\theta 0}$  is the tangential component of speed in peripheral section, outside the boundary layer;

$r_0$  — radius of tube,

there can be obtained:

$$i_0 = i + \frac{c_\theta^2}{2} = (1 - 2\text{Pr}) \frac{c_\theta^2}{2r^2} + \text{const.} \quad (5-81)$$

where  $\bar{r} = \frac{r}{r_0}$  is the relative radius;

$i_0$  is the current value of enthalpy of stagnation.

The constant on the right hand side is found by writing out (5-81) for section  $r = r_0$ ,  $\bar{r} = 1$ . Then

$$\text{const} = i_{00} - (1 - 2\text{Pr}) \frac{c_\theta^2}{2}.$$

Here  $i_{00}$  is the enthalpy of stagnation in section  $\bar{r} = 1$  (in peripheral section of tube).

After substituting the value of constant in (5-81) finally we find

$$\frac{i_0}{i_{00}} = 1 - (1 - 2\text{Pr}) \left(1 - \frac{1}{\bar{r}^2}\right) \frac{c_\theta^2}{2i_{00}}. \quad (5-82)$$

Since  $c_{\text{max}} = \sqrt{2i_{00}}$  is the maximum speed in peripheral section, then

$$\frac{c_\theta^2}{2i_{00}} = \frac{c_\theta^2 \cos^2 \alpha_0}{c^2} = \bar{c}_0^2 \cos^2 \alpha_0.$$

where  $\alpha_0$  is the angle between vector of speed  $c_0$  and plane of rotation of gas.

Consequently,

$$\frac{i_0}{i_{\infty}} = 1 - (1 - 2Pr) \left(1 - \frac{1}{r^2}\right) \frac{c_0^2}{2} \cos^2 \alpha_0. \quad (5-82a)$$

From equation (5-82a) it follows that under condition  $c_v = \text{const}$ , enthalpy of stagnation increases with approach to walls of tube, if the number  $Pr > 0.5$ .

At  $Pr = 0.5$  enthalpy of stagnation is kept constant along radius, and at  $Pr < 0.5$  increases towards axis of pipe.

For a coil of flow on basis of law  $\frac{c_0}{r} = \text{const}$ , from (5-80) it is simple to obtain following formula:

$$\frac{i_0}{i_{\infty}} = 1 - (1 - \bar{r}^2) \frac{c_0^2}{2i_{\infty}} = 1 - (1 - \bar{r}^2) \frac{c_0^2}{2} \cos^2 \alpha_0. \quad (5-83)$$

In this case without the dependence on value of Prandtl number, enthalpy of stagnation decreases towards axis of tube. It is obvious that if for two different laws of the distribution of speeds along the radius, enthalpy of stagnation decreases towards axis of tube, then also for any intermediate law there will take place an analogous change  $i_0^*$ .

It is of interest to evaluate change of enthalpy of stagnation along radius in fractions of kinetic energy  $\frac{c_0^2}{2}$ .

We designate:

$$\Delta i_0 = \frac{2(i_{\infty} - i_0)}{c_0^2} = \frac{i_{\infty} - i_0}{i_{\infty} - i_{10}}$$

where  $i_{10}$  is the enthalpy of a moving gas in section  $r = r_0$ .

By using formula (5-82a) and (5-83), we obtain for the two different laws on distribution of speeds:

$$\begin{aligned} \Delta i_0 &= (1 - 2Pr) \left(1 - \frac{1}{r^2}\right) \cos^2 \alpha_0; \\ \Delta i_0 &= (1 - \bar{r}^2) \cos^2 \alpha_0. \end{aligned}$$

L. A. Vulis considered the more general case of distribution of speeds, corresponding to the equation

$$c_0 = c_{00} \left(\bar{r} + \frac{1}{r}\right).$$

Here integral (5-80) after usual transformations, acquires the form:

$$\frac{i_0}{i_{\infty}} = 1 + Pr \left[ \left(\frac{1}{r^2} - \bar{r}^2\right) + 2 \left(2 \ln \frac{1}{r} - 1\right) \right] \frac{c_0^2}{2} \cos^2 \alpha_0. \quad (5-84)$$

\*Formula (5-82a) at point  $r=0$  gives  $\frac{i_0}{i_{\infty}} = -\infty$ . This result is readily explained, if we remember that on the axis of circulatory flow the speed assumes an infinite value ( $c_v = \text{const}$ ). Here, there is located the point vortex, distribution of speeds in which is linear.

It follows from this that with such circular motion at  $Pr > 0$  enthalpy of stagnation varies along the radius.

For a plane-parallel flow with nonuniform distribution of speeds, enthalpy of stagnation is determined by formula (5-2).

Distribution of static temperature across a section of a rotational flow of gas is established by means of equation of energy (5-80). In considering particular case of a coil on basis of laws  $c_p = \text{const}$  and  $\frac{c_0}{r} = \text{const}$  and by remembering that

$$i_0 = i + \frac{c_0^2}{2},$$

from formulas (5-82a) and (5-83) we find:

$$\frac{i}{i_0} \approx \frac{T}{T_0} = 1 - \left[ 1 + 2 \left( \frac{1}{Pr} - 1 \right) Pr \right] \xi_0^2 \cos^2 \alpha, \quad (5-85)$$

for  $c_p = \text{const}$

$$\text{and} \quad \frac{i}{i_0} \approx \frac{T}{T_0} = 1 - (1 - Pr)^2 \xi_0^2 \cos^2 \alpha, \quad (5-86)$$

for  $\frac{c_0}{r} = \text{const}$ .

The change in static pressure along radius can be found, by using equations of the motion in cylindrical coordinates. By taking into account main assumptions (radial components of speeds and longitudinal pressure gradients are small, field of axial speeds is uniform) first equation of system (1-17) acquires following form:

$$\frac{1}{\rho} \frac{dp}{dr} = \frac{c_0^2}{r}. \quad (5-87)$$

Meaning of equation (5-87) consists of the circumstance that it expresses condition of radial equilibrium of a gas particle, realizing a rotational motion.

In considering that

$$\rho = \frac{p}{gRT} = \frac{kp}{(k-1)i},$$

we present (5-87) in a new form:

$$\frac{dp}{p} = \frac{k}{k-1} \frac{c_0^2}{i} \frac{dr}{r}. \quad (5-88)$$

By substituting here  $i$  from formulas (5-85) and (5-86), after integration there can be obtained the approximate relationships  $p(r)$ .

The above-obtained formulas of the variation of parameters across a section of vortex tube can be used, if the speed on periphery of tube  $c_0$  is known. For

calculating the flow in different sections along length of tube it is necessary to locate by experimental relationships  $c_a(x)$  and  $c_s(x)$  ( $x$  is distance along axis of tube).

In accordance with a change in  $c_a$  along length of pipe\* also the distribution all parameters along the radius varies. In certain sections there occurs an equalizing field of static pressures and temperatures and temperatures of stagnation in which these sections ( $p = \text{const}$ ;  $T = \text{const}$  and  $T_s = \text{const}$ ) do not coincide.

M. G. Dubinskiy theoretically proved that in section with constant static temperature along radius there will be attained a maximum of entropy of a rotating flow of gas. Consequently, twisted flow in a vortex tube tends to an equilibrium state, which also will be attained in the section with  $T = \text{const}$ .

The equalizing of flow in vortex tube is illustrated by graphs in Fig. 5-55.

Thus, in a vortex tube there is detected the effect of temperature separation of the gas, which can be used for cooling of different bodies and, in particular, in refrigerating installations of transient operation et cetera. At the same time this effect deserves further detailed theoretical and experimental study, since it is developed in all cases, when a rotation of the gas (step turbomachine, vortex pump et al. develops).

It must be emphasized that a nonuniform distribution of stagnation temperatures in an adiabatic flow of viscous gas, associated with nonuniform distribution of speeds, is detected also during an external flow around bodies (in boundary layer and wake). In all cases, when the liberated frictional heat\*\* is not equal to quantity of heat, diverted by thermal conductivity there takes place a nonuniform

---

\*We recall that the entire calculation is made without a calculation of the boundary layer; the speed  $c_a$  is taken at the outer boundary of the layer.

\*\*The liberation of frictional heat occurs only in those regions of flow where a nonuniform distribution of the speeds associated with the action of viscosity has been established.

distribution of the total energy.

Of significant interest is the motion of a twisted flow\* in cylindrical annular tubes. In this case original equation of energy (5-79) must be integrated for the annular revolving flow.

---

\* Such a problem occurs in the investigation of a twisted flow in a turbo-machine stage (turbine or compressor).

## CHAPTER 6

### OUTFLOW OF GAS FROM NARROWING NOZZLES AND APERTURES. THE LAVAL NOZZLE.

#### 6-1. Narrowing Nozzles.

Narrowing nozzles are widely used for creating flows of subsonic and transonic speeds. The hydraulic design of such nozzles is very simple and reduces to determining the dimensions of exit section on basis of a given flow of gas and given outflow velocity. In the calculation it is assumed that the flow of gas in the nozzle is adiabatic, since for the brief period of time of the passage of gas particles through a nozzle, a heat exchange with environment virtually is not established. Consequently, for calculating a nozzle there may be used equations of adiabatic flow. If we disregard the effect of friction, then the flow in nozzle can be considered isentropic. As experience shows, frictional losses in short nozzles are small.

After designating, as previously, parameters of total stagnation  $p_0$ ,  $T_0$ , and  $\rho_0$  (in considered case—these are parameters of gas in a reservoir), and parameters of medium after nozzle  $p_a$ ,  $T_a$ , and  $\rho_a$ , we can determine the speed in exit section F of nozzle by equation (2-10):

$$\begin{aligned} c &= \sqrt{\frac{2k}{k-1} \left( \frac{p_0}{\rho_0} - \frac{p_a}{\rho_a} \right)} = \sqrt{\frac{2k}{k-1} \bar{R} T_0 (1 - \epsilon_a^m)} = \\ &= a_0 \sqrt{\frac{k+1}{k-1} (1 - \epsilon_a^m)}, \end{aligned} \quad (6-1)$$

where  $\epsilon_a = \frac{p_a}{p_0}$  is the ratio of pressure after nozzle to pressure in reservoir;

$$m = \frac{k-1}{k}.$$

On the basis of the equation of continuity there may be found the mass flow rate of the gas:

$$G = gF\rho c = F\gamma c = \frac{Fc}{\gamma}.$$

After substituting here the value of speed from formula (6-1), we obtain:

$$G = F \sqrt{\frac{2gk}{k-1}} p_a \gamma_a \epsilon_a^{\frac{1}{k}} \sqrt{1 - \epsilon_a^m}. \quad (6-2)$$

Formula (6-2) gives the flow of gas depending upon pressure and density of gas in a reservoir and pressure of medium. This formula is valid on the assumption of a uniform distribution of speeds in exit section of nozzle F. The outflow of gas G depending upon  $\epsilon_a$  varies the same as the reduced flow q.

Actually, since  $G = gFq\rho_a$ , then after substituting the values p. and a we obtain:

$$\begin{aligned} G &= \left(\frac{2}{k+1}\right)^{\frac{1}{k-1}} F \sqrt{\frac{2gk}{k+1}} p_a \gamma_a q = \\ &= F \sqrt{\frac{2gk}{k+1}} p_a \gamma_a \lambda \left(1 - \frac{k-1}{k+1} \lambda^2\right)^{\frac{1}{k-1}}. \end{aligned} \quad (6-3)$$

From a comparison of equations (6-2) and (6-3) it follows:

$$q = \left(\frac{k+1}{2}\right)^{\frac{1}{k-1}} \sqrt{\frac{k+1}{k-1}} \epsilon_a^{\frac{1}{k}} \sqrt{1 - \epsilon_a^m}. \quad (6-4)$$

Formulas (6-2) and (6-3) show that the maximum value of flow corresponds to the critical speed  $\lambda = 1$  and, correspondingly, critical ratio of pressures  $\epsilon_a = \epsilon_{*}$ .

The maximum or critical flow is obtained after substituting  $\epsilon_a = \epsilon_{*}$  into the equation (6-2) or  $\lambda = 1$  into equation (6-3):

$$\begin{aligned} G_* &= \left(\frac{2}{k+1}\right)^{\frac{1}{k-1}} F \sqrt{\frac{2gk}{k+1}} p_a \gamma_{*} = \\ &= \left(\frac{2}{k+1}\right)^{\frac{k+1}{2(k-1)}} \sqrt{\frac{gk}{R}} F \frac{p_0}{\sqrt{T_0}}. \end{aligned} \quad (6-5)$$

Formula (6-5) is readily obtained by substituting  $\lambda = 1$  into equation (2-38).

For

$$k=1,4 \quad G_*=2,145F\sqrt{p_*\gamma_*}=0,396F\sqrt{\frac{p_*}{T_*}};$$

For

$$k=1,3 \quad G_*=2,09F\sqrt{p_*\gamma_*}\approx 0,305F\sqrt{\frac{p_*}{T_*}}.$$

(6-6)

The equation of flow (6-2) shows that in a given exit section of nozzle with decrease in  $p_a$  at  $p_a > p_*$  the flow of the gas increases, and at  $p_a < p_*$  according to equation (6-2) the flow of gas should decrease. However, the latter does not correspond to reality. Consequently, equation (6-2) incorrectly describes the process of gas outflow at  $p_a < p_*$  if into it we substitute the ratio of pressure of medium  $p_a$  to pressure in reservoir  $p_0$ .

Let us consider the outflow from a narrowing nozzle with fixed values of the pressure and temperature in reservoir and a variable pressure of the medium  $p_a$ .

As long as pressure of the medium is higher than the critical pressure, calculated by parameters of gas in a reservoir, any changes in  $p_a$  are propagated also inside the nozzle. In this case, the flow of the gas changes in accordance with formula (6-2). When a decreasing pressure  $p_a$  attains a critical value  $p_*$ , in exit section of narrowing nozzle there is established a critical speed and subsequent changes of the pressure of environment cannot penetrate inside the nozzle. Consequently, actual differential of pressures, creating a flow of gas through the nozzle at  $p_a < p_*$  irrespective of dependence on magnitude of pressure of environment, will be critical, and the flow of gas—maximum and constant. It follows from this that formula (6-2) at  $p_a < p_*$  only in this case gives correct values of the flow, if into it is substituted the critical pressure, which is established in the exit section of narrowing nozzle. Irrespective of dependence on the magnitude  $p_a$ . At moment when in exit section critical parameters are attained there occurs a unique phenomenon "cutoff of nozzle\*", as a result of which the nozzle and reservoir are

---

\*The same as in the case of outflow from tube (Chapter 5).



found to be isolated from the environment.

Thus, at  $\epsilon_0 < \epsilon$ , into formula (6-2) it is necessary to substitute  $\epsilon_0$ . The flow of gas remains constant and is determined by formula (6-6).

The distribution of speeds in exit section of nozzle exerts an influence on the character of the dependence of  $G$  on  $\epsilon_0$ . The above-obtained formulas are well confirmed by experiment only in the case when the profile of nozzle is made smooth. The smoothly narrowing shape of the nozzle approximates the distribution of speeds in exit section to uniform. For this purpose walls of the nozzle must be calculated in a special manner.

The profile of a narrowing nozzle can be calculated by the Vitoshinskiy formula:

$$r = \frac{r_0}{\sqrt{1 - \left[ 1 - \left( \frac{r_0}{r_1} \right)^2 \right] \frac{\left( 1 - \frac{3x^2}{l^2} \right)^2}{\left( 1 + \frac{x^2}{l^2} \right)^2}}} \quad (6-7)$$

The magnitudes, appearing in formula (6-7), are explained in Fig. 6-1;  $\frac{1}{\sqrt{3}}$ . Such a profile is useful for nozzles, connecting two pipes of different diameters, when the flow during transition into pipe of

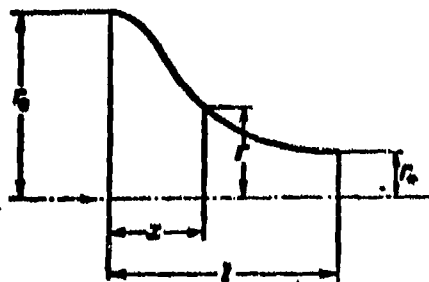


Fig. 6-1. Diagram for constructing a narrowing nozzle.

smaller diameter should be accelerated, but the speed at every point of exit section of nozzle should be identical. Nozzles of such profile are used for wind tunnels of subsonic speeds.

The experiment shows that in wide range of speeds up to  $\lambda = 0.90$  to  $0.95$ , field of speeds after the nozzle are fairly uniform.

In connecting nozzle directly to reservoir its profile can be outlined by arcs of a circle. Sometimes profile of nozzle is outlined by limniscates.

## 6-2. Narrowing Nozzle with Variable Mode of Flow

In the variation of parameters of a gas in the reservoir and after nozzle the flow of gas and spectrum of the discharging stream vary. By using relationships (6-2) and (6-5), it is possible to analyze the change of flow during a simultaneous change of pressure in the reservoir  $p_0$  and pressure of medium  $p_a$ .

We shall designate:

$P_{0 \max}$  is the maximum pressure in reservoir;

$G_{* \max}$  is the maximum critical flow corresponding to this pressure.

$P_0, G_*$  are current values of pressure in reservoir and of the critical flow.

On the basis of formula (6-5) it is possible to express the ratio of the critical flows:

$$\frac{G_*}{G_{* \max}} = \frac{P_0}{P_{0 \max}} \sqrt{\frac{T_{0 \max}}{T_0}}. \quad (6-8)$$

In assuming that with a change of pressure  $p_0$  the temperature of gas in the reservoir  $T_0$  is kept constant, we shall obtain:

$$\frac{G_*}{G_{* \max}} = \frac{P_0}{P_{0 \max}}. \quad (6-9)$$

At  $T_0 = \text{const}$  and constant pressure in the reservoir the change in flow depending on pressure after nozzle  $p_a$  is expressed by the already above-known equation (6-2).

It is readily noted that the ratio of flow with a given counterpressure to the critical flow is equal to:

$$\frac{G}{G_*} = q. \quad (6-10)$$

From expression (6-9) it follows:

$$G_* = G_{* \max} \frac{P_0}{P_{0 \max}} = G_{* \max} \epsilon_0.$$

After substituting  $G_*$  into equation (6-10), we obtain:

$$q_m = \frac{G}{G_{\max}} = \epsilon_0 q = -\left(\frac{k+1}{2}\right)^{\frac{1}{k-1}} \sqrt{\frac{k+1}{k-1}} \epsilon_0^{\frac{1}{k}} \sqrt{1 - \epsilon_0^{\frac{k-1}{k}}} \quad (6-11)$$

It follows from this that with a change of the initial pressure all points of the curve of reduced flow are displaced in proportion to  $\epsilon_0$ , i.e., proportionally to the change of pressure before nozzle.

Consequently, ratio of the flow  $G$  to maximum critical flow  $G_{\max}$  can be presented depending upon  $\epsilon_0$  and  $\epsilon_1$ . This dependence is graphically expressed in the triaxial system of coordinates (Fig. 6-2), where along the three axes there are plotted

$$\epsilon_1 = \frac{P_1}{P_0}, \quad \epsilon_0 = \frac{P_0}{P_{0\max}} \quad \text{and} \quad q_m.$$

As a result, we obtain certain conical surface each point of which determines the flow of gas through a narrowing nozzle depending upon pressures before nozzle and after it. The plane triangle OEB, whose points correspond to regions of critical flows of gas serves as the extension of the conical surface OAB (Fig. 6-2).

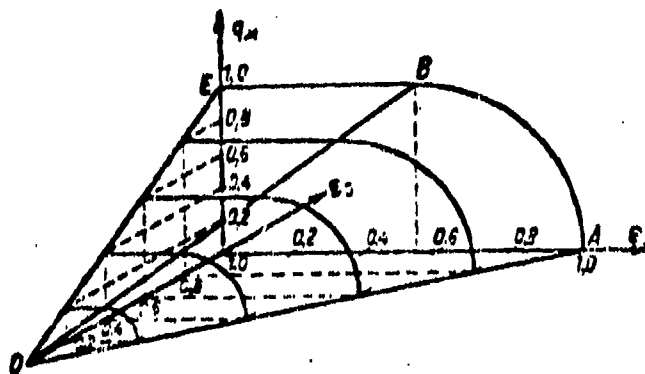


Fig. 6-2. Conical surface of reduced flow rate.

Equation (6-11) can be presented also in a biaxial system of coordinates, after constructing curves  $q_m = f(\epsilon_0)$  for different, but constant values  $\epsilon_1$ . Then, we obtain a grid of relative flows of gas, which is the projection of conical surface

onto plane  $(q, \epsilon)$ . Grid of flows (Fig. 6-3) is very convenient for a graphic calculation of nozzle during variations of the mode.\*

Numerous experiments have shown that equation of surface of flows (6-11) can be simplified by replacing the accurate formula of reduced flow  $q$  by an approximate expression. With subcritical pressure differentials  $(\epsilon_n > \epsilon_*)$  the dependence  $q = q(\epsilon_n)$

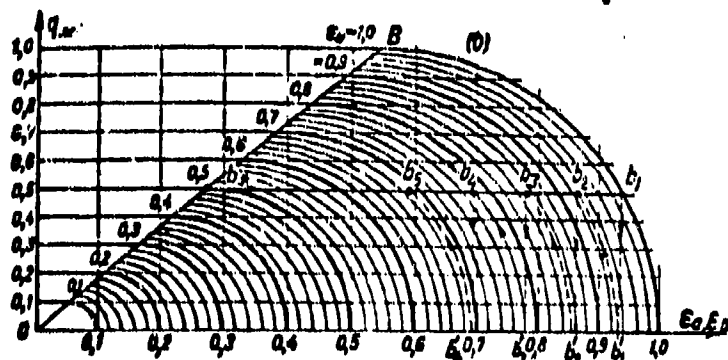


Fig. 6-3. Grid of reduced flows of gas.

can be presented as an arc of an ellipse, whose equation has the form of:

$$\frac{(\epsilon_n - \epsilon_*)^2}{(1 - \epsilon_*)^2} + q^2 = 1. \quad (6-12)$$

Within the entire range of subsonic speeds, this formula very accurately approximates the dependence between  $q$  and  $\epsilon_n$ .

After replacing in equation (6-12)

$$q = \frac{q_n}{q_0},$$

we obtain:

$$\frac{(\epsilon_n - \epsilon_*)^2}{(1 - \epsilon_*)^2} + \frac{q_n^2}{q_0^2} = 1. \quad (6-13)$$

We shall designate:

$$\epsilon' = \frac{P_n}{P_{0 \max}} = \frac{P_n}{P_0} \frac{P_0}{P_{0 \max}} = \epsilon_n \epsilon_0.$$

Then (6-13) will be transformed to:

$$\frac{(\epsilon' - \epsilon_* \epsilon_0)^2}{(1 - \epsilon_*)^2} + q_n^2 = \epsilon_0^2. \quad (6-14)$$

whence

$$q_n = \frac{1}{1 - \epsilon_*} \sqrt{(\epsilon_0 - \epsilon') [\epsilon' - \epsilon_0 (2\epsilon_* - 1)]}. \quad (6-15)$$

\*A. V. Shcheglyayev. Steam turbines, State Power Engineering Publishing House, 1947.

When  $\alpha_0 = \text{const}$ , equation (6-15) gives the relationship  $q_0 = q(\alpha')$ . Since for smoothly narrowing nozzle  $\alpha_0$  depends only on physical properties of the gas and is at  $k = \text{const}$  a constant magnitude.

In the study of a variable nozzle mode of great practical interest is the character of change of spectrum of stream after the nozzle. For subcritical modes of outflow of variations of parameters at the nozzle entry and exit slightly exert an influence on the shape of flow after the nozzle.

With supercritical drops in pressures the transition from a critical speed in exit section to supersonic speed occurs in the free flow after the nozzle.

In this case, the edge of exit section  $AA_1$  (Fig. 6-4,a) is source of disturbance of sonic flow. After the exit section the stream encounters the pressure of the medium  $p_0$  ( $p_0$  is less than critical) and, consequently, at points A and  $A_1$  (Fig. 6-4,a) pressure varies from  $p_*$  to  $p_0$ . As a result, from edges of nozzle there are propagated two waves of rarefaction:  $AA_1B_1$  and  $A_1AB$ , whose outer boundaries are the characteristics. The first boundary  $AA_1$  is the characteristic, whose angle  $\alpha_{m1} = \frac{\pi}{2}$ ; second boundary  $AB_1$  must pass in the free flow at an angle

$$\alpha_{m2} = \arcsin \sqrt{\frac{k-1}{2} \frac{\alpha_0^m}{1-\alpha_0^m}}; \quad m = \frac{k-1}{k}. \quad (6-16)$$

Between these two boundaries are located the characteristics, whose angles vary within the limits

$$\frac{\pi}{2} \gg \alpha_{m1} \gg \alpha_{m2}.$$

In reality, however, all the characteristics, including  $AB_1$  and  $A_1B$ , have a variable angle of slope and, consequently, are curvilinear, since waves of rarefaction from points A and  $A_1$  curvilinear within the limits of the flow intersect. Intersection of the waves occurs in the triangle  $AA_1D$ . Besides, characteristics, falling onto the free edge AB and  $A_1B_1$ , are reflected from it with opposite sign, and waves of rarefaction change into compressional waves.

As a result of intersection, in the flow there will form a wedge of rarefaction  $ADA_1$ , the base of which is located in exit section of nozzle. Within the limits of

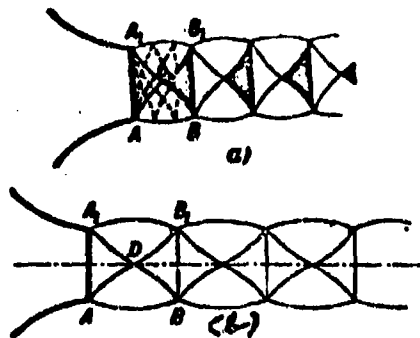


Fig. 6-4. Diagram of spectra of stream after narrowing nozzle with unrated conditions ( $s_2 > s_1$ ).

wedge there occurs a significant decrease of pressure, which in this zone becomes lower than the pressure of the medium  $p_*$ .

Since waves reflected from the free edge intersect within limits of the second wedge  $DBB_1$ , then here pressure increases to value  $p_*$  in section  $BB_1$ ; wedge of rarefaction changes into a wedge of compression. Consequently, the points B and  $B_1$ , the pressure at which varies from  $p_*$  to  $p_a$ , also are sources of waves of rarefaction, and spectrum of stream is repeated. It is readily noted that sectors  $AA_1$  and  $BB_1$  are equal. At the intersection with rarefaction wedge, streamlines are deformed, by being deflected from the axis of nozzle: sections of stream increase, and the stream "swells." Within the limits of the reflected waves flow is compressed, and its sections decrease. Edges of the streams, symmetric with respect to the axis, acquire a wavy form.

On the basis of discussion it is possible to forecast the character of change of pressure along axis of stream. Within the limits of a wedge of rarefaction, the pressure drops from  $p_*$  to certain value  $p_D < p_a$ , and within the limits of wedge the compression increases to  $p_*$ ; farther the process is repeated. Pressure in stream varies by certain periodic law, close to sinusoidal. The character of change of speeds along axis of stream will be corresponding. In the sections  $AA_1$  and  $BB_1$

speeds are critical. Between these sections the speeds are supercritical, where at point D the speed will be maximum. Consequently, the entire region of stream  $ABB_1A_1$  is supersonic.

Spectra of stream in the considered regimes are maintained qualitatively identical for two-dimensional and axially symmetric nozzles, however, in the last case the waves of rarefaction and compression have a conical shape. In an axially symmetric flow, therefore, there will be formed cones (but not wedges) of rarefaction and compression. As the pressure increases in the reservoir or lowers after the nozzle, the spectrum of flow gradually is reconstructed (Fig. 6-4,b). Angles of waves  $AB_1$  and  $A_1B$  decrease, the height of wedges  $ADA_1$  and  $DBB_1$  increases and angles at apex of wedges (cones) decrease. Distances between the sections  $AA_1$  and  $BB_1$  increase.

For an axially symmetric nozzle such a gradual reconstructing occurs up to certain limits. In attaining a certain ratio of pressures  $\epsilon_1$  picture of flow after nozzle varies in a critical manner.

Owing to the intense decrease of pressure of gas within limits of a cone of rarefaction, genatrices AD and  $A_1D$  change into curved shocks AD and  $A_1D_1$  (Fig. 6-5,a), and at cone of flow there will form a normal shock  $DD_1$ , which terminates the curved shocks. In the external flow the curved shocks DB and  $D_1B_1$  appear. Thus, in the flow after nozzle there appears a bridge-like shock  $ADBB_1D_1A_1$ . The shocks DB and  $D_1B_1$  go out beyond free edge of flow and are reflected from it in the form of waves of rarefaction. The waves of rarefaction also are terminated by curved shocks.

At the intersection of normal shock  $DD_1$  speeds of central part of stream become subsonic, and the pressure intensively increases ( $p' > p_a$ ). In the transition through the shocks DB and  $D_1B_1$  the speeds remain supersonic. Consequently, the lines DE and  $D_1E_1$  are lines of the tangential discontinuity of speeds. As a result of the interaction with external supersonic flow, the subsonic core of flow is accelerated, and a section of it decreases to the minimum  $EE_1$ , in which there will be attained

a sonic speed ( $M = 1$ ). After the section  $EE_1$  speeds at all points of the flow are supersonic. As the differential in pressure further increases, the system of shocks gradually is reconstructed (Fig. 6-5,b). The extent of the normal shock increases and the shape of curved shock which limits the overexpanded supersonic core varies. It is necessary to emphasize that external parts of the flow ABFEDA and correspondingly  $A_1 B_1 F_1 E_1 D_1 A_1$ , the same as the core  $ADD_1 A_1$ , at any value  $\epsilon_a < \epsilon^*$ . Thereby will remain supersonic. Subsonic speeds are detected only in small sector within the flow after the shock  $DD_1$ . One should bear in mind that all above-cited considerations do not take into account the influence of viscosity and, in particular, the interaction of the flow with the environment. Spectra of

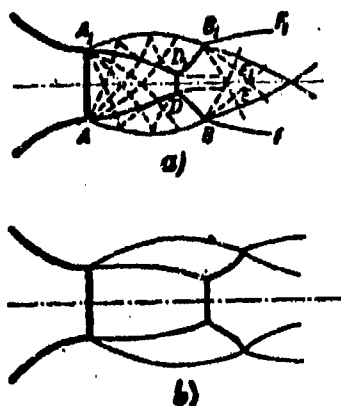


Fig. 6-5.  
Diagram of spectra after narrowing  
nozzle at  $\epsilon_a < \epsilon^*$ .

the outflow from a narrowing axially symmetric nozzle are given in Fig. 6-6.

Here, there clearly are seen all stages in the development of spectrum of stream at

$\epsilon_a < \epsilon^*$ . We note that the supersonic sectors

of the spectrum for a two-dimensional nozzle can be calculated by the method of characteristics. For an evaluation of quality

of nozzle, the coefficient of flow  $\mu_c$ ,

coefficient of speed  $\varphi_c$  and loss factor  $\zeta_c$

are used.

Coefficient of flow is determined by the formula

$$\mu_c = \frac{G}{G_T}, \quad (6-17)$$

where  $G$  is the actual flow of gas through nozzle;

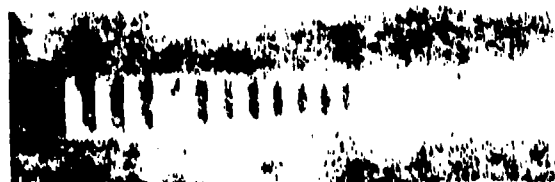
$G_T$  is the theoretical flow (in an isentropic process).

Coefficient of speed is ratio of speeds in real and theoretical processes:

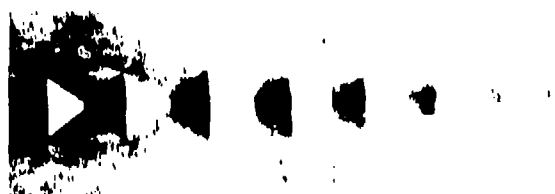
$$\varphi_c = \frac{c}{c_T}. \quad (6-18)$$

In Figs. 6-7 and 6-8 there are presented coefficients  $\mu_c$  and  $\varphi$  for narrowing





a)



b)



c)



d)

Fig. 6-6. Outflow of air from a narrowing nozzle with supercritical differentials of the pressures.  
 a) -  $\pi_0 = 0.51$ ; b) -  $\pi_0 = 0.412$ ; c) -  $\pi_0 = 0.267$ ;  
 d) -  $\pi_0 = 0.05$ .

profiled and conical nozzles depending on  $\epsilon_*$  and  $Re$ . The curves show with an

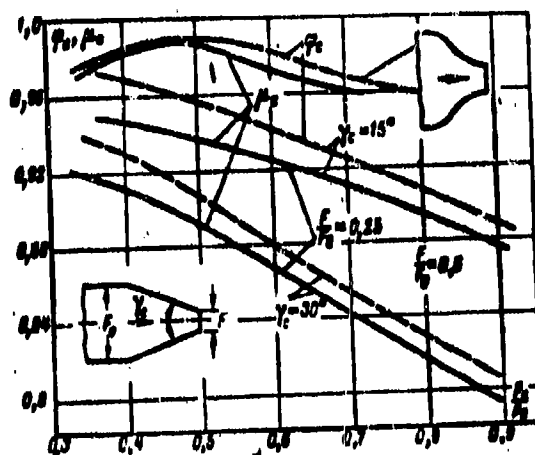


Fig. 6-7. Flow coefficients  $\mu_*$  and coefficients of speed  $\varphi_*$  for conical and profiled nozzles.

increase in the differential of pressures and decrease of angle of conicity the coefficient of flow increases. An analogous result is obtained also for a profiled nozzle. However, maximum  $\mu_*$  in the latter case correspond to near-critical speeds. The absolute values of  $\mu_*$  obtained are higher for a profiled nozzle. At  $\epsilon_* > 0.7$ , curves in Fig. 6-7 reflect not only the influence of compressibility, but also that of the Reynolds number (Fig. 6-8).

Coefficient of speed of conical nozzles varies little depending on the angle of conicity. In a wide range of  $\epsilon_*$  the mean value  $\varphi_*$  amounts to  $\sim 0.97$ . For

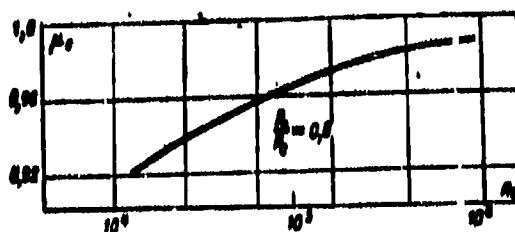


Fig. 6-8. Influence of  $Re$  number on coefficient of flow in narrowing nozzle.

nozzles, profiled by formula (6-7), the values  $\varphi_*$  obtained are higher ( $\varphi_* = 0.985$  to 0.99).

A marked influence of ratio of sections, angle of conicity and  $\epsilon_0$  is explained by the change in structure of flow in stream after nozzle.

With an increase of  $\frac{F}{F_0}$  frictional losses decrease in nozzle, but at the same time field of flow at the exit becomes more nonuniform. Analogously, also, the increase in angle of conicity, with whose increase the field of flow at the exit acquires an increasingly greater nonuniformity, exerts an influence.

As example of the application of grid of flows let us consider the flow of gas in system of consecutively connected nozzles. Suppose in a tube there have been fixed  $n$  narrowing nozzles with an identical area of exit section (Fig. 6-9). We assume that the diameter of tube is much larger than the diameter of the nozzle; speed of gas in the tube can be ignored.

With the outflow through each nozzle the gas expands and its speed increases. In intermediate chamber the process of conversion of kinetic energy into heat takes place. In considered diagram of the apparatus there is realized a complete transformation (complete extinguishing) of kinetic energy. The flow of gas loses speed owing to the interaction with particles in chamber, and also to impact against wall of following nozzle.

The process of extinguishing the kinetic energy in apparatus is isobaric. The state of gas at entry into nozzles is characterized by condition  $i_{01} = \text{const}$  or  $T_0 = \text{const}$  (Fig. 6-10).

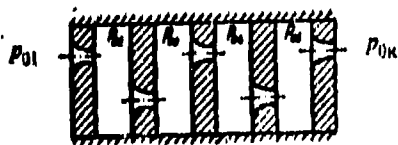


Fig. 6-9. Diagram of nozzle apparatus with complete extinguishing of the speed in intermediate chambers.

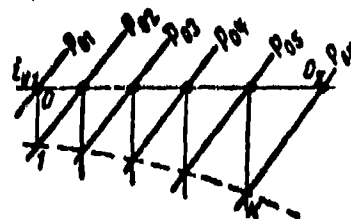


Fig. 6-10. Diagram of process in thermal diagram of nozzle apparatus.

A characteristic peculiarity of process in a nozzle apparatus is the increase of entropy in the intermediate chambers.

The calculation of a nozzle apparatus is realized by means of equations (6-3) and (6-12). In considering that the flow for all nozzles will be identical, from the indicated equations we readily obtain:

$$q_1 = \sqrt{1 - \left(\frac{e_1 - e_2}{1 - e_2}\right)^2} = e_{01} \sqrt{1 - \left(\frac{e_1 - e_2}{1 - e_2}\right)^2} = e_{0n} \sqrt{1 - \left(\frac{e_n - e_2}{1 - e_2}\right)^2} = e_{0n} \sqrt{1 - \left(\frac{e_2 - e_1}{1 - e_2}\right)^2}. \quad (6-19)$$

Here  $q_1$  is the reduced flow through first nozzle;

$$e_{01} = \frac{p_{01}}{p_{01}}; \quad e_{0n} = \frac{p_{0n}}{p_{01}}; \quad e_{0k} = \frac{p_{0k}}{p_{01}}; \quad p_{01}, p_{0n}, p_{0k},$$

$p_{0k}$  is the pressure of stagnation respectively before and after first nozzle, after nozzle (n-1) and after the apparatus;

$$e_n = \frac{p_{0(n+1)}}{p_{0n}}; \quad e_s = \frac{p_{0s}}{p_{0n}} \text{ is the ratio of the pressures in nozzle } n \text{ and } s.$$

The value  $e_n$  is determined by formula (6-19):

$$e_n = e_s + (1 - e_s) \sqrt{1 - \left(\frac{q_1}{e_{0(n-1)}}\right)^2}. \quad (6-20)$$

Hence we conclude that since  $e_{0n} < e_{0(n-1)}$ , then  $e_n < e_{n-1}$ . For each subsequent nozzle, the ratio of the pressures will be less than for the preceding. In accordance with this the dimensionless speeds along nozzle apparatus will increase ( $\lambda_n > \lambda_{n-1}$ ) and, consequently, the critical speed ( $\lambda = 1$ ) will be manifested in the last nozzle (irrespective of whether a complete or partial extinguishing of kinetic energy takes place in intermediate chambers) if  $e_{0n} < e_{0c}$ , where  $e_{0c}$  is the critical ratio of pressures for the nozzle apparatus.

The same conclusion can be reached from simple physical considerations. Actually, with a drop in pressure, also the gas density drops. But since the exit sections of nozzles are identical, then in order that the gas flow remains constant, it is necessary that in each subsequent nozzle the speed increases. Obviously, the maximum speed will be established in the last nozzle.

From equation (6-19) for last nozzle it may be obtained that at

$$e_s = \frac{p_{0s}}{p_{0n}} = e_{0n} \left( \frac{2}{k+1} \right)^{\frac{k}{k-1}}$$

a critical ratio of the pressures for nozzle apparatus will be:

$$\epsilon_{0n} = \left( \frac{p_{0n}}{p_{01}} \right)^{\frac{1}{\gamma}} = \epsilon_1 q_1 \quad (6-21)$$

where  $q_1$  is the reduced flow through first nozzle during a critical outflow from the last.

For each nozzle at  $\epsilon_{0n} = \text{const}$ , it is possible to plot the curves  $q = q(\epsilon)$  (Fig. 6-3). The line of critical flows is determined by equation (6-21) (line OB in Fig. 6-3).

It should be emphasized that formula (6-21) is completely equivalent to formula (5-19), obtained for a tube of constant section. Hence it may be concluded, regardless of the dependence on physical peculiarities of motion of gas (without an energy exchange with environment), but accompanied by an increase in entropy, the limiting mode of this motion, considered within the frames of a one-dimensional diagram, is described by identical equations.

By means of the diagram in Fig. 6-3 it is possible to solve the following problems:

1. If there are given the reduced flow of gas and number of nozzles in apparatus  $n$ , then one can determine  $\epsilon_{0n}$ , and also  $\epsilon_{0n}$  and  $\epsilon_n$ , i.e., establish the distribution of pressures in nozzles.
2. There can be found number of nozzles, if the flow  $q_1$  and relative pressure after last nozzle  $\epsilon_{0n}$  are known.
3. For the known value  $q_1$  one can determine the critical ratio of pressures  $\epsilon_n$  and the number of nozzles  $n$ .

Let us consider corresponding examples.

1. Let us assume that number of nozzles  $n = 4$ , and the reduced flow  $q_1 = 0.5$ . At the intersection of line  $q_1 = 0.5$  with the curve  $q = q(\epsilon)$  for first nozzle we shall find the point  $b_1$ , which determines  $\epsilon_1$ . The curves  $b_1'b_2$  will give the same dependence for the second nozzle. Consequently, at the point  $b'_2$  we obtain

After repeating this construction up to point  $b'_4$ , we shall determine the relative pressure  $\sigma_{0k} = \sigma_0, \sigma_1, \sigma_2, \dots$ .

2. Suppose the flow  $q_1 = 0.5$  and the ratio of pressures  $\sigma_{0k} = 0.69$  are given. Then the original point in grid of flows will be the point  $b_5$  at the intersection of the line  $q_1 = 0.5$  of the arc of ellipse  $\sigma_{0k} = 0.69$ . By shifting along this line up to axis  $\sigma$  and then along the vertical to line  $q_1 = 0.5$ , successively we find

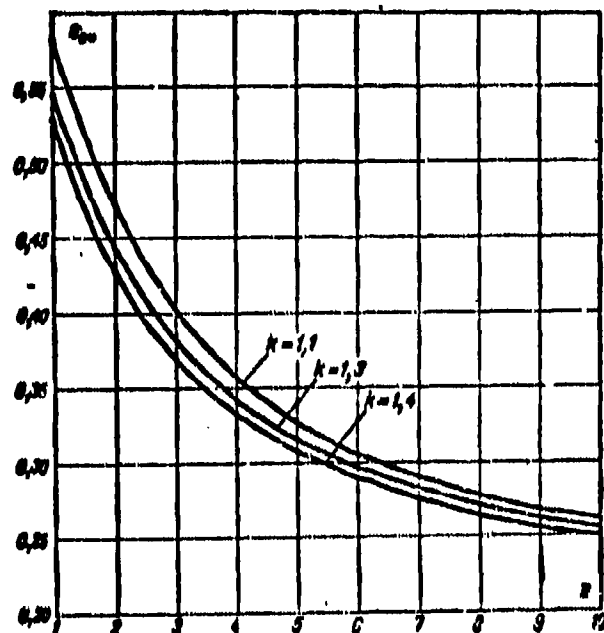


Fig. 6-11. Critical ratios of pressures for nozzle apparatus depending on number of nozzles  $n$  for different values of  $k$ .

the points  $b'_4, b_4, b'_3, b_3$ , etc., up to point  $b_1$ . The number of vertical lines  $b'_4, b_4, b'_3, b_3$ , etc., is equal to the number of nozzles of apparatus  $n$ .

3. We shall now find the number of nozzles at  $q_1 = 0.5$ , corresponding to critical mode of nozzle apparatus  $\sigma_{0k} = \sigma_0$ . After determining on line OB the point  $b_*$ , corresponding to the critical speed in the last nozzle, we find the line  $q = q(*)$ , passing through this point, and further in succession we determine distribution of pressures and the number of nozzles  $n$  just as in the preceding case.

Being given different values of  $q_1$  by (6-21), we find corresponding values

of  $\epsilon_0$ , and, after solving problem 3 by the above described method, we determine the number of nozzles in a critical regime of nozzle apparatus.

Results of such calculations are presented in Fig. 6-11, where we plotted the  $\epsilon_0$ , depending on  $\underline{z}$ .

Of great practical interest also is the possibility of determining the flow of gas through the nozzle apparatus with  $\epsilon_{0k}$  and  $\underline{z}$  given. Such a problem, however, is solved simply only in that case when the nozzle apparatus operates in a critical mode ( $\epsilon_{0k} < \epsilon_0$ ) with the total extinguishing of kinetic energy in intermediate chambers. In this case from graph in Fig. 6-11 we find critical ratio of pressures  $\epsilon_0$  for a given number of nozzles. The magnitude of the reduced flow  $q_{1*}$  can be determined by the formula (6-21) or by Fig. 6-3 (straight line AB).

We note that curves in Fig. 6-11 satisfy the equation

$$\epsilon_0 = \frac{\epsilon_{0k}}{\sqrt{\epsilon_{0k}^2 + (1 - \epsilon_{0k})^2}} \quad (6-22)$$

### 6-3. Outflow of Gas From Aperture with Sharp Edge. Second Critical Ratio of Pressures

Theoretical investigations and experiment detect certain new properties of flow of gas, flowing out of aperture with sharp edge.

Theoretical solutions of this problem have been given in classical works of N. Ye. Zhukovskiy and S. A. Chaplygin both for low speeds, and also for speeds commensurate with the speed of sound. A subsequent development of method of S. A. Chaplygin in reference to outflow from aperture with sharp edge was made by F. I. Frankl for the region of sonic and supersonic speeds.

During outflow from narrowing nozzle the smooth profile of the walls assures gradual expansion of the flow and determines the shape of the streamlines. The developing radial components of the speeds decrease during flow through nozzle and towards exit section vanish. The flow in exit section has a uniform field of speeds. With a supercritical differential of pressures the exit section of nozzle

coincides with critical.

Outflow from aperture with sharp edge occurs otherwise (Fig. 6-12). In the vessel at a sufficiently large distance from the aperture the speed of gas is equal to zero, and the pressure— $p_0$ . After aperture there is maintained a pressure  $p_a < p_0$ .

Near the aperture to the left speeds of the gas intensively increase, the flows of gas contracts and are distorted. The flow of gas is separated from sharp edges of aperture and then moves as a free stream.

The spectrum of the stream in aperture shows that curvature of various streamlines are found to be different. Most distorted are the streamlines along the edge of stream, and the least distorted—streamlines near the axis. Therefore, the speeds

in the outer streamlines will be greater than the speeds at the core of stream. At exit of the aperture there is established nonuniform distribution of speeds and pressures. The irregularity of the flow is increased by the effect of viscosity. It is readily seen that the stream will carry after itself the gas of environment and will be stagnated. The average speed of the stream will decrease, and its cross section will increase. The washing-away of the stream starts directly from the edges of the aperture. However, it proceeds fairly gradually. On this basis it is possible to use following idealized diagram of an outflow through the aperture.

⊙ We assume the gas as perfect, and the motion—irrotational.

On sharp edges A and B there will occur a separation. Since we assume that friction is lacking, then there will be no mixing of surrounding gas into the stream. Consequently, to the right of aperture there will form two regions: a free stream and motionless gas with a pressure  $p_a$ . Since the pressure at the edge of stream is constant, then it is obvious that speed on the edge also is constant.

The problem on determining the shape of such a stream and outflow of gas through aperture was solved in the classical work by S. A. Chaplygin, "On Gas Jets." S. A. Chaplygin considered case of two-dimensional stream, when the ratio of the



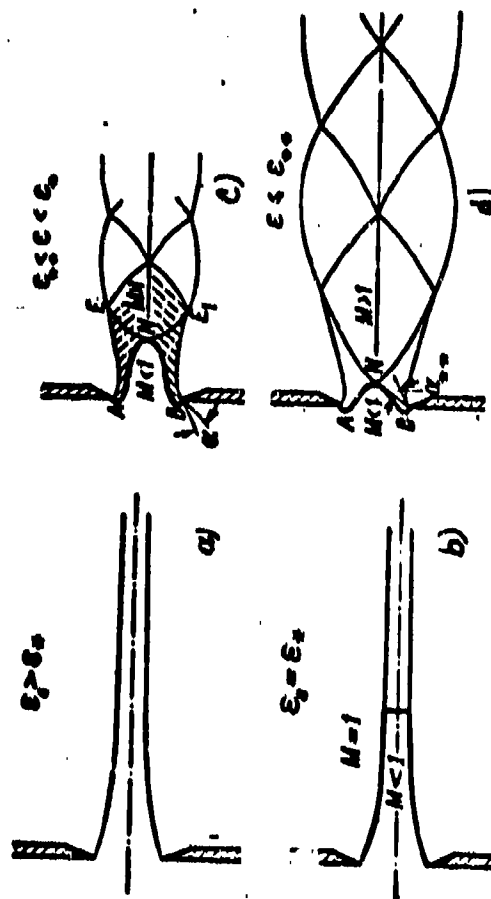


Fig. 6-12. Diagram of outflow of stream from aperture with sharp edge with different modes of flow.

pressures  $\epsilon_a = \frac{p_a}{p_0}$  is greater than the critical or close to it. In this case, stream has shape illustrated in Fig. 6-12 a. The stream continuously narrows down where the maximum constriction takes place at an infinite distance from the aperture. If  $\epsilon_a = \epsilon_c$ , then on the edge of the stream the speed of flow is equal to the critical. Within the stream the speeds are lower than the critical. With distance from aperture, the curves of the speeds level off and at a certain finite distance from aperture the speeds in stream become equal to the speed at the edge, where the leveling-out of the field occurs due to compression of stream and acceleration of core of flow. The stream contraction which forms is characterized by coefficient of the contraction, which is determined as the ratio of minimum width of stream to width of aperture (two-dimensional problem).

Thus, at  $\epsilon_a = \epsilon_c$  the critical speed is detected at the edge of stream and in the cross section at a finite distance from the aperture. The line of the critical speed for such a mode of flow is shown in Fig. 6-12, b. With a subsequent lowering of counterpressure ( $\epsilon_a < \epsilon_c$ ), the stream becomes supersonic.

The transition through speed of sound is realized on the line of sonic speeds ANB, which goes from edges of aperture and juts out into the stream in the form of a "tongue" (Fig. 6-12, c).

Consequently, at  $\epsilon_a < \epsilon_c$  the spectrum of the stream is reconstructed. Line of sonic speeds (line of transition), which coincided at  $\epsilon_a = \epsilon_c$  with edge of stream and minimum section, as  $\epsilon_a$  decreases, is deformed and approaches the exit section of aperture. To the right of transitional line the flow is supersonic. Deformation of line of transition is explained by the rebuilding of the field of speeds in exit section AB and in the exit section, associated with the change of curvature of boundary streamlines.

Within the "tongue" the speeds are subsonic. The character of the deformation of line of transition attests to the fact that supersonic speeds will be attained at first in the external part of stream (on boundary and near it), and later at

the core which completely corresponds to the distribution of speeds in the cross section of the stream. The edge of stream expands. The deformation of the "tongue" during change of  $\epsilon_a$  will occur as long as lines of weak disturbances (characteristics) outgoing from the edges AE and BE<sub>1</sub>, will fall onto the line of transition ANB. Angles of characteristics  $\alpha_m$  with decrease in  $\epsilon_a$  decrease (Fig. 6-12,c).

Consequently, the deformation of line of transition with a decrease in  $\epsilon_a$  will not be infinite. There exists such a value of the external pressure  $p_{**}$ , at which the line of transition occupies a stable position; a subsequent lowering of the pressure of the environment no longer results in its deformation. This mode corresponds to such an angle  $\alpha_{m..}$  of the first characteristics, emanating from points A and B, with which they touch the line of transition, but do not intersect it (Fig. 6-12,d). Pressure  $p_{**}$  F. I. Frankl called the second critical pressure. The corresponding ratio

$$\epsilon_{..} = \frac{p_{..}}{p_a}$$

we shall call the second critical ratio of pressures.

Characteristic peculiarities of a stabilized line of transition are the sectors lying within the nozzle near the points A and B (Fig. 6-12,d), which show that along the edges of aperture from the direction of reservoir the speeds already are supersonic. In addition, at  $\epsilon_a = \epsilon_{..}$  the line of transition in stream occupies nearest position to aperture.

In accordance with picture of flow being reconstructed (depending on  $\epsilon_a$ ) the flow of gas through aperture varies. We shall call the coefficient of flow of aperture  $\mu_{ora}$ , the ratio of the actual flow through aperture to the flow of gas through a narrowing nozzle, having the same area of cross section at exit with one and the same differential of pressures.

Values of coefficient of the flow at  $\epsilon_a > \epsilon_{..}$  calculated by S. A. Chaplygin for air, are presented in the first five columns of Table 6-1. For an incompressible fluid  $\mu_{ora} = 0.63$ .

Above it was indicated that the maximum flow for a nozzle takes place with a

critical counterpressure and subsequent lowering of counterpressure does not exert an influence on the flow. During outflow from aperture owing to change in shape of the line of transition at  $\epsilon_a < \epsilon_{**}$ , the flow of gas will increase as long as  $\epsilon_a > \epsilon_{**}$ .

Table 6-1

$\epsilon_{**} = \frac{P_{**}}{P_0}$	0,676	0,641	0,606	0,559	0,529	0,037
$P_{0,cr}$	0,680	0,700	0,710	0,730	0,740	0,850

At  $\epsilon_a < \epsilon_{**}$  the decrease in counterpressure does not exert an influence on the shape of line of transition and, consequently, on the flow of the gas. If the external pressure is equal to the second critical pressure, then coefficient of flow has a maximum value.

Values of the coefficient of flow  $\mu'_{0,cr}$  and of the second critical ratio of pressure  $\epsilon_{**}$  for apertures of different shapes are presented in Table 6-2.

In Fig. 6-13 there are presented curves of the relative flow through a narrowing nozzle and through an aperture with a sharp edge with identical area of cross

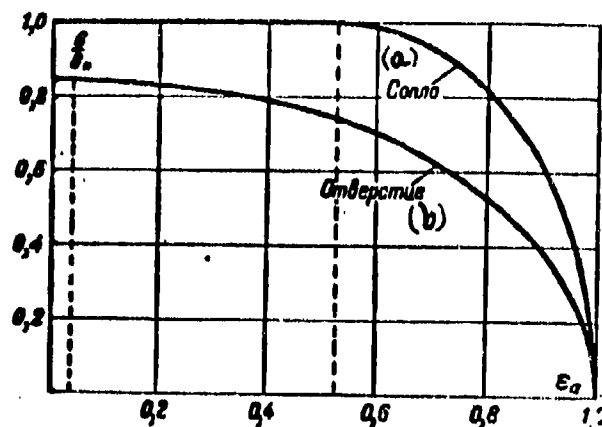

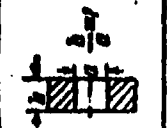





Fig. 6-13. Change of flow of gas through nozzle and aperture with a sharp edge with identical area of cross section ( $k = 1.4$ )  
KEY: a) Nozzle; b) Aperture.

Table 6-2

(a) форма отверстия						
(b) Второе критическое отношение давлений $\epsilon_{cr2}$	(d) Воздух	0.037	0.18	—	0.47	0.528
	(e) Воздух нап (неперпетуи)	0.13	0.27	—	—	0.546
(c) Коэффициент расхода $\mu_{cr2}$	(f) Воздух	0.85	0.88	0.90	0.92	0.99
	(g) Воздух нап (неперпетуи)	—	—	—	—	0.983

KEY: a) Shape of aperture; b) Second critical ratio of pressures; c) Coefficient of flow  $\mu_{cr2}$ ; d) Air; e) Water vapor (superheated); f) Air; g) Water vapor (superheated).

section depending on  $s_a$  for air. In both cases the flow is related to the critical flow through the nozzle.

We shall establish now the shape of curve of relationship  $\frac{G}{G_{**}} = f(s_a)$  for an aperture with a sharp edge. The maximum flow of gas through aperture can be calculated by the formula

$$G_{**} = \left( \frac{2}{k+1} \right)^{\frac{k+1}{2(k-1)}} \sqrt{k} \mu'_{orn} F \sqrt{g p_0 \gamma_0} \quad (6-23)$$

where  $F$  is the area of aperture;

$\mu'_{orn}$  is the coefficient of flow through aperture at  $s_a = s_{**}$ ;

$p_0, \gamma_0$  are parameters of the gas in the reservoir at a significant distance from aperture (parameters of stagnation).

The flow of gas through aperture at an arbitrary  $s_a$  can be found by the equation

$$G = \mu_{orn} F \sqrt{g p_0 \gamma_0} s_a^{\frac{1}{k}} \sqrt{\frac{2k}{k-1} (1 - s_a^m)} \quad (6-24)$$

We shall designate the reduced flow through aperture with sharp edge

$$q_0 = \frac{G}{G_{**}}.$$

Then the flow through aperture

$$G = q_0 G_{**} = \left( \frac{2}{k+1} \right)^{\frac{k+1}{2(k-1)}} \sqrt{k} g \mu'_{orn} q_0 F \sqrt{p_0 \gamma_0} \quad (6-24a)$$

The formula for the reduced flow of gas  $q_0$  on the basis of equations (6-23)

and (6-24) acquires such a form:

$$q_0 = \left( \frac{k+1}{2} \right)^{\frac{k+1}{2(k-1)} \frac{\mu_{orn}}{\mu'_{orn}}} s_a^{\frac{1}{k}} \sqrt{\frac{2k}{k-1} (1 - s_a^m)} \quad (6-25)$$

Values of coefficients of flow  $\mu_{orn}$  and  $\mu'_{orn}$  may be taken from Tables 6-1 and 6-2.

There may be obtained a simple approximate expression for  $q_0$ , assuming that the dependence  $q_0$  on  $s_a$  at  $s_a > s_{**}$  is described by the equation of ellipse:

$$q_0^2 + \frac{(s_a - s_{**})^2}{(1 - s_{**})^2} = 1, \quad (6-26)$$

or

$$(1 - s_{**})^2 q_0^2 = 1 - 2s_{**}(1 - s_a) - s_a^2. \quad (6-27)$$

A comparison between accurate and approximate solutions shows that equation of ellipse with a great degree of accuracy describes the dependence of the reduced flow  $q_0$  on  $\epsilon_1$  for an aperture with a sharp edge, the same as for a narrowing nozzle. The difference consists only in the fact that in the case of an nozzle a maximum flow will be attained with the first critical ratio of pressures  $\epsilon_1$ , and in the case of an aperture with the second critical ratio of the pressures  $\epsilon_{11}$ .

Hence it follows that the effect of the shape of aperture on the flow may be evaluated by an appropriate selection of the second critical ratio of pressures since it should be expected that the elliptic relationship will be accurate for any configuration of the walls if it is accurate for the two extreme cases: nozzles and apertures with sharp edges.

Experiments made for the purpose of determining the flow of air and superheated vapor through apertures of different shape, confirm the elliptic dependence  $q_0$  on

$\epsilon_1$ . For a superheated water vapor, second critical ratio of pressures according to experimental data amounts to  $\epsilon_{11} \approx 0.13$  (Table 6-2). Consequently, with a decrease in  $k$  (coefficient of isentropy)  $\epsilon_{11}$ , the same as  $\epsilon_1$  increases. Hence it may be concluded, that a change of the physical constants of gas exerts an influence on  $\epsilon_{11}$  in the same direction as on  $\epsilon_1$ . This conclusion is clearly corroborated by the data presented in the Table 6-2.

Thus, we see that properties of a stream, flowing from a reservoir, vary considerably depending on the character of the distribution of parameters in the cross section of stream. With a nonuniform distribution of parameters of the flow there are ascertained new properties, and the equations, describing the outflow of a uniform stream, prove to be inapplicable.

We note that the dimensions of the chamber from which the stream flows exerts a certain influence on the spectrum of stream after aperture. The theoretical dependence of coefficient of contraction of two-dimensional stream on dimensions of the chamber and speed in the minimum section  $M_2$ , according to G. A. Dombrovskiy, is

presented in Fig. 6-14. The curves show that with an increase of  $\frac{a}{a_0}$  (with an increase relative to dimension of aperture) and  $M_2$ , the coefficient of contraction increases. Influence of  $\frac{a}{a_0}$  is reflected perceptibly only at  $\frac{a}{a_0} > 0.3$ .

For calculating the aperture or slot at different initial and finite pressures it is possible to use the method, described above for a nozzle. By proceeding from the condition of constant temperature in the reservoir, we construct a grid of relative flows of gas through the aperture, each curve of which  $q_s = f(\epsilon_a)$  corresponds to a constant initial relative pressure  $\epsilon_{0n} = \frac{P_{0n}}{P_{01}}$ .

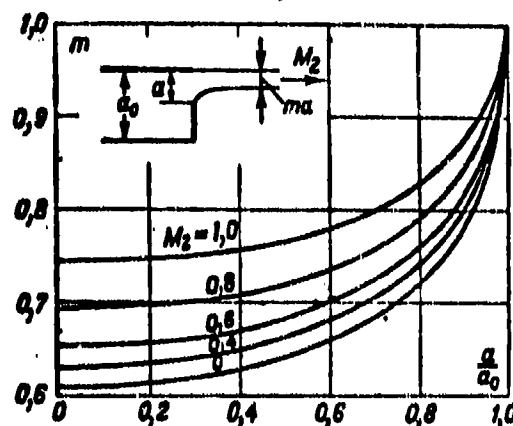


Fig. 6-14. The dependence of coefficient of contraction of a two-dimensional stream on dimensions of chamber and speed in minimum section according to G. A. Dombrovskiy.

#### 6-4. Calculation of Supersonic Nozzle

Supersonic nozzles (Laval nozzles) are used for creating flows of gas with supersonic speeds. These nozzles are used as one of chief elements of jet engines, and also in steam turbines, ejectors and other apparatuses.

An analysis of one-dimensional flow has shown that a flow with supersonic speed can be obtained in a tube with minimum section, if in this section there will be attained a critical speed.\* In accordance with this the Laval nozzle is a tube

---

\*There is considered the particular case of an adiabatic motion of gas in a tube without an energy exchange with the environment. In a general case, the condition of a minimum of a section is not necessary for a transition into a region of supersonic speed.



of variable section, consisting of two parts. The speed of the gas flowing through a normally operating Laval nozzle continuously increases, where in the narrowing part of nozzle the speed is subsonic, and in expanding portion is supersonic (Fig. 6-15).

An elementary calculation of supersonic nozzles is made by the equation of continuity, where there should be given the parameters of gas before nozzle, the

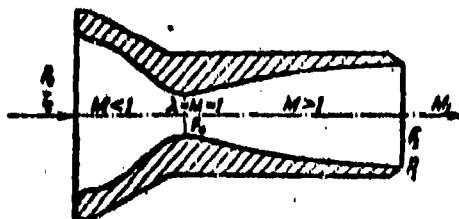


Fig. 6-15. Laval nozzle.

flow of gas and the speed of flow in exit section.

By ignoring the effect of friction, it may be assumed a critical speed is in the minimum section of nozzle. The dimensions of this section are determined by the equation (6-5):

$$F_* = \left(\frac{k+1}{2}\right)^{\frac{1}{k-1}} \sqrt{\frac{R}{gk}} \frac{G_* \sqrt{T_*}}{\rho_*}.$$

The exit section is calculated by the formula

$$F_1 = \frac{F_*}{q_1} = \frac{G_*}{\lambda \sqrt{\frac{2k}{k+1} \rho_* \left(1 - \frac{k-1}{k+1} \lambda^2\right)^{\frac{1}{k-1}}}}. \quad (6-28)$$

Intermediate sections of nozzle can be determined, depending on the speed or ratio of pressures from formula for a reduced flow:

$$\begin{aligned} q &= \frac{F_*}{F} = \left(\frac{k+1}{2}\right)^{\frac{1}{k-1}} \lambda \left(1 - \frac{k-1}{k+1} \lambda^2\right)^{\frac{1}{k-1}} = \\ &= \left(\frac{k+1}{2}\right)^{\frac{1}{k-1}} \sqrt{\frac{k+1}{k-1}} \sqrt{1 - \frac{k-1}{k}}, \end{aligned} \quad (6-29)$$

where  $F$  is the intermediate section;

$\lambda$  and  $\epsilon$  are the speed and relative pressure ( $\epsilon = \frac{p}{p_0}$ ) corresponding to this section.

If there is given the distribution of speeds or pressures along the axis

of nozzle, then formula (6-29) determines the profile of nozzle. However, such a calculation of the intermediate sections, and indeed the profile (shape) of nozzle is approximate and cannot assure a given distribution of the pressures, since the speed in the section is not constant either in magnitude, or in direction, and, consequently, flow is not one-dimensional.

In cases, when it is important to obtain only a given average speed at exit of nozzle, and the character of distribution of speeds along the section are not of great importance, intermediate sections of nozzle are not calculated and for simplicity in manufacturing, both as the narrowing, and also the expanding parts are made conical. In the narrow section and moreover at the exit the field of speeds are nonuniform.

In certain cases for decreasing the non-uniformity of the field of speeds, the narrowing part of nozzle is calculated by the Vitoshinskiy formula (6-7), and aperture angle of conical expanding part is chosen small (up to  $12^\circ$ ). Experience shows, however, that these measures are not always adequate for obtaining of the required field of speeds.

The best results can be obtained by using a shaped nozzle, whose expanding part is calculated by method of characteristics. Considering a two-dimensional nozzle and disregarding influence of friction, we assume that all parameters of flow remain constant along lines, normal to flat walls. Let us assume that in narrow section of the nozzle AA' flow has a uniform field of speeds  $M = 1$  (Fig. 6-16).

For accelerating the flow, having in section AA' a critical speed, it is necessary to enlarge the section of nozzle. For this purpose we shall change the direction of the wall AA<sub>1</sub> and correspondingly A'A'<sub>1</sub> by a small angle from axis of nozzle  $\delta_0$ . Then at points A and A' there will develop weak waves of rarefaction. At the intersection of these waves the flow is accelerated and acquires a speed

$\lambda_{1,2}$ , which one can determine by means of diagram of characteristics (Fig. 6-16,b) or by means of tables.

The state of the flow in the critical section AA' in the diagram of

characteristics is expressed by the point  $(A_1, A_1')$  on the circle  $\lambda=1$ . The speed of the flow in region 1 is determined at the point  $1'$  on the epicycloid  $A_1'1'$ , if we draw a half-line from the origin of the coordinates at an angle of  $\delta_1$  to the direction of nozzle axis  $x$ . Point  $2'$  which corresponds to region 2 of the flow is symmetrically situated. Through points  $1'$  and  $2'$  passes the circle, corresponding to the speed  $\lambda_{1,2}$ .

The continuous expansion of the gas in stationary waves of rarefaction, appearing at points  $A$  and  $A'$ , can be replaced by drawing from these points the sound waves  $AE$  and  $A'E$  at an angle  $\alpha_{m1} + \frac{\delta_1}{2}$  to the direction of axis of nozzle ( $\alpha_{m1}$  is the angle of sound wave, corresponding to speed of flow in region 1).

In diagram of characteristics we shall find the point  $E'$ , corresponding to deflection of flow by an angle  $\frac{\delta_1}{2}$ , and we shall determine the magnitude of speed  $\lambda_{AE}(\lambda_{A'E})$ , corresponding to the direction of sound wave  $AE'$ .

In the transition from regions 1 and 2 into region 3, the streamlines intersect the waves  $EE_1$  and  $EE_2$  (flow is accelerated) and are turned by an angle of  $\delta_2$  to the axis of nozzle. Consequently, in regions 3 the speeds of flow have a direction, parallel to the axis. In the diagram of characteristics there is readily determined point  $3'$ , corresponding to this region of flow.

At points  $A_1$  and  $A_1'$  (Fig. 6-16,a) the walls of the nozzle again change in direction by an angle of  $\delta_2$ . In the transition to regions 4 and 5 the flow is accelerated and acquires a speed  $\lambda_{4,5}=\lambda_2$ . Analogously there can be found the magnitude and direction of speed in regions 6, 7, 8, et cetera, and also directions of the sound waves, which are boundaries of these regions.

As a result of a successive change in direction of walls of nozzle there will be formed two stationary waves of rarefaction of finite intensity, during transition through which the flow expands and attains given value of the speed.

The speed  $\lambda_1(M_1)$  will be attained within limits of zone of intersection of waves of rarefaction in the sector  $HL$ . After last characteristic  $LQ$ , angle of slope of

which is equal to

$$\alpha_{mLQ} = \arcsin \frac{1}{M_1}.$$

flow must have a uniform field of speeds, at each point of which the speed is equal to  $M_1$ . All the streamlines to the right of LQ must be parallel to axis of nozzle.

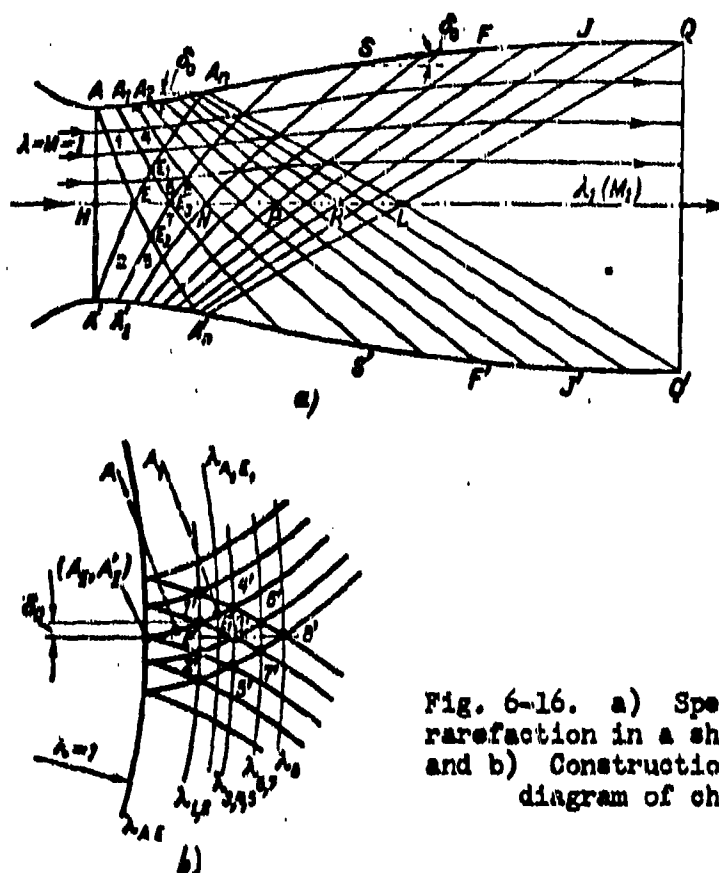


Fig. 6-16. a) Spectrum of waves of rarefaction in a shaped Laval nozzle and b) Construction of process in a diagram of characteristics.

It follows from this that each sound wave from opposite wall, going out beyond the limits A<sub>n</sub>L, must be extinguished by a corresponding change in direction of wall at an angle equal to the angle of deflection of flow in such a wave. Starting from the point A<sub>n</sub>, wall of nozzle changes direction in such a manner that the waves NS, PF, et cetera, incident to it are not reflected.

Thus, in the first sector the walls of nozzle change in direction with respect to axis of nozzle, and in the second sector, where waves from the opposite wall are extinguished, the slope of wall gradually decreases and at the point Q δ<sub>0</sub> = 0.

At the limit of decrease of δ<sub>0</sub>, broken wall AA<sub>n</sub>Q changes into a smoothly curved

wall.

Near the narrow section, where the speed of flow insignificantly exceeds the critical speed, the accuracy of the calculation by the method of characteristics of first section of nozzle is inadequate, especially if calculating value of  $\lambda_1$  is small.

The selection of profile of wall therefore is made by starting from a certain initial section, where flow already possesses a supersonic speed. The distribution of speeds in initial section should be known.

In certain cases initial section of nozzle is made conical. Angle of conicity  $\gamma_0$  is selected depending upon the given value of  $\lambda_1$  and amounts to half of the maximum angle of deflection of flow with an increase of speed from  $\lambda=1$  to  $\lambda_1$ .

Also widely used are the analytical methods of calculating supersonic nozzles, developed by S. A. Khristianovich and others.

The methods of calculating and profiling supersonic nozzles do not take into consideration the influence of viscosity. On wall of nozzle there will form a boundary layer, the thickness of which increases along the length of nozzle. Let us note that in accordance with conclusions of Chapter 5 influence of friction results in the displacement of critical section, which is displaced to the expanding section of nozzle.

Boundary layer on walls causes a certain redistribution of speeds and pressures of the flow along the walls and a displacement of characteristic lines. The actual speeds and pressures in different sections and at the exit of nozzle will differ from the calculated values.

For obtaining a given distribution of speed and calculated value  $\lambda_1$  it is necessary to increase area of cross sections of the nozzle, obtained under the condition of isentropic flow. An accurate solution of such a problem requires a calculation of the boundary layer on walls of the nozzle (Chapter 5).

The approximate solution can be found, if there is known the distribution of

drag coefficients along axis of nozzle.

The specific work of the frictional forces for a tube of variable section (nozzle) can be presented in the following form:

$$dL_{fr} = \tau \frac{c^2}{2g} \cdot \frac{dx}{D}.$$

where  $\frac{dx}{D} = \frac{dx}{D_*}$ ;  $\bar{D} = \frac{D}{D_*}$ ;  $D$  — diameter of throat section of nozzle.

The increment of entropy, caused by the influence of frictional forces is equal to

$$d\bar{S} = \frac{dS}{AR} = \frac{dL_{fr}}{RT} = \tau \frac{c^2}{2gRT} \cdot \frac{dx}{D}, \quad (6-30)$$

where  $\bar{S} = \frac{S}{AR}$  is the reduced entropy.

On the basis of (6-30) after simple transformations we find such expression for drag coefficient:

$$\tau = \frac{k+1}{k} \cdot \frac{\bar{D}}{\lambda^2} \left( 1 - \frac{k-1}{k+1} \lambda^2 \right) \frac{d\bar{S}}{dx}.$$

In considering that according to formula (5-12)

$$\frac{d\bar{S}}{dx} = \frac{1}{c_0} \cdot \frac{dc_0}{dx},$$

where  $c_0 = \frac{p_{01}}{p_0}$  is the ratio of pressures of stagnation at entry into nozzle and in the given section, we can obtain:

$$\ln c_0 = \frac{k}{k+1} \int_0^{\bar{x}} \frac{c_0^2 d\bar{x}}{\bar{D} \left( 1 - \frac{k-1}{k+1} \lambda^2 \right)}. \quad (6-31)$$

If there is known the form of function  $c_0(\bar{x})$ , then by means of (6-31) there is readily found the change in  $c_0$  along the length of nozzle. The values  $c_0(\bar{x})$  may be taken from the graph in Fig. 5-12. In accordance with equation of continuity (2-41) the connection between sections in real ( $F$ ) and isentropic ( $F_0$ ) flows can be presented as:

$$1 = l_0 \frac{q_0}{q} c_0. \quad (6-32)$$

where  $l = \frac{F}{F_0}$ ;  $l_0 = \frac{F_0}{F_0}$ ;  $q_0 = \frac{p_0 c_0}{p_0 a_0}$ ;  $q = \frac{p_0}{p_0 a_0}$ ; and  $q_0$  are the reduced flows for theoretical and real processes.

Investigations, made under the direction of A. A. Gukhman, theoretically and experimentally showed the possibility of a linear approximation of law of change

of entropy along the length of nozzle.

Consequently, if one were to assume

$$\mu = \frac{dS}{dx} = \frac{d \ln i_0}{dx} = \text{const.}$$

then, after substituting in the critical section  $\bar{x} = 0$  by means of (6-32) we shall find ( $i_0 = 1$ ):

$$\ln i_0 = \ln (i_0) = \mu \bar{x},$$

or

$$i = \frac{1}{q} e^{\mu \bar{x}}. \quad (6-33)$$

Experiments show that for nozzles with a polished internal surface it is possible to assume  $\mu \approx 0.011 - 0.018$ .

Equation (6-33) is used for solving direct and inverse problems. In first case,  $i(\bar{x})$  and  $\mu$  are given; according to formula (6-33) there is established the reduced flow  $q(\bar{x})$ ; the distribution of parameters of flow along the length of channel ( $\lambda, p, T$ ) is established by tables of gas-dynamics functions. In solving the inverse problem by the known distribution of  $q(x)$  or  $\lambda(\bar{x})$  there are established those sections in which there are attained the given values  $\lambda(i(\bar{x}))$ . The values  $i_0(\bar{x})$  in both cases can be found by formula (6-32) (here  $q_t = q$ ).

The influence of friction on the speed and other parameters in exit section of nozzle is evaluated by means of the coefficient of speed, which is expressed by the formula

$$\varphi_e \approx \sqrt{1 - \zeta_e} = \sqrt{1 - \frac{2}{k-1} M_{1t}^2 \left( \frac{1}{i_0^m} - 1 \right)}, \quad (6-34)$$

where  $\zeta_e = \frac{2}{k-1} M_{1t}^2 \left( \frac{1}{i_0^m} - 1 \right)$  is the loss factor of energy in nozzle;  
 $i_0 = \frac{p_e}{p_{01}}$  is the ratio of pressures of stagnation at exit and at entry into nozzle;

$M_{1t}$  is the theoretical value of M number in exit section.

From formula (6-34) it follows that magnitude  $\epsilon$ , ambiguously is associated with the coefficients  $\varphi_e$  and  $\zeta_e$ . With identical values  $\epsilon$ , the coefficients  $\varphi_e$  and  $\zeta_e$  vary, depending upon magnitude of available energy, proportional to  $M_{1t}^2$ .

In Fig. 6-17 graphs establishing a connection between  $\varphi$ ,  $\epsilon$ , and  $M_{1t}$  are presented.

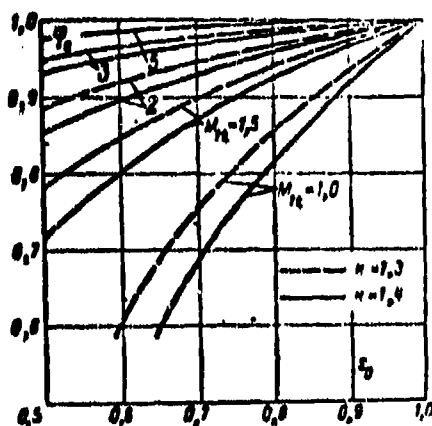


Fig. 6-17. Dependence of coefficient of nozzle speed  $\varphi$  on  $\epsilon$  and  $M_{1t}$ .

#### 6-5. Two-dimensional Laval Nozzle under Nonrated Conditions.

Under operating conditions, parameters and also the flow of gas through a nozzle may vary. Here it is essential that ratios of the pressures  $\epsilon = \frac{p_a}{p_0}$ , where  $p_a$  is as previously the pressure of the environment, change.

We shall consider the operation of a nozzle with variable modes as a first approximation, disregarding friction and thermal conductivity. In Fig. 6-18, there is shown the distribution of pressures in a Laval nozzle, at different pressures of the environment  $p_a$ . The curve AOB, constructed on basis of equation (6-29), corresponds to rated conditions of flow in a nozzle, with which  $\epsilon = \epsilon_1 = \frac{p_1}{p_0}$ .

We assume that at a constant value of  $p_0$ , the pressure of the environment varies within the limits  $p_1 \leq p_a \leq p_0$ , and we shall trace change in structure of flow both within the nozzle, and also after it. It is possible to distinguish four characteristic groups of modes of flow; within the limits of each group of modes the picture of the flow qualitatively is kept constant.

The first group of modes is characterized by lower pressures of medium  $\frac{p_a}{p_0} < \frac{p_1}{p_0}$ . In this case at exit section of nozzle there is established a rated pressure  $p_1$ ,



since the parameters of gas in reservoir, and consequently, also the flow of gas through nozzle do not change. This is obvious also because in supersonic stream the disturbance is not propagated opposite the flow and consequently the drop in pressure of medium will not be reflected in exit section of nozzle. In whole intermediate section of nozzle therefore the pressures also remain rated. Parameters of flow change after the nozzle, in the free supersonic stream.

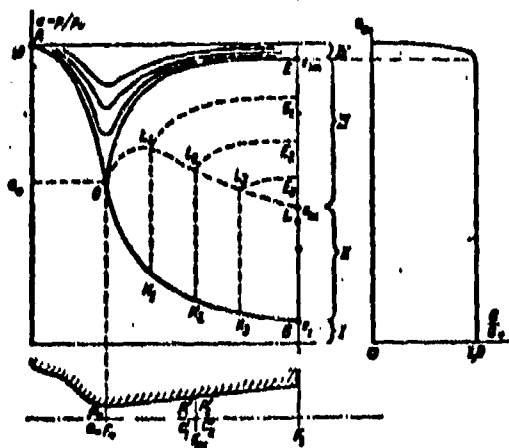


Fig. 6-18. Diagram of distribution of pressures in a Laval nozzle during different modes [of flow].

In Fig. 6-19, there are presented diagrams of spectra of stream at exit of two-dimensional nozzle during a lower counterpressure. At the angular points A and A<sub>1</sub> pressure varies from a value of p<sub>1</sub> up to p<sub>a</sub>. The streamlines at points A and A<sub>1</sub> are deflected by a certain angle  $\theta$  in connection with the generation at these points of waves of rarefaction, which cause an isentropic expansion of the gas from p<sub>1</sub> up to p<sub>a</sub>. Along characteristics AC, A<sub>1</sub>C and AB, A<sub>1</sub>B in accordance with properties of rectilinear characteristics, the pressure does not change. Consequently, in regions 2 there are established a constant speed and pressure p<sub>a</sub>, equal to the ambient pressure. Waves of rarefaction AD<sub>1</sub>E<sub>1</sub>A and A<sub>1</sub>DEA<sub>1</sub> emerge on free edge of stream, along which the pressure remains constant and equal to p<sub>a</sub>. In the zone CBC<sub>1</sub>B<sub>1</sub> of the intersection of these waves, as is already known, there occurs a distortion of the characteristics. As a result the angle of sound wave BD becomes less than the angle of wave A<sub>1</sub>C and  $\alpha_{mBD} < \alpha_{mAC}$ ; correspondingly  $\alpha_{mCD} < \alpha_{mBD}$ ;  $\alpha_{mCH} < \alpha_{mBD}$ .

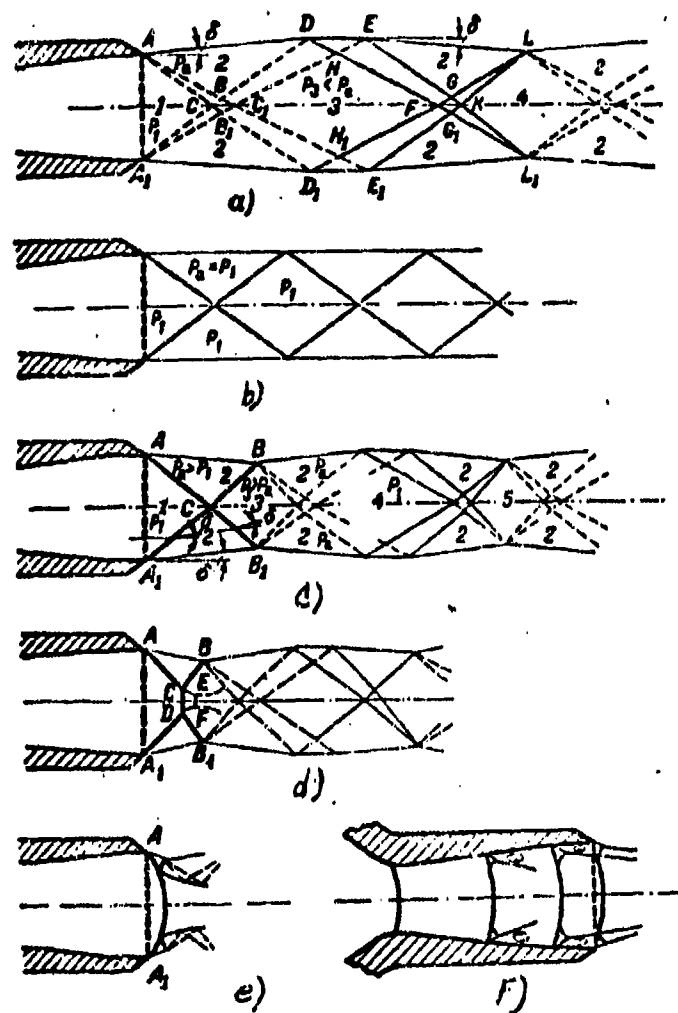


Fig. 6-19. Diagrams of spectra of stream after two-dimensional nozzle during different modes of flow.

From free edge, the wave of rarefaction is reflected, as a compressional wave, in passage through which the streamlines are deformed, by being deflected at an angle  $\delta$  to the axis of stream. At points L and L<sub>1</sub> compressional waves emerge on the free boundary.

After the intersecting waves of rarefaction (in region 3) there is established a pressure, less than pressure of environment (stream is reexpanded). In region 4 after intersection of compressional waves the pressure rises to a pressure  $p_1$  in exit section of nozzle AA<sub>1</sub>. Towards the section LL<sub>1</sub> the stream contracts, and its

width is equal to the width of exit section  $AA_1$ . In regions 1, 3, and 4 the streamlines are rectilinear and parallel to the axis of nozzle. In regions 2, the streamlines also are rectilinear and parallel, but located at an angle  $\delta$  to the axis of nozzle. For the considered first group of modes with the adopted assumptions, there are no losses of energy in the stream.

As the pressure of the medium  $p_a$  increases, the characteristics  $AB$ ,  $ED$ ,  $A_1B_1$ ,  $B_1D_1$ ,  $C_1E$  and  $C_1E_1$  change their position in the stream. Since, the difference between pressures in regions 1 and 2 in this respect decreases, then the angles of indicated characteristics increase and the intensity of waves of rarefaction  $AD_1E_1A$  and  $A_1DEA_1$  decreases. Angles of deflection of streamlines in region 2 also decrease. Reaching a limit, under rated conditions ( $p_a = p_1$ ), the characteristics  $AE_1$  and  $A_1E$  merge with the waves  $AD_1$  and  $A_1D$ . The stream acquires formula given in Fig. 6-19, b.

The second group of modes characterizes the outflow from a Laval nozzle with a higher counterpressure of the medium or with a lower initial pressure ( $p_a > p_1$ ). By knowing the rated speed in exit section of nozzle  $\lambda_1$ , there is readily determined then the value of pressure of medium at which in exit section there will form a normal shock wave [Fig. 6-18 and formula (4-20)]:

$$p_{1k} = p_1 \frac{\lambda_1^2 - \frac{k-1}{k+1}}{1 - \frac{k-1}{k+1} \lambda_1^2} \quad (6-35)$$

The considered second group of modes is characterized by following relationship of the pressures of the medium:  $p_1 < p_a < p_{1k}$ . In this case in section  $AA_1$  (Fig. 6-19, c) there also is established a rated pressure  $p_1$ . If pressure of medium  $p_a$  comparatively slightly exceeds the pressure  $p_1$ , then at points  $AA_1$  there will form two oblique shocks:  $AC$  and  $A_1C$ , intersecting at point  $C$ . The oblique shocks emerge onto the free edge of stream (after intersection at point  $C$  the angles of oblique shocks increase). In the passage through the shocks  $AC$  and  $A_1C$  the streamlines are deflected at angle  $\delta$ , which readily is calculated. In regions 2, the pressure is equal to the ambient pressure; the streamlines are parallel to each other at the free edge of stream  $AB$  and  $A_1B_1$ .

From the condition of symmetry after the shocks  $CB$  and  $CB_1$ , the speed must become parallel to axis of flow, i.e., the streamlines must be turned in the opposite direction by an angle  $\delta$ . In this region, there is established a pressure, higher in comparison with the pressure of medium. Consequently, at points  $B$  and  $B_1$  from the direction of stream the pressure is higher, and from these points there are propagated waves of rarefaction. In the transition through the waves of rarefaction the pressure drops to the ambient pressure, and the streamlines are deflected from the axis: stream expands. After the intersection of waves of rarefaction, the pressure is equal to  $p_1$ . At points of emergence of waves of rarefaction onto free edge stream has a width, equal to  $AA_1$ . The considered group of modes is characterized by losses of energy in the stream, caused by an increase in entropy in the system of oblique shocks. Field of pressures along the axis and in the cross sections acquires significant non-uniformity.

The described scheme of outflow is possible only with a small exceeding of the pressure  $p_a$  above  $p_1$ , when the angle  $\delta$  is small. At a certain pressure of the medium  $p_{1k} < p_a < p'_{1k}$  spectrum of stream at exit of nozzle varies. The existence of a system of two oblique shocks with supersonic speed after the point of their intersection becomes impossible. At  $p_a > p_{1k}$  angle of oblique shocks, going out from the edges  $A$  and  $A_1$ , attains a value, with which in a certain region after the shock the speeds will be subsonic and spectrum of outflow abruptly will change (Fig. 6-19, d and e).

For a two-dimensional nozzle the deflection angle of the streamline  $\delta_{m1}$  (or angle of shock  $\beta_{m1}$ ), with which the picture of outflow will change; it is readily determined by means of a diagram of shock polars.

Shock polar  $AK1$  (Fig. 6-20) corresponds to a rated speed  $\lambda_1$  of the flow in exit section of nozzle (segment  $O1$ ) and, consequently, in entire region 1 (Fig. 6-19, c). At a certain pressure of the medium  $p_a = p'_{1k}$  the speed after the shock is measured by sector  $O2$  (speed in region 2 in Fig. 6-19, c); the limiting speed

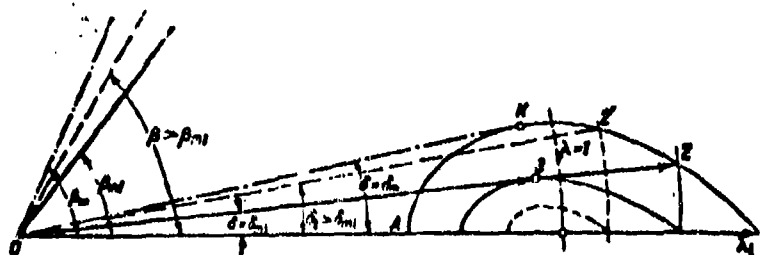


Fig. 6-20. Determination of mode of flow after shocks, forming under nonrated conditions in Laval nozzle, by means of diagram of shock polars.

after oblique shocks CB and CB<sub>1</sub> in region 3, where the streamlines are parallel to axis of stream, is determined by sector 03 (Fig. 6-20).

The magnitude of the pressure  $p'_{1k}$  can be determined by the formula (4-13):

$$p'_{1k} = \frac{2k}{k+1} p_1 \left( \frac{2}{k+1} \cdot \frac{\lambda_1^2 \sin^2 \theta_{m1}}{1 - \frac{k-1}{k+1} \lambda_1^2} - \frac{k-1}{2} \right). \quad (6-36)$$

In this case in the stream after the shocks CB and CB<sub>1</sub> (Fig. 6-19,c) the speeds will be subsonic.

If  $p_u > p'_{1k}$ , then at the intersection of shocks CB and CB<sub>1</sub> the flow no longer can be deflected by an angle  $\delta_1 > \delta_{m1}$  (dotted line in Fig. 6-20), at which it was deflected during transition through AC and A<sub>1</sub>C. Diagram of outflow qualitatively will vary. At exit of nozzle there will form a bridge-like shock.

From the angular points A and A<sub>1</sub> (Fig. 6-19,d) there are propagated oblique shocks AC and A<sub>1</sub>D, changing into normal (or--with a nonuniform distribution of speeds--curved) shock, after which the speeds will be subsonic. After the oblique shocks CB and DB<sub>1</sub> the speeds remain supersonic, but the pressure is found to be higher than the pressure of medium  $p_u$ .

After the normal shock CD, the pressure is much higher than after the shocks CB and DB<sub>1</sub>. Consequently, in the stream there is created a complex distribution of pressures by section: the leveling-off of pressures results in a sharp decrease of  $p$  at the core of stream, i.e., to an acceleration of core which is accompanied by a decrease of its section. The boundaries CE and DF form a narrowing section of core, along which the speeds increase and in the section EF attain sonic values.

In addition, internal flow of subsonic speeds immediately after the shock CD is accelerated by the external supersonic flow. The oblique shocks CB and DB<sub>1</sub> are reflected from the free edge in the form of waves of rarefactions, which also accelerate the core of stream. As a result the speed of the internal flow becomes supersonic. The intensity in the change of pressure in a normal shock CD and after according to data of A. A. Gukhman and A. F. Gandel'sman for two modes of flow, is illustrated by curves in Fig. 6-21. Experiments corroborate that in very short sector after the shock the flow attains a rated pressure p<sub>1</sub> and correspondingly a supersonic speed.

Thus, at the pressure of external medium  $p_a > p'_{1k}$ , the system of intersecting oblique shocks is destroyed and changes into bridge-like shock. This phenomenon analogously is considered in Chapter 4 with cases of irregular reflection of an oblique shock from a rigid wall and the intersection of shocks.

With a further increase of pressure of medium the internal subsonic region of flow expands, and the external supersonic contracts. There exists such a pressure of the medium  $p''_{1k}$ , at which a curved shock is propagated almost over the entire section; in this case, after the shock AA<sub>1</sub> the speeds become subsonic (Fig. 6-19,e), with the exception a narrow peripheral region. This curved shock is situated close to the exit section of nozzle.

Pressure  $p''_{1k}$  will correspond to such a mode, with which angle of rotation  $\delta$  in the shocks AC and A<sub>1</sub>D (Fig. 6-19,d) becomes equal to the maximum angle  $\delta_m$  (dashed line in Fig. 6-20). After determining by means of shock polar the angle  $\beta_m$ , corresponding to angle of rotation  $\delta_m$ , it is possible, by formula (4-13) or (6-36), for an oblique shock to calculate the pressure  $p_{1k}$

$$p''_{1k} = \frac{2k}{k+1} p_1 \left( \frac{2}{k+1} \cdot \frac{\lambda_1^2 \sin^2 \beta_m}{1 - \frac{k-1}{k+1} \lambda_1^2} - \frac{k-1}{2k} \right). \quad (6-37)$$

At pressures of the medium  $p_a > p''_{1k}$  the shock is normalized and at  $p_a = p_{1k}$  [formula (6-35)] the shock has to become normal, being located in exit section of nozzle. Actually as the result of nonuniform distribution of speeds in conical

nozzles and of the influence of the boundary layer (viscosity) the shock enters inside nozzle somewhat distorted (Fig. 6-19,f).

If pressure after nozzle  $p_a > p''_{1k}$ , then in exit section of nozzle the pressure will vary. A further increase of pressure of medium ( $p_a > p_{1k}$ ) causes a displacement of the system of shocks inside nozzle, as was shown in Fig. 6-19,f.

From formula (6-36) for the ratio of the pressures at the boundaries of a shock it follows that a definite increase in pressure in shock corresponds entirely to a given speed  $\lambda_1$  of the supersonic flow before the shock. If pressure of medium exceeds the magnitude  $p_{1k}$ , then, obviously, conditions of equilibrium in normal shock will be disturbed and it will be transferred to that place in the flow which corresponds to an equilibrium position of the shock with new parameters of the medium. It must be remembered that a displacement of the shock inside nozzle is accompanied by new qualitative changes of flow (third group of modes). The pressure after the shock in this case is no longer equal to pressure of the medium; it is found to be less than  $p_a$ . Therefore, after a shock the pressure continues to increase. The distribution of pressures in the flow at intermediate positions of a normal shock is shown in Fig. 6-18 by the lines  $K_1 L_1 E_1, K_2 L_2 E_2$ , etc.

With an increase in pressure of medium, the shock continues to be displaced within nozzle towards minimum section. The relationship between degree of pressure recovery in the shock and the degree of an isentropic recovery of pressures after shock varies. In accordance with the subsequent displacement of shock in region of smaller speeds, the ratio of pressures on boundaries of shock decreases, and the degree of pressure recovery in divergent section of nozzle after shock increases\* (see curves  $L_1 E_1, L_2 E_2$ , et cetera, in Fig. 6-18).

At a certain pressure of the medium  $p_{1m}$  the shocks enters into minimum section of nozzle and disappears here. In minimum section of nozzle the parameters of flow

---

\*There is considered the case of continuous flow after the shock.

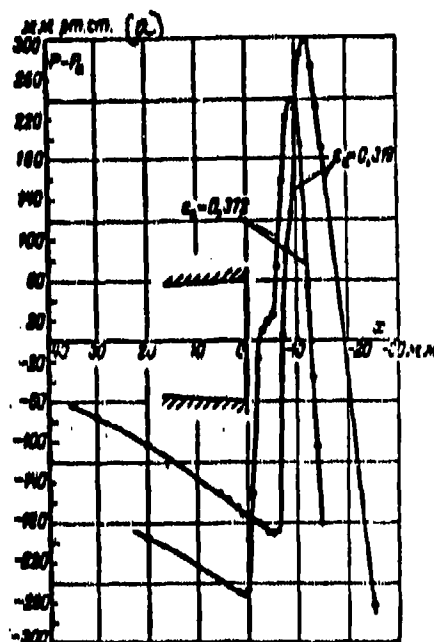


Fig. 6-21. Change of pressure along axis of nozzle and in stream after nozzle in modes with a bridge-like shock in exit section;  $M_1 = 1.5$ . Experiments of MO TsKTI.  
KEY: (a) mm Hg.



are critical, but a transition into the supersonic region does not occur. The line OE is boundary between subsonic and supersonic modes of the nozzle. At  $p_a > p_{1m}$  the speeds at all points of nozzle are subsonic and we obtain fourth group of modes of nozzle. For this group there are characteristic successive expansion of flow in converging part and compression in diverging section of nozzle. The minimum of pressure is attained in narrow section. It is known that such is the character of the distribution of pressures in Venturi tubes used for measurement of gas flows.

As long as  $p_a < p_{1m}$ , the flow of gas through nozzle during different counter-pressure is kept constant (in minimum section of nozzle the parameters of gas are critical, and the initial parameters remain constant). The change of flow starts only with counterpressures greater than  $p_{1m}$ , i.e., within limits of the fourth group of modes. In Fig. 6-18 to the right there is shown the change of gas flow through nozzle depending upon the counterpressure  $p_a$ .

The magnitude of pressure  $p_{1m}$  can be determined, if there are known the geometric characteristics of nozzle and parameters of flow before nozzle. Ignoring the losses in divergent section of nozzle, it is possible by means of the equation of continuity to obtain:

$$q_{1m} = \frac{F_2}{F_1},$$

where  $q_{1m} = \frac{p_{1m} c_{1m}}{p_a a_1}$  is the reduced flow in exit section of nozzle for the mode under consideration.

On the other hand,  $q_{1m}$  can be expressed in terms of the ratio of pressures  $\frac{p_{1m}}{p_a}$  by formula (6-4); then, remembering that

$$c_1 = \left( \frac{2}{k+1} \right)^{\frac{1}{k-1}},$$

we arrive at following equation for  $\epsilon_{1m}$ :

$$\epsilon_{1m}^{\frac{2}{k}} \left( 1 - \epsilon_{1m}^{\frac{k-1}{k}} \right) = \frac{k-1}{k+1} \epsilon_1^{\frac{2}{k}} \frac{1}{f_1^2}, \quad (6-38)$$

where  $f_1 = \frac{F_1}{F_2} = \frac{1}{q_{1m}}$ .

It is readily seen that equation (6-38) at  $f_1 = 1$  (converging nozzle) has a root  $\epsilon_{1m} = \epsilon_1 = \left( \frac{2}{k+1} \right)^{\frac{1}{k-1}}$ , and at  $f_1 = \infty$  (nozzle is designed for maximum speed

$l_{1max}$ )—two roots:  $\epsilon_{1m}=1$  and  $\epsilon_{1m}=0$ . The second value ( $\epsilon_{1m}=0$ ) corresponds to rated conditions of nozzle  $l_1=\infty$  and therefore it is not considered.

The dependence of  $\epsilon_{1m}$  on  $\frac{1}{l_1}$  by formula (6-38) is presented in Fig. 6-22.

For  $\epsilon_{1m}$  there may be obtained the simpler formula, if elliptic dependence between  $q_{1m}$  and  $\epsilon_{1m}$  is used.

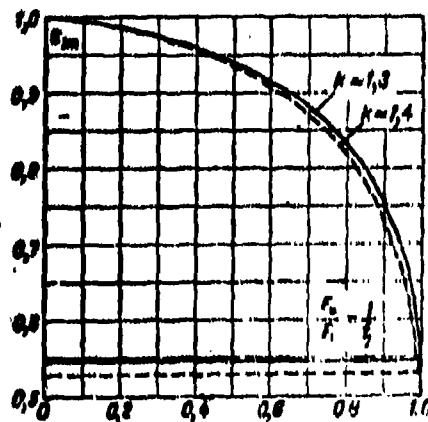


Fig. 6-22. Maximum ratio of pressures in nozzle  $\epsilon_{1m}$  depending on  $1/l_1$ .

According to equation (6-12) it is possible to write out:

hence

$$q_{1m} = \frac{1}{l_1} = \sqrt{1 - \frac{(\epsilon_{1m} - \epsilon_*)^2}{(1 - \epsilon_*)^2}};$$

$$\epsilon_{1m} = \epsilon_* + (1 - \epsilon_*) \sqrt{1 - \frac{1}{l_1^2}}. \quad (6-39)$$

In equation (6-39) it is possible to introduce the correction which takes into consideration losses in divergent section of nozzle. In this case

$$\epsilon_{1m} = \epsilon_* + (1 - \epsilon_*) \sqrt{1 - \frac{1}{T_1^2}}, \quad (6-39a)$$

where

$$T_1 = l_1 \epsilon_* = l_1 \frac{p_{01}}{p_{0*}}.$$

From equation (6-39a) it follows that with an increase in losses in nozzle, the magnitude of the maximum counterpressure  $p_{lm}$  decreases.

In determining  $\epsilon_{lm}$  with a consideration of the losses it is possible to use the graph in Fig. 6-22, plotting along the horizontal axis the magnitude  $\frac{1}{F_1}$ .

We now turn to a consideration of certain peculiarities of third group of modes, with shock waves within nozzle. It is necessary to consider that in reality in nozzle there is created not a normal shock, but a complex system of curved shocks. Of great importance here is the shape of expanding portion of nozzle. At small aperture angles of expanding portion in nozzle there appear shocks close to the normal in shape. Near the walls of nozzle there occurs a branching of the curved shock, acquiring the shape of a bridge-like shock (Fig. 6-19,f).

The third group of modes is characterized by significant losses of energy. Equally with the wave losses in the shocks there appear losses owing to separation of flow from walls of nozzle. The separation is accompanied by the formation of vortices and by the characteristic suction of gas from the environment.

In a number of cases, of practical interest is the determination of position of shock inside nozzle and of losses in nozzle with a given ratio of pressures. Since the structure of the shocks depends on the shape of divergent section of nozzle, then such problem cannot be accurately solved. An approximate solution can be obtained for simplest case, assuming the shock normal and flow in nozzle nondetached.

The problem is solved as follows. Before the shock, the expansion of gas follows along the curve AOB (Fig. 6-18), corresponding to rated conditions. Parameters of gas at entry and in sections K are associated by equations of isentropic flow. The change in state in section K is determined by the formulas of normal shock (line of process K, L, et cetera). Finally, after the shock it is possible to use data, characterizing losses in the diffuser (Chapter 7).

Let us assume that a normal shock appears in certain section of nozzle  $F_{ck}$ . From the equation of continuity there can be obtained the known relationship:

$$l_{ex} = \frac{F_{ex}}{F_1} = \frac{1}{q'_{ex}} \quad (6-40)$$

where  $q'_{ok}$  is the reduced flow before shock.

From formula (6-40) it is possible to express  $l_{ex}$  in terms of  $\lambda'_{ex}$  or by means of equation (6-4) in terms of ratio of pressures  $\epsilon'_{ex} = \frac{P'}{P_0}$ . The reduced flow in the same section after shock is equal to:

$$q''_{ex} = q'_{ex} \frac{P'_0}{P_0} = \frac{q'_{ex}}{\epsilon'_{ex}} \quad (6-41)$$

Here  $P'_0$  is the pressure of stagnation after shock.

From the equation of continuity for sections  $F_{ok}$  and  $F_1$  we shall obtain:

$$\frac{F_{ex}}{F_1} = \frac{q_a}{q'_{ex}} \cdot \frac{P_{0a}}{P'_0} = \frac{q_a}{q'_{ex}} \epsilon_{0a} \quad (6-42)$$

where  $q''_{ok}$  and  $q_a$  are the reduced flows after shock also in exit section with a given pressure  $P_a$ :

$\epsilon_{0a} = \frac{P_{0a}}{P_0}$  is the change in pressure of stagnation in divergent section of nozzle after shock.\*

Then by means of equation (6-40) we obtain:

$$l_{ex} = l_1 \frac{q_a}{q'_{ex}} \epsilon_{0a} \quad (6-43)$$

where  $\epsilon_{ex} = \frac{P'_0}{P_0}$  is the change in pressure of stagnation in the shock.

Substituting in equation (6-43) the values  $q'_{ok}$  and  $q_a$ , we find:

$$l_{ex} = l_1 \frac{\epsilon'_a \frac{1}{2} \sqrt{1 - \epsilon'_a \epsilon_{0ex}}}{\epsilon'_{ex} \sqrt{1 - \epsilon'^m_{ex}}} \left( \epsilon_{0ex} \right)^{\frac{k+1}{k}} \epsilon_{0a} \quad (6-44)$$

Here  $\epsilon'_a = \frac{P_a}{P_0}$  is the relative pressure after nozzle;

$$m = \frac{k-1}{k}.$$

If we disregard the losses in nozzle before the shock, then

$$\epsilon'_a = \epsilon_a = \frac{P_a}{P_0}.$$

---

\*The values  $\epsilon_{0a}$  can be taken according to experimental data, presented in Chapter 7.

Ratio of pressures of total stagnation in a shock is determined by equation (4-35). Formula (6-44) with the substitution  $\frac{P_0''}{P_0}$  from (4-35) become very cumbersome; significantly more convenient to use is equation (6-43), which contains tabular functions of the isentropic flow and of a normal shock. Being given the magnitude  $q'_{ck}$  from  $q'_{ck}=1$  to  $q'_{ck}=q_a$ , we find  $f_{ck}$  by formula (6-43). After determining by tables the corresponding values of  $\frac{P_0''}{P_0}$ , we shall find the magnitude  $q''_{ck} = q'_{ck} \frac{P_0''}{P_0}$ . An evaluation of the coefficient  $\epsilon_{0a}$  is made after calculating  $q''_{ck}$  ( $\lambda''_{ck}$ ) and  $\frac{F_1}{F_{ck}}$ . Then, there is determined the magnitude  $q_a = q''_{ck} \epsilon_{0a}$ . Knowing  $\epsilon_{0a}$  and  $\epsilon_a'' = \frac{P_a}{P_{0a}}$ , we find:

$$\epsilon_a = \epsilon_a'' \frac{P_{0a}}{P_0}.$$

Thus, it is possible to construct the dependence  $f_{ck}$  on  $\epsilon_a$  for different, but constant values  $f_1 = \frac{F_1}{F_0}$ . At  $\epsilon_a = \epsilon_{1m}$  the shock is located in the throat of nozzle and  $f_{ck}=1$ . At  $\epsilon_a = \epsilon_{1n}$  the shock is found in entry section of nozzle.

An analysis of formula (6-43) shows that in interval of changes  $f_{ck}$  from 1 to 2, the dependence  $f_{ck}$  on  $\epsilon_a$  may be expressed by the approximate formula

$$f_{ck} = A(\epsilon_{1m} - \epsilon_a) + 1. \quad (6-45)$$

where  $A$  is a dimensionless coefficient, depending on  $f_1$ .

After calculating  $f_{ck}$  by formula (6-45), it is possible to determine  $q'_{ck}$  and  $\lambda'_{ck}$  (or  $\epsilon'_{ck}$ ) and find  $\frac{P_0''}{P_0}$ ; then loss factor of energy in shock is determined by the formula (4-33) or by tables. Loss factor in expanding part after shock is determined by the formula

$$\zeta_A = \frac{2}{k-1} \frac{1}{M_{ck}^2} \left[ \frac{1}{M_{ck}^2} - 1 \right].$$

The coefficient of total losses in nozzle in modes of the third group is equal to:

$$\zeta_0 = \zeta_{ck} \frac{M_{ck}^2}{M_a^2} + \zeta_A \frac{M_{ck}^2}{M_a^2},$$

where  $M_a$  is the dimensionless speed, corresponding to a ratio of pressures  $\frac{P_a}{P_0}$ .

With a consideration of separation of flow, the losses and position of shock will differ from the calculated in the indicated manner. The separation of flow

after the shock results in a sharp increase of losses.\*

Results of an experimental investigation confirm the indicated peculiarities of flow in nozzle with unrated conditions.

Thus, in Fig. 6-23 there is presented the distribution of pressures along nozzle during different modes. The dashed lines show the results of calculation made by the above-indicated method. With decrease of aperture angle the computed curves approach the experimental. However, the coincidence of the calculated with the experimental is not entirely satisfactory. The increase of pressure at the location of shock occurs, although very intensively, not in a discontinuous manner. Consequently, only at very small aperture angles, shocks, corresponding to the third group of modes, are close to the normal. The experimental fact that the location of shock in nozzle depends on the means by which nozzle mode varies also deserves attention: by the change of initial pressure  $p_0$  or counterpressure  $p_a$ . This result is explained by influence of Reynolds number during interaction of a compression shock with the boundary layer.

The graphs in Fig. 6-24,a show\*\* that the position of system of shocks in nozzle

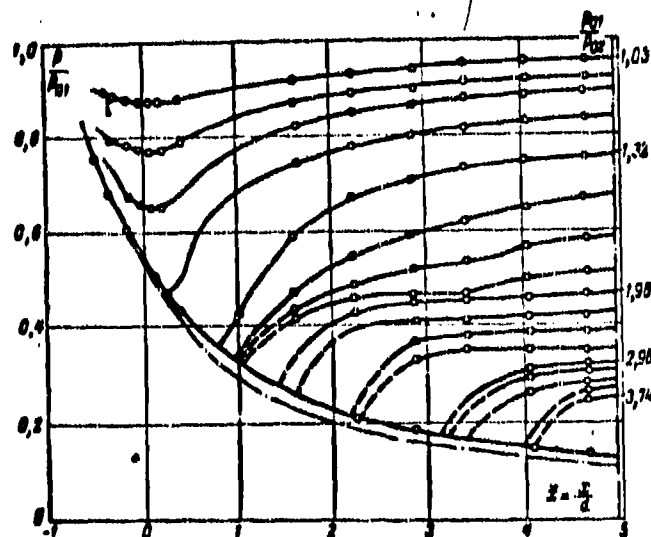


Fig. 6-23. Distribution of pressures in Laval nozzle with different modes and at different angles of aperture  $\gamma_0 = 18^\circ$ .

\*The effect of separation on the position of shock can be evaluated experimentally; in equation (6-45) it is possible to introduce experimental values of the coefficient A.

\*\*According to the data of Oswood and Cross.

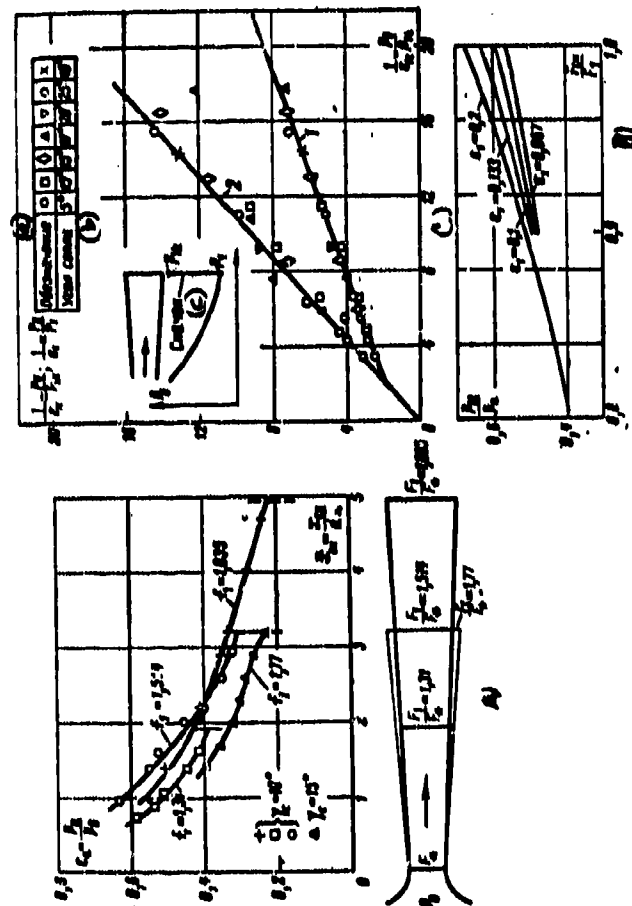


Fig. 6-24. Characteristics of two-dimensional Laval nozzles in third group of modes with shock waves in expanding portion.

A) dimensionless distance of system of shocks depending on ratio of pressure  $p_0/p^*$  and the geometric parameters  $r_1=r_2/r_0$  and  $r$ ; B) position of shock depending upon ratio of pressures in nozzle section and in medium with different calculated ratio of pressures; C) actual ratios of pressures  $p_0$  and  $p_{12}$  depending on the theoretical ratio of pressures  $p_0/p^*$ ; 1—shocks within nozzle,  $p_{12} = \frac{p_0}{p^*}$ ; 2—shocks in exit section  $p_{12} = 1/p^*$ ;

KEY: (a) Designation; (b) Nozzle angle; (c) Shock.

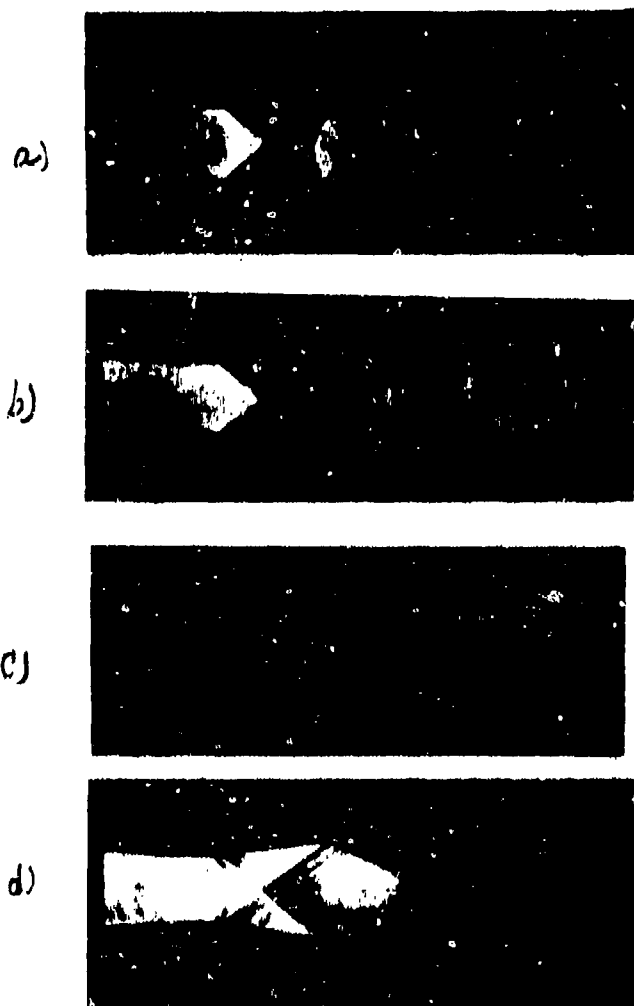


Fig. 6-25. Spectra of flow in a two-dimensional supersonic nozzle under nonrated conditions. Parameters of rated mode:  $\alpha = 0.052$ ;  $M_{tr} = 2.57$ ; aperture angle of nozzle  $\gamma_c = 19^\circ 40'$ .  
 a— $\alpha_a = 0.685$ ; b— $\alpha_a = 0.518$ ; c— $\alpha_a = 0.362$ ; d— $\alpha_a = 0.68$ .



depends on the basic geometric parameter  $f_1 = \frac{F_1}{F_0}$  and the aperture angle  $\gamma_c$ . With an increase of  $\gamma_c$  the system of shocks with the same ratio of pressures  $\epsilon_a$  is displaced towards the minimum section.

The relative pressure after the shock  $\epsilon_{1a}$  does not depend on  $\gamma_c$  (curve 1 in Fig. 6-24,c) (points with different  $\gamma_c$  lie on the same curve).

The change in position of shock depending upon calculated differential of pressures in nozzle  $\epsilon_1$  (or the same on  $f_1$ ) and the ratios of pressures in exit section ( $p_1$ ) and environment ( $p_0$ ) are corroborated by graphs in Fig. 6-24,b.

At the same time the experiments confirmed that in modes, corresponding to the distribution of shocks in exit section of nozzle, the pressure in this section (and speed before shock does not depend on the aperture angle  $\gamma_c$  (curve 2 in Fig. 6-24,c). The ratio of pressures  $\epsilon_1 = \frac{p_1}{p_0}$  differs from the calculated only by a magnitude characterizing the frictional losses.

The gradual development of a spectrum in a two-dimensional nozzle with the aperture angle of expanding part  $\gamma_c = 19^\circ 40'$  is shown in Fig. 6-25. At pressure in medium  $p_{im} > p_a > p_1$  (the third and second groups of modes) inside nozzle there appears a system of shocks. Closing this system is a shock of small curvature

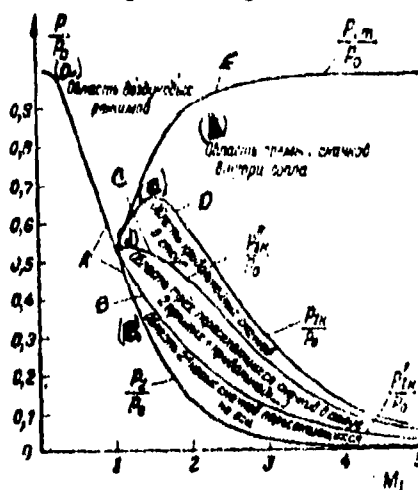


Fig. 6-26. Diagram of nonrated modes of Laval nozzle (after B. Ya Shumyatskiy).

KEY: (a) Region of subsonic modes; (b) Region of normal shocks within nozzle; (c) Region of curved shocks; (d) Region of three intersecting shocks in the flow: two normal plus one curved shocks; (e) Region of two oblique shocks intersecting on axis.

(Fig. 6-25,a) after which the speed is subsonic. In certain modes there are:

ascertained oscillatory motions of flow after point of separation (Fig. 6-25,b).

With the lowering of pressure of medium  $p_a$  the shocks advance from the critical to the exit section: at a certain pressure inside nozzle there will form a system of intersecting oblique shocks (Fig. 6-25c) which with lowering of pressure of medium is transmitted to exit section of nozzle and emerges into flow (Fig. 6-25,d).

Operating conditions of a two-dimensional supersonic nozzle without evaluating the influence of the boundary layer can be determined by means of the diagram constructed by B. Ya. Shumyatskiy (Fig. 6-26). Along vertical axis here is plotted the relative pressure, and along the horizontal—the rated  $M_1$  number for a nozzle. If there is known the ratio of pressures  $s_a = \frac{p_a}{p_0}$  and the rated  $M_1$  number, by using the diagram, it is possible to establish in what mode a given nozzle will operate.

Curve A corresponds to rated values of  $\frac{p_a}{p_0}$ ; the points, lying below this curve, belong to modes of the first group, when in the nozzle section there will form a wave of rarefaction. Curve B corresponds to the limiting case of two intersecting shocks [formula (6-36)]. Between curves A and B there is located a region of modes with oblique shocks in the nozzle section. Curve B corresponds to the case of a maximum ratio of pressures after the first oblique shock [formula (6-37)]. Regions between curves B and C correspond to modes with bridge-like shock in the section. Curve D corresponds to a normal shock in exit section of nozzle [formula (6-35)]. Modes with a curved shock are located in region between the curves C and D. Above the curve D is a region of direct shocks inside nozzle. The upper boundary of this region is curve E, and the lower—curve D. Values of  $\frac{p_a}{p_0}$ , corresponding to curve E, determine the modes with which shocks in nozzle disappear (normal shock is transferred to minimum section of nozzle, where  $M=1$ ).

The diagram in Fig. 6-26 is constructed on the assumption that the flow in nozzle and stream is two-dimensional and symmetric and the flow is continuous.

Results of experiments, presented in Fig. 6-24,c, show that ratio of pressures, corresponding to position of shock in exit section of nozzle, with satisfactory accuracy can be determined by the formula  $s_{1A} = \frac{s_{1I}}{0.4 + s_{1I}}$ .

Losses of energy in two-dimensional Laval nozzles during different modes can be evaluated by Fig. 6-27. Here by the dotted line there are plotted the coefficients of wave losses in compression shocks and of loss factors in expanding section of nozzle. The curves show that in modes of the third group, when the shocks are located near the minimum section, losses in the diffuser after shock (frictional losses also owing to separation) acquire major importance.

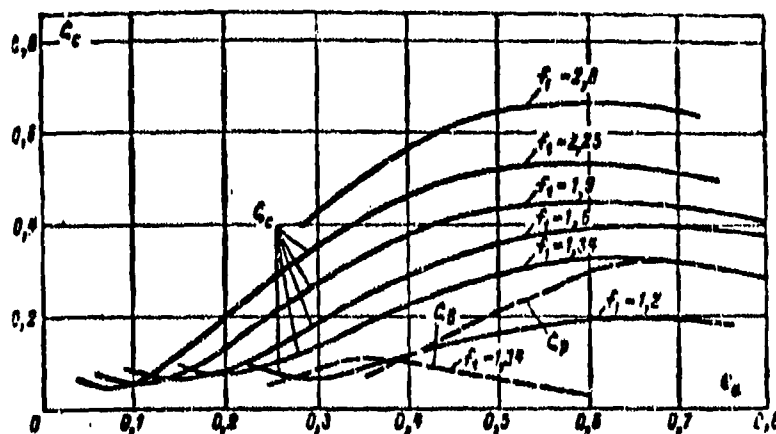


Fig. 6-27. Losses of energy in two-dimensional Laval nozzle during different modes.  
— experimental; --- wave losses (calculation) and losses in expanding part.

#### 6-6. Conical Laval Nozzles under Non-rated Conditions. Reaction Force

The outflow from an axially symmetric nozzle under rated and unrated conditions possesses a number of peculiarities.\*

We shall consider at first the results of an experimental study of the spectrum of flow after nozzle during outflow into medium with lower pressure (first group of modes).

On edge of exit section  $AA_1$  (Fig. 6-28,a) there will form a conical wave of rarefaction, and the pressure falls from  $p_1$  to  $p_a$ . In the core of flow the pressure drops to a lower value. As a result there appears a transverse gradient of

\*These questions are partially discussed in Sec. 6-2.

pressure, directed inside the stream. The expansion of the flow in the conical wave of rarefaction results in the deflection of the streamline from the axis and causes a corresponding deformation of the external boundary in the sector AD. In the sector DC the edge of stream under the influence of the difference of pressures

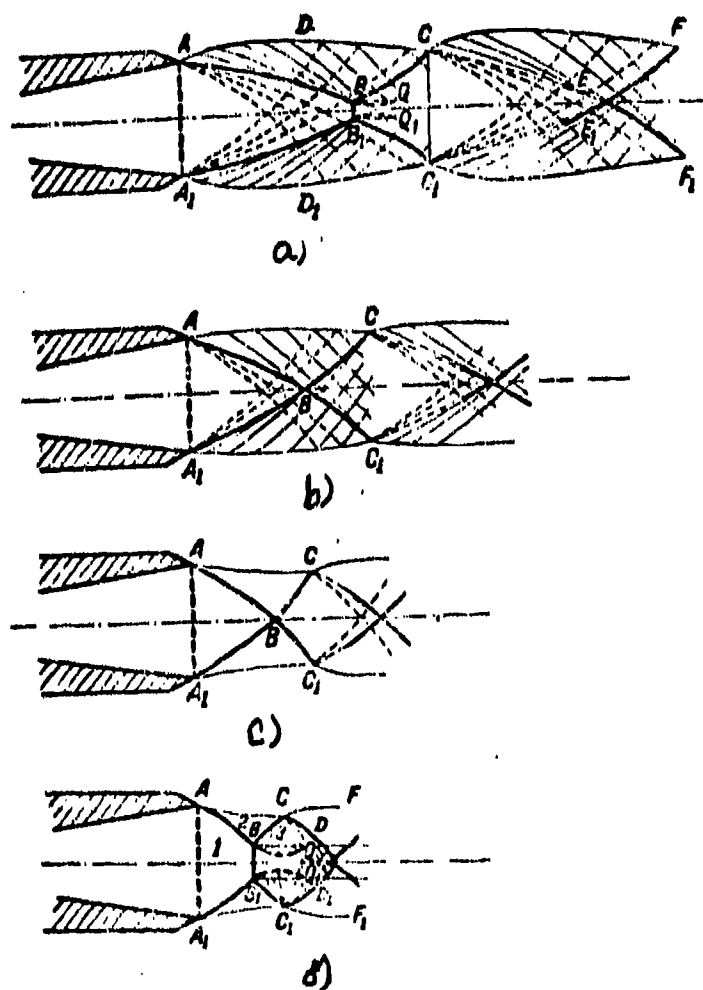


Fig. 6-28. Diagram of spectra of stream after conical nozzle during different modes.

(pressure of medium is higher) is deformed in opposite direction-stream is compressed (Fig. 6-28,a). All the weak waves, going out from the edge, will form with it an identical angle (pressures, speeds and temperatures at all points of boundaries are identical). The characteristics converge towards the axis of flow. As is known, convergent characteristics will form a curved shock. In case of an axially

symmetric flow such a shock has the shape of a surface of revolution with a curvilinear generatrix.

The shock  $ABB_1A_1$  (Fig. 6-28,a) may be generated not at exit edge of nozzle, but at the core of stream, at a certain distance from its boundary.

With a significant deflection of the mode from the calculated ( $p_a < p_1$ ) the shock emerges directly from the edge of nozzle. On axis of flow there appears a normal shock  $BB_1$ , after which the speed of flow becomes subsonic. Consequently, with a lower pressure after the nozzle in this case there appears bridge-like shock.

The curved shock  $CBB_1C_1$  in the external supersonic region is a continuation of the shock  $ABB_1A_1$ . The stream contracts up to that section, where the shock  $CBB_1C_1$  emerges onto surface of flow, and is reflected in the form of a wave of rarefaction. Farther on the stream again expands. From its boundary there emerge sound waves, intersecting at the core of flow. As a result here there will be formed a conical shock  $EE_1FF_1$ , enclosing the wave of rarefaction  $CEE_1C_1$  and emerging onto surface of flow at points F and  $F_1$ . As the pressure of medium increases the system of shocks at exit of nozzle varies little, and under rated conditions after exit section there are maintained two axially symmetric curved shocks (Fig. 6-28,b). With a further increase of pressure of medium (second group of modes) the shape of edge of flow changes. After the first shock the streamlines are deflected from axis of flow (Fig. 6-28,c).

Thus, for conical nozzle, first group of modes continuously changes into the second without essential qualitative changes of spectrum of flow within stream. In distinction from a two-dimensional nozzle in conical nozzle during all modes, shocks generate in the stream.

If aperture angle of nozzle is small, then under rated conditions there are absent the internal normal shock and subsonic core. With a higher counterpressure of the medium, the system of shocks again is reconstructed: two cone shocks are connected by a normal shock, and the internal part of stream becomes subsonic. An

increase in counterpressure results in an expansion of the subsonic region and correspondingly to a contracting of external supersonic flow (Fig. 6-28,d). In this group of modes axially symmetric stream also has a number of peculiarities. The curved shocks AB and  $A_1B_1$  branch at points B and  $B_1$ , as they form the already known bridge-like system. In region 3 there is established a higher pressure and in section  $CC_1$  shock  $BCB_1C_1$  is reflected in the form of wave of rarefaction. However, in this case reflected characteristics are curvilinear.

Characteristics, going out from free boundaries CF and  $C_1F_1$ , intersect. As a result, as in the case indicated in Fig. 6-28,a, wave of rarefaction from points C and  $C_1$  is terminated by shock CD ( $C_1D_1$ ). In the sector to right of second normal shock, located on axis, the flow is accelerated and becomes supersonic. Further process is repeated.

The subsonic core of stream is detected during all modes, different from the rated. However, as in all analysed cases above, the extent of the subsonic core is small. The external supersonic part of stream accelerates the internal part so that already at a small distance after the shock  $BB_1$  (Fig. 6-28,a and d) flow on axis attains supersonic speeds. On axis there will form a Laval nozzle, the edges of which are the boundaries line BQ and  $B_1Q$ .

For all the considered modes a characteristic peculiarity of axially symmetric stream is different curvature of its edge, of the internal streamlines, shocks and waves of rarefaction. Actually, as already indicated in Chapter 4, during transition through cone shock the streamlines immediately after the shock are distorted, where their curvature is variable along the shock. If an axially symmetric shock has a curvilinear generatrix, then the curvature of streamlines increases. The streamlines are distorted also during transition through conical wave of rarefaction.

The shape of diverging section of nozzle exerts a significant influence on the spectrum of stream after nozzle. Experience shows that in a correctly shaped axially symmetric nozzle shock waves after exit section generate only with large

deviations of modes from the rated ( $p_a \ll p_i$ ). In a rated mode and with insignificant deviations it ( $p_a < p_i$ ) nozzle operates without compression shocks in exit.

In conical nozzles shocks in the stream are detected during all modes. With an increase in aperture angle of diverging part the intensity of the shocks and their curvature increase. At a large aperture angle at exit of nozzle under rated conditions there is generated a bridge-like shock (Fig. 6-29).

The diverging part of nonshaped Laval nozzles is made as a rule, conical with a small aperture angle, equal to 8 to 12°. Under rated conditions the flow of gas

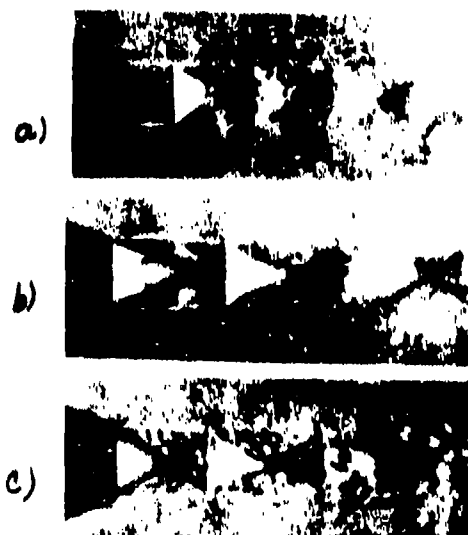


Fig. 6-29. Spectra of flow in stream after axially symmetric Laval nozzle. Rated characteristics of nozzle:  $\lambda = 1.52$ ;  $\mu = 0.066$ ;  $M_{11} = 1.8$   
a—  $\mu_a = 0.546$ ; b—  $\mu_a = 0.04$ ; c—  $\mu_a = 0.16$ .

in nozzle can be continuous also at significantly larger aperture angles.

The magnitude of critical aperture angle of a two-dimensional nozzle, corresponding to a continuous flow, under rated conditions can be readily determined by the diagram of characteristics (Chapter 3) or by means of tables (see Appendix), if the rated value  $\lambda_1$  is given. The angle of nozzle must not be larger than the

angle of deflection in wave of rarefaction during acceleration of flow from  $\lambda = 1$  to  $\lambda_1$ .

At the same time the increase of aperture angle exerts a significant influence on the structure of flow in nozzle under rated and unrated conditions. As the aperture angle increases the magnitude of negative pressure gradient in divergent part increases; nonuniformity of the flow increases along the axis and in the outlet section.

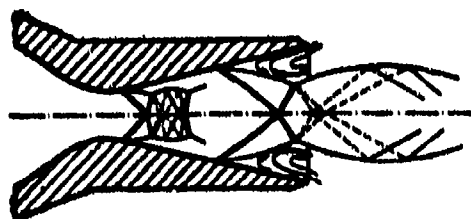


Fig. 6-30. Diagram of location of shocks in Laval nozzle with a large aperture angle.

Above have been presented the spectra of flow in a two-dimensional nozzle with a large aperture angle. Experience shows that also in conical nozzles with large aperture angles, there are detected analogous qualitative changes of the spectrum. Diagram of displacement of system of shocks within conical nozzles with different modes  $\epsilon_n > \epsilon_{n0}$  is presented in Fig. 6-30.

Thus the characteristic modes of a supersonic nozzle with large aperture angle cannot be determined by formulas presented in preceding paragraphs. For such a nozzle the values  $p_{1k}$ ,  $p_{1k}'$  and  $p_{1k}''$  are lower than for a nozzle with small angle  $\gamma_0$  and consequently, the transition into third group of modes occurs with smaller changes of the initial or the final pressure.

In Fig. 6-31, there are presented the loss factors  $\zeta_c$  for several axially symmetric nozzles.

Hence, it may be concluded, that minimum losses correspond to a mode of outflow close to the rated. With an increase in  $\epsilon_n$  the losses in nozzle abruptly increase and attain a maximum magnitude near critical value  $\epsilon_n \approx 0.55$  to  $0.65$ . At still larger values of  $\epsilon_n$  the losses decrease. Such a character of curves  $\zeta_c$  is explained



by change of wave and vortex losses in nozzle for second and third groups of modes. Theoretically, the change of losses must occur only at  $\epsilon_a \geq \epsilon_{1k}$ . However, as

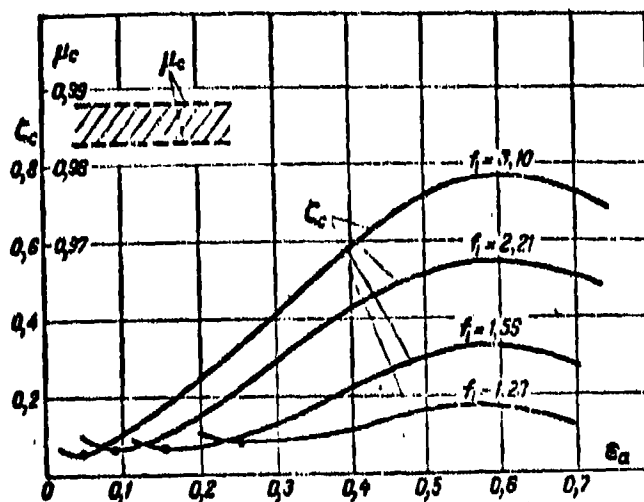


Fig. 6-31. Curves of loss factors  $\zeta_c$  depending on  $\epsilon_a$  and  $f_1$ .

experience shows, an increase of losses with an increase of  $\epsilon_a$  occurs at smaller values of  $\epsilon_a$ . The increase of pressure in the system of shocks, appearing at points A and A<sub>1</sub> during  $\epsilon_a < \epsilon_{1k}$ , are propagated through the subsonic part of boundary layer inside nozzle and result in a redistribution of the parameters in exit section. The maximum wave losses correspond to the mode  $\epsilon_a = \epsilon_{1k}$ . As the shocks within the nozzle ( $\epsilon_a > \epsilon_{1k}$ ) are displaced, the wave losses decrease and the vortex losses increase. In nozzles with a small aperture angle, when the shock approaches the critical section, the separation of the flow has a local character. At a small distance after the shock the flow again approaches the walls of nozzle and the vortex losses decrease. Therefore, the loss factors begin to decrease. In the modes

$\epsilon_a \geq \epsilon_{1m}$  the wave and vortex losses in nozzle are absent. (Venturi tube modes); losses of energy occur only from friction. As can be seen from Figs. 6-27 and 6-31, with an increase of  $f_1 = \frac{F_1}{F_2}$  the losses in modes of third group increase and the region of maximum values of  $\zeta_c$  is displaced somewhat towards the larger  $\epsilon_a$  values.

It should be emphasized that the total losses in nozzle are significantly greater than the wave losses during the given mode  $\alpha_u > \alpha_{1k}$ . We note that the character of the curves  $\zeta_c = \zeta_c(\alpha_u)$  remains identical for two-dimensional and axially symmetrical nozzles; however, the absolute values of  $\zeta_c$  differ somewhat.

In Fig. 6-31 the values of flow coefficients  $\mu_c$  also are indicated.

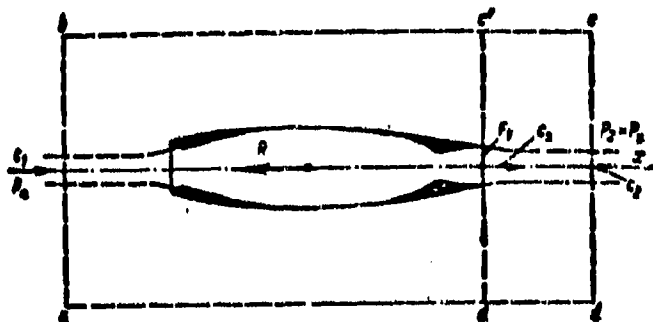


Fig. 6-32. Diagram for deriving formula for computing reaction (force) R.

Laval nozzles are widely used in jet engines. In this connection we shall dwell briefly on characteristics of nozzles necessary for calculating the reaction force.

For determining the reaction force, under the action of which there is realized the flight of a jet aircraft, we shall use the equation of momentum. For this purpose we shall describe around the apparatus a closed cylindrical surface abcd, all elements of which are remote at a fairly great distance (Fig. 6-32). Perturbations, created by apparatus on the defined closed surface, will be infinitely weak. We shall write out the equation of momentum in a projection onto x-axis (Euler equation)

$$\int_0^{\infty} p_a dF - \int_0^{\infty} p_c dF + R = \frac{1}{g} \int_0^{\infty} (c_c - c_a) dG_a + \frac{1}{g} \int_0^{\infty} c_c dG_c. \quad (6-46)$$

Here  $p_a$  is the pressure of incident flow in the section a-b;  $p_c$ ,  $c_c$  are the pressure and speed of flow after apparatus in section c-d;  $F$  is the area of sections a-b and c-d;  $G_a/g$  — mass of air, per second, flowing into contour;  $G_c/g$  — mass of

fuel being given to motor:  $R$  is the reaction (force).

Since the sections a--b and c--d are located at a long distance from the apparatus, then  $p_a = p_1$ . In this case, forces of pressure in indicated sections are compensated everywhere, with the exception of the sector equal to area of exit section of nozzle  $F_1$ . Speeds of individual streams, enveloping the apparatus, also differ little. After designating  $c_a$  as the exhaust velocity from nozzle;  $p_1$  as the pressure in exit section of nozzle  $F_1$ , from (6-46) we shall obtain:

$$R = \frac{1}{g} \int_0^{G_a} (c_a - c_1) dG_a + \frac{1}{g} \int_0^{G_r} c_a dG_r + \int_{F_1}^F (p_1 - p_a) dF_1. \quad (6-47)$$

For an immobile apparatus, not using atmospheric air, from formula (6-47) we find:

$$R = \frac{1}{g} \int_0^G c_a dG + \int_{F_1}^F (p_1 - p_a) dF_1. \quad (6-48)$$

where  $G$  is the flow rate, per second, of the working medium.

At average magnitudes, formula (6-48) can be written as:

$$R = \frac{G}{g} c_a + (p_1 - p_a) F_1.$$

After having replaced here

$$\frac{G}{g} c_a = \rho_1 c_a^2 F_1 = k p_1 M_1^2 F_1 = k \left( \frac{2}{k+1} \right)^{\frac{k}{k-1}} \rho_1 \lambda_1 F_1.$$

Finally we obtain:

$$R = k \left( \frac{2}{k+1} \right)^{\frac{k}{k-1}} \rho_1 \lambda_1 F_1 + (p_1 - p_a) F_1. \quad (6-49)$$

Let us note that the additional term in equation (6-49) is introduced only for first and second groups of operating modes of nozzle, i.e., at supersonic exhaust velocities.

With higher counterpressures ( $p_1 > p_2$ ) the reaction (force) decreases, since the difference  $p_2 - p_1$  is negative. Conversely, with an expansion of the stream after nozzle the difference ( $p_2 - p_1$ ) is positive and  $R$  increases.

If the shocks are located within nozzle, then the outflow occurs with subsonic speeds ( $p_2 = p_1$ ), and the second term drops out. The change in reaction (force) in this case is caused by the deceleration of the outflow, which should be determined

with an evaluation of losses in the system of shocks and in divergent section of nozzle.

The reaction (force) is conveniently presented in dimensionless form. For this purpose we divide (6-49) by the magnitude  $p_1 F_1$ . After simple transformations we obtain:

$$\bar{R} = (\lambda_1^2 + 1) \left( 1 - \frac{k-1}{k+1} \lambda_1^2 \right)^{\frac{1}{k-1}} \frac{p_a}{p_1} - 1. \quad (6-50)$$

For evaluating the effectiveness of nozzle of a reactive apparatus sometimes there is introduced the concept of coefficient of thrust

$$\varphi_R = \frac{R_A}{R_t}, \quad (6-51)$$

where  $R_A$ ,  $R_t$  are the reaction (forces) in actual and theoretical (without loss in nozzle) processes.

The connection between  $R_A$  and  $R_t$  can be found in such a form:

$$R_A = c_s \frac{G}{g} = \mu_c \varphi_c \frac{G_t}{g} c_{1t} = \mu_c \varphi_c R_t,$$

where  $c_s$  is the equivalent speed:

$$c_s = \frac{\frac{G}{g} (c_a - c_1) + (p_1 - p_a) F_1}{\frac{G}{g}};$$

$G$  and  $G_t$  are the actual and theoretical flows through nozzle;

$c_{1t}$  is the theoretical exhaust velocity from nozzle.

Consequently,

$$\varphi_R = \mu_c \varphi_c. \quad (6-52)$$

i.e., coefficient of thrust is product of the coefficients of the flow and speed.

Characteristics of  $\varphi_R$  according to experiments of F. Stepanchuk are indicated in Fig. 6-33 for nozzles with different parameter of  $f_1$  and for various aperture angles.

In modes of first group ( $\epsilon_a < \epsilon_1$ ) the magnitude  $\varphi_R$  is virtually constant. In third group of modes, when the system of shocks enters into divergent section of nozzle, the magnitude  $\varphi_R$  drops in connection with development of significant wave and vortex losses. Minimum value of  $\varphi_R$  sharply decreases with an increase of  $f_1$ . This result is explained by the greater intensity of shocks and increase of losses in diffuser after shocks in nozzles with large  $f_1$ .

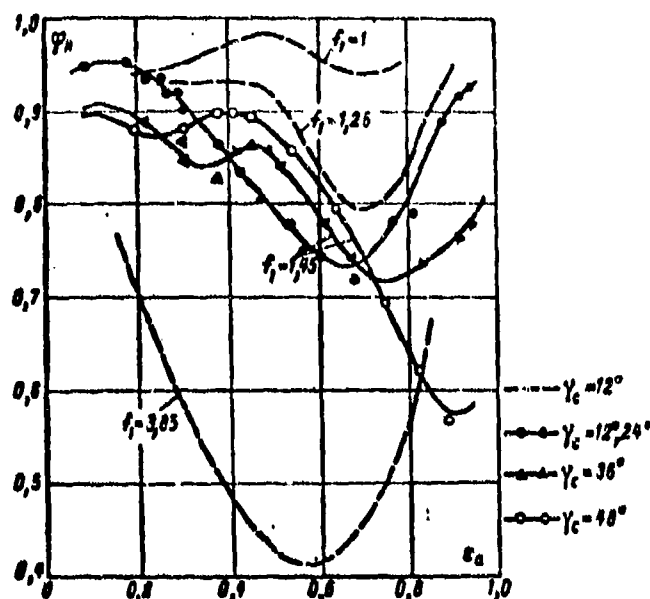


Fig. 6-33. Variation of coefficient  $\varphi_R = p_c/p_0$  depending on mode ( $\epsilon_a$ ), the relation  $f_1$  and aperture angle of nozzle  $\gamma_c$ .

For angles  $\gamma_c = 12^\circ$  to  $24^\circ$  characteristics of the nozzles coincide. A further increase of  $\gamma_c$  results in a sharp decrease of  $\varphi_R$  for the third group of modes.

At  $\gamma_c = 48^\circ$  on the curve  $\varphi_R$  there appear two maxima, the first of which corresponds to the rated conditions, and the second--operating conditions of nozzle, as ordinarily convergent (Fig. 6-33). This means that at large  $\gamma_c$  the separation of flow in modes, corresponding to the third group, occurs close to the critical section. Experiments have confirmed that the value  $\epsilon_a$ , with which in expanding part there will form a separation, depends considerably on the aperture angle and increases with an increase of  $\gamma_c$ .

Thus, in nozzles with aperture angles  $\gamma_c > 5$  to  $8^\circ$  in the modes of third group there appears a complex system of shocks. In accordance with data of the experiment most frequently this system can be approximated by two oblique or cone shocks intersecting on axis. In this case for calculating the third group of operating conditions of nozzle, it is necessary to know angle of oblique shock depending on  $\epsilon_a < \epsilon_a < \epsilon_{a, \text{crit}}$ . At a large aperture angle, when flow after shock is detached, it is possible to assume that  $p_{\text{crit}}'' \approx p_a$ . According to known values of  $M_{\text{lock}}$  and  $\frac{p_a}{p_{\text{crit}}}$

there is readily found the angle of shocks  $\beta$ . If after a shock a separation will not form, then the problem can be solved by trial and error.

#### 6-7. Supersonic Nozzle with Oblique Section

Under rated conditions the outflow from a supersonic nozzle with an oblique section occurs with small changes of spectrum of flow. These changes are caused by the effect of boundary layer on wall of oblique section KA (Fig. 6-34).

Under unrated conditions, when the pressure of medium  $p_a$  is less than the rated (model), an additional expansion of the stream occurs in the oblique section or after its limits. If angle of first characteristic is smaller than the angle of oblique section, then the expansion of flow occurs beyond the oblique section (Fig. 6-34,a). In this case, edges of the nozzle A and  $A_1$  create stationary waves of rarefaction intersecting not on axis of stream, but in a region, lying closer to edge A. For this reason, the symmetry of spectrum of outflow is disturbed and the stream is deflected from axis of nozzle. Waves of rarefaction are reflected from edge of stream, as compression waves ( $BCD_1$  and  $B_1C_1D$ ), intersecting close to opposite boundary. In zones of stream 2, adjoining the boundary, pressure is equal to external pressure  $p_a$ , in zone 3 (after intersection of waves of rarefaction) the pressure is lower, but in zone 4 it is higher and equal to pressure in oblique section of nozzle  $p_1$ .

At the intersection of the asymmetrically located system of waves, angle of deflection of streamlines vary from section to section. Correspondingly the mean angle of deflection of stream varies.

If the first wave of rarefaction from point A partially or completely lies within limits of oblique section, then character of the flow changes (Fig. 6-34,b). The wave of rarefaction reflected from wall of oblique section (partially or entirely) results in a lowering of the pressure, and along the edge A pressure is found to be lower, than  $p_a$ . As a result at point A there will form an oblique shock wave;

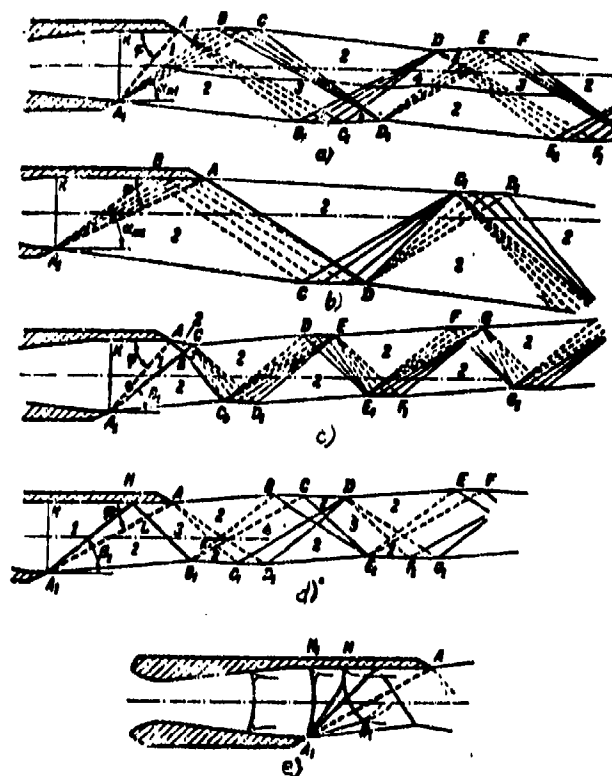


Fig. 6-34. Diagram of spectra of stream after nozzle with oblique section.

the system of waves changes and the angles of deflection will be already different in comparison with the first case. In the oblique shock AD the streamlines are deflected clockwise, therefore, the mean angle of deflection of stream somewhat increases. Such a character of outflow will take place in that case, when angle of oblique section.

$$\varphi < \arcsin \frac{1}{M_1}.$$

For the second group of modes (pressure of medium is higher than the calculated) on the edges A and A<sub>1</sub> there appear oblique shocks (Fig. 6-34,c), intersecting after oblique edge, if angle  $\beta_1$  of shock from point A<sub>1</sub> is smaller than the angle of oblique section  $\varphi$ . Intersection point of the shocks B lies along upper edge of stream. The flow is deflected from axis of stream, passing through an

asymmetric system of shocks and reflected waves of rarefaction; here the deflection of flow occurs in a direction opposite to the first case. Let us note that for first group of modes ( $p_a < p_1$ ), turn of stream occurs with respect to the point  $A$ , and at  $p_a > p_1$  (second group of modes) stream turns with respect to the point  $A_1$ . Angles of deflection of streamlines and, consequently, also of entire stream change along flow, just as in first case, owing to the influence of the reflected waves.

If  $q < \beta_1$  (Fig. 6-34,d), then first oblique shock lies within limits of oblique section. In reflected shock  $HB_1$  the pressure increases to a value, larger than  $p_a$ . As a result in the sector  $HA$  and in region  $LAKB_1$  pressure is higher. From points  $A$  and  $B_1$  there are propagated waves of rarefaction  $AC_1D_1$  and  $B_1BC$ . In zone 2 there is established the pressure  $p_a$ . In zone 4, the pressure is equal to  $p_1$ , and in zone 5 (after intersection of reflected compression waves) the pressure again is higher. Further the process is repeated. It is readily noted that the average angle of deflection of stream in this case may be increased. With a further increase of counterpressure, the shock  $A_1H$  will be deflected toward section  $A_1K$ . At a certain value  $p_a = p'_{1h}$  a normal reflection of the shock  $A_1H$  becomes impossible, since speed after primary shock is close to the speed of sound. The shock acquires the form of an  $\lambda$ -shaped shock  $A_1HB_1$  (Fig. 6-34,b), and on oblique section along wall  $HA$ , a separation of the stream will form.



Fig. 6-35. Spectrum of flow after Laval nozzle with oblique section (wave of rarefaction within limits of oblique section).

If  $p_a \approx p_{1h}$ , then bridge-like shock is located in section of nozzle  $A_1H_1$ , and the spectrum of stream virtually does not differ from that considered above for a nozzle with a normal section.



Calculation of spectrum and the determination of mean angle of deflection at exit of nozzle with oblique section can be made by the method of characteristics (modes I) in combination with the method of shock polars, if  $p_a > p_1$  (modes II)

An approximate evaluation of the angles of deflection can be realized also by simpler methods, presented in Chapter 8, by means of equations of continuity of momentum and energy.

Experiments confirm the above considered spectra of outflow from Laval nozzle with oblique section. In Fig. 6-35, obviously visible is the wave spectrum of stream after oblique section.

Let us note that deflection of stream in oblique section causes a change of the reaction (force), the calculation of which should be made by a revised formula which takes the deflection of flow into account.

## CHAPTER 7

### MOVEMENT OF GAS IN DIFFUSERS. STAGE OF EJECTOR

#### 7-1. Main Characteristics and Design of Diffusers

In diffusers occurs the conversion of the kinetic energy of flow into the energy of pressure. Equations of one-dimensional flow (Chap. 2) show that such a process at subsonic speeds can be realized in a pipe with cross-section increasing along the flow.

The flow of gas in a diffuser is characterized by positive pressure gradients, the presence of which creates conditions for intense build-up of the boundary layer and in a number of cases of flow separation from the walls.

The influence of the positive pressure gradient on the structure of the boundary layer was considered in detail in Sections 5-11. Graphs in Fig 5-29 and 5-30 show that with increase of the positive pressure gradient (parameter  $\Gamma < 0$ ) the momentum thickness  $\delta^{**}$  abruptly increases and the filling of the velocity profile next to the wall is decreased.

At significant pressure gradients in the diffuser, can appear separation (Chap. 5). In this case energy losses abruptly increase and the diffuser does not provide the given increase of pressure.

The main problem of design reduces to establishment of the optimal form of the diffuser, corresponding to continuous flow and a minimum of energy losses at

the given regime parameters (numbers  $Re$  and  $M$ ) and conditions at the entrance.\*

With this aim is chosen a diagram of the distribution of pressures along the diffuser, which gives the least intense growth of momentum thickness to the exit section and does not lead to separation of the layer or displace the separation to the exit cross-section. Such a problem can be solved by means of variant calculations of the boundary layer by methods set forth in Chap. 5.

Having selected a rational distribution of pressures, it is not difficult to calculate flow areas, establish the form of the diffuser and determine the magnitude of losses in it. In the case when form of diffuser is given, the distribution of pressures along the axis is calculated by the channel method (Sections 3-5).

In practice of calculations, it is accepted to consider the losses of energy in diffusers as the sum of two components: losses due to friction in the boundary layer  $\zeta_{fp}$  and expansion losses

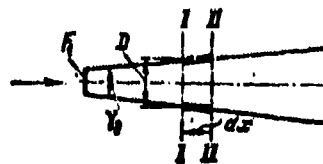


Fig. 7-1. Diagram of diffuser.

$\zeta_p$ . In meaning, the quantity  $\zeta_p$  characterizes losses caused by the turbulent character of motion in zones of separation.

It is assumed that the considered losses are analogous to losses during sudden expansion of flow, when during transition from the narrow part of the pipe into the wider part, the boundary of the stream disintegrates and swirls into vortices. For the maintenance of turbulent motion is expended part of the energy of flow. As a result the sudden expansion is accompanied by a loss of pressure, and the loss factor for an incompressible fluid during sudden expansion (shock loss)

---

\*That is, the length, form and roughness of walls of the entrance section of the diffuser, the initial degree or turbulence of flow, distribution of velocities along the section, and so forth.

can be determined by the formula

$$\zeta_{ya} = \frac{(c_1 - c_2)^2}{c_1^2} = \left(1 - \frac{F_2}{F_1}\right)^2 = \left(1 - \frac{1}{f}\right)^2, \quad (7-1)$$

where  $f = \frac{F_2}{F_1}$  is the expansion ratio of the diffuser ( $F_1$ —the section of the entrance and  $F_2$  is the section of the exit of the diffuser (Fig. 7-1)).

The corresponding loss of pressure is expressed by formula

$$\Delta p_{ya} = p_{2t} - p_2 = \frac{\rho c_1^2}{2} \zeta = \frac{\rho (c_1 - c_2)^2}{2} = \frac{\rho c_1^2}{2} \left(1 - \frac{F_2}{F_1}\right)^2, \quad (7-2)$$

where  $p_{2t}$  is the pressure after sudden expansion during the absence of losses;  $c_1$  and  $c_2$ —velocities in sections  $F_1$  and  $F_2$ .

In the diffuser (Fig. 7-1) the losses of energy and pressure caused by expansion of sections will be less, since the sections change gradually.

Ratio

$$\psi = \frac{\Delta p_A}{\Delta p_{ya}}, \quad (7-3)$$

where  $\Delta p_A$ —loss of pressure in the diffuser, is called the coefficient of shock softening. Consequently, the coefficient  $\psi$  is the ratio of losses of pressure in the diffuser to losses of pressure during sudden expansion.

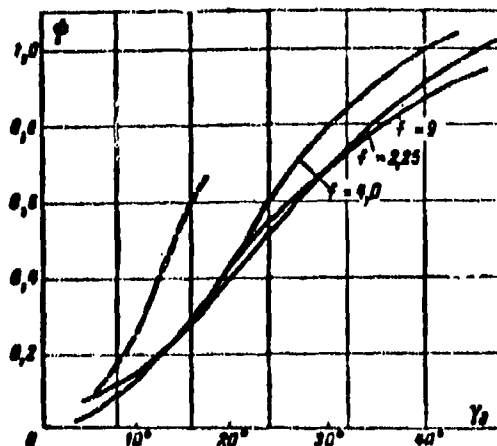


Fig. 7-2. Coefficient of shock softening, depending upon the aperture angle and the parameter  $f$  for diffusers (—round cross-section; ---square cross-section).

As can be seen from Fig. 7-2, the coefficient  $\psi$  depends weakly on the ratio  $f = \frac{F_2}{F_1}$  and the shapes of the section, and mainly is determined by the aperture angle of the diffuser  $\gamma_A$ .

The use of coefficient  $\psi$  for design of diffusers is formal and can be justified only by the fact that the detected losses in diffusers turn out to be larger than frictional losses determined for non-gradient flow.

Indeed, during calculation of frictional losses, as a rule, the known formula (Chap. 5) is used:

$$dL_{fr} = \xi \frac{\rho c_x}{2} \frac{dx}{D} \quad (7-4)$$

with coefficient  $\xi$ , determined by one of the known formulas for non-gradient flow, for example by the formula of Blasius:

$$\xi = 0,3164 Re^{-\frac{1}{4}}. \quad (7-5)$$

Here  $c_x$ —velocity on the axis of the diffuser;  $dx$ —element of length;  $D$ —diameter of cross section of the considered section and

$$Re = \frac{c_x D}{\nu} \quad (7-6)$$

—Reynolds number.

The value of the absolute frictional losses calculated by such a method turn out to be significantly smaller than experimental values, even for continuous flow, since formula (7-5) does not consider the influence of the pressure gradient.

Losses in diffusers of any form for continuous flow can be calculated with use of the theory of the boundary layer; for example by the method of A. Yu. Zaryankin, based on the application of the concept of energy thickness.

For conical diffusers by means of certain simplifications by it is obtained a formula for the loss factor in the following form:

$$\zeta_A = \frac{0.032 f^{1.02}}{Re^{0.2} \sin \frac{\gamma_A}{2}} \left(1 - \frac{1}{f^2}\right). \quad (7-7)$$

Using this coefficient, it is possible to calculate losses of pressure in the diffuser:

$$\Delta p_A = p_{11} - p_2 = \zeta_A \frac{\rho c_1^2}{2}. \quad (7-8)$$

We will compare the results of calculations by the formula (7-7) with data of the experiment.

From curves of losses in Fig. 7-3 it follows that losses in an isogradient diffuser\* are significantly greater than in a conical one. All diffusers had one and the same expansion ratio  $f = 2.25$ . The change of losses depending upon the number  $M_1 < 0.8$  shows that with growth of velocity, losses are somewhat lowered. However, everywhere the value of losses in the isogradient diffuser are approximately 3 times larger than in the conical, which indicates the separation character of the flow in it.

Evaluation of losses by the formula (7-7) for conical diffusers at  $M_1 = 0.7$  gives 5.5 o/o for  $\gamma_A = 10^\circ$  and 5 o/o for  $\gamma_A = 6^\circ$ . These values of  $\zeta_A$ , practically,



Fig. 7-3. Change of losses in different diffusers depending upon the number  $M_1$ .

KEY: (a) Isogradient diffuser; (b) Conical diffuser ( $\gamma_A = 6^\circ$ ); (c) Conical diffuser ( $\gamma_A = 11^\circ$ ).

\*Diffusers with a constant value of the pressure gradient  $dp/dx$  along the axis are called isogradient diffusers.

coincide with the data of the experiment.

For calculation of the distribution of velocities along the axis of the diffuser we will integrate equation (5-10):

$$\frac{d\lambda}{\lambda} (\lambda^2 - 1) - \left( 1 - \frac{k-1}{k+1} \lambda^2 \right) \frac{dF}{F} + \frac{2k}{k+1} \frac{g dL_A}{a_*^3} = 0, \quad (7-9)$$

where the elementary work of friction  $dL_A$  can be expressed by the loss factor in the diffuser.

As a result of integration we obtain:

$$\frac{F_1}{F} = \frac{\lambda \left( 1 - \varphi \frac{k-1}{k+1} \lambda^2 \right)^3}{\lambda_1 \left( 1 - \varphi \frac{k-1}{k+1} \lambda_1^2 \right)^3}, \quad (7-10)$$

where

$$\varphi = 1 + \frac{k}{k-1} \frac{16\zeta_A}{1 - \beta^2}; \quad (7-11)$$

$$\beta = \frac{1}{2} \left( \frac{1}{\varphi} \frac{k+1}{k-1} - 1 \right). \quad (7-12)$$

Following the method described in work [L.4] we will introduce by analogy with the reduced expenditure in the given section  $q(\lambda)$  function

$$q_R(\lambda) = \left( \frac{k+1}{2} \right)^{\frac{k-1}{2}} \lambda \left( 1 - \varphi \frac{k-1}{k+1} \lambda^2 \right)^3. \quad (7-13)$$

During the absence of losses  $q_R(\lambda) = q(\lambda)$ , therefore function  $q_R(\lambda)$  can be called the generalized reduced expenditure. Knowing the distribution of speed along the axis of the diffuser, by the equation of inseparability with the help of this formula can be found the relation of pressures of full deceleration in an arbitrary section of the diffuser [see formula (2-41)]:

$$\frac{p_0}{p_{01}} = \frac{1}{\beta} \frac{q(\lambda_1)}{q_R(\lambda)} \quad (7-14)$$

and the corresponding relation of static pressures:

$$\frac{p}{p_1} = \frac{1 + \epsilon(\lambda_1)}{1 + \epsilon(\lambda)} \quad (7-15)$$

Here  $\epsilon(\lambda) = \frac{p_0}{p} q(\lambda)$  (see Chap. 2).

Calculation of the distribution of the parameters of flow along the axis of the diffuser, taking into account viscosity, shows that the velocity of flow in an arbitrary section is larger, but static and total pressure are less than the corresponding values of these quantities obtained without calculation of the influence of viscosity. Curves  $\bar{p}$  show that restoration of static pressure in the conical diffuser occurs most intensely in the initial section. Further growth of  $\bar{p}$  is abruptly slowed down, and, starting from some limiting value  $f_{\text{пред}}$  the pressure starts to drop.

Formula (7-15) also reflects the influence of compressibility: with an increase of velocity at the entrance the positive pressure gradients increase especially intensely on the initial section.

For evaluation of the accuracy of calculation by the formula (7-14) in Fig. 7-4 are presented values of  $\epsilon_0$  according to data of K. S. Szilard for a diffuser with  $f = 4.92$  and  $\gamma_1 = 4$  and  $8^\circ$ . The coincidence of calculated and experimental data should be recognized as satisfactory in the entire range of numbers  $M_1 < M_{1*}$ .

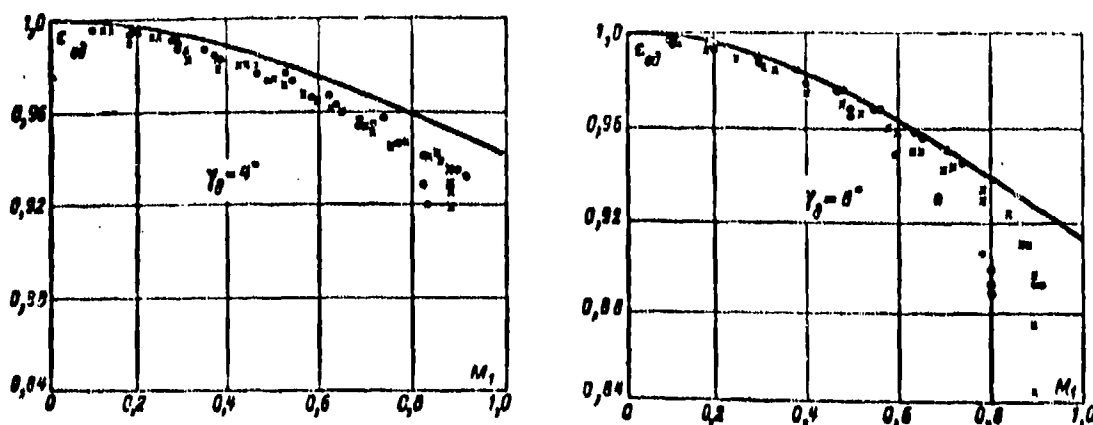


Fig. 7-4. Comparison of calculated and experimental values  $\epsilon_0$  for conical diffusers with different aperture angles (experiments of K. S. Szilard).



We will conclude now with the characteristics of diffusers obtained during experimental investigation.

Let us consider in the thermal diagram the change of state of gas in a subsonic diffuser. Parameters of full stagnation of flow at the entrance in the diffuser are determined by point  $O_1$  (Fig. 7-5), and the parameters of moving gas up to the diffuser by point 1.

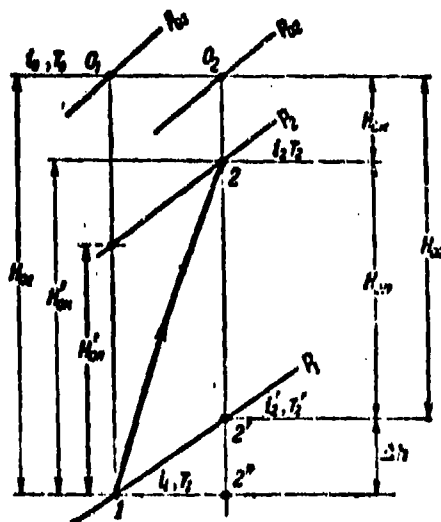


Fig. 7-5. Process of change of state of gas in subsonic diffuser in the thermal diagram.

Compression in the diffuser occurs with the increase of entropy. This process will be depicted by line 1-2, and point 2 corresponds to the parameters of gas after the diffuser. Point  $O_2$  corresponds to the state of completely stagnant flow after the diffuser. In the thermal diagram it is easy to find corresponding power characteristics: loss of kinetic energy  $\Delta h$ , change of potential energy  $H_{01}$ , and kinetic energy of flow in the exit section  $H_{02}$ . The energy loss factor in the diffuser, as in the case of a shock, is determined by the formula (4-33a):

$$\zeta_1 = \frac{H_{01} - H_{02}}{H_{01}} = \left( \frac{k+1}{k-1} \lambda_1^2 - 1 \right) \left( \epsilon_{01}^{\frac{k-1}{k}} - 1 \right). \quad (7-16)$$

where  $\epsilon_{a1} = \frac{P_{02}}{P_{01}}$  is the coefficient of restoration of stagnation pressure in the

diffuser.

The effectiveness of the diffuser may be characterized also by power efficiency

$$\eta_A = \frac{H_{02}}{H_{01}} = 1 - \zeta_A. \quad (7-16a)$$

In certain cases for evaluation of the diffuser is used another concept of efficiency; this quantity is determined by the formula

$$\eta_A' = \frac{H_{0H}}{H_{0K}}.$$

where  $H_{0H}$  ---change of potential energy of flow in the diffuser;

$H_{0K}'$  ---difference of kinetic energies of flow at the entrance and exit sections of the diffuser.

After substitution of  $H_{0H}$  and  $H_{0K}'$  can be obtained the efficiency of the diffuser in the form of:

$$\eta_A' = \frac{1}{2} \frac{k+1}{k-1} \frac{1 - \frac{k-1}{k+1} \lambda_2^2}{\lambda_1^2 - \lambda_2^2} \left[ 1 - \left( \frac{P_1}{P_2} \right)^{\frac{k-1}{k}} \right]. \quad (7-16b)$$

The power efficiency depends only on losses of energy in the diffuser at the time when  $\eta_A'$  changes during the change of the compression ratio. It is easy to see that  $\eta_A > \eta_A'$ .

Selection of the optimal diagram of velocities (or pressures) along the diffuser is accomplished on the basis of variant calculations.

The quantities  $\delta^{**}$  and  $dp/dx$ , determining the state of flow in the diffuser, depend on the expansion ratio (ratio  $f = F_2/F_1$ ) and the aperture angle of the diffuser  $\gamma$ , etc. It follows from this that the form of the optimal diagram of pressures depends on these geometric parameters.

In diffusers with a smooth change of section (with small aperture angles)

with continuous flow it is expedient to select diagrams with large gradients at the entrance sections (diagrams 2 or 5 in Fig. 7-6,a) and with decreasing values of  $dp/dx$  in the middle and exit sections; satisfactory results can be obtained in the diffuser with rectilinear walls (diagram 3 in Fig. 7-6a).

In diffusers with large aperture angles separation occurs in cross-sections of the entrance section. In order to displace the separation to the exit section, it is necessary to decrease the pressure gradients at the entrance, i.e., to cross

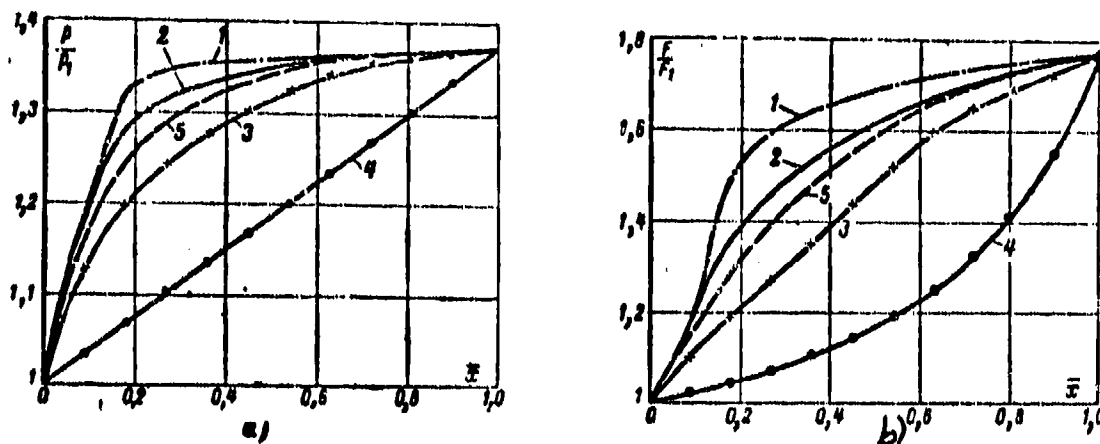


Fig. 7-6. Diagrams of pressures and flow areas of diffusers of different form.

to the curve  $dp/dx = \text{const}$  (diagram 4 in Fig. 7-6a, etc.). Changes of flow areas of diffusers providing diagrams of the shown pressures are presented in Fig. 7-6b.

## 7-2. Subsonic Diffusers

Let us consider influence of basic geometric and regime parameters on effectiveness of flat and conical diffusers. As it was shown, the most important geometric parameters are the aperture angle  $\gamma_a$  and the expansion ratio  $f$ .

From the presented formulas (Section 7-1) it follows that at the given distribution of velocities, the value of the parameter  $r$  does not depend on  $\gamma_a$  and this quantity can be selected arbitrarily. On the basis of formula (7-11) it may

be concluded that at large angles  $\gamma_n$  losses in the diffuser are decreased.

However, as experiments show, at  $\gamma_n \geq 8$  to  $12^\circ$  in conical diffusers there appears separation; losses of energy at this time abruptly increase.

It is possible to consider that the formation of separation at a large aperture angle is combined with a nonuniform distribution of velocities at the entrance. In most cases the transition from the convergent channel part to the conical diffuser takes place with a sharp change of curvature of the walls, and the jump in curvature increases with the increase of  $\gamma_n$ . Such a local disturbance of boundary conditions is the cause of the early separation of the boundary layer during the increase of angle  $\gamma_n$ . The influence of the shown disturbance is especially great in those cases, when the boundary layer at a significant distance from the input is laminar.

Let us note that the character of nonuniformity of the velocity field at the entrance has considerable influence on losses in the diffuser. Especially unfavorable is the diagram of velocities 1, drawn out in the middle part (Fig. 7-7); less important is the influence of nonuniformity, if the flow is characterized by increased speeds at the walls (diagram 2). In this case the losses can be smaller, as compared to the uniform velocity field (diagram 3). Nonuniformity, characterized by diagram 2 in Fig. 7-7, is favorable because in this case the boundary layer in the diffuser becomes thinner, and the point of separation is displaced along the flow.

During regular organization of the flow at the entrance into the diffuser, the aperture angle  $\gamma_n$  may be assumed to be increased.

During determination of the optimum aperture angle  $\gamma_{n, \text{opt}}$ , i.e., the maximum angle at which flow separation has not yet occurred, it is possible for round diffusers at low velocities to use the formula of I. Ye. Idel'chik:

$$\gamma_{n, \text{opt}} = 0.43 \left( \frac{\xi}{\xi_n} \cdot \frac{f+1}{f-1} \right)^{0.115},$$

where  $\gamma_n$  —experimental coefficient, taking into account the influence of the non-uniformity of the velocity field at the entrance to the diffuser.

One should note that the formulas for  $\gamma_{A,opt}$  represent this quantity in dependence upon the Reynolds number, a function of which is the drag coefficient  $\lambda$ . Calculations show that with the growth of  $Re_1$ ,  $\gamma_{A,opt}$  is increased.

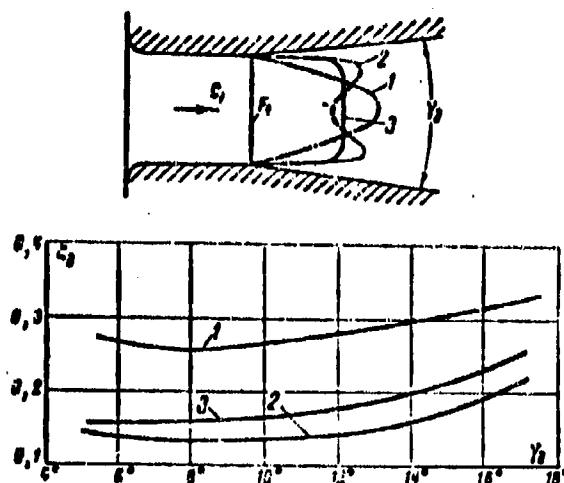


Fig. 7-7. Influence of character of nonuniformity of velocity field at the entrance section of the diffuser on losses;  
 $Re_1 = 3 \cdot 10^5$ ;  $M_1 = 0.5$ .

According to the experimental data of K. S. Szilard, with the growth of Mach number  $M_1$  the advantage of small angles increases. Consequently, with an increase of  $M_1$  the optimum aperture angle should decrease (Fig. 7-4). This result is evident, since the influence of compressibility appears in the fact that the longitudinal pressure gradients increase. So, during increase of Mach number  $M_1$  from 0 to 0.8,  $\gamma_{A,opt}$  is decreased by  $0.7-0.9^\circ$  ( $Re_1 = 10^6$ ). This dependence of  $\gamma_{A,opt}$  on Mach number  $M_1$  is less intense, than on  $Re_1$ .

Experiments show that for round conical diffusers, optimum values of  $\gamma_{A,opt}$  can be taken within the limits  $\gamma_{A,opt} = 6$  to  $15^\circ$ . The most commonly used are the average values  $10-12^\circ$ .

An important geometric characteristic of diffuser is the ratio of sections  $f$ . At a given speed at the entrance, increase of pressure occurs only up to definite

limits, and in the conical diffuser and in the diffuser of optimal form, the most violent increase of pressure corresponds to the initial section.

The value of parameter  $f$  corresponding to the maximum compression ratio in the diffuser is called limit  $[f_{\text{npex}}]$ . Design of diffuser with the largest ratio  $f$  is not expedient, since, in this case, at the exit section is detected a lowering of pressure.

Results of calculation show that  $f_{\text{npex}}$  depends on the aperture angle of the diffuser  $\gamma_1$ , the dimensionless speed of flow  $\lambda_1$  and Reynolds' number  $Re_1$  at the entrance. With increase of  $\gamma_1$  and  $\lambda_1$ , the value of  $f_{\text{npex}}$  decreases. Physically this result is explained by the fact that with increase of  $\gamma_1$  and  $\lambda_1$ , are increased the pressure gradients. Increase of Reynolds number leads to increase of  $f_{\text{npex}}$ , since in this case are decreased the functional losses in the diffuser.

One should note that values of  $f_{\text{npex}}$  taken in practice should be less than the calculated values. Indeed, the most intense compression of gas occurs in the entrance section of the diffuser, so that in sections  $f = 2.5$  to  $3.5$  increase in pressure is nearly 90 o/o of the maximum, corresponding to  $f_{\text{npex}}$  (for diffusers with aperture angles  $\gamma_1 = 8$  to  $15^\circ$ ). Upon final selection of  $f_{\text{npex}}$  one should make a detailed calculation of the boundary layer and evaluate the probability of formation of separation by the parameter  $l' < l'_s$ .

Results of corresponding calculations for conical diffusers are shown in Fig. 7-8. It is clear that the limiting values  $f_{\text{npex}}$  determined by the conditions of continuous flow ( $l' < l'_s$ ) and maximum increase of pressures in the diffuser  $p_2/p_1 = 0.9(p_2/p_1)_{\text{max}}$  are considerably lower than the theoretical  $f_{\text{npex}}$ , depicted by the solid lines.

For diffusers constructed according to rational distribution of pressures, the values of  $f_{\text{npex}}$  can be selected larger, since in this case flow in the diffuser is continuous.

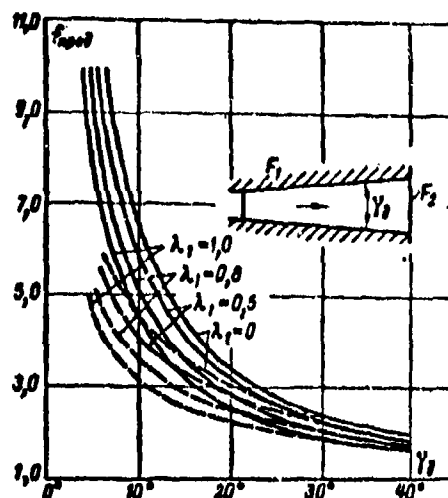


Fig. 7-8. Limiting expansion ratios of diffuser in dependence upon the aperture angle and dimensionless velocity at the entrance.

The influence of the form of the diffuser on its basic characteristics was partially considered in section 7-1. As was shown, the solution of this problem is not universal; the optimum diagram of pressures changes in dependence upon two basic geometric parameters—the ratio of sections  $f$  and the length of the diffuser. At small length and large  $f$ , when the pressure gradients at the entrance very abruptly increase, the formation of separation in the entrance sections is possible.

In these cases it is necessary to decrease  $dp/dx$  at the entrance, and diffusers with constant pressure gradient turn out to be more effective for large aperture angles, i.e., small length and large  $f$ . This fact is clearly confirmed by the experiments of I. Ye. Idel'chik with flat diffusers (Fig. 7-9).

Since in isogradient diffusers, frictional losses are greater (in connection with the fact that  $\delta^{**}$  increases at the exit more intensely), the application of such diffusers should be considered to be expedient only during aperture angles  $\gamma_1 \geq 18^\circ$ . In the interval  $\gamma_1 = 12$  to  $18^\circ$ , the best results are given by diffusers with rectilinear walls ( $\gamma_1 = \text{const}$ ). At small angles  $\gamma_1 < 12^\circ$  one should change to diffusers with curvilinear convex walls (curves 2 in Fig. 7-6).

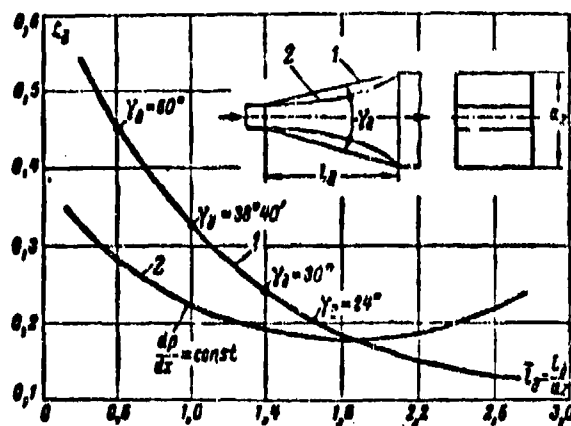


Fig. 7-9. Change of the loss factor in flat diffusers is dependent upon the relative length  $\bar{l}_d$ .

Also possible is the application of combined diffusers, the basic diagrams of which are shown in Fig. 7-10. Special interest is presented by the step diffuser. Increase of pressure here occurs in the beginning in the usual smoothly expanding channel, and then the pressure increases during sudden expansion of the cross section. Such diffusers should be applied for small length and large ratios  $f$ . For each value of  $f$  there exists a definite optimum length  $l_1$ , which corresponds to the minimum losses. At the selected optimum aperture angle  $\gamma_{d, \text{opt}}$  and  $l_1$ , the area of the exit section of the smooth part of the diffuser  $F'_2$  is determined uniquely.

Step diffusers have important advantages in those cases, when it is necessary to shorten the length of the diffuser. At small  $\gamma_d$ , the application of the step diffuser is not expedient, since total losses during the sudden expansion increase.

Experiments show also that the effectiveness of a diffuser is influenced by the form of its cross sections. In round and flat diffusers, losses of energy are minimal. In diffusers with square or rectangular cross-section with broadening in two planes losses are higher. This is explained by a different change of pressures along the flow: pressure gradients in round and flat diffusers at identical  $F_1$  and  $F_2$  will be less than in square ones. In non-circular diffusers, losses are increased due to the interference of the boundary layers in the corners.



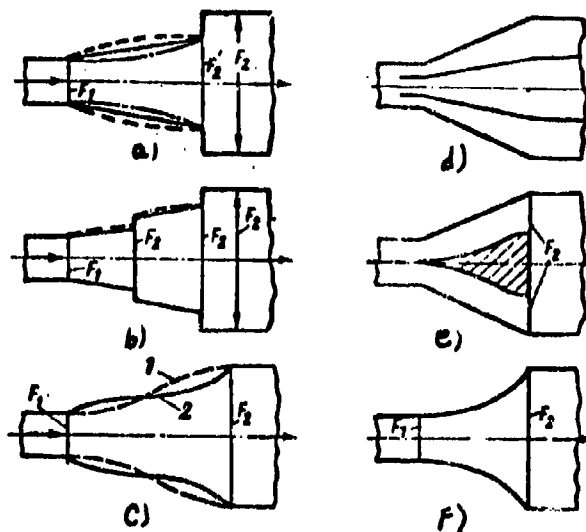


Fig. 7-10. Diagrams of combined diffusers. a, b and e—step diffusers, c—diffusers with small (1) and large (2) pressure gradients at the entrance; d—diffuser with separating walls; f—isogradient diffuser.

Experiments confirm the significant influence of initial turbulence on characteristics of the diffuser in full conformity with that which was obtained during investigation of the boundary layer (Chapter 5). Loss factors intensely increase with increase of initial turbulence.

We will conclude with the evaluation of the influence of the basic regime parameters, the numbers,  $Re_1$  and  $M_1$ , on the characteristics of diffusers.

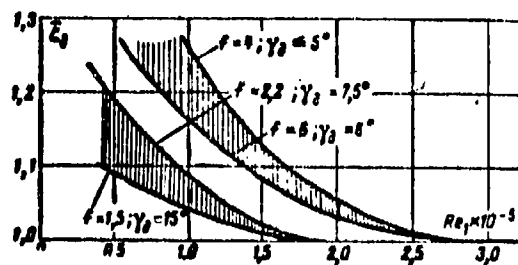


Fig. 7-11. Influence of numbers  $Re_1$  and  $M_1$  on the loss factor in conical diffusers.  $\xi_d = \xi_{d1} \xi_{d2} Re_1 = 3 \cdot 10^4$ .

Experiments show that the character of curves  $\xi_d (Re_1)$  depends on the geometric characteristics of the diffuser:  $\gamma_d$  and  $f$ . The corresponding curves according to data of different investigations are shown in Fig. 7-11. As can be seen, the

influence of  $Re_1$  is observed at  $Re_1 < 3 \cdot 10^5$  in dependence upon  $\gamma_1$ ,  $f_2$  and the form of the diffuser. Let us note that the characteristics  $\xi_1(Re_1)$  at large aperture angles and  $f > 4$  proceed with more gentle slope. Here is observed an analogy with the influence of initial turbulence: at large  $\gamma_1$  the influence of  $E_0$  weakens.

Increase of the number  $M_1$  leads to increase of pressure gradients; in accordance with this, frictional losses in the diffuser, with increase of  $M_1$  starting from  $M_1 > 0.7$ , are increased. Compressibility leads to increase of windage losses in the diffuser; during separated flow, with increase of  $M_1$  the point of separation of flow is transferred to the entrance section.

At transonic speeds at the entrance (at  $M_1 < 1$ ) losses in the diffuser increase especially intensely, since the pressure gradients in the entrance section abruptly increase, which leads to early separation even for small aperture angles (Fig. 7-4). One should note that the curves in Fig. 7-3 reflect the influence not only of the compressibility, but also the Reynolds number. Decrease of  $\xi_1$  with increase of  $M_1$  for  $0.1 < M_1 < 0.5$  is caused by change of  $Re_1$ , since in this range of Mach numbers  $M_1$  the influence of compressibility still is not apparent.

Let us consider in conclusion certain results of experiments, carried out for the purpose of lowering of losses in diffusers with large aperture angles. According to the data of I. Ye. Idel'chik, along with the application of isogradient diffusers, lowering of losses may be attained by installation of grids, separating walls and by the organization of drawing or blowing off of the boundary layer, and also by the application of step diffusers.

Experiments of V. Kmonichk showed that the installation of a wire bundle leads to a noticeable decrease of losses in a flat diffuser with large aperture angles (Fig. 7-12, a, b and c). Analogous results were obtained for round diffusers with a radial distribution of the wires (Fig. 7-12, d).

The detected effect is explained by the fact that the resistance introduced

into the diffuser equalizes the velocity field at the exit from the diffuser. Equalizing of velocities leads to displacement of the point of separation along the flow, since the velocity profile by the walls becomes fuller (Fig. 7-7).

The optimal position and the form of the wire grids introduced into diffuser depend considerably on the form and aperture angle of the diffuser, and also on the flow regime (numbers  $M_1$  and  $Re_1$ ).

Investigations of V. Kmonichk were carried out with resistances, introduced inside the diffuser. It turned out that for a flat diffuser with an aperture angle  $\gamma_n = 15^\circ$ , the variant in Fig. 7-12,a is optimal; for  $\gamma_n = 30^\circ$  the best results were showed by variants b and c. Improvement of the flow of gas in the diffuser with large aperture angles can be provided also with the help of deep grooves, turned at some distance from the entrance section (Fig. 7-12,e). The drawing off of the layer due to the grooves displaces the separation along the flow, as shown by experiments of V. K. Migaya.

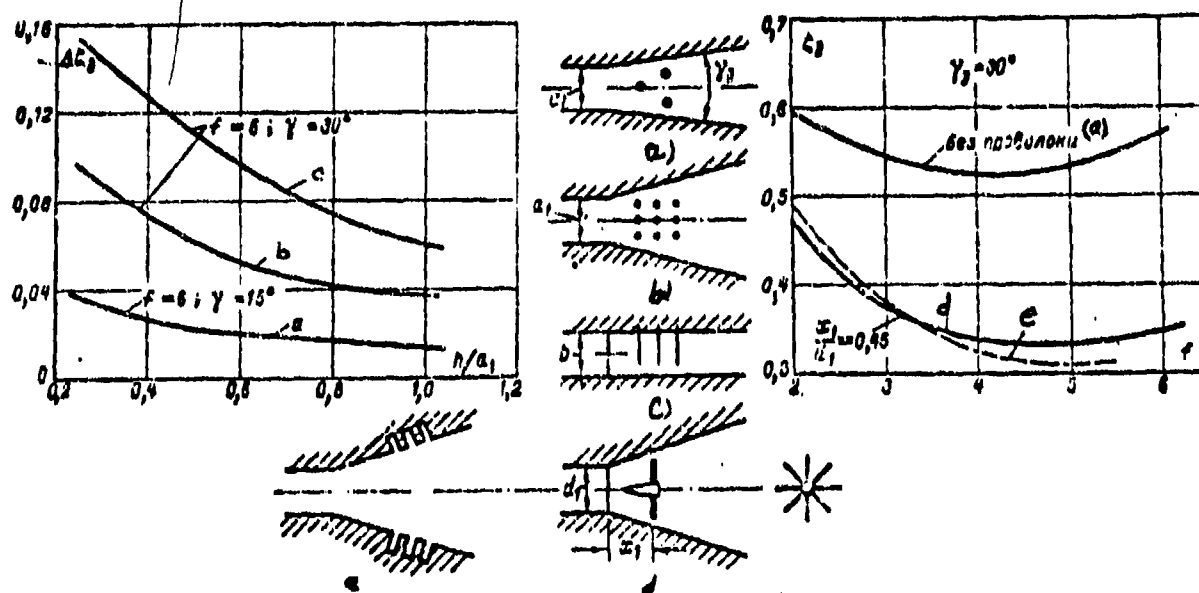


Fig. 7-12. Influence of local resistances on losses in flat diffusers at small velocities.

KEY: (a) Without wires.

### 7-3. Exhaust Ducts of Turbomachines

Exhaust of gas from a turbomachine is carried out along the axis of rotation or according to structural conditions at a right angle to it. Partial conversion of the kinetic energy of the exhaust into potential energy allows an increase in efficiency of the turbomachine. Such conversion is realizable in diffusion

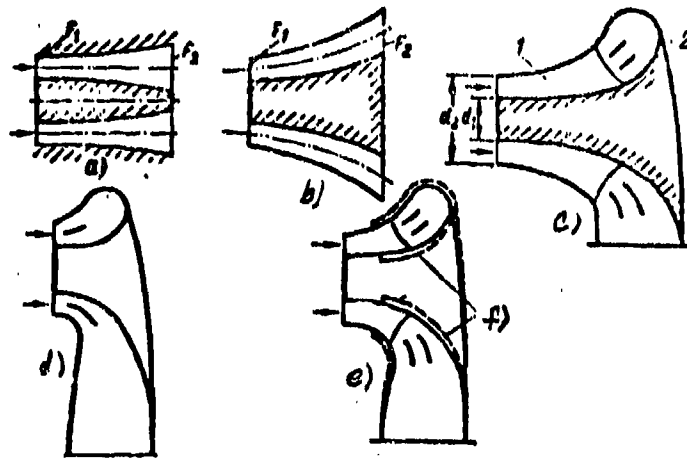


Fig. 7-13. Rational diagrams of exhaust ducts of turbomachines.

exhaust ducts, various diagrams of which are shown in Fig. 7-13.

The first two diagrams (a and b) show the simplest curvilinear annular diffusers  $F_2 > F_1$  with axial or diagonal flow of gas.

The three other ducts must provide a turn of the flow at an angle of  $90^\circ$  to the axis of rotation. In the diagram of the duct in Fig. 7-13, c is applied the developed annular diffuser 1 with a diagonal or axial direction of flow. In such a diffuser basically occurs the conversion of kinetic energy into potential; the turn of the flow by an angle of the order of  $90^\circ$  is realized even at low velocities in the scroll 2. The exit part of the duct (radial diffuser) has relatively small length.

The other diagram (Fig. 7-13,d) ensures pressure recovery after the turn in the radial diffuser. In such a duct it is desirable to make the turn in the converging flow or, in an extreme case, at constant speed.

As can be seen from comparison of diagrams c and d, the first diagram has significantly larger axial dimensions, and the second--radial.

The third diagram (Fig. 7-13,e) is combined. Here are designed relatively short axial (or diagonal) and radial diffusers. Consequently, pressure recovery in such a duct is realized partially before the turn and partially after it. Such a problem is solved in the diagram f, realized with a step diagonal diffuser. The effectiveness of each diagram depends considerably on the method of turn of the flow in the scroll (during transition from axial to radial diffuser). This problem is solved by the corresponding selection of a rational system of annular turning guide blades and vanes, established at the turn.

As it was shown in Section 5-15, in curvilinear channels, there appear secondary motions of the liquid, combined with nonuniform pressure distribution at the turn.

In annular curvilinear channels, the structure of the secondary flows, depending upon the ratios of diameters  $d_2/d_1$ , can differ considerably from the usual for the simple turn. At large values of  $d_2/d_1$  experiment confirms the existence of two vortices in the cross-section of annular channel. If the ratio of the diameters is near to unity, then in the cross-section will appear four vortices, located in the section of the annular channel (two internal and two external).

Bearing in mind what was said above about the influence of the form of the section of the channel, it may be concluded, that inescapable reforming of the section of flow in the ducts of turbomachines should be organized taking into account additional losses, which can arise with this.

Structurally, stiffening ribs are necessary in ducts. Selection of a rational diagram of the location of ribs and their form, which insures minimum losses, constitutes an important problem in the designing of ducts.

Especially complicated constructionally are exhaust ducts of powerful steam turbines. Large volume expenditures of steam in the condensor with constructionally limited axial and radial dimensions leads to a complicated diagram of the duct with a large number of stiffening ribs. An example of the rational distribution of ribs at the turn is shown in Fig. 7-13 and 7-17.

During investigation of exhaust ducts, the main characteristics are determined, experimentally, among which are included: a) a coefficient evaluating power losses

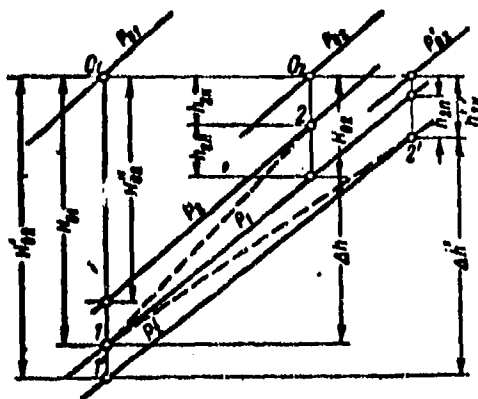


Fig. 7-14. Process in exhaust duct in thermal diagram.

in the duct; b) coefficient of pressure recovery, showing the change in static pressure; c) variation factor of the velocity field in the exit section.

It is convenient to consider the process in the duct in the thermal diagram (Fig. 7-14). Designating by  $p_{01}$  and  $p_{02}$  the stagnation pressures at the entrance the exit from the duct, by  $p_1$  and  $p_2$ —the static pressures in these sections, we find the power loss factor by the formula (7-16).

Having obtained the loss factors in the exit section of the duct, its mean value can be found by the equation of energy.

In Fig. 7-14 are considered two possible cases: a) the exhaust duct of a turbomachine works as a diffuser (process 1-2); b) in the exhaust duct occurs lowering of pressure due to large losses (process 1-2'). Here it is possible to indicate magnitude of kinetic energy after the branch pipe ( $h_{2k}$ ), change of potential energy in the branch pipe ( $h_{2n}$ ) and losses ( $\Delta h$  or correspondingly  $\Delta h'$ ).

In the practice of laboratory investigations of exhaust ducts, other evaluation coefficients also find application. Thus, for example, the laboratory of turbines LMZ uses for evaluation of a duct the quantity

$$\zeta_n = \frac{H_{02}''}{H_{01}}.$$

where  $H_{02}''$  -- isentropic drop corresponding to expansion from the stagnation pressure at the entrance  $p_{01}$  to the static outlet pressure  $p_2$ .

The connection between the power loss factor  $\zeta_1$  and  $\zeta_n$  is established by the following obvious relationships (Fig. 7-14):

$$H_{02}'' \approx H_{01} - h_{2n} = H_{01} - (H_{01} - h_{2k}) = \zeta_n H_{01} + h_{2k},$$

therefore

$$\zeta_n = \zeta_1 + \frac{h_{2k}}{H_{01}} = \zeta_1 + \bar{h}_{2k}.$$

It follows from this that  $\zeta_n$  includes the kinetic energy at the outlet from the branch pipe  $\bar{h}_{2k} = h_{2k} / H_{01}$ . It is easy to see that if  $\zeta_n > 1$  ( $H_{02}'' > H_{01}$ ), then  $p_2 < p_1$  (exhaust duct is not a diffuser); if  $\zeta_n < 1$ , then  $p_2 > p_1$ .

For an incompressible fluid, the coefficient of the duct is defined by the formula

$$\zeta_n = \frac{p_{01} - p_2}{p_{01} - p_1}.$$

Taking into account the compressibility,  $\zeta_n$  can be obtained in the form:

$$\zeta_n = \frac{1 - \left(\frac{p_2}{p_{01}}\right)^{\frac{k-1}{k}}}{1 - \left(\frac{p_1}{p_{01}}\right)^{\frac{k-1}{k}}}. \quad (7-17)$$

The coefficient  $\zeta_n$  allows the calculation of the powerloss in the exhaust duct:

$$\Delta N_n = \frac{\zeta_n H_{01}}{850} G_n, \quad (7-18)$$

where  $G_n$  -- flow of gas through the exhaust duct.

The second characteristic of the exhaust duct, the recovery factor, is determined by the formula

$$\zeta_p = \frac{p_2 - p_1}{\frac{\rho_1 c_1^2}{2}} = \frac{k+1}{k} \frac{\frac{p_2}{p_{01}} - \frac{p_1}{p_{01}}}{\frac{p_1}{p_{01}} \lambda_1^2}. \quad (7-19)$$

From formula (7-19) it is clear that for the determination of the quantity  $\xi_p$ , is necessary measurement of static pressures at entry into the duct. Such an experiment is labor-consuming. Using the discharge coefficient  $G_u = f(p_{01})$  and the table of gas-dynamic functions, pressure  $p_1$  can be obtained by means of calculation.

The third characteristic of the duct allows the evaluation of nonuniformity of the field of static pressures and velocities in the outlet section. As was shown, an important element of the exhaust duct is the curvilinear annular diffuser. Experiments of M. Khibsha showed that the loss factor for such a diffuser depends on the following geometric parameters (Fig. 7-15,a):

The ratio of the areas of sections  $f = \frac{F_2}{F_1}$ ; relative height of the ring at the entrance  $a_1/r_{m1}$ ; relative curvature of the middle line  $\frac{r_{m1}}{R}$ ; relative length of the middle line  $\frac{L}{r_{m1}}$  and the law of change of area  $f(x)$ .

Examples of corresponding dependences are shown in Fig. 7-15,b. Curves show that the optimum value of  $\frac{r_{m1}}{R}$  lies within the limits 0.25--0.4, and with growth of  $f$  this magnitude is increased.

During design of curvilinear diffusers is used the concept of the equivalent conical diffuser, the length of which, and also the areas  $F_1$  and  $F_2$  coincide with the corresponding geometric parameters of the original diffuser. In accordance with this is introduced the concept of the equivalent aperture angle.

An analogous characteristic can be used also for annular curvilinear diffusers.

Losses in the annular curvilinear diffuser increase with an increase in  $f$  and with a decrease in  $a_1/r_{m1}$ .

A significant influence on the loss is rendered by the form of the diffuser in the longitudinal section. The form of the function  $f(x)$  determines the change of pressures along the diffuser, i.e., the structure of the boundary layer and  $\delta^*(x)$ .

Selection of the rational function  $f(x)$  can be carried out, for example, by means of evaluation of the change of  $\xi^{**}$  for different pressure diagrams. Thus, it



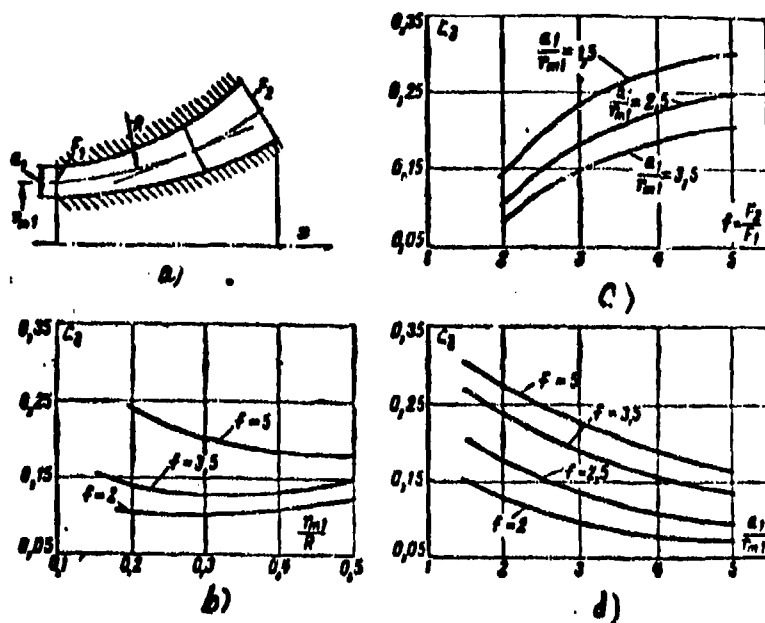


Fig. 7-15. Diagram (a) and loss factors in a curvilinear annular diffuser independence upon the main geometric parameters (b, c and d).

is necessary to consider the design features of the planned machine.

Diagrams of frequently applied annular exhaust ducts are shown in Fig. 7-16. One should note that losses in such diffusers, as a rule, are small, if the indicated geometric parameters are near to optimum. An alternate design of diffuser 4 (Fig. 7-16) with maximum curvature of forms gives maximum losses, but the alternate design of diffuser 2 gives minimum.

Results of the investigation of annular diffusers were used as the basis of development of the exhaust ducts of the turbine, the diagram of which is shown in Fig. 7-17, a. The duct consists of a curvilinear annular diffuser 1 and scroll 2

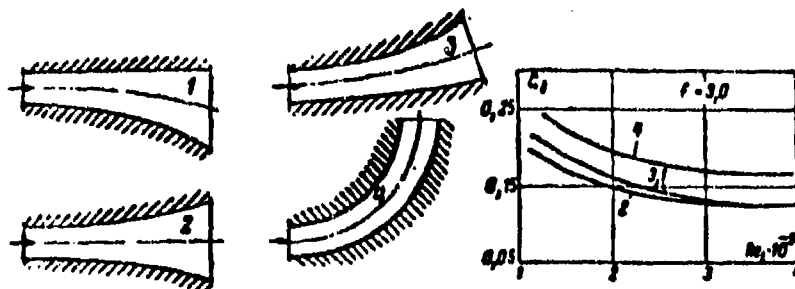


Fig. 7-16. Diagram of the applied annular exhaust ducts (a) and dependence of loss factors on Reynolds number  $Re_1$  (b).

(exhaust part), in which occurs the turn of the flow by  $90^\circ$ . At the entrance to the scroll during the turn, the flow is divided by the central rib 3 and spreads along the curvilinear channels formed by ribs 4, 4', 5, 5' etc. Design of the channels between the ribs is carried out in such a way that losses from secondary flows are minimal. This will be attained by design of the channel to be diffuser-type at the start and then convergent ( $\frac{a_m}{a_1} > 1$  and  $\frac{a_m}{a_2} > 1$ ).

The results of the investigation presented in Fig. 7-17 b of the branch pipe show that its effectiveness considerably depends on the relationship of the areas of the annular diffuser and the scroll  $f = \frac{F_2}{F_1}$  and  $f_1 = F_3/F_1$ . The largest values of the coefficients  $\zeta_u$  are obtained for the variants  $f = 2.5$  and  $f_1 = 1.46$ . With increase of  $f$  to 3.32 and during the corresponding decrease of  $f_1$  to 1.1,  $\zeta_u$  was decreased to 0.75. The variant near to optimum corresponded to the ratios of sections  $f = 3.04$  and  $f_1 = 1.2$ .

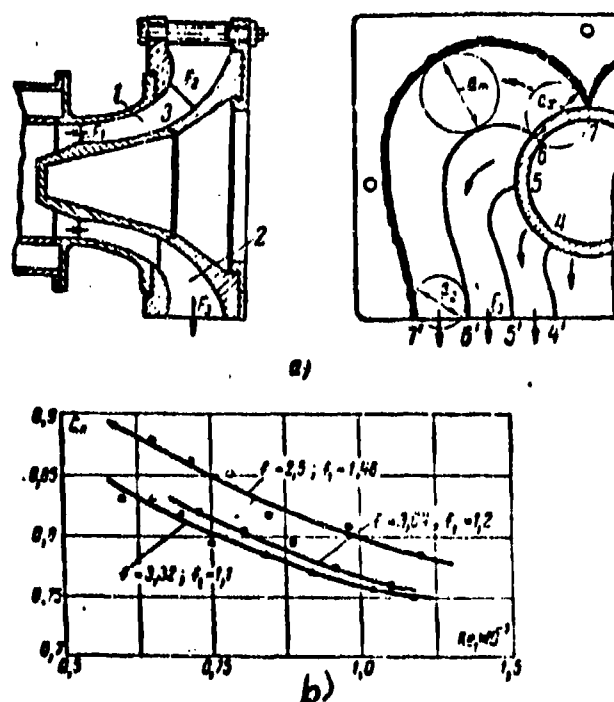


Fig. 7-17. Diagram of exhaust duct of turbine (a) and its characteristics (b).

The obtained values of the coefficients  $\zeta_n$  and their change in dependence upon Reynolds number  $Re_1$  clearly show that for correct selection of the ratio of flow areas, the exhaust duct reacts less abruptly to change of this regime parameter.

A variant of the combined duct with short axial and radial diffusers for the condition of correct selection of relationships of flow areas gives results near to those obtained for the first variant.

The influence of compressibility on characteristics of an exhaust duct can be evaluated by the curves in Fig. 7-18. With an increase of  $M_1$  is noted an increase of losses ( $\zeta_n$  is increased), especially intense at  $M_1 > 0.8$ . It is characteristic that ducts with well-developed annular diffusers are less sensitive to change of  $M_1$  (curves 1 and 2 in Fig. 7-18). The branch pipe without a diffuser practically does not react to a change in  $M_1$  (curve 4) and has  $\zeta_n > 1$ .

Thus, the experiments carried out have shown that introduction of axial and radial diffusers into the design of the exhaust duct allows a considerable improvement of its characteristics and the providing of partial pressure recovery after the turbomachine.

By correct selection of the form and flow areas of diffusers and scroll, and also by rational location of stiffening ribs, it is possible to increase the effectiveness of the duct.

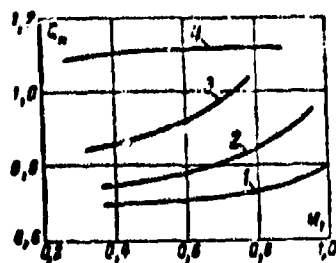


Fig. 7-18. Characteristics of exhaust duct with diffuser (1, 2 and 3) and without diffuser (4).

Experiments show that in certain cases an exhaust duct with vane cascades of the diffusion type established on the turn (Fig. 7-13) have noticeable advantages.

Practical interest has the question concerning the influence of irregularity

(spin) of flow at the entrance into the duct. Corresponding experiments have shown that deflection from the axial entrance within the limits  $\pm 15^\circ$  do not lead to a

noticeable change of characteristics of the duct.

#### 7-4. Supersonic Diffusers

From the fundamental equation of one-dimensional flow it follows that deceleration of supersonic flow can be realized in a pipe of variable section, the inlet of which is narrowed, and the outlet of which is widened. In the first part speed is decreased and will attain a critical value in the minimum section. Then, in the expanded part is continued the process of compression of subsonic flow.

It follows from this that, in principle, it is possible to utilize a supersonic nozzle with contoured walls, as an "ideal" diffuser, considering the flow in it turned (Fig. 7-19). Due to the smoothness of the contoured walls, at every point of which the flow accomplishes a turn on a small angle, in the inlet of the diffuser should appear a system of weak compressional waves (characteristics). Passing through this system, flow is decelerated isentropically. A system of weak compressional waves completely coincides with the system of weak wave of rarefaction

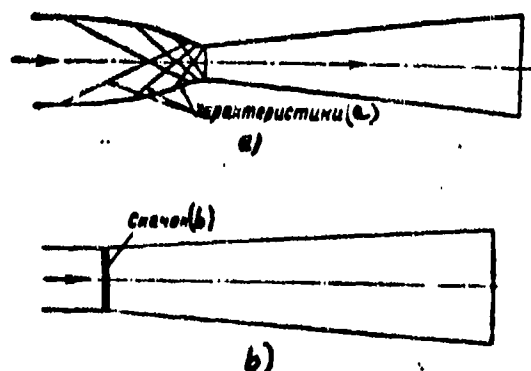


Fig. 7-19. Diagrams of a supersonic (a) and transonic (b) diffuser with straight shock wave at the inlet.

KEY: (a) characteristics; (b) shock.

(characteristics) in the widened part of the nozzle.

In the throat, flow attains critical speed  $\lambda = 1$ . In the widened part of the diffuser velocities are subsonic, decreasing in the direction of flow.

In reality, however, such a diffuser cannot be realized, since flow in it is unstable: small disturbances of flow in the inlet lead to final disturbances at the outlet. This is explained by the fact that for a small decrease of Mach number  $M$  at the inlet into the throat critical velocity will not be established, as a result of which, in front of the diffuser will appear a departed wave. Actually the field of the flow proceeding into the diffuser from the Laval nozzle, as a rule, is non-uniform and saturated with shocks. Besides, due to the appearance of losses in the inlet and formation of a boundary layer, the character of change of flow areas will not correspond to the calculated change. As a result, in the inlet appears a system of shocks.

The process of movement of gas in a diffuser is constructed in the thermal diagram by a known method (Fig. 7-20). Point 1 corresponds to the state of flow at the inlet into the diffuser. Line 1--2 conditionally depicts the process of compression of gas in the system of shocks in the supersonic part of the diffuser. The corresponding increase of entropy  $\Delta s_1$  characterizes basically the wave losses in the inlet of the diffuser. Behind the shocks is established pressure  $p_{2s}$ . If  $p_{2s}/p_{01} < \epsilon$ , then behind the shocks the flow is still supersonic and in the narrowed part of the diffuser compression of the gas is continued. If  $p_{2s}/p_{01} > \epsilon$ , then flow behind the shocks is subsonic. This means that in the narrowed part up to the minimum section the flow will be accelerated and its pressure will fall. If in the minimum section the velocity of flow will attain the critical value, then in the widened part  $\lambda > 1$ . In this case deceleration of flow will occur in the system of shocks after the narrow section. Increase of entropy  $\Delta s_2$  is caused by losses in the subsonic part of the diffuser.

Let us note that full change of potential energy in a supersonic diffuser  $H_{01}$  can be considered as the sum of the change of potential energy in the system of shocks  $h_{0s}$  and in the subsonic part  $h_{0R}$ .

At small supersonic speeds at the inlet ( $M_1 < 1.5$ ) it is possible to apply



ratio of sections  $F_1/F_{*A}$  is increased. Hence, it also follows that for a fixed value of  $F_1/F_{*A}$  change of parameters at the inlet leads to change of losses in the narrowed part. Comparing the two flow regimes for identical initial conditions with different losses, from expression (7-22) can be obtained the formula, showing that the minimum section of the diffuser must be increased in proportion to the change of stagnation pressure in section  $F_{*A}$  :

$$\frac{F_{*A}}{F'_{*A}} = \frac{p_{0*}}{p'_{0*}},$$

or

$$\frac{F_1}{F'_{*A}} = \frac{F_1}{F_{*A}} \cdot \frac{p_{0*}}{p'_{0*}}. \quad (7-23)$$

Here  $p_{0*}$  is the stagnation pressure in the critical section for the given regime;  $p'_{0*}$  is the same for another regime.

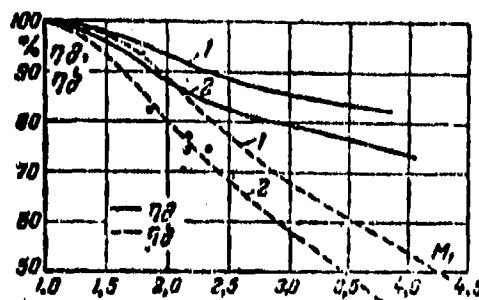


Fig. 7-21. Efficiencies of a supersonic diffuser in dependence upon  $M_1$ : 1--with a normal shock in the throat; 2--with a normal shock at the inlet.

For design of the inlet of the diffuser it is necessary to know the value of the loss factor  $\zeta_{*1}$  and, consequently, the structure and position of shock waves in this section. In the simplest case it is possible to assume that in the inlet is located only one normal shock. The magnitude of  $\zeta_{*1}$ , depends on the location of the normal shock. If the shock appears in section  $F_1$ , energy losses will be maximum; if the shock is located in the narrow section, losses will be significantly lowered.

For illustration, in Fig. 7-21 are shown the corresponding efficiencies of the

diffuser  $\eta_A$  and  $\eta_A'$  for two extreme cases (1--with a normal shock in the throat, and 2--with a normal shock in the inlet), and also experimental values of efficiency. Comparison shows satisfactory coincidence of calculated and experimental values.

The outlet of the diffuser is determined by the equation of continuity. The loss factor in the widened part of the diffuser  $\zeta_{A2}$  in the first approximation can be obtained by the data of tests of subsonic diffusers. They are given as velocities from the outlet of the diffuser.

The full loss factor in the diffuser can be found by the formula (for  $\lambda_1' = 1$ )

$$\zeta_A = 1 - \eta_A = \zeta_{A1} + \frac{v_{A2}^2}{\lambda_1^2}.$$

Stagnation pressure behind the diffuser is determined by equation

$$\frac{p_{02}}{p_{01}} = \left( \frac{k-1}{k+1} \cdot \frac{\lambda_1^2 \zeta_A}{1 - \frac{k-1}{k+1} \lambda_1^2} + 1 \right)^{\frac{k}{k-1}}. \quad (7-24)$$

Wave losses at the inlet can be decreased by introducing stepped deceleration of flow in the inlet (Chapter 4).

Deceleration in the system of shocks is realized by different methods. One of the methods consists of constructing the walls of the inlet section with fissures (Fig. 7-22a). The best result can be obtained with the help of a contoured needle (Fig. 7-22,b). In diffusers of jet engines an analogous system of stepped deceleration is applied (Fig. 7-22,c).

For decrease of wave losses at the inlet a system of reflected shocks is also used (Fig. 7-22,d and -22,e).

Design of a supersonic diffuser with stepped deceleration consists of several stages. In the beginning a system of shocks is established at the inlet and total pressure recovery and wave loss factor in the system of shocks are determined. Then according to the given flow the critical section is calculated:

$$G_* = K F_{*1} p_{01} e_{01} / \sqrt{T_{01}},$$

where  $e_{01} = \frac{p_{02}}{p_{01}}$  is the coefficient of total pressure recovery in the system of shocks.



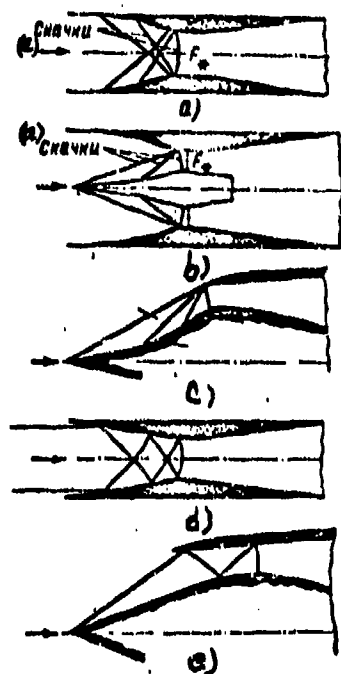


Fig. 7-22. Diagrams of supersonic diffusers with stepped deceleration of flow in a system of shock waves.  
KEY: (a) shocks.

flow of gas G) and outlet pressure  $p_2$ .

Let us assume in the beginning that the parameters of flow at the inlet and flow through the diffuser remain constant, and we will follow the influence of the changing counterpressure  $p_2$ . Let us assume that in section  $F_{*}$  the velocity is equal to critical, but the pressure of the medium is significantly lower than calculated ( $p_a < p_*$ ). In this case the widened part of the diffuser operates as a supersonic nozzle. On the outlet in dependence on  $p_a$  appear waves of rarefaction or slanting shocks. With increase of  $p_a$  the system of shocks is reconstructed; at pressure  $p_a = p_{2k}$  at the outlet section a bridge-like shock is located; upon further increase in  $p_a$ , the shock is transferred inside of the expanded part and moves to the minimum section. At a certain limiting counterpressure  $p_a = p_{2m}$ , the shock is located in the throat of the diffuser (narrow section); flow in the widened part is completely subsonic. To such a regime with a shock in the throat corresponds

It is expedient to make the initial section of the widened part of the diffuser conical. The outlet part of the diffuser is designed according to the selected rational distribution of pressures (Section 7-1). By the results of calculation of the boundary layer, losses of energy in the subsonic part of the diffuser  $\zeta_{A1}$  and, for the selected area of the outlet section  $F_2$ , the velocity at the outlet from the diffuser  $\lambda_2$  are determined.

Let us consider certain characteristics of operation of the supersonic diffuser for off-design conditions. The regime in the diffuser can change as a result of change of the parameters of flow at the inlet ( $\lambda_1, p_1, p_{01}$ ) and, consequently,

the maximum compression ratio in the diffuser.

The corresponding graphs of the distribution of pressures along the diffuser at  $p_a < p_{2m}$  is shown in Fig. 7-23, a (curves OAC, OADE, etc.). This part of the diagram of pressures completely corresponds to the diagram of pressures in the nozzle for the second and third groups of regimes.

Further increase of counterpressure leads to change of the parameters of flow (pressure and density) in the narrow section and in the inlet.

Let us consider now the influence of change of parameters of flow at the inlet into the diffuser. Let us assume that the pressure behind the diffuser is maintained constant ( $p_a < p_{2m}$ ). Velocity at the inlet  $\lambda_1'$  is increased. At subsonic speeds at the inlet ( $\lambda_1' < 1$ ) in the narrowed part, flow is accelerated and maximum velocity will be attained in the narrow section  $F_{*1}$ . With increase of  $\lambda_1'$  the flow of gas and the velocity in the narrow section  $\lambda_1$  increase.

At some value  $\lambda_1'' < 1$  the velocity in section  $F_{*1}$  equals critical ( $\lambda_1' = 1$ ). Further increase of flow at constant static pressure in front of the diffuser becomes impossible. In accordance with this, the increase of speed  $\lambda_1' > \lambda_1''$  will entail an increase in pressure in the inlet section of the diffuser and in all other sections of the narrowed part; as a result, at  $\lambda_1' > 1$  in front of the diffuser will appear a shock. With increase of  $\lambda_1'$  the shock approaches the diffuser and at a certain value of  $\lambda_1'$  is located in the inlet section  $F_1$ . If the shock in the inlet is normal, then in the narrowed part flow is subsonic and accelerated toward the minimum section. So that the normal shock (or system of shocks) penetrates into the narrowed part of the diffuser, further increase of velocity  $\lambda_1'$  is necessary ( $\lambda_1' > \lambda_1$ ).

Since during movement of the shock toward the throat, losses of energy are decreased, then in the minimum section the critical velocity can occur again. In certain cases at  $p_a = p_{2m}$  during transition to the widened part, the flow continues to be accelerated and becomes supersonic. Then in the widened part of the diffuser appear shocks. In such regimes losses in the diffuser abruptly increase.\*

\*The considered case is shown by the dashed and dotted line in the diagram 1--s in Fig. 7-20.

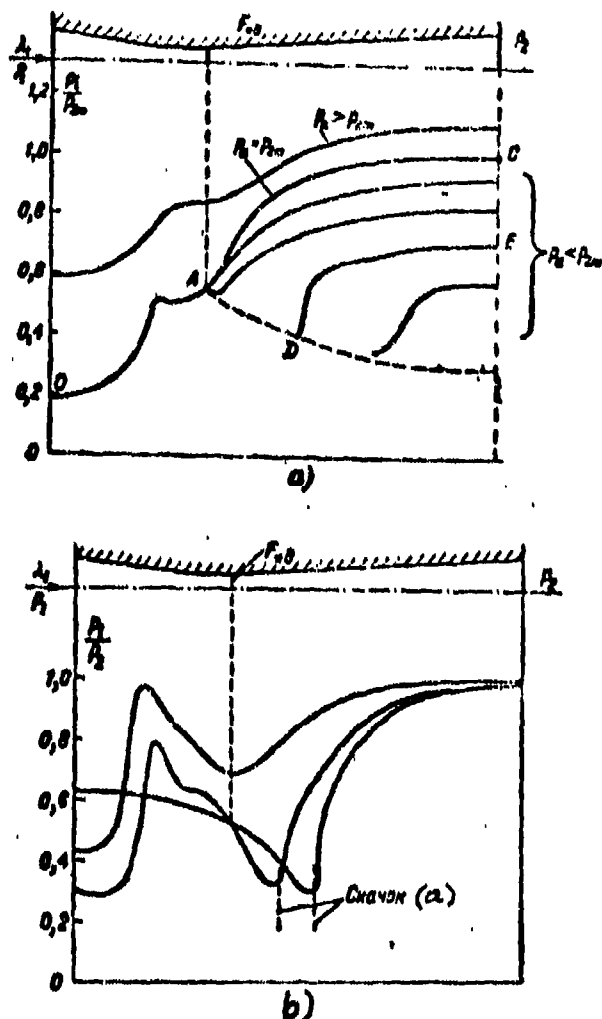


Fig. 7-23. Distribution of pressures in a supersonic diffuser at different regimes.  
KEY: (a) shock.

The considered regimes are illustrated by graphs of the distribution of pressures in Fig. 7-23, b. At the simultaneous appearance of shocks in the narrowed and widened parts of the diffuser, distribution curves of pressures assume the characteristic loop-shaped form.

Consideration of operational conditions of a supersonic diffuser at off-design conditions shows that the ratio of sections  $F_{x,0}/F_1$  must change during change of the parameters of flow at the inlet or outlet. In the period of starting the ratio  $F_{x,0}/F_1$  must be maximum. In operation any disturbance of the regime can be

partially compensated by corresponding change of the ratio  $F_{1,2}/F_1$ .

Will analyze in more detail the variable regimes of a diffuser with changing minimum section in the process of operation. If the minimum section is decreased gradually from  $F_{1,2} = F_1$  to that value with which velocity  $M_* = 1$ , then flow of gas through the diffuser will be kept constant ( $G = gF_1 \rho_1 c_1$ ). However, if the area of the throat is further decreased, then flow through the diffuser will be decreased. Near the narrow section will appear a shock wave, since the narrowed throat represents additional resistance. Due to increase of entropy in the shock, the pressure in the minimum section drops, but velocity and temperature are kept maintained constant. Due to the decrease in density, flow is decreased to a still larger degree and the shock will move against the flow. The intensity of the shock will grow. Movement of the shock in the direction against the flow will continue until it goes beyond the inlet section  $F_1$ ; the shock will occupy a position relative to  $F_1$ ; at which a part of the gas will go out into the external flow passing the diffuser (Fig. 7-24,a).

Upon further decrease of  $F_{1,2}$ , the shock will move against the flow, providing the necessary decrease of flow through the diffuser; the intensity of the shock will be maintained practically constant.

Considering now the reverse process—increase in  $F_{1,2}$ , it may be concluded that if  $F_{1,2}$  attains that value at which the shock first appeared, then the shock will not disappear, since the decreased density in the throat causes partial expulsion of the mass of gas into the external flow. Consequently,  $F_{1,2}$  must be increased to such limits in order to to compensate for the decrease in density in the throat. Subsequent increase in  $F_{1,2}$  will lead to displacement of the shock inside the diffuser and will provide a constant maximum flow through the diffuser.

That which was stated shows that in the diffuser with a throat of variable section are observed hysteresis phenomena. Graphs in Fig. 7-24,b additionally illustrate these phenomena. In the diagram of the dependence of  $G/G_0$  on  $F_{1,2}$ ,

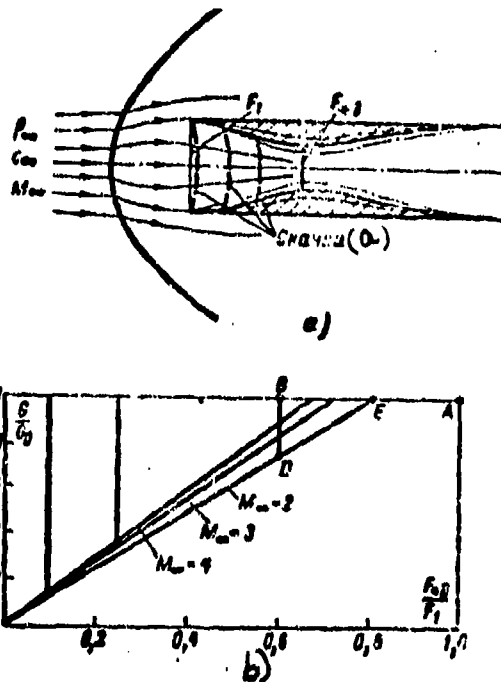


Fig. 7-24. Diagram of a diffuser with regulated minimum section (a) and its discharge characteristic (b) different regimes.  
KEY: (a) shocks.

( $G$  is the flow through the diffuser;  $G_0 = gF_1 \rho_{\infty} c_{\infty}$ ), it is possible to indicate the point A, corresponding to  $F_{2A} = F_1$  ( $G = G_0$ ). With decrease of  $F_{2A}$  flow is kept constant up to point B, which corresponds to  $M_1 = 1$  in the throat; in front of the diffuser appears a shock, and flow falls to the value at point D. Further decrease of  $F_{2A}$  leads to change of flow along the line DO.

With increase in  $F_{2A}$  the shock in front of the diffuser is maintained up to that value of  $F_{2A}$  which corresponds to point E. The diffuser returns along the line ODEA to the original point A. As a result, a hysteresis loop EBDE will be formed, and in order to establish the state of flow in the diffuser at arbitrary  $F_{2A}$ , it is necessary to know what the direction of change of  $F_{2A}$  was.

It is necessary to underline the fact that regimes with shock waves in front of the diffuser are characterized by a sharp increase of resistance. The dimension of the hysteresis loop depends on Mach number  $M_1$ , with whose growth segment BD is displaced to the left (Fig. 7-24,b). One should note that the region between curves

1 and 2 in Fig. 7-24 characterizes unstable operating regimes of the diffuser, with which a shock can appear and disappear.

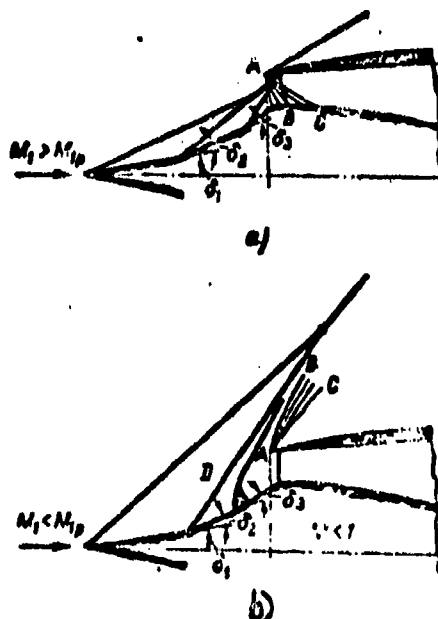


Fig. 7-25. Diagrams of spectra in diffusers with stepped deceleration at the inlet for different regimes.

As it was shown, in practice, controlled supersonic diffusers (Fig. 7-23) with stepped deceleration at the inlet are applied.

In those cases when the internal cone has the possibility of axial displacements, it is possible not only to improve the conditions of starting and operation of the supersonic diffuser, but also to provide higher efficiency of the diffuser at rated and off-design conditions.

Change of velocity of flow at the inlet in such diffusers leads to change of the angles of slope of the shocks: at  $M_1 > M_{1p}$ , the angles of shocks are decreased

but at  $M_1 < M_{1p}$ , they are increased.

In the first case (Fig. 7-25,a) interaction of the shocks with the opposite wall will occur inside the throat or in the widened part. Also possible is distortion of the shock near the external surface of the diffuser. During flow around the edge there appears a wave of rarefaction ABC; as a result flow at the inlet in the diffuser becomes nonuniform.

In the second case, when  $M_1 < M_{1p}$ , shocks do not occur at the entrance of the diffuser (Fig. 7-25,b). For this reason the flow of gas through the diffuser is decreased and the wave losses in the shocks (Chapter 4) increase. At the entrance of the diffuser appears a wave of rarefaction ABC.

At decrease of  $M_1$  the velocity of flow before the second turn (point D) can become less than that value at which is still possible the existence of a rectilinear shock (angle  $\delta_s > \delta_{lim}$ ). In this case distortion and departure of the shock from the corner occur; losses at the inlet in the diffuser noticeably increase.

Characteristics of a controlled diffuser for variable velocities at the inlet are presented in Fig. 7-26.

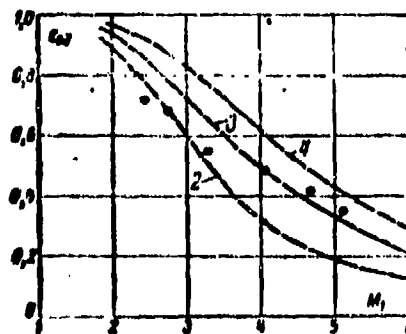


Fig. 7-26. Coefficients of stagnation pressure recovery in supersonic diffusers for variable regimes. Numbers on the dotted curves indicate the number of shocks (by calculation). Experimental points are drawn for a four-shock diffuser.

The position of the normal shock, closing the system, depends on the outlet

of the diffuser. If the outlet becomes larger than rated, then the normal shock in the throat does not occur--flow remains supersonic in the widened part, where, as it was shown above, there appears a system of shocks, in which flow changes to subsonic velocities.

Upon decrease of the outlet, the normal shock is displaced from the throat in the direction against the flow. In both cases wave losses in the diffuser increase.

#### 7-5. The Ejector Stage\*

Gas ejectors find wide and varied application in technology. In such apparatuses mixing of gas flows occurs (in the simplest and most wide-spread case--two). As a result of mixing, parameters of deceleration and the static parameters of mixing flows change. The main characteristic of the physical process in the ejector is that the mixing of flows occurs at high velocities of the ejecting (active) gas.

The principle of action of the ejector stage can be comprehended from consideration of the diagram presented in Fig. 7-27. Main elements of the stage are

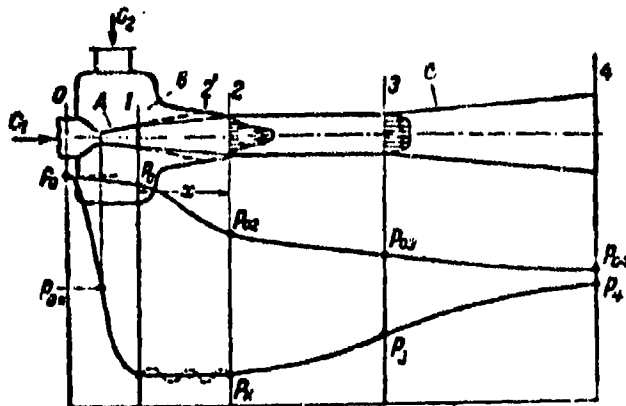


Fig. 7-27. Diagram of ejector stage.

nozzle A, mixing chamber B and diffuser C\*\*. Ejecting gas under pressure moves to the nozzle A. Expanding in the nozzle, the flow of gas acquires in section 1 supersonic speed. In the mixing chamber B a stream of active gas interacts with the ejected (passive) medium and carries it along into the diffuser, where compression

\*Article A 7-5 was composed with the participation of M. V. Polikovskiy; Articles 7-6 and 7-7 were written jointly with A. V. Robozhevyy.

\*\*The diffuser of the supersonic ejector usually consists of a conical inlet section, cylindrical throat and widened outlet section.



of the formed mixture occurs.

Experimental study of the mechanism of ejection in the mixing chamber shows that the most important influence on the process of mixing is rendered by the turbulence of the flows and the wave structure of the supersonic ejecting stream.

Study of the spectra of the axially-symmetric supersonic stream (Fig. 6-28 and 6-29) allows us to establish that with moving away from the nozzle, on the periphery of the stream a boundary layer will be formed. In the annular boundary layer speeds change from small subsonic on the periphery to supersonic in the section adjacent to the flow core. Let us note that in accordance with the wave spectrum of the stream the static pressure along the axis of the flow core periodically changes. Along the diameter of the stream, pressures are also distributed nonuniformly: in the stream will be formed transverse pressure gradients. In sections behind shocks pressure gradients are directed toward the periphery of the stream, and in sections behind waves of rarefaction--toward the axis of the stream. In the subsonic section of the boundary layer static pressure is near to the pressure of the medium. At some distance from the nozzle the entire stream becomes subsonic: in this region static pressure is distributed along the axis and the section practically uniformly.

These properties of the field of the axially symmetric supersonic flooded stream allow us to conclude that between the external medium and the stream there occurs continuous exchange of particles. Transverse displacements of particles from the boundary layer into the core and from the core into the boundary layer take place with an intensity which is variable along the axis.

We will return to consideration of the process in the ejector stage (Fig. 7-27). In section 2 mixed flow with a nonuniform velocity profile fills the inlet part of the diffuser. In section 2-3 in the throat of the diffuser further mixing of flow occurs\*. In section 1-2 the process of mixing can be considered approximately isobaric. In section 2-3 mixing and equalizing of flow are accompanied by an increase of average pressure in the section. In the outlet part of the diffuser

\*The inlet part and throat of the diffuser sometimes are called the mixing chamber.

(section 3-4) there occurs further increase of pressure.

In the literature sometimes another diagram of the process of mixing is considered, when the distance between the exit of the nozzle and the inlet of the throat of the diffuser  $x = 0$ . Such ejectors (compressors) are called ejectors with a cylindrical mixing chamber or with constant area of mixing.

However, the indicated difference has no special meaning, since the considered diagram (Fig. 7-27) can be changed into the other by means of continuous decrease of the magnitude of  $x$  to zero.

For determination of the parameters of mixed flow in the outlet of the throat (section 3) we will use the equations of momentum, energy conservation and continuity. In the first approximation we will consider that the field of pressures and velocities in sections 1 and 3 are uniform; influence of force of the wall on flow is absent; the pressure forces acting on the flow from the wall of the throat do not leave axial components; frictional forces in the first approximation also can be disregarded. Therefore the change of momentum between section 1 and 3 equals the difference of the pulses of pressure forces in these sections. Consequently, the equation of momentum for sections 1--3 can be written in the form:

$$\begin{aligned} \frac{G}{g} c_{1t} + p_1 F_1 + \frac{G_2}{g} c_2 + p_3 (F_{3x} - F_1) = \\ = \frac{G_1 + G_2}{2} c_3 + p_3 F_{3x}, \end{aligned} \quad (7-25)$$

where  $G$ —rate of flow of ejecting (active) gas;

$c_{1t}$ ,  $p_1$ —speed and pressure in the outlet of the nozzle during isentropic outflow;

$c_2$ ,  $G_2$ —flow rate and velocity of ejected (passive) gas;

$c_3$ ,  $p_3$ —velocity and pressure of mixed flow in the outlet of the throat of the diffuser;

$F_{3x}$ ,  $F_1$ —area of section of throat of diffuser and outlet of nozzle.

In the general case the sum of momentum and pressure forces i.e. pulse of flow, is expressed by the formula of B. M. Kiselev [(2-44) and (2-45)].

Placing expression (2-44) into the equation (7-25), we obtain after simple

transformations:

$$\begin{aligned} \frac{k+1}{2k} \frac{G_1}{g} a_{*1} \left( \lambda_{*1} + \frac{1}{\lambda_{*1}} \right) + \frac{G_2}{g} \lambda_{*2} a_{*2} + p_k (F_{*2} - F_{*1}) = \\ = \frac{k+1}{2k} a_{*3} \frac{(1+x) G_1}{g} \left( \lambda_{*3} + \frac{1}{\lambda_{*3}} \right), \end{aligned} \quad (7-26)$$

where  $x = G_2/G_1$  — coefficient of ejection;

$a_{*1}$ ,  $a_{*2}$  and  $a_{*3}$  critical velocities of active, passive and mixed flows;

$\lambda_{*1}$  — dimensionless velocity at outlet from nozzle for isentropic outflow.

It is possible to express the flow of active gas by the formula

$$G_1 = g F_{*c} \rho_* a_{*1},$$

where  $\rho_*$  is the density in the critical section of the nozzle:

$$\rho_* = \left( \frac{2}{k+1} \right)^{\frac{1}{k-1}} \rho_0 = \left( \frac{2}{k+1} \right)^{\frac{1}{k-1}} \frac{p_0}{g R T_{01}}; \quad (7-27)$$

bearing in mind that  $a_{*1} = \sqrt{\frac{2kg}{k+1} R T_{01}}$ , and introducing function  $\psi$  [formula (2-45)], we will represent equation (7-26) in the form:

$$\begin{aligned} \psi(\lambda_{*1}) + \frac{2k}{k+1} x \sqrt{\frac{T_{02}}{T_{01}}} \lambda_{*2} + \left( \frac{k+1}{2} \right)^{\frac{1}{k-1}} \frac{p_k}{p_*} \left( \frac{F_{*2}}{F_{*c}} - \frac{F_{*1}}{F_{*c}} \right) = \\ = (1+x) \sqrt{\frac{T_{03}}{T_{01}}} \psi(\lambda_{*3}), \end{aligned} \quad (7-28)$$

where  $T_{03}$  — stagnation temperature of mixed flow.

The ratio of stagnation temperatures  $T_{02} / T_{01}$  and  $T_{03} / T_{01}$  can be expressed with the help of the equation of energy:

$$G_1 i_{01} + G_2 i_{02} = (G_1 + G_2) i_{03}.$$

Hence, considering the heat capacities of the mixed flows to be identical, we come to the expression

$$\frac{i_{02}}{i_{01}} = \frac{T_{02}}{T_{01}} = \tau_2 = \frac{1+x\tau_1}{1+x}, \quad (7-29)$$

where  $\tau_1$  is the relative stagnation temperature of passive flow:

$$\tau_1 = \frac{i_{02}}{i_{01}} = \frac{T_{02}}{T_{01}}.$$

Let us note that critical velocities  $a_{*1}$  and  $a_{*2}$ ,  $a_{*1}$  and  $a_{*3}$  of the flows are connected by the obvious relationships:

$$\frac{a_{*2}}{a_{*1}} = \sqrt{\frac{T_{02}}{T_{01}}} = \sqrt{\tau_1} \quad \text{and} \quad \frac{a_{*3}}{a_{*1}} = \sqrt{\frac{T_{03}}{T_{01}}} = \sqrt{\tau_2}.$$

Placing expression (7-29) into the equation (7-28), we obtain:

$$\begin{aligned} \psi(\lambda_{11}) + \frac{2k}{k+1} x \sqrt{\tau_1} \lambda_1 + \left( \frac{k+1}{2} \right)^{\frac{1}{k-1}} \frac{p_k}{p_0} \left( \frac{F_{*1}}{F_{*c}} - \frac{F_1}{F_{*c}} \right) = \\ = \sqrt{(1+x)(1+x\tau_1)} \psi(\lambda_1). \end{aligned} \quad (7-30)$$

Equation (7-30) establishes the connection between the dimensionless gas-dynamic parameters  $p_k/p_0$ ,  $x$ ,  $\tau_1$ , and  $\lambda_1$ , and the geometric characteristics of the ejector  $F_{*1}/F_{*c}$  and  $F_1/F_{*c}$ . One should bear in mind that the ratio  $F_1/F_{*c}$  also is a function of  $\lambda_{11}$ . The velocity  $\lambda_1$  is usually small, and in practical calculations it is possible to disregard the second term of the equation.

Analysis of equation (7-30) shows that for the given values of  $x$ ,  $\lambda_1$ ,  $p_k/p_0$ , and  $\tau_1$ , the velocity in the inlet of the throat  $\lambda_1$  is determined ambiguously; equation (7-30) is satisfied by two values of  $\lambda_1$ , connected by the equation

$$\lambda_1' \lambda_1'' = 1.$$

The physical meaning of the ambiguity of determination of  $\lambda_1$  is obvious, if one considers that in a normal shock wave the velocities in front of the shock and behind it are connected by the same kind of relationship. Inasmuch as in the shock the pulse, flow of gas and stagnation temperature do not change, the fundamental equation of the ejector stage (7-30) remains correct, independently of whether or not there appears a shock in the throat. With a sufficiently long throat which provides equalizing of the mixed flow, there usually is realized a subsonic solution of equation (7-30). Transition to subsonic flow occurs in the system of shocks in the throat.

Equation (7-30) serves for determination of the basic geometric characteristic of the ejector stage  $F_{*1}/F_{*c}$ , or, if this magnitude is known, equation (7-30) can be used for determination of the gas-dynamic parameters  $x$  and  $p_k/p_0$ , or  $x$  and  $p_k/p_0$  under the conditions of variable regime. In the last case, it is necessary to use still one equation--continuity, which allows us to determine the stagnation pressure in section 3.

The equation of continuity for the outlet of the throat is presented in

the form:

$$G_1 + G_2 = F_{\infty} \rho_{\infty} c_{\infty} g.$$

After division by  $G_1$  we find:

$$(1 + x) = \frac{F_{\infty} \rho_{\infty} c_{\infty}}{F_{\infty} \rho_{\infty} c_{\infty}} \cdot \frac{c_2}{a_1}.$$

Since

$$\rho_2 c_2 = q_2 \rho_2 a_{23},$$

then

$$(1 + x) = q_2 \frac{F_{\infty}}{F_{\infty}} \cdot \frac{\rho_{23} a_{23}}{\rho_{\infty} a_{21}}.$$

Noticing that

$$\frac{\rho_{23}}{\rho_{\infty}} = \frac{\rho_{21}}{\rho_{\infty}} \cdot \frac{1}{\tau_2} = \frac{\rho_{21}}{\rho_{\infty}} \cdot \frac{1+x}{1+x_1} \quad \text{and} \quad \frac{a_{23}}{a_{21}} = \sqrt{\tau_2} = \sqrt{\frac{1+x_1}{1+x}},$$

we finally obtain:

$$\frac{\rho_{23}}{\rho_{\infty}} = \frac{F_{\infty}}{F_{\infty}} \cdot \frac{1}{q_2} \sqrt{(1+x)(1+x_1)}. \quad (7-31)$$

From equation (7-31) it follows that the stagnation pressure in the outlet of the throat depends on velocity  $\lambda_1(q_2)$ ,  $x$ ,  $\tau_2$  and  $F_{\infty}/F_{\infty}$ .

Static pressure  $p_4$  after the diffuser is connected with the stagnation pressure  $p_{04}$  and dimensionless velocity  $\lambda_1$  at the outlet from the diffuser by the obvious relationship:

$$\frac{p_4}{p_{04}} = \left(1 - \frac{k-1}{k+1} \lambda_1^2\right)^{\frac{k}{k-1}}. \quad (7-32)$$

Usually velocity  $\lambda_1$  is small and in first order of approximation it is possible to consider that  $p_4 \approx p_{04}$ . If in the widened part of the diffuser losses are small, then the stagnation pressure in sections 3 and 4 can be approximately taken as identical, i.e., considered as

$$p_{03} \approx p_{04}.$$

Thus, assuming that velocity  $\lambda_4$  is small and losses in the widened part are absent, we can determine the pressure behind the diffuser  $p_4 \approx p_{03}$  by the formula (7-31). If the velocity  $\lambda_1$  cannot be considered as a negligibly small quantity, then  $p_4$  is determined by the formula (7-32).

The equations obtained in the assumption of the simplest one-dimensional

character of the process in the ejector, (7-30) and (7-31), evaluate only losses of mixing, which are basic in the considered problem. However, along with losses of mixing, it is necessary to consider also other losses in separate elements of the ejector: losses in the nozzle, in the inlet of the diffuser and in the throat\*, and also losses in the widened part. Besides, the process in the inlet of the diffuser in reality can deviate from the isobaric process assumed during derivation of equation (7-30). Change of pressure in the general case does not start exactly in the inlet of throat 2, but higher or lower along the flow in the initial section of the diffuser. Further, the fundamental equation of momentum must be supplemented by a term expressing the influence of pressure forces from the wall of the inlet section of the diffuser. At the same time, even for a significant length of the throat, one should consider the nonuniformity of the field of flow in section 3, which considerably affects the effectiveness of the diffuser.

Calculation of all enumerated factors characterizing the actual process in the ejector stage is carried out on the basis of the following considerations.

Losses in the nozzle are taken into account by the velocity coefficient. The actual outflow velocity from the nozzle equals:

$$\lambda_1 = \varphi_c \lambda_{1u} = \sqrt{1 - \zeta_c} \lambda_{1u}.$$

The coefficient  $\varphi_c \approx \sqrt{1 - \zeta_c}$  is determined with the help of the curves presented in Fig. 6-31.

Losses in the widened part of the diffuser, taken into account by the coefficient  $\zeta_{01}$ , can be taken according to the graph in Fig. 7-4 in dependence upon the velocity  $\lambda_3$  in the outlet of the throat.

The force influence on flow of the wall of the inlet of the diffuser is considered by introduction into the equation of momentum the pulse from the walls

---

\*In the inlet and the throat, except for basic losses of mixing, there appear losses caused by friction and wave losses.

$I_{ct}$ . The specific impulse from the walls of the initial section of the diffuser is calculated, equal to:

$$\xi_{cy} = \frac{I_{cy}}{\frac{k+1}{2k} \cdot \frac{G_1}{g} a_{11}} = \left( \frac{k+1}{2} \right)^{\frac{1}{k-1}} \frac{I_{cy}}{p_0 F_{c0}} \quad (7-33)$$

The absolute value  $\xi_{cy}$  depends on the operating regime and geometric parameters of the stage, first of all on the coefficient of ejection  $\alpha$ , the ratio  $p_k/p_0$ , the angle of conicity of the inlet of the diffuser, the distance from the exit edge of the nozzle to the beginning of the throat of the diffuser and the ratio  $F_{*k}/F_{*0}$ .

Experimental investigation of the influence of nonuniformity of flow in the outlet of the throat shows that this factor also should be considered during design of the stage.

It is established that incomplete equalizing of flow in the throat leads to a redistribution of the compression work between the throat and the widened part of the diffuser. With increase of nonuniformity in section 3 the compression work and losses in the throat are decreased, and in the widened part increased. Detailed analysis shows that into the fundamental equation of the ejector should be introduced coefficients which take into account the influence of irregularity.

Taking into account all losses and nonuniformity of the field in section 3, the equations of the ejector stage take the form:

$$\psi(\lambda_1) + \frac{2k}{k+1} \alpha \sqrt{\varphi_1 \lambda_1} + \left( \frac{k+1}{2} \right)^{\frac{1}{k-1}} \frac{p_k}{p_0} \left( \frac{F_{*k}}{F_{*0}} - \frac{F_{*1}}{F_{*0}} \right) -$$

$$-\xi_{cy} = \sqrt{(1+\alpha)(1+\alpha\varphi_1)} \varphi_1(\lambda_1); \quad (7-34)$$

$$\frac{p_{01}}{p_0} = \frac{e_{01}}{q_0} \frac{F_{*0}}{F_{*k}} \sqrt{(1+\alpha)(1+\alpha\varphi_1)}; \quad (7-35)$$

$$\psi(\lambda_1) = \varphi_c \lambda_{11} + \frac{1}{\varphi_c \lambda_{11}}; \quad (7-36)$$

where

$$\varphi_1(\lambda_1) = \varphi_n \lambda_1 + \frac{1}{\lambda_1};$$

$$e_{01} = \frac{p_{01}}{p_{00}};$$

$\varphi_n$  is the coefficient which takes into account the nonuniformity of the field

in the outlet of the throat; it can be calculated if the velocity profile is known.

By experiment it is established that in the limit regime (see below) for a definite (optimum) length of throat, the average velocity of mixed flow in the outlet of the throat of the diffuser attains a critical value, and the velocity profile approaches a quadratic parabola. This allows the calculation of this coefficient for a particular case and setting  $\varphi_n = 1.22$  to  $1.26$ . According to experimental data, values of the coefficient  $\varphi_n$  in variable regimes oscillate on the average within the limits  $\varphi_n = 1.0$  to  $1.3$ . Smaller values of  $\varphi_n$  correspond to a more uniform field of velocities. All coefficients  $\varepsilon_{01} = \frac{p_{01}}{p_{02}}$ ,  $\varphi_c$ ,  $\varphi_n$  and  $\varepsilon_{n,y}$  change during change of the operating regime of the stage and the contour of the flow through part of the stage (form of nozzle and diffuser) and for the time being can be obtained only by experimental means.

Design of the stage for  $x=0$  is carried out by analogous equations. The equation of impulses for this case has the form:

$$\psi(\lambda_1) + x \sqrt{\varepsilon_1} \psi(\lambda_1) = \psi_1(\lambda_1) \sqrt{(1 + \gamma)(1 + x \varepsilon_1)}, \quad (7-37)$$

where

$$\psi(\lambda_1) = \varphi_{c2} \lambda_{21} + \frac{1}{\varphi_{c2} \lambda_{21}}; \quad (7-38)$$

$\varphi_{c2}$  is the velocity coefficient of the nozzle of the passive gas.

Equation (7-37) does not contain the basic geometric parameter of the stage  $F_{21}/F_{c2}$ . The connection between  $F_{21}/F_{c2}$  and the coefficient of ejection, as before, is expressed by equation (7-35).

#### 7-6. Ejector Stage at Variable Regimes; Limit Regime

Under operating conditions the ejector stage frequently operates in regimes which are difficult from the intended one. Causes of deviations from rated conditions may be changes of the initial parameters (and consequently flow) of the ejecting



gas, parameters and flow of the ejected gas and pressures of the mixed flow behind the diffuser.

The number of independent parameters determining the regime of the stage and the connection among these parameters is established by equations (7-34) and (7-35), which at  $F_{0,2}/F_{0,1} = \text{const}$  are fundamental equations of the variable regime the stage.

According to equation (7-34) and (7-35) in the number of dimensionless parameters determining the regime of the step are included:

- a) coefficient of ejection  $\alpha = \frac{G_2}{G_1}$ ;
- b) compression ratio (increase of pressure) in the stage  $\epsilon_2 = p_4/p_k$ ;
- c) net drop of pressures  $p_k/p_0$ ;
- d) ratio of stagnation temperatures of mixed flows  $\tau_1 = \frac{T_{0,2}}{T_{0,1}}$ .

During change of regime of the stage, the operating conditions of its separate elements are changed: nozzle, mixing chamber and diffuser. There occurs a redistribution of losses in the indicated elements of the stage. Under the operating conditions simultaneous change of all four parameters is possible. In this case all elements of the stage operate under off-design conditions.

We will analyze the behavior of the stage during deviations of the regime caused by change of pressure behind the diffuser  $p_4$  or change of pressure in the mixing chamber  $p_k$ , assuming that the pressure of ejecting gas before nozzle  $p_0$  and the ratio  $\tau_1$  remain constant.

At constant pressure before the nozzle, change of pressure in the mixing chamber  $p_k$  or of pressure after the stage  $p_4$  leads to change of the quantity of ejected gas. It is obvious that in this case the compression ratio in the diffuser  $\epsilon_2 = p_4/p_k$  changes.

According to equations (7-34) and (7-35), between the coefficient of ejection  $\alpha$  and the compression ratio  $\epsilon_2$  there exists a definite dependence, which is called the characteristic of the stage or regime diagram. The form of this characteristic is determined according to which of the two basic parameters ( $p_k$  or  $p_4$ ) changes

during change of the regime.

1. Operation of the stage at constant intake pressure. We will follow the character of the change of basic parameters of the regime during increase of the coefficient of ejection from  $\alpha=0$  (idle running) to the maximum  $\alpha=\alpha_{np}^*$  at  $p_k = \text{const.}$

At  $\alpha=0$ , the gate valve on the line of intake is completely closed and the pressure after the diffuser will attain the maximum value  $p_4 = p_{4m}$  for the given  $p_k$ . For increase of  $\alpha$  it is necessary to decrease the counterpressure  $p_4$ , i.e., the resistance of the flow through part, maintaining  $p_k$  constant; in this case the

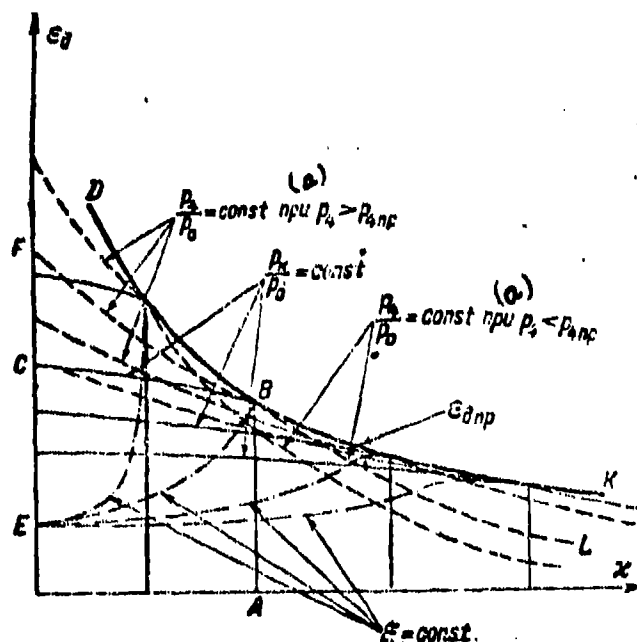


Fig. 7-28. Characteristics of ejector stage.  
KEY: (a) at.

compression ratio in the stage is lowered. On segment CB of the considered characteristic (Fig. 7-8) velocities in sections 2 and 3 ( $\lambda_2$  and  $\lambda_3$ ), shown in Fig. 7-27, are increased (from the condition of continuity).

\*  $\alpha_{np}$  is the limit coefficient of ejection.

At a certain value of the coefficient of ejection  $\kappa = \kappa_{np}$  the velocity in the initial section of the throat of the diffuser will attain the maximum value, and the velocity in the outlet section of the throat is near to critical ( $\lambda_3 \approx 1$ ). The ratio of pressures  $p_3/p_{04}$  in the widened part of the diffuser is also near to critical. Further decrease of the counterpressure does not lead to change of the coefficient of ejection. In this section the characteristic of the stage  $\varepsilon_{\Delta} = f(\kappa)$  is located parallel to the axis  $\varepsilon_{\Delta}$  (segment AB). This means that in the considered regime the capability of the stage does not depend on the compression ratio, and the coefficient of ejection is equal to the limit ( $\kappa = \kappa_{np}$ ).

The maximum coefficient of ejection for a given value of  $p_k/p_0$  is called the limit coefficient; the corresponding counterpressure is called the limit counterpressure. This regime, corresponding on the diagram to point B, is called the limit regime. The mechanism of development of the limit regime is presented by the following. With increase of  $\kappa$  in some section of the inlet of the diffuser, the average velocity of flow becomes supersonic. The subsonic layer next to the wall in this section has a minimum transverse extent and is not capable of transmitting a disturbance against the flow. Therefore, lowering of the counterpressure

( $p_4 < p_{4np}$ ) does not influence the conditions in the mixing chamber and the coefficient of ejection is maintained constant. It can be increased only at the expense of increase of flow density, i.e., the pressure in the mixing chamber  $p_k$ . Therefore on segment BA, the characteristic  $p_k = \text{const}$  is parallel to the y-axis. The process in the stage of the ejector on this segment of the characteristic differs in principle, as can be seen from a distance, from the process on segment CB; after the zone of maximum velocity located in the initial section of the throat of the diffuser, mixed flow is decelerated in the throat, crossing a complicated system of shock waves, to subsonic speed in the inlet (if the length of the throat corresponds to optimum), after which further (now smooth) braking in the widened section is realized. The described picture is illustrated by the graph of distribution of pressures along the contour of the diffuser in Fig. 7-29. If the length

of the throat is less than that, which ensures deceleration of flow to subsonic velocity, then in the widened part of the diffuser flow accelerates, and then in they system of shocks changes to subsonic (the widened part of the diffuser operates as a Laval nozzle under off-design conditions). With lowering of  $p_h$  the system of shocks is displaced toward the outlet of the diffuser.

Returning to the curves of change of pressure along the contour of the diffuser (Fig. 7-29), in the limit ( $p_h / p_{hnp} = 1$ ) and beyond-limit ( $p_h / p_{hnp} < 1$ ) regimes, we see that disturbances from lowering of  $p_h$  are not transmitted higher than the determined section, which is located in the initial section of the diffuser.

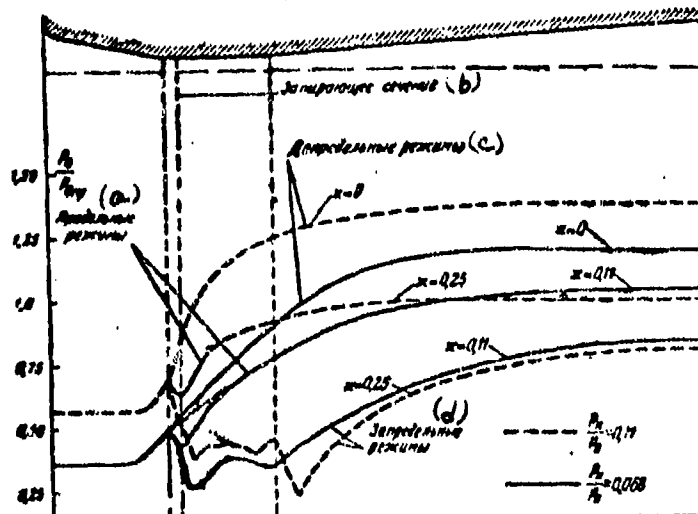


Fig. 7-29. Distribution of pressures along the contour of the diffuser at different operating regimes of the ejector stage;  $\bar{t}_x = 4$ ;  $\bar{x} = 6$ . Experiments of Moscow Power Engineering Institute.  
KEY: (a) limit regimes; (b) blocking section; (c) sub-limit regimes; (d) translimit regimes.

This section (more accurately, the zone adjacent to it), as was shown above, is blocking. In Fig. 7-30 it is possible to see that during transition from the limit regime to the beyond-limit, the velocity profile in the initial section of the diffuser and the coefficient of ejection  $x$  practically do not change. At the same time in the outlet of the throat at a constant coefficient of ejection, the average

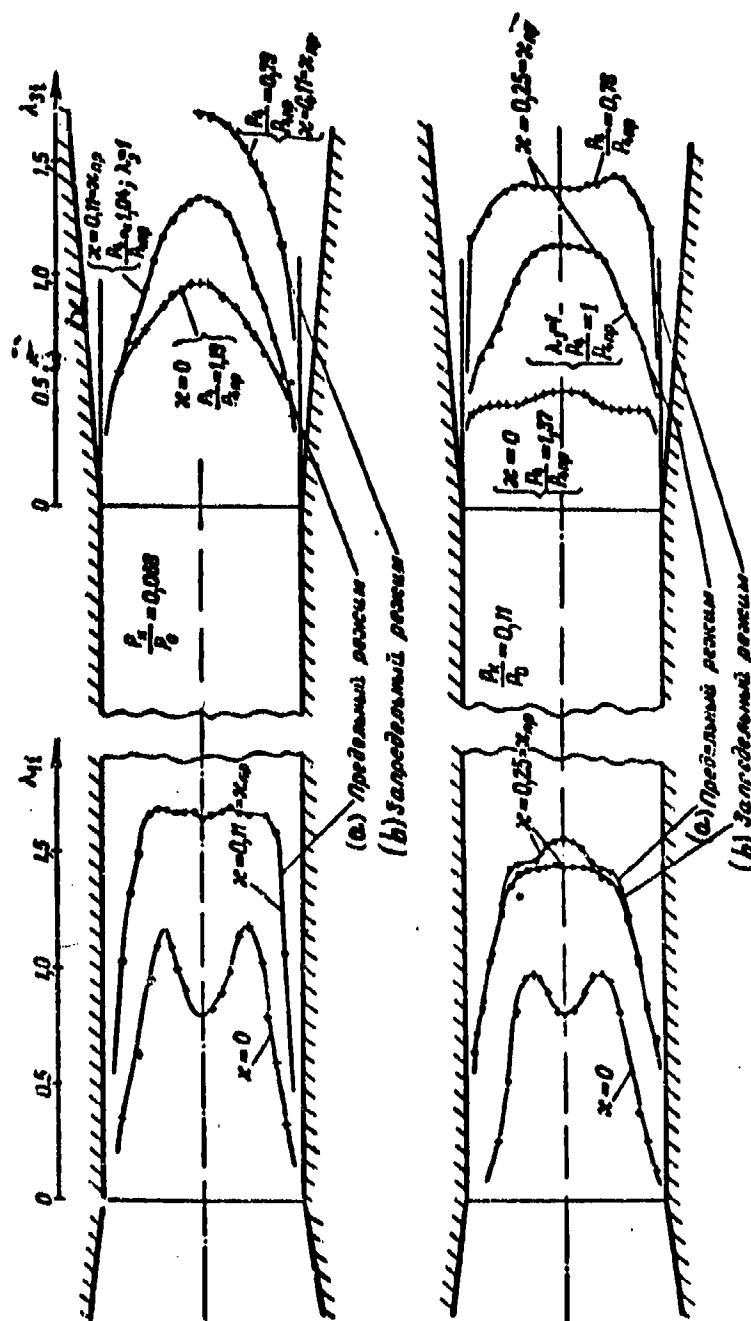


Fig. 7-30. Distribution of dimensionless velocities  $\lambda_1$  in the inlet and outlet of a throat of length  $l_t = 4$  during different regimes. The distance between the nozzle and the diffuser  $\bar{x} = 6$ . Experiments of Moscow Institute of Energetics. KEY: (a) limit regimes; (b) beyond-limit regimes.

velocity is increased. Experiments showed that in the limit regime, the velocity profile in the outlet of the throat acquires a form near to parabolic which is characteristic for flow in a pipe when the average velocity is near to critical (Chapter 5).

In Fig. 7-31 is shown the "universal profile" of relative average velocities  $\lambda_1/\lambda_0$  ( $\lambda_0$  is the velocity on the axis of the diffuser), obtained as a result of superposition of velocity fields in the outlets of throats of different diffusers in limit regimes\*. As can be seen, all curves practically coincide and differ little

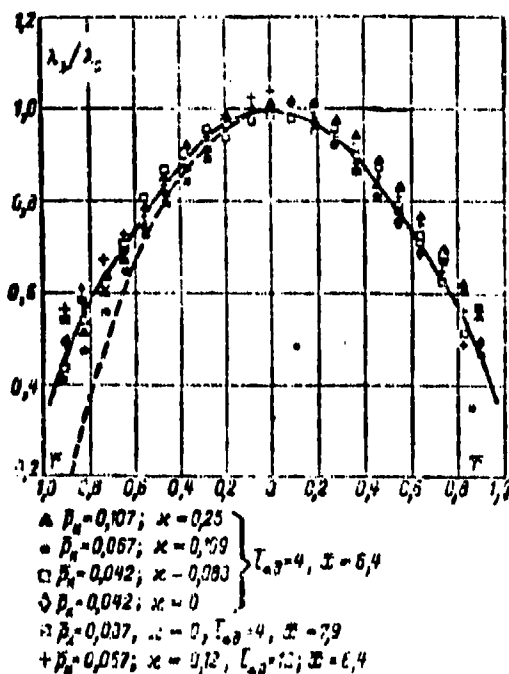


Fig. 7-31. Universal velocity profile in the outlet of the throat in regimes near to limit regimes.

from the quadratic parabola independently of the relative length of the throat  $\bar{l}_a = l_a/d_a$ . Such reconstruction of the velocity profile at transonic speeds is explained by the influence of viscosity in transonic flow which is very sensitive to any external influence.

Calculation of characteristics of the ejector  $p_k/p_0 = \text{const}$  is carried out by

\*Experiments were conducted for different dimensionless pressures in the mixing chamber  $p_k = p_k/p_0$  and optimum dimensionless distances between the nozzle section and inlet into the throat  $\bar{x} = x/d_1$  ( $d_1$  is the diameter of the nozzle at the outlet).

equations (7-34) and (7-35). For the limit regime ( $x = x_{np}$  and  $\epsilon_A = \epsilon_{A,np}$ ) after substitution of  $\lambda_1 = 1$  and  $q_3 = 1$  these equations take the form (velocity  $\lambda_1 \approx 0$ ):

$$\psi'(\lambda_1) + \left(\frac{k+1}{2}\right)^{\frac{1}{k-1}} \frac{p_0}{p_c} \left(\frac{F_{A,1}}{F_{c,1}} - \frac{F_1}{F_{c,1}}\right) - \epsilon'_{Ay} =$$

$$= (\varphi'_n + 1) \sqrt{(1 + x_{np})(1 + x_{np}\epsilon_1)}; \quad (7-39)$$

$$\frac{p_{A,1}}{p_0} \approx \frac{p_{A,np}}{p_0} = \epsilon_{0,1} \frac{F_{c,1}}{F_{A,1}} \sqrt{(1 + x_{np})(1 + x_{np}\epsilon_1)}, \quad (7-40)$$

where

$$\psi'(\lambda_1) = \varphi'_c \lambda_{1c} + \frac{1}{\varphi'_c \lambda_{1c}};$$

$\varphi'_c$ ;  $\varphi'_n$ ;  $\epsilon'_{Ay}$  are coefficients, characterizing the considered limit regimes, and  $\varphi'_c$  maintains constant value for all points of the given curve  $p_k / p_0 = \text{const}$ .

By equation (7-39) for a given value of  $p_k / p_0$ , the limit coefficient of ejection  $x_{np}$  is determined, and by the formula (7-40), the maximum counterpressure  $p_{A,np}$  is determined. With the help of these dependences can be constructed the curves

$$x_{np} = f_1\left(\frac{p_k}{p_0}\right) \quad \text{and} \quad \epsilon_{A,np} = f_2\left(\frac{p_k}{p_0}\right).$$

Values of  $\epsilon_{Ax} = f_3(p_k / p_0)$  for idel running can be easily obtained from expressions (7-34) and (7-35) after substitution of  $x = 0$ .

Characteristics  $\epsilon_A(x)$  at  $p_k / p_0 = \text{const}$ , as a rule, are very gently sloping, and therefore, with sufficient accuracy for practice, can be constructed by two points:  $x = 0$  and  $x = x_{np}$ . Let us note that with decrease of  $p_k / p_0$ , the range of controlled capability of the stage is lowered [segment of characteristic corresponding to sub-limit regimes,  $p_k > p_{A,np}$ , is shortened (Fig. 7-28)]. In this case the limit coefficient of ejection is decreased, but the maximum compression ratio increases. At  $x = 0$  and  $\epsilon_A = \epsilon_{A,np}$  the segment of characteristic  $p_k / p_0 = \text{const}$  connecting points  $x = 0$  and  $x = x_{np}$ , becomes a point.

Line DBK on the regime diagram of the stage which corresponds to the limiting values  $\epsilon_A = \epsilon_{A,np}$  and  $x = x_{np}$  for various  $p_k / p_0$  is called the limit line. In all points of this line for correct selection of the length of the throat, velocity

$\lambda \approx 1$ .

## 2. Characteristics of the stage at constant pressure after behind the ejector

$p_4/p_0 = \text{const}$ . Just as in regimes  $p_k = \text{const}$ , characteristics  $p_4 = \text{const}$  have two branches: the sub-limit and beyond-limit, corresponding respectively to the conditions  $p_4 > p_{4np}$  and  $p_4 = p_{4np}$ . We will trace the flow of processes in the ejector during change of the intake pressure  $p_k$ .

Let us point F (Fig. 7-28)  $p_4 > p_{4np}$ ; here  $\epsilon_A < \epsilon_{A, np}$ ,  $p_A > p_{A, np}$ . In order to increase the coefficient of ejection at the given counterpressure, it is necessary to increase the pressure in front of the diffuser, i.e., in the mixing chamber,  $p_k$ . The compression ratio  $\epsilon_A$  in this case will be decreased, but the average speed of the mixed flow will increase. It will continue in this way with increase of  $\epsilon_A$  until the average velocity of flow in the blocking section attains maximum value  $\lambda = 1$ .

Upon further growth of  $\epsilon_A$  the process in the ejector changes. Increase of the coefficient of ejection as before will be attained at the expense of increase of pressure in front of the diffuser  $p_k$ , but velocities in the blocking and exit section cannot be increased and the capability of the apparatus increases only at the expense and the capability of the apparatus increases only at the expense of increase of current density.

Static pressure and stagnation pressure in section 3,  $p_3$  and  $p_{03}$ , also increase. In the widened part of the diffuser flow acquires supersonic velocities. As a result there appears here a shock (or system of shocks), and the position of which depends on the counterpressure  $p_4$ . Upon lowering of  $p_4$  the leap is displaced toward the outlet of the diffuser.

Points of the considered segment of the characteristics  $p_4/p_0 = \text{const}$  with shocks in the widened part lie on vertical segments of the corresponding characteristics  $p_k/p_0 = \text{const}$ . In regimes with shock waves, losses in the widened part of the diffuser increase, due to decrease of the stagnation pressure in the shocks and



flow separation. The considered regimes are accompanied by increase by  $p_k$ , and the compression ratio  $\pi$  continues to decrease.

Thus, characteristics of the stage corresponding to the condition  $p_k / p_o = \text{const.}$  are depicted by lines whose form is shown by the dotted line in Fig. 7-28 (line FBL); on segment FB the counterpressure  $p_i > p_{\text{imp}}$ , and on section BL the counterpressure  $p_i < p_{\text{imp}}$ .

Calculation of the characteristics  $p_k / p_o = \text{const.}$  is carried out with the help of equations (7-34) and (7-35), if the geometric parameters of the ejector

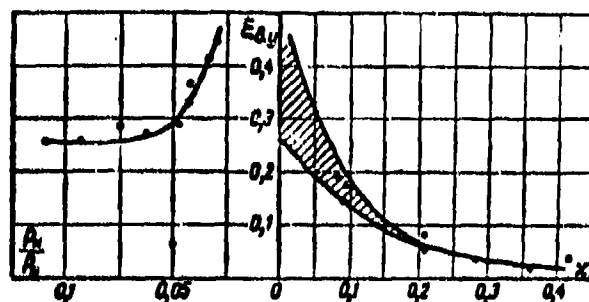


Fig. 7-32. Change of coefficient of entrance section of diffuser dependence from  $p_k / p_o$  and  $x$ .

( $F_{*1} / F_{*2}$  ;  $F_1 / F_{*o}$  ) and two parameters of the regime (for example  $p_k / p_o$  and  $x$ ) are known. In this case, by the formula (7-35) the value of  $x$  is determined (assuming  $\frac{p_{*1}}{p_i} \approx \frac{p_1}{p_i}$ ), and by equation (7-34) is determined the value of  $p_k / p_o$ .

Graphs of the distribution of pressures in Fig. 7-29 allow us to establish the character of change of the specific impulse  $\epsilon_{ay}$  in dependence upon  $x$  and  $p_k / p_o$ . In Fig. 7-32 is presented such a dependence for the inlet part with an angle of conicity of  $20^\circ$ . Hence it may be concluded that for large values of  $x$ , corresponding to the conditions of filling of the free stream of the inlet of the throat, the value of  $\epsilon_{ay}$  is near to zero. With decrease of  $x$  increases the pressure behind the diffuser and in the inlet of the throat (on the wall of the inlet). Increase of pressure from  $p_k$  to the pressure in the inlet of the throat (regimes  $p_k / p_o = \text{const.}$  are considered) is realized in the inlet of the diffuser.

At decreased  $x$  in the inlet of the throat there appear reverse currents: an excess of gas entering into the active stream is ejected near the inlet of the

throat. Part of the small streams in this case is decelerated and then accelerated in the direction, opposite to the motion of the main flow. Deceleration and turn of the separate small streams are not able, obviously, to occur without an increase of pressure in the direction of motion of the main flow. It follows from this that independently of the form of the contour of the flow-through part of the ejector, decrease of  $x$  always leads to intensification of compression in the initial section of mixing.

Pressure in the chamber  $p_k$  has an influence on the value of  $i_{uy}$  only for substantial deviations of the regime from the designed one. Decrease of pressure leads to growth of  $i_{uy}$ . This fact is explained by the increase of inflow into the stream and corresponding intensification of reverse currents.

3. Regimes with variable counterpressure at constant position of the gate valve on the suction line\* (i.e., for simultaneous change of  $p_k$  and  $p_h$ ). It is obvious that for  $p_h < p_{hnp}$  such a characteristic of the stage coincides with the characteristic  $\frac{p_k}{p_0} = \text{const}$ . At  $p_h > p_{hnp}$ , with increase of  $p_h$ , the coefficient of ejection decreases, since  $p_k$  abruptly increases (curve ABE in Fig. 7-29). In this case the compression ratio falls simultaneously. The more the gate valve is opened on the line of inflow, the less intense is the change of the compression ratio. All lines  $i = \text{const}$  converge at the point  $x = 0$  (point E), where the pressure  $p_k$  equals the pressure of the environment.\*\*

The region between the limit line and the axis  $x$ , we will call the regime diagram of the stage. The regime diagram obtained by experimental means is shown in Fig. 7-33. One should underline that the calculation, performed with the help of the experimental (variable) coefficients  $\varphi'_0, \varphi'_n, i'_{uy}$ , satisfactorily coincides with the data of the experiment.

---

\*The considered regimes are sometimes called regimes with constant throttling on the suction line.

\*\*Letter  $i$  is arbitrarily designated the magnitude of opening of the gate valve on the suction line.

Till now we assumed that the pressure of the active gas before the nozzle is held constant. According to experimental data change of  $p_0$  renders a very great influence on the effectiveness of the stage, since the flow and the distributed energy of the active gas change.

In a stage of given dimensions, the flow of active gas is directly proportional to  $p_0$ . If the pressure after the stage  $p_k$  and the position of the gate valve on the

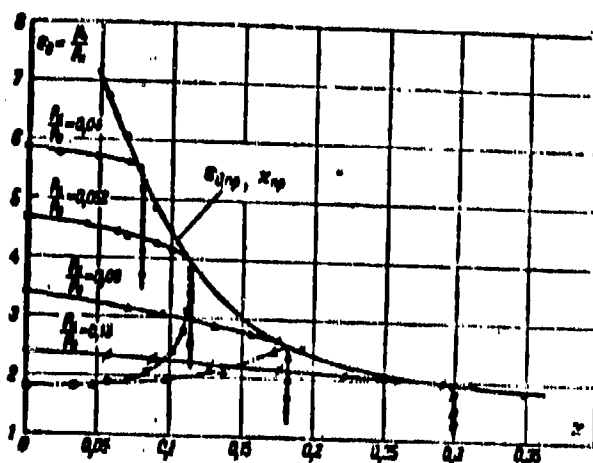


Fig. 7-33. Experimental diagram of regimes of ejector stage.

suction line are held constant, then with increase of  $p_0$  the pressure in the mixing chamber  $p_k$  decreased, and the flow of ejected gas increases. Upon attainment of some optimum value of  $p_0$ , the pressure  $p_k$  acquires the minimum value.

Further increase in  $p_0$  leads to increase of  $p_k$  and decrease of the flow of ejected gas.

The distribution of pressures along the diffuser allows us to explain the influence of  $p_0$  (Fig. 7-34). At  $p_0 > p_0'$  a sharp increase of pressure in the inlet part of the diffuser is noticeable, which is caused by the appearance of a system of shocks. Flow in the narrowed part behind the shocks becomes subsonic and is accelerated, attaining critical speed in the throat. In the widened part of the

diffuser acceleration of flow is continued, which is ended by the system of shocks.

The limiting counterpressure is proportional to the initial pressure [equation (7-29)]. For a given opening of the gate valve and  $p_4 = \text{const}$ , with increase of  $p_0$  the ejector from the sub-limit regime ( $p_4 > p_{4\text{lim}}$ ) approaches the limit regime ( $p_4 = p_{4\text{lim}}$ ). Therefore the compression ratio increases, but  $p_k$  decreases. Upon

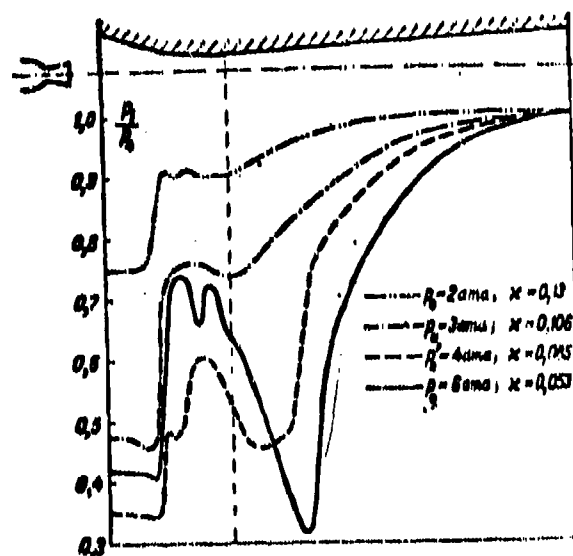


Fig. 7-34. Distribution of pressure along contour of diffuser at various initial pressures of active gas.

further increase of  $p_0$  ( $p_{4\text{lim}} > p_4$ )  $p_{11}$  is increased, i.e. the ejector changes to the beyond-limit regime.

Visual investigations of flow in the ejector stage clearly show that in all regimes with excessive initial pressure ( $p_0 > p'_0$ ) in the widened part there appears a shock (Fig. 7-35,a). An analogous picture, as we have seen, is observed also in regimes  $x = x_{\text{ap}}$  at  $p_4 < p_{4\text{lim}}$ . The shocks lead to breakdown to vorticity in the widened part of the diffuser (Fig. 7-35,b).

In a stage with a small distance between the nozzle and the diffuser ( $x = 0$ ), except for the considered first limit regime (the critical velocity will be attained



Fig. 7-35. Spectra of flow in ejector stage. a--shock wave in widened part of diffuser;  $p_0 = 5.02$  at.,  $p_k = 0.81$  at.; b--breakdown of flow in diffuser (visualization of flow by vapors of ammonium chloride, experiments of Moscow Power Engineering Institute).

in the outlet of the throat:  $\lambda_1 = 1$ , a second limit regime also can appear, corresponding to the critical speed of the passive gas in section 2 ( $\lambda_2 = 1$ )

#### 7-7. Selection of Geometrical Parameters of the Ejector Stage

For design of the ejector stage, as a rule, parameters and flow of active gas ( $p_0, T_{01}, G_1$ ), parameters and flow of passive gas ( $p_{0k}, p_k, T_{02}, \dots$ ) and the necessary compression ratio  $\epsilon_1$  are given. Then by equations (7-34) and (7-35) the main geometric parameter of the stage  $F_{*1}/F_{*2}$  (for the condition  $\lambda_1 = 1$ ) is determined. As it is simple to note, increase of design coefficients of ejection leads to increase of the parameter  $F_{*1}/F_{*2}$ ; increase of design compression ratios leads to decrease of this parameter.

Before determination of  $F_{*1}/F_{*2}$  it is necessary to design the nozzle. At given values of  $p_0, p_k, \varphi_0$ , design of the nozzle is carried out simply by tables of

gas-dynamic functions. In this case the pressure in the outlet in the design regime should be selected somewhat larger than  $p_k$ . For low-pressure ejectors it is possible to apply a narrowed nozzle.

The influence of all basic geometric parameters of the ejector, which do not lend themselves to calculation can be estimated by experimental data. Different variants of the stage are compared under the most favorable conditions: at optimum flow of ejecting gas (optimum initial pressure) and at optimum distance between the nozzle and the diffuser. Comparison of the investigated variants are expediently carried out by the maximum characteristics of the stage:  $\dot{m}_{\text{max}} = f(x_{\text{np}})$ .

The character of the dependence of the pressure in the mixing chamber on  $\bar{x}$  at constant pressure  $p_k$  shows that  $p_k/p_0$  changes periodically during change of  $\bar{x} = x/d_1$  ( $d_1$ —diameter of the outlet of the nozzle), if the flow at the inlet into the diffuser is supersonic (Fig. 7-36). For large values of  $\bar{x}$ , the pressure  $\bar{p}_k$  continuously increase with increase of  $\bar{x}$  (in this case velocity at the inlet into the diffuser is subsonic). The periodic character of the dependence of  $\bar{p}_k$  on  $\bar{x}$  at  $M_1 > 1$  is explained by the wave structure of the flow. If during motion of the nozzle relative to the diffuser shocks hit the wall of the inlet part, the impulse from the wall decreases ( $t_{\text{np}}$  is lowered) and the pressure in the chamber increases. Conversely, if at the inlet into the diffuser are located waves of rarefaction, the pressure in the mixing chamber increases. Change of the coefficient of ejection in this case occurs according to the characteristic of the stage, which corresponds to constant pressure behind the diffuser ( $p_k / p_0 = \text{const}$ ).

As experiments show,  $\bar{x}_{\text{opt}}$  corresponds to the position of the nozzle, at which the mixed stream is approximately joined to the throat of the diffuser; however in this case this basic requirement should be satisfied: the surface of mixing of the active stream must be sufficient for attachment of the given quantity of passive gas. It is possible to calculate approximately the distance between

the nozzle and the diffuser throat\* by the empirical formula

$$\bar{x} \approx 5\sqrt{x}$$

and, the, for control, to determine the diameter of the stream at a distance  $\bar{x}$  from the outlet of the nozzle  $d_{cr} \approx 1 + 0,35\bar{x}$ .

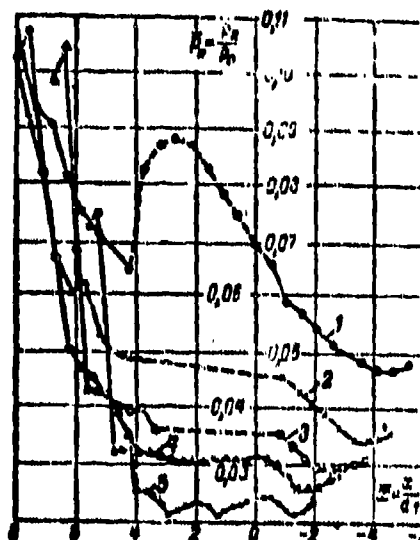


Fig. 7-36. Dependence of pressure in the mixing chamber  $p_k/p_0 = \bar{p}_k$  on the distance between the nozzle and the diffuser  $\bar{x} = x/d_1$ .  
1— $M_1 = 1$ ; 2— $M_1 = 1.59$ ; 3— $M_1 = 1.94$ ; 4— $M_1 = 2.31$ ; 5— $M_1 = 2.95$ .

During design of the ejector for a given coefficient of ejection, the diameter of the stream should somewhat exceed (approximately by 10%) the diameter of the diffuser throat.

The curves presented in Fig. 7-37 curves illustrate the influence of the basic geometric parameter  $F_{*1}/F_{*0}$  (at  $F_{*0} = \text{const}$ ). With increase of  $F_{*0}$  (or  $G_1$ ) for other equal conditions the curves  $\bar{p}_k(x)$  are lowered. Explanation of this fact gives an analysis of the equation of continuity (7-40). Since in the limit regime for optimum length of the throat, the velocity  $u_3 \approx u_1$ , and consequently,  $q_3 \approx 1$ ,

\*Negative values of  $\bar{x}$  correspond the location of the nozzle, at which its outlet is farther to the right of the inlet of the throat.

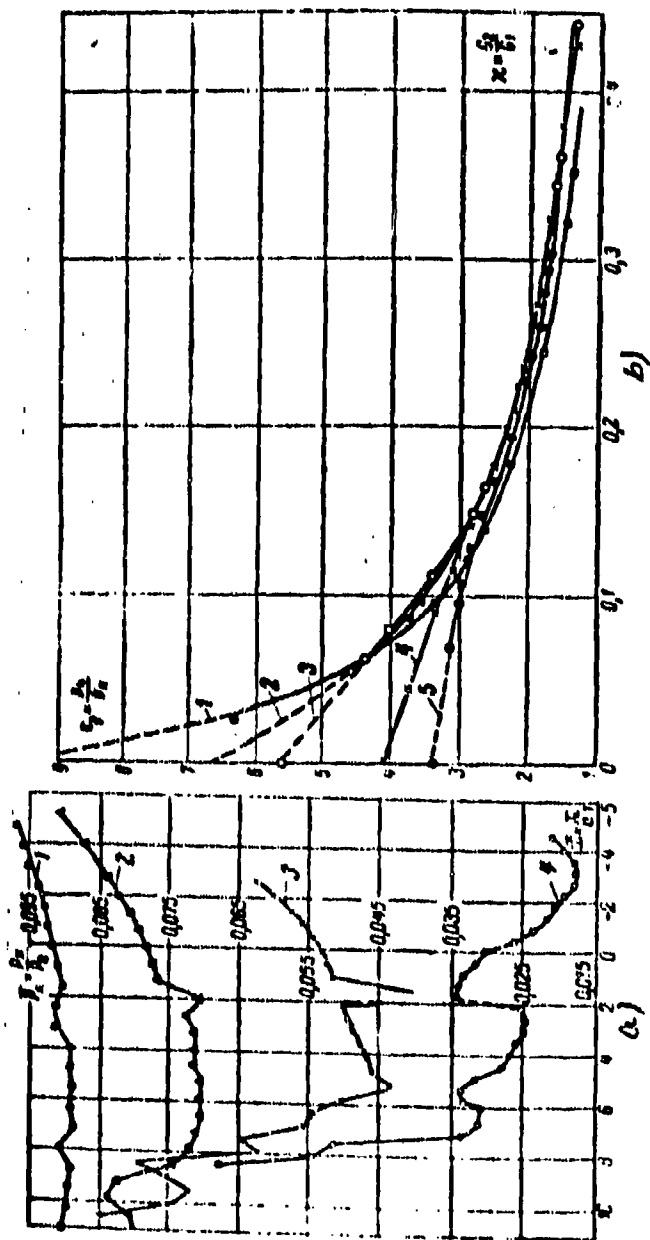


Fig. 7-37. Influence of the parameter  $F_c/F_{c1}$  on the pressure in the mixing chamber of the ejector (a) and parameter  $F_1/F_{1c}$  on the limiting characteristic of the ejector (b).

as  $1 - \frac{F_{1c}}{F_{1A}} = 1.8$ ; 2 -  $\frac{F_{1c}}{F_{1A}} = 2.0$ ; 3 -  $\frac{F_{1c}}{F_{1A}} = 2.2$ ; 4 -  $\frac{F_{1c}}{F_{1A}} = 2.5$ ; 5 -  $\frac{F_{1c}}{F_{1A}} = 3.0$ ; 1 -  $\frac{F_{1c}}{F_{1A}} = 1.8$ ; 2 -  $\frac{F_{1c}}{F_{1A}} = 2.0$ ; 3 -  $\frac{F_{1c}}{F_{1A}} = 2.2$ ; 4 -  $\frac{F_{1c}}{F_{1A}} = 2.5$ ; 5 -  $\frac{F_{1c}}{F_{1A}} = 3.0$ .



then for  $\tau_1 = 1$  we have (assuming that  $p_{03} = p_4$ ):

$$p_{4up} = p_0 \frac{F_{*c}}{F_{*A}} (1 + \kappa).$$

With increase of flow of the active gas  $G_1$ , i.e., the ratio  $F_{*c}/F_{*A}$ ,  $p_{4up}$  (at  $p_0$  and  $\kappa$  constant) also grows. Consequently, at constant counterpressure  $p_k$ , the difference  $p_4 - p_{4up}$  will decrease until  $p_4$  becomes equal to  $p_{4up}$ . During further increase of the ratio  $\frac{F_{*c}}{F_{*A}} p_4 - p_{4up}$  becomes less than zero, i.e., the apparatus changes to beyond-limit regimes, which should be accompanied by a decrease of  $\kappa$  and increase of  $p_k$  ( $p_k = \text{const}$ ).

The influence of the ratio  $\frac{F_{*c}}{F_{*A}}$  (or  $M_1$ ) on the value of pressure in the mixing chamber can be traced by Fig. 7-37, b. With increase of number  $M_1$  the minimum pressure in the mixing chamber decreases and at  $M_1 = M_{\max} = 2.95$  will attain the smallest value. In this case the pressure in the mixing chamber and the pressure in the nozzle section approach each other; the losses in the stream decrease.

It is characteristic that with increase of  $\kappa$ , the influence of the parameter  $F_1/F_{*c}$  is abruptly lowered and at values  $\kappa = 0.1$ , it is almost not detectable; the curves  $\kappa_1(\kappa)$  in this section practically merge.

Experiments showed also that the optimum values of cone angles of the nozzle are  $\gamma_c = 12$  to  $24^\circ$ .

The effectiveness of the ejector stage is greatly influenced by the length of the throat. For all flows of ejected gas, increase of the length of the throat from  $\bar{l}_{*1} = 0$  to  $\bar{l}_{*1} = 4$  leads to a sharp increase of the maximum compression ratio (Fig. 7-38). Further lengthening of the crater does not cause a noticeable change of the limiting characteristic for a given value of  $F_{*A}/F_{*c}$ . The value of  $\bar{l}_{*1, \text{opt}}$  changes during change of the basic geometric parameter of the stage  $F_{*A}/F_{*c}$ . For conditions in which ejectors usually operate with an isobaric section of mixing, the length of the throat should be selected within the limits of 4-8 diameters of the throat. For stages with  $\bar{\kappa} \approx 0$   $\bar{l}_{*1, \text{opt}}$  is increased to 10-12.

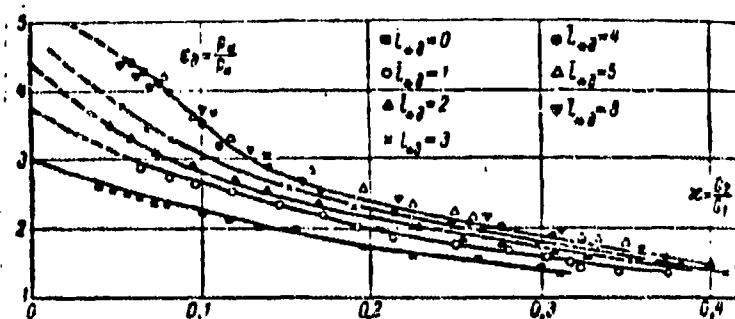


Fig. 7-38. Influence of the length of the throat of the diffuser on the limiting characteristic of the ejector.

Diffusers of ejectors with a short throat operate poorly in variable regimes. In this case flow at the inlet in the widened part can be supersonic, which leads to formation of a shock and sharp growth of losses in the widened part.

During interaction of the stream with the wall of the inlet section, the latter receives a part of the impact pressure, which is larger, the larger the angle of conicity of the inlet section. Therefore, it is desirable to make the inlet section with a small, convergence angle near  $20^\circ$ . However in this case the length of the inlet section is increased.

In those case when the ejector operates stably in regimes near to design, it is possible to allow an angle  $\gamma_{01}$  of up to  $50^\circ$ , providing a smooth inlet section with the throat.

For a normal throat ( $L_{0,1} = 4L_{0,2}$ ) the best characteristic is obtained with a short inlet section and angle  $\gamma_{01} = 19^\circ$ . For  $L_{0,1} = 0$ , good results are shown by an elongated inlet section.

Results of the investigation of different outlet sections of the diffuser showed that outlet sections with aperture angles of  $5^\circ$  and  $8^\circ$  were best. Smaller angles of conicity  $\gamma_{01}$  and  $\gamma_{02}$  are expediently chosen for a small length of the throat; in this case in the inlet and outlet parts of the diffuser there occurs a partial equalizing of the mixed flow.

## CHAPTER 8

### FLOW OF GAS THROUGH TURBOMACHINE CASCADES

#### 8-1. Geometric and Gas-Dynamics Parameters of Cascades. Peculiarities of the Flow in Cascades \*

The transformation of energy in a turbomachine stage occurs as the result of the interaction of a flow of gas with the stationary and rotating blades, which form the guide and rotating cascades.

The cascades of turbomachines in a general case are a system of blades of identical shape, evenly distributed on a certain surface of revolution. A particular case of a three-dimensional cascade is an circular cylindrical cascade with radially-fixed blades, located between coaxial cylindrical surfaces of revolution.

In flowing through a cascade the flow of gas changes speed and the direction of its motion. The reaction acts on the cascade. On the rotating cascades of a turbine this force accomplishes work; rotating cascades of compressors, conversely, increase energy of the flowing gas. In stationary cascades with an energy exchange with the environment this does not occur; here there are realized necessary conversions of energy for obtaining required speed and turn of flow.

A classification of cascades can be made according to different parameters.

Depending upon the rated conditions of the flow around and the corresponding geometric parameters of the profile and channel, three main types of cascades are distinguished.

---

\*Sec. 8-1 was written for the first edition by G. Yu. Stepanov.

a) nozzle cascades--are used in turbines both as nozzle or guide (stationary), and also reactive moving (rotating) cascades;

b) impulse cascades--are used in turbines as moving (rotating) cascades;

c) diffuser cascades--are used in compressors both as guide (stationary), and moving (rotating) cascades.

Depending upon the general direction of motion of the gas in reference to the axis of rotation the cascades are subdivided into axial and radial. In certain

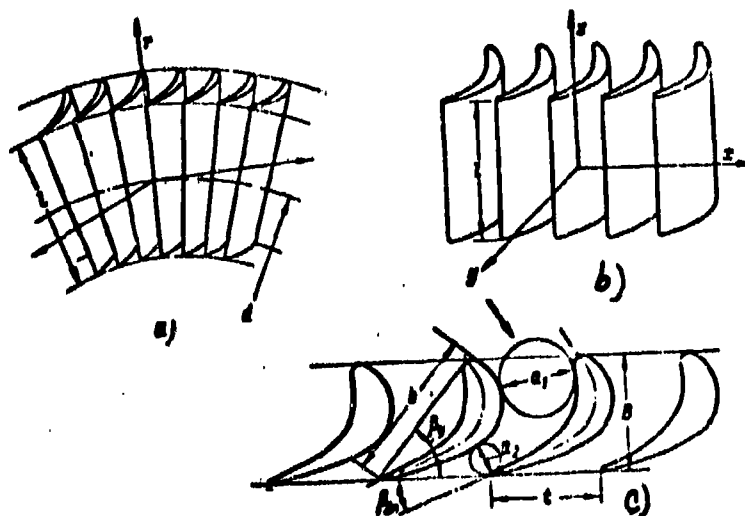


Fig. 8-1. Geometric parameters of a cascade  
a--circular (cylindrical) cascade; b--rectilinear cascade; c--two-dimensional cascade.

designs of machines, the flow of gas moves at an angle to the axis of rotation (diagonal cascade).

Some of the most important geometric parameters of circular (cylindrical) cascades are: average diameter  $d$ , length (height) of blade  $l$ , width of cascade  $B$ , pitch of profiles on average diameter  $t$ , chord  $b$ , angle of incidence  $\beta$ , and other parameters of the profile and channel (Fig. 8-1), and also the form of meridional contours of cascades.

There exist various methods of assigning the form of profiles of blades. Most widely used are the coordinate method (Fig. 8-2,a), and also the method of constructing a profile by adjoining arcs of a circle (Fig. 8-2,b).

If the ratio of the average diameter of cascade  $d$  to height of blade  $l$  is large, then for simplifying the problem it is possible to assume the cascade rectilinear. Here the shape of the vane channel by height is kept constant. In simplest case, assuming that diameter of cascade, the number and length of blades infinitely increase, we obtain a two-dimensional infinite cascade (Fig. 8-1, c).

The transformation from a cylindrical to a two-dimensional cascade is realized in the following manner. We draw two coaxial cylindrical sections of a circular

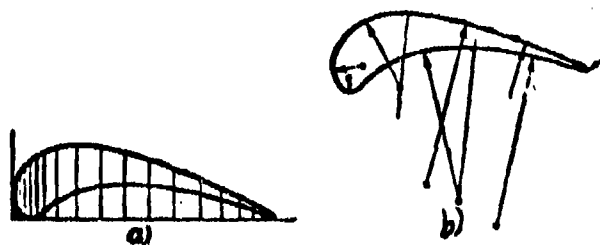


Fig. 8-2. Different methods of prescribing profile of blade.  
a--coordinate; b--by arcs of circle.

cascade along the average diameter  $d$  and along a diameter  $d + \Delta d$ . Assuming that  $\Delta d$  is small, we shall develop into a plane the obtained circular cascade of minute height. By increasing the number of blades to infinity, we obtain a two-dimensional infinite cascade, shown in Fig. 8-1c. Hypothesis of two-dimensional sections, assumed as the basis of investigations and calculations of contemporary turbomachines, was for the first time fruitfully used by N. Ye. Zhukovskiy in 1890. The value of this hypothesis has been confirmed by numerous experiments.

Geometric characteristics of cascades, as a rule, are given in dimensionless form. For example, relative pitch of profiles is determined by the formula

$$\bar{t} = \frac{t}{b} \quad \text{or} \quad \bar{t}_s = \frac{t}{B}.$$

The relative height (or length) of a blade

$$\bar{l} = \frac{l}{b} \quad \text{or} \quad \bar{l}_a = \frac{l}{a_2}.$$

where  $a_2$  is the width of minimum (narrow) section of channel (Fig. 8-1).

A rectilinear cascade is located in the system of coordinate  $x, y, z$ , where the direction of  $x$  is called the axis of cascade (Fig. 8-1,b). All profiles must coincide with progressive transference along axis of cascade. Cascade pitch  $t$  is distance between any two corresponding points.

With a given profile, the shape of the vane channel of cascade depends on relative pitch and angle of setting of the profile, which is determined as angle  $\beta_v$  between shaft of cascade and chord of profile (Fig. 8-1,c).

Process of a gas flow through cascades of a turbomachine is very complicated. The theoretical solution of problem of a nonstationary three-dimensional motion of a viscous compressible fluid in a cascade represents great difficulties. The correct approach to the solution of this problem consists in investigating simplified models of an actual process, which conserve its the most essential features with a consideration and subsequent analysis of influence of secondary factors.

At present the most developed is the theory of a two-dimensional stationary periodic flow of an ideal fluid through a cascade at subcritical speeds. Such flow may be considered as the limiting case of an actual flow in cascade with little influence of the viscosity (at large  $Re$  numbers).

This simplified scheme makes it possible to establish main characteristics of a potential flow in a cascade. However, the obtained solutions need essential correction. The maximum errors occur owing to the ignoring of viscosity. Therefore, an important problem is experimental and theoretical evaluation of influence of viscosity.

We shall consider certain peculiarities of a two-dimensional potential flow of ideal incompressible fluid as exemplified by the flow around a reactive cascade (Fig. 8-3). Owing to the periodicity of flow it suffices to study the flow in one inter-vane channel or the flow around a single profile. In Fig. 8-3, with solid curves there are drawn lines of flow  $\psi = \text{const}$ , with dotted curves showing isopotential lines  $\phi = \text{const}$ , normal to the lines of flow. A fairly dense net of these lines

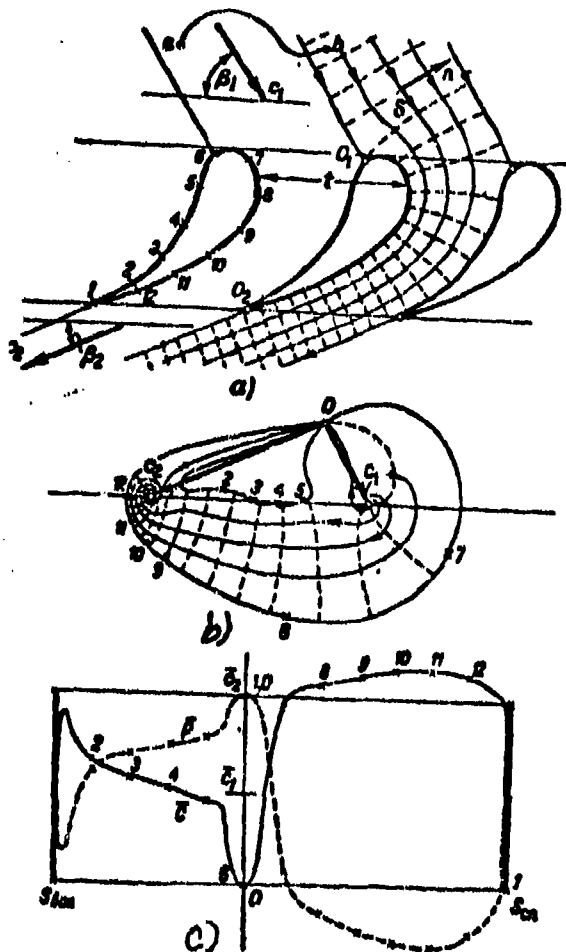


Fig. 8-3. Flow of ideal incompressible fluid through a guide cascade.  
 a--isopotential lines and lines of flow in cascade; b--hodograph of speed; c--distribution of relative speeds and pressure coefficients along profile.

characterizes the flow well. Speed  $c$  at any point of flow is equal to:

$$c = \frac{d\Phi}{dS} = -\frac{d\Psi}{dn},$$

where  $S$  and  $n$  are curvilinear coordinates respectively along lines of flow and the isopotential lines.

The differentials approximately can be replaced by finite increments and there can be obtained:

$$c \approx \frac{\Delta\Phi}{\Delta S} \approx -\frac{\Delta\Psi}{\Delta n}.$$

At  $\Delta\Phi = \Delta\Psi = \text{const}$  at each point  $\Delta S \approx \Delta n$ . In this case individual cells of orthogonal net of lines  $\Phi = \text{const}$  and  $\Psi = \text{const}$  at the limit (at  $\Delta S \rightarrow 0$  and  $\Delta n \rightarrow 0$ ) becomes squares, therefore the flow net of an ideal incompressible fluid is called square.

Another important characteristic of flow is the design of the speeds, or hodograph of speed (Fig. 8-3,b). To each line of flow and isopotential line there corresponds in plane of hodograph the locus of ends of vectors of speed on this line. Corresponding loci in plane of hodograph also will form orthogonal net, which may be considered as the net of certain flow in plane of hodograph, limited by locus of ends of vectors of speed on surface of profile and caused by the so-called vortex-source at end of vector of speed  $c_1$  at infinity prior to cascade and a vortex sink at end of vector of speed  $c_2$  after the cascade. Point  $O_1$ ,  $c_1$  and  $c_2$  will form the triangle of speeds of the cascade. On the basis of equality of flow rates of fluid prior to and after the cascade

$$c_1 l \sin \beta_1 = c_2 l \sin \beta_2$$

it follows that projection of speeds  $c_1$  and  $c_2$  onto the normal to the front (axis) of cascade are equal or that the straight line passing through ends of vectors  $c_1$  and  $c_2$  in plane of hodograph is parallel to the front of cascade. In considering hodograph of speed of a cascade, it is possible to reach the conclusion that at points along back edge of profile, the tangents to which are parallel to directions of speeds at infinity prior to and after the cascade the speeds should be higher than  $c_1$  and  $c_2$  respectively.

Of great interest is the distribution of the speed or pressure on the surface of profile. In Fig. 8-3,c there is shown exemplary distribution of relative velocities  $\bar{c} = \frac{c}{c_1}$  and relative pressures  $\bar{p} = \frac{p - p_1}{\frac{\rho}{2} c_1^2} = 1 - \bar{c}^2$  as a function of length of arc of profile  $S$ . If magnitude  $c_1$  and direction  $\beta_1$  of the speed at infinity prior to the cascade are known and also position of point of descent of flow  $O_2$  (on outgoing edge), then the flow through a given cascade is determinate. In the flow of ideal incompressible fluid with a change in magnitude of speed  $c_1$  the



form of the lines of flow and of the isopotential lines, as well as the magnitude of relative velocities or pressures, do not change.

At a finite distance from the cascade the field of speeds and pressures is nonuniform. The lines of flow (at  $\beta_1 \neq 90^\circ$ ) have wave-like form; they periodically are deflected from their own direction at infinity. In accordance with conditions of continuity and in the absence of vortexes, the average speed along any line ab (Fig. 8-3,a) between two points, distant a whole number of periods  $t$  of the cascade, constant and equal to the speed at infinity. One of the lines of flow branches at entry edge of profile, as it approaches it along a normal. At point  $O_1$  (called otherwise the point of entry) the speed becomes equal to zero, and the pressure <sup>is</sup> maximum.

Beginning from point of branching, at which  $S = 0$  (Fig. 8-3,c), speed on profile abruptly increases. Depending upon form of entry edge, and also on the direction of speed at entry (the re-entrant angle  $\beta_1$ ) the speed near point of branching may have one or two maxima. On the back edge of profile the speed on an average is higher, and the pressure lower, than on the concave surface. General character of distribution of speed along the profile can be evaluated, by considering width of the intervane channel and curvature of contour of profile. In particular, the narrowing of the channel, characteristic for turbine cascade of reactive type, results in an acceleration of the flow; in the sector of channel between profiles of turbine grid of impulse type with approximately constant width and curvature mean values of the speed and pressure vary little (Fig. 8-4); in a compressor cascade the intervane channel expands and the speed correspondingly decreases (Fig. 8-5).

The distribution of local speeds at points of the contour profile considerably depends on form of concave and convex surfaces and the degree of narrowing of channel and also on the geometric parameters and cascade parameters.

Increase of curvature in the convex sectors of profile results in an increase of speed, and conversely. With an abrupt change in curvature, for example, at points of intersection of arcs of circles, the theoretical curves of the distribution

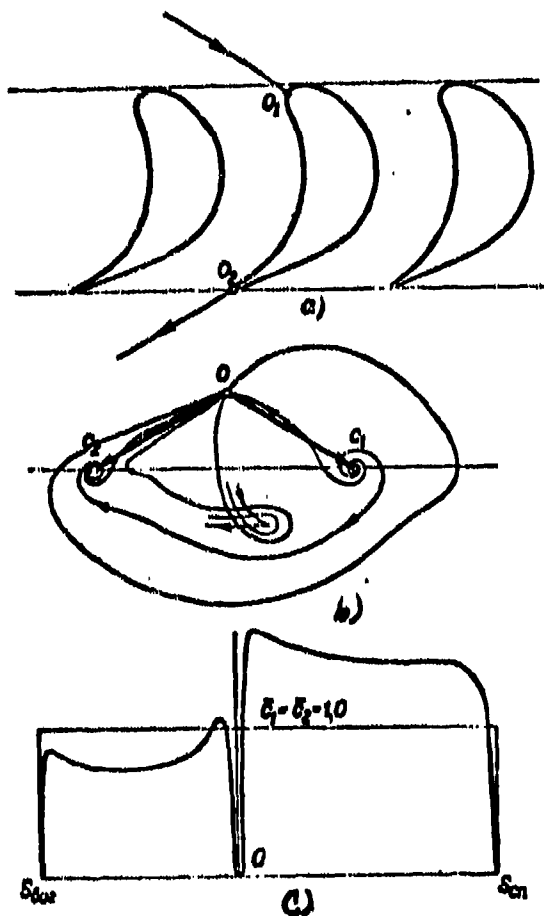


Fig. 8-4. Flow of ideal incompressible fluid through an impulse cascade. a--profile of impulse cascade; b--hodograph of speed; c--distribution of relative speeds along profile.

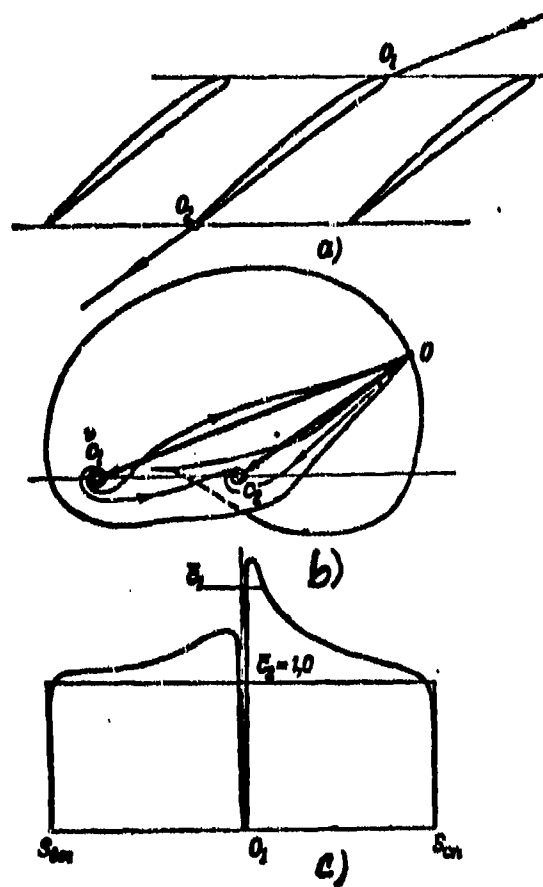


Fig. 8-5. Flow of ideal incompressible fluid through compressor cascade. a--profile of cascade; b--hodograph of speed; c--distribution of relative velocities along profile.

of pressures and speeds experience a discontinuity. On the protruding angles of profile the speed theoretically increases ad infinitum. Owing to this the contours of profile of contemporary cascades are made from smoothly changing curvature.

Along a trailing edge of finite thickness\*, as on the leading edge, the speed has one or two maxima and it theoretically drops to zero at point of descent, which is located on trailing edge in region of maximum curvature. At a great distance after the cascade direction of flow is determined by the angle  $\beta_2$ .

Above there was considered the flow of ideal incompressible fluid through a cascade. In reality with a consideration of influence of viscosity the picture

\*The case of an infinitely thin edge is not considered, that is, as having no practical value.

of flow in cascade may differ considerably from the considered case.

In the flow of real viscous fluid on surface of profile a boundary layer will form where there are concentrated loss of energies, caused by friction.

In sectors of the channel with an increase of pressure (diffusor sections) there may occur a separation of the flow. The diffusor sections depending upon form of profile may develop within the channel; the manifestation of diffusor regions <sup>is</sup> inevitable on leading and trailing edges of profile. On trailing edge there always occurs a separation of the flow; in the zone forming beyond the edges there is a vortex motion. At boundaries of zones beyond edges there occurs an abrupt change in speed. In a real flow of viscous fluid such change in speed would result in the appearance of infinitely great forces of friction; therefore boundary of separation zones break up into individual vortexes which are removed by the flow.

As the result of the separation the pressure after trailing edges is found to be lower. At a certain small distance beyond the edges there occurs an equalization of the flow, accompanied by change of static pressure, of angle of outlet of flow and speed.

In the equalizing of flow after the cascade there develop losses of kinetic energies, constituting a second portion of profile losses in the cascades (edge losses).

In case of high speeds ( $M > 0.5$ ) the distribution of speeds in the cascade experiences a change (effect of compressibility is developed). Here besides, usual gradients of speeds along lines of flow increase, the form of lines of flow changes, and also regions of maximum and minimum speeds are displaced. At certain values  $M < 1$  in certain portions of surface of profile supersonic speeds manifest themselves. The character of flow around cascade in this case abruptly changes; at supersonic speeds additional losses develop in the shocks.

Profile losses characterize a two-dimensional cascade. In rectilinear and cylindrical cascades additional losses will form, caused by finite length of blades

(end losses) and the fanwise arrangement of cascade.

Losses of energy in the cascades, during low speeds, caused by the influence of viscosity and periodic nonstationariness, and also by high turbulence of the flow, and at transonic and supersonic speeds as well as nonreversible processes of change of energy in the shocks, to a significant degree determine efficiency of the turbine machine.

In designing blades cascades it is necessary to assure given conversion of the energy of the flow with minimum losses. Hence there is the necessity of a detailed study of process of flow around cascades and establishment of influence of the profile's form and other geometric parameters of cascade on its efficiency and angle of exit of flow in wide range of modes, determined by angle of entry of flow,  $M$  and  $Re$  numbers, et cetera.

Above in part there was given a classification of cascades depending upon character of variation of parameters of flow in the intervane channel and direction of motion of gas in relation to the shaft of the turbomachine.

The classification of the applied cascades can be considerably broadened. Thus, depending upon speed ( $M$  number) all cascades should be divided into three groups: subsonic, transonic and supersonic. Within the limits of each group the cascades differ by angle of deflection of flow (i.e., angles of entry  $\beta_1$  and exit  $\beta_2$ ).

In addition, the applied cascades are distinguished by their relative height, which is characterized by the ratio  $\bar{l} = \frac{l}{b}$  : cascades of low height ( $\bar{l} < 1.0$  to 1.5) and cascades of great height ( $\bar{l} > 1.5$  to 2.0).

At the same time various cascades are distinguished by the degree of their fanwise arrangement  $\theta = \frac{d}{r}$ ; at small  $\theta$  ( $\theta < 10$ ) the blades are made with a profile varying in height (twisted blades).

Considering that characteristics of cascades within definite range of variations of model and geometric parameters change insignificantly, number of profiles, satisfying the requirements of turbine construction, can be reduced to the required minimum.

## 8-2. Calculation of Potential Flow in Cascades According to Channel Theory

In theory of cascades and in experimental investigation on them two basic problems arise. One of them, the so called direct problem, consists of determining the field of speeds of potential flow through a cascade, consisting of profiles of given form, and in a subsequent evaluation of the losses of energy during different regime (angle of entry,  $M$  and  $Re$  numbers) and geometric (pitch, angle of setting of profile, height of cascade and so forth) parameters. Consequently, the direct problem is very important in the study of variable systems of cascades and the construction of their aerodynamic properties.

Inverse problem consists in the construction of a cascade, which corresponds to a selected or given flow in a cascade.\* In this statement of the problem practically important is problem of construction of a cascade with a rational distribution of speeds (pressures) along the surface of profile to assure minimum losses of energy.

At present, methods of calculating the potential flow in cascades, using apparatus of functions/<sup>of a</sup> complex variable, have been developed. However these methods are found to be cumbersome. They in detail have been discussed in special literature.\*\*

Significantly more simple are methods of calculation, which make it possible with sufficient accuracy to solve the direct and inverse problems, based on the channel theory.\*\*\* To present time there are known several methods of designing cascades according to theory of channel. One of the first was the proposed method of G. Flyugel' developed later by G. Yu. Stepanov.

---

\*It is readily seen that the direct and inverse problems are mutually associated.

\*\*See, for example, monograph by M. Ye. Deych and G. S. Samoylovich "Fundamentals of aerodynamics of axial turbomachines." (Machine-Construction Publ. House, 1959), and also N. I. Zhukovskiy [11].

\*\*\*3. See. 3-5.

The problem of flow around cascades may be successfully reduced to the calculation <sup>of</sup> flow in channel only at moderate values of the relative pitch. In addition, the channel theory provides the possibility of calculating the flow only in intervane channel; in region of entrance section of back and in an oblique cross section it is necessary to use additional methods, and accuracy of the calculation in these sections drops.

In calculating the flow at entrance and in an oblique cross section of cascade it is necessary with known approximation to determine the boundary lines of flow.

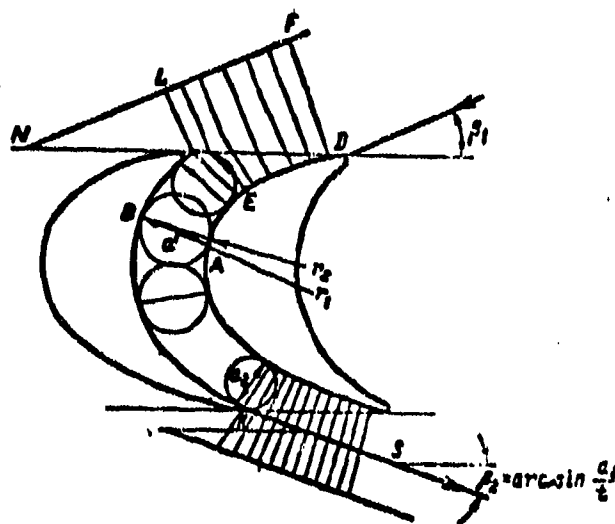


Fig. 8-6. [Chart] for calculating flow around cascade by channel method.

In simplest case, the boundary lines of flow before and after cascade may be selected in the form of segments of straight lines (Fig. 8-6). Direction of these lines at entrance to cascade is given (angle  $\beta_1$ ), and at exit it may be determined by one of the known methods.

Actually, the isolated boundary lines of flow before and after the cascade are distorted near leading and trailing edges, where the greater is the distortion then the greater will be the relative pitch of the blade, and the circulation integral. Certain influence is exerted by flow conditions: angle of entrance,  $M$  and  $Re$  numbers. According to the proposal of the LMZ in the calculation of flow at

entrance there is considered a certain fictitious entrance sector EDFL (Fig. 8-6), which serves as an immediate continuation of the intervane channel. One boundary line of the sector crosses at an angle  $\beta_1$  and is line of undisturbed flow, and second is the back of profile. The sector DN may be assumed equal to  $(1.5 \text{ to } 2.0)t$ .

At exit of channel the boundary lines of flow KS (Fig. 8-6) are constructed on the assumption that beams, orthogonal to back of profile, are isopotential. The lines of flow KS in this case serve as the continuation of the concave surface of neighboring profile. At a certain distance after the cascade (from point S) the lines of flow change to straight line drawn at an angle  $\beta_2^*$ .

The distribution of speeds through the section of channel of cascade in accordance with Sec. 3-5 is expressed by formula (3-43).

At small M numbers ( $M < 0.4$ ) the calculation of distribution of speeds can be made by means of graphs, presented in Fig. 3-14. For a compressible fluid it is necessary to consider the variation of density. In this case it is possible to use method indicated in Sec. 3-5.

The procedure of the calculation reduces to the following:

1. In the channel there are inscribed circles (Fig. 8-6). Through point of tangency of these circles with the walls of the channels A and B there are drawn equipotential lines (in the form of arcs of a circle). There are determined the lengths of these equipotential lines  $a$  and the lengths of radii of curvature of boundary lines at points A and B ( $r_1$  and  $r_2$ ).

2. For each equipotential line there are calculated the dimensionless geometric parameters:  $\bar{a} = \frac{a}{r_1}$ ;  $\bar{r}_1 = \frac{r_1}{r_2}$ ;  $x = \frac{r_2 - 1}{\bar{a}}$ ;  $k_1 = \frac{x - 1}{2\bar{r}_1 - \bar{a}}$ .

3. There are determined parameters of gas at entrance into the cascade: dimensionless speed  $\lambda_1 = \frac{C_1}{a}$ ; the reduced flow rate  $q = q(\lambda)$  and ratio of densities  $\frac{\rho_1}{\rho_0} = f(\lambda_1)$  from the tables of gas-dynamics functions.

\*Angle  $\beta_2$  is calculated on the basis of empirical formulas, for example, by formula (B-36) (Sec. 8-6).

4. The average reduced flow rate can be determined by the reduced flow rate at entrance:

$$q_m = \frac{Q}{Q_1} = \frac{p_1 c_1 / \sin \beta_1}{a p_1 a_1} = q_1 \frac{t}{a} \sin \beta_1. \quad (8-1)$$

5. The ratio of the densities  $\frac{\rho_m}{\rho_1}$  is determined by calculated average reduced flow rate  $q_m$  by means of tables of gas-dynamics functions.

6. The volumetric flow rate  $Q$  through considered section  $a$  is determined by the formula

$$Q = Q_1 \frac{\frac{p_1}{p_2}}{\frac{p_2}{p_1}}. \quad (8-2)$$

where  $Q_1 = c_1 t_1 \sin \beta_1$  is the volumetric flow rate at entrance into channel.

7. By formula (3-44), which in our designations has the form:

$$\delta = \frac{1}{a} \cdot \frac{1}{1 + 4K_1} \cdot \frac{1 - \frac{2K_1 a}{1 - \sqrt{1 + 4K_1}}}{1 - \frac{2K_1 a}{1 + \sqrt{1 + 4K_1}}},$$

(or from the graph in Fig. 3-14) we find  $\delta$ .

8. Speed of gas at the point A is determined by the relationship

$$c_a = \frac{Q}{\delta a},$$

and by it there is determined the magnitude  $\lambda_a$ .

9. Speed (dimensionless, and by it--the dimensional) at point B is determined by the formula

$$\frac{\lambda_B}{\lambda_a} = \frac{1}{1 + a - K_1 a^2}. \quad (8-3)$$

As to the accuracy of determining speeds in cascade by channel method it is possible to judge from Fig. 8-7, in which there is presented a comparison of the calculated and experimental data for an impulse cascade. As is evident from Fig. 8-7, the marked divergence between the calculation and the experiment is observed only near the leading and trailing edges which is entirely as expected.



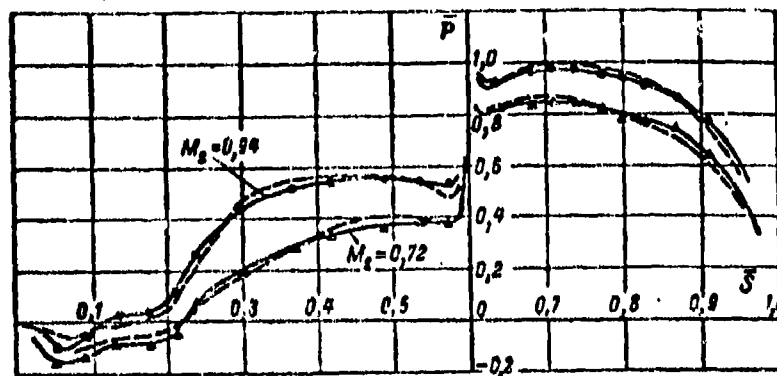


Fig. 8-7. Comparison of calculation of potential flow in cascade by channel methods with the experiment (---empirical curves;—calculated curves).

### 8-3. Forces Acting on Profile in Cascade. Theorem of N. Ye. Zhukovskiy for a Cascade

For determining the forces, operating on a profile, we shall isolate a portion of flow, as is shown in Figs. 8-8 and 8-9. The outer boundaries of the isolated

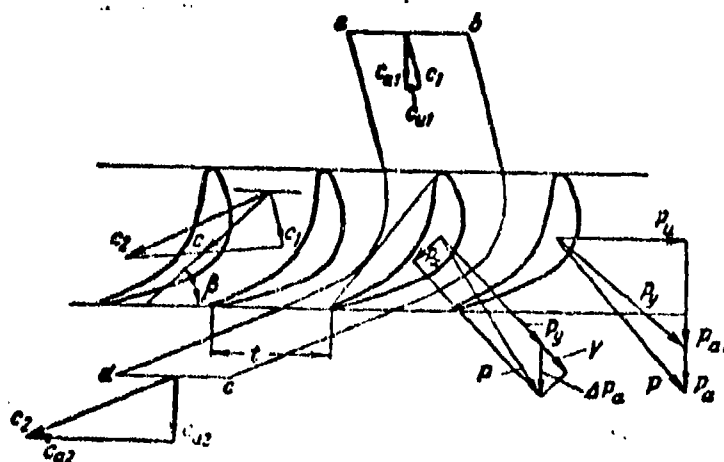


Fig. 8-8. Forces, acting on profile in turbine (nozzle) cascade.

region are the sectors  $\underline{ab}$  and  $\underline{dc}$ , parallel to axis of cascade and equal to the pitch  $t$ , and the lines of flow  $\underline{ad}$  and  $\underline{bc}$ . The lines  $\underline{ab}$  and  $\underline{dc}$ , strictly speaking, must be found at an infinitely great distance from the cascade, since parameters of flow along these lines are assumed to be constant. The inner boundary of the region is the contour of profile.

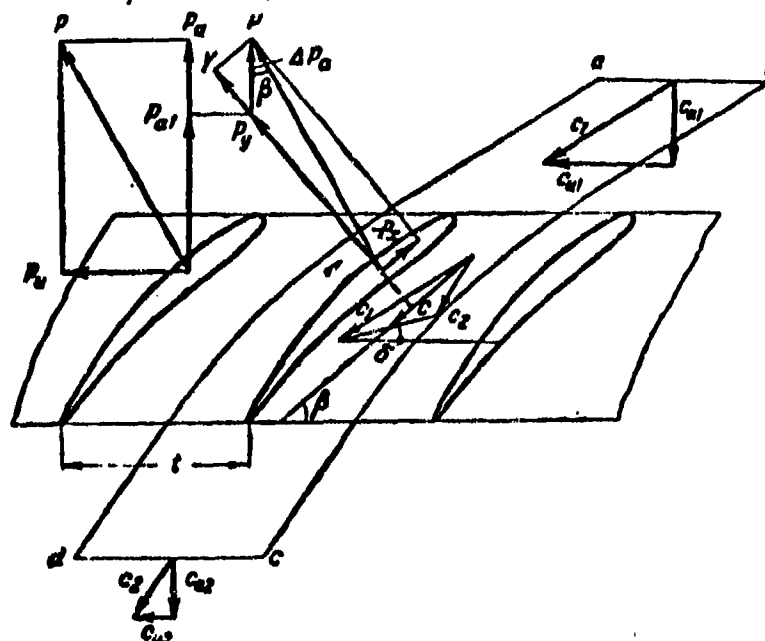


Fig. 8-9. Forces, acting on profile in compressor (diffusor) cascade.

Projections of the force, with which flow acts on a profile of unit length, we shall designate as  $P_u$  and  $P_a$ . Magnitude of these forces can be determined by equation of momentum. Since the lines of flow  $ad$  and  $bc$  <sup>are</sup> equidistant, then the resultant forces acting on that portion of flow isolated by these lines are equal in magnitude and opposite in sign. In the projection in a direction normal to axis of cascade variation of the momentum is equal to:

$$m = (c_{u1} - c_{u2}) = l(p_2 - p_1) - P_a,$$

where  $P_a$  is a component of the force  $P$  in a direction, normal to axis of cascade.

The mass of gas per second is determined by the formula

$$m = \rho_1 c_{u1} l = \rho_2 c_{u2} l,$$

therefore

$$P_a = l[(\rho_2 c_{u2}^2 - \rho_1 c_{u1}^2) + p_2 - p_1]. \quad (8-4)$$

The projection of the force  $P$  onto the axis of cascade can be expressed by the equation

$$P_u = l\rho_1 c_{u1} (c_{u1} - c_{u2}). \quad (8-5)$$

Equations (8-4) and (8-5) can be presented in another form, expressing the forces  $P_u$  and  $P_a$  by the circulation integral  $\Gamma$  and parameters of flow at entrance and exit of cascade.

According to the equation of continuity

$$\rho_1 c_{u1} = \rho_2 c_{u2} = \rho c_u,$$

where  $\rho$  is the average density of gas.

The speed  $c_u$ , contained in this expression, we shall determine as the arithmetical average of the speeds at entrance and exit:

$$c_u = \frac{c_{u1} + c_{u2}}{2}.$$

It is readily shown that here

$$\rho = \frac{2\rho_1\rho_2}{\rho_1 + \rho_2}. \quad (8-6)$$

Circulation integral around the profile is equal to:

$$\Gamma = l(c_{u1} - c_{u2}), \quad (8-7)$$

since the circulations along the equidistant lines ad and bc are identical in magnitude and opposite in sign.

After simple transformations from (8-4) and (8-5) we obtain:

$$P_a = l(p_2 - p_1 - \rho c_u(c_{u1} - c_{u2})); \quad (8-8)$$

$$P_u = \rho l' c_u. \quad (8-9)$$

We shall use equation of energy (2-11). Since

$$c_1^2 = c_{u1}^2 + c_{n1}^2 \quad \text{and} \quad c_2^2 = c_{u2}^2 + c_{n2}^2,$$

then, designating  $c_u = \frac{c_{u1} + c_{u2}}{2}$ , we obtain:

$$c_u(c_{u1} - c_{u2}) = \frac{k}{k-1} \left( \frac{p_2}{\rho_2} - \frac{p_1}{\rho_1} \right) - c_u(c_{u1} - c_{u2}). \quad (8-10)$$

After substituting this expression in equation (8-8) and taking into consideration formula (8-7), we obtain:

$$P_a = l \left[ p_2 - p_1 - \frac{k}{k-1} \rho \left( \frac{p_2}{\rho_2} - \frac{p_1}{\rho_1} \right) \right] + \rho l' c_u. \quad (8-11)$$

Force  $P_a$  is conveniently represented in the form of the sum of two forces:

$$P_a = P_{a1} + \Delta P_a,$$

where

$$P_{a1} = \rho l' c_u$$

and

$$\Delta P_a = l \left[ p_2 - p_1 - \frac{k}{k-1} \rho \left( \frac{p_2}{p_1} - \frac{p_1}{p_2} \right) \right]. \quad (8-12)$$

The resultant forces  $P_a$  and  $P_u$  we shall designate by  $P_y$ , and total resultant force—by  $P$  (Fig. 8-9).

The force  $P_y$  we shall determine by the formula

$$P_y = \sqrt{P_u^2 + P_{a1}^2}.$$

After substituting here the values  $P_u$  and  $P_{a1}$ , we obtain:

$$P_y = \rho l \sqrt{c_u^2 + c_a^2}.$$

But

$$c_u^2 + c_a^2 = c^2,$$

where  $c$ —is the mean vector speed.

Consequently, the expression for  $P_y$  during flow around cascade has the same form, as in case of single profile (Sec. 3-4).

$$P_y = \rho l c. \quad (8-13)$$

Direction of force  $P_y$  is perpendicular to the direction of the vector speed  $c$ . This follows from evident equality

$$\tan \beta = \frac{c_a}{c_u} = \frac{P_u}{P_{a1}}.$$

Thus, the Zhukovskiy force, operating on profile in a cascade is equal to the product of the average density of gas and circulation integral around profile and the mean vector speed. The direction of the force  $P_y$  is determined by rotating the vector of speed  $c$  by  $90^\circ$  in a direction opposite to the direction of the circulation.

We recall that the density  $\rho$  corresponds to average specific volume, i.e.,

$$\frac{1}{\rho} = \frac{1}{2} \left( \frac{1}{\rho_1} + \frac{1}{\rho_2} \right).$$

Thus, we established that in distinction from a single profile, the resultant force, acting on profile in cascade is equal to the sum of the Zhukovskiy force  $P_y$  and the additional force  $\Delta P_a$ , perpendicular to axis of cascade:

$$\vec{P} = \vec{P}_y + \Delta \vec{P}_a.$$

It is important to note that nature of the forces  $P_y$  and  $\Delta P_a$  varies. While the force  $P_y$  depends on circulation of flow and vanishes at  $\Gamma=0$ , the force  $\Delta P_a$  does not directly depend on circulation.

The force, acting on profile, has been determined for the general case of motion of gas. By means of the general relationships obtained there is readily obtained the magnitude of aerodynamic force, acting on the profile, for certain particular cases. Thus, for example, by changing from a cascade to single profile, by increasing the cascade pitch ad infinitum, we obtain  $p_2=p_1$  and  $\rho_2=\rho_1$ ; then  $\Delta P_a = P_u = 0$  and, consequently, in the case of an isentropic flow around an isolated profile, the resultant force, acting on the profile, is equal to the Zhukovskiy force:

$$P = P_z = \rho l c,$$

where  $\rho$  and  $c$  are density and speed of incident flow.

Direction of force is perpendicular to the direction of speed of incident flow.

In changing to the case of flow around a cascade by an incompressible fluid, first of all we should turn our attention to the fact that in equation (8-12) the second term on right-hand side is proportional to the change in potential energy of flow (taking into account hydraulic losses), i.e.,

$$\frac{k}{k-1} \left( \frac{p_2}{\rho_2} - \frac{p_1}{\rho_1} \right) = \frac{c_1^2 - c_2^2}{2}.$$

For an incompressible fluid ( $\rho_1=\rho_2=\rho$ ) from equation of energy we find:

$$\frac{c_1^2 - c_2^2}{2} = \frac{p_{2t} - p_2}{\rho},$$

where  $p_{2t}$  is the theoretical pressure when there are no losses.

Consequently,

$$\Delta P_a = -t(p_{2t} - p_2) = -t\Delta p_n.$$

Difference of pressures  $\Delta p_n = p_{2t} - p_2$  is equal to the loss of pressure in cascade. Thus, in case of a flow around a cascade by a flow of an incompressible fluid the supplemental force is negative and is determined by the loss of pressure in cascade (one should not confuse loss of pressure  $\Delta p_n$  with the difference of

pressures  $p_2 - p_1$ ).

In the absence of losses  $\Delta p_n = 0$  and  $\Delta p_a = 0$ . In this case the resultant force for an incompressible fluid is equal to the Zhukovskiy force:<sup>\*</sup>

$$P = P_z = \rho l'c.$$

#### 8-4. Classification of Losses and Fundamental Characteristics of Cascades

In the motion of a gas through turbomachine cascades energy losses develop: part of the kinetic energy of flow owing to viscosity irreversibly will be converted into heat.

Certain results, under consideration in the present chapter, of the theoretical and experimental investigations of a flow of gas in cascades make it possible to classify the losses of energy according to the following scheme:

A. Profile losses (in two-dimensional cascade with an infinitely great height), including: 1) loss to friction in boundary layer; 2) vortex losses during separations on profile; 3) vortex losses after trailing edge (edge losses).

B. End losses in rectilinear three-dimensional cascade (additional to group A").

C. Wave losses (additional to groups "A" and "B" during transonic and supersonic speeds) in shock waves.

D. Losses caused by non-stationariness and high turbulence of flow.

E. Fan losses in circular (cylindrical) cascade caused by deflections of geometric parameters of cascade from optimum values and radial leakage of gas.

It is necessary to emphasize that the profile losses in cascade are analogous to the profile drag during flow around an individual airfoil profile (Chapter 5).

---

\*Possibility of generalizing Zhukovskiy's theorem in the case of a flow of incompressible fluid through a cascade was pointed out for the first time by B. S. Stechkin in 1944. An accurate solution was obtained by L. I. Sedov in 1948. The basis of Zhukovskiy's approximate theorem for a cascade in the flow of compressible fluid was proposed by L. G. Loytsyanskiy in 1949. The discussed generalization, presented in the above paragraph, of Zhukovskiy's theorem for a cascade in adiabatic flow of gas, was given by A. N. Sherstyuk.

The difference consists only in the fact, during an investigation of cascades there are established the relative losses of energy, and the profile drag is characterized by a drag force, related to the velocity head of incident flow. Physical nature of the profile losses and the profile drag is identical. Vortex losses during separation of flow on profile and after trailing edge are equivalent to the pressure drag. Consequently the profile losses may be considered as the sum of frictional losses and "losses of pressure."

Losses, related to groups "B", "D", and "E", are specific for cascades. Wave losses (group "C") develop in cascades in a specific form. However this group of losses, caused by irreversible processes in shocks is analogous to the wave impedance during flow around a single profile.

In calculating the stage of a turbomachine it is necessary to know the direction of flow at exit of cascade (flow angle at exit) and the energy or power characteristics of cascades. Below there are considered individual components of the losses and there are pointed out methods of calculating the basic aerodynamic properties of cascades.

For evaluating of a turbine cascade in distinction from single profile there are introduced chiefly the energy characteristics. Compressor cascades are characterized chiefly by power coefficients.

Power characteristic of a cascade is the coefficient of losses determined as the ratio of the portion of kinetic energy, which irreversibly has transformed into heat, to the available kinetic energy:

$$\zeta = \frac{2}{k-1} \frac{1}{M_{2t}^2} \left[ \left( \frac{p_{01}}{p_{02}} \right)^{\frac{k-1}{k}} - 1 \right], \quad (8-14)$$

where  $p_{01}$ ,  $p_{02}$  are the pressures of absolute stagnation before and after cascade;

$M_{2t}$  is the M number after cascade in case of an isentropic flow.

Considering that numerator of expression (8-14) is the square of certain fictitious number  $M_\phi$ , calculated on the basis of stagnation parameters:

$$M_\phi^2 = \frac{2}{k-1} \left[ \left( \frac{p_{01}}{p_{02}} \right)^{\frac{k-1}{k}} - 1 \right],$$

The formula for the coefficient of losses can be presented in the form:

$$\zeta = \frac{M_2^2}{M_1^2} \quad (8-15)$$

The efficiency of cascade is determined by evident expression

$$\eta = 1 - \zeta. \quad (8-15a)$$

During an experimental investigation of cascades there is determined the field of stagnation pressures before and after cascade  $p_{011}$  and  $p_{021}$  and static pressures  $p_{11}$  and  $p_{21}$ . From these data by means of formula (8-14) there are calculated the pointwise values  $\zeta$ .

The actual flow at entry and at exit of cascade is nonuniform: the speeds, flow angles and static pressures vary according to the pitch, therefore values of local loss coefficients of energy, and also other characteristics of cascade must be averaged according to the pitch. For determination of averaged characteristics there must be formulated the concept of an ideal (theoretical) process in a cascade during nonuniform flow. As an ideal process it is possible to consider such an isentropic process, during which in the investigated section there are maintained constant, in comparison with actual process, the fields of static pressures and directions of speeds.\*

The efficiency of the cascade in a nonuniform flow is calculated by the formula

$$\eta = \frac{\int_0^l \rho_1 c_1^2 \sin \beta_1 dl}{\int_0^l \rho_2 c_2^2 \sin \beta_2 dl} \quad (8-16)$$

where  $c_2$  is the actual speed;

$\rho_1$  -- density of gas in actual flow.

Introducing in this expression the reduced flow rate  $q$  after elementary

---

\*In another definition of an ideal process it is assumed that the entry and exit angles of the cascades are equal to the average angles  $\beta_1$  and  $\beta_2$ , determined by equation of momentum.



transformations we obtain:

$$\eta = \frac{\int_0^l \lambda_{2l}^2 \frac{p_{01}}{p_{01}} \sin \beta_{2l} dt}{\int_0^l \lambda_{2l}^2 q_{2l} \frac{p_{01}}{p_{01}} \sin \beta_{2l} dt} \approx \frac{\int_0^l \eta_l q_{2l} \frac{p_{01}}{p_{01}} \sin \beta_{2l} dt}{\int_0^l q_{2l} \frac{p_{01}}{p_{01}} \sin \beta_{2l} dt} \quad (8-17)$$

The last expression is obtained on the assumption  $\lambda_{2l}$  const. The magnitude  $\eta_l = \frac{\lambda_{2l}^2}{\lambda_{2l}^2}$ ;  $\lambda_{2l}$ ,  $q_{2l}$  is the theoretical speed and reduced flow rate at point after cascade.

For calculations on the basis of formula (8-17) it is convenient to use diagram proposed A. V. Gubarev (Fig. 8-10).

Diagram is constructed for separate determination of magnitudes

$$A = \eta_l q_{2l} \frac{p_{01}}{p_{01}} \quad \text{and} \quad B = q_{2l} \frac{p_{01}}{p_{01}}.$$

The order of construction and uses of the diagram are readily understood by means of Fig. 8-10. On the basis of the values  $p_{02l}/p_{01}$  and  $p_{2l}/p_{01}$  at the point of investigated flow there are determined  $A_l$  and  $B_l$  respectively. Then there is made separate summation of magnitudes  $A_l \sin \beta_{2l}$  and  $B_l \sin \beta_{2l}$ . Final expression for cascade efficiency has the form:

$$\eta = \frac{\sum_{l=1}^n A_l \sin \beta_{2l}}{\sum_{l=1}^n B_l \sin \beta_{2l}},$$

where  $n$  is the number of selected sectors within limits of cascade pitch.

In addition to coefficient of losses of a cascade in calculating the stage there is used the coefficient of flow rate, equal to the ratio of actual flow rate to flow rate in an ideal process. Since the flow rate of a gas through one and the same channel

$$G_l = g \int_0^l \rho_l c_l \sin \beta_l dt = g \int_0^l \rho_l c_l \sin \beta_l dt, \quad (8-18)$$

then, by using formula (2-38), we find coefficient of flow rate in such a form:

$$\mu = \frac{\int_0^l q_{2l} \frac{p_{01}}{p_{01}} \sin \beta_{2l} dt}{\int_0^l q_{2l} \sin \beta_{2l} dt} \quad (8-19)$$

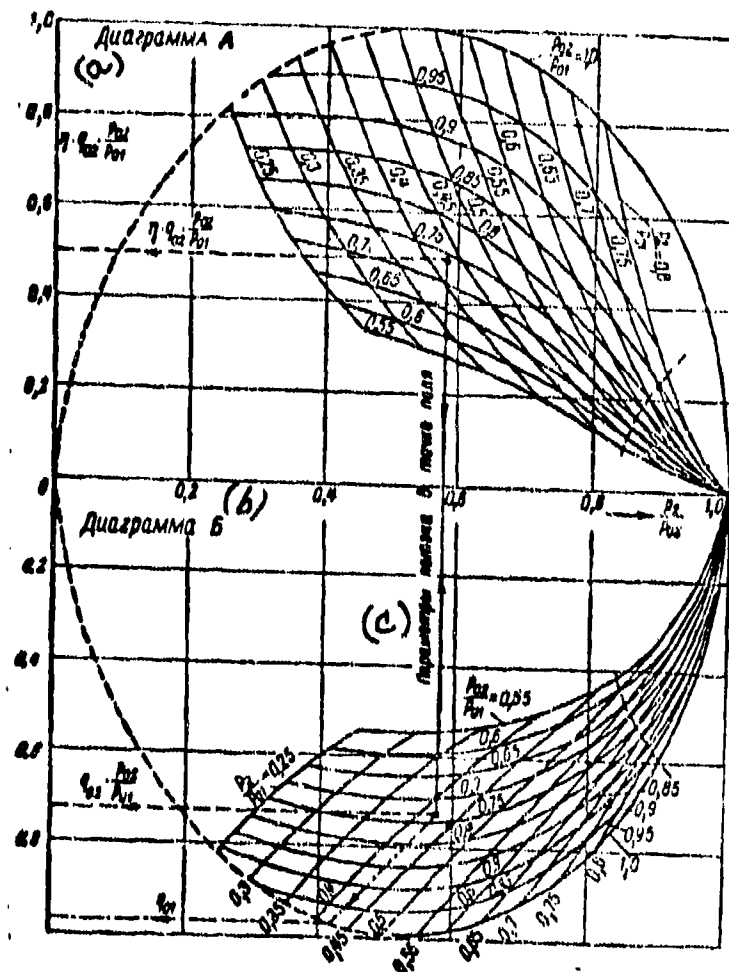


Fig. 8-10. Diagram for determining losses in adiabatic flow ( $k = 1.4$ ).  
KEY: (a) Diagram A; (b) Diagram B; (c) Flow parameters at point of field.

By means of formulas (8-18) and (2-38) momentum after cascade can be presented in this form:

$$\frac{G_1}{g} c_2 = k_1 \int_0^l p_{01} q_2 \lambda_2 \sin \beta_2 dt.$$

Then the utilisation factor of impulses\*

$$\eta = \frac{\int_0^l q_{21} \frac{P_{02}}{P_{01}} \sin \beta_2 dt}{\int_0^l q_{21} \frac{P_{02}}{P_{01}} \sin \beta_2 dt} \quad (8-20)$$

\*The coefficient  $\eta$  frequently is called the velocity coefficient. Formulas (8-19) and (8-20) are obtained by means of equations of continuity and momentum on the assumption that in an ideal process the field of angles and pressures is kept the same as in an actual process.

where  $\varphi_i = \frac{\lambda_i}{\lambda_{2i}}$ .

It is readily shown that the diagram constructed for determining  $\eta$  (Fig. 8-10) makes it possible also to find  $\mu$  and  $\varphi$  in a nonuniform flow. For determining  $\mu$  it is sufficient in diagram B to find the value  $B_i = q_{2i} \frac{p_{02i}}{p_{01}}$  (at intersection of experimental values  $p_{02i}/p_{01}$  and  $p_{2i}/p_{01}$ ) and  $B_t = q_{2t}$  (at intersection of curves  $p_{2i}/p_{01}$  and  $p_{02i}/p_{01} = 1$ ); then

$$\mu = \frac{\sum_{i=1}^n B_i \sin \beta_{2i}}{\sum_{i=1}^n B_i \sin \beta_{2i}}.$$

For determining  $\varphi$  it is necessary to construct additional diagram of the function  $\varphi_i = f\left(\frac{p_{02i}}{p_{01}}; \frac{p_{2i}}{p_{01}}\right)$ .

Since

$$\varphi_i \approx \sqrt{\eta_i} = \sqrt{1 - \zeta_i},$$

then

$$\varphi = \frac{\sum_{i=1}^n \frac{A_i}{\varphi_i} \sin \beta_{2i}}{\sum_{i=1}^n B_i \sin \beta_{2i}}.$$

The averaged value of flow angle at exit is determined by the equation of momentum. Mean values of projections of speed after the cascade are equal to:

$$(c_x \cos \beta_x)_{x=A} = \frac{kR}{G_1} \cdot \int_0^1 p_{01} q_2 \lambda_2 \cos \beta_2 \sin \beta_2 dt;$$

$$(c_x \sin \beta_x)_{x=A} = \frac{kR}{G_1} \cdot \int_0^1 p_{01} q_2 \lambda_2 \sin^2 \beta_2 dt.$$

Then the average angle

$$\beta_{x=A} = \arctan \frac{2 \int_0^1 p_{01} q_2 \lambda_2 \sin^2 \beta_2 dt}{\int_0^1 p_{01} q_2 \lambda_2 \sin 2\beta_2 dt}. \quad (8-21)$$

### 8-5. The Boundary Layer and Frictional Losses in Cascades

The determination of the structure of the boundary layer forming in a profile, the establishment of points of transition and separation of layer are important part of the problem on profile losses in cascades. The scheme of the formation of a boundary layer on a profile in a two-dimensional cascade is shown in Fig. 8-11, a.

Using a graph of distribution of speeds along contour of profile, we shall trace character of change of layer on concave and convex surfaces of blades.

On the concave surface after the point of stagnation (critical point), the thickness of the layer increases slightly. At places of greater curvature, where speed of external flow either remains constant or drops the thickness of boundary layer increases. At these points there may develop a transition from a laminar layer to a turbulent, and under certain flow conditions—even a local separation of the layer. In nozzle section near contraction section, where pressure rapidly falls, and the speed increases, thickness of boundary layer decreases and attains minimum values on descent from profile.

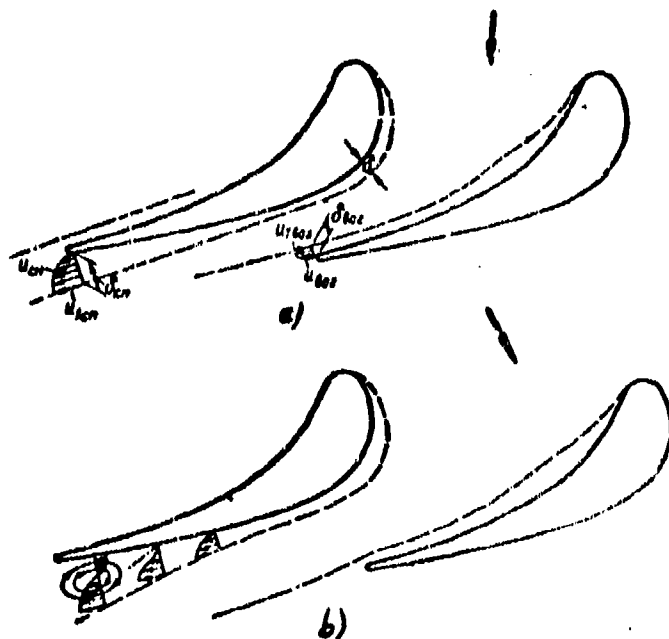


Fig. 8-11. Schematic diagram of formation of boundary layer on profile in cascade.  
a--without separation; b--separation on back of blade.

On the back edge in the direction of contraction section the thickness of the layer also decreases. Along back edge in an oblique cross section there is a marked rapid increase in thickness of layer, which attains along trailing edge maximum values. A certain portion of back edge in oblique cross section is flowed around, as a rule, with a positive gradient of pressure (diffusion sector of back edge) which sometimes may result in a separation (Fig. 8-11,b).

In designing a cascade, practically essential is the determination of location of transition region of laminar layer into turbulent and conditions of continuous flow around a profile. As the calculations and experiments show, point of transition most frequently coincides with point of minimum pressures on back edge or it is somewhat displaced into diffuser region. In those cases when flow is strongly turbulized point of transition may be considerably displaced against flow (into nozzle region).

We shall consider certain results of an experimental investigation of boundary layer in impulse and reactive turbine cascades.

In Fig. 8-12 there are presented results of measurements in boundary layer on back edge of profile TC-2A. The high degree of contraction of the channels in cascade (Fig. 8-12,a) creates favorable conditions for the maintenance of a laminar mode in the layer. However, at the exit to oblique cross section ( $\bar{x}_{en} = 0.5$ ) laminar layer loses stability and transforms into a turbulent layer. Zone of transition is determined entirely satisfactorily by the described method in Chapter 5 and occupies about 4% of total contour of profile. The further flow in boundary layer bears an obviously pronounced turbulent character (Fig. 8-12,b). After region of transition in oblique cross section on back edge there is noted an intense increase in the momentum thickness.

Boundary layer on the concave surface up to trailing edge is laminar. Hence it may be concluded that the point of separation on trailing edge is located asymmetrically with respect to center line of profile.

Results of investigation of boundary layer in an impulse cascade, composed of profiles of the Moscow Power Engineering Institute TP-0A, showed that also here with a calculated entrance angle there exist three zones of flow in the layer, which are arranged in the same manner, as in channel of reactive cascades.

With optimum entrance angle  $\beta_1 = 23^\circ$  (Fig. 8-13) the distribution of speeds along the back edge is that of a nozzle. Transitional zone at all values of  $M_2$  is located after the minimum section of channel at the entrance in an oblique cross section and a change of flow condition according to the  $M$  and  $Re$  numbers does not result in a marked redistribution of extent of laminar and turbulent sections of the layer.

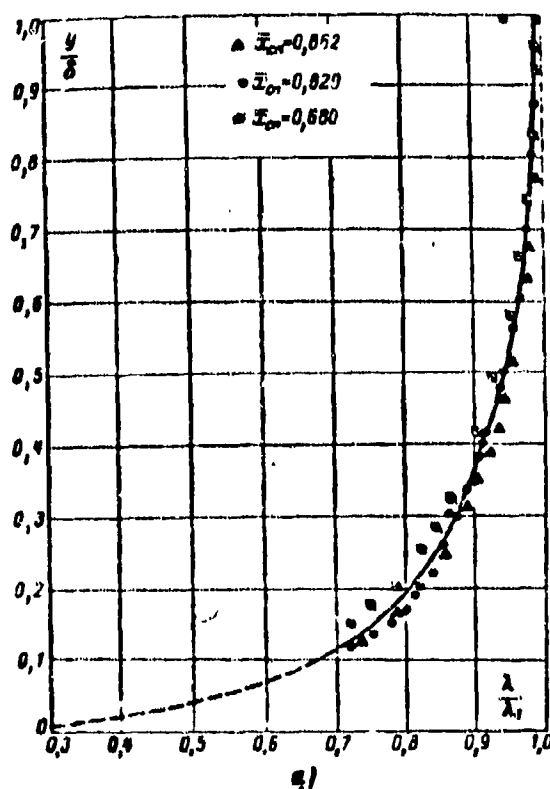
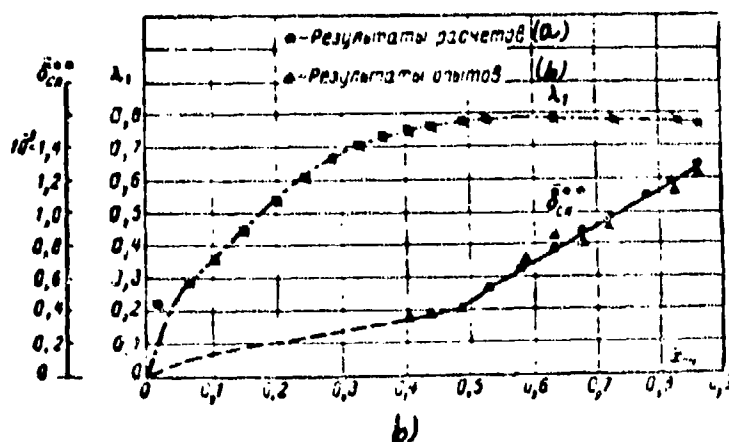


Fig. 8-12. Distribution of speeds in boundary layer on back edge of profile a) and distribution of momentum thicknesses along back edge b) for reactive cascade TC-2A.  
KEY: (a) Results of calculation;  
(b) Results of experiments.



At small entrance angles ( $\beta_1 = 14^\circ$ ) the entire boundary layer on back edge is found to be turbulent and the momentum thickness for trailing edges on back edge increases by 2.0 to 2.5 times in comparison with  $\beta_1 = 23^\circ$  (Fig. 8-14).

Essential changes in the distribution of the thickness  $\delta^{**}$  are marked also on the concave surface (Fig. 8-15). If at  $\beta_1 = 23^\circ$  ( $M_2 = 0.52$ )  $\delta_{\text{cor}}^{**}$  were found to be

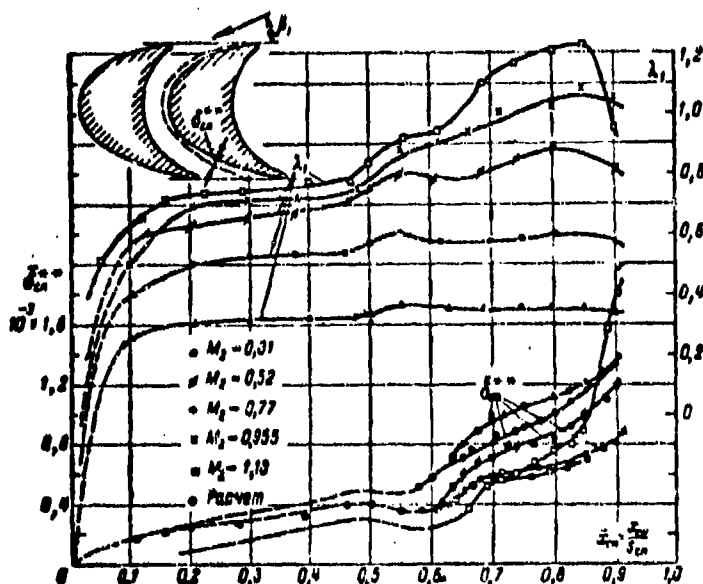


Fig. 8-13. Change of momentum thickness on back edge of profile of impulse cascade TR-OA at different  $M_2$  numbers (experiments at Moscow Power Engineering Institute (MEI)).

of an order  $0.7 \cdot 10^{-3}$ , then with transition to  $\beta_1 = 14^\circ$  the thickness  $\delta_{\text{cor}}^{**}$  decreased to  $0.27 \cdot 10^{-3}$ . The total momentum thickness with a decrease in flow angle at entrance increases by 60 to 70%. With an increase in  $\beta_1$ ,  $\delta^{**}$  increases on concave surface and decreases on back edge. However, the total momentum thickness increases less intensely than with a decrease in flow angle at entrance. Hence it directly follows that at a certain optimum entrance angle  $\Sigma\delta^{**}$  is minimal. The dependence of the thickness  $\delta^{**}$  along trailing edges on  $\beta_1$  for a reactive cascade is shown in Fig. 8-15,b. The less is the contraction of the flow in cascade the more intensive is the change of  $\Sigma\delta^{**}$  depending on  $\beta_1$ .

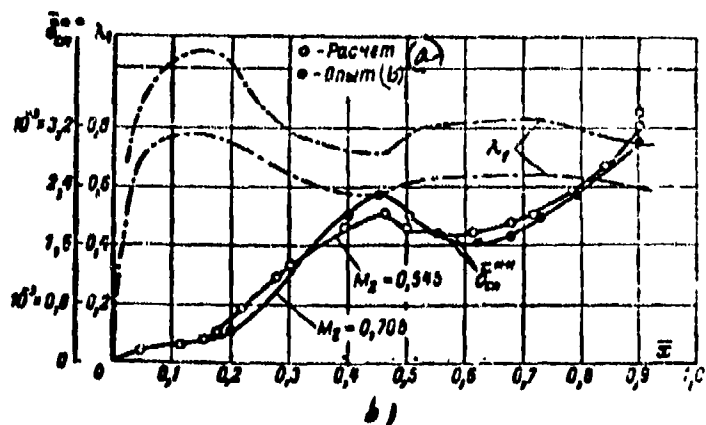
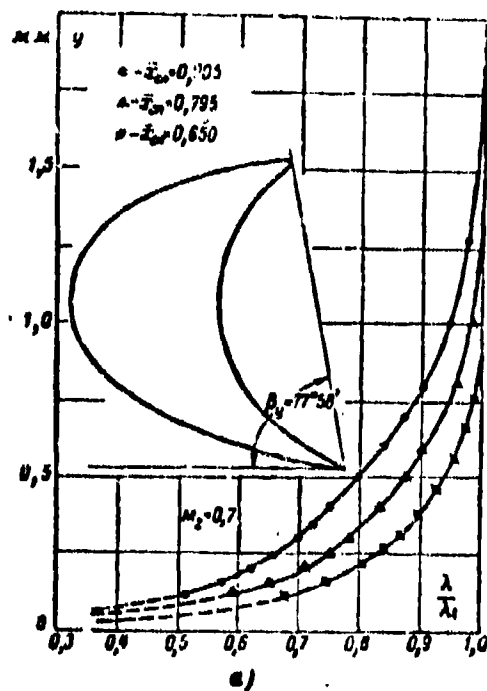


Fig. 8-14. Profiles of speed a) and change in momentum thickness along back edge b) for impulse cascade at  $\beta_1 = 14^\circ$ .  
KEY: (a)  $\circ$  calculation; (b)  $\bullet$  experiment



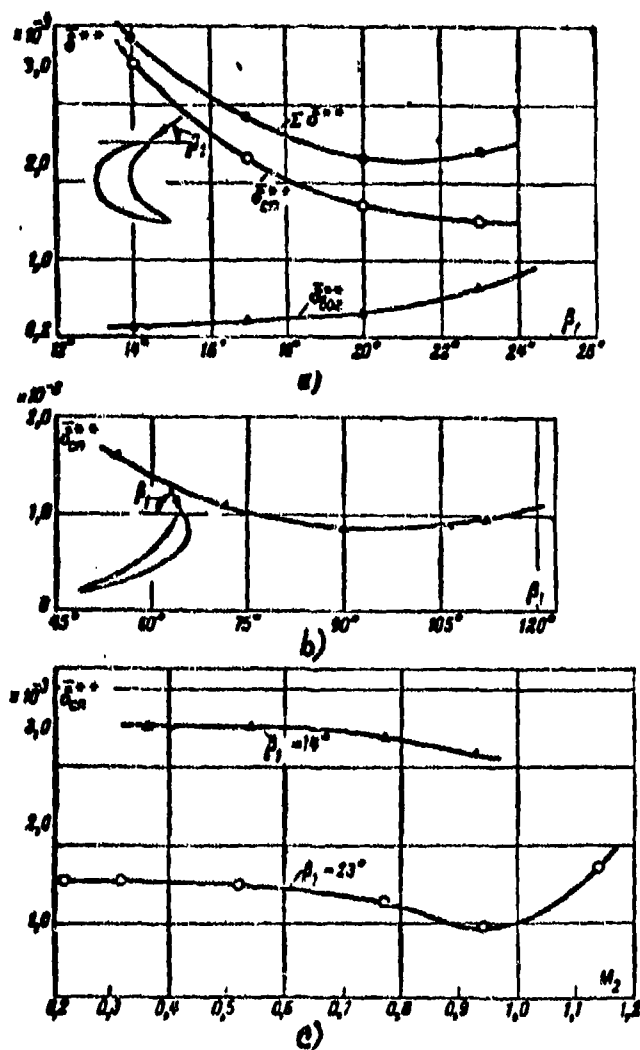


Fig. 8-15. Dependence of  $\bar{\delta}^{**}$  on flow angle at entrance  $\beta_1$  for impulse and reactive cascades (experiments at Moscow Power-Engineering Institute).

The influence of two other flow mode parameters ( $Re_2$  and  $M_2$ ) on structure of layer in cascades can be traced by graphs in Figs. 8-13 and 8-15,c. With an increase in  $Re_2$  and  $M_2$  thickness  $\delta_{en}''$  markedly decreases.

An intensive decrease in  $\delta_{en}''$  with an increase in  $M_2$  is explained to a significant degree by the change in gradients of speed in the intervane channel. From the distribution of speeds given in Fig. 8-13 there is readily seen the increase in contraction on back edge with an increase of  $M_2$ .

With a transition to supersonic speeds the magnitude  $\delta''$  markedly increases as a result of interaction between a compression wave and the boundary layer. In place where the shock falls onto back edge in oblique cross section there may be observed a separation of the layer.

Very significant influence on structure of boundary layer is exerted by the degree of turbulence in the flow; its magnitude in turbomachine stages may attain large values.

Influence of degree of turbulence on structure of boundary layer\* on back edge of reactive and active profiles can be evaluated by Figs. 8-16,a and b. With an increase in turbulence there occurs a rebuilding of profiles of speed in the layer: a filling-in of the speed profiles occurs (Chapter 5). An increase in the degree of turbulence results in reducing the laminar layer section and an increase in thickness of turbulent layer.

The character of change in profile losses and frictional losses depending on degree of turbulence for two types of cascades can be evaluated by curves in Fig. 8-16,b. In a reactive cascade TC-1A an increase of  $E_0$  from 1 to 4% results in an increase of  $\zeta_p$  from 2.6 to 4%. For active cascade TP-0A, the curve  $\zeta_p$  has minimum at  $E_0 = 3\%$ . In the sector  $1\% < E_0 < 3\%$ . There occurs a turbulization of the layer at point of separation on back edge and the losses decrease. At  $E_0 > 3\%$  with an increase of  $E_0$  the frictional losses increase more intensely than in a nozzle

---

\*The experiments were made by V. A. Vrublevska.

reactive cascade.

The calculation of the boundary layer in cascades is made by means of the procedure presented in Chapter 5. Here, as a preliminary measure there must be calculated or experimentally determined the distribution of the speeds along the contour of profile. It is used to make a calculation of the momentum thicknesses.

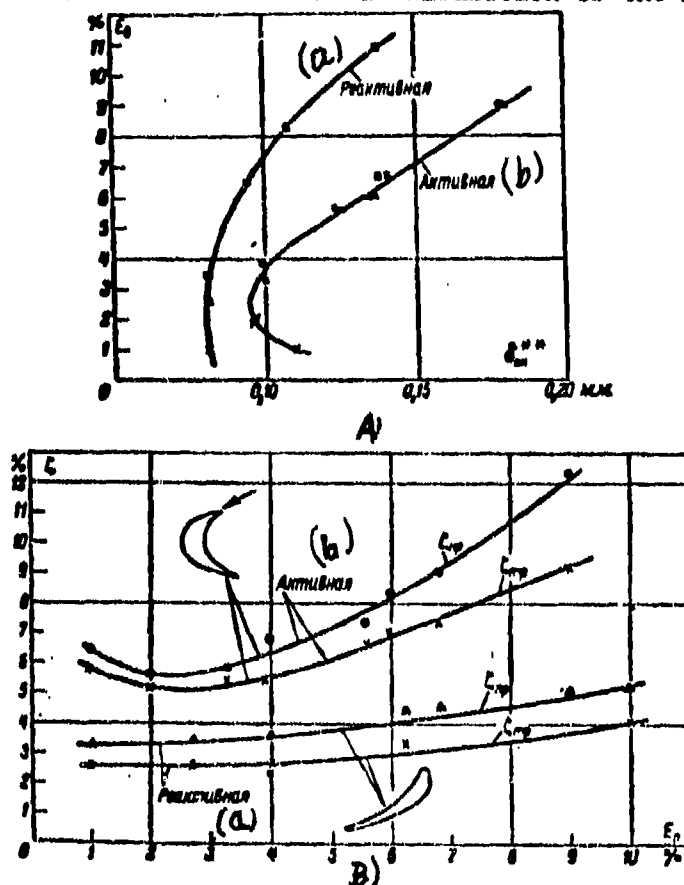


Fig. 8-16. Influence of degree of turbulence on distribution of thicknesses of  $\delta''$  along back edge A) and on profile losses and frictional losses in reactive and impulse cascade TC-1A and TR-OA B) (experiments at Moscow Power-Engineering Institute).

KEY: (a) Reactive; (b) Impulse

As a preliminary it is necessary to determine correctly the location of transitional region on back edge and concave surface.

If there are no experimental data for  $\delta''$  in the zone of transition they may be determined by the formulas presented in Sec. 5-10. During high degrees of turbulence the transition is realized near the leading edge; in this case necessity

of considering the laminar section becomes superfluous.

The loss of kinetic energy in boundary layer (frictional loss) is determined by the equation of energy, written out for exit section of cascade:

$$\Delta E_{rp} = \frac{1}{2} \left\{ \left[ \int_0^{\infty} \rho u (u_1^2 - u^2) dy \right]_{cn} + \left[ \int_0^{\infty} \rho u (u_1^2 - u^2) dy \right]_{cor} \right\}. \quad (8-21)$$

where  $u$  is the speed at given point of layer;

$u_1$  is the speed at external boundary of layer;

$y$  is the coordinate, normal to profile at a given point.

In the absence of losses the kinetic energy after the cascade will be:

$$E_t = \frac{G u_1^2}{2g}. \quad (8-22)$$

where  $G$  - the actual flow rate through one channel - is determined by the formula

$$G = G_t - g \left[ \int_0^{\infty} (\rho_1 u_1 - \rho u)_{cn} dy + \int_0^{\infty} (\rho_1 u_1 - \rho u)_{cor} dy \right]. \quad (8-23)$$

where  $G_t$ ,  $u_t$  are the theoretical flow rate and speed at exit of cascade.

The coefficient of frictional losses is equal to:

$$\zeta_{rp} = \frac{\Delta E_{rp}}{E_t}.$$

After expressing  $\Delta E_{rp}$  and  $E_t$  by formulas (8-21), (8-22) and (8-23) after certain transformations there may be obtained:

$$\zeta_{rp} = \frac{\Sigma(k_1 k_2 // k_1'')}{t \sin \beta_2 - \Sigma(k_1 k_2 // k_1')}. \quad (8-24)$$

where

$$k_1 = \left( \frac{1 - \xi_1^2}{1 - \xi_1'^2} \right)^{\frac{1}{k-1}}; \quad k_2 = \left( \frac{\xi_1}{\xi_{1t}} \right)^2; \quad k_3 = -\frac{\xi_1'}{\xi_{1t}};$$

$\xi_1 = \frac{u_1}{c_{max}}; \quad \xi_{1t} = \frac{u_{1t}}{c_{max}}$  are dimensionless speeds after cascade for actual and theoretical processes. The sign  $\Sigma$  indicates summation along the back edge and the concave surface.

Results of verifying the accuracy of the calculation of layer for several

cascades may be seen in Figs. 8-13 and 8-14. A comparison shows satisfactory agreement between the experimental and calculated values of  $\delta^{***}$  over entire region of subsonic speeds (up to  $M_2 = 0.955$ ).

After calculating the thickness  $\delta^{***}$  the determination of frictional losses presents no difficulty, if the magnitude  $H^* = \frac{\delta^{***}}{\delta^{**}}$  is known. For calculating turbine (nozzle) cascades it is possible to assume  $H^* = 1.8$ .

In diffuser (compressor) cascades the magnitude  $H^*$  is somewhat higher. Thus, frictional losses as a first approximation may be considered proportional to the momentum thickness on trailing edge of profile and from its magnitude to judge the relative efficiency of the cascades.

#### 8-6. Edge Losses in Cascades

In the descent from trailing edges of the profile there occurs a separation of the boundary layer. As the result of separation and interaction between the layers, flowing down from the concave and convex surfaces, with the external flow after trailing edge there develop vortices, which will form the initial sector in the wake of trailing edge (Fig. 8-17).

Within the limits of initial sector and at that place after it, where there will be form vortex street, the interaction between edge wakes and core of flow reduces to an equalizing of the flow after the cascade. In certain section after cascade the vortex wakes of neighboring profiles are closed and field of speeds, static pressures and angles become uniform. In the sector prior to a complete equalization average static pressure of flow increases, and the exit angle decreases.

For supporting the vortex motion after the edge there is expended a portion of kinetic energy of flow; additional losses of kinetic energy will form on boundary of the wake of edge and of the core of flow, where there develops an intense turbulent exchange.

The formation of a vortex motion in wake of edge is corroborated experimentally.

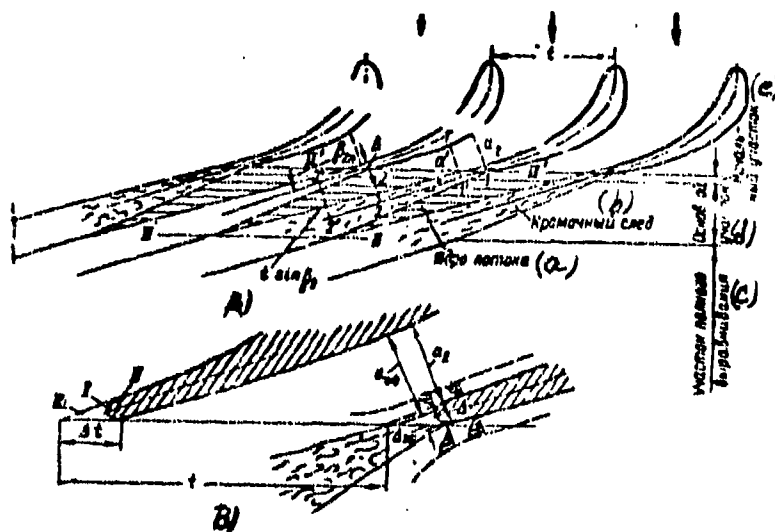


Fig. 8-17. Schematic diagram of flow of gas after cascade.  
KEY: (a) core of flow; (b) wake of edge; (c) sector of total equalization; (d) primary sector; (e) initial sector.

In Fig. 8-18 are presented curves of distribution of total and static pressures, angles and temperatures of stagnation at a certain distance after edges of a reactive cascade. At small distances from edge there is detected a significant nonuniformity of fields of pressures, angles and of, especially important, stagnation temperatures. In wake of edge the pressure and stagnation temperature which is characteristic for vortex motion decreases. A change in  $T_0$  is explained by the nonuniform distribution of speeds and vortex effect after edge (Sec. 5-1 and 5-16). The rapid equalization of  $T_0$  attests to the intense exchange between the core of flow and the wake of edge.

With a small thickness of edge, the thickness of boundary layer and distribution of speeds close to the points of separation of flow as well as the pressure difference between these points exert a decisive influence on the structure of the wake of the edge.

As the thickness of the edge increases, the losses associated with sudden expansion of flow acquire a marked effect.

In Fig. 8-19 there are shown results of drainage of trailing edge. As is

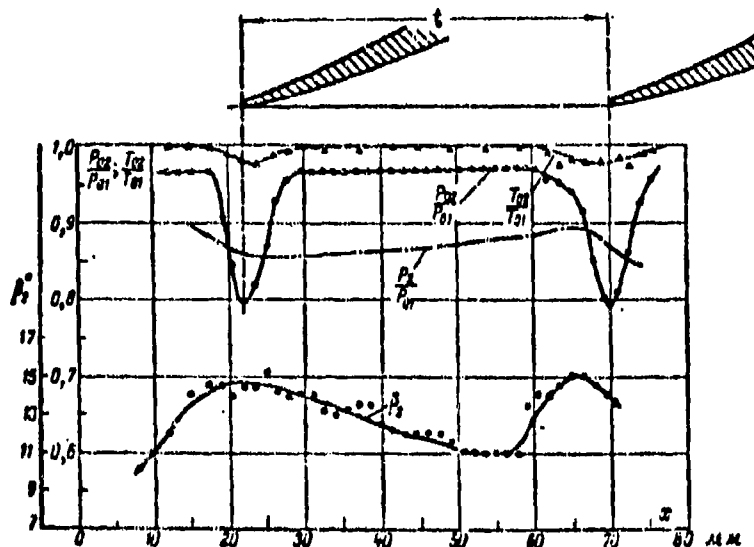


Fig. 8-18. Distribution of parameters of flow after trailing edges of reactive cascade.

evident, pressure along edge abruptly changes. From side of concave surface the flow is a nozzle flow and from side of back edge diffuser. Consequently, the point of separation is displaced to back edge of blade.

With a change in thickness of trailing edge  $\Delta$  (Fig. 8-17) the distribution of speeds along contour of profile varies and, consequently, there occurs certain reconstruction of boundary layer close to trailing edge. The frictional losses here vary in accordance with variation of energy thickness on trailing edge. Experiments by V. S. Yelizarov (Fig. 8-20) have clearly corroborated that with increase in  $\Delta$  the sum  $\delta_{a.k.t}^{***} + \delta_{concur}^{***} = H^* \Sigma \delta^{***}$  varies.

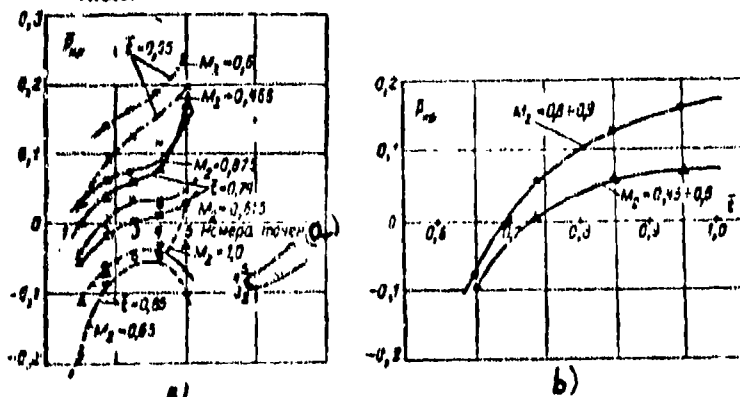


Fig. 8-19. Distribution of pressures on trailing edge of reactive cascade during different modes of flow. KEY: (a) Numbers of the points.

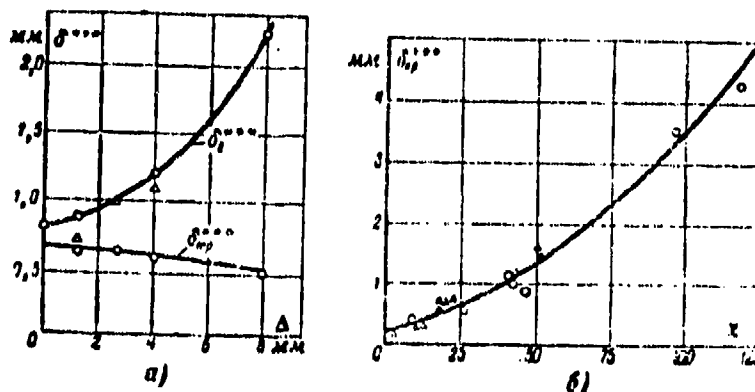


Fig. 8-20. Variation of energy thickness on profile and after cascade (a) and  $\delta'''_{np}$  depending on the parameters  $x$  (b) according to V. S. Yelizarov.

A significant influence on structure of flow after the edge is exerted by the pitch of the blades. With a small pitch (Fig. 8-19) after edge is detected rarefaction, which increases somewhat with an increase of  $M_2$ . As the pitch increases average pressure after edge increases and with a specific pitch attains values, larger than the pressure after the cascade. Consequently, with an increase of pitch both the relative and also absolute values of edge losses must decrease; these circumstances have been corroborated experimentally.

Certain influence on edge losses is exerted by the shape of edge, which determines under known conditions the location of points of separation. Experiments show that in case of a rounded edge at subsonic speeds the initial sector of the wake is narrower (point of separation displaced along flow) than along a flat truncated edge.

A theoretical calculation of edge losses is very complicated, and this problem up to present is still unsolved. Available semiempirical methods make it possible to evaluate the edge losses and angle of exit of cascade on the basis of experimental data, obtained for specific classes of profiles.

Parameters of an equalized flow after cascade may be found by means of a common solution of equations of continuity, momentum and energy. For a fluid, enclosed



between control surfaces (Fig. 8-17), parallel to each other at a distance, equal to the sector of equalization, the indicated can be written out under the following assumptions: a) the flow density varies slightly in the process of mixing (between sections II--II and II'--II'); b) field of speeds and pressures between edges and in section II--II are uniform; c) back edge of profile in nozzle section is made rectilinear.

In this case equation of continuity can be presented as:

$$\rho c_1 (l - \Delta l) \sin \beta_{2n} = c_{2\infty} \rho l \sin \beta_1,$$

or

$$c_1 (1 - \tau) \sin \beta_{2n} = c_{2\infty} \sin \beta_1, \quad (8-25)$$

where  $\tau = \frac{\Delta l}{l}$ ;

$\Delta l$  is the thickness of edge in plane of exit section (Fig. 8-17).

Equation of momentum in direction of axis of cascade gives:

$$c_1^2 \cos \beta_{2n} \rho (l - \Delta l) \sin \beta_{2n} = c_{2\infty}^2 \cos \beta_1 \rho l \sin \beta_1. \quad (8-26)$$

Equation of momentum in direction, perpendicular to axis of cascade, can be written in the form:

$$\begin{aligned} c_{2\infty}^2 \rho \sin^2 \beta_{2n} (l - \Delta l) + p_1 (l - \Delta l) + p_{2\infty} \Delta l = \\ = c_{2\infty}^2 \rho \sin^2 \beta_1 l + p_{2\infty} l. \end{aligned} \quad (8-27)$$

From equations (8-25) and (8-26) there readily is obtained:

$$\beta_1 = \arccos[(1 - \tau) \sin \beta_{2n}]. \quad (8-28)$$

Equation (8-25) and (8-27) make it possible to find the increase of pressure after cascade:

$$\Delta \bar{p}_1 = \frac{p_{2\infty} - p_1}{\frac{1}{2} \rho c_1^2} = [2(1 - \tau) \sin^2 \beta_{2n} + \frac{\bar{p}}{\rho}] \tau. \quad (8-29)$$

For determining the theoretical speed at infinity after a cascade, we use equation of energy, which under the adopted assumption  $\rho_1 = \rho_{2\infty} = \rho$  can be presented in the form:

$$\frac{c_{2\infty}^2}{2} + \frac{p_{2\infty}}{\rho} = \frac{c_1^2}{2} + \frac{p_1}{\rho}, \quad (8-30)$$

where  $c'_{2\infty}$  is the theoretical speed in the section II—II.

By means of equations (8-27), (8-28), and (8-30) we obtain the coefficient of the edge losses

$$\zeta_{\text{ep}} = \frac{v \sin^2 \beta_{2n} \bar{p}_{\text{ep}}}{1 - \delta p_{2\infty}} \quad (8-31)$$

In equations (8-29) and (8-31) dimensionless pressure after edges  $\bar{p}_{\text{kp}}$  must be determined by experimental data.

According to (8-31) with an increase of thickness of trailing edges  $\Delta l$  it is expedient simultaneously to increase the relative pitch  $t$  and to decrease the blade angle in order to maintain a given exit flow angle and to assure moderate losses.

The above-mentioned formulas, obtained by G. Yu. Stepanov, satisfactorily agree with experimental data; however practical use of equations (8-31) is made difficult because the magnitude  $\bar{p}_{\text{kp}}$  may vary in very wide limits depending upon the mode and geometric parameters of the cascade.

V. S. Yelizarov proposed the method of approximation for determination of edge losses as the difference between losses at a certain distance after cascade (profile losses) and frictional losses. Coefficients of the profile losses and frictional losses can be expressed in terms of corresponding arbitrary energy thicknesses [formula (8-24)].

In accordance with considered method the energy thickness in wake of an edge is expressed by the formula

$$\delta_{\text{kp}}''' = \delta_i''' - H \delta_{\text{rp}}''',$$

where  $\delta_i'''$  is the energy thickness in section of wake of edge at selected distance after cascade.

The relative energy thickness in the wake

$$\bar{\delta}_{\text{kp}}''' = \frac{\delta_i'''}{H \delta_{\text{rp}}'''} = \frac{\delta_i''}{\delta_{\text{rp}}''} - 1 \quad (8-32)$$

depends basically on the complex

$$\chi = \frac{\Delta \Sigma'''_{\text{back concave}}}{\delta'''_{\text{back concave}}} = \frac{\Delta \Sigma''_{\text{back concave}}}{H \cdot \delta''_{\text{back concave}}} \quad (8-33)$$

A corresponding dependence, obtained experimentally for a continuously streamlined profiles, is presented in Fig. 8-20, b. The formula, approximating this dependence, has the form:

$$\delta'''_{kp} = (0,21 \chi^2 + 12,4 \chi + 220) \cdot 10^{-3} \quad (8-34)$$

Consequently,

$$\delta'''_z = H \cdot \delta'''_{kp} (\delta''_{kp} + 1).$$

The coefficient of the profile losses is determined by the formula

$$\zeta_{sp} = \frac{\delta'''_z}{a_1 \sqrt{1 - \zeta_{fp}}} \quad (8-35)$$

where  $a_1$  -- width of narrow section of channel;

$\zeta_{fp}$  is the coefficient of frictional losses determined by formula (8-24).

Thus, the considered method of calculating the profile losses is based on establishing an association between edge losses and the frictional losses,\* and besides these losses are determined separately.

An evident advantage of the method consists in the fact that it makes it possible to consider influence of different geometric and mode parameters of the cascade on the edge and profile losses. With a change in these parameters there change the arbitrary thicknesses of boundary layer, in terms of which there are expressed coefficients  $\delta'''_{sp}$  and  $\zeta_{sp}$ .

However, actually the form of the function  $\delta'''_{sp}(\chi)$  may change depending not only on the type of cascades but also on the mode of flow around; this is a defect of the method.

For cascades with thick edges, thickness of which considerably greater than the thickness of the layer ( $\bar{\Delta} = \Delta/a_1 > 0.3$ ), a method of solution has been

\*For cascades with sharp edges a method of calculating the profile losses was worked out by L. G. Loytysanskiy. V. S. Yelizarov's solution is an extension of L. G. Loytysanskiy's method for cascades with edges of finite thickness.

proposed by A. N. Sherstyuk. There is considered the flow in one intervane channel whose boundaries after the trailing edges are straight lines made by the exit flow angle  $\beta_2$  to the front of cascade (Fig. 8-17).

Approximately the exit flow angle is determined by the empirical formula

$$\beta_{2,\phi} = \arcsin \left( m \frac{a_2}{t} \right), \quad (8-36)$$

where  $m$  is the experimental coefficient.

With a great thickness of trailing edges it may be assumed that transitions from section 1-1 to section 1'-1' and from section 2-2 to 2'-2' (Fig. 8-17) cause the same loss of energy, as during an abrupt expansion of the flow. After determining the magnitude of these losses there can be obtained the approximate formula

$$\zeta_{ep} = \frac{1}{\gamma_0} \left[ \frac{\Delta_{ep}^2 \left( \frac{0.25m^2}{(1+0.7\Delta_{ep})^2} + \frac{1}{(2m-\Delta_{ep})^2} \right)}{1 + \gamma_0^2 \Delta_{ep}^2 \left( \frac{0.25m^2}{(1+0.7\Delta_{ep})^2} + \frac{1}{(2m-\Delta_{ep})^2} \right)} \right]. \quad (8-37)$$

Here (Fig. 8-17)  $\Delta_{ep} = \frac{\Delta_{ep}}{a_2}$ ;  $\Delta_{ep}$  is the effective "thickness" of trailing edge, determined as the distance between the points of separation  $\Delta_{ep} \approx 0.7 \Delta$ ;  $a_{2,\phi} = a_2 + \frac{\Delta}{6}$  is the effective "width" of narrow section;  $\gamma_0$  is the coefficient of speed for infinitely thin edge.

The simplest empirical formula for determining edge losses was proposed by G. Flyugel:

$$\zeta_{ep} = K \frac{\Delta}{a_2},$$

where  $K = 0.2$ . However, experiments show that the coefficient  $K$  may vary within very wide limits depending upon geometric and mode parameters of the cascade (Fig. 8-21).

A comparison of different method of calculating edge losses shows that the best results are given by formula (8-34), which takes into consideration the influence of  $Re_2$  and  $M_2$  numbers and the basic geometric parameters.

The influence of  $Re_2$  and  $M_2$  numbers (Fig. 8-21, b and c) is explained chiefly by the displacement of points of transition and separation along the edge, and also

by the variation of frictional losses (Chapter 5). Especially characteristic is the curve  $\zeta_{ep}(M_2)$  for  $\bar{\Delta} = 0.42$ . The first maximum of curve is explained by displacement of points of separation against flow (laminar separation). The turbulization of layer in zone of separation reduces to a displacement of points of separation along the flow (critical region of the Re number). The second maximum is associated with the formation of local supersonic zones on edge and the displacement of separation against the flow ( $\Delta_{ep}$  increases). Transition to supersonic speeds is accompanied by improvement of the flow around the edge. Thus, the flow around a thick edge at different  $Re_2$  and  $M_2$  is qualitatively reminiscent of the spectrum of the flow around a poorly streamlined body (Sec. 5-14).

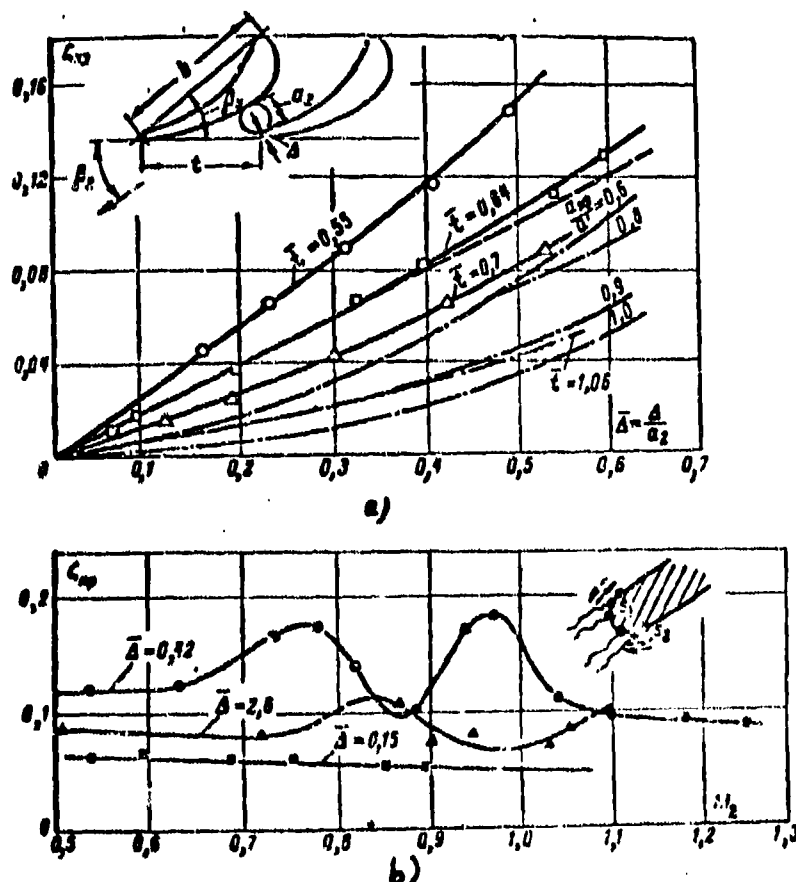


Fig. 8-21. Change of edge losses depending on thickness of edge and relative pitch (a),  $M_2$  numbers (b).

Influence of thickness of edge on the exit flow angle (Fig. 8-22) is found to vary depending on manner of the edge's formation. In trimming the edge by method I the angle  $\beta_2$  decreases with a decrease of  $\delta$ . A trimming of the concave surface (by method II) results in an increase of  $\beta_2$  as  $\delta$  decreases. It must be emphasized that the effective angle, determined by formula (8-36), as a rule, does not coincide with the actual  $\beta_2$  angle in which  $\beta_{2\text{эф}} \leq \beta_2$ . (Fig. 8-22,b). Correction factor  $m$  in formula (8-36) makes it possible to convert from  $\beta_{2\text{эф}}$  to  $\beta_2$ . In accordance

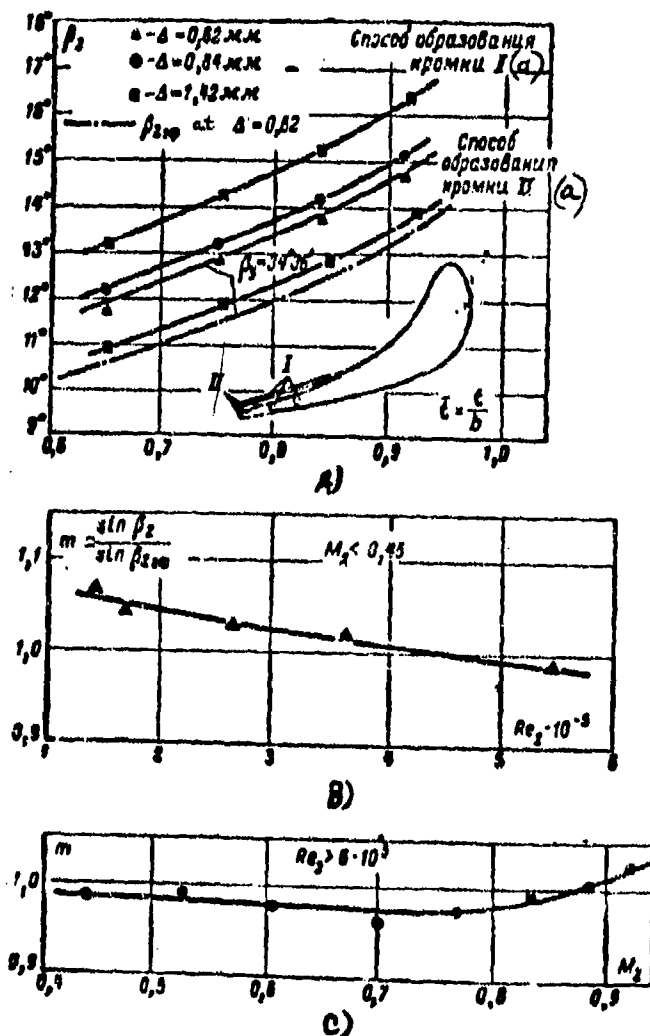


Fig. 8-22. Dependence of exit flow angle on the relative spacing and thickness of edge (A)  $Re$  numbers (B) and  $M_2$  numbers (C).

KEY: (a) Method of edge formation.

with the physical nature of phenomena after edges the coefficient  $\mu$  depends on  $Re_2$  and  $M_2$  numbers, and also on thickness of edge  $\Delta$  (Fig. 8-22) and shape of back edge in nozzle section. Experiments show that for profiles with a rectilinear back edge in nozzle section the angle  $\beta_2 \approx \beta_{20} (m \approx 1)$ . For convex back edge  $\beta_2$  is somewhat less than  $\beta_{20}$ .

#### 8-7. Certain Results of an Experimental Investigation of Two-Dimensional Cascades at Subsonic Speeds

We shall consider the results of an experimental investigation of profile losses and flow angles at exit depending on geometric and mode parameters and shape of profile for cascade in reactive and impulse cascades.

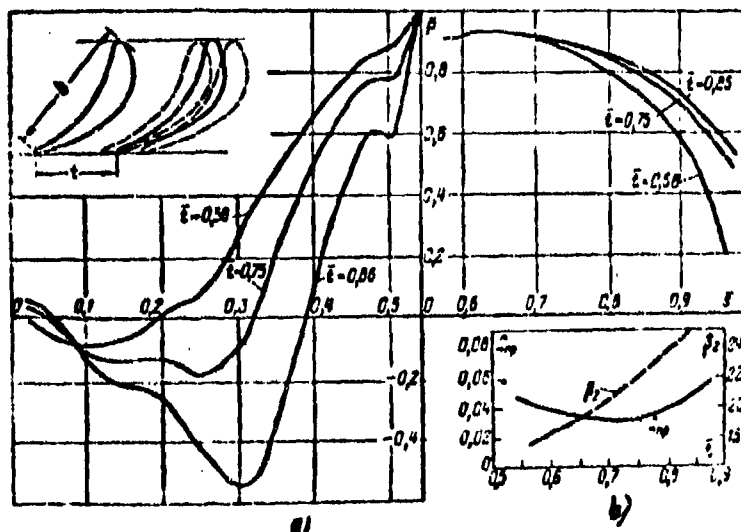


Fig. 8-23. Influence of pitch on distribution of pressures about profile in cascade of reactive type (a); profile losses and flow angle at exit (b).

The influence of pitch and angle of setting of the profiles. Distribution of pressures about profile to reactive cascade (Fig. 8-23) shows that at  $\bar{t} = 0.7$  to 0.8 nozzle flow is along entire contour of profile, with the exception of short sections close to leading and trailing edges. As the pitch increases the point of minimum of pressures on back edge is displaced against flow, regions of nozzle flow are reduced in oblique cross section; gradients of pressures in nozzle

and diffuser regions increase. Consequently, region of transition is displaced against flow, and the frictional losses increase somewhat in nozzle section. The flow around the concave surface with an increase in the pitch becomes favorable, because the nozzle flow near the trailing edge increases. With small pitch the flow along back edge in nozzle section is more contracted; however gradients

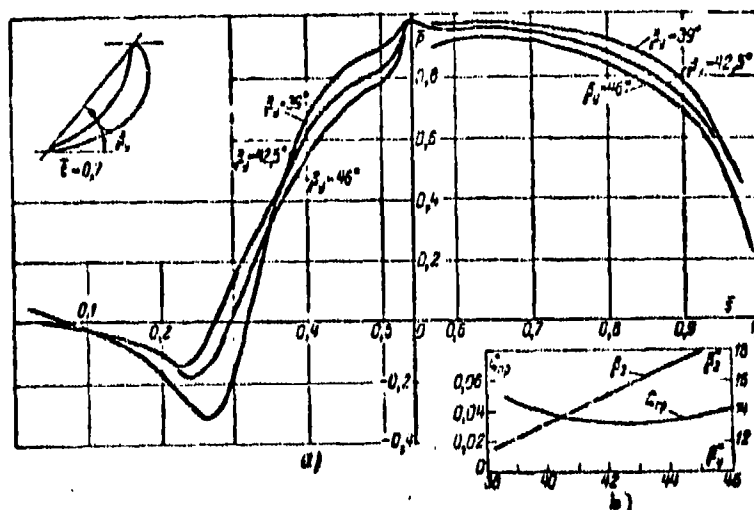


Fig. 8-24. Influence of setting angle of profile in reactive-type cascade on distribution of pressures (a), profile loss and flow angle at exit (b).

of pressures decrease.

Consequently, with an increase of the pitch during a continuous flow around of profile the frictional and edge losses vary differently  $\zeta_{fp}$  (frictional loss) at first decreases, since the relative value of the momentum thickness  $\frac{\Sigma \delta^{**}}{a_1}$  decreases and with large pitches increases owing to an increase in momentum thickness; the edge losses with an increase of  $\bar{t}$  decrease continuously. As a result the profile losses at first decrease, and later increase. Range of relative pitches, corresponding to a minimum of profile losses, is called optimal (Fig. 8-23,b). Experiments clearly show that range of optimal pitches depends on the shape of profile.

A change in angle of setting of profile  $\beta_1$  evokes change of distribution of pressures along the profile (Fig. 8-24). In accordance with this the gradients of pressure in the diffuser and nozzle sections in profile and structure of boundary layer vary. As a result the profile losses with an increase of  $\beta_1$  at first



decrease, and later increase (Fig. 8-24,b), i.e., there is definite range of optimal setting angles. It must be noted that this range depends on the pitch of the cascade.

The flow angle at exit of cascade increases with an increase of pitch and of setting angle. In interval value  $\bar{\tau}_{opt}$  and  $\beta_{y,opt}$  angle at exit with a change of pitch varies approximately proportionally to  $\arcsin a_2/t$ .

The slight change in  $\zeta_{np}$  within a wide range of changes of the pitch and  $\beta_y$  is important peculiarity of reactive cascades composed of well-streamlined profiles. The absolute values of  $\zeta_{np}$  do not exceed 2-3%.

Analogously change the profile losses and flow angle at exit depending on  $\bar{\tau}$  and  $\beta_y$  for cascades of active type; however, range of  $\bar{\tau}_{opt}$  and  $\beta_{y,opt}$  for impulse cascades is found to be narrower, since the geometric and aerodynamic contraction of the channels of such cascades will be less.

We note that presence of diffuser sectors on back edge in nozzle section with small pressure gradients does not result in a sharp increase of the losses, since with small degrees of turbulence, the transition in boundary layer proceeds more rapidly and the separation at trailing edges is displaced along the flow.

The Influence of Mode Parameters on Profile Losses. In preceding paragraph it was shown that depending on flow angle at entrance  $\beta_1$  distribution of thicknesses  $\delta^{**}$  varies on the concave and convex surfaces, since the distribution of pressures varies about the profile (Fig. 8-25,a). The most unfavorable are modes with small angles at entrance ( $\beta_1 \sim 45^\circ$ ), when in entrance sector of back edge there is a marked diffuser section. Here the boundary layer sharply thickens in the contour of back edge, the distribution of speeds in layer deteriorates and even with moderate gradients in diffuser region in nozzle section a separation

---

\*Reactive and impulse rotating cascades with small profile losses have been developed at the Moscow Power Engineering Institute (MEI). The Central Scientific Research and Design-Engineering Boiler-Turbine Institute (TsKTI) and the Kiylov Central Scientific Institute.

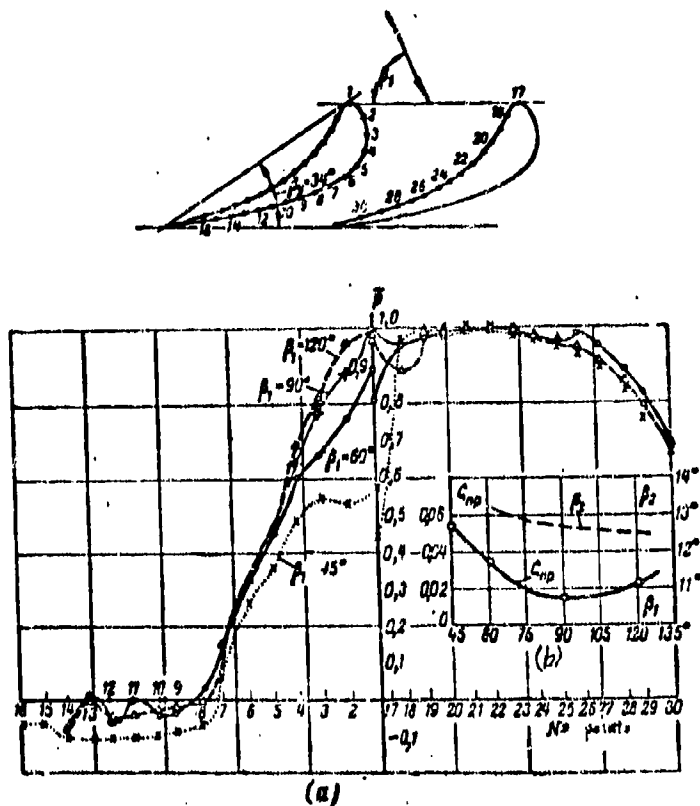


Fig. 8-25. Distribution of pressures about profile of reactive cascade (a), profile losses and flow angle at exit (b) depending upon exit angle  $\beta_1$ ;  $M_2 = 0.5$ ;  $Re = 3.46 \cdot 10^5$ .

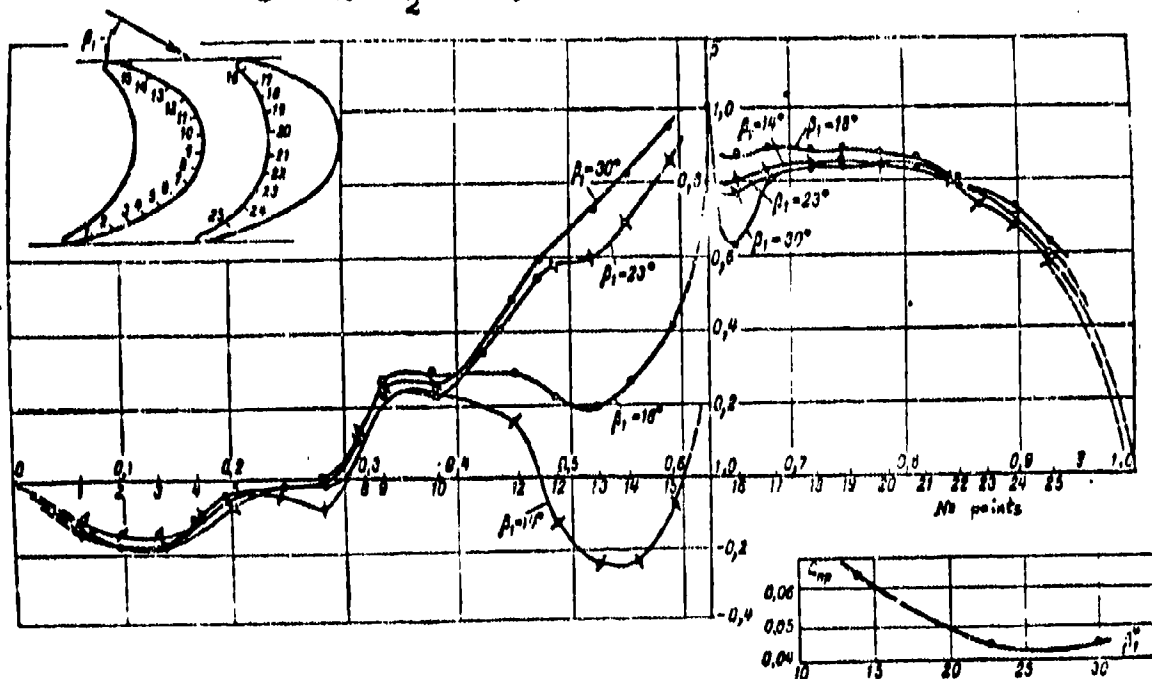


Fig. 8-26. Distribution of pressures about profile of cascade of impulse type (a); profile losses depending on  $\beta_1$  (b);  $M_2 = 0.7$ ;  $Re_2 = 4 \cdot 10^5$ .

develops; sometimes the separation may develop also on entrance section of back edge. With  $\beta_1$  larger than the design value the diffuser region is detected on concave surface. However, in connection with the fact that on descent from this surface, the flow is of nozzle type, the separation, as a rule, does not extend to the trailing edge.

An analogous, but more distinct picture is detected in cascades of active type (Fig. 8-26). Consequently, at small angles at entrance there is noted a significantly sharper increase of losses, than at large angles (see also Fig. 8-15).

A comparison between reactive and impulse cascades at different  $\beta_1$  obviously shows that cascades with a smaller geometric constriction  $\frac{a_1}{a_2}$  are more sensitive to a change in  $\beta_1$ .

At low subsonic speeds, when influence of compressibility can be ignored, the profile losses depend on the Reynolds number. Influence of  $Re_2$  is especially great with a separation of flow around the back edge of profile, when the separation occurs up to the point of transition of laminar layer into a turbulent. In this case with an increase in  $Re_2$ , the point of separation is displaced along the flow. Here losses depending upon  $Re_2$  number sharply change (Fig. 8-27).

The influence of  $Re_2$  on the profile losses must be considered at different angles at entrance  $\beta_1$  and degrees of turbulence of incident flow. The geometric constriction also exerts an influence on the character of the dependence  $\zeta_{np}(Re_2)$ .

With small degrees of turbulence and design angles at entrance there is obviously seen the significant influence of  $Re_2$  on  $\zeta_{np}$  at  $Re_1 \leq (6 \text{ to } 8) \cdot 10^5$ . With an increase in  $E_0$  (Fig. 8-27, b) region of practical self-simulation is displaced towards the smaller  $Re_2$  (Sec. 5-14). A decrease in  $Re_{self}$  is noted also during small  $\beta_1 < \beta_{1 \text{ design}}$  and for cascades with small constriction of the channels. Thus, value of the  $Re_2$  numbers determining region of self-simulating flow in cascades may vary within wide limits depending upon shape of profile, geometric parameters of the cascade the degree of turbulence and the angle of entrance.

Influence of compressibility (number  $M_2$ ) on characteristics of cascades at subcritical speeds is detected, beginning approximately from  $M_2 \approx 0.5$  (Fig. 8-28). With an increase in  $M_2$ ,  $\zeta_{np}$  decreases and attains a minimum value  $M_2 \approx 0.75$  to  $0.95$  depending upon type of cascade and shape of profile.

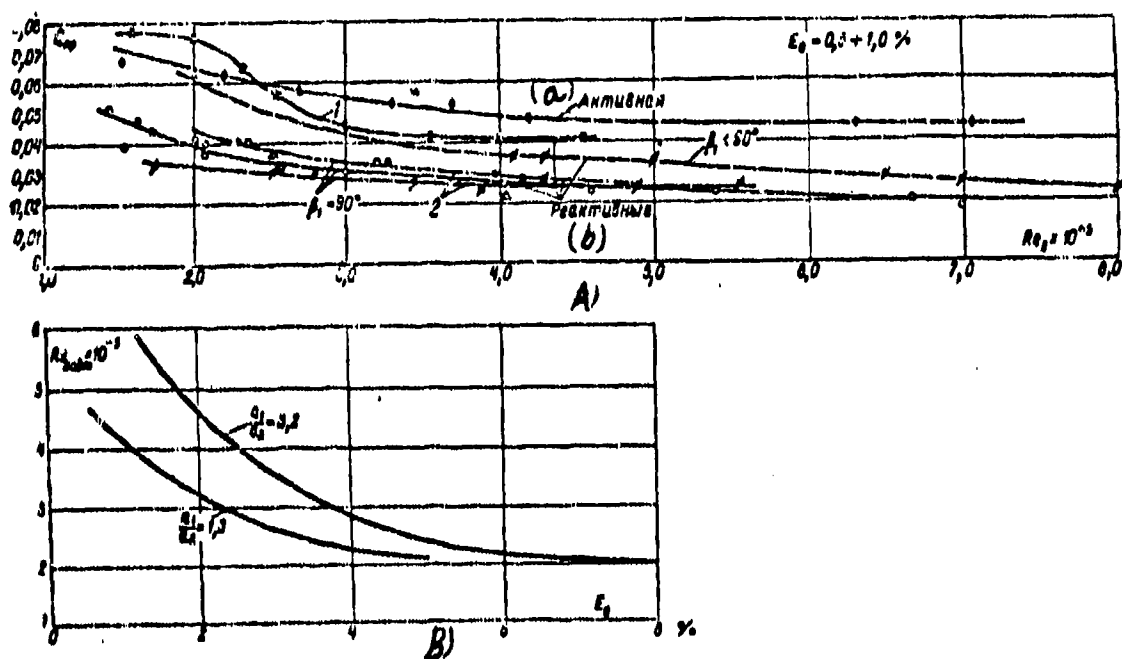


Fig. 8-27. A--influence of  $Re_2$  number on losses in cascade of reactive and impulse types, streamlined with separation (Curve 1) and with continuous flow around (Curve 2); Leningrad Metallurgical Mill experiments (profile 2339); experiments at TsKTI (profile TH-2); experiments at MEI (profile TC-2A); B--influence of degree of turbulence on number  $Re_{self}$  corresponding to beginning of auto-modelling region.  
KEY: (a) Impulse; (b) Reactive

The variation of  $\zeta_{np}$  depending upon  $M_2$  in subcritical region during continuous flow around is readily explained by the fact that gradients of pressure in a compressible fluid increase with an increment of  $M_2$  (Chapter 3).

In a nozzle flow around the profile the momentum thickness  $\delta^{**}$  decreases, and in a diffuser flow around--correspondingly increases (Sec. 8-5).

As  $M_2$  increases, the point of minimum of pressures in nozzle section is somewhat displaced along the flow and value  $\bar{p}_{min}$  diminishes. As a result the extent of the nozzle section on back edge increases. For these reasons the losses decrease.

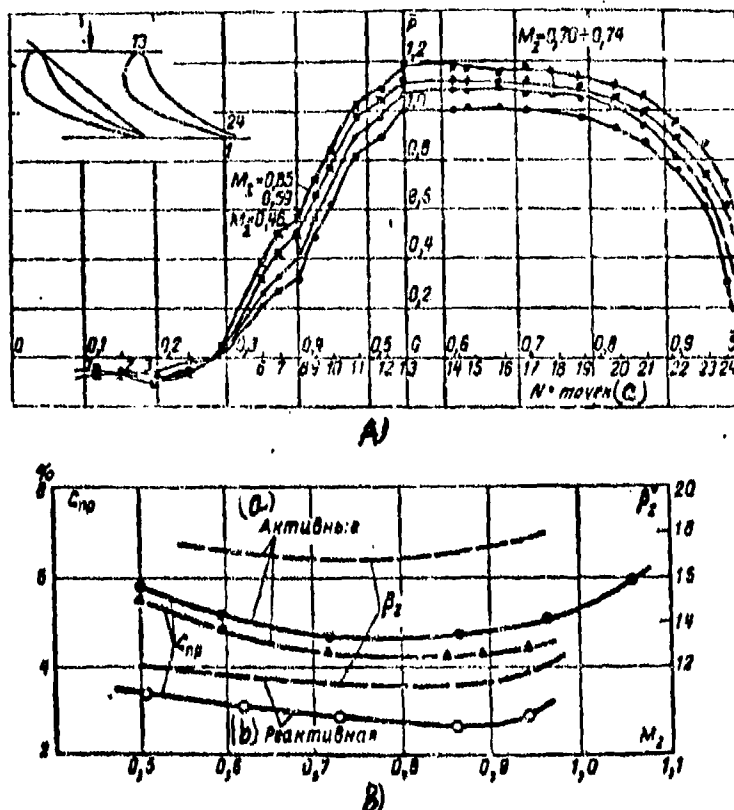


Fig. 8-28. The influence of  $M_2$  number on distribution of pressures, profile losses and flow angle at exit for cascades reactive and impulse types.  
KEY: a) Impulse; b) Reactive; c) No. of points.

Analogous results are obtained also for impulse cascades.

At high subsonic speeds (beginning with  $M_2 = M_{2*}$  and with large  $M_2$ ) in nozzle section of channel and on edges of profile there appear supersonic regions, which are terminated by shock waves. For this reason there appear additional wave losses and  $\zeta_{np}$  (profile loss) increases.

The flow angle at exit depending upon  $M_2$  varies insignificantly (Fig. 8-28,b). With an increase in  $M_2$  angle  $\beta_1$  decreases somewhat and at  $M_2 > M_{2*}$  it increases, this explained by the increase of losses in the local supersonic region.

Profile Characteristics of Cascades. Results of measurements of  $\zeta_{np}$  and  $\beta_1$  in cascades of different types show that the profile characteristics are composite functions of a large number of parameters:  $\zeta_{np} = \zeta(\beta_1, \beta_2, Re, M_1, \bar{\Delta}, \text{shape of profile})$  and can be established only experimentally.

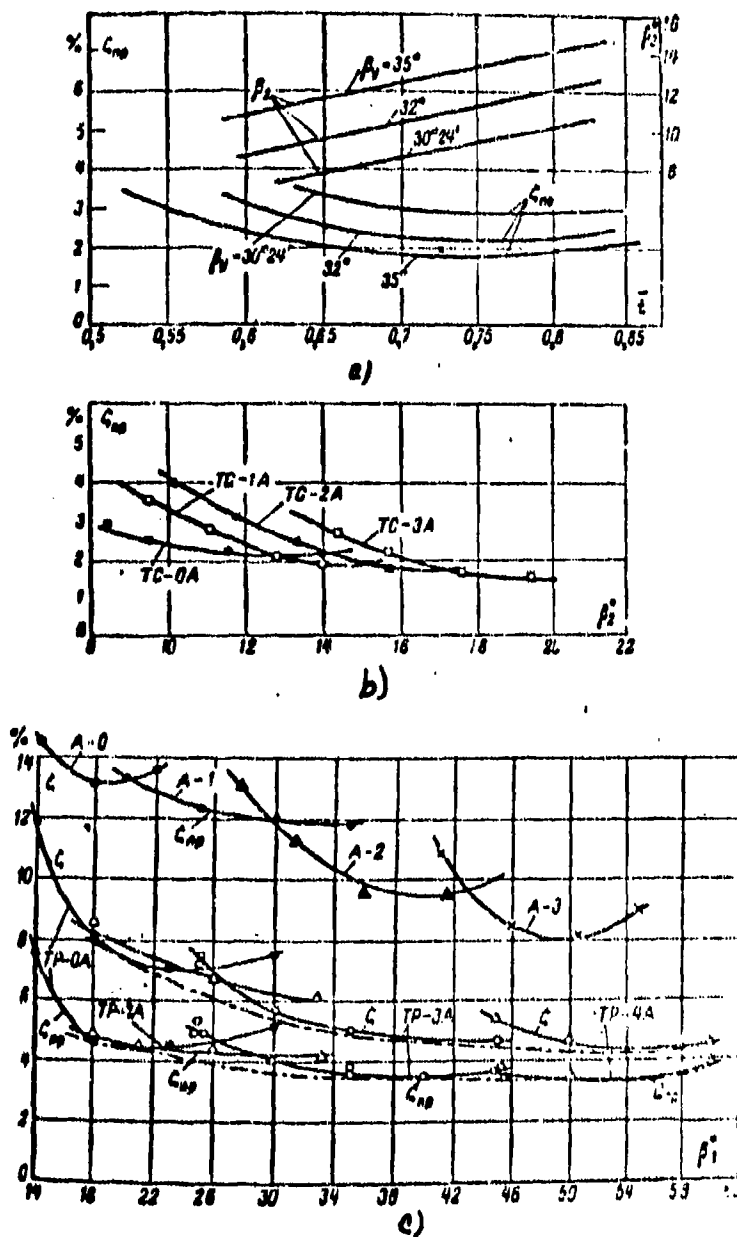


Fig. 8-29. Profile characteristics of reactive (a and b) and impulse cascades (A-0, A-1, A-2 and A-3--cascade of old type).

Examples of constructing such characteristics for Moscow Power-Engineering Institute (MEI) cascades of reactive and impulse types may be seen from Fig. 8-29. As is evident in Fig. 8-29, b, the profile losses in reactive cascades at  $\beta_1 = 90^\circ$  slightly depend on angle  $\beta_2$  in the interval  $\beta_2 = 12$  to  $18^\circ$ .

Profile losses in impulse cascades are small (3.0 to 7%) and for each cascade within a wide range of  $\beta$ , very insignificantly (Fig. 8-29,c). The curves  $\zeta_{np} = f(\beta)$  for this group of cascades have a sloping envelope. In Fig. 8-29, also curves of losses in cascades of old type, formed by arcs of circles and segments of straight lines, are presented. It is readily seen that modern cascades, developed by aerodynamic methods, have by far the best characteristics. This result is corroborated also by graphs of distribution of pressures for comparable shapes of profiles at identical flow angle at entrance.

#### 8-8. Three-Dimensional Flow of Gas in Cascades. End Losses and Methods of Decreasing Them

In intervane channels of cascade of finite height, as in a single curvilinear channel\*, secondary flows develop: under the influence of transverse pressure gradient there occurs an overflowing of gas along flat (or cylindrical) walls\*\* from the concave surface to the back edge (Fig. 8-30).

On the back edge, at a certain distance from tips of blades, boundary layer, streaming from the flat walls, merges with the main boundary layer, moving along trajectories, parallel to the flat walls; as a result here there occurs an intense bulging of boundary layer and there develop components of the speed, directed to the core of flow. In the core at tips of blade there develops a flow, directed from back edge to concave surface, forming, together with peripheral flow along end walls, vortex regions. Thus, along back edge of profile at tips of blade there develop a paired vortex, consisting of two eddy regions. The vortices have opposite senses of rotation.

In a photograph of wakes of flow (Fig. 8-31) clearly evident is the overflow of boundary layer on flat walls and on back edge. Since after region of generation of

---

\*An analysis of secondary flows in curvilinear channels is given in Sec. 5-15.

\*\*Henceforth secondary flows only in a belted cascade are considered.

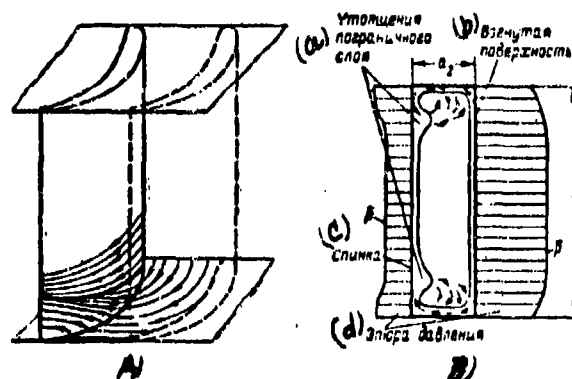


Fig. 8-30. Scheme of the formation of secondary flows in intervane channel of cascade.

A—lines of flow on flat wall and on back edge, B—peripheral flow in boundary layer at tips of blade.

KEY: (a) Bulges of boundary layer; (b) Concave surface; (c) Back edge; (d) Pressure curve.

vortices the inflow of gas continues from the end walls, then the vortex motion increases towards exit section of channel; region of swelling of boundary layer, and also the core of the paired vortex are displaced to the middle section. At low heights eddy regions extend over the entire section of channel, forming a paired vortex, characteristic for curvilinear channels of a square section (Sec. 5-15).



Fig. 8-31. Traces of peripheral over-flow in an intervane channel.



The distribution, presented in Fig. 8-32, of losses and exit angles according to height of cascade shows the characteristic change of these magnitudes for vortex regions. With distance from the end walls, the losses at first decrease (Fig. 8-32,a), then sharply increase and then again decrease towards middle section (losses in middle section with sufficient height of cascade are equal to the profile losses). Maximum losses correspond to region of building of boundary layer on back edge. The minimum value of  $\zeta$  along flat walls may be larger or smaller than  $\zeta_{np}$  depending on intensity of the secondary flows; for a reactive cascade the minimum of losses, as a rule, is not detected (Fig. 8-32,b). In the zone of secondary flows in

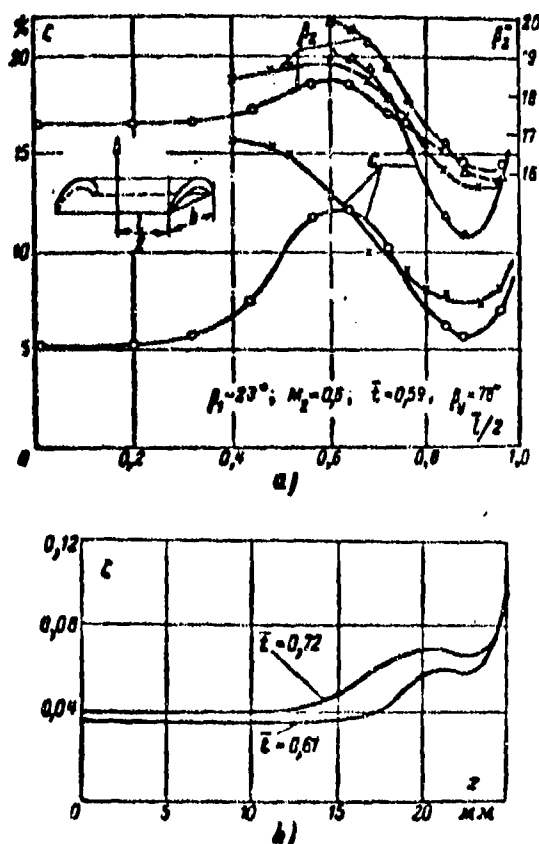


Fig. 8-32. Influence of secondary overflows on distribution of losses and flow angles at exit according to height of impulse (a) and reactive (b) cascades at different heights.

accordance with the change of  $\zeta$ ; the exit angles at first increase and then towards middle section decrease.

End losses are defined as the difference between total and the profile losses. An evaluation of influence of height, pitch, setting angle, shape of profile and channel, and also angle of entrance,  $Re_2$  and  $M_2$  numbers can be made on the basis of experimental data.

Experiments show that, as in case of single curvilinear channel, any changes of geometric and mode parameters causing an increase of transverse gradients of pressure in a cascade, the bulging of boundary layer and the manifestation of diffuser sections at exit results in an increase of tip losses.

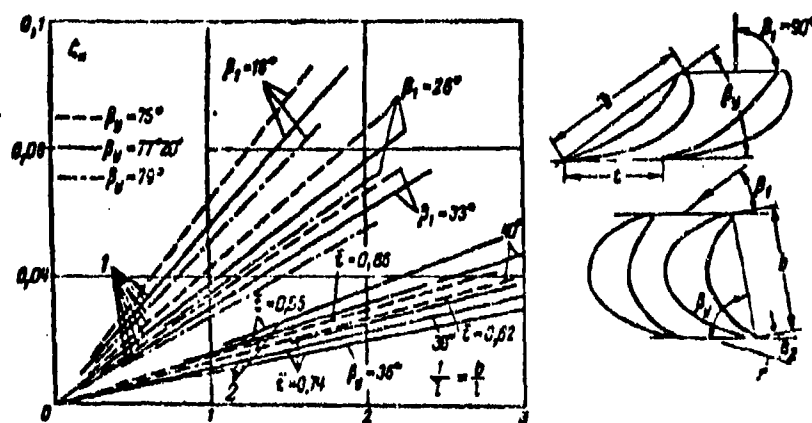


Fig. 8-33. Variation of end losses depending upon height, flow angles at entrance, setting angles and pitch in impulse (Curve 1) and reactive (Curves 2) cascades.

With a decrease in height of cascade down to known limits the two-dimensional section of flow in middle sections of channel contracts; the region of increased losses in the zone of vortices practically remains constant. Consequently, coefficients of end losses linearly vary depending on  $\frac{1}{l} = \frac{b}{l}$ . With a certain minimum height there occurs closing of secondary flows; the region of greater losses occupies all the middle section of the channel (Fig. 8-32a).

Character of dependence of end losses on  $\bar{l}$  greatly varies for cascades of different types. The slope of the lines  $\zeta_A = f\left(\frac{1}{l}\right)$  decreases with decrease of angle of deflection of flow in cascade  $\Delta\beta = 180 - (\beta_1 + \beta_2)$  (Fig. 8-33). The minimum values of  $\zeta_A$  correspond to reactive cascades, which are characterized by a

great constriction of the channels and small angle of the flow's deflection.

With an increase in pitch of reactive cascade, the end losses at first decrease, because the constriction of the flow increases; they attain a minimum, and then increase in connection with the increment in transverse pressure gradient. An increase in the setting angle of profile with an optimal pitch results in a lowering of end losses, because the angle of deflection of flow and transverse gradient of pressures decrease, and with small pitch with an increase of  $\beta_1$ , the end losses increase. The influence of the pitch is especially great for impulse cascades, where minimal end losses correspond to a pitch, with which the intervane channels at first expand (at entrance), and then contract.

The great influence of flow angle at entrance  $\beta_1$  on  $\zeta_k$  (Fig. 8-33) is explained by the change of transverse pressure gradients in channel, the occurrence of diffuser sectors at entrance and in nozzle section and in certain cases by formation of a separation. End losses markedly increase with a decrease of  $\beta_1$  (increase of  $\Delta\beta$ ). With a constant value of  $\beta_1$ ,  $\zeta_k$  increases with a decrease in exit angle  $\beta_2$  (at small  $\beta_2 < 11$  to  $12^\circ$ ), because here the curvature of the channel (Fig. 8-33) increases.

The variation of end losses depending upon the Reynolds number can be evaluated by curves in Fig. 8-34. With an increase of  $Re_2$  the end losses decrease. The influence of the  $Re_2$  number on  $\zeta_k$  is great if  $Re_2 < 5 \cdot 10^5$ . This is explained by the fact that with an increase of  $Re_2$  the boundary layer becomes thinner.

Influence of compressibility at subcritical speeds is reflected in the decrease of end losses with an increase of  $M_2$  number (Fig. 8-34) in connection with the fact that transverse pressure gradients in the channel decrease (Sec. 5-15) (See also Fig. 8-69).

The structure of a three-dimensional flow in circular (cylindrical) stationary cascades possesses certain peculiarities. Most important we assume, is the presence of a radial gradient of pressure; pressure along the periphery is higher than along the root section.\* As a consequence radial overflows develops along the blades

\*See Secs. 9-3 and 9-4.

directed from the periphery to root section. These radial overflows are superposed onto the transverse overflows (Fig. 8-35). In addition in a circular (cylindrical) cascade the shape of the channel varies according to the height (owing to the change in pitch and cylindricity of end walls) and therefore the intensity of peripheral

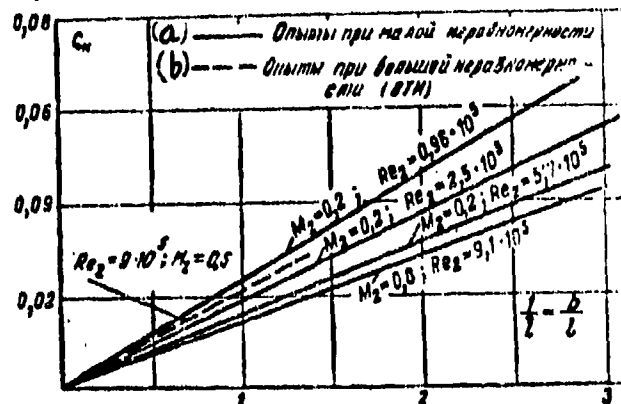


Fig. 8-34. Influence of  $Re_2$  and  $M_2$  numbers on end losses in cascade.

KEY: (a) Experiments with little nonuniformity; (b) Experiments with great nonuniformity (VTI).

overflows for end walls is different. As a rule, energy losses near the root section, where radial overflows coincide with transverse, in a circular cascade are higher than on the periphery. The marked influence of fan-like behavior depends on parameter  $d/l$ , with the decrease of which the difference in speeds and pressures in root and peripheral sections increases.

Of great practical interest is the development of methods of decreasing end losses. A lowering of  $\zeta_n$  may be assured by increasing the relative height of blade, which with a given absolute height is attained by decreasing the chord (width) of profile. However, in connection with the fact that with a change in the chord not only the tip, but also, the profile losses vary, there arises a problem of establishment of an optimal chord of a cascade.

A decrease in the end losses may be attained also by a corresponding selection of geometric parameters of cascade and shape of profile (of intervane channel).

Results of investigation of flow in curvilinear channels show that minimum intensity of secondary flows in channels of impulse type is ascertained in those

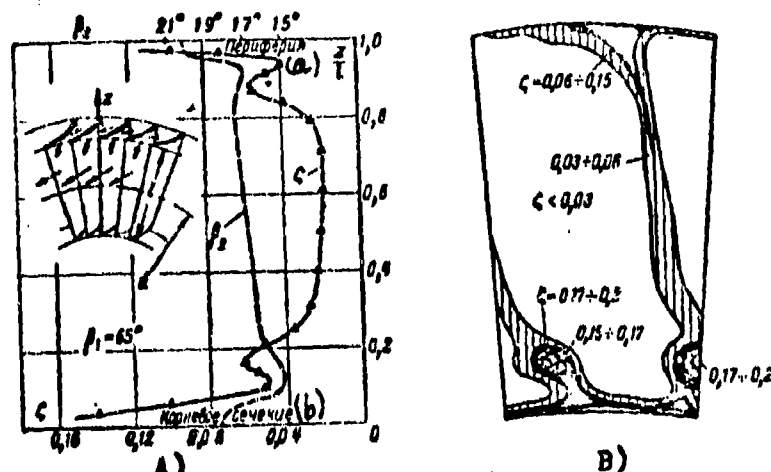


Fig. 8-35. Structure of secondary flows in a circular (cylindrical) cascade.  
Key: (a) Periphery; (b) Root section.

cases, when entry portion of channel is made as a diffuser. Analogous data have been obtained also for cascades of impulse type.\*

In Fig. 8-36 results of investigation of two cascades having identical relative height,  $\bar{l}$  and  $\beta_{y_1}$ , and also shape of back edge, are presented. The concave surfaces of profiles being compared differ in radius of curvature: the TP-1A cascade has a smoothly contracting and the TP-1A cascade, diffuser-nozzle channels. The distribution of losses by height for different modes shows that in the TP-1A cascade, the level of losses is much lower. Total losses in the cascades being compared, depending on the angle of entrance  $\beta_1$  and  $M_2$  number, vary analogously (Figs. 8-36, a and 8-36, b). Especially important are the advantages of TP-1A cascade with low speeds and small angles of entrance.

Efficiency of diffuser nozzle cascades and the optimal geometric ratios  $\frac{a_m}{a_1}$ ,  $\frac{a_1}{a_2}$  and others) depends on angle of deflection of flow in cascade and the relative height  $\bar{l}$  (Fig. 8-37). With an increase in angle of deflection of flow and a decrease in relative height of cascade the optimal ratio  $\frac{a_m}{a_1}$  at first increases, and later decreases. Results of experiments show that cascades with diffuser-nozzle channels

\*Diffuser-nozzle channels of impulse cascades for the first time were proposed by AIL-Union "Order of the Red Banner of Labor" Scientific. Research Institute of Heat Engineering im. F. E. Dzerzhinskiy (VTI).

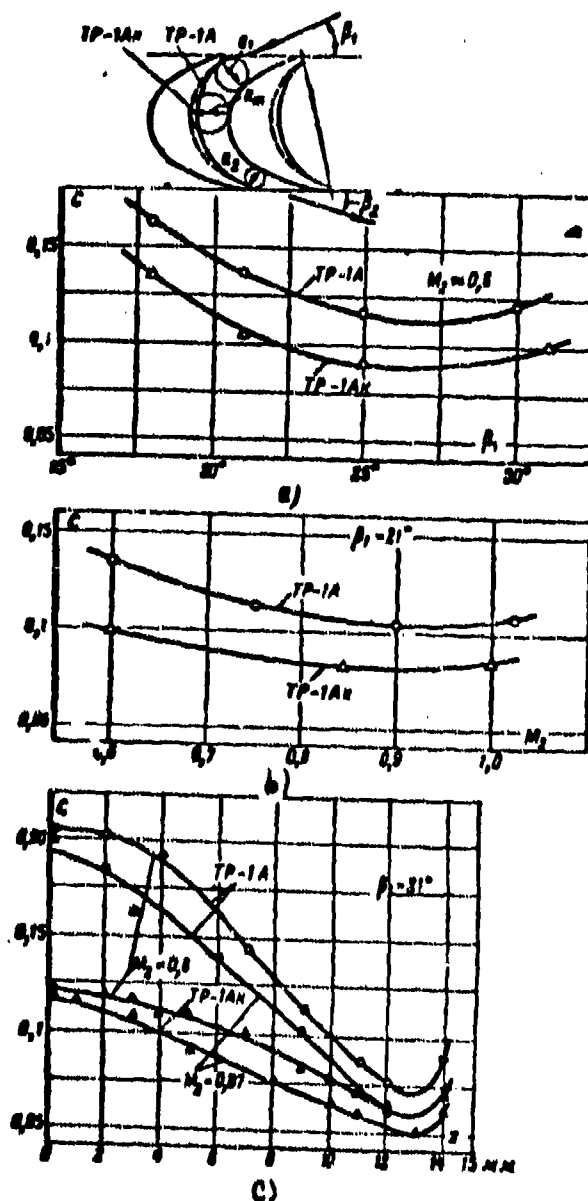


Fig. 8-36. Influence of shape of channel on losses in impulse cascade.  
a--variation of  $\zeta$  depending upon  $\beta_1$  for two types of cascades; b--influence of  $M_2$  number on losses in cascades of two types; c--distribution of losses according to height of cascade.

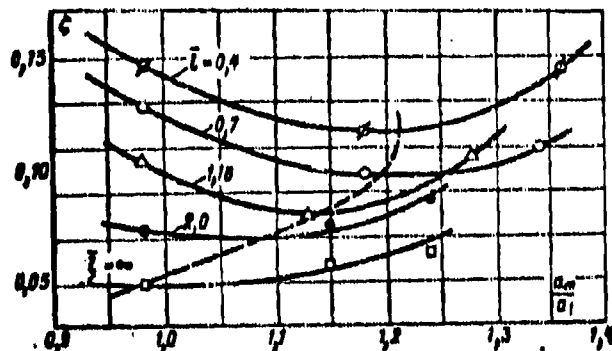
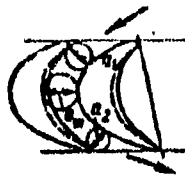
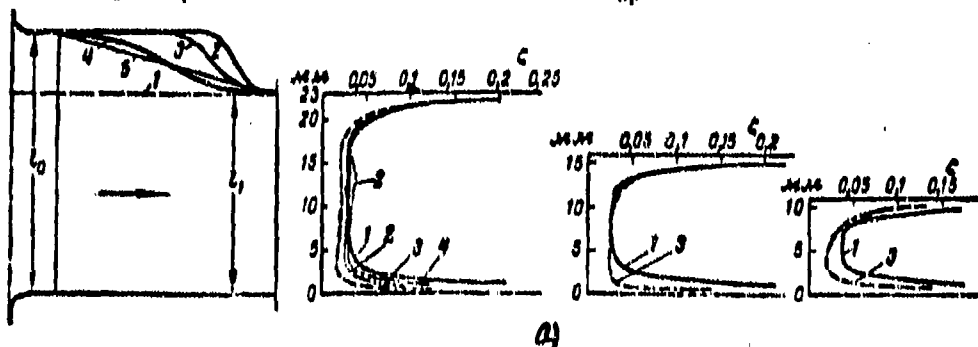


Fig. 8-37. Optimal values of  $\bar{a}_m$  depending upon relative height  $l$ .

are expedient to use at  $l_{up} < 1.2$  to  $1.8$  depending upon angle of deflection of flow; at large  $\Delta\beta$  we see the limiting value  $\bar{l}_{up}$  increases.



a)

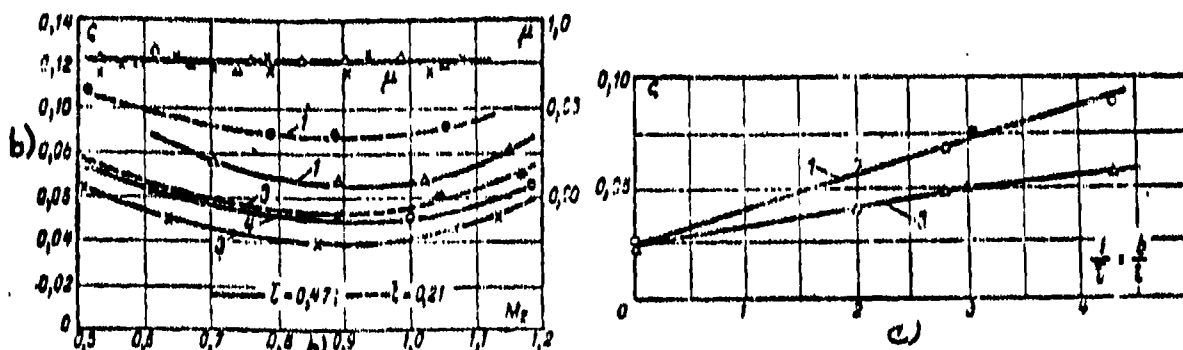


Fig. 8-38. Influence of meridional cascades on losses in guide cascades. a--forms of upper band of investigated and distribution of losses by height for different forms of the upper contours and heights; b--influence of  $M_2$  number on loss in cascades with a different shape of upper contour; c--influence of relative height on losses in cascades with two variants of band. Figures on curves indicate the variant of contour. Profile TC-2A;  $M_2=0.87$ ;  $\mu=0.724$ ;  $\alpha_y=34^\circ$ .

In reactive (nozzle) cascades an appreciable decrease of end losses can be attained by profiling the channels by height (profiling in the meridional plane). This method is especially important for circular (cylindrical) cascades in whose root section usually there are detected higher losses.

In Fig. 8-38,a there are shown schematic diagrams of variants of guide cascades with different shapes of upper band, and in Fig. 8-38,b and c--corresponding results of tests of a rectilinear cascade under static conditions. Here there is presented the curve of losses in a circular (cylindrical) cascade with cylindrical bands of the same height.

Experiments show significant decrease of losses in cascade with profiled upper band. Essential also is the redistribution of losses by height of cascade: for the lower band the losses sharply decrease.

The profiling of upper band makes it possible also to decrease difference between reactions in root and peripheral sections, that is, to increase the efficiency of the turbine stage.

Curves in Fig. 8-39 make it possible to explain advantage of cascades with a profiled band: in such cascades there is assured a greater nozzle flow on back edge in nozzle section and the point of minimum pressure is displaced towards trailing edge; besides, speed of flow before main deflection of flow in channel decreases and results in a lowering of transverse gradient in the sector of maximum curvature and, consequently, of the intensity of secondary flows. By being given a rational distribution of pressure along the channel, there may be found optimal shape of band.

The losses presented in Fig. 8-38,c depending on  $\bar{l}$  show that described method of profiling is especially effective at small relative heights.

It must be noted that an asymmetric compression of the upper contour of cascade expands range of optimum pitches and setting angles.

The optimum magnitude of the compression, determined by the ratio  $\frac{l_2 - l_1}{l_1}$ ,



varies depending upon height of cascade (Fig. 8-39,b).

It is necessary to emphasize, that the indicated methods of diminishing tip losses in impulse (diffuser-nozzle channels) and reactive (asymmetric compression) cascades are physically identical. In both cases there are attained a decrease in speeds at turn of flow in channel and greater constriction at exit of cascade.

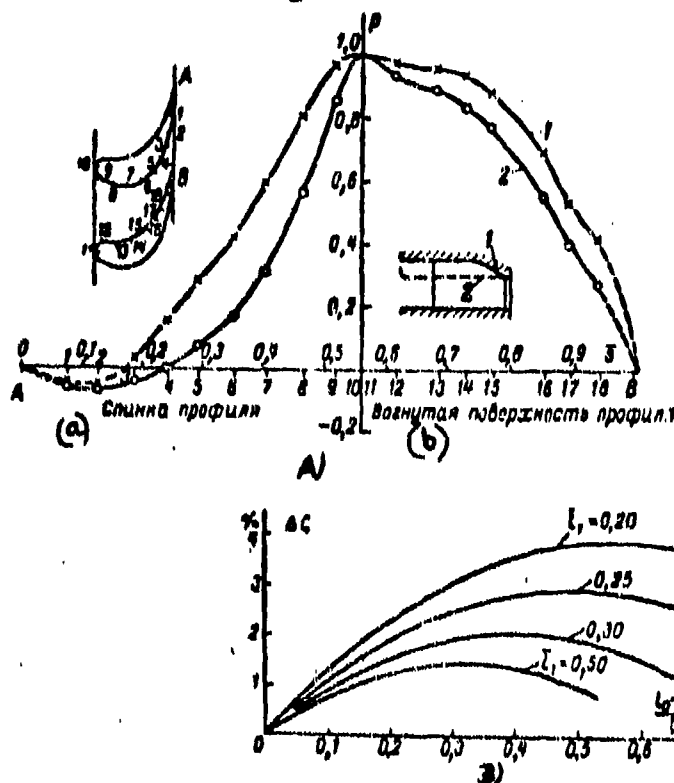


Fig. 8-39. A--the influence of a meridional profiling of cascades on distribution of pressures about the profile; B--decrease of losses depending upon  $I$ , and on the degree of compression  $l_0 - l_1 / l_1$ . KEY: a) Back edge of profile; b) Concave surface of profile.

Conditions at entrance into cascade and, in particular, the irregularity of field of speeds by height and the high turbulence of the flow exerts a great influence on the end losses. The increase in irregularity according to the data VTI cause an increase in the end losses (Fig. 8-34). An increase in the initial turbulence results in a decrease of the slope angle of the straight lines  $\zeta_{\text{th}} = 1 \left( \frac{1}{I} \right)$ , but total losses in a reactive cascade increase. Physically this result is explained by the fact that with an increase in the irregularity and turbulence the thickness of

boundary layer on the end walls and the mass of gas participating in peripheral motion increase.

### 8-9. Procedure for Calculating End Losses in Cascades

The strict solution of problem on end losses in cascades should be based on equation of three-dimensional motion of a viscous compressible fluid. In connection with evident difficulties of such a solution it is possible to use another method: on the basis of theory of dimensionality construct, proceeding from considerations about physical nature of secondary flows, a structural formula and introduce experimental correctives [ L.5].

In the general case the end losses of energy can be presented as the sum:

$$\Delta E_e = \Delta E_1 + \Delta E_2 + \Delta E_3,$$

where  $\Delta E_1$  is that part of end losses, caused by the interaction of the boundary layers and by the peripheral motion;

$\Delta E_2$  represents frictional losses along end walls of channel;

$\Delta E_3$  additional vortex losses, including losses from compensating motions at the tips.

It is readily seen that the vortex losses  $\Delta E_2$  and  $\Delta E_3$  depend on circulation of speed  $\Gamma$ , and  $\Delta E_1$  does not depend on  $\Gamma$ .

An analysis of experimental data shows that magnitude of  $\Delta E_e$  may be expressed by the following functional dependence:

$$\Delta E_e = f(\Gamma, \rho, c_{a2}, b, T_1, \nu_1, \beta_1) \quad (8-38)$$

We now write out (8-38) in dimensionless form:

$$\frac{\Delta E_e}{\rho \Gamma^2 c_{a2}^2 b^3} = f_1 \left( \frac{\Gamma}{c_{a2} b}, \sin \beta_1, Re_1, M_1 \right). \quad (8-39)$$

By expanding expression (8-39) into a series in parameters of  $\bar{\Gamma} = \frac{\Gamma}{c_{a2} b}$  and  $\sin \beta_1$ , there can be obtained the function (8-39) in explicit form. By considering that function (8-39) is even with respect to arguments of  $\bar{\Gamma}$  and  $\sin \beta_1$  and at

$\bar{\Gamma} = 0$  is independent of  $\beta_1$ , we obtain:

$$\frac{\Delta E_k}{\rho_0 c_{a2}^3 \delta^3} = \psi_0 (Re, M_2) \left( 1 + \frac{\psi_1}{\psi_0} \bar{\Gamma}^2 \sin^2 \beta_2 \right). \quad (8-40)$$

If it is assumed that the coefficients  $\psi_1$  and  $\psi_0$  with a change of  $M$  and  $Re$  numbers vary proportionally, i.e.,  $\psi_1 / \psi_0 = B$ , where  $B$  is a certain experimental constant, then there is readily obtained an expression for the coefficient  $\psi_0$ .

With a zero circulation ( $\bar{\Gamma} = 0$ )

$$\frac{\Delta E_k}{\rho_0 c_{a2}^3 \delta^3} = \psi_0.$$

The magnitude  $\Delta E_k$  may be expressed by the energy thickness  $\delta^{***}$  according to the equation

$$\Delta E_k = \rho_0 c_{a2}^3 \delta^{***} l \sin \beta_2 = \frac{\rho_0 c_{a2}^3 \delta^{***} l}{\sin^2 \beta_2};$$

then

$$\psi_0 = \frac{\delta^{***} l}{\delta^3 \sin^2 \beta_2} = \frac{\bar{\delta}^{***} l}{\sin^2 \beta_2}. \quad (8-41)$$

For determining the coefficient of the end losses  $\xi_k$  we shall determine the kinetic energy of flow after a cascade:

$$E = \frac{G v^2}{2g}.$$

Here  $G = \rho_0 c_{a2} F$  is the actual flow rate through channel of cascade;  $F$  is the effective area of channel, which is readily determined, if one were to use the displacement thickness:

$$F = l - 2\delta_{top}^* - \delta_{cn}^* - \delta_{nor}^*,$$

where  $\delta_{top}^*$ ,  $\delta_{cn}^*$ ,  $\delta_{nor}^*$  are the thicknesses of displacement on end wall, on back edge and on concave surface of profile.

$$\begin{aligned} \text{Consequently,} \quad E &= \frac{\rho_0 c_{a2}^3 l}{2 \sin^2 \beta_2} \left[ l - 2\delta_{top}^* - \frac{l}{l} (\delta_{cn}^* + \delta_{nor}^*) \right] = \\ &= \frac{\rho_0 c_{a2}^3 l}{2 \sin^2 \beta_2} \left[ l - 2\delta_{top}^* - \frac{l}{l} \delta_{na}^* \right], \end{aligned} \quad (8-42)$$

where  $\delta_{cn}^* + \delta_{nor}^* = \delta_{na}^*$ .

The magnitude of  $\bar{\Gamma} \sin \beta_1$  we present as:

$$\begin{aligned} \bar{\Gamma} \sin \beta_1 &= \frac{l(c_{n1} + c_{n2})}{c_{a2} b} \sin \beta_2 = \bar{\Gamma} \left( \frac{c_{a1}}{c_{a2}} \cot \beta_1 + \cot \beta_2 \right) \sin \beta_2 = \\ &= \left( 1 + \frac{c_{a1}}{c_{a2}} \frac{\cot \beta_1}{\cot \beta_2} \right) \bar{\Gamma} \cos \beta_1 = \left[ 1 + \varphi(\lambda) \frac{\cot \beta_1}{\cot \beta_2} \right] \bar{\Gamma} \cos \beta_1. \end{aligned} \quad (8-43)$$

where

$$\gamma(\lambda) = \frac{c_{a1}}{c_{a2}} = \frac{p_1}{p_2} \quad (8-44)$$

For incompressible fluid during a turbulent condition of flow in boundary layer on a fairly adequate basis it may be assumed:

$$\delta_{\text{top}}^{**} = \delta_{\text{en}}^{**} = \delta_{\text{cor}}^{**} = \delta^{**}; H = \frac{\delta^{**}}{\delta^{*}} = 1.4;$$

$$H^{**} = \frac{\delta^{***}}{\delta^{**}} = 1.8; \delta^{**} = \frac{0.036}{\text{Re}_2^{1/2}}.$$

By means of formulas, (8-40) to (8-43) and by ignoring the magnitude  $0.1^2$  ( $\frac{T}{T} - 1$ ) in comparison with the term  $\text{Re}_2^{0.2} \bar{1}$ , we obtain for an incompressible fluid:

$$\zeta_{\text{en}} = \frac{0.13}{\text{Re}_2^{0.2} T} \left[ 1 + B \left( 1 + \frac{\text{cor } p_1}{\text{cor } p_2} \right)^2 \cos^2 \beta_1 \right]. \quad (8-45)$$

In a general case for a compressible fluid the coefficient of end losses is determined by the formula

$$\zeta_{\text{en}} = \frac{Ak_1}{\text{Re}_2^{0.2} T} \left\{ 1 + B \left[ 1 + \gamma(\lambda) \frac{\text{cor } p_1}{\text{cor } p_2} \right]^2 \cos^2 \beta_1 \right\}. \quad (8-46)$$

Here  $k_1$  is a correction factor, which takes into consideration influence of compressibility. Its dependence on dimensionless speed  $M_2$  is presented in Fig. 8-40.

For determining the numerical values of coefficients of A and B in Fig. 8-41 there have been plotted experimental data on the end losses, obtained both for impulse, and also for reactive cascades with different pitches, heights, flow entrance and exit angles.

Here, as the argument, there has been adopted the complex

$$\left[ 1 + \gamma(\lambda) \frac{\text{cor } p_1}{\text{cor } p_2} \right]^2 T \cos^2 \beta_1$$

and along axis of ordinates is plotted the function  $\frac{\zeta_{\text{en}} \text{Re}_2^{0.2} T}{k_1}$ . In the adopted system of coordinates formula (8-46) is expressed by a straight line, cutting off along axis of ordinates a sector, equal to A, sloping to axis of abscissas at an angle  $\delta = \arctan AB$ .

Results of the indicated processing\* of the experimental data make it possible

\*The procedure discussed was worked out in collaboration with A. Ye. Zaryankin.

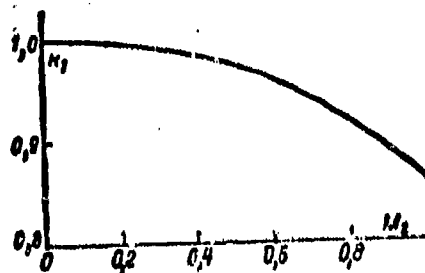


Fig. 8-40. Dependence of correction factor  $k_1$  on dimensionless speed.

to conclude that the coefficients A and B depend considerably on the mode of flow in boundary layer and type of cascade. For reactive cascade with flat end walls

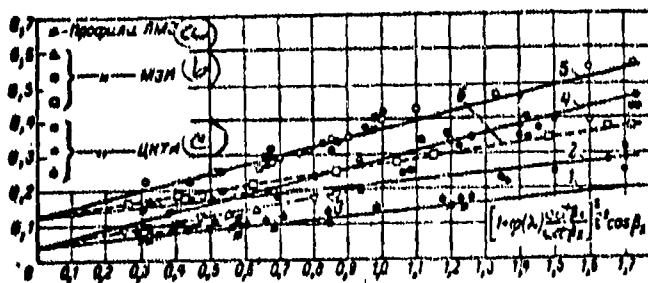


Fig. 8-41. Comparison of design and experimental values of end losses for reactive (rectilinear 1, 2 and 3) and impulse (rectilinear 4, 5 and 6) cascades.  
KEY: (a) LMZ-Leningrad Metallurgical Mill Profiles.  
(b) M E I-Moscow Power-Engineering Institute Profiles.  
(c) TBTI-Central Boiler-Turbine Institute Profiles.

the experimental points are fairly well grouped depending upon mode of flow in boundary layer near the straight lines 1 and 2. For reactive cascades with asymmetric compression the slope of the line varies (straight line 3).

Straight lines 4 and 5 characterize impulse cascades with smoothly contracting channels and straight line 6-with diffuser-nozzle channels.

Values of the coefficients, obtained on the basis of processing of experimental data, are presented in Table 8-1.

It is interesting to note that for impulse and reactive cascades, if there is a diffuser sector at the entrance into cascade, coefficient  $A = 0.13$ ; this corresponds to turbulent mode of flow in the boundary layer. In the transition from or

mode of flow to another there occurs parallel displacement of the straight line, corresponding to a given type of cascade. The influence of the shape of intervane channels is characterized by a coefficient, whose value varies very differently for various types of cascades.

Formula (8-46) makes it possible to establish the influence of certain geometric and mode parameters on the end losses. The coefficient  $\zeta$  varies inversely proportional to the relative height  $\bar{l}$ . With an increase in pitch  $\bar{T}$ , the coefficient  $\zeta$  at first decreases, and then increases. A decrease in angle at exit  $\beta_1$  and increase in angle of turn of flow in cascade reduces an increase in  $\zeta$ . With an increase in the  $Re_2$  and  $M_2$  numbers the end losses diminish. These results agree very well with the experimental data\*, presented in Sec. 8-8.

Table 8-1.

(a) Активные решетки без диффузорного участка на входе				(b) Реактивные решетки без поджатия по высоте			
(c) Ламинарный пограничный слой		(d) Турбулентный пограничный слой		(e) Ламинарный пограничный слой		(f) Турбулентный пограничный слой	
A	B	A	B	A	B	A	B
0,45	5,5	0,13	1,90	0,45	2,0	0,13	0,7
(g) Активные решетки с диффузорно конфузорными каналами				(h) Реактивные решетки с несимметричным поджатием в каждом срезе			
—	—	0,13	1,0	—	—	0,13	0,3

KEY: a) Impulse cascade without diffuser section at entrance; b) Reactive cascade without contraction by height; c) Laminar boundary layer; d) Turbulent boundary layer; e) Laminar boundary layer; f) Turbulent boundary layer; g) Impulse cascade with diffuser nozzle channels; h) Reactive cascades with asymmetric contractions in nozzle section.

\*Formula (8-46) does not take into consideration the influence of the non-uniformity and high turbulence of the flow. Appropriate correctives can be introduced after the accumulation of the necessary experimental data.

# 8-10. Structure of Flow and Losses in Reactive Cascades at Transonic and Supersonic Speeds

In reactive cascades speeds at the entrance are subsonic; transition to supersonic speeds occurs in the intervane channels. Depending on the position of minimum (transitional) section in channel reactive cascades are divided into two types: with contracting and expanding intervane channels.

a) Cascades with contracting channels. In such cascades the transition to supersonic speeds occurs in the nozzle section.

In many cases, the transition to the transonic region is accompanied by significant change in the characteristics of the cascades. In this connection it is necessary to know critical  $M_2$  number, with which in cascade there appear local regions of supersonic speeds.

In Fig. 8-42, a there are given curves of maximum speeds on back edge of profile of guide cascade depending upon  $M_2$  and relative pitch. Beyond the line  $M_1=1$  there will form enclosed regions of supersonic speeds. Local supersonic speeds may also generate in region of flow, adjoining trailing edge.

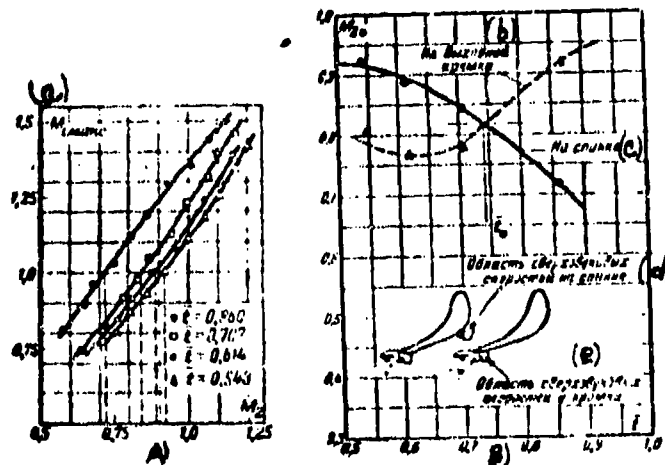


Fig. 8-42. Local maximum speeds on back edge of profile depending upon  $M_2$  (A); critical values  $M_{2*}$  depending upon the pitch for  $\lambda$  reactive cascade (B).  
 KEY: (a)  $M_{1\max}$ ; (b) on trailing edge; (c) on back edge; (d) region of supersonic speeds on back edge; (e) region of supersonic speeds along edge.

The critical  $M_2$  numbers depending upon the pitch for reactive cascades are presented in Fig. 8-42,b. It follows from this that for cascades there exists a pitch  $\bar{t}_*$  at which, sonic speeds are attained simultaneously for the back edge and in region of edge. This pitch corresponds to the maximum value of the  $M_{2*}$  number.

$M_{2*}$  values for a grid, the character of the change of  $M_{2*} = f(\bar{t}, \beta)$ , and also the location and extent of supersonic region depend on the shape of profile (curvature of exit sector of back edge, thickness and shape of trailing edge). With an increase of  $M_2 > M_{2*}$  the supersonic region increases and its boundary is displaced inside the channel.

With a  $M_2 \approx 1$  number the line of transition approximately coincides with narrow section of channel\* and the supersonic region on back edge of profile is connected with region of supersonic speeds after the trailing edge.

The most characteristic peculiarity of flow around of cascades by a flow of

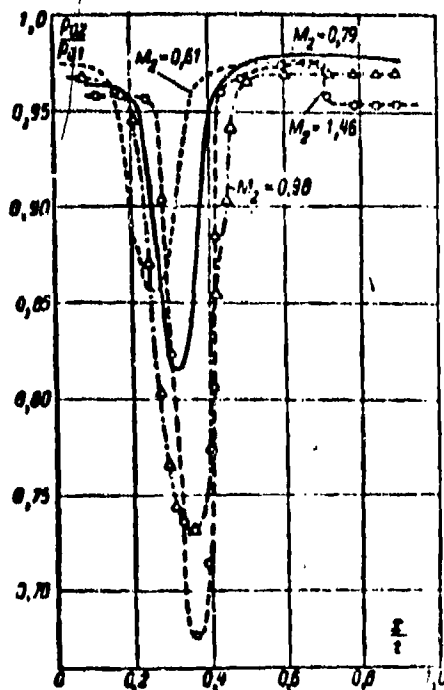


Fig. 8-43. Distribution of stagnation pressures according to pitch in reactive cascade at different  $M_2$ .

\*With a greater curvature of back edge this line is displaced in the channel.



transonic speeds is the increment of pressure gradients in the nozzle and diffuser regions and the displacement of points  $\bar{p}_{min}$  along the flow.

In Fig. 8-43 the presented graphs of the distribution of stagnation pressures according to the pitch of guide cascades, makes it possible to conclude that with an increase in  $M_2$  the nonuniformity of the flow increases: the depth of the edge wakes increases in the transition to transonic speeds, the edge wake expands.

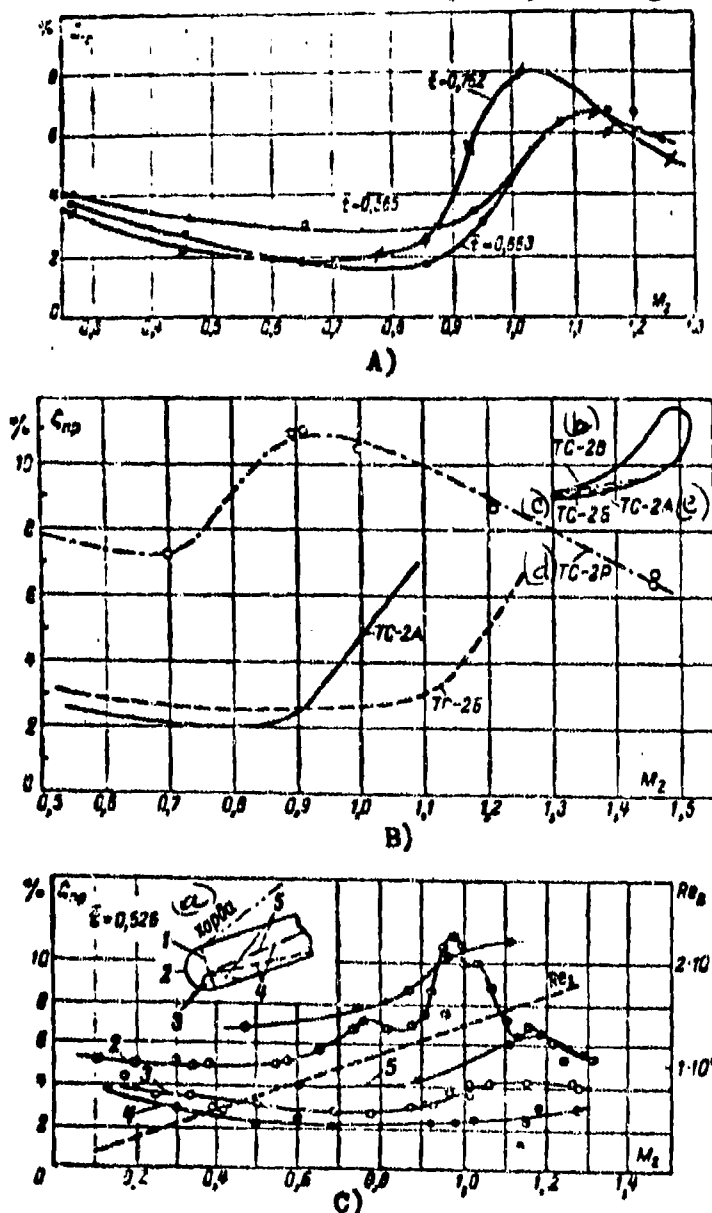


Fig. 8-44. Influence of  $M_2$  number on profile losses in a reactive cascade.

A--with a change of relative pitch  $\bar{t}$ ; B--with a change in shape of back edge of profile in nozzle section; C--with a change in thickness and shape of trailing edge.  
KEY: (a) chord; (b) TS-2C; (c) TS-2B; (d) TS-2A; (e) TS-2R.

An analysis of curves of profile losses, presented in Fig. 8-44, shows that character of change in  $\zeta_{np}$  depending on  $M_2$  is determined by shape of profile (mainly), curvature of back edge in nozzle section, the shape and thickness of edge and the geometric parameters of cascade. Here there must be distinguished two main zones of change: the subcritical ( $M_2 < M_{2*}$ ) and the supercritical ( $M_2 > M_{2*}$ ). In the subcritical region with an increase of  $M_2$  the coefficient of losses for a majority of cascades is somewhat diminished. With a separation of flow around back edge of profile an increase in  $M_2$  usually reduces to an increase in  $\zeta_{np}$ .

With a decrease in the pitch the intensity of the increase  $\zeta_{np}$  in transonic zone decreases, and the  $M_{2*}$  value, after which there occurs an increase of losses, becomes larger.

The influence of the Reynold's number, detected in experiments by N. A. Sknar' should be considered important because with its increase the rate of increase of

$\zeta_{np}$  in the transonic zone diminishes. These data pertain to a low degree of turbulence of the flow\*. With an artificial turbulization of the flow also there is observed decrease in degree of increase in losses ( $M_2 > M_{2*}$ .)

The influence of the shape of back edge in nozzle section on losses in cascade is shown in Fig. 8-44, b. Losses in the TS-2A cascade greatly increase at  $M_2 > 0.85$ , this is caused by the great curvature of back edge. For the TC-2B cascades, whose profiles have in the nozzle section a smaller curvature, the increase in losses is observed only at  $M_2 \geq 1.05$  to 1.10. The realization of a profile back edge concave in nozzle section makes it possible to displace the region of critical losses to a zone of still larger  $M_2$  numbers.

In the study of the influence of compressibility on characteristics of cascades

\*The influence of degree of turbulence on characteristics of reactive cascades during transonic speeds explains the nonconformity of the curves  $\zeta_{np} = f(M_2)$ , obtained in various tubes, having a different turbulence. With low turbulence the transition through the speed of sound is accompanied by a sharp increase of profile losses, since shocks in local supersonic zone on the back edge results in a separation of the laminar boundary layer. With high turbulence boundary layer in supersonic zone is turbulent and a separation, as a rule, does not generate or it is displaced along the flow.

the thickness and shape of trailing edge must be taken into consideration. In Fig. 8-44, c the results of experiments shown confirm influence of these parameters on the function  $\zeta_{mp}(M_2)$ .

With supercritical pressure differentials in the cascade in the zone of narrow section intervane channel\* there is established a critical speed. After the trailing edge the pressure is lower than the critical; therefore in a flow around edge (point A, Fig. 8-45) pressure falls—in nozzle section of channel wave of rarefaction ABC extends. It must be emphasized that intensity of wave ABC is determined by the pressure in wake of edge and not the pressure at infinity after the cascade. In primary waves and waves of rarefaction reflected from the back edge of profile the flow reexpands: static pressure on back edge of profile after wave ABC will be lower, than at infinity after the cascade.

A subsequent development of spectrum depends on the structure of flow after trailing edge and degree of reexpansion of flow in the wave ABC. The boundary streams of gas, converging from the concave and convex surfaces of the profile approach each other and at a certain distance after edge turn sharply. On the boundaries of initial sector of edge wake there develops a system of shocks and compression waves, which merge to the diagonal shocks FC and FH.

The reexpansion of the flow in the primary and reflected waves of rarefaction partially "is corrected" by the primary shock FC. The shock, interacting with boundary layer on back edge of profile in nozzle section, is reflected and again occurs in wake of edge. Depending upon mean value of the M number in this section in wake of edge the reflected shock FC either intersects the wake of edge ( $M_{kp} > 1$ ), or is reflected from its boundary. Thus, flow, moving in nozzle section, successively passes through primary and reflected waves of rarefaction, the primary and reflected

---

\*Surface of transition approximately coincides with narrow section of channel. Actually owing to the nonuniformity of the flow in channel and influence of viscosity the surface of transition has certain curvature and is displaced against the flow.

shocks\*.

The behavior of the limiting lines of flow during descent from edge (from side of back edge of profile) essentially depends on the ratio of the pressures at point D and after trailing edge. If the pressure at point D is higher, than after the edge,

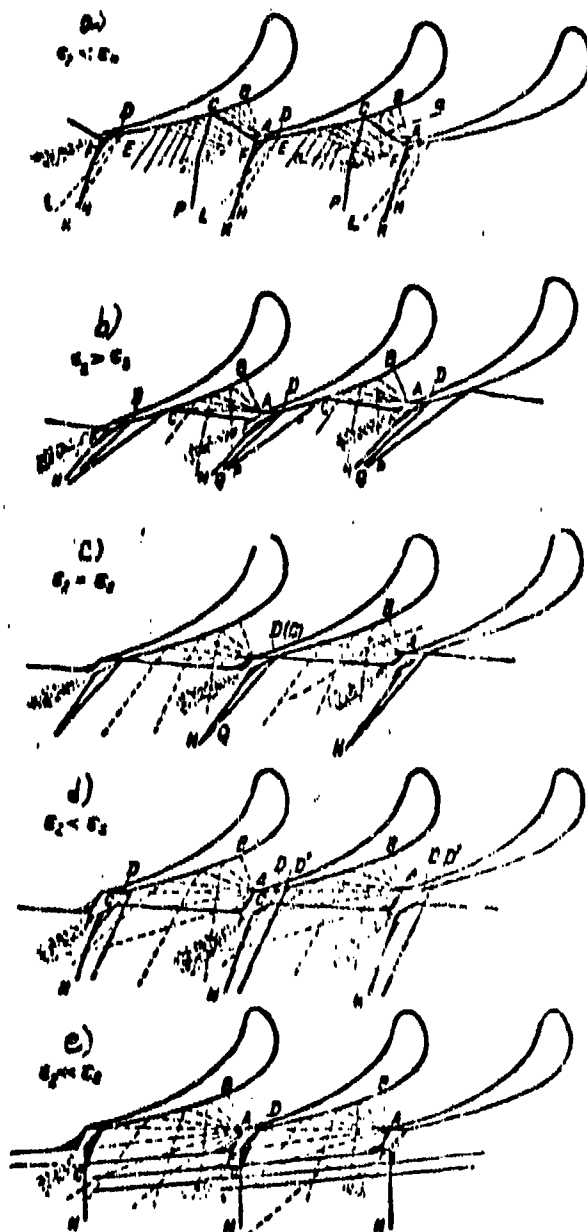


Fig. 8-45. Schematic diagram of outflow of gas from a guide cascade at supersonic speeds.

\*Intensity of primary and reflected shocks is variable along the front, since they are propagated in a nonuniform flow and they interact with the waves of rarefaction.

then at the point D there will form a wave of rarefaction and the flow around the edge improves. The line of flow descends from profile not at point D, but at the point E. The wave of rarefaction DLKD is enclosed by system of weak compression waves, merging into curvilinear shock FH. The system of shocks FC and FH will form the tail shock wave of the profile.

If pressure near the point D is lower than pressure after edge, then a shock will form at point D. In this case the wake of edge is found to be more broken up. In certain cases the shock is located higher along the flow with respect to the point D.

The re-expansion of flow in waves of rarefaction, intensity of edge shocks FC and FH, and also their location are determined by curvature of back edge of profile in nozzle section and by the thickness and shape of trailing edge. Thus, with a decrease in curvature of back edge, the re-expansion of the flow decreases and, consequently, the intensity of the shocks lowers. By specifying for the back edge of profile in nozzle section an inverse curvature, it is possible to reduce the re-expansion of the flow to a minimum; the edge shocks in this case will be weakened.

In the intersection of system of waves of rarefaction and diagonal shocks individual lines of flow repeatedly and variously are deformed, in which at  $M_2 < M_1$  the average flow angle at exit increases in comparison with the subsonic mode: flow is deflected in the nozzle section.

With an increase of differential in pressures the spectrum of the flow in nozzle section of channel and after cascade changes; the intensity and character of location of waves of rarefaction and compression waves vary. The extent and intensity of primary wave of rarefaction increase. Angles of primary, reflected and edge shocks decrease, and point of fall of diagonal shock FC onto back edge of profile (point C) is displaced along the flow. In accordance with this also the character of deformation of individual lines of flow varies. However, the intensity of the shocks increases only to a certain value of the  $M_2$  number, depending on geometric

parameters of cascade.

The expansion of flow in nozzle section of cascade terminates with the relation of pressures  $p_2 = p_3$ . Accurate determination of value  $p_2$  is difficult,

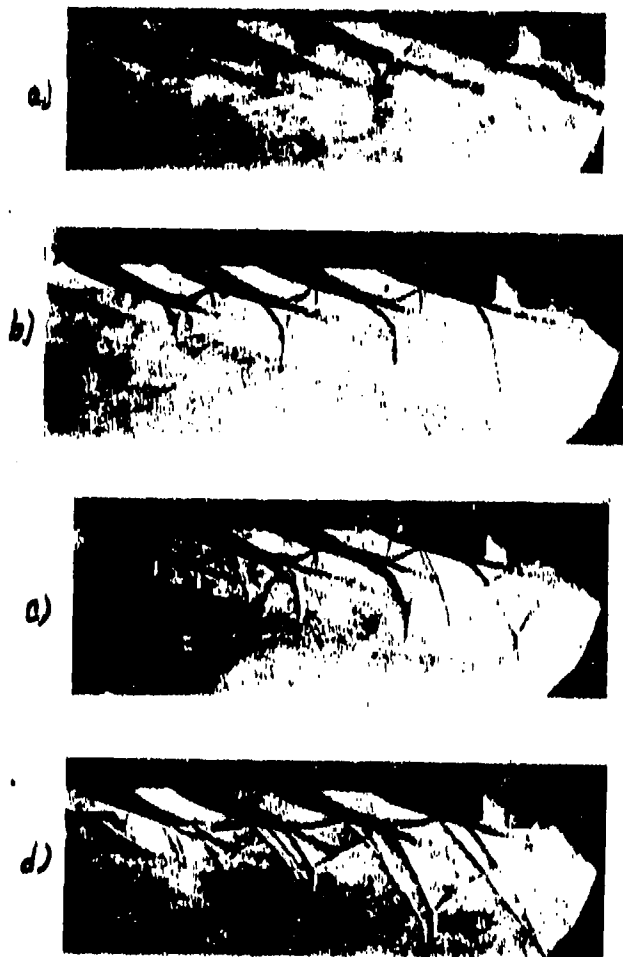


Fig. 8-46. Spectra of flow of air through reactive cascade with contracting channels transonic and supersonic speeds. Relative step  $\bar{t} = 0.543$ ; exit angle of profile  $15^\circ 52'$ ;  
a---  $\epsilon_2 = 0.528$ ; b---  $\epsilon_2 = 0.450$ ; c---  $\epsilon_2 = 0.370$ ; d---  $\epsilon_2 = 0.264$ .

however it is possible to consider limiting such a mode, during which a primary shock occurs at point D (Fig. 8-54,c). In this case instead of three shocks only two will form: the reflected shock CP merges with the edge shock FH.

If  $\varepsilon_2 < \varepsilon_{*}$ , then the expansion of the flow partially occurs beyond the limits of the cascade (Fig. 8-45,d). System of shocks on the trailing edge remains basically as previously but the structure of the wake of edge varies. The left branch of the edge shock FC occurs in subsonic part of wake of edge and sharply deforms it. The pressure after the edge in this case is determined by the shock, and consequently, also the counterpressure. With a significant decrease of  $\varepsilon_2 < \varepsilon_{*}$ , the primary shock occurs in supersonic part of wake of edge (Fig. 8-45,b). Here the flow around trailing edge of profile and the edge pressure are determined only by geometric parameters of the cascade and do not depend on counterpressure. This value of  $\varepsilon_2$  corresponds to a secondary limiting mode of flow in cascade.

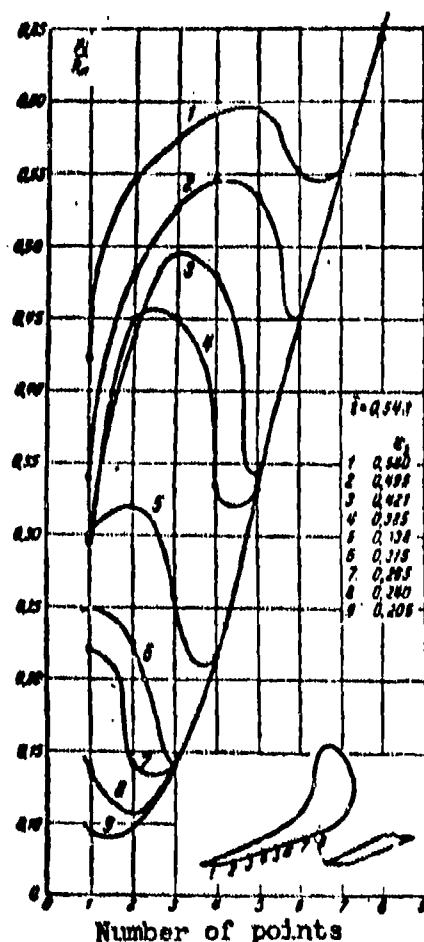


Fig. 8-47. Distribution of pressures along back edge of profiles in nozzle section of reactive cascade with contracting channels during a supercritical outflow.

The considered schematic diagrams of outflow from reactive cascade are corroborated by visual observations by means of an optical instrument (Fig. 8-46).

In Fig. 8-47 there is given the distribution of pressures in sector of back edge of profile in nozzle section of cascade during different ratios  $\varepsilon_2 = p_2/p_0$ . After the narrow section (Points 2-6) it is possible to note significant re-expansion of the flow, which is terminated by a sharp increase of pressure caused by interaction of primary and reflected shocks with the boundary layer. After the shocks the pressure along back edge falls. With decrease of  $\varepsilon_2$ , the zone of maximum rarefaction is displaced along the flow towards trailing edge. In a mode of limiting expansion

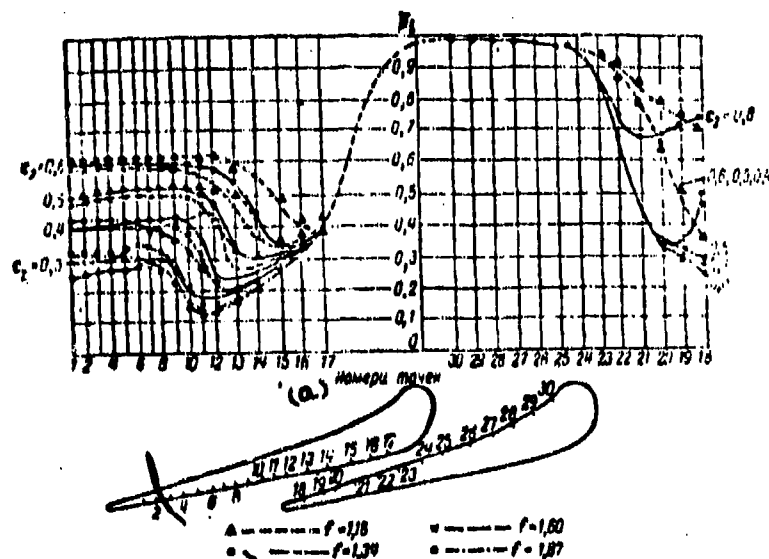


Fig. 8-48. Distribution of pressures about profile in cascades with expanding intervane channels.

KEY: (n) Number of points.

( $\epsilon_1 \approx 0.205$ ) the pressure along back edge of profile continuously falls.

b) Reactive cascades with expanding intervane channels. We shall consider results of an experimental investigation of such cascades. In Fig. 8-48 the distribution of pressures about profile for four cascades is shown. Hence it is evident that under certain modes of flow in the intervane channels as in a single Laval nozzle, shock waves (diffuser section) appear, where their position and intensity depend on the mode  $\epsilon_1$  and geometric parameter  $\lambda = \frac{F_1}{F_2} = \frac{a_1}{a_{min}}$  (Fig. 8-53). As  $\epsilon_1$  decreases the shocks are displaced towards exit of channel. Under design conditions, determined by the ratio  $\lambda$ , only edge shocks will form.

The character of the change of flow spectra in intervane channels of cascade can be traced by the photographs in Fig. 8-49.

Curves of the loss coefficients (Fig. 8-50) show that the flow in cascade with expanding channels is accompanied by a sharp increase of losses during deflections of flow mode from the designed mode. The variation of the coefficient of losses is found to be greater more significant, the larger is the geometric parameter  $\lambda$ , i.e., the greater is the design value of  $M_{2p}$  (See Chapter 6).





Fig. 8-49. Spectra of flow in cascades with expanding channels.  
a—  $\epsilon_2 = 0.4$ ; b—  $\epsilon_2 = 0.3$ ; c—  $\epsilon_2 = 0.2$ .

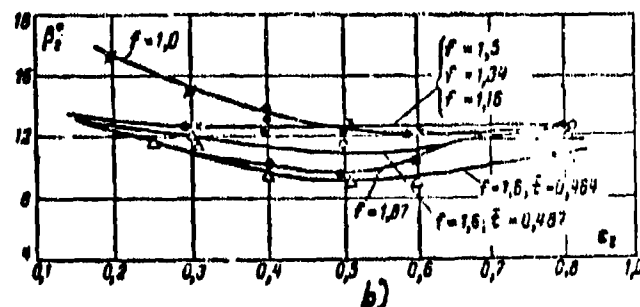
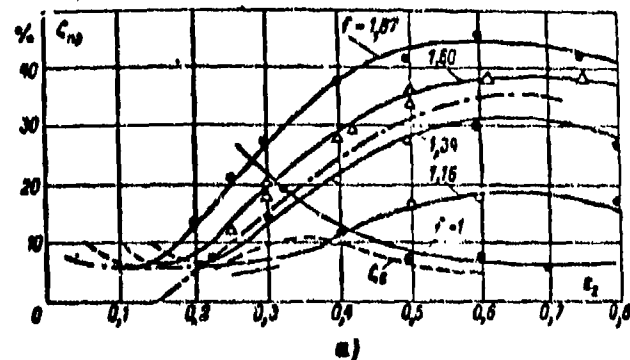


Fig. 8-50. Characteristics of cascades with expanding channels.  
a—variation of  $\zeta_{wp}$  depending on  $\epsilon_1$  and  $\epsilon_2$ ; b—dependence of flow angle at exit on  $\epsilon_1$  and  $\epsilon_2$ .

The maximum variation of losses occurs with an increase of  $\epsilon_2$  from the design value up to 0.5–0.6. With larger  $\epsilon_2$  the shocks are located near the minimum section; the intensity of the shocks decreases, and  $\zeta_{wp}$  lowers.

Under the design conditions  $\epsilon_2 < \epsilon_2$  the losses increase, since there occurs an expansion of the flow in nozzle section of the cascade. Under flow conditions close to the designing, the losses for all cascades are small, whereupon profiling of the expanding part by method of characteristics makes it possible only insignificantly to lower the losses under such flow conditions.

In Fig. 8-50,a, there is presented a curve of wave loss coefficient  $\zeta_w$  for a

cascade with  $\beta = 1.6$ , constructed according to the curves of pressure distribution (Fig. 8-48) on the assumption that the shocks are normal. Hence, it is evident that the wave losses are small; the chief losses under nondesign conditions are caused by a separation of the flow. In Fig. 8-50,a there is plotted also a curve of  $\zeta_{np}$  for a cascade with contracting channels. Intersection points of the curve  $\zeta_{np}$  for this cascade with curves for cascades with expanding channels makes it possible to establish regions of the rational use of the cascades being compared.

The variation of the central angle of flow after cascade depending upon  $\alpha_2$  is shown in Fig. 8-50,b. For cascades with  $\beta > 1$  the central flow angle slightly varies over entire range of variations of  $\alpha_2$ . For a cascade with  $\beta = 1.0$  characteristic is the increase of  $\beta_2$  at supersonic speeds, caused by a deflection of the flow in the nozzle section.

#### 8-11. Calculation of Angle of Deflection of Flow in Nozzle Section and the Profiling of Reactive Cascades at Transonic and Supersonic Speeds\*.

There are several methods of calculating angle of deflection of flow in a nozzle section of cascade. The most widely used and simplest are methods, based on equations of a one-dimensional flow.

In assuming the field of flow in sections AA (Fig. 8-51) and EF (selected at a great distance after cascade) even, it is possible to write out the equation of continuity in the following form:

$$\rho_1 c_1 \sin \beta_1 = \rho_{2\infty} c_{2\infty} \sin \beta_{2\infty}, \text{ where } \sin \beta_2 = \frac{AA}{EF}.$$

We divide both sides of this expression by  $\rho_1 c_1$ ; then we obtain:

$$c_1 \sin \beta_1 = c_{2\infty} \sin \beta_{2\infty}.$$

In taking into consideration that at  $\alpha_2 < \alpha$ ,  $q_2 = 1$  and  $\beta_{2\infty} = \beta_2 + \delta$ , where  $\delta$  is the angle of deflection of flow in nozzle section, we arrive at Baire's formula:

$$\delta = \arcsin\left(\frac{1}{c_{2\infty}} \sin \beta_1\right) - \beta_1. \quad (8-47)$$

\*Paragraphs 8-11 to 8-14 were written by A. V. Gubarev.

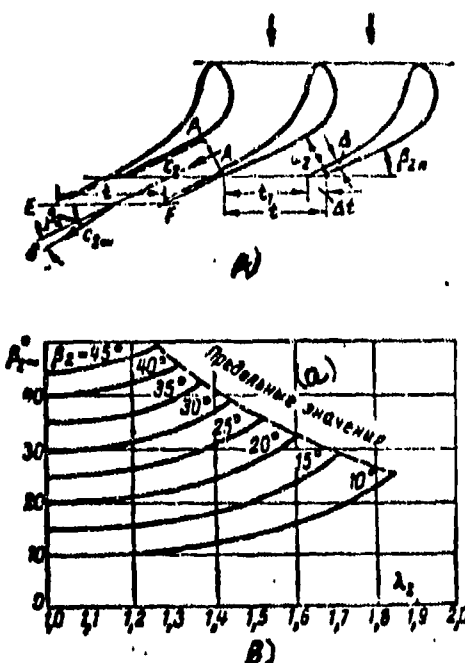


Fig. 8-51. A--chart for determining angle of deflection of flow in nozzle section of cascade; B--designed relationship between flow angle at exit of cascade on the speed  $\lambda_2$  and  $\beta_{2n}$ .

KEY: (a) Limiting values

With a consideration of losses between sections AA and EF Baire's formula acquires the form:

$$\delta = \arcsin \left( \frac{1}{q_{2\infty}} \cdot \frac{P_{01}}{P_{02\infty}} \sin \beta_1 \right) - \beta_1. \quad (8-48)$$

It follows from this that with an increase in losses, the angle of deflection increases. Essential also is the fact that the angle of deflection  $\delta$  depends not only on the rate of outflow and losses, but also on the design exit angle  $\beta_1$  (Fig. 8-51,b).

Baire's formula is valid only at  $s_2 > s_1$ , i.e., as long as primary wave of rarefaction is within limits of the nozzle section. The angle of deflection, corresponding to maximum expansion in nozzle section, is determined approximately by the relationship

$$\beta_2 = \alpha_{m2} - \beta_1,$$

where  $\alpha_{m2}$  --angle of characteristic, coinciding with exit section.

Hence, by means of (8-47) we obtain the obvious equality

$$\sin(\beta_1 + \delta) = \sin \alpha_{m2} = \frac{1}{M_{2s}} = \frac{\sin \beta_1}{q_{2s}}. \quad (8-49)$$

In expressing  $q_{2s}$  in terms of  $q_1$ , we find the ratio of pressures for the mode under consideration:

$$q_2 = q_1 (\sin \beta_2)^{\frac{2k}{k+1}}.$$

From equation (8-49) there readily is determined the critical angle of deflection  $\delta_*$ .

By means of equations of continuity, momentum and energy, there can be obtained an accurate solution for angle of deflection of flow in nozzle section of cascade with edges of finite thickness.

By assuming that in sections AA and EF (Fig. 8-51,a) the flow is uniform, we use the equations of conservation presented in Sec. 8-6. By solving these equations commonly there can be obtained the computing formula proposed by A. S. Natalevich:

$$\tau_{2s} \delta = \frac{\sqrt{\left(\frac{k}{k-1} \bar{p} n \cos \beta_2\right)^2 - (k+1-N\bar{p})\left(k+1-N\bar{p} + \frac{2k}{k-1} \bar{p} n + \frac{k^2(k+1)}{k-1}\right)}}{k+1-N\bar{p}} - \frac{\frac{k}{k-1} \bar{p} n \cos \beta_2}{k+1-N\bar{p}}. \quad (8-50)$$

At  $\delta < 10^\circ$  it is expedient to use the approximate expression

$$\tau_{2s} \delta = \left[ \frac{\frac{k(k+1)}{k+1-N\bar{p}} - \frac{k-1}{k} (k+1-N\bar{p})}{2n\bar{p}} - 1 \right] \tau_{2s} \beta_2. \quad (8-51)$$

Here and above it is designated:  $n = \frac{1}{1-\tau}$ ;  $\tau = \frac{\Delta t}{t}$ ;  $\bar{p} = \frac{p_{2s}}{p_1}$ ;  $N = \frac{1}{1-\tau} \left( 1 - \tau \frac{p_{2s}}{p_{2s0}} \right)$ ;  $p_{2s}$  is the pressure after the edge.

For the case of an infinitely thin edge formulas (8-50) and (8-51) were for the first time given by G. Yu. Stepanov.

The solution of system of three equations provides the possibility also to determine wave losses in nozzle section. For the case of infinitely thin edges the wave losses are determined by G. Yu. Stepanov's formula:

$$\zeta_s = 1 - \frac{\left[ \frac{1}{k} (1-\bar{p}) - 1 \right]^2}{\frac{k+1}{k-1} \left[ 1 - \frac{k-1}{k} \right]} \frac{1}{\cos^2 \delta}. \quad (8-52)$$

It must be noted that the coefficient of wave losses considers only losses, associated with turn of flow in nozzle section.

Losses, caused by the interaction of shock waves with boundary layer, frictional losses and losses for equalizing the flow usually greatly exceed the wave losses, calculated for an ideal fluid. Therefore the angle of deflection both by formula (8-47), and also by G. Yu. Stepanov's and A. S. Natalevich's formulas are found to be less than real. Baire's formula with a consideration of losses in nozzle section (8-48) gives close agreement with an experiment, but its use is limited, because it is necessary as a preliminary to determine the losses.

In Sec. 8-10 it was shown that flow angle at exit from cascade with expanding channels remains virtually constant in wide range of modes  $M_1 < M_{2n}$ . By using such character of dependence  $\beta_2(M_2)$ , it is possible by calculating to determine losses in a cascade under various flow conditions.

We write out the equation of continuity for the critical section  $F = a_{\text{min}}$  and section at infinity after the cascade in the form:

$$a_{\text{min}} a_1 = \rho_1 c_1 t \sin \beta_1,$$

where  $\rho_1, c_1$  are the actual parameters of the flow.

We shall divide and then multiply right side by  $\rho_{21} c_{21}$  and after transformations we obtain:

$$\frac{a_{\text{min}}}{t \sin \beta_1} = \varphi \lambda_{21} \frac{\rho_1}{\rho_2} \frac{c_{21}}{c_1} \frac{p_1}{p_2} \quad (8-53)$$

After solving this equation with respect to  $\varphi$ , we find:

$$\varphi = \frac{F}{2} \pm \sqrt{\left(\frac{F}{2}\right)^2 + \frac{1}{\lambda_{21}^2} \frac{k+1}{k-1}}, \quad (8-54)$$

where

$$F = \frac{t \sin \beta_1}{a_{\text{min}}} q_{21} \left(1 - \frac{1}{\lambda_{21}^2} \frac{k+1}{k-1}\right). \quad (8-55)$$

Sign minus in equation (8-54) has not physical meaning, since  $\varphi > 0$ .

In the case, when  $\beta_1 = \text{const}$ ,  $t \sin \beta_1 = a_1$  and

$$F = f q_{21} \left(1 - \frac{1}{\lambda_{21}^2} \frac{k+1}{k-1}\right). \quad (8-55a)$$

In Fig. 8-52 there are presented the computed curves showing the relationship between  $\varphi$  and  $\epsilon_1$  and the parameter  $l = \frac{a_1}{a_{\min}}$  at  $\beta_1 = \text{const}$ . The proposed procedure provides the possibility with sufficient accuracy to determine the additional loss

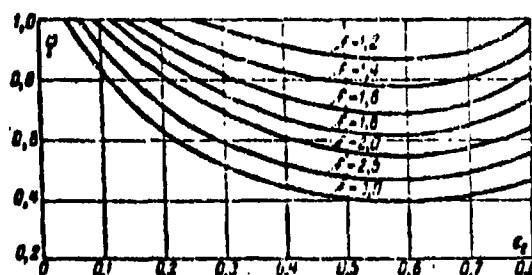


Fig. 8-52. Calculating dependence of  $\varphi$  on  $\epsilon_1$  for cascade with expanded channels ( $k = 1.4$ ).

under off-design conditions, if the dependence of  $\beta_1$  on  $\epsilon_1$  is known.

It is readily seen that for decrease of losses in a wide range of modes  $\epsilon_1 > \epsilon_{1p}$ , it is necessary that the exit angle  $\beta_1$  is variable.

Ideal in this sense is the cascade, for which a variation of  $\beta_1$  would correspond to equation (8-54) at  $\varphi = 1$ . Hence, after a number of transformations there may be obtained the following optimum law for the change of flow angles:

$$\beta_1 = \arcsin \left( \frac{1}{q_{2t}} \frac{a_{\min}}{l} \right).$$

Consequently, at  $M_{2t} = 1$  ( $q_{2t} = 1$ ) the flow angle at exit should be at a minimum, but at  $M_{2t} > 1$ —it increases. However experiments have shown that for cascades with expanding channels such character of change of  $\beta_1$  is possible.

For a cascade with contracting channels,  $a_{\min}/l = \sin \beta_{1p}$ . Under this condition we obtain the usual Baire equation for flow angle at exit (8-47).

Thus, for cascades with contracting channels, the law of variation of  $\beta_1(M_{2t})$  coincides with the theoretical.

However, as is well known, in such cascades under off-design conditions ( $\epsilon_1 < \epsilon_{1p}$ ) the losses intensively increase (Fig. 8-44).

This is caused by the occurrence of wave losses and interaction of shocks with boundary layer on back edge in nozzle section.

As has already been indicated, intensity of shocks in nozzle section at  $M_2 > 1$  depends on curvature of back edge, where the minimum wave losses may be obtained with the back edge having a reverse concavity in nozzle section.

Investigations, made at the Moscow Power-Engineering Institute have shown the possibility of creating reactive cascades with small losses at  $M_2 > 1$  under design and off-design conditions. In such cascades rationally there are combined the positive features of cascades with expanding and contracting channels. At moderate supersonic speeds  $M_2 \leq 1.3$  to 1.4 the intervane channel are made contracting and the back edge in nozzle section is calculated by method of characteristics in such a way that along the back edge there does not occur a re-expansion of the flow. Method of characteristics can be used only for evaluating indicators of the flexure on back edge. Point of change of curvature on back edge should be located inside the channel.

At high supersonic speeds  $M_2 > 1.3$  to 1.4, it is expedient to make the cascade channels with a small expansion ( $f = 1.05$  to 1.15), by displacing narrow section within the channel. Here the necessary design concavity of back edge diminishes

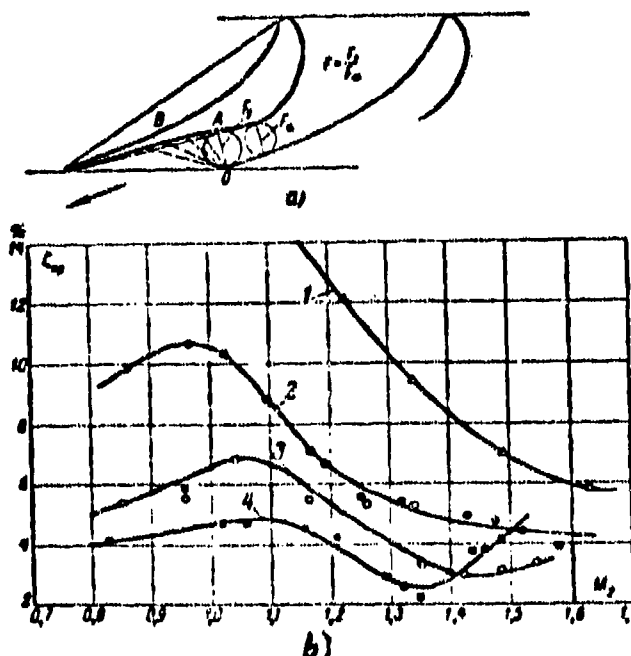


Fig. 8-53. a--supersonic reactive cascade of Moscow Power-Engineering Institute (MEI) with concave nozzle section and small expansion of intervane channels; b--influence of expansion of channel on characteristics of supersonic cascades with concave back edge in nozzle section (experiments at MEI). 1-- $f = 1.17$ ;  $t = 0.46$  (flat back edge in nozzle section); 2-- $f = 1.17$ ;  $t = 0.53$ ; 3-- $f = 1.10$ ;  $t = 0.581$ ; 4-- $f = 1.0$ ;  $t = 0.680$  (curves 2, 3 and 4--concave back in nozzle section).

and contours of the profile are simplified. The expediency of introduction of a small expansion of channel up to nozzle section is based on curves of losses, presented in Fig. 8-50: with small values of parameter  $f$  intensity of increase of  $\bar{\eta}_{np}$  under off-design conditions sharply lowers. With a decrease of  $M_2$  number the flow angle at exit in such cascades will vary more intensely, than in cascades with expanding channels.

In Fig. 8-53 there are presented certain results of investigating cascades profiled by the indicated method. A comparison of curves shows that such cascades have significant advantages not only under variables, but also under design conditions in comparison with cascades, having a wide expansion of channel ( $f > 1.2$ ). Experiments have shown also that for transonic speeds ( $M_2 < 1.2$ ) satisfactory results may be obtained by means of a rectilinear back edge in nozzle section; here the point of discontinuity of curvature on back edge is disposed inside the channel.

#### 8-12. Structure of Flow in Impulse Cascades at Transonic and Supersonic Speeds.

The flow around impulse cascades by a flow with transonic speeds is characterized by supersonic zones both on back edge in nozzle section, and also on entrance sector of back edge. Therefore, equally with  $M_{2*}$  the critical  $M_2$  number, with which sonic speeds generate in nozzle section, the introduction of the concept of a second critical number  $M_{2**}$  which determines such a mode of flow around, at which sonic speeds generate on leading edge is meaningful. Thus, like  $M_{2*}$ , the magnitude  $M_{2**}$  depends on the spacing and stagger angle. Besides, the second critical number  $M_{2**}$  decisively depends on the flow entrance angle.

In Fig. 8-54 are presented the  $M_{2*}$  and  $M_{2**}$  values depending on  $f$ ,  $\beta$ , and entrance flow angle  $\beta_1$ . As can be seen, at small  $\beta$ , and large  $t$   $M_{2**} < M_{2*}$ , i.e., sonic speeds in an impulse cascade are generated first on leading edges of blades. With an increase of the spacing,  $M_{2*}$  increases. The character of the change  $M_{2*}$  and  $M_{2**}$  to a significant degree is determined also by the shape of profile: curvature of back



edge in nozzle section and at entrance sector and in the thickness of edges.

Under conditions  $M_2 > M_{2**}$  in entrance sector of back edge of each profile of cascade there will form an  $\lambda$ -shaped shock. With an increase in speed this shock is developed into a forward shock for the neighboring profile (Fig. 8-55). Directly after each forward shock the flow is subsonic, however such scheme of flow around, obviously, takes place only in the case, when after each shock flow is accelerated and before the subsequent shock the speed is  $M > 1$ . As the speed of incident flow increases the forward shocks approach the leading edges and are distorted. Here the flow after the shock is vortical and along front of cascade the speeds vary in magnitude and direction.

At a certain value of  $M_1 > \frac{1}{\sin \beta_1}$ , when axial component of the speed is supersonic, shocks, occurring before each profile, merge into a single wave-like shock (Fig. 8-55,b). The left branches of forward shocks are turned in a direction toward the concave surface of profile. With a further increase in  $M_1$  the shocks enter into the intervane channel. Consequently, under the conditions  $M_1 > \frac{1}{\sin \beta_1}$  neighboring profiles do not exert an influence on the flow before the leading edges and therefore the flow around entrance sector by such a supersonic flow may be assumed isolated.

However in majority of encountered cases speeds at entrance into cascade are insufficiently great and axial speed of flow is significantly less than the sonic. In this case, the influence of profiles is propagated in a direction against the flow.

We shall consider the flow around by supersonic flow of ideal fluid of a cascade with a finite number of profiles under the condition that axial speed is less than the sonic. Let us assume that thickness of leading edge is equal to zero, the design angle of edge is extremely small and back edge of profile up to entrance sector of channel is formed by a straight line whose slope angle to front of cascade is equal to  $\beta_c$ .

If vector of speed at entrance in cascade is directed at an angle  $\beta_c$  from side of back edge onto leading edge there appears a slight discontinuity--the characteristic.

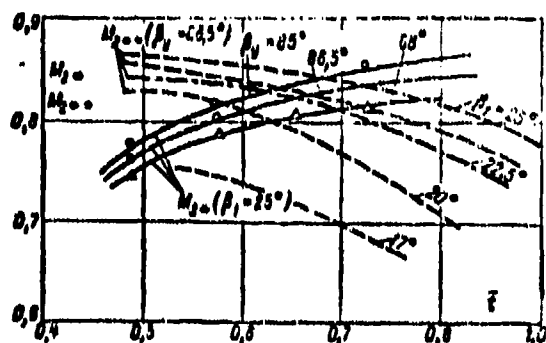


Fig. 8-54. Influence of relative pitch  $\bar{t}$ , the setting angle  $\bar{\beta}$ , and entrance flow angle  $\beta_1$  on critical values of  $M_{2*}$  for an impulse cascade.

Along the rectilinear sector of back edge, the speed is maintained constant and, consequently, before edges of following profiles the speed of the flow is equal to

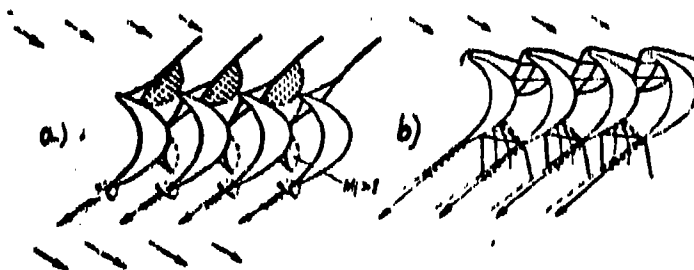


Fig. 8-55. Schematic diagram of flow of supersonic flow in an impulse cascade.

speed before first profile (Fig. 8-56,a). Thus, in this case flow before cascade with an infinite number of profiles does not differ from the flow at infinity.

In the case when vector of speed at entrance into cascade is directed at an angle, smaller than  $\beta_c$ , on leading edge of first profile (from side of back edge) there will form a wave of rarefaction, in which the flow is accelerated and is turned by an angle  $\delta = \beta_c - \beta_1$  (Fig. 8-56,b).

Along the rectilinear sector of back edge of profile the speed is maintained higher than speed at infinity before the cascade, and its vector is directed at an angle  $\beta'_1 = \beta_c > \beta_1$ . Therefore on edge of following profile there develops a compression wave and all the lower located profiles are flowed around by a flow of

greater speed, than the first.

At  $\beta_1 > \beta_c$  on leading edge of first profile there appears shock wave, in which there occur a decrease in speed and turn of flow by an angle  $\delta = \beta_1 - \beta_c$ . Further discussions are analogous to the case, when  $\beta_1 < \beta_c$ .

If at  $\beta_1 \neq \beta_c$  we consider a cascade with an infinite number of profiles, then it is necessary to admit that at infinity before the cascade there must either exist a wave of rarefaction (at  $\beta_1 < \beta_c$ ), in which flow is turned by angle  $\delta = \beta_c - \beta_1$ , or shock wave (at  $\beta_1 > \beta_c$ ). This contradicts the condition  $\beta_1 \neq \beta_c$ . Consequently, at a supersonic speed before cascade flow at infinity can be directed only at an angle  $\beta_1 = \beta_c$ .

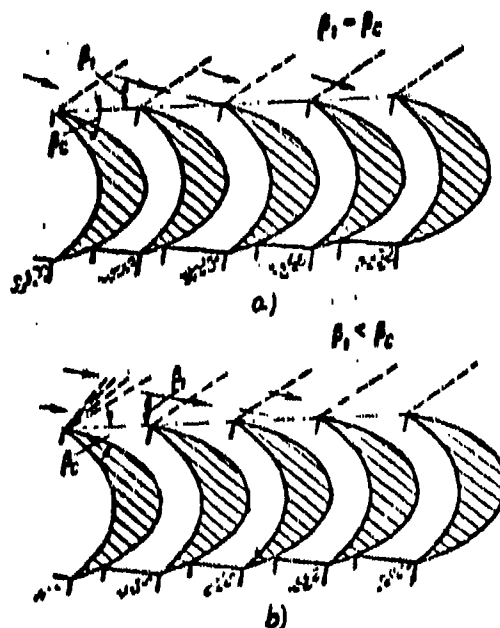


Fig. 8-56. Structure supersonic flow at entrance into impulse cascade.

Under actual conditions a rotating cascade is flowed around concurrently with the guide cascade. In this case the entire change in structure of flow on leading edges of first profile are localized in nozzle sector of guide channel, where in a such system it is possible to assure a flow around cascade by a supersonic flow at any entrance angle  $\beta_1 \neq \beta_c$  (up to the arrival of modes of "cutoff", Sec 8-13). Here the flow around lower located profiles to a significant degree is determined by the system of shocks and waves of rarefaction, reflected from wall of oblique section

of nozzle. Structure of flow before cascade is complicated, and the monotonous flow around all profiles is disturbed. The periodicity of the flow at entrance into rotating cascade at supersonic speeds will be observed in the interval, a brief spacing of guide cascade.

K. Ovatich observed that even in case of knife-sharp leading edge at design entrance angles of flow in the cascade there may appear a complicated system of shocks. An analysis of these results shows that the head shocks developing before the cascade formally may be divided into three main groups: shocks caused by the thickness and shape of leading edge, shocks depending on shape of inter-vane channel (shocks from "cut-off" of inter-vane channel) and shocks (or waves of rarefaction) caused by off-design entrance flow angle into cascade ( $\beta_1 \neq \beta_c$ ). Under actual conditions it is virtually impossible to divide these shocks, because they will form a single complex system.

### 8-13. Reduced Flow Rate of Gas Through a Cascade. Peculiar Operating Conditions of Impulse Cascade in a Supersonic Flow.

We now write out the equation of continuity for sections of entrance and exit of cascade (Fig. 8-57) in following form which we know (See Sec. 8-11):

$$q_1 \sin \beta_1 = q_2 s_2 \sin \beta_2; \quad s_2 = \frac{P_{01}}{P_{02}}. \quad (8-56)$$

This equation may be used for a graphic calculation of parameters of flow in a cascade.

We note that the axial projection  $q_1$  is equal to:

$$q_{1a} = q_1 \sin \beta_1 = q_2 s_2 \sin \beta_2 = q_{2a} s_2. \quad (8-57)$$

On the other hand,

$$q_2 = \left( \frac{k+1}{2} \right)^{\frac{1}{k-1}} \lambda \left( 1 - \frac{k-1}{k+1} \lambda^2 \right)^{\frac{1}{k-1}} \sin \beta. \quad (8-58)$$

It follows from this that constant value  $q_{1a}$  may correspond to different values of  $\lambda$  and  $\beta$ . Consequently, at  $q_{1a} = \text{const.}$  the end of vector  $\lambda$  describes in the polar system of coordinates  $(\lambda, \beta)$  certain transcendent curve. This curve we shall call the hodograph of the vector  $\lambda$ .

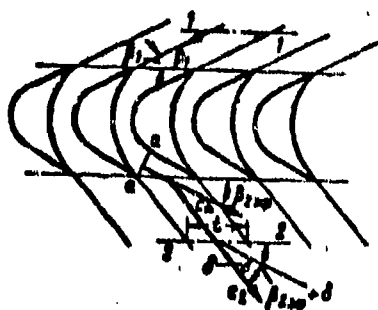


Fig. 8-57. Chart for deriving equation of hodograph.

In being given different, but constant  $q_a$  from  $q_a = 0$  to  $q_a = 1$  and  $\beta_1$  from 0 to  $\pi$ , in plane of hodograph it is possible to construct group of curves, making it possible to calculate graphically the flow in rotating cascades.

The form of hodograph  $\lambda$  for certain  $q_a$  is shown in Fig. 8-58. The circle, corresponding to  $\lambda = 1$ , divides plane of hodograph into two regions [subsonic ( $\lambda < 1$ ) and supersonic ( $\lambda > 1$ )].

At subsonic speeds at entrance the use of the graphic method does not cause unusual difficulties. Actually, at  $\alpha_1 = 1$  (ideal fluid)  $q_{2a} = q_{1a}$  and the vector  $\lambda_1$  with a given  $\beta_1$  is found on the same curve ( $q_a = \text{const}$ ) that also the vector  $\lambda_2$  is. Consequently, by the known  $\lambda_1$  and  $\beta_1$  we find the point A, and the determining curve  $q_{1a} = \text{const}$ , and by  $\beta_2$  at points B and B' we determine the vector  $\lambda_2$  (or  $\lambda'_2$  if speed at exit is supersonic).

The hodograph method may be extended also to the case of flow with losses. For this purpose we construct the curve (dotted line in Fig. 8-58) from the equation

$$\frac{\lambda}{c_0} \left( 1 - \frac{k-1}{k+1} \lambda^2 \right)^{\frac{k}{k-1}} \sin \beta = \frac{q_a}{c_0} = \text{const.} \quad (8.59)$$

On this curve, we find the points E and E', corresponding to speeds of flow after cascade with a consideration of the losses. Hence, it is evident that at  $\lambda_1 < 1$  the exit speed of flow from the same cascade with losses will be greater, than in the case  $\alpha_1 = 1$ , and at  $\lambda_1 > 1$ —less (under the condition of maintaining the same exit flow angle).

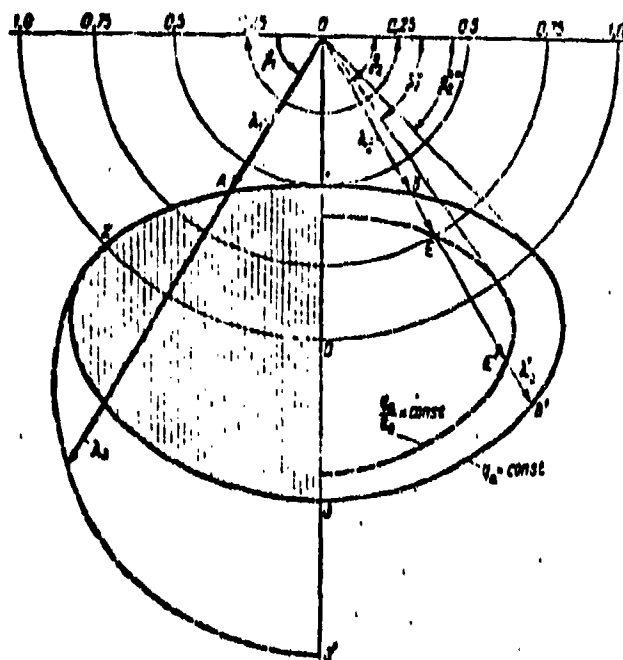


Fig. 8-58. Graphic determination of parameters of flow in cascade.

Of great interest is the determination of conditions, which at entrance or at exit of cascade the speeds attain critical values. From (8-56) there may be obtained that at  $\lambda_1 = 1$ .

$$\beta_1^* = \arcsin(q_{2e} \sin \beta_e) = \arcsin(q_{2u} e_e). \quad (8-60)$$

During absence of losses

$$\beta_1^{**} = \arcsin q_{2u}.$$

It is readily seen that at

$$q_{2u} = \text{const and } \beta_1^* < \beta_1^{**}. \quad (8-60a)$$

The critical speed at exit of cascade is established in the case, when

$$\beta_1^* = \arcsin\left(q_{1u} \frac{1}{\lambda_e}\right). \quad (8-61)$$

During absence of losses

$$\beta_1^{**} = \arcsin q_{1u}. \quad (8-61a)$$

It follows from this that during

$$q_{1u} = \text{const and } \beta_1^* > \beta_1^{**}.$$

The values  $\beta_1^*$ ,  $\beta_2^*$ ,  $\beta_2^{**}$ , and also  $\beta_1^{**}$  can be determined by means of the hodograph (Fig. 8-58).

During supersonic speeds at entrance not all the modes, corresponding to hodograph

of speed, are actually admissible. Experiments show that in certain cases at

$\lambda_1 > 1$ , at entrance into cascade there develop systems of shocks, not associated with flow around the profiles; in intersecting this system of shocks the flow becomes subsonic. Such modes of flow around active cascades are called "cutoff" modes.

At the same time according to the condition of continuity of motion there is found to be inadmissible a certain other group of modes with subsonic and supersonic speeds at entrance. We shall establish at first range of inadmissible values of  $\lambda_1$ . We consider the motion of the gas in the system inlet nozzle--cascade (Fig. 8-59a). Passage sections in this system are determined by evident relationships:

$$F_0 = a_0 l; F_1 = l \Sigma \sin \beta_1; F_2 = l \Sigma \sin \beta_2. \quad (8-62)$$

We write out the equation of continuity with a consideration of the losses:

$$q_0 F_0 = q_1 \frac{p_{01}}{p_{02}} F_1 = q_2 \frac{p_{02}}{p_{03}} F_2. \quad (8-63)$$

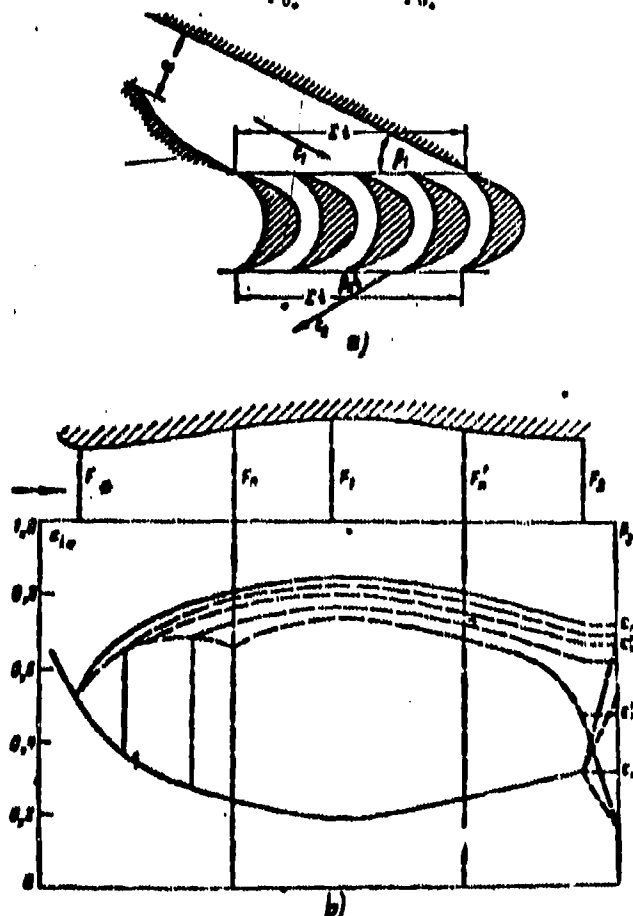


Fig. 8-59. Chart for the analysis of "cutoff" modes of rotating cascade.

Hence it is evident that the critical speed in section  $F_*$  and, consequently, supersonic flow at entrance into cascade (in section  $F_1$ ) can develop only under the conditions  $F_1 < F_2$  and  $F_* \leq F_2$ . At  $F_* > F_2$  the flow before cascade will be subsonic, and consequently, "cutoff" modes cannot be observed.

After substituting (8-62) and (8-63) and assuming that  $q_1 \sin \beta_1 = q_{1a}$ , and maximum flow rate through the system corresponds to  $q_2 = 1$ , we obtain:

$$q \cdot \frac{a}{\Sigma} = q_{1a} = \sin \beta_1.$$

It follows from this that the modes, corresponding to condition

$$q \cdot \frac{a}{\Sigma} = q_{1a} > \sin \beta_2, \quad (8-64)$$

are not realisable.

In plane of hodograph (Fig. 8-58) region, corresponding to the inadmissible values of  $\lambda_1$ , at entrance into cascade, is cross-hatched. Thus, before the cascade there cannot be realized either certain supersonic speeds (region 0-2-3), or

certain subsonic (0-1-2). It is necessary once again to emphasize that region of impossible modes at entrance into cascade does not coincide with region of "cutoff" modes. In last case before the cascade shocks appear and, consequently, the "cutoff" may form only in the case, when in the stator there is attained a supersonic speed.

For the solution of this problem it is convenient to use a simplified scheme of inlet nozzle--channel, in which the cascade is replaced by a contracting channel (Fig. 8-59,b). In such a tube of variable section at  $\epsilon > \epsilon_m$  the speeds everywhere are subsonic ( $\epsilon_m$  -- maximum ratio of pressure, at which in critical section  $\lambda_* = 1$ ). In case  $\epsilon < \epsilon_m$  in initial section after section  $F_*$  there occurs a supersonic zone, which is enclosed by a compression wave. The modes  $\epsilon < \epsilon'_m$ , where  $\epsilon'_m$  is the ratio of the pressures, with which the shock is located in section  $F = F_2$ , theoretically may be realized in three ways: with a shock in exit section and in intermediate sections of nozzle  $F_n$  and channel  $F'_n$ . However, first and third methods of attaining  $\epsilon < \epsilon'_m$  cannot be realized, since even weak perturbations above the flow result in a separation of mode. Thus, in the modes  $\epsilon_m > \epsilon > \epsilon'_m$  with a decrease in counter-pressure the supersonic region in initial section of supersonic nozzle increases--shock wave is displaced towards exit section  $F_1$ .



At  $\lambda \leq \lambda_m'$  supersonic zone remains constant and the shock is located in section  $F_n$ , which can be determined from the condition, at which in section  $F_2$  there is established a critical speed. A further lowering of counterpressure does not alter the mode of flow in the system. With the specific ratio  $F_2/F_*$  and  $F_1/F_*$  the section  $F_n$  coincides with  $F_1$ . In this case before the channel and in channel there is possible the existence of supersonic speeds.

Consequently, in system nozzle—channel supersonic speeds may be attained only at  $F_2 > F_*$ . With the specific ratio  $F_2/F_1$  and  $F_1/F_*$  in the modes  $\lambda \leq \lambda_m'$  at entrance into channel there is possible the existence of supersonic speeds.

By returning to the system nozzle—cascade (Fig. 8-59,a) we note that the ratio  $\frac{F_1}{F_*} = \frac{M \sin \beta_1}{a}$  determines the value of  $\lambda_1$  for diverging nozzle, and  $\frac{F_1}{F_*} = \frac{\sin \beta_{1,sh}}{\sin \beta_1}$ .

As has been shown above, supersonic speeds before cascade are possible only in the case, when the equation of continuity with a consideration of the losses is satisfied:

$$q_1 \sin \beta_1 = q_2 \frac{p_{01}}{p_{02}} \frac{p_{02}'}{p_{02}} \sin \beta_2.$$

Here  $p_{02}/p_{01}$  is the change in stagnation pressure in a normal shock with the change depending only on  $\lambda_1$ ;  $p_{02}'/p_{02}$  is the change in stagnation pressure in cascade.

At  $p_{02}'/p_{02} = 1$  and  $\lambda_2 = 1$  from equation of continuity we obtain:

$$\left(\frac{k+1}{2}\right)^{\frac{1}{k-1}} \frac{1}{\lambda_1} \left(1 - \frac{k-1}{k+1} \frac{1}{\lambda_1^2}\right)^{\frac{1}{k-1}} \sin \beta_1 = \sin \beta_{1,sh}. \quad (8-65)$$

Formula (8-65) determines in the plane of hodograph the curve, limiting region of modes, under which supersonic speeds at entrance into cascade is unattainable.

At  $\lambda_1 = 1$   $\beta_1 = \beta_{1,sh}$ . i.e., curves, governed by formula (8-65), coincide with curves, constructed by formula (8-59).

For practical use it is expedient to construct diagram of hodographs, corresponding to different, but constant values of  $q_{a1}$  (Fig. 8-60).

Diagram is constructed in following manner. In being given the constant  $q_a$  and a number of values of  $q_2$  we determine by (8-59) the corresponding values of  $\beta$ . In region  $\lambda > 1$  we construct also a family of curves by formula (8-65), where in

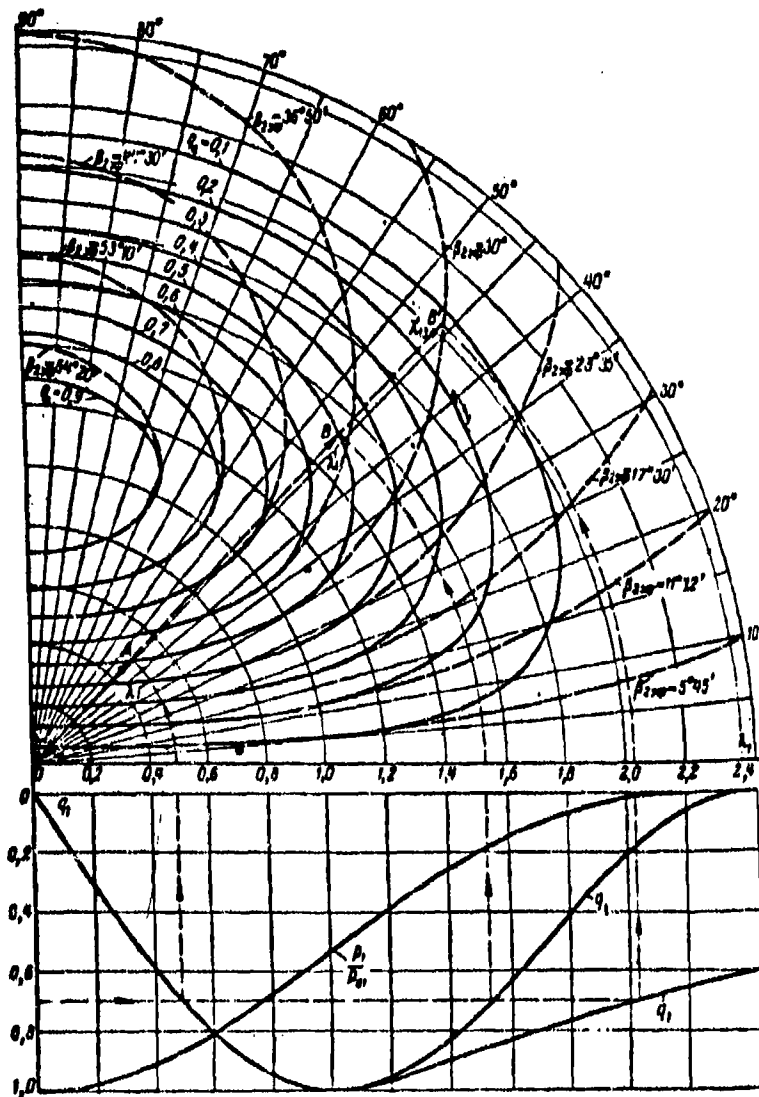


Fig. 8-60. Diagram of hodograph  $\lambda$ .

this case  $\sin \beta_{1\phi} = q_a$ . These curves are used for determining the zone of possible supersonic speeds at entrance into cascade.

For convenience in constructing and using the diagram below there have been plotted functions of the one-dimensional isentropic flow:

$$q_1, \frac{p}{p_0}, \frac{T}{T_0} \text{ et cetera, and also } q_2 = \frac{p_{01}}{p_{02}} q_1.$$

We consider in a particular example the use of this diagram. We shall assume as given the values  $q_a = 0.5$  and  $q_1 = 0.7$ .

Then  $\sin \beta_1 \frac{0.5}{0.7} = 0.714$  and  $\beta_1 = 45^\circ 30'$ . On horizontal axis we find two values:

$\lambda_1$  and  $\lambda'_1$ . By drawing from point O two circles with radii  $\lambda_1$  and  $\lambda'_1$  we shall obtain at intersection with the radial line  $\beta_1 = 45^\circ 30'$  the points A and B, corresponding to the hodograph  $q_a = 0.5$ . After determining by the indicated method of entrance and exit triangles of speeds, we can find the parameters of the flow. As a preliminary it is necessary to make check of the possibility of attaining a speed  $\lambda'_1$  at entrance into cascade.

For such an evaluation it is necessary to know  $\beta_{2,p}$ . We assume  $\beta_{2,p} = 36^\circ 50'$ . Then during a supersonic speed at exit of cascade  $q_{2a} = \sin \beta_{2,p} = 0.6$ . Consequently, before the cascade a supersonic speed is unattainable, since the point B is found in the region limited by dotted curve  $\beta_{2,p} = 36^\circ 50'$ .

The hodograph 1 can be used also for an approximate calculation of angles of flow deviation in nozzle section both in guide and also rotating cascades.

For this purpose as a preliminary from equation of continuity (8-56) during an absence of losses ( $\epsilon_1 = 1$ ) we obtain:

$$q_2 = q_1 \frac{\sin \beta_1}{\sin \beta_2},$$

whence

$$\delta = \beta_2 - \beta_{2,p} = \arcsin \left( \frac{q_1}{q_2} \sin \beta_1 \right) - \beta_{2,p}.$$

In considering that at  $p_2 = p_1$  and  $q_2 = q_1$ , the angle of deflection of flow is equal to  $\delta = \beta_1 - \beta_{2,p}$ , we reach the conclusion that  $\beta_1 = \beta_2$ .

At  $\beta_1 = \beta_2 - \delta = 0 = 0$  and, consequently, at any supersonic speed of the incident flow a deflection in nozzle section does not occur. In the case, when  $\beta_1 < \beta_{2,p} < 0$ , i.e., in nozzle section, a contraction occurs instead of an expansion. An analogous conclusion can be reached also in the analysis of flow in the plane of hodograph.

Such behavior of a supersonic flow in impulse cascades is associated with the fact that at supersonic speeds perturbations are not propagated against the flow and the pressure before the cascade  $p_1$  may be selected arbitrarily. This condition is disturbed only in "cutoff" modes i.e., in the case when vector  $\lambda'_1$  lies in region, limited by the dotted curve  $q_{2a} = \sin \beta_{2,p}$ .

Thus, prior to the arrival of "cutoff" modes the exit flow angle from cascade can be determined by the value  $\lambda_2 = f(p_2/p_{2i})$  in the basic family of curves  $q_2 = \text{const}$ , in which  $\beta_2$  is independent of the geometric parameters of cascade and the Mach number. In "cutoff" modes the vector  $\lambda_2$  is found inside region bounded by the dotted curve  $q_2 = \text{const}$ ; angle of exit is determined by  $\lambda_2$  on the curve  $q_2 = \sin \beta_{2,b}$ , i.e. it depends on geometric parameters of the cascades.

In Fig. 8-61 there are presented the design curves of the dependence of exit flow angle from cascade on  $\beta_1$  and  $M_{2t}$  at  $\beta_{2,b} = 18^\circ 20'$  and  $M_{lp} = M_{2t}$ , where  $M_{lp}$  is the design value of M number for inlet nozzle. On the graph there have been plotted also experimental points, obtained at  $M_{2t} = 1.62$ . There may be noted a satisfactory agreement between the calculation and the experiment.

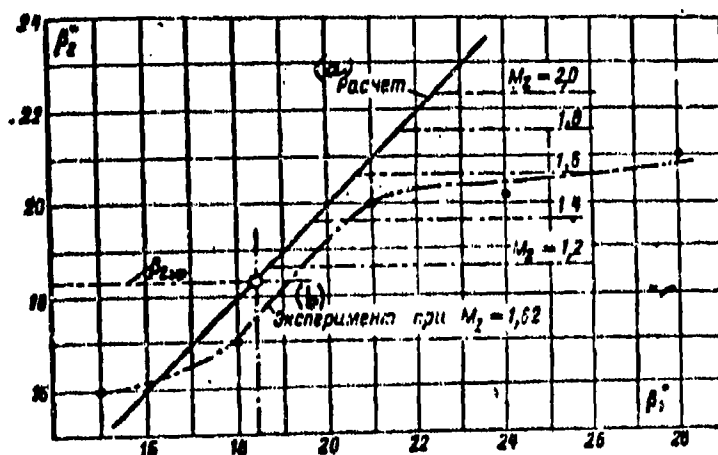


Fig. 8-61. Dependence of exit flow angle  $\beta_2$  from impulse cascade on  $\beta_1$  at  $M_{2t} = M_{2p}$  and  $\beta_{2,b} = 18^\circ 20'$ . KEY: a) Calculation; b) Experiment at  $M_2 = 1.62$ .

#### 8-14. Profiling and Results of Experimental Investigation of Impulse Cascades during High Speeds

The designing and manufacturing of cascades profiles for transonic and supersonic speeds are realized experimentally. Experience shows that supersonic impulse cascades have small losses only in the case, when at entrance into cascade flow is stagnated down to low supersonic speeds. We discuss two possible methods of profiling of supersonic impulse cascades with the deceleration of flow at entrance.

First method consists in the fact that the deceleration is controlled in entrance

sector of back edge of profile. For this purpose the entrance sector of back edge is made concave for a smooth deceleration of the supersonic flow (with the possible formation of an isolated curvilinear shock) or with angular breaks for a stepwise deceleration\* in a system of diagonal shocks.

The second method is based on decelerating flow in curvilinear or diagonal shocks, organized in entrance section of channel. Here the entrance section of back

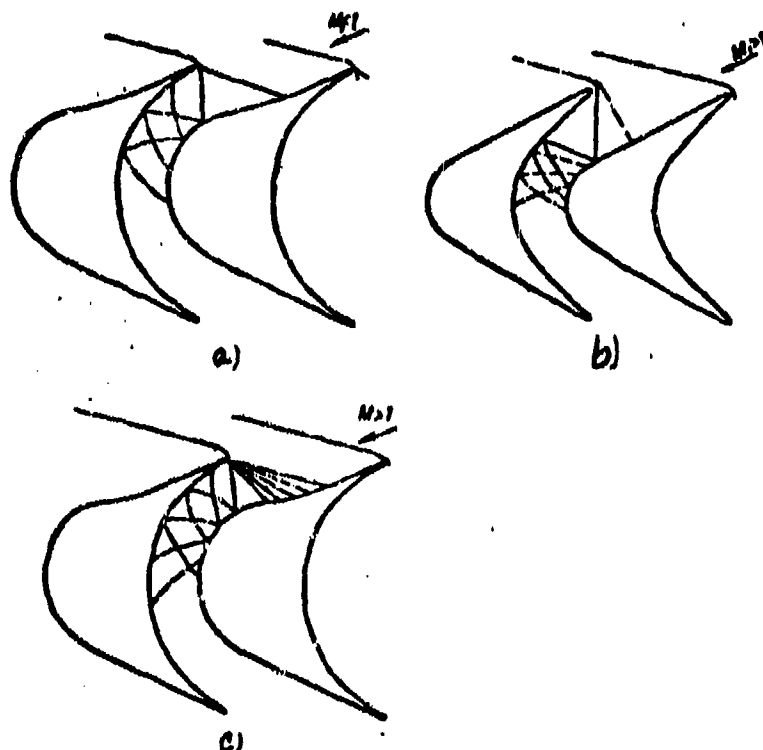


Fig. 8-62. Schematic diagram of active supersonic cascades.

a--with stepwise deceleration at entrance; b--with smooth deceleration along back edges at entrance; c--with deceleration in diagonal or normal shocks on concave surface.

edge is made rectilinear or with a very small curvature, and the design angle of leading edge is selected in such a way that deceleration of the flow occurs in the shock, developing from side of concave surface.

At small supersonic speeds ( $M_1 < 1.25$ ) losses in a normal shock are small

\*See Chapter 4.

(1-1.5%). Losses with an expansion of the flow in nozzle section also can be reduced to a minimum. Therefore the intervane channel of cascade, operating at low supersonic speeds, can be designed as contracting in such a manner that ahead of it a normal "cutoff" shock generates. At high supersonic speeds it is expedient that the intervane channel is made convergent-divergent.

The possible shapes of profiles and channels of active supersonic cascades are shown in Fig. 8-62.

As a theoretical analysis shows even in an intervane channel of relatively great curvature it is possible to avoid formation of compression waves. This conclusion is corroborated also by experimental data.

In Figs. 8-63a-d, there are presented a schematic diagram and photographs of spectra of flow around an TR-2A impulse cascade\* by a supersonic flow. Ahead of a thick leading edge there appears the shock wave 1. At entrance edge and on back edge of profile the flow is accelerated in waves of rarefaction. The waves of rarefaction terminate in shock 2 which in combination with shock 1 forms the bow  $\lambda$ -shaped shock. At point A there is observed a separation of the boundary layer, the  $\lambda$ -shaped bow shock causes a discontinuity in the boundary of vortex zone at point B. However the separation of boundary layer is maintained up to exit section of intervane channel, where boundary of vortex zone and the concave surface of profile will form hypothetical channel of practically constant width. At the place where an edge shock occurs on back edge there occurs a local separation of boundary layer owing to the curvature of back edge; after the shock (point C) the flow is accelerated. In approaching the trailing edge there will form the isolated shock wave 3. After the edge, there appears a second edge shock 5. Both shocks merge into one  $\lambda$ -shaped shock.

In cascades of group A at supersonic speeds there occur additional losses: in

---

\*Cascades in group A have been designed for a flow-around by a flow of subsonic speeds.

the compression waves at entrance, in vortex zone, forming as a consequence of separation of boundary layer after shock 2, in the edge and reflected shocks 4 and in the  $\lambda$ -shaped shock. With an increase of speed these losses intensively increase.

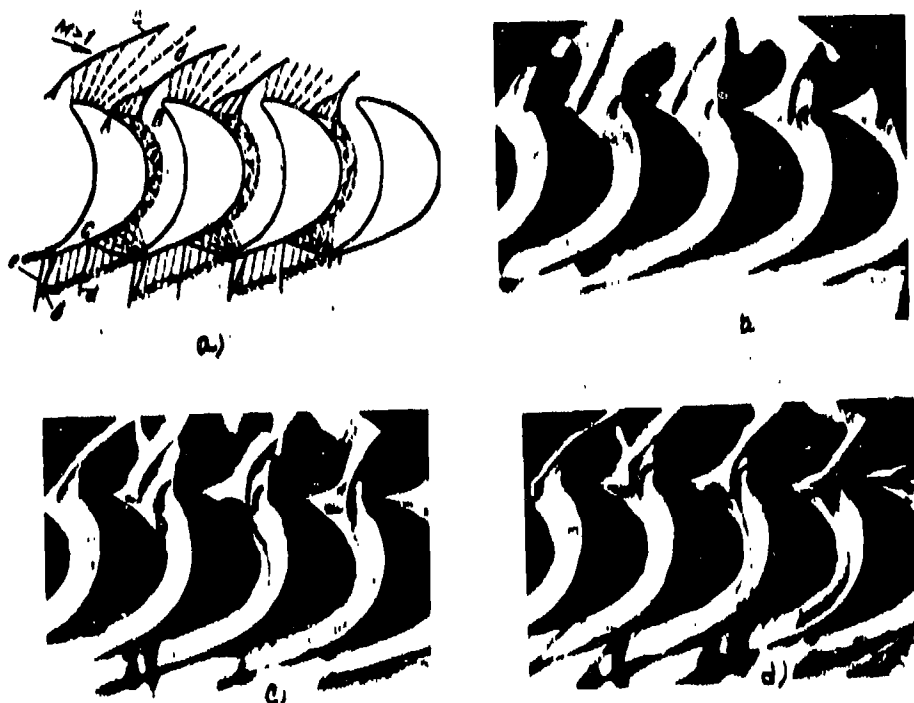


Fig. 8-63. a-schematic diagram of shocks 1-5 and points A, B, C; Figs. 8-63-b - 8-63d-photographs of spectra of air flow in TR-2A impulse cascade; b- $M_1 = 1.205$ ; c- $M_1 = 1.395$ ; d- $M_1 = 1.1635$ .

Cascades of group B, developed at Moscow Power-Engineering Institute for transonic speeds, are characterized by smaller thickness of leading edge and curvature of back edge in entrance section and nozzle section. In these cascades before leading edge there develops a curvilinear shock a (Fig. 8-64) of lesser intensity. On the curvilinear surface of back edge (terminating A) there occurs an intense acceleration of the flow. The shock enclosing the zone of expansion is located inside channel (channel No 1 in Fig. 8-64). In case the re-expansion is small, the stagnation occurs only in the forward shock (at point B, channel No. 2 in

Fig. 8-64).

With a great constriction of the channel ahead of it (not ahead of edge) there appears a shock wave ("cutoff" mode, channel No. 3 in Fig. 8-64). Such a location of the shock assures a stable subsonic flow in the intervane channel. If by profiling the exit section of back edge small losses are added during an expansion of the flow in nozzle section, then such a cascade may be found to be highly economical up to  $M_1 \approx 1.25$  numbers.

In Fig. 8-65 curves of losses in cascades of groups A and B are presented. At  $M_2 \leq 0.95$  losses in a TR-1A cascade are lower than in cascades of group B. However at  $M_2 > 1$  losses in the TP-1A cascade sharply increase; in cascades of group B at  $M_2 \geq 0.95$  to 1.25 the losses are lower.

Value of critical  $M_{2*}$  number for a cascade of group B in all cases is higher than for a cascade of type A.

In a TR-2B cascade the decrease in losses occurs up to  $M_2 = 1.0$ . However, at  $M_2 > 1.1$  there is observed a more intensive increase of losses, than in the TR-1B cascade. This is caused by the greater curvature of back edge of profile of TR-2B in nozzle section.



Fig. 8-64. Schematic diagram of supersonic flow in cascades of group B.

In Fig. 8-66 there are presented curves of the pressure distributions about the profile of a TR-IV cascade at the Moscow Power-Engineering Institute for supersonic speeds by decelerating the flow in oblique shock, developing inside channel from direction of concave surface. The intervane channel of the cascade is a convergent-divergent channel. The minimum section is located in entrance section (points 8 and 7 and 13-14).



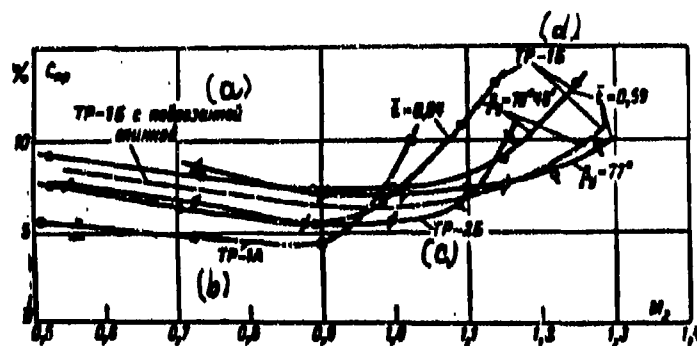


Fig. 8-65. The relationship between profile losses in cascades of groups A and B on the  $M_1$  numbers.

KEY: (a) TR-1B with a truncated back edge; (b) TR-1A; (c) TR-2B; (d) TR-1B.

The stagnation of the flow occurs ahead of entrance section of channel (point 10-12). At  $M_1 > 1.0$  before channel there generates a normal shock which with an increase in  $M_1$  number approaches the entrance section.

At  $M_1 > 1.5$  the bow shocks enter into the intervane channel and the deceleration occurs in a system of diagonal shocks; in the channel the flow is accelerated, where in some of minimum section on back edge of profile there is detected a deep rarefaction. With an increase of  $M_1$  the minimum pressure decreases, and the beginning of diffuser section is displaced along the flow.

In Fig. 8-67 there are shown spectra of the flow around cascades of group B. It is characteristic that at fairly sufficient large  $M_1$  numbers, speeds in the intervane channels are supersonic, but shock waves are absent, despite the greater curvature of the channels. In entrance section of profile, before edge, there will form a system of forward shocks.

In case the cascade is designed by the method of stepwise deceleration of flow along back edge of profile (system of diagonal-normal shocks), at high supersonic speeds there will form two shocks one of which is located at place of discontinuity (Fig. 8-67,b). In Fig. 8-68 there is given a comparison of losses in impulse cascades, designed by the method of decelerating flow along back edge of profile and by method of decelerating in oblique shock on concave surface. It is possible to note that first method makes it possible to attain somewhat the better

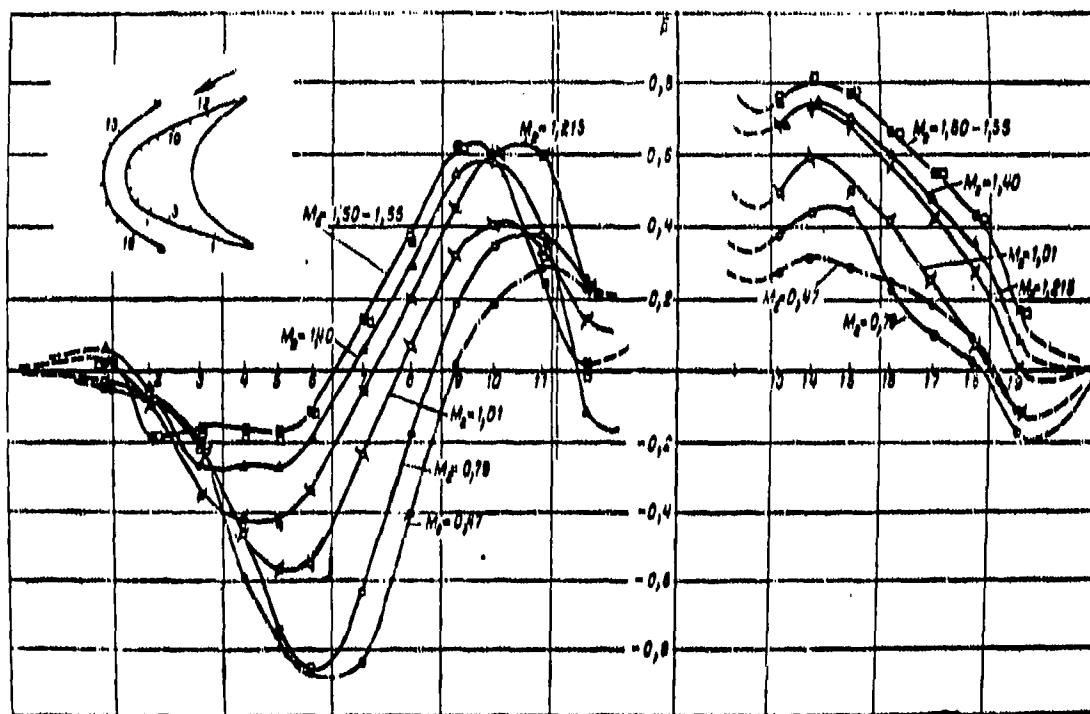


Fig. 8-66. Distribution of pressures about profile TR-IV (convergent-divergent channels) in cascade.

$t = 0.575$ ;  $\beta_y = 89^\circ 05'$ ;  $\beta_1 = 20^\circ$ .

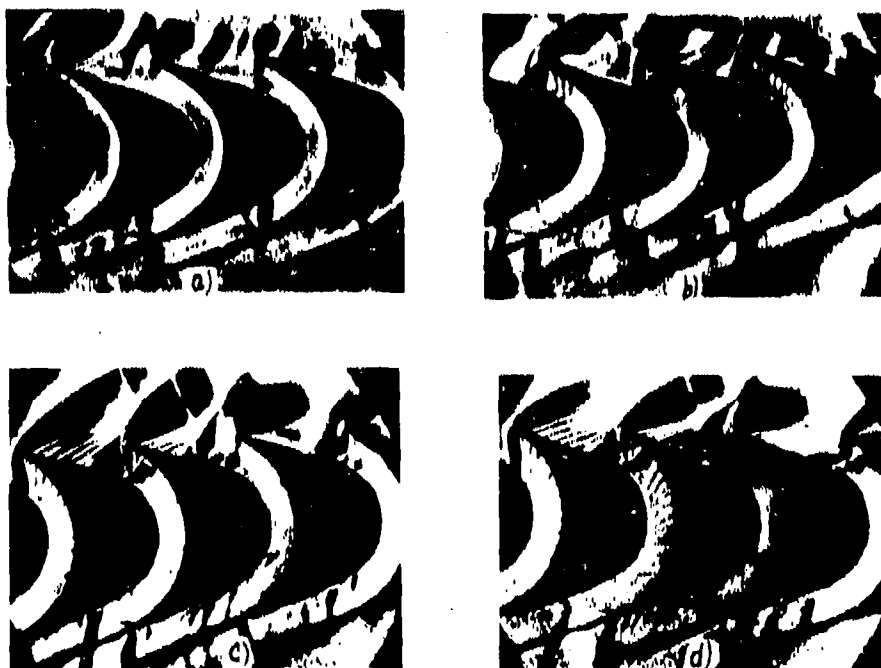


Fig. 8-67. I--spectra of air flow in cascade with convergent-divergent channels (TR-IV);  $t = 0.575$ ;  $\beta_y = 89^\circ 05'$ ;  $\beta_1 = 18^\circ$ ; a-- $M_1 = 1.34$ ; b-- $M_1 = 1.64$ ; II--spectra of air flow in cascade with stepwise deceleration at entrance;  $t = 0.625$ ;  $\beta = 90^\circ$ ;  $\beta_1 = 22^\circ 30'$ ; c-- $M_1 = 1.47$ ; d-- $M_1 = 1.67$ .

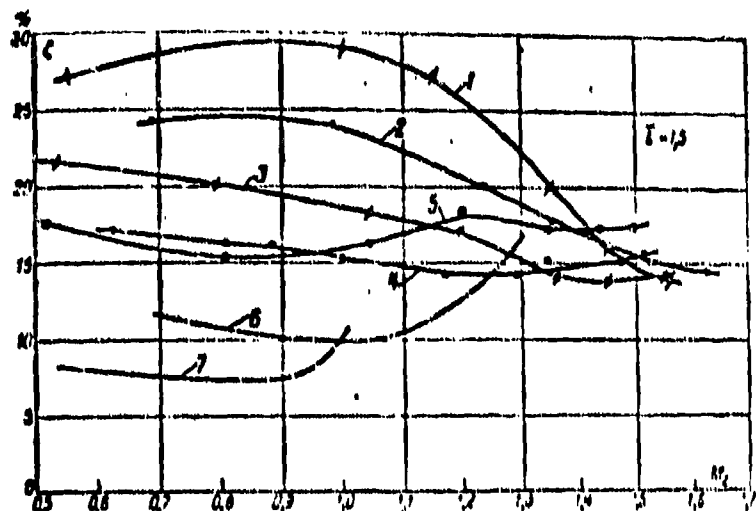


Fig. 8-68. Comparison of characteristics of supersonic impulse cascades of different types.  
1, 2, 3, 4—cascades with convergent-divergent channels;  
1, 3—with deceleration in entrance shocks; 5—with constant section of channel; 6—TR-1B; 7—TR-1A.

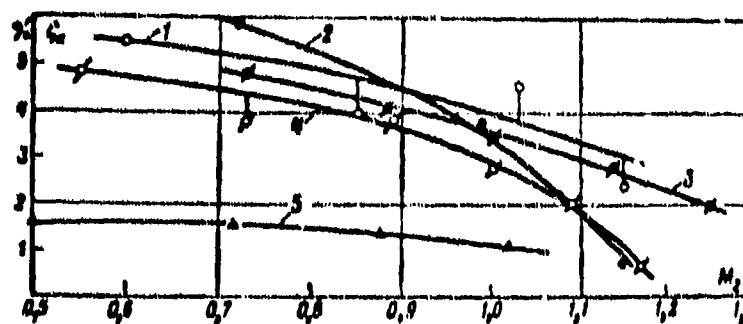


Fig. 8-69. Relationship between end losses in cascades and  $M_2$  number.  
1—TR-1B at  $\beta_1 = 18^\circ$ ; 2—TR-1B at  $\beta_1 = 21^\circ$ ; 3—TR-1B-1 at  $\beta_1 = 18^\circ$ ; 4—TR-2B at  $\beta_1 = 24^\circ$ ; 5—TS-1A at  $\beta_1 = 90^\circ$ .

characteristics of a cascade at  $M_2 > 1.3$  (by 1 to 2.5%). However, this conclusion is made on the basis of a limited amount of experimental data.

Experiments show that at transonic and supersonic speeds end losses for all cascades greatly decrease (Fig. 8-69). Also the nonuniformity of exit flow angles decrease according to the height of the cascades.

## CHAPTER 9

### FLOW OF GAS IN A TURBOMACHINE STAGE

#### 9-1. Fundamental Equations

In a turbomachine stage there occurs a conversion of the potential energy of gas into mechanical work (turbine) or mechanical work into potential energy of gas (compressor). In both cases, flow of gas makes an energy exchange with the environment.

We shall consider the scheme in principle of a turbine stage with an axial flow of gas. In Fig. 9-1 there are shown the basic elements of such a stage. Through inlet duct 1 gas is supplied to stationary guide row 2, where part of its potential energy will be converted into kinetic energy. Acquiring in the guide row significant speeds, the flow of gas passes through clearance 3 and impinges on moving blades 4, fastened on wheel 5. Here there occurs a transfer of energy to rotor of turbine.

With the radii  $r$  and  $r+dr$  we draw two cylindrical sections, the axis of which will coincide with axis of turbine. By these sections we shall divide the elementary stage of turbine; developing it into a plane (Fig. 9-2,a), it is possible to trace character of change of speeds in the flow part of stage.\*

We shall introduce, in distinction from preceding, the following designations

---

\*The guide and moving rows of the stage will be called the flow part.

of speeds:

$c$ —speed of absolute motion of gas;

$w$ —speed of gas in relative motion;

$u$ —speed of migratory motion (peripheral speed);

$c_u$  and  $w_u$ —projections of speeds of absolute and relative flows onto direction of speed  $u$ ;

$c_a$ ,  $w_a$ —projections of speeds of absolute and relative flows onto direction of axis of rotation;

$c_r$ ,  $w_r$ —radial components of speeds of absolute and relative flows.

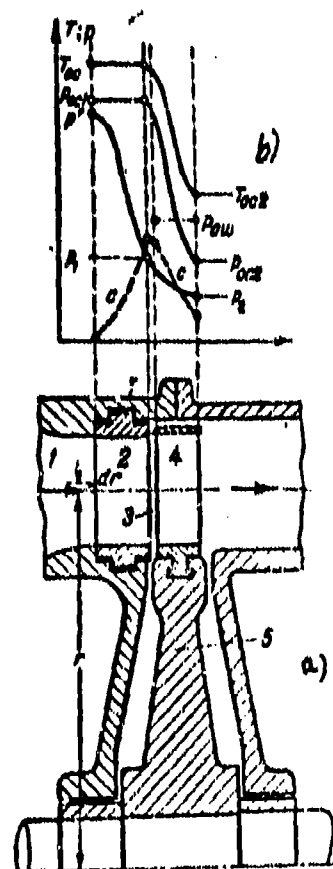


Fig. 9-1. Schematic diagram of turbine stage in an axial flow of gas (a) and distribution of parameters of stagnation, static pressures and speeds in flow part (b).

The subscript 1 designates speeds referring to entry to, and the subscript 2 to

exit from moving blades.

The operation of turbine stage can be traced by Figs. 9-1 and 9-2. In the vane channels of guide row, the flow of gas accelerates and simultaneously turns, leaving it with a speed  $c_1$  directed at an angle  $\alpha_1$  to axis of row (Fig. 9-2,a). The potential energy of gas is transformed into the kinetic energy of flow.

Onto moving blades the flow enters with a relative velocity  $w_1$ , which readily is obtained, after constructing the entry triangle of speeds.

In the vane channels of moving row there occurs a turn of the flow in the relative motion; in this connection, the forces of gas pressure gas produces work

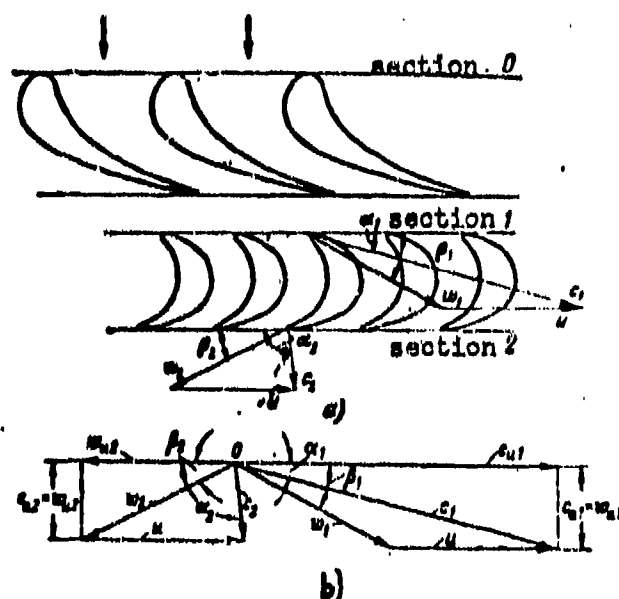


Fig. 9-2. Development of flow portion (a) and triangles of speeds of axial stage (b).

of rotation of turbine rotor. The flow emerges from moving blades with a relative velocity  $w_2$  at an angle  $\beta_2$  to axis of grid. Knowing the peripheral speed  $u$  it is easy to construct the exit triangle of speeds and to determine speed of the absolute flow at exit of stage  $c_2$  (Fig. 9-2,a). Frequently the entry and exit triangles of speeds are expressed from one pole, as is indicated in Fig. 9-2,b.

Thus, energy of gas is transmitted to rotor of turbine owing to the fact that the forces of pressure during turning of flow on the blades produce the work of rotation of rotor. As a result temperature and pressure of stagnation of absolute

flow decreases so that

$$T_{ac1} > T_{ac2}$$

and

$$P_{ac1} > P_{ac2}$$

A characteristic peculiarity of the considered process is its multistage character: the potential energy at first is transformed into the kinetic energy of moving gas, and then on the moving wheel the kinetic energy will be converted into mechanical work. Such process in pure form takes place in an active stage: the static pressures at entry and exit of moving row are approximately identical, and the speeds  $w_1$  and  $w_2$  differ only on account of the losses in moving row.

In a purely reaction stage both components of the process proceed simultaneously on the moving wheel. The flow of gas in the moving channels, in the relative motion is accelerated and simultaneously realizes the work of rotating the rotor. Widely used are intermediate types of stages, in which rationally there are combined both principles--the active and reactive. In this case conversion of potential energy of gas into kinetic is realized partially in the stationary row and partially in the moving channels.

The change in static parameters of flow and of parameters of stagnation in flow part of such a stage is shown in Fig. 9-1,b.

The stage may be realized also with a radial flow of gas. In such a stage the gas moves in radial planes from the axis of rotation to periphery or, conversely, to axis of rotation. The radial stage can be of active, reactive, or intermediate type.

Diagrams of the flow parts of stages of turbine with radial flow of gas are shown in Fig. 9-3. In radial section there are evident the shapes of profiles of the guide and moving rows of the stage and triangles of speeds at entry and exit of moving channels. We note that in radial stage the peripheral speed varies from entry to exit section of row.

In certain stages the flow of gas is directed at an angle to the axis of rotation. The radial components of the speed  $c_r$  are not equal to zero and in a analysis of properties of the flow must be considered (Fig. 9-4).

In a compressor stage (axial or centrifugal) there occurs a transformation of mechanical work into potential energy of the gas. Channels of the moving row 1 of the

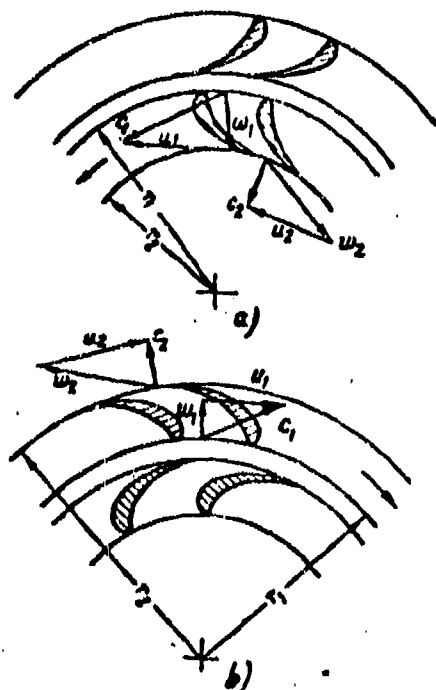


Fig. 9-3. Diagram of centrifugal (a) and centripetal (b) radial stages of turbines.

axial compressor are expanding channels (Fig. 9-5). The pressure of gas in the relative motion increases, and the speed decreases. This process is continued in stator 2. The enthalpy of total stagnation in the absolute motion increases.

In the centrifugal compressor stage the motion of gas is realized from center to periphery (Fig. 9-6); the moving blades of wheel 1 form expanding channels in which there occurs a stagnation of the relative flow. The compression of the gas can be continued in the vaned diffuser 2.

In an accurate posing of problem the flow of gas in a turbomachine stage is described by differential equations of the three dimensional flow of a viscous compressible fluid. Approximate solutions are based on equations of an ideal



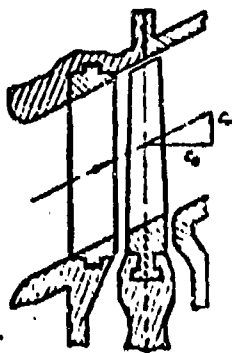


Fig. 9-4. Diagram of diagonal stage.

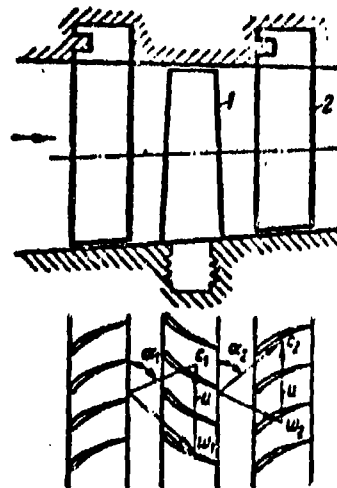


Fig. 9-5. Diagram and development of flow part of axial compressor stage.

compressible fluid, derived in Chapter 1.

The initial equations (conservation of momentum, continuity and energy) are expediently written in a cylindrical system of coordinates. As the independent variables, as previously, there are selected: radius-vector  $r$ , the vectorial angle  $\Theta$ , and the  $z$  axis. The direction of axis  $x$  coincides with axis of rotation of turbine. Then the system of equations of conservation in absolute steady motion

$$(\partial p / \partial t = \partial c_r / \partial t = \partial c_\theta / \partial t = \partial c_z / \partial t = 0)$$

at  $R=0=Z=0$  reduces to equations (1-14) and (1-17a).

For investigation of flow in moving row, the fundamental equations of ideal fluid expediently are written for the relative motion. Here there are used the evident relationships (Fig. 9-2):

$$w_a = c_a; w_r = c_r; \text{ and } w_\theta = c_\theta - u = c_\theta - \omega r,$$

where  $\omega$  is the angular velocity of rotation of moving row.

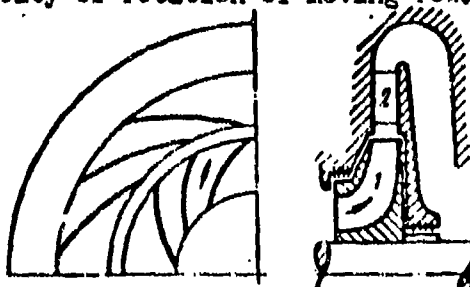


Fig. 9-6. Diagram of centrifugal compressor stage.

After substituting these relationships in equation (1-17a) for steady relative motion we obtain:

$$\left. \begin{aligned} \omega_r \frac{\partial \omega_r}{\partial r} + \frac{\omega_u}{r} \frac{\partial \omega_r}{\partial \theta} + \omega_a \frac{\partial \omega_r}{\partial z} - \frac{\omega_u^2}{r} - \\ - \omega^2 r + 2\omega\omega_u = -\frac{1}{\rho} \frac{\partial p}{\partial r}; \\ \omega_r \frac{\partial \omega_u}{\partial r} + \frac{\omega_u}{r} \frac{\partial \omega_u}{\partial \theta} + \omega_u \frac{\partial \omega_u}{\partial z} + \\ + \frac{\omega_r \omega_u}{r} + 2\omega\omega_r = -\frac{1}{\rho r} \frac{\partial p}{\partial \theta}; \\ \omega_r \frac{\partial \omega_a}{\partial r} + \frac{\omega_u}{r} \frac{\partial \omega_a}{\partial \theta} + \omega_a \frac{\partial \omega_a}{\partial z} = \\ = -\frac{1}{\rho} \frac{\partial p}{\partial z}. \end{aligned} \right\} \quad (9-1)$$

Differential equation of continuity for a steady relative flow has the form:

$$\frac{\partial(\rho\omega_r)}{\partial r} + \frac{1}{r} \frac{\partial(\rho\omega_u)}{\partial \theta} + \frac{\partial(\rho\omega_a)}{\partial z} = 0. \quad (9-2)$$

System of equations of motion (1-17a) and (1-14) or (9-1) and (9-2) is supplemented by conservation of energy and isentropic process equations. The system of equations determining the three-dimensional steady motion of an ideal compressible fluid in a turbomachine stage is closed.

We turn now to the derivation of equation of energy for stream of gas in the flow part of stage. The equation of energy can be written in parameters of absolute or relative motion. In first case in equation of energy there are introduced terms, considering the energy exchange between flow and the environment. In second case (for a relative flow) it is necessary to consider additional forces, the introduction of which makes it possible to consider the relative motion as if it were absolute. Such additional forces are the Coriolis force of inertia and centrifugal force.

The equation of energy for absolute flow we shall write in the form of the first law of thermodynamics. Taking into account the assumptions made we obtain:

$$di + cdc - g dL_r = 0. \quad (9-3)$$

Here  $L_r$  is the work being done by the gas.

The magnitude  $L_r$  can be determined by means of the equation of moments of momentum. Moment of forces acting on the moving blades during a steady motion

will be:

$$M_u = \frac{G}{g} (c_2 \cos \alpha_2 r_2 - c_1 \cos \alpha_1 r_1),$$

where  $G$  is the flow of gas through the row per second.

Multiplying  $M_u$  by angular velocity of rotation of row  $\omega$ , we shall find the work or power per second which the blades exchange with the gas flow:

$$M_u \omega = \frac{G}{g} (c_2 u_2 \cos \alpha_2 - c_1 u_1 \cos \alpha_1).$$

Consequently, the work relating to weight of flowing gas is equal to:

$$L_r = \frac{1}{g} (c_2 u_2 - c_1 u_1). \quad (9-4)$$

Equation (9-4) was obtained by Euler. In differential form, the Euler equation is:

$$dL_r = \frac{1}{g} d(c_u u). \quad (9-5)$$

Since in a turbine the gas performs work, then along stream of absolute flow  $d(c_u u) < 0$ . For a compressor stage expression of the external work is analogous, but in this case  $d(c_u u) > 0$ . Using expressions (9-3) and (9-5), we obtain the differential equation of energy for the flow in absolute motion:

$$di + cdc - d(c_u u) = 0. \quad (9-6)$$

In accordance with the law of conservation of energy the change of kinetic and internal energy of gas in the relative motion is equal to the amount of supplied (or diverted) heat and to work of actual and secondary forces. Since the Coriolis force of inertia is directed normal to axis of stream in the relative motion (to vector  $w$ ), then the work of this force is equal to zero.

Thus, of the number of secondary forces in the equation of energy for a flow of gas in relative motion, it is necessary to introduce the centrifugal force, directed along a radius normal to axis of rotation. In the particular case of an axial stage, the vector of centrifugal force is normal to lines of flow, and work of centrifugal forces also is equal to zero.

Equation of energy for a flow in relative motion is obtained on the basis of first law of thermodynamics (9-3).

Considering that  $c^2 = c_r^2 + c_a^2 + c_u^2$  and using the connection between absolute and relative velocities, we transform expression (9-6). We obtain:

$$dl + wdw - udu = 0. \quad (9-7)$$

The integration of equation of energy (9-6) for a flow in absolute motion gives:

$$l + \frac{c^2}{2} - c_u u = \text{const.} \quad (9-8)$$

The integral of equation of energy of flow in a relative motion (9-7) is equal to:

$$l + \frac{w^2 - u^2}{2} = \text{const.} \quad (9-9)$$

The transition from equation (9-8) to equation (9-9), obviously, is made by means of formula (Fig. 9-2, b)

$$w^2 = c^2 + u^2 - 2c_u u. \quad (9-10)$$

The obtained equations for the relative motion can be used for calculating the stage of not only a turbine, but also of other turbomachines (compressor, fan). The direction of the energy exchange (removal or supply of mechanical work) is not important. This remark is entirely valid only on the assumption of an isentropic flow in a turbomachine stage. Under actual conditions the motion of the gas is accompanied by losses. The direction of the energy exchange considerably affects structure of flow (the nature of distribution of parameters in flow part) and, consequently, the efficiency of the stage.

In the absence of losses, the change of state of gas in the absolute and relative motion is subject to the isentropic law, which for an ideal gas can be represented by formula  $p/p^* = \text{const.}$

In this case, integrals of equations of momentum and energy coincide. Indeed, for a one-dimensional flow in the absolute motion the equation of momentum has the form:

$$c dc + \frac{dp}{\rho} - d(c_u u) = 0. \quad (9-11)$$

Considering relative motion of gas in the stage as steady, we shall write the equation of momentum in such a form:

$$w dw + \frac{dp}{\rho} - r \omega^2 \cos(r, x) dx = 0,$$

where  $r\omega^2 \cos(r \cdot x) dx$  is the impulse of centrifugal forces.

Since  $r\omega = u$ , then

$$u du + \frac{dp}{\rho} - u du = 0. \quad (9-12)$$

Integrals of equations (9-11) and (9-12) coincide with equations (9-8) and (9-9), if  $di = dp/\rho$ , which corresponds to an isentropic process.

Equations of momentum for absolute and relative motions taking into account losses can be obtained by introducing in (9-11) and (9-12) the impulse of forces of friction; in this case  $i$ ,  $c$  and  $w$  also are parameters of the actual flow.

In investigating a stage within frameworks of a simplified one-dimensional diagram of the flow there is used equation of continuity:

$$m = F_c \rho c = F_w \rho w = F_w q_w \rho_w a_{w,c} = F_c q_c \rho_c a_{c,c},$$

where  $F_c$ —area of section, normal to vector of speed  $c$ ;

$F_w$ —area section, normal to vector of relative speed  $w$ ;

$q_c$  and  $q_w$ —are the reduced flows during absolute and relative motions.

From the equation of continuity we find:

$$\frac{F_c}{F_w} = \frac{w}{c} = \frac{q_w}{q_c} \cdot \frac{\rho_w}{\rho_c} \cdot \frac{a_{w,c}}{a_{c,c}},$$

where  $\rho_c$ ,  $\rho_w$ ,  $a_{c,c}$ ,  $a_{w,c}$  are the critical densities and speeds for absolute and relative flows.

Obviously, the static parameters  $\rho$ ,  $p$ ,  $T$  both in the absolute and also in the relative motions are identical.

The actual process of motion of gas in flow part of stage has a number of peculiarities not considered by the above derived equations. Thus, the flow of gas in the clearance between guide and moving rows possesses nonuniformity. In the moving channels, receiving the flow from the clearance, flow of gas turns out to be periodically non-stationary, with continuous pulsation of the speeds and pressures.

In addition, the flow realizes a heat exchange with the environment in connection with unproductive losses of heat and owing to the arranged artificial cooling of blades subjected to high loads. In equation of energy this peculiarity can be

considered by the introduction of an appropriate term which takes into account the external heat exchange.

In the motion in the flow part, the main flow branches; a certain quantity of gas, unpassing through the moving row, flows into clearances between stator and rotor. Depending upon distribution of the pressures in flow part there may occur a suction of the gas through the clearances into main flow.

Thus, in the general case, the flow of gas in a stage is subjected to different external effects exerting an influence on process of conversion of energy. An evaluation of these influences is made on the basis of experimental data.

## 9-2. Parameters of Flow in Absolute and Relative Motions. One-dimensional Flow Diagram.

The magnitude of the right-hand constant in energy equations (9-8) and (9-9)

$$\frac{c^2}{2} - c_a u + i = \frac{w^2 - u^2}{2} + i = \text{const} \quad (9-13)$$

can be determined from boundary conditions.

In calculating the stage of a turbine usually there are known the parameters of flow at entry to rotor wheel. For the entry we have:

$$\frac{c_1^2}{2} - c_{a1} u_1 + i_1 = \frac{w_1^2 - u_1^2}{2} + i_1 = \text{const.}$$

Designating, as before,

$$\frac{c^2}{2} + i = i_{oc}, \quad (9-14)$$

where  $i_{oc}$  is the enthalpy of a total isentropic stagnation in an arbitrary section of flow in absolute motion, we write (9-13) as

$$\frac{c^2}{2} - c_a u + i = i_{oc1} - c_{a1} u_1, \quad (9-15)$$

or for a perfect gas:

$$\frac{c^2}{2c_p} - \frac{c_a u}{c_p} + T = T_{oc1} - \frac{c_{a1} u_1}{c_p}, \quad (9-15a)$$

where  $i_{oc1}$ ,  $T_{oc1}$  are the enthalpy and temperature of the isentropic stagnation at entry into rotor wheel in the absolute motion.

On the other hand, during total isentropic stagnation of flow in

relative motion, its kinetic energy reversibly changes into heat. The enthalpy of stagnation is determined by the obvious equation

$$\frac{w^2}{2} + i = i_{ow}. \quad (9-16)$$

Consequently, equation of energy acquires the form:

$$\frac{w^2 - u^2}{2} + i = i_{owl} - \frac{u_1^2}{2}, \quad (9-17)$$

where  $i_{owl}$  is the enthalpy of total stagnation of relative flow at entry to rotor wheel.

Let us note that if the flow at entry is not swirling and  $c_{u1} = 0$ , then from (9-15) it follows

$$\frac{c^2}{2} - c_u u + i = i_{oe} - c_u u = i_{owl}.$$

Such a case can take place only for a purely reaction stage or for a centrifugal compressor stage.

Taking into account expressions (9-14) and (9-16) equation (9-13) can be written as:

$$i_{oe} - c_u u = i_{ow} - \frac{u^2}{2}. \quad (9-18)$$

The connection between  $i_{owl}$ ,  $i_{owl}$ ,  $i_{oe}$  and  $i_{ow}$  can be presented in the form:

$$i_{owl} = i_{owl} - \frac{c_1^2 - w_1^2}{2}; \quad (9-19)$$

$$i_{oe} = i_{oe} - \frac{c^2 - w^2}{2}. \quad (9-19a)$$

Correspondingly we obtain dependence between temperatures of stagnation in absolute and relative flows:

$$T_{oe} - \frac{c_u^2}{c_p} = T_{owl} - \frac{c_{u1}^2}{c_p} = T_{ow} - \frac{u^2}{2c_p} = T_{owl} - \frac{u_1^2}{2c_p}. \quad (9-20)$$

Equation (9-20) shows that temperature of stagnation in the general case is variable along the stream not only for the absolute, but also for relative motion. We shall present (9-20) in a somewhat different form:

$$\frac{T_{ow}}{T_{owl}} = 1 - \frac{u_1^2 - u^2}{2c_p T_{owl}}; \quad (9-20a)$$

$$\frac{T_{oe}}{T_{owl}} = 1 - \frac{c_{u1}^2 - c_u^2}{c_p T_{owl}}. \quad (9-20b)$$

The difference between temperatures of stagnation

$$T_{oc} - T_{ow} = \frac{c^2 - w^2}{2c_p} = \frac{(2c_u - u)u}{2c_p}. \quad (9-21)$$

From equation (9-20a) it follows that temperature of stagnation of relative flow changes corresponding to a change of peripheral speed along the tube of flow. At  $u = \text{const}$ , temperature  $T_{ow}$  is constant. On this basis it may be concluded that the temperature of stagnation  $T_{ow}$  is constant in a stage with an axial flow of gas. In a radial stage  $T_{ow}$  along the tube of flow changes. If in such a stage the flow is directed from the axis of rotation to the periphery, then  $T_{ow}$  increases. In the case when flow moves towards the axis of rotation,  $T_{ow}$  decreases.

The obtained result has a simple physical explanation.

The total energy of the relative flow, proportional to  $T_{ow}$ , varies owing to the work of centrifugal forces, into the field of which the gas moves. If the radial components of the speed are not equal to zero ( $c_r = w_r \neq 0$ ) and stream of gas moves not only along axis of rotation, but also radially, then centrifugal forces perform the work of displacing the particles in a radial direction and increase or decrease the total energy of particle depending upon direction of flow. If the direction of relative flow coincides with direction of the centrifugal forces (radial stage with flow of gas towards periphery), then  $T_{ow}$  increases. Otherwise (radial stage with flow of gas towards axis of rotation) the total energy decreases.

Formula (9-20b) shows that temperature of stagnation in the absolute motion in all cases diminishes. From a consideration of the principle of operation of a turbine stage it follows that in arbitrary section of a tube of flow  $c_{u2} < c_{u1}$  and diminishes along the direction of flow, since gas performs work in rotating the wheel.

In the compressor stage, conversely,  $c_{u2} > c_{u1}$  and increases in the direction of flow, since work is supplied to the gas.

We now turn to equation of energy (9-13). We note that the magnitude of the constant on the right-hand side of equation (9-13) is different for different streams,



since  $c_{ul}$  may change during transition from one stream to another. Hence, we conclude that, strictly speaking, the equation of energy must be used individually for each stream. For the channel as a whole, equation (9-13) can be used, if all the magnitudes entering into this equation are calculated as averages along the section of channel.

To the equation of energy in a relative motion it is possible to ascribe the well-known form, replacing  $i$  by the formula

$$i = \frac{k}{k-1} \frac{p}{\rho} = \frac{a^2}{k-1};$$

then according to equation (9-16)

$$\frac{w^2}{2} + \frac{k}{k-1} \frac{p}{\rho} = \frac{k}{k-1} \frac{p_{ow}}{\rho_{ow}} \quad (9-22)$$

or

$$\frac{w^2}{2} + \frac{a^2}{k-1} = \frac{a_{ow}^2}{k-1} \quad (9-22a)$$

where  $p_{ow}$ ,  $\rho_{ow}$ ,  $a_{ow}$  are the pressure, density and speed of sound in an isentropically stagnated relative flow.

We emphasize once again that the speed of sound and static parameters of the flow  $p$ ,  $\rho$  and  $T$  for absolute and relative motions have one and the same magnitude.

The speed of sound of a stagnated relative flow changes along the stream in accordance with change of enthalpy  $i_{ow}$ . With any changes  $i_{ow}$  along stream the sum of the kinetic and potential energy of relative flow in given section by equation (9-16) is equal to  $i_{ow}$ . In a particular case, the speed of relative flow in a certain section can attain the local speed of sound; then

$$w = a = a_{ow}.$$

From equations (9-16) there can be obtained value on right-hand side of the equation of energy in the form:

$$\frac{w^2}{2} + \frac{a^2}{k-1} = \frac{a_{ow}^2}{2} \cdot \frac{k+1}{k-1}. \quad (9-22b)$$

After equating right-hand side of equations (9-22), (9-22a) and (9-22b), we obtain:

$$\begin{aligned} i_{ow} = c_p T_{ow} &= \frac{a_{ow}^2}{k-1} = \frac{a_{ow}^2}{2} \frac{k+1}{k-1} = \frac{k}{k-1} \frac{p_{ow}}{\rho_{ow}} = \\ &= \frac{w_{max}^2}{2} = i_{ow1} - \frac{1}{2} (u_1^2 - u^2). \end{aligned}$$

Analogous transformations for a flow in absolute motion results in the relationship

$$i_{oc} = c_p T_{oc} = \frac{a_{oc}^2}{k-1} = \frac{a_c^2}{2} \frac{k+1}{k-1} = \frac{k}{k-1} \frac{p_{oc}}{\rho_{oc}} =$$

$$= \frac{c_{max}^2}{2} = i_{oc1} - (c_{u1} u_1 - c_u u).$$

By means of these relationships it is simple to obtain an expression for the characteristic speeds  $a_{*0}$ ,  $c_{max}$ ,  $a_{*w}$ , etc. Thus, for example, for relative flow we find:

$$a_{*w} = \sqrt{\frac{2k}{k+1} \frac{p_{ow}}{\rho_{ow}}} =$$

$$= \sqrt{2 \frac{k-1}{k+1} \left[ i_{ow1} - \frac{1}{2} (u_1^2 - u^2) \right]}. \quad (9-23)$$

For an absolute flow

$$a_{*w} = \sqrt{\frac{2k}{k+1} \frac{p_{oc}}{\rho_{oc}}} =$$

$$= \sqrt{2 \frac{k-1}{k+1} \left[ i_{oc1} - (c_{u1} u_1 - c_u u) \right]}. \quad (9-24)$$

From equation (9-24) it follows that characteristics of the absolute flow, depending on magnitude of total energy  $i_{oc}$  (from parameters of stagnation), change along the tube of flow. Consequently,  $a_{*0}$ ,  $c_{max}$ , and  $a_{oc}$  are variable magnitudes for a stream of gas in the absolute motion.

In the relative motion the critical and maximum speeds may change or remain constant depending upon whether or not the peripheral speed  $u$  changes. If along the stream  $u = \text{const}$  (stage with axial flow), then  $i_{ow} = \text{const}$ , and correspondingly  $a_{*w} = \text{const}$  and  $w_{max} = \text{const}$ . With a variable peripheral speed along stream these basic characteristics of the flow of gas change according to the change in  $u$ .

Equation (9-21) makes it possible to establish a connection between temperatures of stagnation in relative and absolute flows in following form:

$$\frac{T_{ow}}{T_{oc}} = 1 - \frac{(2c_u - u)u}{2c_p T_{oc}}.$$

After substituting

$$2c_u u = c^2 + u^2 - w^2,$$

we obtain:

$$\frac{T_{ow}}{T_{oc}} = 1 - \frac{c^2}{2c_p T_{oc}} \left(1 - \frac{w^2}{c^2}\right). \quad (9-25)$$

After substituting (see, for example, triangles of speeds in (Fig. 9-2,b))

$$\frac{w^2}{c^2} = 1 + \left(\frac{u}{c}\right)^2 - 2 \frac{c_u u}{c^2} = \frac{\sin^2 \alpha}{\sin^2 \beta} \quad (9-26)$$

equation (9-25) is transformed to the form:

$$\frac{T_{ow}}{T_{oc}} = 1 - u_0^2 \left(2 \frac{c_u}{u} - 1\right) = 1 - u_0^2 \frac{\sin^2 \beta - \sin^2 \alpha}{\sin^2 (\beta - \alpha)}, \quad (9-25a)$$

where  $u_0 = \frac{u}{c_{max}}$ .

Equation (9-25a) shows that along the stream ratio of the temperatures of stagnation changes. At  $u = 0$  and  $u = 2c_u$  the ratio  $T_{ow}/T_{oc} = 1$ . The first case corresponds to a stationary wheel ( $u = 0$ ), when mechanical work by the gas is not done ( $c_u u = 0$ ). Second value  $u$  determines that section of the stream, in which temperature of stagnation in the absolute and relative motions are identical.

The dimensionless speeds  $M_w$ ,  $M_c$ ,  $\lambda_w$  and  $\lambda_c$  are associated with the temperature of stagnation in a given section by well known relationships (Chapter 2):

for a relative flow

$$\frac{T_{ow}}{T} = 1 + \frac{k-1}{2} M_w^2 = \frac{1}{1 - \frac{k-1}{k+1} \lambda_w^2}; \quad (9-27)$$

for an absolute flow

$$\frac{T_{oc}}{T} = 1 + \frac{k-1}{2} M_c^2 = \frac{1}{1 - \frac{k-1}{k+1} \lambda_c^2}. \quad (9-28)$$

Hence, by well-known formulas of the isentropic process:

$$\frac{p_{ow}}{p} = \left(\frac{T_{ow}}{T}\right)^{\frac{k}{k-1}}; \quad \frac{p_{oc}}{p} = \left(\frac{T_{oc}}{T}\right)^{\frac{k}{k-1}} \quad \text{et cetera.}$$

there can be obtained a connection between  $\frac{p_{ow}}{p}$  and  $\lambda_w$ ,  $\frac{p_{oc}}{p}$  and  $\lambda_c$ , etc.

By means of equations (9-27) and (9-28) it is possible also to obtain a relationship between parameters of the isentropic stagnation in absolute and relative flows:

$$\frac{T_{ow}}{T_{oc}} = \frac{1 + \frac{k-1}{2} M_w^2}{1 + \frac{k-1}{2} M_c^2} = \frac{1 - \frac{k-1}{k+1} \lambda_c^2}{1 - \frac{k-1}{k+1} \lambda_w^2}; \quad (9-29)$$

$$\frac{p_{ow}}{p_{oc}} = \left(\frac{T_{ow}}{T_{oc}}\right)^{\frac{k}{k-1}} \quad (9-30)$$

and

$$\frac{p_{ow}}{p_{oc}} = \left( \frac{T_{ow}}{T_{oc}} \right)^{\frac{1}{k-1}}. \quad (9-31)$$

Taking into account expression (9-25a), we express the ratio  $P_{ow}/P_{oc}$  in the form:

$$\frac{p_{ow}}{p_{oc}} = \left[ 1 - u_0^2 \left( 2 \frac{c_u}{u} - 1 \right) \right]^{\frac{k}{k-1}}. \quad (9-32)$$

By means of equation (9-20) there is readily obtained a relationship between parameters of total stagnation at entry and at exit of wheel.

For a relative flow we obtain [see formula (9-20a)]

$$\frac{T_{ow1}}{T_{oc1}} = 1 - \frac{k-1}{k+1} u_{w1}^2 \left( 1 - \frac{u_2^2}{u_1^2} \right) = 1 - u_{oc1}^2 \left( 1 - \frac{u_2^2}{u_1^2} \right), \quad (9-33)$$

where

$$u_{w1} = \frac{u_1}{a_{w1}}; \quad (9-34)$$

$$u_{oc1} = \frac{u_1}{\sqrt{2} l_{oc1}} = \frac{u_1}{w_{max1}}. \quad (9-35)$$

Correspondingly for the absolute flow [see formula (9-20b)]

$$\frac{T_{oc2}}{T_{oc1}} = 1 - \frac{c_{u1} u_1 - c_{u2} u_2}{l_{oc1}} = 1 - \frac{u_1^2}{l_{oc1}} \sum (c_u u), \quad (9-36)$$

where

$$\sum (c_u u) = \frac{c_{u1} u_1 - c_{u2} u_2}{u_1^2}. \quad (9-37)$$

We shall express  $l_{oc1}$  by  $c_{max1}$ ; then

$$\frac{T_{oc2}}{T_{oc1}} = 1 - 2u_{01}^2 \sum (c_u u) \quad (9-38)$$

and

$$\frac{p_{oc2}}{p_{oc1}} = \left[ 1 - 2u_{01}^2 \sum (c_u u) \right]^{\frac{k}{k-1}}. \quad (9-39)$$

Into formulas (9-27)--(9-39) enter the dimensionless speeds of the absolute and relative flows. The connection between  $M_c$  and  $M_w$  is expressed as:

$$\frac{M_w}{M_c} = \frac{\sin \alpha}{\sin \beta}. \quad (9-40)$$

From the equation

$$w^2 = c^2 + u^2 - 2c_u u \quad (9-41)$$

we find:

$$\lambda_w^2 = [\lambda_c^2 + (u_c - 2\lambda_{cu}) u_c] \frac{T_{oc}}{T_{ow}}, \quad (9-42)$$

where  $u_{*c} = \frac{u}{a_{*c}}$ .

The last equation shows that the ratio of temperatures of stagnation  $T_{ow}/T_{oc}$  serves as the conversion factor from an absolute flow to a relative. This magnitude varies along the stream. At the entry and at exit of rotor wheel  $\frac{T_{ow}}{T_{oc}}$  for a given pattern acquires definite values.

The basic gas-dynamics relationships presented above are valid both for axial and also for radial stages of a turbomachine.

Practical calculations show that influence of the centrifugal effect in the axial stage is small.\* This conclusion is readily reached by means of equation (9-33), from which it follows that if the ratio  $u_2/u_1$  differs little from unity, then a change in the temperature of stagnation of the relative flow is negligible. Only with a significant change in the peripheral speed along tube of flow, as, for example, takes place in a centrifugal compressor or radial turbine stage the influence of indicated effect will be significant.

For an ordinary turbine radial stages the ratio of the peripheral speeds  $u_2/u_1$  fluctuates between 1.02 and 1.10. On the basis of Fig. 9-7 we conclude that for

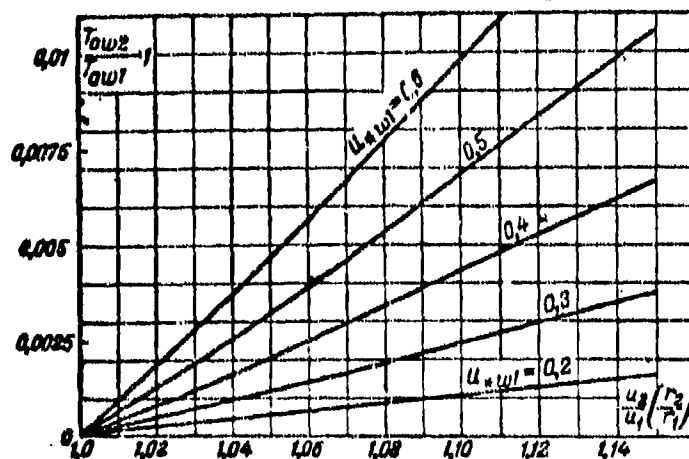


Fig. 9-7. Change of temperature of stagnation of relative flow depending on  $u_2/u_1$  and  $u_{*w1}$ .

\*Here there are not considered the influence of centrifugal forces on boundary layer in the vane channels and also other peculiarities of a three-dimensional flow of a viscous fluid in a stage with radial speed components.

$u_2/u_1 = 1.10$ , the relative change in temperature of stagnation  $T_{0w}$  at  $u_{*w1} = 0.3$  to 0.5 amounts to  $0.25=0.70\%$  i.e., it is small.

We shall illustrate the change of state of gas along stream in thermal diagram taking into account losses of energy in elements of the turbine stage. Parameters of the total stagnation at entry in the guide row, we find at point 0 (Fig. 9-8):  $p_{0c}$  and  $i_{0c1}$ . The corresponding static parameters are determined by point 0'. If we designate the static pressure after guide row  $p_1$ , then point 1' fixes state of gas during isentropic expansion, and point 1 shows the actual state of flow (taking into account losses). The loss of energy is expressed by the sector 1-1'.

Pressure of stagnation of the absolute flow after the guide row will be  $p_{0c1}$  (enthalpy of stagnation remains constant). The difference  $p_{0c} - p_{0c1}$  is equivalent to the losses of energy  $\Delta h_c$ .

The loss factor in guide row is equal to:

$$\zeta_1 = \frac{\Delta h_c}{H_0} = \left( \frac{k+1}{k-1} \frac{1}{\lambda_0^2} - 1 \right) \left[ \left( \frac{p_{0c1}}{p_{0c}} \right)^{\frac{k-1}{k}} - 1 \right],$$

where  $\lambda_0$  is the dimensionless speed, equivalent to an isentropic differential in heat in the stage  $H_0$ .

The difference between enthalpies in the absolute and relative flows is determined by equation (9-19). Plotting the magnitude  $i_{0c1} - i_{0w1}$  from point 0' on line  $i_{0c1} = \text{const}$ , we find point 2, which determines state of stagnated relative flow at entry to rotor wheel.

In the moving channels as a result of losses, part of the kinetic energy irreversibly changes into heat. As a result the pressure of stagnation in the relative motion falls. If along the stream of gas, the peripheral speed does not change, then the corresponding process is expressed by the line 2-3 ( $i_{0w1} = \text{const}$ ). With an increase of  $u$  along stream (radial flow from axis of rotation to periphery)  $i_{0w}$  increases (dotted line 2-3'). If  $u$  decreases, then  $i_{0w}$  diminishes (line 2-3'').

The static parameters at exit of moving row are determined at point 4, where the sector 3-4' (or correspondingly 3'-4' and 3''-4') is equal to  $\frac{Aw_2}{2g}$ .

The loss factors of kinetic energy in the moving row will be:

$$\zeta_s = \frac{\Delta h_w}{H_s} = \frac{A(\omega_{21}^2 - \omega_2^2)}{2gH_s} =$$

$$= \left( \frac{k+1}{k-1} - \lambda_{w1}^2 \right) \left[ \left( \frac{p_{0c1}}{p_{0c2}} \right)^{\frac{k-1}{k}} - 1 \right] \frac{T_{0c1}}{T_{0c1} - \frac{1}{\lambda_0^2}}.$$

The flow leaves the stage with a certain absolute velocity  $c_2$ . Part of kinetic energy, equivalent to speed  $c_2$ , is the loss  $(\Delta h_s)$ .

The loss factor with exit velocity

$$\zeta_s = \frac{\Delta h_s}{H_s} = \frac{T_{0c2}}{T_{0c1}} \frac{\lambda_{c2}^2}{\lambda_0^2} = \left( \frac{p_{0c2}}{p_{0c1}} \right)^{\frac{k-1}{k}} \frac{\lambda_{c2}^2}{\lambda_0^2},$$

where  $p_{0c2}$  is the pressure of stagnation of absolute flow after the stage;

$p_{0c}''$  is the theoretical pressure of stagnation after stage (Fig. 9-8).

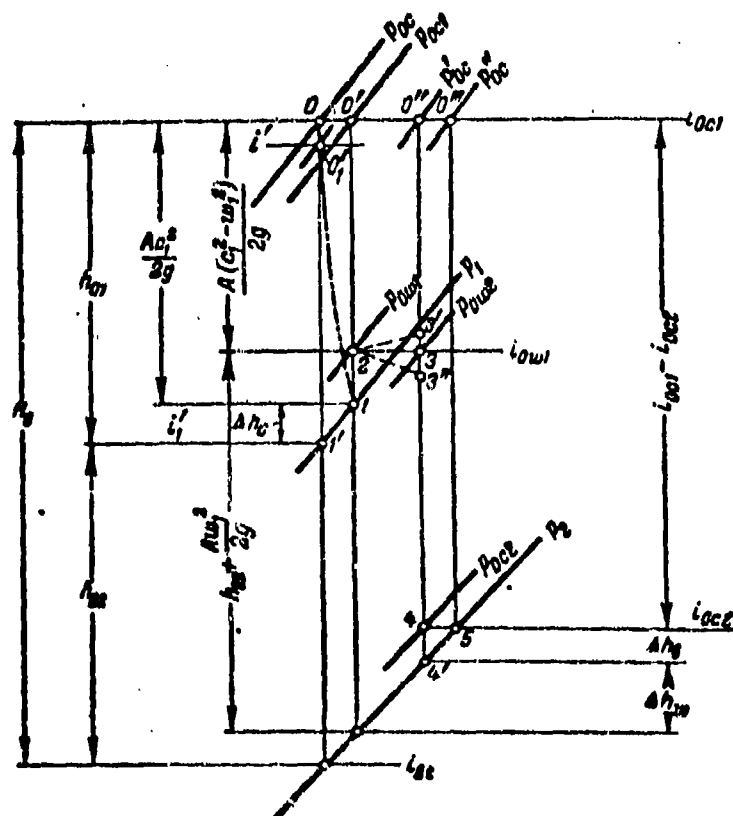


Fig. 9-8. Process in a thermal diagram for a turbine stage.

As can be seen from formulas, loss factors  $\zeta_s$  and  $\zeta_s$  depend in implicit form on  $\frac{u_1}{c_0}$ , since on this magnitude the ratios of the temperatures  $\frac{T_{0w1}}{T_{0c1}}$  and  $\frac{T_{0c2}}{T_{0c1}}$  depend. The magnitude  $\zeta_s$ , characterizing the loss in the stationary row, also depends on  $\frac{u_1}{c_0}$ ; with a change of  $\frac{u_1}{c_0}$  the M and Re numbers change at exit of the guide row.

In the thermal diagram we plot from point 4' upwards the magnitude  $\Delta h_s$ ; then we obtain point 4, characterizing state of stagnated absolute flow after the stage. Let us assume that all kinetic energy of the absolute flow after the stage irreversibly changes into heat; then on isobar  $p_2$  at point 5 there is determined the state of gas after the stage (process of stagnation after stage is assumed isobaric).

We introduce now the concept of degree of reaction. The degree of reaction is the ratio of the available thermal differential in moving row to the total available thermal differential in the stage. Consequently, the degree of reaction indicates that part of the available potential energy of gas (heat) which will be converted into mechanical work directly in the moving row (on wheel).

By definition (Fig. 9-8)

$$\rho = \frac{h_{02}}{h_{01}} = \frac{i_1' - i_{2f}}{i_{0c1} - i_{2f}} = 1 - \frac{i_{0c1} - i_1'}{i_{0c1} - i_{2f}},$$

where  $h_{02}$  is the isentropic available thermal differential in moving row.

The formula for the degree of reaction can be converted to the form:

$$\rho = \frac{1}{\lambda_0^2} \left( \lambda_{w2}^2 \frac{T_{0c2}}{T_{0c1}} - \lambda_{w1}^2 \right) \frac{T_{0c1}}{T_{0c1}}.$$

It follows from this that for an axial stage ( $\frac{T_{0c2}}{T_{0c1}} = 1$ ) the degree of reaction vanishes at  $\lambda_{w2} = \lambda_{w1}$ . For a radial stage  $\rho = 0$  at

$$\frac{\lambda_{w1}}{\lambda_{w2}} = \sqrt{\frac{T_{0c2}}{T_{0c1}}} = \sqrt{1 - u_{0c1}^2 \left( 1 - \frac{u_2^2}{u_1^2} \right)}.$$

From this formula it follows that the stage of reaction can be equal to zero with the motion of gas in a radial stage from the axis of rotation towards periphery ( $u_2 > u_1$ ) at  $\lambda_{w1} > \lambda_{w2}$ . With the motion of gas towards axis of rotation  $\rho = 0$ , if  $\lambda_{w1} < \lambda_{w2}$ .

The actual specific work developed in a stage for any degree of reaction  $\rho$  can be calculated by the formula

$$\begin{aligned} \Delta L_T &= i_{0c1} - i_{0c2} = \\ &= i_{0c1} \left( 1 - \frac{T_{0c2}}{T_{0c1}} \right) = \frac{\Delta h}{k-1} gRT_{0c1} \left[ 1 - \left( \frac{p_{0c2}}{p_{0c1}} \right)^{\frac{k-1}{k}} \right]. \end{aligned}$$



Hence, by means of equation (9-36) we find:

$$AL_T = 2i_{a1} u_{01}^2 \Sigma \bar{c}_u u.$$

Then the efficiency of the stage on the rim can be found by the formula  $\eta_u = \frac{AL_T}{H_0}$ . After substituting here the values  $AL_T$  and  $H_0$ , we obtain:

$$\eta_u = 2 \frac{k+1}{k-1} \left( \frac{u_{01}}{u_1} \right)^2 \Sigma \bar{c}_u u = 2 \left( \frac{u_1}{c_u} \right)^2 \Sigma \bar{c}_u u.$$

From the formula it is clear that even in the case, when energy losses in the guide and moving rows are absent ( $\zeta_1 = \zeta_2 = 0$ ), the efficiency of stage on the rim is equal to zero at  $\Sigma \bar{c}_u u = 0$ .

Formula (9-37) shows that such a condition is fulfilled, if

$$c_{u1} u_1 = c_{u2} u_2.$$

It is obvious that in this case, flow of gas in the stage does not perform work. The magnitude  $\Sigma \bar{c}_u u = 0$  also for a stationary wheel ( $u_1 = u_2 = 0$ ). The maximum value of  $\eta_u$  corresponds to  $(\Sigma \bar{c}_u u)_{\max} = c_{u1} u_1$ .

It is readily seen that in the considered case

$$c_{u2} u_2 = 0, \text{ or } c_{u2} = 0 \text{ (} u_2 \neq 0 \text{)}.$$

From the triangles of speeds it may be concluded, that in this connection the exit losses are minimal, since at  $c_{u2} = 0$   $c_a = c_{2\min}$ .

### 9-3. Equations for Calculating the Distribution of Flow Parameters along a Radius within the Scope of Flow Theory\*.

We now consider the flow of gas through an axial turbomachine stage. We select three control sections: 0-0—before guide row, 1-1—between guide and moving rows, and 2-2—after moving row.

We shall find the distribution of flow parameters along radius in the two control sections (1-1 and 2-2), if there are known: the distribution of parameters in section 0-0, pressure of gas on root or average radius of section 2-2, geometric dimensions of stage, number of rotations of turbine rotor and the aerodynamic characteristics of the rows.

---

\*Questions discussed in this section have been worked out in collaboration with G. S. Samoylovich.

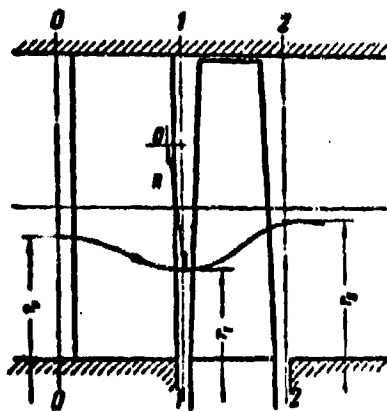


Fig. 9-9. Diagram of flow part of stage with long blades.

By considering difficulties connected with an investigation of a three-dimensional flow of a compressible fluid, it is possible in first approximation to consider a simplified axially symmetric diagram of flow in a turbomachine stage.

Thus, if it is assumed that the flow in the stage is steady and axially symmetric ( $\partial/\partial\theta=0$ ), while the radial components of the speed ( $c_r=w_r$ ) and also their derivatives ( $\frac{\partial c_r}{\partial z}$ ;  $\frac{\partial c_r}{\partial r}$ ;  $\frac{\partial w_r}{\partial z}$ ;  $\frac{\partial w_r}{\partial r}$ ) are extremely small, then equations (1-17a) and (9-1) are simplified and acquire the form ( $R=\theta=z=0$ ):

$$\left. \begin{aligned} \frac{1}{\rho} \frac{dp}{dr} &= \frac{c_u^2}{r}; & c_u \frac{dc_u}{dz} &= 0; \\ c_u \frac{dc_u}{dz} &= -\frac{1}{\rho} \frac{dp}{dz}. \end{aligned} \right\} \quad (9-43)$$

$$\left. \begin{aligned} \frac{w_u^2}{r} + (rr - 2w_u) &= \frac{1}{\rho} \frac{dp}{dr}; & w_u \frac{dw_u}{dz} &= 0; \\ w_u \frac{dw_u}{dz} &= -\frac{1}{\rho} \frac{dp}{dz}. \end{aligned} \right\} \quad (9-44)$$

The first equation (9-43) expresses the condition of radial equilibrium of a particle of gas, with which centrifugal forces on any of the coaxial cylindrical surfaces are balanced by forces of static pressure of gas. Thus, according to designations in Fig. 9-9 for a unit of length of the clearance (section 1-1) it is possible to write out:  $2\pi r dp_1 = 2\pi r dr \rho_1 c_{u1}^2 / r$  and to obtain from it the first equation (9-43).

The second equation (9-43) expresses condition of invariability of  $c_u$  along the axis of stage. From the third equation there is readily obtained  $dc_u/dz=0$

at  $dp/dz=0$ , i.e. if pressure along the axis does not change, then the axial components of the speed also remain constant.

The flow conforms with the adopted assumptions to a maximum degree in control sections 1-1 and 2-2; the motion in the intervane channels is not subject to such simplified law-governed principles.

We introduce in addition a number of simplifications. We shall disregard periodic non-stationariness of the flow, caused by the rotation of rotor wheel or, more precisely, we believe that a consideration of averaged speeds by time also introduces no significant error. We assume also that after a rearrangement the flow in control sections moves along cylindrical surfaces (i.e. radius of curvature of meridian section of surface of flow R in Fig. 9-9 is fairly large). We assume that an external and an internal heat exchange is lacking and the rows of the stage are flowed around continuously.

We shall consider the flow after the guide row. We shall use the simplified equation of radial equilibrium (9-43), after writing it out in the following form:

for the section 0-0

$$\frac{1}{\rho_0} \frac{dp_0}{dr} = -\frac{c_0^2 \cos^2 \alpha_0}{r}; \quad (9-43a)$$

for section 1-1

$$\frac{1}{\rho_1} \frac{dp_1}{dr} = -\frac{c_1^2 \cos^2 \alpha_1}{r}, \quad (9-43b)$$

where  $p_0, \rho_0, p_1, \rho_1, c_0, \alpha_0, c_1, \alpha_1$  are the pressures, densities, speeds and angles of flow before and after the guide row.

We assume that the function  $\alpha_1 = \alpha_1(r)$  is known. The form of this function is determined by the law of torque of guide vanes. It is obvious that a flow of gas has to satisfy equations of energy and continuity. For each elementary annular stream, flowing through guide row, equation of energy can be written out in such a form:

$$i_0' = i_1 + \frac{c_1^2}{2} = i_{11} + \frac{c_{11}^2}{2} = i_1 + \frac{c_{11}^2}{2}, \quad (9-45)$$

where  $i_0^*$  -- enthalpy of stagnation in clearance;

$c_{1t}, c_1, i_{1t}, i_1$  -- are the speeds and enthalpy of gas at the termination of the isentropic and actual processes of expansion in the guide row;  
 $\eta_1$  -- is the efficiency of the guide row (approximately determined as  $\eta_1 = \varphi^2$ ).

We shall differentiate equation (9-45) with respect to the radius  $r$ :

$$\frac{di_0^*}{dr} = \frac{di_{1t}}{dr} + \frac{1}{2} \left( \frac{2\eta_1 c_1 dc_1 - c_1^2 d\eta_1}{\eta_1^2 dr} \right). \quad (9-46)$$

The derivative  $\frac{di_{1t}}{dr}$  describes the change in enthalpy of flow in the clearance after guide row along the radius and, as is known, can be written as:

$$\frac{di_{1t}}{dr} = \frac{1}{\rho_{1t}} \frac{dp_1}{dr} = \frac{\rho_1}{\rho_{1t}} \frac{1}{\rho_1} \frac{dp_1}{dr}. \quad (9-47)$$

Here  $\rho_{1t}$  is the density of gas at the termination of isentropic expansion in guide row;  $\rho_1$  is the density of the gas at the termination of actual expansion (in the presence of losses).

The ratio of the densities can be expressed by the formula

$$\gamma_e = \frac{\rho_1}{\rho_{1t}} = \frac{\rho_1}{\rho_0} = \left( \frac{1 - \frac{k-1}{k+1} \lambda_{1t}^2 \eta_1}{1 - \frac{k-1}{k+1} \lambda_{1t}^2} \right)^{\frac{1}{k-1}}. \quad (9-48)$$

where  $\lambda_{1t} = c_{1t}/a_{e,1}$  is the theoretical dimensionless speed after the guide row.

Consequently, the derivative

$$\frac{di_{1t}}{dr} = \gamma_e \frac{1}{\rho_1} \frac{dp_1}{dr},$$

or taking into account (9-43b)

$$\frac{di_{1t}}{dr} = \gamma_e \frac{c_1^2 \cos^2 \alpha_1}{r}. \quad (9-49)$$

By substituting (9-49) in equation of energy (9-46), we obtain a differential equation of distribution of absolute velocities along the radius in the clearance:

$$\frac{dc_1}{dr} + \left( \gamma_e \eta_1 \frac{\cos^2 \alpha_1}{r} - \frac{1}{2\eta_1} \frac{d\eta_1}{dr} - \frac{1}{2h_{e,1}} \frac{di_0^*}{dr} \right) c_1 = 0, \quad (9-50)$$

where  $h_{e,1} = c_1^2 / 2\eta_1$  is the available thermal differential in guide row in a given section along the radius.

Integrating equation (9-50), we find:

$$c_1 = K_1 \exp \left[ - \int_{r_0}^r \left( \frac{\gamma_e \eta_1 \cos^2 \alpha_1}{r} - \frac{1}{2\eta_1} \frac{d\eta_1}{dr} - \frac{1}{2h_{e,1}} \frac{di_0^*}{dr} \right) dr \right], \quad (9-51)$$

where  $K_1$  is a constant, corresponding to initial (average or root) section.

Equation (9-51) within the scope of the considered flow problem is the most general.

From (9-48) it follows that at subsonic speeds and moderate losses in the guide row the ratio of the densities  $\rho_1/\rho_{11}$  is close to unity. Calculations make it possible to establish that range of values of  $\lambda_{11}$  and  $\eta_{11}$  in which it is possible to take  $\gamma_c = 1$ . Without significant error, such a simplification is admissible at  $\lambda_{11} < 1$ .

At supersonic speeds function  $\gamma_c$  should be retained in equation (9-50). However, in certain cases it is possible to use simplified relationships  $\gamma_c(\lambda_{11}, \eta_{11})$ , and with a slight change in  $\lambda_{11}$  and  $\eta_{11}$  along radius  $\gamma_c$  is assumed for each sector as constant. Recalling that  $\gamma_c$  depends on  $\lambda_{11}$  and  $\eta_{11}$ , it must be concluded that in an accurate calculation of a stage at supersonic speeds, the method of successive approximations becomes inevitable.

It is necessary to emphasize also that the effect of compressibility indirectly is considered in equation (9-51) by the functions  $\alpha_1$  and  $\eta_{11}$ . Depending upon the  $M_1$  number the losses and the angle of exit of guide row vary. Consequently, the form of the functions  $\eta_{11}(r)$  and  $\alpha_1(r)$  depends on  $M_1$ ; according to (9-51) with a change of these functions also the character of distribution of absolute velocities  $c_1(r)$  in the clearance varies.

It is necessary also to note that equations (9-50) and (9-51) are valid for any law of torque.

Let us turn now to calculating the flow after the moving row. Under the above made assumptions, condition of radial equilibrium in section 2-2 is expressed by the first equation (9-44):

$$\frac{1}{\rho_2} \frac{dp_2}{dr} = \frac{w_{u2}^2 - 2uw_{u1} + u^2}{r} = \frac{(w_2 \cos \beta_2 - u)^2}{r} = \frac{c_2^2 \cos^2 \alpha_2}{r}, \quad (9-52)$$

where  $p_1$  and  $\rho_1$  are the pressure and density, and  $c_1$  and  $\alpha_1$  are the speed and angle of flow after moving blades in the absolute motion;  $u$  is the peripheral speed

on current radius  $r$ ;  $\beta_1 = \beta_1(r)$  is the angle of exit in the relative motion which is a given function of the radius;  $w_2$  is the relative speed after the moving row.

Assume further that the radial dislocation of the flow during the transition from control section 1-1 into the control section 2-2 will be small ( $u_1 \approx u_2$ ). Then the equation of energy for the relative flow can be presented in the well-known form:

$$i_1 + \frac{w_1^2}{2} = i_{2t} + \frac{w_2^2}{2\eta_2}, \quad (9-53)$$

where  $w_1$  is the relative velocity at entry to moving row;

$i_1$  is the enthalpy of gas before moving row;

$\eta_2$  is the efficiency of moving row ( $\eta_2 \approx \psi^2$ );

$i_{2t}$  is the enthalpy of gas after a moving row in an isentropic process.

The theoretical and actual speeds after the row are associated by the relationship

$$w_2 = \sqrt{\eta_2} w_{2t}.$$

It is obvious that  $i_{2t} = i_{2t}(r)$  and  $w_2 = w_2(r)$  are the functions being sought and  $\eta_2 = \eta_2(r)$  and  $w_1 = w_1(r)$  can be considered as the given functions of radius  $r$ .

The enthalpy of the flow after the guide row is determined by the equation of energy:

$$i_0 = i_1 + \frac{c_1^2}{2}.$$

After substituting  $i_1$  in (9-53) we find:

$$i_0 = i_{2t} + \frac{w_2^2}{2\eta_2} + \frac{c_1^2 - w_1^2}{2}.$$

After differentiating the equation of energy, we obtain (we assume  $di_0/dr = 0$ ):

$$\frac{di_{2t}}{dr} + \frac{w_2}{\eta_2} \frac{d\eta_2}{dr} - \frac{w_2^2}{2\eta_2} \frac{d\eta_2}{dr} + \frac{d}{dr} \left( \frac{c_1^2 - w_1^2}{2} \right) = 0. \quad (9-54)$$

We substitute in equation (9-54)

$$c_1^2 - w_1^2 = 2uc_1 \cos \alpha_1 - u^2. \quad (9-55)$$

We use the equation of radial equilibrium

$$\frac{di_{2t}}{dr} = \frac{p_2}{\rho_2} \frac{1}{r} \frac{dp_2}{dr} =: \gamma_w \frac{(w_2 \cos \beta_2 - u)^2}{r}, \quad (9-56)$$

where

$$\gamma_w = \frac{p_2}{\rho_{2t}}.$$

Equations (9-54), (9-55) and (9-56) we solve in common. After certain simplifications we obtain the sought differential equation:

$$w_2 \frac{dw_2}{dr} + \left( \frac{\gamma_w \eta_2 \cos^2 \beta_2}{r} - \frac{1}{2\eta_2} \frac{d\eta_2}{dr} \right) w_2^2 - 2\gamma_w \eta_2 w \cos \beta_2 w_2 + \eta_2 \frac{d(c_{u1} r)}{dr} = 0. \quad (9-57)$$

Equation (9-57) is nonlinear. It is linearized only in the particular case, when  $d(c_{u1} r)/dr = 0$ .

Integrating (9-57) in this case, i.e. taking into account  $\frac{d(c_{u1} r)}{dr} = 0$ , we find:

$$w_2 = K_2 \exp \left[ \int_{r_n}^r \left( \frac{\gamma_w \eta_2 \cos^2 \beta_2}{r} - \frac{1}{2\eta_2} \frac{d\eta_2}{dr} - 2\gamma_w \eta_2 w \cos \beta_2 \right) dr \right], \quad (9-58)$$

where  $K_2$  is a constant, determinate for the initial (average or root) section.

The condition  $d(c_{u1} r)/dr = 0$  is satisfied strictly with a torque of the stage on method of constant circulation\*. However, as experience shows, this condition is realized approximately and in a number of other practically important cases.

The constant  $K_1$  and  $K_2$  in equations (9-51) and (9-58) are determined if there are known the speeds  $c_1$  and  $w_2$  in any section according to height of blades. This problem is solved by using the equation of continuity for sections 1-1 and 2-2:

$$\dot{G} = 2\pi g a_{c1} \rho_{c1} \int_{r_n}^r q_1 \sin \alpha_1 dr; \quad (9-59)$$

$$\dot{G} = 2\pi g a_{w2} \rho_{w2} \int_{r_n}^r q_2 \sin \beta_2 dr. \quad (9-60)$$

The function  $\gamma_w$  appearing in equation (9-58) in simplified solutions may be assumed equal to  $\gamma_w = \text{const}$  for the entire stage or for individual annular flows\*\*.

It must be also noted that the differential equation (9-57) for motionless moving wheel ( $w=0$ ) transforms to equation (9-50).

#### 9-4. Calculation of Flow in a Stage with Long Blades of Constant Profile.

We now consider a stage with an axial flow of gas, assuming that the flow

\*See Sec. 9-5.

\*\*The flow of gas in the stage after the guide and moving rows is whirled, i.e. it has a nonuniform field of speeds both in the absolute, and also in the relative motion. As it was shown in Sec. 5-16, in such flow the field of total energy will be nonuniform.

at entry to guide row has a uniform field of speeds. We pose the following problem: to establish distribution of parameters in the clearance and after moving row along the radius, if the blades have a constant profile by height. The solution of this problem allows, in addition, obtaining initial data for calculating a stage with blades of constant profile by the aerodynamic characteristics of the rows and may be used for determining that limiting state of radiating rows at which it is possible to use a blade of constant profile.

The calculation of stages with blades of constant profile can be made by assuming as constant the angles along the radius  $\alpha_1$  and  $\beta_2$ . A more accurate method of calculating discussed below consists in the fact that the angles  $\alpha_1$  and  $\beta_2$  are given as functions of the radius  $r$ . This method is expediently used in those cases when the fanwise arrangement of the stages is found to be significant.

Numerous experiments show that the angle  $\alpha_1$  can be expressed depending on relative spacing or radius by the formula

$$\tau_{2\alpha_1} = \tau_{2\alpha_{1k}} + \frac{\Delta \tau_{2\alpha_1}}{2} (\theta - 1) (\bar{r} - 1), \quad (9-61)$$

where

$$\Delta \tau_{2\alpha_1} = \tau_{2\alpha_{1k}} - \tau_{2\alpha_{1a}};$$

$\alpha_{1a}, \alpha_{1k}$  are the angles of flow exit in the apex and in root sections respectively;  $\bar{r} = r/r_k$ ;  $r_k$  is the radius of root section;  $r$  is the radius of flow section;

$$\theta = \frac{d}{l} = 2 \frac{r_k}{l} + 1.$$

After substituting (9-61) in equation (9-50) and integrating the latter we obtain:

$$\bar{c}_1 = \frac{c_1}{c_{1k}} \approx \frac{F(\bar{r})}{r^2}, \quad (9-62)$$

here

$$\left. \begin{aligned} F(\bar{r}) &= \left[ 1 + \frac{2n_1 b_1}{1 + n_1^2} (\theta - 1) (\bar{r} - 1) + \frac{b_1 (\theta - 1)^2}{1 + n_1^2} (\bar{r} - 1)^2 \right]^{\frac{1}{2}}; \\ n_1 &= \frac{\eta_1}{1 + [n_1 - b_1 (\theta - 1)]^2}; \\ n_1 &= \tau_{2\alpha_{1k}}; \\ b_1 &= \frac{1}{2} (\tau_{2\alpha_{1a}} - \tau_{2\alpha_{1k}}). \end{aligned} \right\} \quad (9-63)$$



For determination of speed  $c_1$  it is necessary to know the magnitude of  $c_{1k}$  in the root section. For this purpose we shall transfer the equation of continuity (9-59), after writing it out for sections 0-0 and 1-1:

$$\frac{c_{a0}^2}{2}(\bar{r}_0^2 - 1) = \int_1^{\bar{r}_0} \bar{\rho}_1 c_{a1} \bar{r}_1 d\bar{r}_1, \quad (9-64)$$

where  $c_{a0}, c_{a1}$  are the axial components of the speed in sections 0-0 and 1-1;  $\bar{\rho}_1 = \rho_1/\rho_0$  is the relative density in the clearance.

The function  $c_{a1}$  in equation (9-64) can be determined by the formula

$$c_{a1} = c_1 \sin \alpha_1 = \frac{c_1 r_{a0} \alpha_1}{\sqrt{1 + r_{a0}^2 \alpha_1^2}},$$

or approximately

$$c_{a1} = c_{1k} \bar{c}_1 \sin \alpha_1 = c_{1k} \frac{F(\bar{r})}{\bar{r}^4} \sin \alpha_1, \quad (9-65)$$

where  $\alpha_1$  is taken according to formula (9-61).

The above-presented relationships are valid, if the flow in clearance is subsonic. With mixed flows in the clearance, when in lower part of stage (in root sections)  $c_1 > a_{*1}$ , formula (9-62) is not applicable. In this case it is necessary to consider the deflection of flow in an oblique section of the guide row.

Let us turn now to calculating the flow after the stage. We shall use the fundamental equation (9-57) and will integrate it at  $r_1 = \text{const}$  and  $d(c_{u1}) = 0$  for the assumed law of change in angles along the radius

$$\sin \beta_1 = \sin \beta_{2k} + \frac{\Delta \sin \beta_1}{2} (\theta - 1)(\bar{r} - 1).$$

As a result of the integration we find the approximate expression

$$\bar{w}_1 = \frac{w_1}{w_{2k}} = \bar{r}^\varphi. \quad (9-66)$$

Here  $w_{2k}$  is the value of  $w_2$  in root section;

$\beta_{2k}$  is the angle of vector  $w_{2k}$ ;

$$\varphi = \{1 - [n_1 - b_1(\theta - 1)]^2\}; \quad n_1 = \sin \beta_{2k};$$

$$b_1 = \frac{1}{2} \Delta \sin \beta_1 = \frac{1}{2} (\sin \beta_{2k} - \sin \beta_{1k}).$$

With the known values  $\bar{w}_2$ , there is readily determined the available thermal differential in the stage.

By means of the derived equations, it is possible to calculate the distribution of parameters along radius in clearance and after stage with blade of constant profile.

The available thermal differential in the guide row according to (9-62) will

be:

$$\bar{h}_{01} = \frac{h_{01}}{h_{01k}} = \bar{c}_1 = \frac{[F(\bar{r})]^2}{r^{2k}}. \quad (9-67)$$

We find change in reaction stage along the radius:

$$p = 1 - \frac{h_{01}}{H_0} = 1 - \frac{h_{01k}}{H_0} \bar{h}_{01} = 1 - h_{01k} \frac{H_{0k}}{H_0} \frac{h_{01k}}{H_{0k}};$$

$$\frac{h_{01k}}{H_{0k}} = 1 - p_k.$$

where  $p_k$  is the stage of reaction in the root section.

After using (9-67), we obtain:

$$p = 1 - (1 - p_k) \frac{[F(\bar{r})]^2}{r^{2k} H_0}, \quad (9-68)$$

where  $H_0 = \frac{H_0}{H_{0k}}$ .

Hence there can be obtained an approximate formula for determining the reaction on average diameter of a stage with nontwisted blades, by proceeding from the given value  $p_k$  in the initial--root--section. Noting that  $\bar{r}_m = \theta/\theta - 1$  and assuming  $b_1 \approx 0$ , from formula (9-68) we obtain:

$$p_m = 1 - \frac{1 - p_k}{H_0} \left( \frac{\theta - 1}{\theta} \right)^{2k}. \quad (9-69)$$

Formula (9-69) has a limited area of application. It is obvious that it is valid for relatively large  $\theta$ , since only in this case difference of  $\alpha_1$  for the vertex and for the root is small and it is possible to assume  $b_1 \approx 0$ .

Minimum degree of reaction in mean section can be determined, by assuming that in the root section  $p_k \geq 0$ . Then, from (9-69) we obtain:

$$p_m^{\min} \geq 1 - \frac{1}{H_0} \left( 1 + \frac{2n_1 b_1}{1 + n_1^2} \right) \left( \frac{\theta - 1}{\theta} \right)^{2k},$$

or approximately ( $b_1 \approx 0$ )

$$p_m^{\min} \approx \left( \frac{\theta - 1}{\theta} \right)^{2k}.$$

The change of work on rim along radius can be found by the formula:

$$\bar{L}_m = \frac{L_m}{L_{m0}} = \bar{r} \frac{c_{u1} + c_{u2}}{c_{u1k} + c_{u2k}},$$

where  $c_{u2} = w_{2k} \cos \beta_2 = u$ .

The function  $c_{u1}(\bar{r})$  also is known. Consequently, magnitude  $\bar{L}_m(\bar{r})$  is determined.

The field of axial components of the speeds after the stage is calculated by the formulas:

$$c_{a2} = c_{a1} \quad a_2 = w_{a2} r_{a2}^2 = (c_{a2} + u) \quad \dot{r}_2$$

In conclusion we note that the initial formula for the reaction stage (9-68) makes it possible to determine difference in  $\dot{r}$  at vertex and at root of blade.

Since 
$$\dot{r}_2 = \frac{\theta + 1}{\theta - 1},$$

then after substituting in (9-68) we obtain:

$$\frac{1 - \dot{r}_2}{1 - \dot{r}_1} \approx \left( 1 + \frac{4n_1 b_1}{1 + n_1^2} \right) \left( \frac{\theta - 1}{\theta + 1} \right)^2,$$

where  $\dot{r}_2$  is the stage of reaction at vertex.

For rough calculations it is possible to recommend the formula

$$\frac{1 - \dot{r}_2}{1 - \dot{r}_1} \approx \left( \frac{\theta - 1}{\theta + 1} \right)^2 \quad (9-70)$$

Using the obtained relationships, it is possible to analyze the variation of parameters along radius in clearance and after stage and to evaluate additional losses, appearing in stage with blade of constant profile.

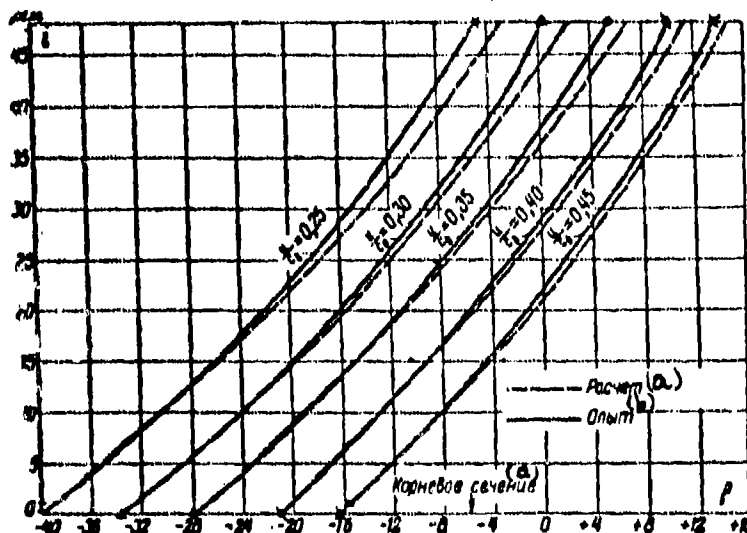


Fig. 9-10. Comparison between experimental and calculated values of reaction stage in different sections along radius of stage with blades of constant profile;  $\theta = 7.73$ ;  $M_0 = 0.65$ .

KEY: a) Calculation; b) Experiment; c) Root section.

Results of corresponding calculations show that additional losses in the stage with nontwisted blades are caused by an increase of exit losses, by the change of angle of entry of flow into moving row, and also by change of work being yielded along the radius. After the stage the flow is vortical; a levelling-off of the field of speeds is accompanied by losses of kinetic energies, which must be included in the

total balance of losses of the stage.

Results of calculations by the proposed method satisfactorily agree with the experimental data.

Detailed experimental investigations of the flow in the clearance and after a stage with cylindrical blades were made at the Moscow Power-Engineering Institute (MEI) at  $\theta = d/l = 7$ . The calculation of the experimental stages was made on basis of the method of approximation discussed above. Corresponding curves of the change of reaction along radius are presented in Fig. 9-10. The comparison shows satisfactory convergence of the experimental and calculated values of the reaction. The experimental and calculated values of the angles, pressures and speeds also satisfactorily agree.

In conclusion, we mention that at large  $\theta$  the change in the angles  $\alpha_1$  and  $\beta_2$  along the radius is small.

The calculation of the speeds  $c_1$  and  $w_2$  in such stages can be made by formulas, which readily are obtained from the fundamental equations (9-50) and (9-57) under the following assumptions:  $\eta_1 = \text{const}$ ;  $\eta_2 = \text{const}$ ;  $\alpha_1 = \text{const}$  and  $\beta_2 = \text{const}$ .

#### 9-5. Certain Methods of Profiling Long Blades of Stages with an Axial Flow of Gas

Above-discussed method of calculating stages with blades of constant profile makes it possible to evaluate additional losses of the stages, caused by a variation of the parameters and angles of flow along radius in clearance and also by an increase of exit losses.

Results of such calculation are presented in Fig. 9-11. Here there are given curves, establishing additional losses in a stage with blades of constant profile depending on  $\theta = d/l$ . In addition, in the graphs there have been plotted the experimental values of supplemental losses  $\Delta\eta_{\text{sup}}$ . At  $\theta \leq 10$  the supplemental losses exceed 1%. Consequently, in such stages it is necessary in a special manner to organize the flow, assuring minimal losses of energy. For this purpose the blades

of the guide and moving rows are made twisted (helical) with a profile variable with height.

The twist of the blades can be realized by different methods. Initial differential equation of the distribution of speeds in the clearance (9-50) has infinite number of solutions. In accordance with this the number of methods of twisting the blades theoretically can be infinitely large. However, only a insignificant part of these methods corresponds to conditions of rational arrangement of flow in stage of turbine. For this reason, and also remembering that equation (9-50) is approximate, one should develop those methods of profiling which are constructed on clear physical premises.

In practice of turbine construction, the following are the most widely adopted methods of arranging flow in clearance: a) constant circulation of speed with a uniform field of axial speeds ( $c_{u1}r = \text{const}$ ); b) constant direction of

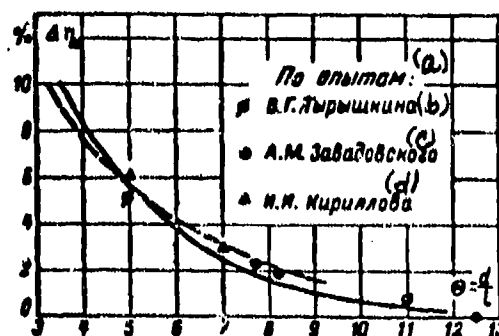


Fig. 9-11. Decrease of stage efficiency from nontwisting of blades depending on  $e = d/l$ ; a comparison between the calculated and experimental values  $\Delta\eta$ .

KEY: a) According to experiments of b) V. G. Tyryshkin; c) A. M. Zavadovskiy; d) I. I. Kirillov.

absolute flow along radius  $\alpha_1 = \text{const}$ ); c) special selected law of change of direction of absolute flow  $[\alpha_1 = f(r)]$ , including guide vanes of constant profile.

The arrangement of flow after moving blade is realized on the assumption: a) of a uniform field of absolute velocities; b) of the constancy of work, being developed by flow in different sections along radius; c) of the constancy of available thermal differential along the radius.

The number of combinations of any of the enumerated methods of arranging the flow in clearance and after the stage is limited by the condition of continuity, associating the flow in these sections.

We shall consider as an example the isentropic flow of gas in a stage with a uniform field of axial speeds in clearance and after stage (method of constant circulation of speed).

In this case, the coefficients  $\eta = \chi = 1$ ,  $di_0 = 0$  and equation (9-50) acquires the simple form:

$$\frac{dc_1}{c_1} + \cos^2 \alpha_1 \frac{d\bar{r}}{\bar{r}} = 0. \quad (9-50a)$$

Since

$$c_1 dc_1 = c_{a1} dc_{a1} + c_{u1} dc_{u1}$$

and according to the adopted assumption  $c_{a1} = \text{const}$ , then equation (9-50a) is transformed to the form:

$$\frac{dc_{u1}}{c_{u1}} + \frac{d\bar{r}}{\bar{r}} = 0.$$

Integrating this equation, we obtain:

$$c_{u1} \bar{r} = \text{const}.$$

The latter condition expresses the constancy of circulation of speed around guide row. Actually, in the simplest case of axial entry into guide row ( $c_{u0} = 0$ ) circulation of speed is equal to:

$$\Gamma = l(c_{u1} - c_{u0}) = lc_{u1} = \frac{2\pi r}{z} c_{u1} = \text{const},$$

where  $z$ —number of blades in the row.

The initiator of the considered method is N. Ye. Zhukovskiy. As early as 1912 in investigating propellers N. Ye. Zhukovskiy showed that axial speeds are constant in a radial direction, if change of the peripheral components of the speed corresponds to the law of constancy of circulation. It is well-known that propellers, and later also fans, constructed according to vortex theory by N. Ye. Zhukovskiy, were distinguished by their great economy. For calculating long blades of steam and gas turbines, this method was for the first time applied by V. V. Uvarov.

By means of equation (9-50a) there is readily found the distribution of the absolute velocities in clearance:  $\bar{c}_1^2 = \frac{1}{\bar{r}^2} [1 + (\bar{r}^2 - 1) \bar{c}_{u1}^2]$ .

where

$$\bar{c}_1 = \frac{c_1}{c_{1k}}; \quad \bar{c}_{a1} = \frac{c_{a1}}{c_{1k}} = \text{const.}$$

The change in reaction along radius is established by means of the evident relationships

$$p = 1 - \frac{h_{a1}}{H_0} = 1 - \frac{c_1^2 c_{1k}^2}{2gH_0}$$

or

$$p = 1 - \frac{1-p_2}{\bar{r}^2} [1 + (\bar{r}^2 - 1) \sin^2 \alpha_{1k}]. \quad (9-71)$$

In accordance with condition  $c_{u1} \bar{r} = \text{const}$  there can be found the change of angles of absolute velocity along radius in the form:

$$\tan \alpha_1 = \frac{c_{a1}}{c_{u1}} = \frac{\bar{r} c_{a1}}{\sqrt{1 - c_{a1}^2}}.$$

The twist of blades on the basis of the condition of constancy of circulation of speed can be realized by taking into account the losses in rows.

For an adiabatic flow (taking into account losses) the calculated relationships, obtained by means of integrating initial differential equations, are given in Table 9-1.

For a flow with losses, as is evident from formulas presented in Table 9-1, the conditions  $c_{u1} r = \text{const}$  and  $c_{a1} = \text{const}$  are incompatible. Under the condition of a uniform field of axial speeds in clearance the circulations of speed around guide blades must be increased towards its vertex. If, as the basis of profiling of stage there is assumed the condition of constancy of circulation of speed, then the axial speeds in clearance also increase somewhat towards the vertex.

The adiabatic flow in clearance at  $\eta_1 = \text{const}$  and  $\alpha_1 = \text{const}$  is subject to equation, obtainable by the integration of (9-50), in following form:

$$\bar{c}_1 = \frac{r c_1}{c_{1k}} = r^{-\tan^2 \alpha_1}.$$

Consequently, the available thermal differential in guide row will be:

$$\bar{h}_{a1} = c_1^2 = r^{-2 \tan^2 \alpha_1}.$$

The ratio of speeds varies along the radius in accordance with formula

$$\frac{u}{c_1} = x_{u1} r^{1 + \tan^2 \alpha_1}.$$

Table 9-1

A) Величина	B) Расчетная формула
$\bar{c}_1, \bar{c}_{u1}$	$\sqrt{1 - \gamma_1 \cos^2 \alpha_{1K} (1 - \bar{r}^2)} \bar{r}^{-1}$
$\bar{c}_{a1} = c_{a1}/c_{u1K}$	$\sqrt{1 - \cos^2 \alpha_{1K} [\gamma_1 + (1 - \gamma_1) \bar{r}] \frac{1}{\sin \alpha_{1K}}}$
$\cos \alpha_1$	$\frac{\cos \alpha_{1K}}{\bar{r} \sqrt{1 - \gamma_1 \cos^2 \alpha_{1K} (1 - \bar{r}^2)}}$
$\bar{K}_{a1}$	$1 - \gamma_1 \cos^2 \alpha_{1K} (1 - \bar{r})$
$\lambda = \frac{u}{c_1}$	$\frac{x_K \bar{r}}{\sqrt{1 - \gamma_1 \cos^2 \alpha_{1K} (1 - \bar{r}^2)}}$
$\tan \beta_1$	$\frac{\bar{r} \sqrt{1 - \cos^2 \alpha_{1K} [\gamma_1^2 + (1 - \gamma_1) \bar{r}^2]}}{\cos \alpha_{1K} - x_K \bar{r}^2}$
$\rho$	$1 - (1 - \gamma_1) \frac{1 - \gamma_1 \cos^2 \alpha_{1K} (1 - \bar{r}^2)}{1 - \frac{c_{a1K}^2}{H_{0K}} (1 - \bar{r}^2)}$
$\bar{w}_1$	$\sqrt{\frac{H_{0K}}{\frac{\gamma}{2} \left[ 1 - \frac{c_{a1K}^2}{H_{0K}} (1 - \bar{r}^2) \right]} - \mu_K^2 \left( \frac{2 \cos \alpha_{1K}}{x_K} - 1 \right)}$

A) Magnitude; B) Standard working formula.

where  $x_K = u_K/c_{1K}$  is the ratio of speeds for root section.

The angle of relative flow

$$\tan \beta_1 = \frac{\sin \alpha_1}{\cos \alpha_1 - x_K \bar{r} \sqrt{1 + \gamma_1 \cos^2 \alpha_1}}.$$

It must be emphasized that the realization of method of twist at  $\alpha_1 = \text{const}$  results in guide vanes of variable profile by height, since with small  $\theta$  the spacing of the blades and the speed  $c_1$  along radius varies significantly. Consequently in order to realize the condition  $\alpha_1 = \text{const}$ , it is necessary to change the adjusting angle of profile  $\alpha_{adj}$ , i.e., to make the blade twisted. At high speeds it is necessary also to consider influence of compressibility on the mean angle after row which also results in the necessity of twisting the guide vanes.

For a large number of stages it seems possible to make the guide vanes without twists. The calculation of the guide rows is made by formulas, presented in Sec. 9-4. By means of these relationships there are calculated parameters of flow in clearance.



The calculation of moving blades both at  $u_1 = \text{const}$ , and also at  $u_1 = f(r)r$  is made by proceeding from conditions adopted after the stage. As it has been shown, there may be assumed a condition of without a swirl of flow at exit ( $c_{u2} = 0$ ), of constancy of work along radius ( $L_{u1} = \text{const}$ ) and others.

The calculation of a stage with a flow, nearly cylindrical, it is possible to realize, by dividing the flow into a number of elementary annular flows. Within limits of each flow it is possible to assume the problem one-dimensional and to use ordinary calculation procedure. The twist of a guide vane, in general, can be selected any:  $\alpha_1 = \text{const}$ ;  $c_{u1} r = \text{const}$ ;  $\alpha_1 = f(r)$ . In this connection, naturally, for determining parameters in the clearance it is possible to one of the particular solutions (9-50). After determining parameters in clearance, we write out the equation of continuity for each flow in the control sections 1-1 and 2-2:

$$\frac{\Delta Q}{f_{11}} = g \mu_1 c_{1t} / \lambda_1$$

$$\frac{\Delta Q}{f_{21}} = g \mu_2 w_{2t} / \lambda_2$$

where  $\Delta Q$  is the flow of steam through an elementary stream;

$\mu_{11}$  and  $\mu_{21}$  are the densities at termination of isentropic expansion in guide and moving rows;

$c_{1t}$ ,  $w_{2t}$  are the theoretical exit velocities of the flow;

$f_1$  and  $f_2$  are areas of exit sections within the limits of one elementary flow;

$\mu_1$ ,  $\mu_2$  are coefficients in a given annular section of the guide and moving rows.

From equation of continuity and triangles of speeds we determine the parameters, necessary for designing a moving row. The total flow of gas through the stage G is equal to the sum of flows through all the elementary flows. The total efficiency of the stage is found on the basis of the efficiency of the elementary flows as neutralized along the flow.

With such a calculation method, the flow factors  $\mu_1$  and  $\mu_2$  and coefficients

of speed  $\varphi$  and  $\psi$  should be assumed variable, depending on geometric and regime parameters in considered sections of the rows. The described method of calculation is very simple and gives reliable results.

The construction of guide and moving blades is realized by design data of the twist. From the calculated values of  $M_{c1}(r)$  and  $\alpha_1(r)$  the profiles in the root, middle and upper sections of the guide vanes are selected. With large heat differentials in the stage, in root sections  $M_{c1} > 1$ , and in peripheral  $M_{c1} < 1$ . Correspondingly the root sections will form profiles of group C (with reverse concavity in oblique section and a small expansion of channel), middle sections—profiles of group B (rectilinear sectors of back edge in oblique section), and the upper—profiles of group A (convex back edge in oblique section). Analogously there is constructed a moving blade, for which the following parameters serve as the initial:  $\beta_1(r)$ ,  $M_{u1}(r)$ ,  $M_{u2}(r)$  and  $\beta_2(r)$ . In the construction it is desirable to select spacings and adjusting angles of profiles in a range of optimum values.

The above-considered methods of profiling give virtually a coincident character in the change of reaction along radius which directly ensues from the approximate equation (9-50).

Certain differences are ascertained in the distribution of angles of absolute and relative flows  $\alpha_1$  and  $\beta_1$ , and also axial components of the speed.

A comparison of three methods of twist ( $c_{u1}r = \text{const}$ ,  $\alpha_1 = \text{const}$  and for cylindrical flow  $\rho_1 c_{a1} = \text{const}$ ) is presented in Fig. 9-12. A somewhat larger twist of moving row is given by the method  $\alpha_1 = \text{const}$ . In this connection the guide vanes prove to be the least twisted. For method of profiling  $c_{u1}r = \text{const}$ , the twist of the moving blades decreases and of the guide blade—increases. Intermediate results are obtained for cylindrical flow, corresponding to regularities of flow, arranged according to the method  $c_{u1}r = \text{const}$  at  $\rho_1 = \text{const}$ .

Experiments show that stages, profiled by the indicated methods, have virtually an identical effectiveness. A further increase in the efficiency obviously may be assured by selecting a rational distribution of the reaction along radius. Such a

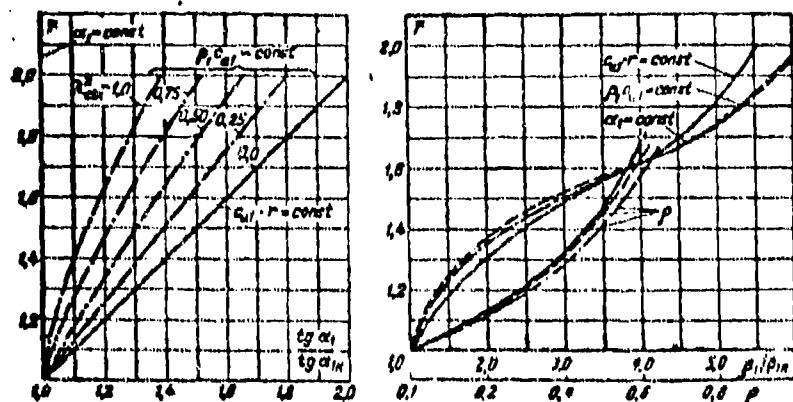


Fig. 9-12. Comparison of certain methods of twists of blades.

condition corresponds to law  $p(\bar{r})$ , with which radial pressure gradients in root sections will be minimal.

#### 9-6. Axial Stage with a Small Variation of the Reaction along Radius

The possibility of realizing a turbomachine stage with a small change of reaction along the radius is of great practical interest. In a turbine stage an equalizing of the reaction results in a more uniform field of speeds in clearance, to decrease in difference of angles at entry of flow  $\beta_1$  in upper and root sections, to a lowering of losses from leaks, to a decrease of axial stresses at cetera. For a compressor stage with a reaction  $p = 0.5$  owing to the equalizing of the field of speeds by height, there may be displaced the maximum limit with respect to M number, higher peripheral speeds and, consequently, a larger coefficient of pressure head with the maintenance of a high economy of the stage.

For stages of turbines with low heights of blades ( $I < 0.8$  and  $\Theta > 13$ ) the equalizing of the reaction can be realized by the use of meridional profiling of channels in guide row by height.

The condition of equality of centrifugal forces, acting within channel on an element of the mass of the peripheral and axial components of the speed, i.e. the condition of constancy of static pressure of channel by height can be

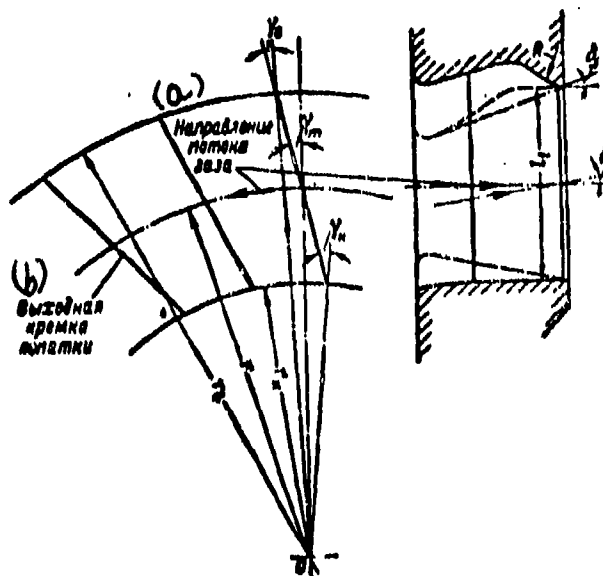


Fig. 9-13. Diagram of annular row of guide profiles with oblique edges and a meridional profiling.  
KEY: a) Direction of flow of gas; b) Exit edge of blade.

presented as:

$$\frac{r_k^2}{r_k} \approx \frac{r_k^2}{R} \quad (9-72)$$

Here  $R$  is radius of curvature of upper contour in the meridional plane;  $r_k$  is the radius of root section (Fig. 9-13).

From (9-72) we find:

$$R = r_k \tan^2 \alpha_1$$

As has been indicated (Sec. 8-8), the use of meridional profiling in stage with low heights of blades makes it possible not only to decrease the difference between reactions, but also significantly to decrease losses in the guide rows. In Fig. 9-14 there are illustrated the results of tests of two stages ( $T_1 = 0.5$ ;  $\Theta = 16$ ) with curvilinear and cylindrical contours of the upper band. It is evident that the stage with a meridional profiling has a higher efficiency (by 1.5—2%), and the difference between the reactions  $\Delta p = p_a - p_k$  decreases more than threefold (from 16 to 5%).

From a stage with a  $\Theta < 10$  meridional profiling it is difficult to attain

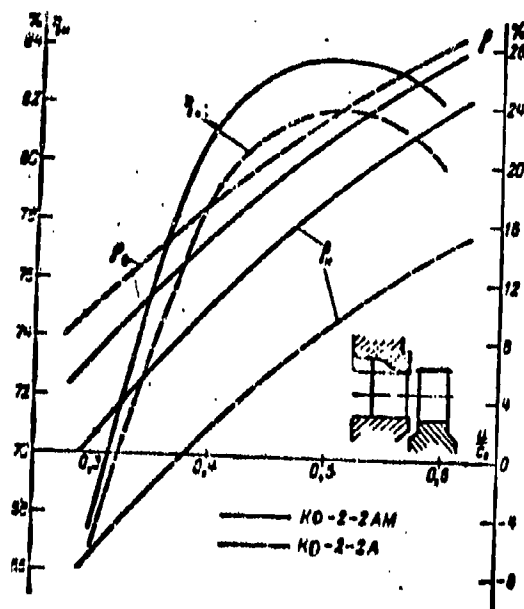


Fig. 9-14. The dependence of the efficiency of  $\eta$  and reaction on  $u/c$  for a stage with meridional profiling (KD-2-2AM) and for a stage with cylindrical contours (KD-2-2A)  $\theta = 16$ ;  $\bar{r}_1 = 0.5$

significant equalizing of the reaction without a significant increase of losses in guide row.

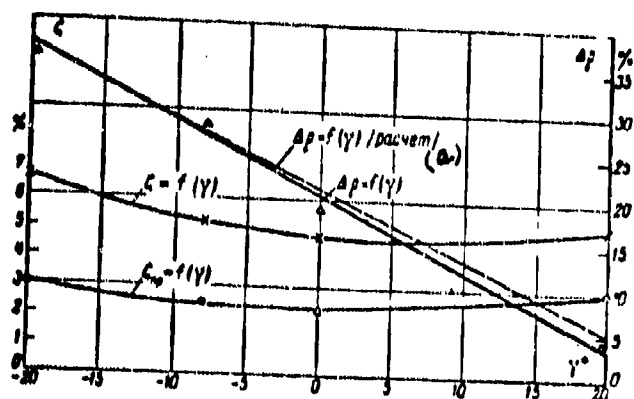


Fig. 9-15. Variation of difference of reaction  $\Delta P$  of profile and total losses in rows as a function of slope angle of blades  $\gamma$  ( $\theta = 8.5$ ;  $\bar{r}_1 = 1.0$ ;  $a_1 = 15$ ).  
KEY: a) Calculation.

For the limiting values  $2.5 \leq \theta \leq 5$  for the purpose of lowering gradient of static pressure along radius, it is expedient to use slope of blades in the radial plane. Actually, from equation of radial equilibrium, written out taking into

account forces of the action of blades on flow,

$$\frac{1}{r} \frac{\partial p}{\partial r} = \frac{c_a^2}{r} - c_r \frac{\partial c_r}{\partial r} - c_a \frac{\partial c_r}{\partial x} + F_r \quad (9-73)$$

(where  $F_r$  is the radial component of the force of the action of blades on the flow) it is evident that at  $F_r < 0$  (slope of blades along the flow, Fig. 9-12) the pressure gradient is less than with a radial arrangement of the blades. Physically this means that on element of gas there acts a force, whose direction is opposite to the direction of the centrifugal force. Consequently, in this case, there is decreased difference between static pressures which assure the equilibrium of the gas element decreases.\*

Thus, slope of the guide vanes in plane of rotation can change the distribution of static pressure in the clearance and the distribution of the reaction along the radius.

In Fig. 9-15 there are shown results of tests of four annular rows with different angles of slope  $\gamma = 20^\circ; 0^\circ; -8^\circ; -20^\circ$ , made at the Moscow-Power Engineering Institute (MEI). As can be seen from the graph, with an increase of slope angle of blade along the flow difference between reactions in peripheral and root sections significantly decreases; for  $\Theta \approx 8$ ,  $\Delta p \approx 0$  can be attained at  $\gamma \approx 25^\circ$ . In the same graph there have been plotted the profile and total losses in the rows.

Within limits of variations of the slope angle  $\gamma$  from  $-8$  to  $+8^\circ$  profile losses virtually do not change and amount to 2-2.5%. At  $\gamma \approx +20^\circ$  and  $\gamma \approx -20^\circ$  the profile losses increase to 3%. This result is explained by the distortion of shape of vane channels with a large slope of the blades.

The total losses in the rows remain virtually constant within limits of varying the angle  $\gamma$  from  $-8$  to  $+20^\circ$ . An intensive increase of losses is observed with slope angles of  $-8^\circ > \gamma > +20^\circ$ . Graphs of the variation of losses by height of rows (Fig. 9-16) show that for negative slope angles the losses increase in the

\*An investigation of stages with oblique blades was made by Yu. I. Mityushkin (Leningrad Metalworking Plant) and G. A. Filippov (Moscow Power-Engineering Institute).

root sections, where there appears a separation of the flow. For rows with a slope of the blades along the flow, when there is realized a compression of the flow in root sections, the losses increase in the peripheral sections.

Experiments have shown that with a simultaneous introduction of meridional profiling of the upper contour of row and with the slope of blades it is possible to decrease losses in upper sections ( $\gamma > 0$ ). In this connection, both factors, the slope of blades along the flow and the profiling of upper contour make it possible to lower sharply differences between reactions  $\Delta p = p_s - p_k$ .

An approximate formula for determining the reaction in stage with different slope angles of blades  $\gamma$  can be obtained by means of a common solution of equations of momentum and of radial equilibrium of cylindrical flow (9-73). The force of the effect of blades on the flow is determined in terms of the peripheral component

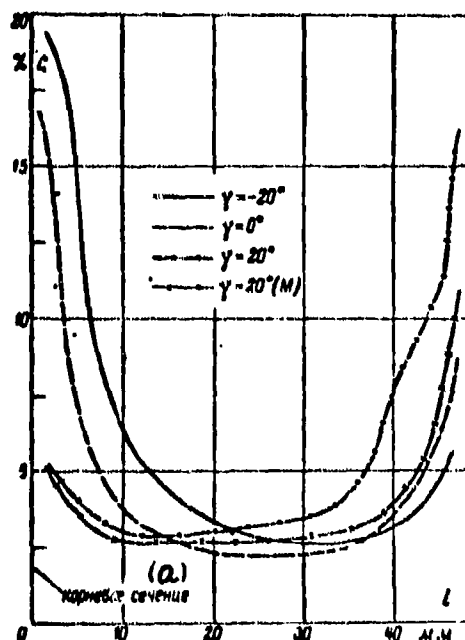


Fig. 9-16. Character of change of losses along height of row at various angles of inclination of blades ( $\theta = 8.5$ ;  $\bar{I}_1 = 1.0$ ;  $\alpha_1 = 15^\circ$ ). KEY: a) Root section.

by the equation ( $c_r \approx 0$ ):

$$F_r = \frac{p_n}{\tau_{2n}(90-\gamma)} - \frac{c_a}{\tau_{2n}(90-\gamma)} \frac{dc_a}{dx},$$

where  $P_u$  is the peripheral component of force of effect of blades on the flow.

After assuming a linear law of the change in  $c_u$  across width of row for a middle line of channel  $c_u = xc_{u1}/B$ , we obtain:

$$F_p = c_1 \sin \alpha_1 \frac{c_1 \cos \alpha_1}{B \tan(90 - \gamma)}.$$

Substituting  $F_p$  in equation (9-73), we find:

$$\frac{dp}{r} = \frac{c_1^2 \cos^2 \alpha_1}{r} dr - \frac{c_1^2 \sin \alpha_1 \cos \alpha_1}{B (90 - \gamma)} dr.$$

From the latter equation jointly with equation of energy we obtain:

$$\frac{dc_1}{c_1} = \frac{\sin \alpha_1 \cos \alpha_1}{B \tan(90 - \gamma)} dr - \cos^2 \alpha_1 \frac{dr}{r}.$$

After integrating this equation for the case  $\alpha_1 = \text{const}$ , we obtain the distribution of speeds by height of blades:

$$\frac{c_1}{c_{1k}} = \left(\frac{1}{r}\right)^{\cos^2 \alpha_1} \exp \left[ \frac{\sin \alpha_1 \cos \alpha_1 (r_1 - r_k)}{B \tan(90 - \gamma)} \right]. \quad (9-74)$$

The reaction in arbitrary section of clearance is calculated by the formula

$$p = 1 - (1 - p_k) \frac{v_{1k}}{v_1} \left(\frac{1}{r}\right)^{2 \cos^2 \alpha_1} \exp \left[ \frac{2 \sin \alpha_1 \cos \alpha_1 (r_1 - r_k)}{B \tan(90 - \gamma)} \right]. \quad (9-75)$$

The difference between reactions at  $p_k = 0$  and  $b \approx 1.5B$  ( $b$  is the chord of profile)

$$\Delta p = 1 - \left[ \left( \frac{b-1}{b+1} \right) \exp \left( \frac{3 \tan \alpha_1 \tan \gamma}{2 \tan(90 - \gamma)} \right) \right]^{2.1 \cos^2 \alpha_1} \frac{v_{1k}}{v_1}. \quad (9-76)$$

The obtained formulas give values somewhat too high for the difference between reactions which is connected basically with the deflection of flow in clearance of stage from coaxial, by the presence of radial overflows of gas in the boundary layer of blades, by leaks in the stage, by the effect of moving wheel. The error of calculation is explained also by the assumed approximate law of variation of  $c_u$  along axis of channel et cetera.

The influence of the enumerated factors is considered the basis of experimental data introduced by the coefficient  $A = 0.65$  in formula (9-76).

The calculation of the reaction in stage with slope of blades along flow and meridional profiling of upper contour is realized by the formula

$$p = 1 - (1 - p_k) \frac{v_{1k}}{v_1} \left( 1 + \frac{l_1 \sin^2 \alpha_1}{2R} \right) \left( \frac{1}{r} \right)^{1.3 \cos^2 \alpha_1} \times \exp \left[ \frac{1.3 \sin \alpha_1 \cos \alpha_1 (r_1 - r_k)}{B \tan(90 - \gamma)} \right]. \quad (9-77)$$



obtained by taking into account the influence of curvature of upper contour on the distribution of the speeds along the radius in the clearance.

Experience confirms the satisfactory accuracy of formula (9-77) at  $\theta > 6$ .

For stages with small  $\theta < 5$  and supercritical heat differentials the application of slope of blades also is expedient. Actually, with a significant degree of fanwise arrangement of blades of the flow part (Fig. 9-17) the compression of flow makes it possible to improve the flow around the root sections; the flow around the upper sections is virtually constant since the slope angle  $\gamma_u$  at the periphery is much smaller than at the root. For example, for a stage with  $\theta = 2.6$  and  $\gamma_m = 9^\circ$ , the slope at vertex is  $\gamma_u = 5^\circ 40'$  and at the root  $\gamma_u = 14^\circ$ . The decrease of reaction in the upper sections and correspondingly decrease of angle at entry of flow for the moving blades  $\beta_1$  will result in a decrease of twist of moving blade.

The redistribution of the heat differential between guide and working rows and decrease of angle  $\beta_1$  in the peripheral sections, caused by the slope of blades along the flow, facilitates the profiling of upper sections of moving rows at supersonic speeds.

Influence of the slope of guide vanes in the stage  $\theta = 2.6$  and  $s_u = 0.27$  on the distribution of parameters along radius is shown in Fig. 9-17. With a slope in middle section  $\gamma_m = +3^\circ$  the reaction in upper section lowered from 75 to 56%, angle at entry of flow  $\beta_1$  decreased from  $155^\circ$  to  $127^\circ$ . The  $M_{c1}$  number increased at vertex of blade to 0.9, and the  $M_{w2}$  number decreased to  $M_{w2} = 1.08$ .

The latter turbine stages frequently must be realized with conical contours (Fig. 9-12). The presence of conicity results in a decrease of the reaction in stage.

For a conical guide row, the change in reaction along the radius can be determined approximately by the formula

$$\rho = 1 - (1 - \rho_u) \left( \frac{1}{r} \right)^{2 \cos^2 \alpha_1 \frac{\eta_{1u}}{\eta_1} K_1},$$

where  $K_1 = 1 + \sin^2 \alpha_1 \delta_u^2$  is the coefficient, which considers the effect of conicity;  $\delta_u$  is the angle of conicity at vertex.

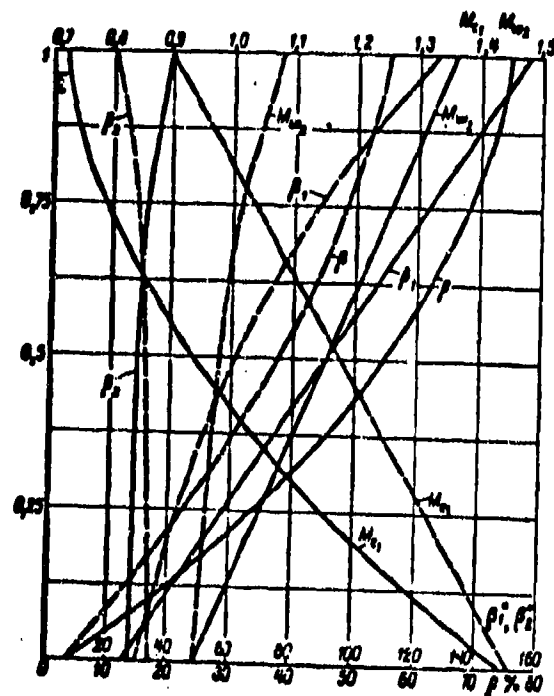


Fig. 9-17. Variation of parameters by height of blades ( $\theta = 2.6$ ;  $\alpha_s = 0.27$ ).  
 ----with slope of edges: ——— - radial edges.

## CHAPTER 10

### METHODS OF EXPERIMENTAL INVESTIGATION OF GAS FLOWS AND BLADING OF TURBOMACHINES

#### 10-1. Experimental Stands For Investigation of Bladings of Turbomachines

Problems of experimental investigation of the blading of turbomachines can be divided into three groups. In the first group are included questions connected with the investigation of the structure of flow in separate elements of the stage, considered as isolated and, in the first place, in the guide row and moving row.

The second group of problems consists of a differentiated study of the physical phenomena occurring in the stage.

The third group of problems reduces to the determination of the experimental coefficients necessary for thermal design of the turbomachine and for the explanation of the dependence of these coefficients on the basic structural, geometrical and regime parameters of the stage.

Main requirements for experiment under laboratory conditions are formulated by theory of analogy. In practice, not all of these requirements can be realized with an identical degree of accuracy, since actual processes in the turbomachine are distinguished by great complexity. Therefore, for the experimental setup, one should establish the most important characteristics of the process in each individual case, disregarding its secondary characteristics. Correct solution of this problem determines the direction and method of the experiment and also the theoretical and practical value of the results of the investigation. If the main goal of the

experiment is the obtaining of integral characteristics of the stage, then it is obvious that in the model conditions there must be reproduced all of the most essential characteristics of the process. Therefore experimental investigation of the characteristics of the stage must be conducted on a special experimental turbine or experimental compressor, allowing the establishment of reliable values of characteristics and the study of the main properties of flow in the cascades.

The last problem, however, is difficult to solve in an experimental machine since this requires the application of complicated special measuring equipment. Therefore for detailed study of flow around cascades during the study of the mechanism of formation and development of losses in individually considered cascades, it is necessary to resort also to other simpler methods of experiment, waiving certain requirements of the theory of similitude. It follows from this that along with the use of an experimental turbomachine as the main method of investigation, it is necessary to apply also the simpler and therefore more wide-spread methods of test of stationary rows.

Investigations of elements of the blading of steam and gas turbines can be carried out with water vapor or with air, and the diagram of the test stand depends considerably on the applied working fluid. Investigations of elements of the compressor are carried out, naturally, on air.

The fundamental diagram of the air experimental stand for the investigation of bladings of turbines and compressors is presented in Fig. 10-1.

Air is compressed by compressor 2 and, passing through receiver 3, is purified in filter 4. When necessary, the temperature of the air can be raised in the air pre-heater 5. This is especially important during the attainment in the investigated row of high velocities when the temperature of the air abruptly drops, which causes condensation of the water vapors, which are always in air.

With the cleaned and warmed up air are fed: experimental installations for investigation of flat stationary rows 6 and for investigation of annular stationary rows 7, the air experimental turbine 8, the installation operating on the principle

of measurement of reactive stresses 10, wind tunnel 11 with optical instruments 12 and the block 17 for tests of ejectors, ducts, valves, etc.

The annular wind tunnel 7 is designed so that, besides pneumometric measurements, it allows the measurement of torque and axial stress on the investigated row. The air experimental turbine 8 with hydraulic or induction brake 9 is analogously designed.

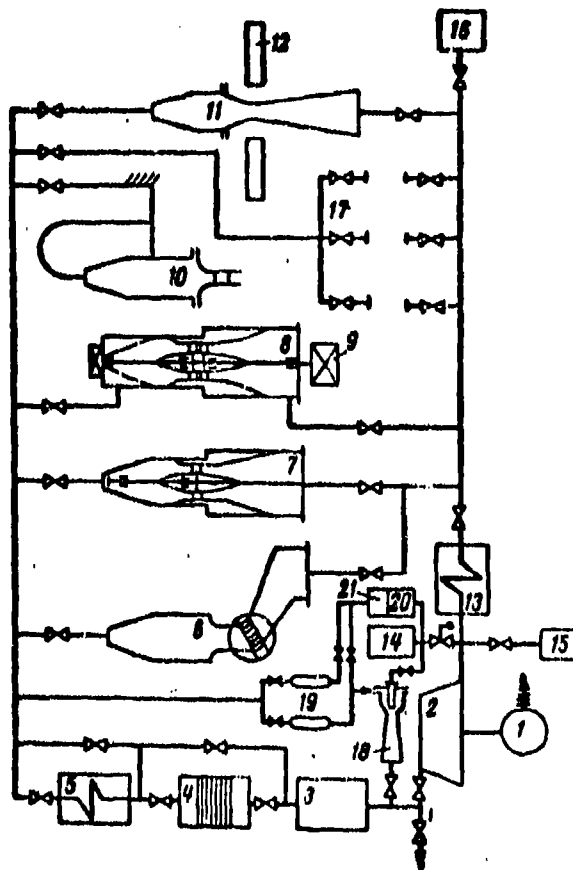


Fig. 10-1. Fundamental diagram of an air experimental stand.  
1-motor; 2-compressor; 3-receiver; 4-filter; 5-preheater; 6 and 7-static installations; 8, 9-experimental turbine; 10-installation for measurement of reactive stress; 11-wind tunnel; 12-optical installation; 13-refrigerator; 14-additional compressor; 15-filter; 16-muffler; 17-stand for test of valves, ejectors, etc.; 18-ejector; 19-tanks; 20 and 21-filter and moisture separator.

The wind tunnel is a necessary element of the stand and is designed for calibration tests of different measuring instruments and necessary systematic operations. On the plane installation 6 or in wind tunnel 11 are conducted experiments with the application of the optical apparatus 12. The stand can work by the opened, as well as by the closed diagram. The closed diagram, being the more complicated, makes possible, however, the independent change of numbers  $M$  and  $Re$ , i.e., allows the investigation separately of the influence of compressibility and viscosity. For the setup of a number of experiments, this requirement is basic.

During the use of the open diagram air is ejected into the atmosphere through the muffler 16. During operation by the closed diagram, air moves through the cooler 13 into the suction line of the compressor.

For creation in the closed circuit of the stand of increased pressure and compensation of leaks through cracks and seals, the supplementary compressor 14 is necessary with a pressure exceeding the maximum pressure in the suction duct of the main compressor. If compressor 14 has sufficient compression ratio and efficiency, then, for a number of regimes, instead of the main compressor 2, compressor 14 and ejector 18, can be used, feeding the experimental installations with air at lowered pressure.

In case it is necessary to carry out an experiment requiring large flow rates and high velocities, the tank set-up can be applied, consisting of compressor 14 and a group of tanks 19. For a definite time the tanks 19 are filled by compressor 14 through filter 20 and moisture separator 21. Then air from the tanks is directed through regulating valves into the experimental installation. Since during operation, the pressure in the tanks will fall, for maintenance of the constant regime of the experimental installation it is necessary to use automatically controlled valves. Briefness of the action is the main shortcoming of the tank set-up.

The method of experiment with air at temperatures of the order of  $50-100^{\circ} C$

is significantly more simple than with steam at temperatures of 250°-350° C.

This determined the wide application of air in laboratory investigations of bladings of turbomachines.

However, a number of problems connected with extended operation of experimental installations with large flow rates and at high velocities require extraordinarily powerful and cumbersome compressor installations. Work connected with the investigation of the last stages of condensation steam turbines can be conducted with air only partially, and these problems in general cannot be solved on the air stand.

The optimum solution, giving the greatest possibility of conducting different investigations of bladings of turbines with minimum expenditure of time and means, is the use of a composite steam-air stand, whose basic diagram is shown in Fig. 10-2.

The majority of installations of such a stand can operate on air as well as on steam, which allows us to select the optimum type of working fluid for the given experiment. The air circuit of the stand does not differ from the one presented in Fig. 10-1. Use of steam allows us easily to obtain large flow rates and high velocities, and to change independently the numbers  $M$  and  $Re$ ; it also provides for the conduction of all investigations connected with humidity. Steam moves through the reducing-cooling installation 29 to the experimental installations of the stand, passes through them and heads into the main condensor 21. The condensate by means of the condensate pump 24 moves into the measuring tank 25, and then into the return line of the condensate of the heat and electric power plant.

The steam-air stand consists of an installation for the investigation of annular stationary rows 7, the high-speed single-stage experimental axial turbine 8, the two-shaft experimental turbine 14, intended basically for investigation of the last stages, the experimental turbine for investigation of radial-axial stages 20, axial 26 and centrifugal 27 experimental compressors with steam turbine drive 28, and the installation for testing of the plane cascades 6.

If necessary, in the steam-air stand ejector wind tunnels 18 and 19 can be used, the air flow in which is created by a steam ejector, sucking in air from

the atmosphere.

In the diagram of the stand is included block 17, allowing us to establish for periodic tests different auxiliary components of turbines.

For drawing off of steam from seals of the experimental turbines the auxiliary condensor 23 is used. Vacuum in the condensers is maintained by steam ejectors 22.

It is desirable to supply the exhaust ducts of turbines with throttling mechanisms, allowing us to raise the counterpressure after the rotor wheel to 3-5 atm (abs). For the majority of experiments a pressure of fresh steam of 5-7 atm (abs) at a temperature of 250°-350° C is sufficient.

The reducing-cooling installation must allow feeding of stands not only with superheated steam of lowered parameters, but also with wet steam.

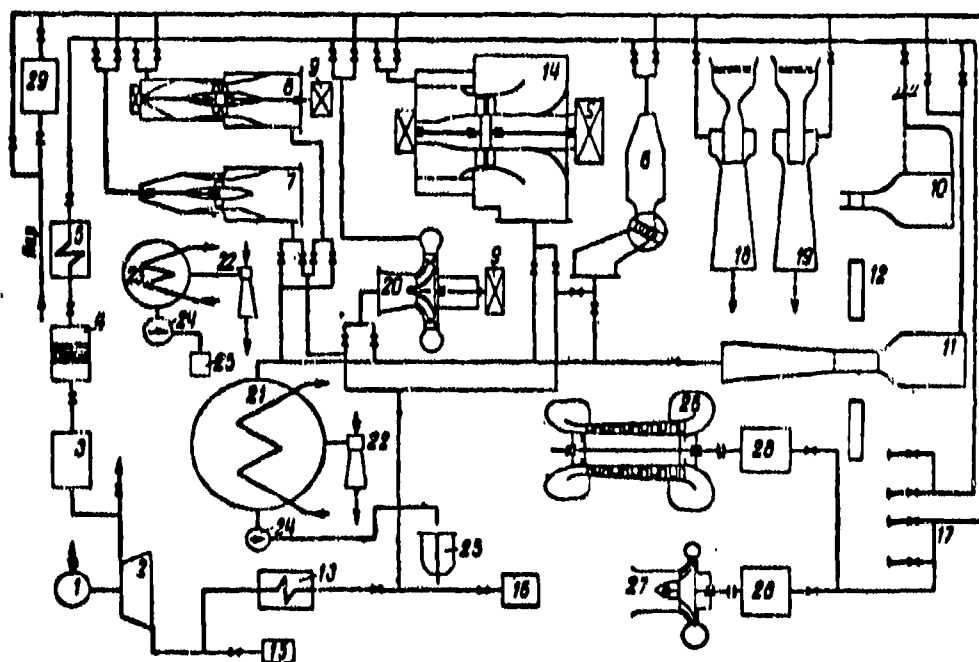


Fig. 10-2. Basic diagram of steam-air stand of Moscow Power-Engineering Inst. 1 and 2-motor and compressor; 3-receiver; 4-filter; 5-pre-heater 6, 7, 10, 11, 18 and 19-wind tunnels; 9-load mechanisms; 8, 14 and 20-experimental turbines; 21 and 23-condensers; 22-ejectors; 24-pump; 25-measuring tank; 26 and 27-experimental compressors; 28-drive turbines; 29-reduction-cooling installation.



## 10-2. Methods of Measurement of Parameters of the Working Fluid During the Investigation of Gas Flows

The basic parameters of the working fluid directly measured in the process of experiment are: total stagnation pressure and temperature, static pressure, and also the direction and magnitude of the vector of velocity. During investigation of non-stationary phenomena, the frequency, amplitude and form of change of these parameters with time are measured.

For measurement of pressures in flows various heads are applied.

Dimensions of the investigated cascades are usually small, especially during tests at high velocities. Consequently, the dimensions of the head should be minimum, so that perceptible distortion of the investigated field does not occur. Significant nonuniformity of flow after the cascade also causes a maximum decrease of the dimensions of the receiver and a change of its design in distinction from widely known heads, which are applied for measurement in relatively uniform flows.

We will consider certain designs of heads.

Total stagnation pressure is measured by the heads, schematically depicted in Fig. 10-3. The perfection of the nozzle is characterized by the dimensionless coefficients:

$$K_{p_0} = \frac{p_0 - p_{0u}}{\frac{1}{2} \rho c^2}; \quad \nu_{p_0} = \frac{p_{0u}}{p_0},$$

where  $K_{p_0}$  is the coefficient characterizing the sensitivity of the head to change of the angle of incidence;  $\nu_{p_0}$  is the coefficient characterizing the quality of the receiver;  $p_0$  is the actual total stagnation pressure for an angle of incidence  $\delta = 0$ ;  $p_{0u}$  is the measured stagnation pressure for given  $\delta \neq 0$ ;  $p_{0u}$  is the measured stagnation pressure at  $\delta = 0$ .

It is experimentally established that at  $\delta = 0$  the coefficient  $\nu_{p_0}$  is approximately identical for all forms of the heads presented in Fig. 10-3 and is near to unity. Magnitude of  $K_{p_0}$  considerably depends on the form of the head, which is illustrated by the characteristics in Fig. 10-3.

For measurement of stagnation pressure near the walls, where there are significant gradients  $p_0$ , micro-heads are applied. For measurements in bounded regions, for example in gaps between the guide and moving apparatuses, heads of types  $f$  and  $g$  are applied. Nozzle  $f$  is more useful at low velocities and is distinguished from nozzle  $g$  only by lower rigidity.

For measurement of static pressure, the heads whose diagram and characteristics are shown in Fig. 10-4 are applied. Measurement of static pressure is difficult due to the necessity of stricter orientation of the axis of the head in the direction of the velocity vector of flow.

The sensitivity of the head to change of the angle of incidence of the flow and the quality of the receiver of static pressure are characterized by the following dimensionless coefficients:

$$K_p = \frac{p_s - p}{\frac{1}{2} \rho v^2} \quad \text{and} \quad v_p = 1 - \frac{p - p_u}{p_s - p},$$

where  $p_s$  is the pressure, shown by the instrument at the given angle of incidence;  $p$  is the static pressure of undisturbed flow;  $p_u$  is the measured pressure at  $\alpha = 0$ .

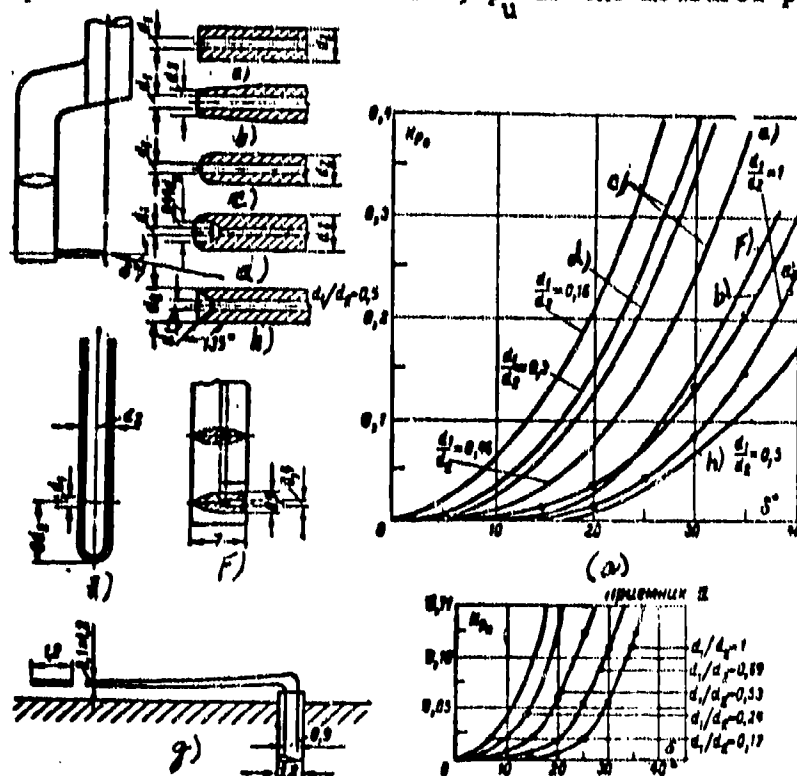


Fig. 10-3. Heads for the measurement of stagnation pressure. a-h are forms of receivers and results of calibration. KEY: (a) receiver a.

For measurement of static pressure in flows of subsonic velocity, the head of type b gives satisfactory results. The head consists of a pipe with a spherical end; diameter  $d = 0.9$  to  $1.2$  mm with two receiving apertures of diameter  $d_1 = 0.2$  to  $0.3$  mm. Measurements in gaps and other places accessible with difficulty

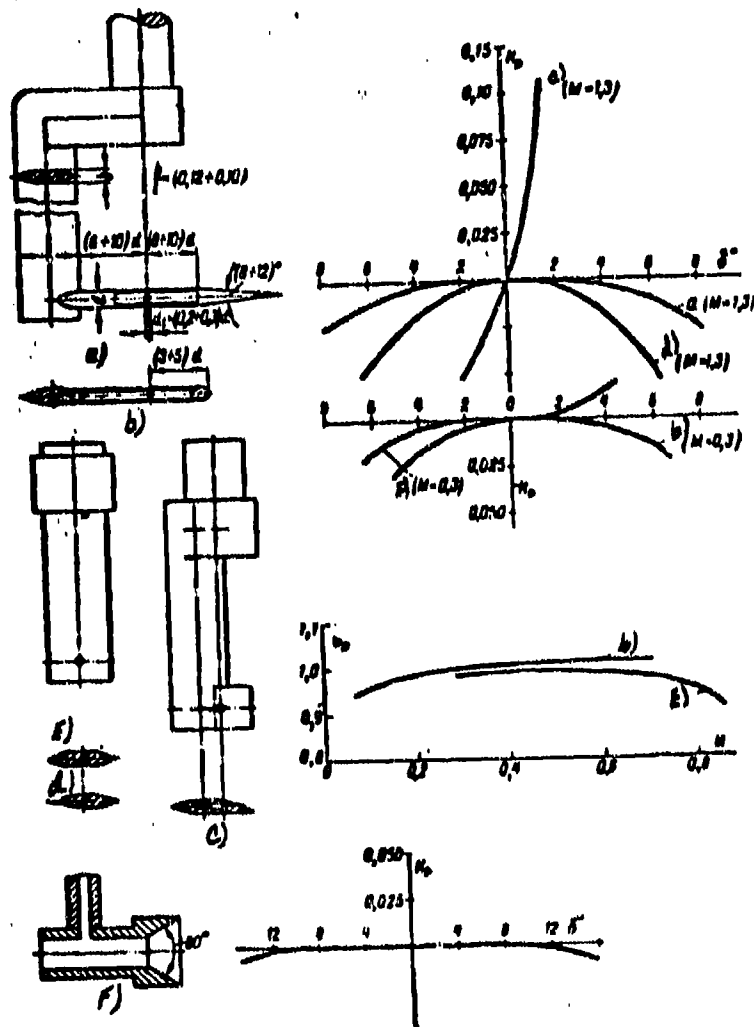


Fig. 10-4. Heads for the measurement of static pressure in the flow a-f are forms of receivers and results of calibration.

sometimes require the application of heads of the types c, d and e, distinguished by large rigidity, smaller linear dimensions, but also by worse characteristics.

For measurements of static pressure at supersonic velocities the head  $a_1$ , which has a favorable characteristic, is applied. Independently of the design of the head, its receiving apertures are conveniently located on the axis of rotation.

During total supersonic stagnation flow around the head a curved shock will be formed. Assuming that the neutral flow line crosses an element of the normal shock, it is possible to use already known equations for the determination of

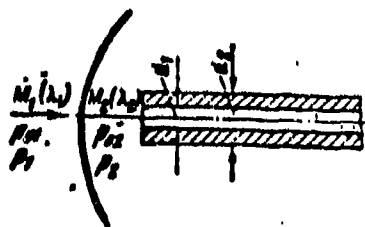


Fig. 10-5. Curved shock before a pitot head.

stagnation pressure if the dimensionless velocity of the incident flow  $M_1$  and the static pressure  $p_1$  (Fig. 10-5) are known.

Under the conditions of the experiment it is usually possible to measure  $p_1$  and the stagnation pressure behind the shock  $p_{02}$ . With help of the equations of the normal shock, it is simple to find the connection between  $p_{02}/p_2$  and  $p_2/p_1$  and finally to obtain the dependence for  $\frac{p_1}{p_{01}} = \frac{p_2}{p_{01}} \frac{p_1}{p_2}$ , allowing the determination of  $M_1$  (or  $\lambda_1$ ):

$$\frac{p_1}{p_{01}} = \left( 1 - \frac{k-1}{k+1} \frac{1}{\lambda_1^2} \right)^{\frac{k}{k-1}} \frac{1 - \frac{k-1}{k+1} \lambda_1^2}{\lambda_1^2 - \frac{k-1}{k+1}} -$$

$$- 2 \left\{ \frac{[4kM_1^2 - 2(k-1)]^{\frac{1}{k-1}}}{(k+1)^{\frac{k-1}{k-1}} M_1^{\frac{k-1}{k-1}}} \right\}.$$

Instead of direct calculations by this formula, it is convenient to use tables of functions of the normal shock or the diagram of shocks.

For measurement of the direction of the velocity vector in gas flow, are applied various designs of goniometrical heads: spherical, cylindrical, tubular and wedge-shaped. The most convenient are the tubular and wedge-shaped goniometrical heads (Fig. 10-6). Spherical and cylindrical heads cannot be recommended due to the complexity of their manufacture, and calibration and significant errors during

measurements in nonuniform flow.

With the help of a tubular or wedge-shaped head, the direction of velocity is determined by the difference of pressures which are measured on the surface of the wedge at an identical distance from the edge.

In flows of high subsonic and supersonic velocities, the heads of types a and b have an approximately identical characteristic. A head of type a has large linear

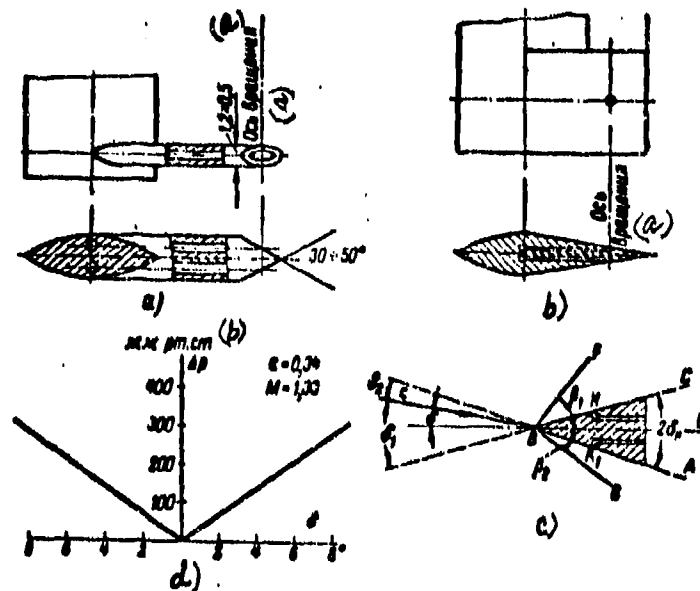


Fig. 10-6. Heads for measurement of direction of the velocity vector at a point; d is the result of calibration. KEY: (a) axis of rotation; (b) mm of Hg.

dimensions, is less vibrationally stable, but is more accurate and in a smaller stage disturbs flow near the point of measurement. A head of type b is more rigid and compact, but does not allow measurements near the walls confining the flow.

If the wedge ABC (Fig. 10-6,c) is located at an angle of incidence  $\delta$  to the flow line, then the bow wave appearing at point B, at  $M_1 > 1$  will be asymmetric with respect to the axis of the wedge BE. Consequently, the pressure at point K will be higher than at point K1. At  $\delta > \delta_k$ , instead of the shock EG, a wave of rarefaction may appear. The difference of pressures  $p_k - p_{k1}$  in this case is increased still more. Since the initial orientation of the axis of the head is known, then, turning the head until the pressures  $p_k$  and  $p_{k1}$  are equal by the

indicator, the direction of the velocity of flow is determined. It is desirable that the angle of sharpness of the nozzle be less than the critical angle at which the curved shock will be formed, considerably lowering the sensitivity of nozzle.

Measurement of the static temperature of the moving gas causes significant difficulties. The stagnation temperature can be measured comparatively simply; methods of its measurement are considered below.

There exists a large number of designs of thermal heads for measurement of stagnation temperature based on one and the same principle: the stream of investigated gas by one method or another is decelerated, and the thermally sensitive element is placed in the zone of decelerated flow.

The stagnation temperature  $T_0$  is connected with the flow velocity and static temperature  $T$  by the known relationship:

$$T_0 = T \left( 1 + \frac{k-1}{2} M^2 \right) = T + \frac{Ac^2}{2gc_p}$$

The thermoreceiver introduced into the region of decelerated flow, due to heat exchange with its environment and incomplete deceleration, will have some temperature  $T_1$ , bounded by the limits  $T < T_1 < T_0$  and determined by the equation  $T_1 = T + r \frac{Ac^2}{2gc_p}$ , where  $r < 1$  is the recovery factor of the thermoreceiver. Measuring temperature  $T_1$  and knowing from calibration tests the value of  $r$ , it is simple to calculate the true stagnation temperature  $T_0$  by the formula

$$T_0 = T_1 + \frac{Ac^2}{2gc_p} (1 - r).$$

The principle requirements of the thermal head reduce to the following: 1) the value of  $r$  should as near as possible to unity, since at  $r = 1$ ,  $T_1 = T_0$ ; 2) the value of  $r$  must remain constant in a range of numbers  $M$  and  $Re$  which is as wide as possible; 3) overall dimensions of the thermal head must be minimum.

As a rule, a thermocouple serves as the sensitive element in the thermal head. Lately semiconductor thermoelements (thermistors), which have higher sensitivity, have received widespread use.

In Fig. 10-7 and 10-8 are presented several diagram and characteristics of

thermal heads, which are the most suitable for the conditions of experimental investigation of bladings of turbomachines. For investigation of temperature fields after the stage it is possible to recommend thermal heads of type d, which have very stable characteristics. Such heads are insensitive to rake angle within the limits  $\pm (10^\circ \text{ to } 12^\circ)$ . For measurements in clearance spaces of turbomachine stages, the most suitable is the thermal head of type b.

A somewhat improved modification of the transversely streamlined quick-response head, which allows measurement at elevated pressures with full hermetic sealing, is shown in Fig. 10-7,c. One electrode of this head is made in the form of a thin-walled, for example copper, pipe of dimensions  $1.1 \times 0.8 \text{ mm}$ , inside of which, in a porcelain tube, is inserted a second electrode.

After installation of the internal electrode, the end of the pipe is ground and covered with a thin layer of electrolytic copper. The "junction" of such a thermocouple for a diameter of the internal electrode of the order of  $0.05 \text{ mm}$  possesses insignificant inertia, and the thermoreceiver itself is very easily sealed. In Fig. 10-8 are presented designs and characteristics of heads which are applied at high supersonic velocities and significant temperatures. Good results were shown by the nozzles of type a.

The casing of the shield and the sensitive element of this head is made from quartz, covered by layer of platinum, which significantly decreases convective and radiant heat exchange at high values of  $T_0$ .

For measurement of the stagnation temperature in the boundary layer and in flows with small free flow section, the thermal head c can successfully be applied; however, manufacture of a head with such small dimensions presents definite difficulties.

During investigations in the region of elevated temperatures, where it is essential to consider radiant heat exchange, the thermal head d can be used, which is insensitive to wash of flow within the limits of  $\pm 12^\circ$  and is shielded by a double screen.

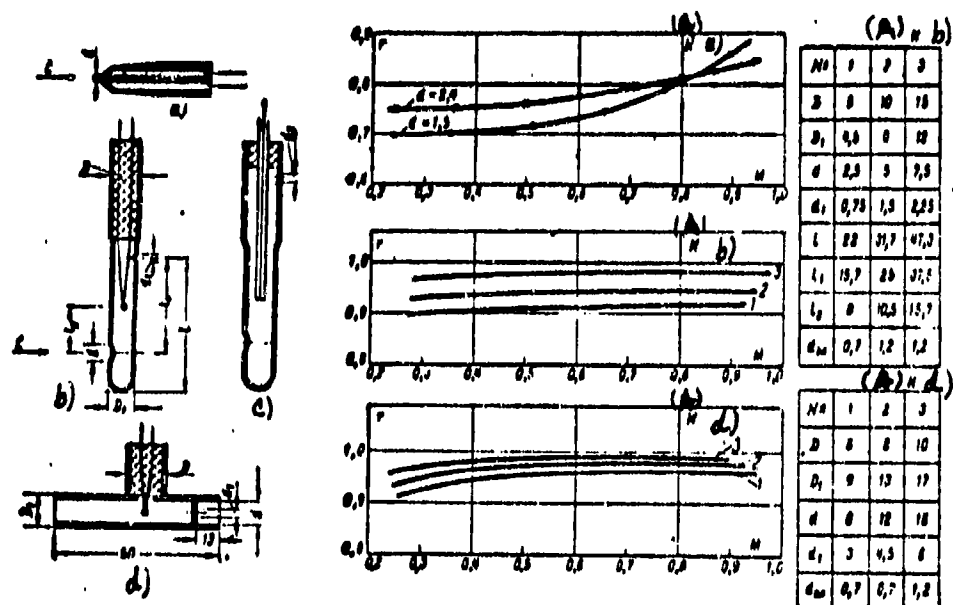


Fig. 10-7. Thermal heads for measurement of stagnation temperature and results of their calibration.

KEY: (a) for.

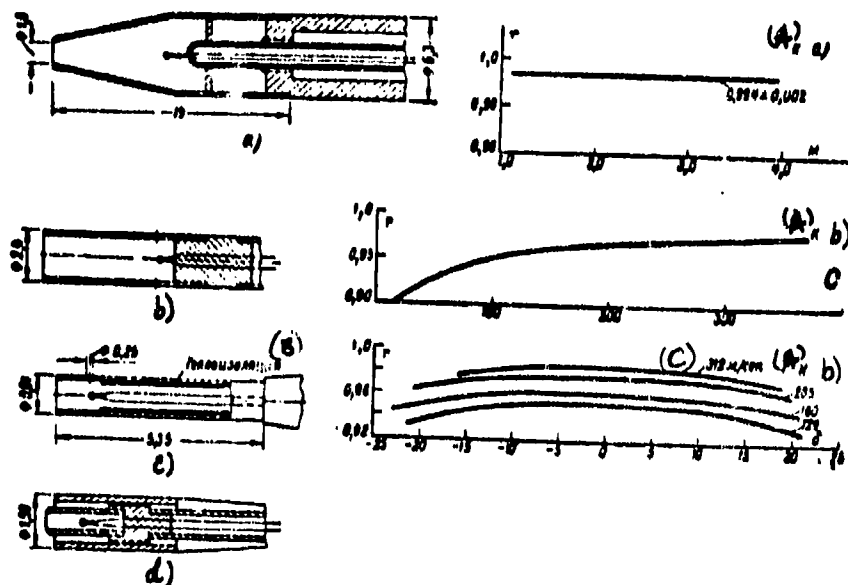


Fig. 10-8. Longitudinally streamlined thermal heads and results of third calibration.

KEY: (a) for; (b) thermal insulation; (c) m/sec.



For comparatively large dimensions of the investigated field, it is convenient to apply combined heads, which give simultaneously values of two or more parameters. Several designs of such heads are shown in Fig. 10-9. The head a is used for simultaneous measurement of total stagnation pressure and the direction of two-dimensional subsonic flow.

The head b is widely used in the Moscow Power-Engineering Inst. during the simultaneous measurement of total stagnation pressure and the direction of two-dimensional and supersonic flows and is the most perfect of the heads of this type.

The comb-like head is convenient for the measurement of total stagnation pressures in flows with small change of angles over the section.

The disk can be applied for simultaneous measurement of static pressure and direction of two-dimensional flow. Heads a and b in Fig. 10-10 are used for the simultaneous measurement of total stagnation pressure and static pressure.

Head c, consisting of tubes of complete deceleration and a Venturi tube, is insensitive to rake angle right up to  $40^{\circ}$ - $45^{\circ}$ , which makes it very convenient for a number of experiments in which turning the head for orientation of its axis is difficult.

In Fig. 10-10,d is represented a combined nozzle for the measurement of total stagnation pressure and temperature, proposed by I. Tsuber.

Processes, proceeding in turbomachine stages are periodically non-steady-state. Therefore a significant interest is presented by methods of measurement of the parameters of non-steady gas flows.\*

Since during the investigation of non-steady-state processes it is necessary to be concerned with frequencies reaching thousands of cycles per second, direct measurement of the parameters by the usual instruments becomes impossible.

---

\*Below are considered only some of the developed methods of measurement in non-steady flows. Electrical circuits of the measuring devices, which are described in applied special literature, are beyond the scope of this book and are not considered.

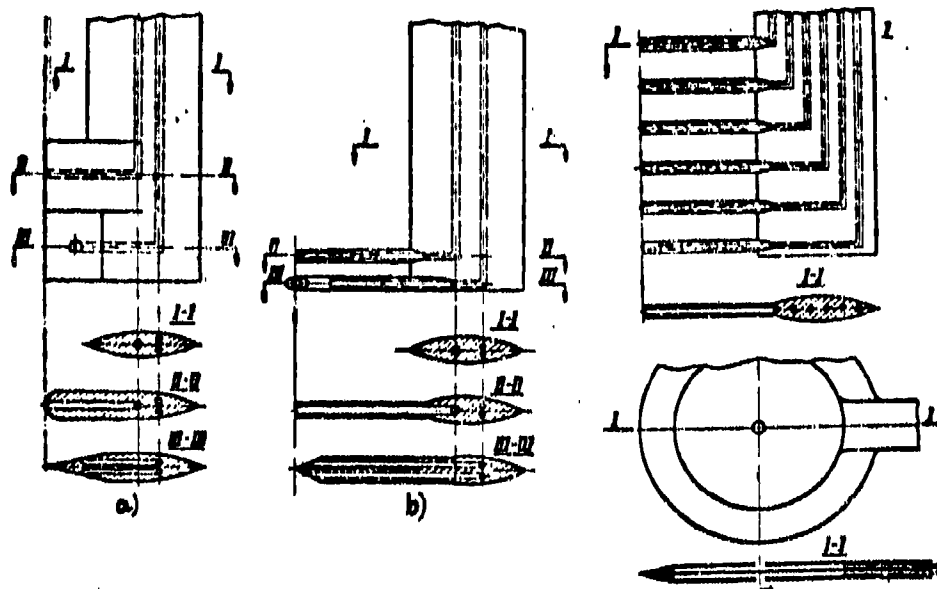


Fig. 10-9. Combined heads for measurement of stagnation pressure, static pressure and direction of the velocity vector.

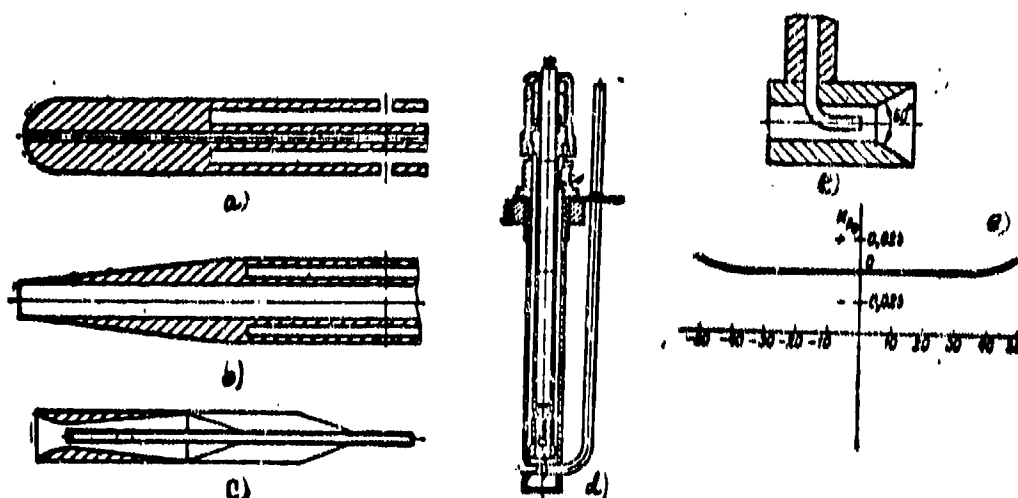


Fig. 10-10. Combined heads for the measurement of stagnation pressure and static pressure.

In this case special low-inertia heads are used, which uniquely convert the measured parameter into a current or emf of a certain value. By the change with time of the current or emf, the change in the measured parameter is determined.

At the basis of the design of a low-inertia nozzle with an electrical transducer there can be assumed various physical principles (change of resistance, capacitance, etc., as a function, for example, of pressure).

It is desirable, that the selected principle provide for the measurement of as large a number of parameters as possible of non-steady state flow.

For registering the form of the investigated process as accurately as possible, the natural frequency of the transducer should exceed the maximum frequency of change of the investigated parameter by at least an order of magnitude. Amplifying equipment, usually applied jointly with the sensors, must have a linear frequency response.

Realization of the amplifying and registering parts of the measuring installation with such requirements presents special difficulties, and the high natural frequency of the system of the transducer is attained with difficulty.

The head must have a sensitivity, as high as possible, linearity of characteristics in the region of measurement and time stability; it must also allow temperature compensation and have minimum over-all dimensions.

On the whole, the measuring system must allow simultaneous measurement and fixation of different parameters at several points for the manifestation of a time connection between them, and be, insofar as possible, simple in operation and insensitive to mechanical, thermal and electrical external influences.

The main difficulty in the creation of such equipment consists in the satisfaction of all, or in any case, of the majority of these requirements. For measurement in the flow core of rapidly varying total stagnation pressures and of static pressures and angles, in the Moscow Power-Engineering Inst. a number of quick-response

heads with tensometric transducers were developed; one of them is depicted in Fig. 10-11.

Actually, the head of such an instrument is a short pipe of total stagnation. The transducer of pressure into emf is located in a small box 1. of streamlined form fastened to the lens-holder. The pulsating measured pressure is brought under the diaphragm 2, on the reverse side of which is wound the spiral tensometric sensor of resistance 3.

The diameter of the mica diaphragm is nearly 5 mm; thickness is 0.012—0.050 mm. The spiral tensometric sensor with a diameter of 3 mm is wound from constantan wire,  $\varnothing$  0.03 mm, and has a resistance of  $\sim$  100 ohm. A strain gauge is included in the bridge input circuit of the measuring device, which consists of a stabilized power supply, an electronic multichannel amplifier and an oscillograph.

The described heads with strain transducers have fully satisfactory characteristics. This is illustrated by the oscillogram presented in Fig. 10-11,b, which was obtained on a special calibrating installation, which gives trapezoidal pulses of pressure of various magnitudes and frequencies.

As was shown above, one of the most important characteristics of a head with a transducer is the natural frequency of oscillation of the elastic system.

Increase of the natural frequency of the transducer and increase of its relative sensitivity may be attained by replacing the tensometric principle of measurement of strain in the diaphragm by a capacitive principle, which does not require placing on the diaphragm of any kind of additional mass.

In the Moscow Power-Engineering Inst. have been developed samples of quick-response heads with capacitive transducers. The basic circuit of the converter is clear from Fig. 10-12. As a mobile electrode of the converter serves a mica diaphragm 1, covered with a thin layer of aluminum. The fixed electrode 2 is completely isolated from the housing. The operating diameter of the diaphragm is 5 mm. The amplifying

electronic circuit is conveniently located directly on the holder of the head, since this prevents errors arising from the variable capacitance of connecting wires.

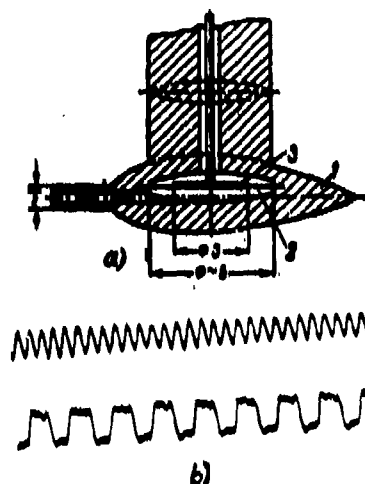


Fig. 10-11. Tensometric head for measurement of stagnation pressure and results of calibration.

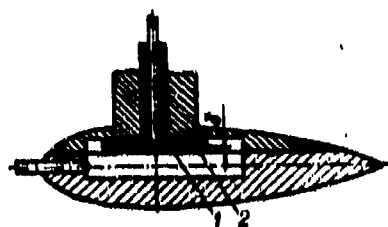


Fig. 10-12. Head with capacitive transformer.

For measurement of variable pressures on surfaces of streamlined bodies inductive transformers are very widely applied.

In spite of the relative complexity of their design, they are convenient due to the fact that, with the observance of certain conditions, they can operate directly on the loop of the oscillograph without electronic amplifiers.

Inductive transformers allow us to measure constant as well as variable

component pressures and are especially suitable when many-point remote measurements are necessary.

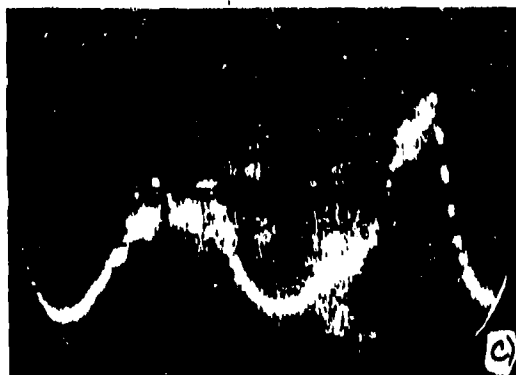
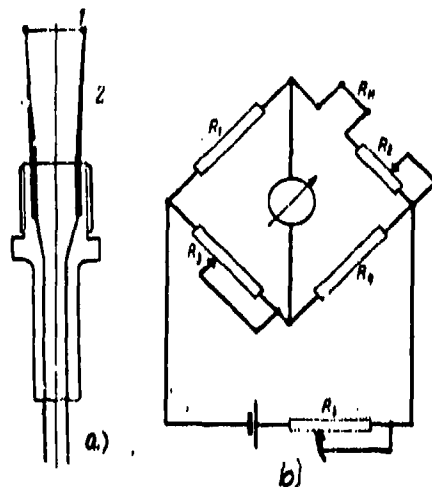


Fig. 10-13. Heads of electrothermoanemometer (a), fundamental electrical circuit (b) and an oscillogram of the pulsation of velocity (c).

At the present time, the best developed method of investigation of non-steady-state gas flows is thermoanemometry. A contemporary thermoanemometric installation, allowing the determination of pulsation of velocity, the magnitude and direction of velocity and the temperature of the investigated flow, is quite a complicated system, consisting of several heads, a measuring bridge, a special electronic amplifier and oscillographs.

The head of the thermoanemometer (Fig. 10-13,a) consists of a thin ( $\varnothing 0.01$  to  $0.02$  mm) platinum or tungsten wire 1, welded to two nickel holders 2, which are current conductors.

There exist two main fundamental circuits of the measuring system of thermoanemometers. In both cases the head  $R_x$  (Fig. 10-13,b) is connected into one of the arms of the bridge, whose remaining arms are made from resistances which are not dependent on temperature.

The bridge, balanced at  $c = 0$ , becomes unbalanced upon the introduction of the head into a flow with some velocity  $u$ . Balance of the bridge can be restored either by increase of the current with the help of the rheostat  $R_1$  or compensation of the change of resistance  $R_x$  with the help of  $R_2$ .

The first method is called "constant resistance." The more wide-spread is the second method--the method of direct current.

During measurements in non-stationary flows, into the measuring diagonal is connected an electronic amplifier with a special selected characteristic, which allows, within definite limits, the compensation of the thermal inertia of the filament.

Thermoanemometers allow carrying out of experiments within a wide range of velocities and frequencies of pulsation of gas flows.

### 10-3. Optical Methods of Study of Gas Flows

At high velocities in the field of flow there appear significant density gradients. The nonuniformity of flow in this case allows the wide application of optical methods of study. In certain cases nonuniformities of the field are created in the flow artificially by means of local heating. With such a method of visualization optical methods can be applied also for subsonic flows of low velocities.

Optical instruments are based on the use of the known properties of light rays, which are deflected from their initial direction upon passing through a medium of variable density and, consequently, variable refracting ability.

If  $n$  is the index of refraction of light rays at a given point of the field, then the value of density of the flow at the point is determined by the

relationship

$$\frac{1}{\rho} \frac{n^2 - 1}{n^2 + 2} = \text{const.}$$

which can be replaced by the approximate expression:

$$\frac{n - 1}{\rho} = \frac{n_1 - 1}{\rho_1} = \text{const.} \quad (10-1)$$

where  $n_1, \rho_1$  are the index of refraction and density at a certain initial point; usually these quantities refer to standard atmosphere conditions ( $t_1 = 0^\circ \text{C}$  and  $p_1 = 760 \text{ mm Hg}$ ).

From formula (10-1) it follows that the field of densities of the flow will be determined, if we find by an experimental method the field of indexes of refraction of light rays in the investigated region. Pressure and temperature can be determined, if two more equations, connecting the parameters of flow  $p, \rho$  and  $T$ , are known. For this purpose serve the equation of state and the equation of an isentropic process.

Differentiation of equation (10-1) leads to the evident relationships:

$$\frac{\partial n}{\partial y} = K \frac{\partial \rho}{\partial y}; \quad \frac{\partial n}{\partial z} = K \frac{\partial \rho}{\partial z}$$

and

$$\frac{\partial^2 n}{\partial y^2} = K \frac{\partial^2 \rho}{\partial y^2}; \quad \frac{\partial^2 n}{\partial z^2} = K \frac{\partial^2 \rho}{\partial z^2}.$$

where  $K$  is a constant.

Hence we conclude that, depending on the principle of action and the setup of optical instruments, either the first or second derivative can be used for direct measurement of density. For qualitative study of flow all instruments are useful, without regard to what method is used to determine the field of densities during quantitative investigation. However, the accuracy and clarity of the obtained qualitative picture of flow, and also the accuracy and labor-consuming character of processing of the results of qualitative analysis essentially depend on the setup and design of the instrument.

The simplest are optical system in which the shadow method of determination of densities is used. The diagram of such a mechanism is shown in Fig. 10-14, a. A diverging beam of light from source  $S$  passes through lens  $L$  and becomes parallel.



The parallel beam crosses the air flow, in which model A is located, and falls on the screen or photographic plate J. During flow around the model there appear density gradients. Thus, for example, if the flow line 1-2 crosses the bow shock near the model, then the density in the zone of intersection changes intermittently (Fig. 10-14,b). In this case  $\frac{\partial \rho}{\partial z} \neq 0$  and  $\frac{\partial^2 \rho}{\partial z^2} \neq 0$ .

In those points of the field, where  $\frac{\partial^2 \rho}{\partial z^2} > 0$ , rays of the parallel beam disperse and on the screen a dark region will be formed. There, where  $\frac{\partial^2 \rho}{\partial z^2} < 0$ , rays converge and the illumination on the screen is increased. At point 1 Fig. 10-14,b  $\frac{\partial^2 \rho}{\partial z^2} > 0$  and at point 2  $\frac{\partial^2 \rho}{\partial z^2} < 0$ . Hence, it follows that the image of the bow shock for the model will consist of two lines, black and white located next to each other. In the simplest case, the shadow method can be realized in the diverging beam of light (without a lens). This method, simpler and cheaper, finds application during the study of shocks in the flow.

The other, the more sensitive and accurate optical instrument which allows the measurement of the first derivatives of density, is based also on the shadow method. In this instrument, rays, before falling on the screen, are focused to a point, to which is brought a blade. In the presence of nonuniformity in the flow, the point of focusing of part of the rays will be displaced and will hit the blade, which does not prevent their further propagation. As a result, the picture formed on the screen will have greater contrast than in the simple instrument (Fig. 10-14).

Wide use has been received by mirror system of shadow optical instruments. The most perfect is the instrument with a mirror-meniscus system proposed by Prof. D. D. Maksutov (Fig. 10-15). From the source, the beam of light passes through a condenser K and a slot D. The flat diagonal mirror  $S_1$  changes the direction of the rays. Rays hit the concave spherical mirror  $S_2$ , which transforms the diverging beam of light into a parallel beam. Spherical mirror  $S_2$  together with

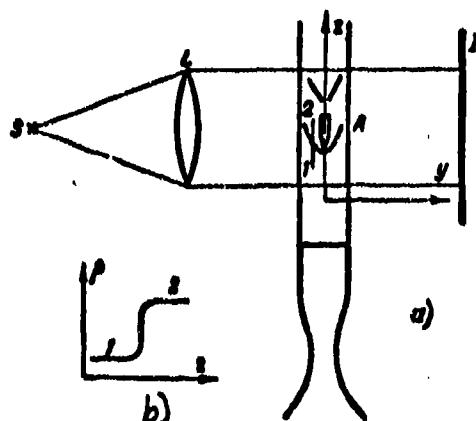


Fig. 10-14. Diagram of shadow method.

a dispersing meniscus lens  $L_1$ , will form mirror-meniscus system.

This part of the apparatus, consisting of the illuminating assembly, mirror  $S_2$  and lens  $L_1$ , makes a parallel beam of light and is called a collimator.

The receiving part of the instrument is made up of the meniscus lens  $L_3$ , spherical mirror  $S_3$ , flat diagonal mirror  $S_4$ , blade H, rotating mirror  $S_5$ , screen I and photoattachment  $\phi$ . The rotating mirror  $S_0$  in the illuminating assembly serves for control of focusing of the slot.

In order that the source of light, which must be on the optical axis of the system, does not close the center of the field of the image, the optical axis of the system is displaced to its edge. Therefore the system is asymmetric with respect to the geometrical axis, which one may readily see in Fig. 10-15.

The main advantage of the mirror-meniscus system consists of the fact that at identical candle-power, it has significantly smaller spherical and chromatic aberrations as compared with the lens system.

Thus, in the considered system, the main subassemblies are the main optics of the apparatus (mirror-meniscus), the illuminating assembly, the actuating mechanism of movement and change of the slot and focusing of the source of light and the mechanism of movement of the blade with the photoattachment.

In the process of experiment, work with the apparatus reduced to operation of the illuminating assembly, the mechanism of movement of the slot, the

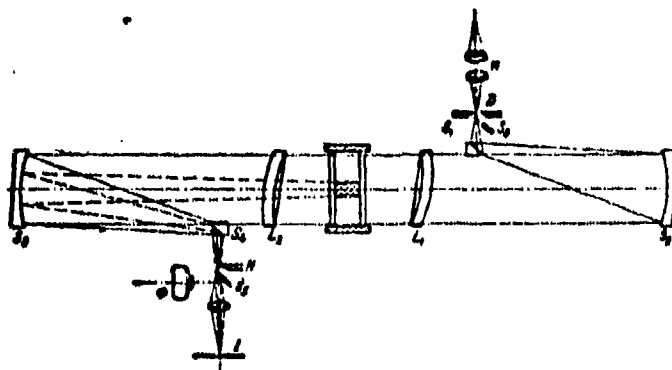


Fig. 10-15. Diagram of mirror-meniscus instrument of D. D. Maksutov.

photoattachment and the mechanism of movement of the blade.

As the source of light different illuminators can be applied, including the mercury arc lamp, motion picture projection lamp, spark discharger and so forth. In a number of cases the consecutive use of two illuminators turns out to be expedient.

During qualitative study of flow, the main problem consists of correct selection of the degree of intensity of illumination of the field, which depends on the dimensions of the slot, the position of the blade and the type of illuminator. The highest intensity of illumination occurs for the maximum slot and withdrawn blade.

It is necessary, however, to remember that, with increase of the degree of illumination, the sensitivity of the instrument decreases. Therefore the region of flow with small density gradients should be photographed at small dimensions of the slot and with the blade introduced into the beam of light. If the main interest is the investigation of a system of shocks, then the dimensions of the slot are increased.

The location of the blade relative to the studied object has an important significance also. Depending upon the position of the blade, (horizontal, vertical or diagonal) beams, passing through a nonuniform field and being deflected, can be stopped by the knife or, on the otherhand, pass to the screen. In the first case nonuniformity appears on the screen as dark, and in the second as light. Definition of the image therefore is kept the same. The best results are obtained when the

edge of the knife is located normal to the direction of the maximum density gradient.

Thus, the type of illuminator, dimension of the slot and position of the blade must in each separate case be found by selection which depends upon the flow regime, the object and the problem of the investigation.

During quantitative investigation of flow, the blade turns out to be unsuitable, since it stops the beams and does not allow measurement of the angles of deviation, which are necessary for determination of the field of refractive indices. In this case diaphragming of the beam of light is produced by a thin filament. Such a method of quantitative investigation with the help of the optical apparatus received the name, "the method of filament and slot."

For direct measurement of the field of densities of the stream the optical instrument known by the name of interferometer is applied. The principle of action of the interferometer can be comprehended from consideration of the diagram presented in Fig. 10-16.

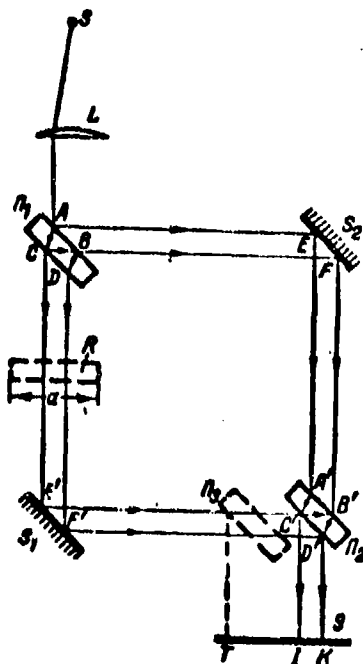


Fig. 10-16. For explanation of the principle of action of the interferometer.

The instrument consists of two reflecting mirrors  $S_1$  and  $S_2$  and two semitransparent mirrors  $P_1$  and  $P_2$  located at the corners of a rectangle at an angle of  $45^\circ$ . Let us consider at first the case when the surfaces of mirrors are strictly parallel. The diverging beam of light from source  $S$  passes through lens  $L$  and becomes parallel. Rays of the parallel beam are divided during passage through the semitransparent mirror  $P_1$ . Part of the rays  $ACE'$  pass through the semitransparent mirror and, being reflected from

mirror  $S_1$  and  $P_2$ , strike the screen at point  $I$ . The other part of the rays are

reflected from  $P_1$  and  $S_2$  and, passing through mirror  $P_2$ , strike the same point of the screen I (trajectory of this beam is AEA'C'I). Reflection of the rays will occur also at points C and B (rays CB and BD) and C' and B' (rays C'B' and B'D') of the semitransparent mirrors. These rays strike the screen at point K. Consequently, the part of the rays striking point I pass through the semitransparent mirrors ( $P_1$ ,  $P_2$ ) once, but that part which strike point K pass through  $P_1$  or  $P_2$  twice. Therefore, at point K the intensity of light will be lower.

Since all four mirrors have parallel surfaces, the length of the optical path (product of the trajectory of the ray by the index of refraction) of both beams striking point I will be identical. In this case the screen will be evenly illuminated.

The character of illuminance of screen abruptly changes if the mirrors ( $S_1$  or  $S_2$ ) are turned by some small angle with respect to the axis perpendicular to the plane of the drawing. In this case the length of the optical path of one of the beams reflected by the corresponding mirror  $S_1$  and  $S_2$  and striking in point I changes. As a result there occurs interference of the rays meeting at point I, due to the fact that part of the rays extinguish one another, and there will be formed intermittent dark and light bands\* on the screen, located at some identical distance  $\Omega$  from one another (Fig. 10-17,a).

If, between mirrors  $P_1$  and  $S_1$  is located the investigated field R, whose density  $\rho$  differs from the density of the medium between  $P_2$  and  $S_2$ , then, due to the change of the optical path of beam CE' the difference of path of beams CE' and EA' will change. In this case the interference bands will be displaced by some distance parallel to themselves (Fig. 10-17,b).

The magnitude of displacement of the interference bands is determined

\*Rays striking point K also interfere with each other; however, as it was shown, due to the considerably smaller intensity of light at point K, the interference here will be weaker. By a small supplement to the design of the instrument, it is possible to exclude it.

by

$$\xi = -\frac{l(n'-1)}{l'} \frac{\rho - \rho'}{\rho} \Omega, \quad (10-4)$$

where  $l$  and  $l'$  are lengths of the optical path of the beam in media with densities  $\rho$  and  $\rho'$  respectively.

Hence we obtain the difference of densities:

$$\rho - \rho' = m \frac{\xi}{\Omega},$$

where  $m = \frac{\rho' l'}{l(n'-1)}$  is a quantity depending on the conditions of the experiment: the angle of rotation of the mirror, density  $\rho'$  and the refractive index of medium  $n'$ .

Values of  $m$ ,  $\xi$  and  $\Omega$  are determined

in the course of the experiment.

In those cases when the investigated field is characterized by a nonuniform distribution of densities, displacement of the interference bands will be different on various sections of the screen; as a result, the bands will be curved. Thus the lines of identical displacements of

the bands of interference ( $\xi/\Omega = \text{const}$ )

correspond to lines of constant density ( $\rho - \rho' = \text{const}$ ) in the investigated region.

Thus, the principal of action of the interferometer is based on measurement of the differences of lengths of the optical paths of the light. The interference method allows a detailed investigation of the structure of flow in interblade channels of cascades and with sufficiently high accuracy to determine quantitative characteristics at all points of the field of flow.

With the help of the interferometer, it is easy to establish the change of thickness of the boundary layer along the profile, and also the position of points of separation of the layer. This instrument allows us to separately determine frictional losses and edge and wave losses in two-dimensional cascades.

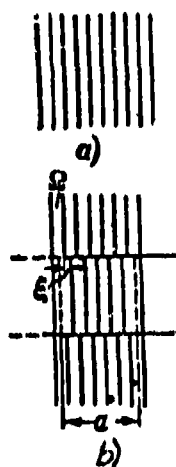


Fig. 10-17. Schematic diagram of interference spectrum.

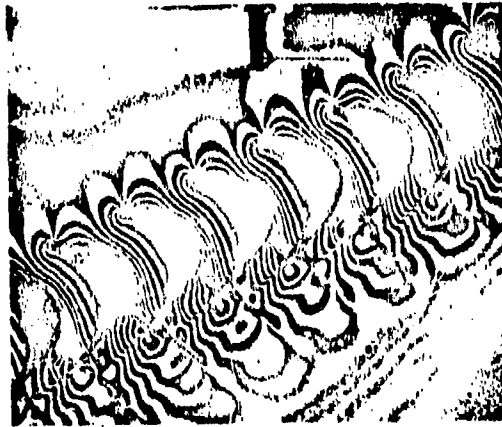


Fig. 10-18. Interference photograph of flow of gas in a turbine cascade (experiments of Central Scientific Research Institute for Boilers and Turbines).

As an example, in Fig. 10-18 is presented an interference photograph of flow in a turbine row. Comparison of the pictures of the distribution of pressures along the contour, obtained by pneumometric and interference methods shows good agreement of results of the optical measurements with the data of direct measurements.

The design of the interferometer by means of a small addition allows us simultaneously to obtain interference and shadow photographs of flow spectra. With this goal, it is possible to introduce one more semitransparent mirror  $P_3$  (Fig. 10-16) into the design of the instrument. Then part of the rays reflected by the mirror  $P_3$ , will give a shadow image of the spectrum on the screen at point T. The other part of the rays, passing through mirror  $P_3$ , will be reflected by mirror  $P_2$  just as in the usual design of the instrument.

#### 10-4. Installations For Investigation of Cascades Under Static Conditions

Tests of stationary rows are carried out on installations of various types, whose design and construction are determined by the problems of the investigation and the adopted method of experiment.

Tests under static conditions, as already was indicated, are carried out for the purpose of comparative evaluation of cascades and for study of properties of the physical process of flow around different cascades. Obtained experimental characteristics in certain cases can be used also for thermal design of the stage.

For determination of characteristics and for investigation of the structure of flow in the cascade various methods of aerodynamic experiment are used. In these are included the following:

A. Methods of study of the spectrum of flow, including: 1) measurements of the field of flow in characteristic sections of the cascade by heads and also by various electrical instruments which establish the total and static pressure, total stagnation temperature, direction of velocity at the point; 2) study of the field of density by optical methods (shadow and interference); 3) visualization of flow by means of mixing of foreign particles.

B. Methods of study of flow at the boundaries of profile, including: 1) measurement of temperatures and pressures on the surface of the profile of the blade by means of draining ; 2) study of the velocity profile in the boundary layer with the help of micro-tube or electrical instruments; 3) visual investigation of the structure of the boundary layer on the profile by means of coloring the surface of the blade.

C. Methods of force measurement including: 1) determination of the total impulse of flow after the cascade; 2) determination of forces, acting on the cascade as a whole and on an individual blade in the infinite cascade with the help of special scales.

D. Methods of study of non-steady-state processes, connected with flow around a separate blade or cascade. Oscillations of a streamlined profile are investigated, also pulsation of velocities, pressures and temperatures of the circumfluent flow.

Without dwelling on the comparative evaluation of different methods of investigation, let us note that their simultaneous use in one installation is



unpractical. Realization of such a requirement makes the installation universal, but it is structurally too complicated, expensive and inconvenient in operation.

It is necessary to consider that to the diagram and design formulation of the installation are presented additional requirements, stipulated by design parameters of the investigated cascades and gas-dynamic parameters of flow before the cascade and after it. Thus, in the investigated cascade there can change the form of the profile, pitch and height of the blades and the angle of their setting..

The most important gas-dynamic parameters are the angle of the flow onto the cascade, whose change must be anticipated in any installation, velocity of flow after the cascade  $M_2$  (or at the inlet into the cascade  $M_1$ ) and Reynolds number  $Re$ . Also in a number of cases it is necessary to provide for a separate study of the influence of compressibility and viscosity on the characteristics of the cascade by means of independent change of numbers  $M$  and  $Re$ . The range of change of regimes is dictated in the final result by the given conditions of the experiment and the requirements of practical modeling.

Among the latter, except for the obvious conditions  $M = idem$  and  $Re = idem$ , are included the special requirements for the organization of flow before the cascade. In certain cases it turns out to be necessary to introduce artificial turbulization of the flow, in others--to thoroughly equalize the flow at the inlet, and also to provide the conditions of flow around the infinite cascade.

The statements above show that the fundamental diagrams and design forms of installations for static tests of cascades can be classified according to objects of investigation (installations for test of flat or cylindrical cascades), according to conditions of testing of cascades (installations with open moving part or with chamber of counterpressure for testing in uniform or turbulent subsonic or supersonic flow at the inlet) and according to the adopted method of investigation (installations for detailed study of aerodynamic fields, for determination of forces, acting on a profile in the cascade for investigation of cascades by optical methods, etc.).

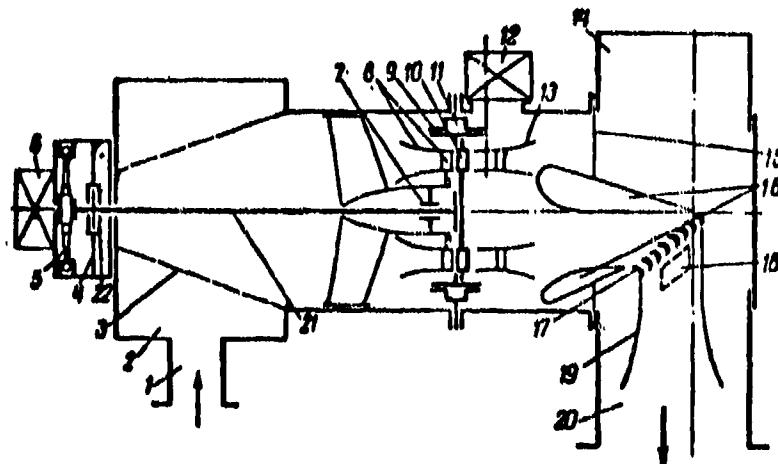


Fig. 10-19. Fundamental diagram of wind tunnel for static investigation of flat and annular cascades. 1-air inlet; 2-annular chamber; 3-grid; 4-meter of  $P_a$ ; 5-meter of  $M_{up}$ ; 6-calibration mechanism; 7-bearing; 8 and 13-shell; 9-11-seal; 10-investigated cascade; 12-coordinator; 14 and 20-exhaust chamber; 15-detachable flange; 16-nozzle of flat bank; 17-flat bank; 18-field of coordinator; 19-diffuser; 21-shaft; 22-thrust bearing.

It is possible to classify installations also depending upon the applied working fluid (steam, air, steam-air and others) and the method of organization of the working flow (installations with excess or atmospheric inlet pressure, ejector installations, steam installations, operating with a condenser).

Laboratory stands should, as a rule, include several experimental installations. In this case the number of problems solved on each installation is limited by its design, adopted by the method of investigation and maximum values of the parameters of the working fluid.

We will consider the basic schemes of certain testing installations. In Fig. 10-19 is presented a diagram of a wind tunnel, in which is provided the possibility of simple replacement of moving parts. Air from the compressor moves into the tunnel through the duct 1 and arrives in the annular chamber 2. Passing through cone 3, which has a large number of apertures, the air goes into the receiver and flows around the investigated annular row 10. The necessary direction of flow at

the inlet into the investigated row is created by lip with guide cascade 8.

The investigated annular package is fastened to a flange of the shaft 21, installed in the ball support bearing 7 and support-thrust bearing 22. Axial force through the bearing 22 is transmitted to the elastic element 4, and torque from the shaft on the housing is transmitted through the symmetrical elastic elements 5. On the elastic elements are fastened wire strain gauges, with the help of which torque and axial force are determined with sufficient accuracy.

Row 10 is supplied with a seal 9, into the chamber 11 of which moves air under pressure equal to the pressure in the receiver. Thus, overflow from the receiver into the exhaust chamber is removed and the flow passing through row 10 is equal to measured flow through the duct 1. Such a determination of flow is necessary with the application of a method of force measurement. For increase of the accuracy of measurement of  $M_{\text{ex}}$  and  $P_{\text{ex}}$  there is provided the special calibrating mechanism 6.

For investigation of the field of flow before the row and after it are used heads, moved by an automated transversing gear 12.

During investigation of the annular row, flange 15 is absent and air is expelled into the exhaust box 20.

If investigations of rows in a flat bank are necessary the annular bank 10,

8, 13 and seal 9 are removed. Flange 15 is installed and on it the flat moving part of the needed design with nozzle 16, the investigated row 17, the transverse gear 18 and the diffuser 19.

Moving parts for the investigation of flat banks have different design formulations. In Fig. 10-20 is presented the general form of one of the moving parts for the flat row.

Here the upper wall of nozzle 5 by bolts 6 is immovably fastened to the housing 3 so that its trailing edge coincides with the common axis of the two disks 8, 9. Disks 8 with the help of inserts 7 are immovably and coaxially fastened together. The lower wall of nozzle 4 by sliding keys 10 and screws 11 is fastened to vertical

slider 1, fastened with housing 3 by screw 2.

Moving wall 4 relative to slider 1 and the slider relative to housing 3, it is possible to change the distance OC within the limits of CB for a given angle of inlet depending upon the length of the investigated bank. Change of the inlet angle is produced by turn of disks 8 relative to the body 3. The coordinator after the row, rigidly fastened with disks 8, ensures four independent movements of the nozzle: linear movement in directions of axes  $xyz$  and turn around axis  $z$ .

Three of these movements (in directions  $x$  and  $z$  and turn around axis  $z$ ), are realized by electric motors, remotely controlled by the operator by a given program.

On installations of the considered type rows can be tested in uniform or turbulent flow. For the purpose of artificial turbulization of flow in the parallel section before the row it is possible to place the turbulizing grids. Depending upon the density of the grid (dimensions of cells) and diameter of tubing during constant speed of flow there can be obtained a different degree of turbulence before the row.

Along with the considered diagrams of installations which operate with excess pressure, application of the diagram with atmospheric pressure in the prechamber

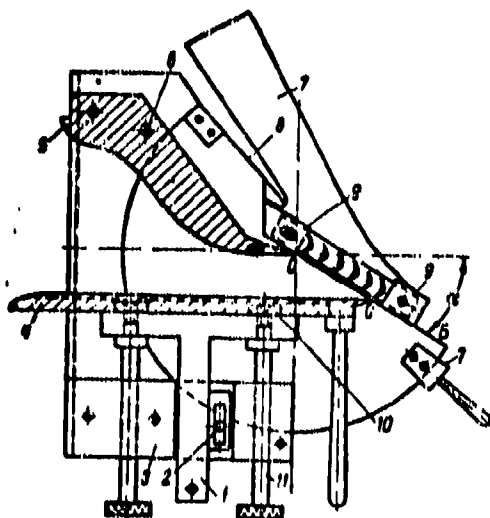


Fig. 10-20. Flat moving part with variable length of bank and automatic transverse gear (transverse section).  
1-slider; 2, 6 and 11-screw; 3-housing; 4 and 5-nozzle; 7-inserts; 8-disk; 9-bank attachment; 10-key.

is found, including the installation of the ejector type. In such installations air is sucked into the prechamber from the atmosphere, is accelerated in a nozzle and directed toward the row. Flow in the row is induced by the ejector. Such an installation operates with open flow and allows the attainment of low pressures after the row (and correspondingly low Reynolds numbers  $Re$ ).

The presented short survey shows that the number of possible designs of installations for static tests of cascades is quite large. Selection of one or the other design is determined by the problems of the experiment, and at the basis of comparison of different set-ups considerations of economy and the requirement of the theory of modelling should be made.

Considering the earlier designations, it is possible to write the expressions for numbers  $M$  and  $Re$  in the known form:

$$M = \frac{c}{a} = \frac{1}{\sqrt{k g R}} \cdot \frac{c}{\sqrt{T}}; Re = \frac{\rho L}{\mu} = \frac{\sqrt{T}}{R \mu} L \frac{p c}{T^{1.5}}.$$

where  $L$  is the characteristic linear dimension;  $p$ ,  $T$ ,  $c$  are parameters of flow in the working part of the installation (after the row).

We will exclude speed  $c$  from the expressions for  $M$  and  $Re$ ; then

$$L = \sqrt{\frac{R T}{k \mu}} \cdot \frac{T}{p} \frac{Re}{M} = K_L \frac{T}{p} \frac{Re}{M}. \quad (10-5)$$

We will designate  $K_y$  as the coefficient of quality of the installation, determined as the ratio of the power of the flow to the required power of the compressor in the working section of the installation. The required power of the compressor is determined by the formula

$$N_k = K_N \frac{1}{K_H} \frac{T^{2.5}}{p} M Re^3. \quad (10-6)$$

In equations (10-5) and (10-6)  $K_L$  and  $K_N$  are constants.

From formula (10-6) it follows that for identical parameters of the gas ( $p$  and  $T$ ) the dimensions of the installation in the working section are increased proportional to the ratio  $Re/M$ . With increase of pressure, the dimensions of the installation are reduced. The power of the installation is proportional to  $M Re^2$ .

Increase of the coefficient of quality of the installation  $K_y$  is attained by

means of introduction of a diffuser, lowering of losses in the installation and use of a compressor with high efficiency within limits of the operating regimes.

With the help of formulas (10-5) and (10-6) it is possible to compare two designs of installations which are different in principle: with excess and with atmospheric pressure in the prechamber.

During maintenance of the similarity simultaneously of  $M$  and  $Re$ , the power of the installation with atmospheric pressure is significantly larger than the power of the installation with excess pressure. At the same time, in the first case the dimensions of the investigated models also increase, which is especially important during investigation of the boundary layer in the row. The installation with excess pressure can operate with a chamber of counterpressure and with an open working part. In the latter case, the technique of experiment is significantly simplified.

Consequently, in installations with excess pressure it is possible to carry out a separate investigation of the influence of compressibility and viscosity at the time that in installations with atmospheric pressure in the prechamber separate modeling is unrealizable. For small values of  $M$ , the economy of both designs is identical.

Thus, we see that installations with excess pressure in the prechamber in the general case (similarity of  $M$  and  $Re$ ) possess high economy and are more universal. They have, therefore, the wider use. In certain cases, however, installations with atmospheric pressure are more economical (if the influence only of compressibility is investigated) and are the only possible solution. Only by such a design, for example, can the steam-air installation with steam ejector operate.

#### 10-5. Experimental Turbines

Experimental investigation of the characteristics of a turbine or compressor stage is carried out on special experimental turbines or compressors.

The stand of the experimental turbine consists of the turbine, an electric or hydraulic load mechanism, air, steam or other gas supply and exhaust devices.

of measuring devices.

In certain cases the turbine and load mechanism are structurally consolidated. In installations of high power the turbine and load mechanism are usually separate and are connected by a coupling.

A general and very important requirement made of the load mechanisms of experimental turbines is the possibility of maximum accuracy of measurement of torque on the shaft of turbine. The possibility of measurement of the axial force of the rotor is desirable.

An experimental turbine must provide the possibility of testing of stages with different geometrical dimensions, reliable operation in a wide range of numbers of revolutions, convenient and correct arrangement of the measuring equipment and simplicity of assembly operations.

In principle it is possible to design a universal experimental turbine providing for tests of separate stages, as well as groups of them and work with different revolutions, allowing testing of models of control, intermediate and last stages. However design and operation of such a machine will be very complicated and its creation is hardly advisable. Obviously, it is more rational to have several experimental machines, each of which is oriented to the investigation of definite types of stages.

In Fig. 10-21 as an example is presented the longitudinal section of a high speed experimental air-driven turbine, intended for detailed investigation of stages with relatively long blades ( $\theta = d/l = 2.8 - 4.5$ ). The turbine is designed for a maximum flow rate of air  $G = 4.5$  kg/sec;  $T_0 = 200^\circ\text{C}$  at a maximum pressure  $p_0 = 3$  atm (abs) and  $n_{\text{max}} = 20,000$  rpm.

The receiver part of the turbine 1 is welded without a horizontal split. Air moves through duct 2 into the annular chamber 3, from where it goes through perforation 18 uniformly into air box 19. For organization of flow before the guide row 22 serve the fairings 20 and the row of plates 21, which allow change of the angle of entry into the guide row. The housing of the turbine 26 is welded with

horizontal split. Air passing through the working part is ejected through the exhaust duct 37. The operation of the machine as an experimental turbine or wind tunnel for the investigation of annular rows is stipulated by design.

The design allows measurement of torque and axial force on the rotor wheel, as well as on the guide apparatus. The latter is fastened onto the hollow shaft 17. The front ball bearing of the shaft does not receive an axial load. The axial load is received by the rear thrust-support bearing 13 and is transmitted through the spherical insert 14 to the elastic element 15.

Torque is transmitted through the key 8 to the three-beam measuring coupling 9, two elastic symmetrical beams of which 6 are intended for measurements of torque and one rigid beam 10 of which is for calibration of the measuring coupling.

So that friction in the contacts of elastic beams of the measuring coupling does not introduce error in the measurement of axial force, the contact is realized through the needle bearing in the spherical housing 5. Torque is transmitted through the ring 12 to the worm pair 4. For measurement of torque and axial force on the diaphragm electrical resistance tensometers glued on flexible elements 6 and 15 are applied.

The measuring device of the described machine allows us easily to conduct calibration in the process of the experiment, and, if necessary, before each measurement.

If necessary highly accurate mechanical or optical-mechanical indicators can be applied simultaneously with the tensometers for measurement of  $M_{\text{н.р}}$  and  $P_{\text{а}}$ .

The rotor wheel 23 of the experimental turbine is made with a flanged attachment. The shaft is flexible, rotating in special precision roller bearings. The load mechanism is a single-disk hydraulic brake of cantilever construction. The question concerning measurement of the moment of friction in bearings is specific for experimental turbines. In a number of existing machines the moment in the bearings in general is not measured, and into the design there is introduced a correction, obtained on the basis of calculations. However, for accurate measurement



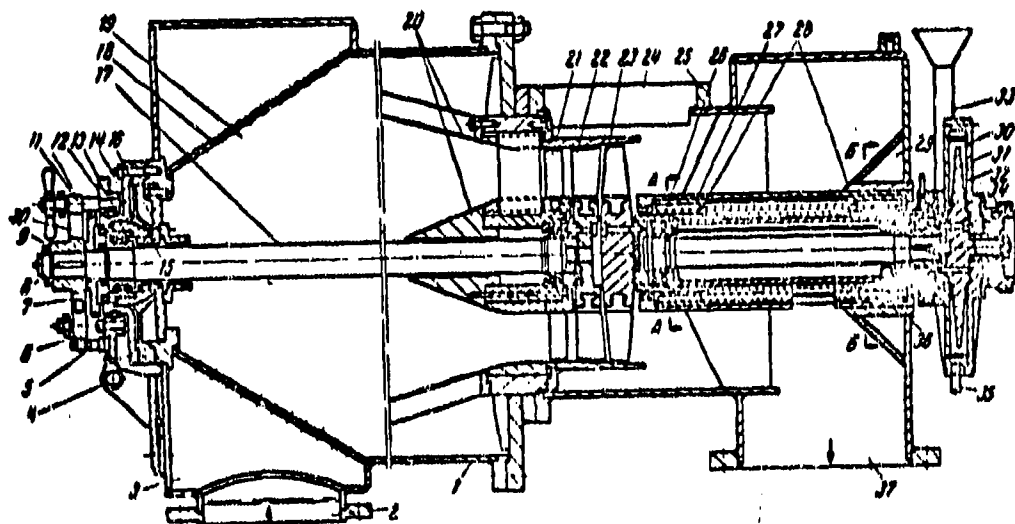


Fig. 10-21. High speed air-driven experimental turbine of the Moscow Power-Engineering Inst. with measurement of  $M_{kp}$  and  $P_a$  on the diaphragm and rotor.

1-and 25-housing; 2-admission duct; 3-annular chamber; 4-turn actuating unit of nozzle apparatus; 5-needle bearing; 6-elastic beam of scales  $M_{kp}$ ; 7-toothed wheel; 8-key; 9-measuring coupling; 10-rigid beam of measuring coupling  $M_{kp}$ ; 11-eccentric; 12-ring; 13-bearing; 14-spherical insert; 15-elastic element of scales; 16-seal; 17-shaft of diaphragm; 18-cascade; 19-receiver; 20-fairings; 21-guide row of plates; 22-nozzle apparatus; 23-rotor wheel; 24-hatch of transverse gear; 26-floating bushing; 27-bushing; 28 and 36-chambers; 29-annular chamber; 30-brake disk; 31 and 32-brake housing; 33-feed channel; 34-induction pickup; 35-drain; 37-exhaust duct.

turbines such a method is not permissible, since the moment in the thrust bearing depends on the axial load, and, consequently, also on the operating regime of the turbine.

In the experimental turbine (Fig. 10-21), the housings of the journal and journal-thrust bearings are distributed in the split "floating" bushing 26. In the non-detachable bushing 27, immovably connected with the housing in sections AA and BB, are four symmetrical chambers 28, each fed through throttling washers with compressed air with a pressure  $\sim 6$  atm (abs), from the annular chamber 29. In operating conditions due to the difference of gaps between bushings 26 and 27 above and below, the pressure in the upper chambers 28 will be less than the pressure in the lower chambers 36. The difference of pressures, directed upward, under determined conditions will balance the weight of the construction included in bushing 26, and will force it to "float."

The main load moment from the disk of the hydraulic brake 30 is transmitted to the housing of the hydraulic brake 32, rigidly joined with the "floating" bushing 26. Therefore moments of bearings and load moment of the disk of the brake are added and are balanced by the moment of the measuring device applied to the housing 32. Thus, the measuring device measures the sum of three moments: moment of the journal bearing, moment of the journal-thrust bearing and moment on the disk of the hydraulic brake. The moment developed as a result of friction of disk 23 against air, is not considered by scales, but can be determined with necessary accuracy by means of calibration.

The axial force of the rotor wheel, transmitted to the "floating" bushing through the journal-thrust bearing, is measured by a special measuring head.

Water in the hydraulic brake moves by an open stream into the feed channel 33 and departs through the drain valve 35. The tachometer, revolution counter and automatic safety device in the described machine are electrical, operating from the general induction data pickup 34.

For measurement of aerodynamic fields after the initial guide apparatus

during work without a wheel a special transverse gear with an automatic electrical drive installed in the hatch 24 is applied.

# APPENDIX

1. Table of gas-dynamic functions for  $k = 1.4$  and  $k = 1.3$ .

2. Shock wave diagrams for  $k = 1.3$  and  $k = 1.4$

## GAS-DYNAMIC FUNCTIONS FOR $k = 1.4$

$\lambda$	$\frac{p}{p_0}$	$\frac{\rho}{\rho_0}$	$\frac{T}{T_0}$	$q$	$\frac{a}{a_0}$	$l$	$l_0$	$\phi(\lambda)$	$m$	$t$	$M$
0.02	0.9998	0.9998	0.9999	0.0315	1.0054	0.00816	0.0002	50.02	—	—	0.0182
0.04	0.9990	0.9993	0.9997	0.0631	1.0053	0.0163	0.0009	25.04	—	—	0.0265
0.06	0.9979	0.9985	0.9994	0.0945	1.0051	0.0245	0.0021	16.72	—	—	0.0348
0.08	0.9963	0.9974	0.9993	0.1259	1.0049	0.0327	0.0037	12.58	—	—	0.0431
0.10	0.9941	0.9958	0.9983	0.1571	1.0045	0.0408	0.0058	10.10	—	—	0.0514
0.12	0.9916	0.9940	0.9976	0.1882	1.0041	0.0490	0.0083	8.453	—	—	0.1097
0.14	0.9886	0.9919	0.9967	0.2190	1.0036	0.0571	0.0113	7.282	—	—	0.1280
0.16	0.9851	0.9893	0.9957	0.2497	1.0031	0.0653	0.0148	6.410	—	—	0.1464
0.18	0.9812	0.9865	0.9940	0.2801	1.0025	0.0735	0.0186	5.736	—	—	0.1648
0.20	0.9768	0.9834	0.9933	0.3102	1.0018	0.0816	0.0229	5.200	—	—	0.1832
0.22	0.9720	0.9799	0.9919	0.3401	1.0010	0.0898	0.0277	4.765	—	—	0.2016
0.24	0.9668	0.9762	0.9904	0.3696	1.0002	0.0980	0.0328	4.407	—	—	0.2201
0.26	0.9611	0.9721	0.9887	0.3987	1.0003	0.1061	0.0383	4.106	—	—	0.2387
0.28	0.9550	0.9667	0.9869	0.4274	1.0003	0.1143	0.0442	3.851	—	—	0.2573
0.30	0.9485	0.9629	0.9850	0.4557	1.0002	0.1225	0.0505	3.633	—	—	0.2759
0.32	0.9415	0.9579	0.9829	0.4835	1.0001	0.1306	0.0572	3.445	—	—	0.2946
0.34	0.9341	0.9525	0.9807	0.5109	1.0000	0.1388	0.0642	3.281	—	—	0.3134
0.36	0.9264	0.9469	0.9784	0.5377	1.0000	0.1470	0.0716	3.138	—	—	0.3322
0.38	0.9183	0.9409	0.9759	0.5640	1.0002	0.1551	0.0793	3.012	—	—	0.3511
0.40	0.9097	0.9346	0.9733	0.5897	1.0007	0.1633	0.0872	2.90	—	—	0.3701
0.42	0.9008	0.9281	0.9706	0.6149	1.0002	0.1715	0.0955	2.801	—	—	0.3892
0.44	0.8911	0.9213	0.9677	0.6394	1.0076	0.1796	0.1040	2.713	—	—	0.4083
0.46	0.8819	0.9142	0.9647	0.6633	1.0060	0.1878	0.1128	2.634	—	—	0.4275
0.48	0.8719	0.9067	0.9616	0.6865	1.0042	0.1960	0.1219	2.563	—	—	0.4468
0.50	0.8616	0.8991	0.9583	0.7091	1.0024	0.2041	0.1311	2.500	—	—	0.4662
0.52	0.8509	0.8911	0.9549	0.7309	1.0005	0.2123	0.1405	2.443	—	—	0.4858
0.54	0.8400	0.8829	0.9514	0.7521	1.0005	0.2204	0.1502	2.392	—	—	0.5054
0.56	0.8287	0.8744	0.9477	0.7724	1.0064	0.2286	0.1599	2.346	—	—	0.5251
0.58	0.8171	0.8657	0.9439	0.7920	1.0043	0.2368	0.1699	2.304	—	—	0.5450
0.60	0.8053	0.8567	0.9400	0.8108	1.002	0.2449	0.1799	2.267	—	—	0.5649
0.62	0.7931	0.8474	0.9359	0.8288	1.000	0.2531	0.1900	2.233	—	—	0.5850
0.64	0.7808	0.8379	0.9317	0.8460	1.007	0.2613	0.2002	2.202	—	—	0.6053
0.66	0.7681	0.8283	0.9274	0.8623	1.005	0.2694	0.2105	2.175	—	—	0.6256
0.68	0.7553	0.8183	0.9229	0.8778	1.002	0.2776	0.2207	2.151	—	—	0.6461
0.70	0.7422	0.8082	0.9183	0.8924	1.000	0.2858	0.2310	2.129	—	—	0.6668
0.72	0.7289	0.7978	0.9136	0.9062	1.007	0.2939	0.2413	2.109	—	—	0.6876
0.74	0.7153	0.7872	0.9087	0.9189	1.004	0.3021	0.2514	2.091	—	—	0.7086
0.76	0.7017	0.7764	0.9037	0.9308	1.001	0.3103	0.2616	2.076	—	—	0.7298
0.78	0.6879	0.7655	0.8986	0.9418	1.008	0.3184	0.2717	2.062	—	—	0.7511
0.80	0.6738	0.7553	0.8933	0.9518	1.005	0.3266	0.2816	2.050	—	—	0.7727
0.82	0.6597	0.7429	0.8879	0.9610	1.002	0.3348	0.2914	2.039	—	—	0.7944
0.84	0.6454	0.7314	0.8824	0.9692	1.009	0.3429	0.3011	2.030	—	—	0.8163
0.86	0.6310	0.7197	0.8767	0.9764	1.006	0.3511	0.3105	2.023	—	—	0.8384
0.88	0.6165	0.7079	0.8709	0.9826	1.002	0.3593	0.3198	2.016	—	—	0.8608
0.90	0.6020	0.6959	0.8650	0.9880	1.019	0.3674	0.3288	2.011	—	—	0.8834
0.92	0.5873	0.6837	0.8589	0.9923	1.015	0.3756	0.3376	2.007	—	—	0.9062
0.94	0.5726	0.6715	0.8527	0.9956	1.011	0.3837	0.3461	2.004	—	—	0.9292
0.96	0.5579	0.6591	0.8464	0.9981	1.008	0.3919	0.3544	2.002	—	—	0.9526

## Continuation

$\lambda$	$\frac{p}{\lambda}$	$\frac{p}{\lambda^2}$	$\frac{r}{T_0}$	$q$	$\frac{a}{u_0}$	$k$	$f_0$	$\psi(\lambda)$	$\alpha_m$	$\delta$	$M$
0.98	0.5430	0.6465	0.8399	0.9095	1.004	0.4901	0.3626	2.0004	—	—	0.9761
1.00	0.5283	0.6339	0.8333	1.0	1.0	0.4682	0.3698	2.000	90°	0	1.00
1.02	0.5135	0.6212	0.8266	0.9995	0.9960	0.4164	0.3770	2.0004	70°33'	0°10'	1.024
1.04	0.4987	0.6084	0.8197	0.9981	0.9918	0.4246	0.3838	2.0015	72°30'	0°30'	1.049
1.06	0.4840	0.5955	0.8127	0.9957	0.9876	0.4327	0.3903	2.0034	68°22'	0°55'	1.073
1.08	0.4693	0.5825	0.8056	0.9924	0.9832	0.4409	0.3963	2.006	65°33'	1°25'	1.098
1.10	0.4546	0.5694	0.7983	0.9881	0.9788	0.4491	0.4019	2.009	62°51'	1°55'	1.124
1.12	0.4400	0.5563	0.7909	0.9829	0.9742	0.4572	0.4071	2.013	60°20'	2°25'	1.150
1.14	0.4255	0.5432	0.7834	0.9768	0.9690	0.4654	0.4118	2.017	58°15'	2°55'	1.176
1.16	0.4111	0.5300	0.7757	0.9698	0.9648	0.4736	0.4160	2.022	56°15'	3°30'	1.202
1.18	0.3968	0.5168	0.7718	0.9619	0.9600	0.4817	0.4197	2.027	54°20'	4°10'	1.229
1.20	0.3827	0.5035	0.7600	0.9531	0.9550	0.4899	0.4229	2.033	52°43'	4°50'	1.257
1.22	0.3687	0.4903	0.7519	0.9435	0.9409	0.4981	0.4257	2.040	51°08'	5°35'	1.284
1.24	0.3548	0.4770	0.7437	0.9331	0.9347	0.5062	0.4279	2.046	49°38'	6°15'	1.313
1.26	0.3410	0.4638	0.7354	0.9218	0.9304	0.5144	0.4295	2.054	48°12'	7°50'	1.341
1.28	0.3275	0.4505	0.7269	0.9097	0.9340	0.5226	0.4306	2.061	46°51'	7°55'	1.370
1.30	0.3141	0.4373	0.7183	0.8968	0.9284	0.5307	0.4311	2.069	45°35'	8°45'	1.400
1.32	0.3010	0.4241	0.7096	0.8832	0.9228	0.5389	0.4311	2.078	44°21'	9°35'	1.430
1.34	0.2880	0.4110	0.7007	0.8688	0.9170	0.5470	0.4305	2.086	43°11'	10°30'	1.461
1.36	0.2753	0.3980	0.6917	0.8538	0.9111	0.5552	0.4294	2.095	42°04'	11°30'	1.493
1.38	0.2628	0.3849	0.6826	0.8380	0.9050	0.5634	0.4276	2.105	40°59'	12°25'	1.525
1.40	0.2500	0.3720	0.6733	0.8216	0.8980	0.5715	0.4253	2.114	39°53'	13°15'	1.557
1.42	0.2385	0.3592	0.6639	0.8045	0.8926	0.5797	0.4225	2.124	38°57'	14°10'	1.591
1.44	0.2267	0.3464	0.6544	0.7869	0.8861	0.5879	0.4190	2.134	37°59'	15°15'	1.625
1.46	0.2152	0.3338	0.6447	0.7687	0.8796	0.5960	0.4151	2.145	37°03'	16°15'	1.660
1.48	0.2040	0.3212	0.6349	0.7499	0.8729	0.6042	0.4104	2.156	36°08'	17°20'	1.695
1.50	0.1930	0.3088	0.6250	0.7307	0.8660	0.6124	0.4053	2.167	35°16'	18°25'	1.732
1.52	0.1823	0.2965	0.6149	0.7110	0.8590	0.6205	0.3996	2.178	34°25'	19°40'	1.769
1.54	0.1720	0.2844	0.6047	0.6908	0.8519	0.6287	0.3934	2.189	33°35'	20°55'	1.808
1.56	0.1619	0.2724	0.5944	0.6703	0.8446	0.6369	0.3867	2.201	32°47'	22°02'	1.847
1.58	0.1521	0.2606	0.5839	0.6494	0.8371	0.6450	0.3794	2.213	32°00'	23°11'	1.887
1.60	0.1427	0.2489	0.5733	0.6282	0.8294	0.6532	0.3717	2.225	31°14'	24°22'	1.929
1.62	0.1335	0.2374	0.5626	0.6067	0.8216	0.6614	0.3634	2.237	30°29'	25°37'	1.971
1.64	0.1249	0.2261	0.5517	0.5849	0.8137	0.6695	0.3547	2.250	29°45'	26°48'	2.015
1.66	0.1162	0.2150	0.5407	0.5630	0.8055	0.6777	0.3456	2.262	29°02'	28°01'	2.061
1.68	0.1081	0.2041	0.5296	0.5409	0.7972	0.6859	0.3360	2.275	28°20'	29°20'	2.107
1.70	0.1002	0.1934	0.5183	0.5187	0.7887	0.6940	0.3261	2.288	27°38'	30°30'	2.155
1.72	0.0927	0.1830	0.5069	0.4964	0.7799	0.7022	0.3157	2.301	26°58'	31°50'	2.205
1.74	0.0856	0.1727	0.4954	0.4741	0.7710	0.7103	0.3051	2.315	26°18'	32°48'	2.257
1.76	0.0787	0.1627	0.4837	0.4518	0.7619	0.7185	0.2940	2.328	25°39'	34°29'	2.310
1.78	0.0722	0.1530	0.4719	0.4296	0.7525	0.7267	0.2828	2.342	25°01'	35°49'	2.365
1.80	0.0660	0.1435	0.4600	0.4076	0.7430	0.7348	0.2712	2.355	24°23'	36°37'	2.424
1.82	0.0601	0.1342	0.4482	0.3855	0.7334	0.7430	0.2593	2.369	23°45'	38°38'	2.482
1.84	0.0546	0.1253	0.4367	0.3637	0.7231	0.7512	0.2475	2.383	23°09'	40°00'	2.541
1.86	0.0494	0.1166	0.4251	0.3423	0.7128	0.7593	0.2354	2.398	22°32'	41°30'	2.609
1.88	0.0445	0.1082	0.4139	0.3210	0.7022	0.7675	0.2232	2.414	21°56'	43°00'	2.677
1.90	0.0399	0.1001	0.3983	0.3001	0.6913	0.7757	0.2109	2.426	21°20'	44°40'	2.748
1.92	0.0356	0.0923	0.3856	0.2790	0.6802	0.7838	0.1985	2.441	20°45'	45°40'	2.823
1.94	0.0316	0.0848	0.3727	0.2595	0.6688	0.7920	0.1862	2.455	20°10'	47°40'	2.901
1.96	0.0279	0.0776	0.3597	0.2400	0.6570	0.8002	0.1739	2.470	19°35'	49°20'	2.983
1.98	0.0245	0.0707	0.3466	0.2209	0.6449	0.8084	0.1617	2.485	19°01'	51°10'	3.070

Continuation

$\lambda$	$\frac{r}{r_0}$	$\frac{r}{r_0}$	$\frac{r}{r_0}$	$\theta$	$\frac{a}{a_0}$	$i$	$i_0$	$\psi(\lambda)$	$\theta_m$	$\lambda$	$M$
2.00	0.0214	0.0041	0.3333	0.2023	0.0324	0.8105	0.1497	2.500	18°20'	52°46'	3.162
2.02	0.0185	0.0079	0.3199	0.1845	0.0196	0.8247	0.1378	2.515	17°51'	54°31'	3.260
2.04	0.0159	0.0520	0.3064	0.1672	0.0064	0.8328	0.1261	2.530	17°18'	56°17'	3.364
2.06	0.0136	0.0404	0.2927	0.1506	0.5927	0.8410	0.1148	2.545	16°44'	58°08'	3.476
2.08	0.0115	0.0411	0.2789	0.1348	0.5785	0.8492	0.1037	2.561	16°09'	60°02'	3.598
2.10	0.0096	0.0361	0.2650	0.1198	0.5639	0.8573	0.0930	2.576	15°35'	61°53'	3.724
2.12	0.0079	0.0315	0.2509	0.1055	0.5487	0.8655	0.0827	2.592	15°00'	63°57'	3.863
2.14	0.0065	0.0273	0.2367	0.0920	0.5330	0.8736	0.0728	2.607	14°26'	65°59'	4.105
2.16	0.0052	0.0233	0.2224	0.0795	0.5166	0.8818	0.0635	2.623	13°51'	68°07'	4.181
2.18	0.0041	0.0197	0.2079	0.0678	0.4995	0.8900	0.0546	2.639	13°15'	70°18'	4.364
2.20	0.0032	0.0164	0.1933	0.0570	0.4816	0.8991	0.0464	2.654	12°39'	72°35'	4.654
2.22	0.0024	0.0135	0.1786	0.0472	0.4629	0.9063	0.0387	2.670	12°02'	74°57'	4.796
2.24	0.0018	0.0108	0.1637	0.0383	0.4432	0.9145	0.0318	2.686	11°25'	77°25'	5.054
2.26	0.0013	0.0085	0.1487	0.0304	0.4224	0.9226	0.0254	2.702	11°47'	80°01'	5.350
2.28	0.0009	0.0065	0.1336	0.0235	0.4004	0.9308	0.0198	2.719	11°07'	82°30'	5.695
2.30	0.0006	0.0048	0.1183	0.0175	0.3768	0.9390	0.0149	2.735	10°26'	85°42'	6.104
2.32	0.0004	0.0034	0.1029	0.0124	0.3514	0.9470	0.0107	2.751	9°43'	88°46'	6.601
2.34	0.0002	0.0023	0.0874	0.0083	0.3238	0.9553	0.0072	2.767	8°57'	92°08'	7.226
2.36	0.0001	0.0014	0.0717	0.0051	0.2933	0.9635	0.0045	2.784	8°08'	95°48'	8.005
2.38	0.00004	0.0009	0.0559	0.0029	0.2590	0.9716	0.0026	2.800	7°17'	99°54'	9.188
2.40	0.00001	0.00032	0.0400	0.0012	0.2100	0.9798	0.0011	2.817	6°14'	104°42'	10.96
2.42	0.000002	0.00009	0.0239	0.00032	0.1694	0.9880	0.0003	2.833	4°01'	110°32'	14.29
2.44	0	0.000005	0.00077	0.00005	0.0962	0.9961	0.00002	2.850	2°15'	119°08'	25.37
2.4495	0	0	0	0	0	1.0	0	2.858	0	130°21'	$\infty$

# GAS-DYNAMIC FUNCTIONS FOR $k = 1.3$

$\lambda$	$\frac{P}{P_0}$	$\frac{P}{P_0}$	$\frac{T}{T_0}$	$\rho$	$\frac{a}{a_0}$	$l$	$\frac{1}{r_0}$	$u_m$	$\delta$	$M$
0.02	0.9998	0.9998	0.9999	0.03187	1.072	0.00722	0.00023	—	—	0.01865
0.04	0.9991	0.9993	0.9998	0.06369	1.072	0.0144	0.00090	—	—	0.03730
0.06	0.9980	0.9985	0.9995	0.09546	1.072	0.0217	0.00203	—	—	0.05596
0.08	0.9964	0.9972	0.9992	0.1271	1.072	0.0289	0.00361	—	—	0.07463
0.10	0.9944	0.9957	0.9987	0.1581	1.072	0.0361	0.00563	—	—	0.09331
0.12	0.9919	0.9937	0.9981	0.1900	1.071	0.0433	0.00809	—	—	0.11200
0.14	0.9890	0.9915	0.9974	0.2212	1.071	0.0500	0.01098	—	—	0.1307
0.16	0.9855	0.9888	0.9967	0.2521	1.071	0.0578	0.01431	—	—	0.1494
0.18	0.9818	0.9860	0.9958	0.2828	1.070	0.0651	0.01806	—	—	0.1682
0.20	0.9776	0.9827	0.9948	0.3170	1.070	0.0722	0.02222	—	—	0.1870
0.22	0.9729	0.9791	0.9937	0.3482	1.069	0.0795	0.02679	—	—	0.2058
0.24	0.9679	0.9752	0.9925	0.3729	1.068	0.0867	0.03175	—	—	0.2246
0.26	0.9623	0.9700	0.9912	0.4022	1.068	0.093	0.03710	—	—	0.2435
0.28	0.9564	0.9663	0.9898	0.4311	1.067	0.1011	0.04282	—	—	0.2624
0.30	0.9501	0.9614	0.9883	0.4596	1.066	0.1083	0.04891	—	—	0.2814
0.32	0.9434	0.9562	0.9866	0.4875	1.065	0.1156	0.05543	—	—	0.3004
0.34	0.9363	0.9506	0.9849	0.5150	1.064	0.1229	0.06211	—	—	0.3195
0.36	0.9288	0.9448	0.9831	0.5420	1.063	0.1300	0.06921	—	—	0.3386
0.38	0.9209	0.9386	0.9812	0.5683	1.062	0.1372	0.07660	—	—	0.3577
0.40	0.9127	0.9321	0.9791	0.5941	1.061	0.1444	0.08430	—	—	0.3769
0.42	0.9040	0.9253	0.9770	0.6193	1.060	0.1517	0.09226	—	—	0.3962
0.44	0.8951	0.9183	0.9747	0.6438	1.059	0.1589	0.1005	—	—	0.4156
0.46	0.8851	0.9109	0.9724	0.6677	1.057	0.1661	0.1089	—	—	0.4340
0.48	0.8751	0.9033	0.9699	0.6909	1.056	0.1733	0.1176	—	—	0.4545
0.50	0.8642	0.8951	0.9674	0.7133	1.055	0.1806	0.1265	—	—	0.4740
0.52	0.8530	0.8872	0.9647	0.7351	1.053	0.1878	0.1356	—	—	0.4937
0.54	0.8415	0.8788	0.9620	0.7561	1.052	0.1950	0.1448	—	—	0.5134

## Continuation

$\lambda$	$\frac{P}{P_0}$	$\frac{P}{P_0}$	$\frac{P}{P_0}$	$\rho$	$\frac{a}{u_0}$	$l$	$l_0$	$a_m$	$\delta$	$M$
0.50	0.8344	0.8700	0.9501	0.7703	1.050	0.2022	0.1542	—	—	0.5332
0.55	0.8233	0.8610	0.9501	0.7958	1.049	0.2095	0.1637	—	—	0.5531
0.60	0.8119	0.8519	0.9530	0.8145	1.047	0.2167	0.1733	—	—	0.5731
0.62	0.8002	0.8424	0.9499	0.8322	1.045	0.2239	0.1830	—	—	0.5932
0.64	0.7883	0.8328	0.9466	0.8493	1.043	0.2311	0.1928	—	—	0.6134
0.66	0.7760	0.8229	0.9432	0.8653	1.041	0.2384	0.2026	—	—	0.6337
0.68	0.7637	0.8127	0.9397	0.8806	1.039	0.2456	0.2124	—	—	0.6541
0.70	0.7511	0.8024	0.9361	0.8950	1.038	0.2528	0.2222	—	—	0.6747
0.72	0.7384	0.7919	0.9324	0.9085	1.035	0.2600	0.2320	—	—	0.6953
0.74	0.7253	0.7811	0.9286	0.9211	1.033	0.2672	0.2418	—	—	0.7161
0.76	0.7122	0.7702	0.9247	0.9327	1.031	0.2745	0.2514	—	—	0.7370
0.78	0.6989	0.7591	0.9206	0.9435	1.029	0.2817	0.2610	—	—	0.7580
0.80	0.6854	0.7478	0.9165	0.9533	1.027	0.2889	0.2705	—	—	0.7792
0.82	0.6718	0.7364	0.9123	0.9622	1.024	0.2961	0.2799	—	—	0.8006
0.84	0.6581	0.7248	0.9080	0.9702	1.022	0.3034	0.2891	—	—	0.8220
0.86	0.6443	0.7130	0.9035	0.9771	1.019	0.3106	0.2981	—	—	0.8437
0.88	0.6304	0.7012	0.8990	0.9833	1.017	0.3178	0.3070	—	—	0.8655
0.90	0.6164	0.6892	0.8943	0.9884	1.014	0.3250	0.3155	—	—	0.8874
0.92	0.6023	0.6771	0.8896	0.9925	1.011	0.3323	0.3239	—	—	0.9096
0.94	0.5882	0.6649	0.8847	0.9958	1.009	0.3395	0.3320	—	—	0.9310
0.96	0.5740	0.6525	0.8798	0.9982	1.006	0.3467	0.3399	—	—	0.9524
0.98	0.5599	0.6401	0.8747	0.9996	1.003	0.3539	0.3475	—	—	0.9741
1.00	0.5457	0.6276	0.8696	1.0000	1.000	0.3612	0.3547	90°	0	1.0000
1.02	0.5315	0.6150	0.8643	0.9995	0.9970	0.3684	0.3616	77°47'	0°10'	1.0231
1.04	0.5171	0.6024	0.8589	0.9982	0.9939	0.3756	0.3683	72°52'	0°30'	1.046
1.06	0.5032	0.5897	0.8534	0.9960	0.9907	0.3828	0.3745	69°00'	0°55'	1.069
1.08	0.4891	0.5769	0.8479	0.9928	0.9874	0.3900	0.3803	66°06'	1°25'	1.091
1.10	0.4750	0.5641	0.8422	0.9887	0.9841	0.3973	0.3858	63°20'	1°55'	1.118
1.12	0.4611	0.5513	0.8364	0.9838	0.9807	0.4045	0.3909	61°07'	2°25'	1.142
1.14	0.4471	0.5384	0.8305	0.9789	0.9773	0.4117	0.3955	59°00'	2°5'	1.163
1.16	0.4333	0.5268	0.8245	0.9737	0.9737	0.4189	0.4000	57°05'	3°28'	1.191
1.18	0.4193	0.5127	0.8184	0.9680	0.9701	0.4262	0.4035	55°18'	4°19'	1.216
1.20	0.4050	0.4998	0.8122	0.9618	0.9664	0.4334	0.4068	53°38'	4°52'	1.242
1.22	0.3925	0.4870	0.8059	0.9567	0.9627	0.4406	0.4097	52°00'	5°37'	1.267
1.24	0.3791	0.4742	0.7994	0.9510	0.9588	0.4478	0.4121	50°38'	6°20'	1.293
1.26	0.3659	0.4614	0.7929	0.9454	0.9549	0.4551	0.4149	49°10'	7°08'	1.319
1.28	0.3528	0.4487	0.7863	0.9392	0.9500	0.4623	0.4155	47°59'	7°52'	1.346
1.30	0.3399	0.4360	0.7796	0.9332	0.9448	0.4695	0.4165	46°45'	8°44'	1.373
1.32	0.3272	0.4234	0.7727	0.9268	0.9387	0.4767	0.4170	45°35'	9°32'	1.400
1.34	0.3147	0.4109	0.7658	0.9203	0.9324	0.4839	0.4170	44°27'	10°16'	1.428
1.36	0.3023	0.3984	0.7588	0.9134	0.9251	0.4912	0.4165	43°23'	11°18'	1.456
1.38	0.2901	0.3860	0.7516	0.9060	0.9177	0.4984	0.4155	42°28'	12°01'	1.484
1.40	0.2782	0.3738	0.7444	0.8988	0.9102	0.5056	0.4141	41°24'	13°17'	1.513
1.42	0.2665	0.3616	0.7370	0.8912	0.9026	0.5128	0.4121	40°20'	14°04'	1.542
1.44	0.2550	0.3495	0.7295	0.8820	0.8949	0.5201	0.4097	39°30'	14°52'	1.572
1.46	0.2438	0.3370	0.7220	0.8754	0.8872	0.5273	0.4068	38°37'	15°50'	1.602
1.48	0.2327	0.3258	0.7144	0.8683	0.8803	0.5345	0.4034	37°44'	16°50'	1.633
1.50	0.2219	0.3142	0.7065	0.8610	0.8734	0.5417	0.3996	36°50'	18°00'	1.664
1.52	0.2114	0.3026	0.6986	0.8533	0.8663	0.5490	0.3952	36°08'	18°51'	1.696
1.54	0.2011	0.2912	0.6907	0.8456	0.8591	0.5562	0.3904	35°38'	20°05'	1.728
1.56	0.1911	0.2800	0.6826	0.8361	0.8500	0.5634	0.3852	34°59'	21°00'	1.761
1.58	0.1814	0.2689	0.6744	0.8272	0.8406	0.5706	0.3795	34°23'	22°08'	1.794
1.60	0.1719	0.2581	0.6661	0.8180	0.8312	0.5778	0.3745	33°40'	23°15'	1.828
1.62	0.1627	0.2474	0.6577	0.8087	0.8219	0.5851	0.3690	32°58'	24°21'	1.863
1.64	0.1538	0.2369	0.6492	0.8001	0.8124	0.5923	0.3632	32°17'	25°29'	1.898
1.66	0.1452	0.2266	0.6406	0.7914	0.8028	0.5995	0.3579	31°38'	26°38'	1.934
1.68	0.1368	0.2165	0.6319	0.7826	0.7931	0.6067	0.3524	30°59'	27°47'	1.971
1.70	0.1287	0.2066	0.6231	0.7736	0.7835	0.6140	0.3475	29°52'	28°55'	2.008
1.72	0.1209	0.1969	0.6141	0.7646	0.7740	0.6212	0.3422	29°15'	30°07'	2.047



## Continuation

$\lambda$	$\frac{p}{r_0}$	$\frac{p}{r_0}$	$\frac{r}{r_0}$	$\theta$	$\frac{a}{a_0}$	$l$	$l_0$	$\alpha_m$	$\alpha$	$M$
1.74	0.1134	0.1874	0.6051	0.5196	0.8342	0.6284	0.3207	28°37'	31°13'	2.086
1.76	0.1062	0.1781	0.5960	0.4996	0.8279	0.6356	0.3119	28°03'	32°27'	2.126
1.78	0.09922	0.1691	0.5867	0.4796	0.8214	0.6429	0.3028	27°29'	33°45'	2.167
1.80	0.09256	0.1603	0.5774	0.4598	0.8149	0.6501	0.2936	26°55'	35°04'	2.209
1.82	0.08718	0.1517	0.5680	0.4400	0.8082	0.6573	0.2841	26°22'	36°24'	2.252
1.84	0.08007	0.1434	0.5584	0.4204	0.8014	0.6645	0.2744	25°49'	37°33'	2.296
1.86	0.07424	0.1353	0.5488	0.4010	0.7944	0.6717	0.2645	25°17'	38°53'	2.341
1.88	0.06870	0.1274	0.5390	0.3818	0.7873	0.6790	0.2545	24°46'	40°22'	2.388
1.90	0.06341	0.1193	0.5291	0.3628	0.7801	0.6862	0.2445	24°14'	41°33'	2.436
1.92	0.05840	0.1125	0.5192	0.3441	0.7727	0.6934	0.2344	23°44'	43°06'	2.485
1.94	0.05364	0.1054	0.5091	0.3257	0.7652	0.7006	0.2241	23°18'	44°14'	2.535
1.96	0.04915	0.09851	0.4989	0.3077	0.7575	0.7079	0.2139	22°44'	45°36'	2.587
1.98	0.04491	0.09191	0.4887	0.2900	0.7496	0.7151	0.2037	22°10'	47°04'	2.641
2.00	0.04092	0.08556	0.4783	0.2727	0.7416	0.7223	0.1934	21°46'	48°25'	2.697
2.02	0.03717	0.07946	0.4678	0.2555	0.7334	0.7295	0.1833	21°17'	49°52'	2.754
2.04	0.03366	0.07363	0.4572	0.2383	0.7251	0.7368	0.1732	20°49'	51°14'	2.813
2.06	0.03038	0.06804	0.4465	0.2233	0.7166	0.7440	0.1632	20°21'	52°45'	2.875
2.08	0.02732	0.06271	0.4357	0.2078	0.7079	0.7512	0.1533	19°54'	54°10'	2.938
2.10	0.02448	0.04762	0.4248	0.1928	0.6990	0.7584	0.1430	19°26'	55°53'	3.004
2.12	0.02185	0.05280	0.4138	0.1784	0.6904	0.7656	0.1341	18°59'	57°24'	3.073
2.14	0.01942	0.04822	0.4027	0.1644	0.6805	0.7729	0.1248	18°32'	58°52'	3.145
2.16	0.01718	0.04389	0.3915	0.1511	0.6710	0.7801	0.1157	18°06'	60°30'	3.219
2.18	0.01513	0.03979	0.3801	0.1382	0.6612	0.7873	0.1069	17°39'	62°15'	3.297
2.20	0.01325	0.03595	0.3687	0.1260	0.6512	0.7945	0.09835	17°13'	64°22'	3.378
2.22	0.01155	0.03234	0.3572	0.1144	0.6409	0.8018	0.09008	16°47'	66°00'	3.464
2.24	0.01050	0.02895	0.3455	0.1033	0.6304	0.8090	0.08210	16°21'	67°21'	3.553
2.26	0.00961	0.02580	0.3338	0.09291	0.6196	0.8162	0.07448	15°55'	68°08'	3.647
2.28	0.00770	0.02288	0.3220	0.08313	0.6085	0.8234	0.06723	15°29'	71°06'	3.747
2.30	0.00525	0.02017	0.3100	0.07392	0.5971	0.8307	0.06031	15°03'	72°44'	3.852
2.32	0.00527	0.01767	0.2980	0.06531	0.5854	0.8379	0.05370	14°37'	74°36'	3.963
2.34	0.00440	0.01538	0.2858	0.05735	0.5733	0.8451	0.04760	14°11'	76°30'	4.081
2.36	0.00354	0.01329	0.2736	0.04997	0.5609	0.8523	0.04184	13°45'	78°29'	4.208
2.38	0.00298	0.01130	0.2612	0.04320	0.5481	0.8596	0.03647	13°19'	80°31'	4.342
2.40	0.00241	0.00968	0.2487	0.03702	0.5348	0.8668	0.3152	12°52'	82°52'	4.487
2.42	0.00192	0.00814	0.2361	0.03139	0.5211	0.8740	0.02694	12°26'	84°31'	4.644
2.44	0.00151	0.00677	0.2235	0.02632	0.5069	0.8812	0.02278	11°59'	86°51'	4.813
2.46	0.00117	0.00557	0.2107	0.02183	0.4922	0.8884	0.01905	11°32'	89°04'	4.998
2.48	0.00089	0.00451	0.1978	0.01781	0.4769	0.8957	0.01568	11°05'	91°24'	5.2000
2.50	0.00066	0.00360	0.1848	0.01434	0.4610	0.9029	0.1272	10°37'	93°48'	5.423
2.52	0.00048	0.00281	0.1717	0.01128	0.4444	0.9101	0.01008	10°09'	96°22'	5.671
2.54	0.00034	0.00210	0.1585	0.00875	0.4270	0.9173	0.00788	9°40'	98°54'	5.940
2.56	0.00024	0.00161	0.1452	0.00656	0.4086	0.9246	0.00596	9°11'	101°37'	6.264
2.58	0.00015	0.00117	0.1318	0.00481	0.3893	0.9318	0.00440	8°41'	104°27'	6.627
2.60	0.00010	0.00081	0.1183	0.00330	0.3698	0.9390	0.00310	8°09'	107°20'	7.040
2.62	0.00006	0.00054	0.1047	0.00225	0.3740	0.9462	0.00210	7°36'	110°37'	7.551
2.64	0.00003	0.00034	0.09096	0.00143	0.3234	0.9535	0.00134	7°02'	114°21'	8.162
2.66	0.00002	0.00020	0.07713	0.00084	0.2978	0.9607	0.00080	6°25'	117°37'	8.891
2.68	0.000006	0.00010	0.06320	0.00043	0.2698	0.9679	0.00041	5°46'	121°41'	9.941
2.70	0.000002	0.00005	0.04917	0.00022	0.2378	0.9751	0.00020	5°09'	126°08'	11.35
2.72	0	0.00001	0.03503	0.00005	0.2007	0.9823	0.00004	4°14'	131°28'	13.55
2.74	0	0.000002	0.02078	0.000008	0.1546	0.9896	0.00001	3°13'	137°47'	17.72
2.76	0	0	0.00644	0	0.08606	0.9968	0	1°46'	147°19'	32.07
2.76887	0	0	0.00601	0	0.00679	1.0	0	159°12'		∞

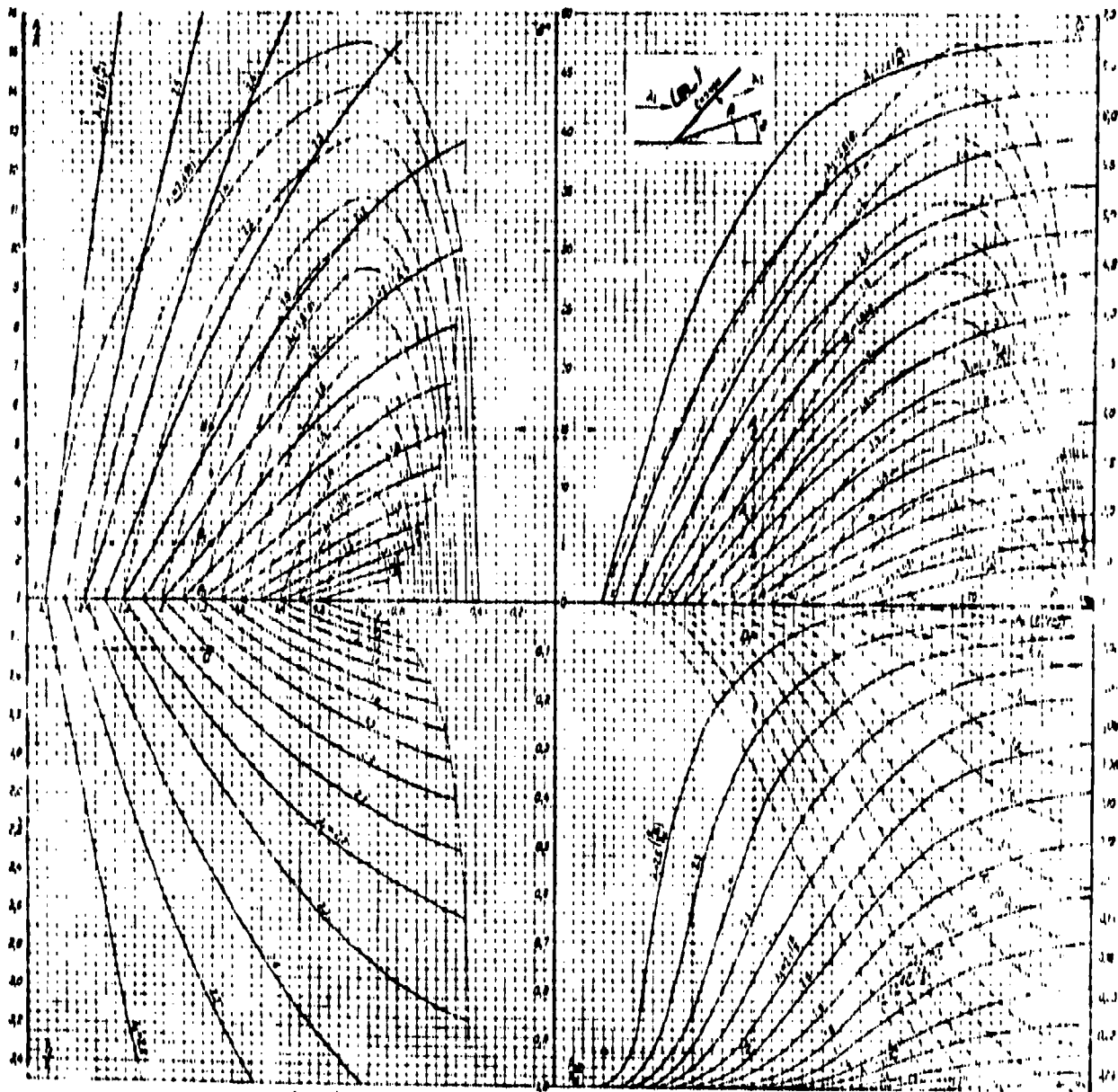


Diagram for calculation of shock waves ( $k=1.3$ )  
 KEY: (a) shock

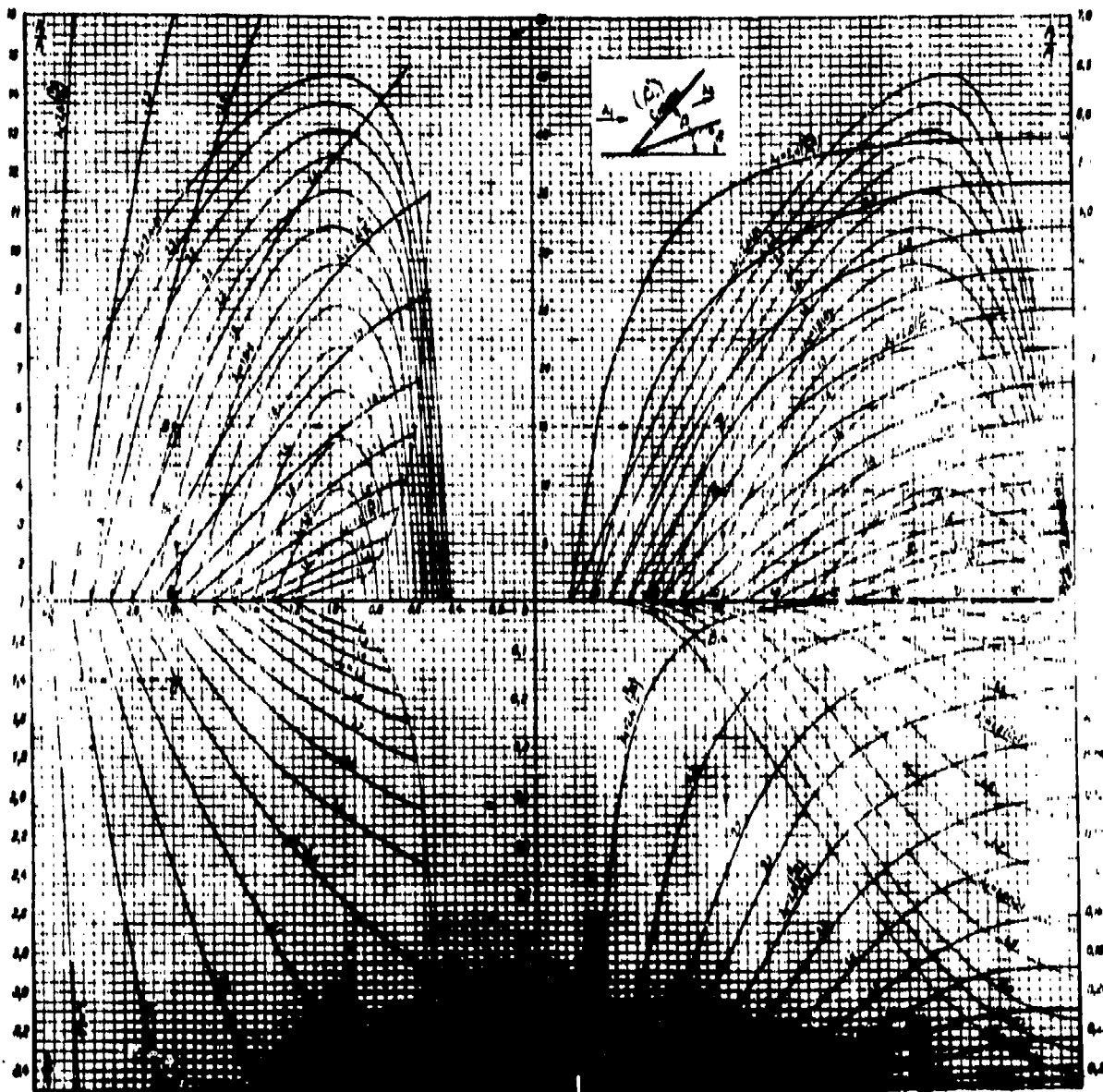


Diagram for calculation of shock waves ( $k = 1.4$ )  
 KEY: (a) Shock.

## LITERATURE

### Basic References

1. N. Ye. Zhukovskiy. Modification of method of Kirchhoff, Complete collection of compositions, vol.III, ONTI, 1936.
2. N. Ye. Zhukovskiy. On connected vortices, Complete collection of compositions, vol. V, ONTI, 1936.
3. N. Ye. Zhukovskiy. Vortex theory of a screw propeller, Complete collection of compositions, vol.VI, ONTI, 1936.
4. S. A. Chaplygin. Theory of a lattice-type foil, Collection of compositions, vol.II, Hydrodynamics, Aerodynamics, Gostekhizdat, 1948.
5. S. A. Chaplygin. Concerning gas streams, Collection of compositions, vol. II, GITTL, 1948.
6. L. G. Loytsyanskiy, Mechanics of liquids and gases, Gostekhizdat, 1957.
7. L. I. Sedov. Two-dimensional problems of hydrodynamics and aerodynamics, Gostekhizdat, 1954.
8. N. S. Arshanikov, V. N. Mal'tsev. Aerodynamics, Oborongiz, 1957.
9. G. N. Abramovich. Applied gas dynamics, Gostekhizdat, 1953.
10. L. I. Sedov. Methods of analogy and dimension in mechanics, Gostekhizdat, 1950.
11. V. S. Zhukovskiy. Engineering thermodynamics, Gostekhizdat, 1952.
12. L. A. Vulis, Thermodynamics of gas flows, State Power-Engineering Publishing House, 1950.
13. L. Prandtl. Hydroaeromechanics, Publishing House of Foreign Literature, [PHFL] 1949.
14. Contemporary state of hydroaerodynamics of a viscous liquid, Collection Ed.: S. Goldstein, PHFL, 1948.
15. Contemporary state of aerodynamics of high speeds, Collection under editorial office of R. Khouert, PHFL, 1955.
16. N. Ye. Kochin. Hydrodynamic theory of blade rows, GITTL, 1949.
17. T. Karman. Supersonic aerodynamics, PHFL, 1948.

### For Chapter 1

1. N. Ya. Fabrikant. Aerodynamics, Gostekhizdat, 1955.
2. A. P. Mel'nikov. Foundations of theoretical aerodynamics, Izd. LKVVIA, 1953.

## For Chapter 2

1. F. I. Frankl', S. A. Khristianovich, and R. N. Alekseyev, Principles of gas dynamics, Proceedings of Central Aero-Hydrodynamic Institute, No. 364, 1938.
2. S. A. Khristianovich, V. G. Gal'perin, M. D. Millionshchikov, and L. A. Simonev. Applied gas dynamics, Izd. TsAGI, 1948.
3. B. M. Kiselev. Calculation of one-dimensional gas flows, "Applied mathematics and mechanics," 1947, No. 1.

## For Chapter 3

1. S. A. Khristianovich. Flow of gas around bodies at high subsonic velocities, Trans. of Central Aero-Hydrodynamic Institute, No. 481, 1940.
2. S. A. Khristianovich. Concerning supersonic flows of gas, Trans. of Central Aero-Hydrodynamic Institute, No. 543, 1941.
3. A. N. Sherstyuk. Design of wing profiles at high subsonic speeds, News of Academy of Sciences of USSR, OTN, 1956, No. 8.
4. G. F. Burago, Theory of wing profiles taking into account the influence of the compressibility of air, Izd. VVIA im. N. Ye. Zhukovskiy, 1949.
5. L. I. Sedov. Two-dimensional problems of hydrodynamics and aerodynamics, Gostekhnizdat, 1950.
6. N. Ya. Fabrikant. Aerodynamics, Gostekhnizdat, 1949.
7. G. F. Burago, and B. Ya. Shymyatskiy, Fundamentals of theoretical aerohydrodynamics, ch. I, Izd. VVIA IM. N. E. Zhukovskiy, 1951.
8. V. S. Polyadskiy. Calculation of distribution of pressure at high velocities of flight, Bureau of New Technology Press, 1943.
9. G. V. Lipman, and A. Ye. Paket. Introduction to the aerodynamics of a compressible fluid, PHFL, 1949.
10. Problems of flight at high velocities, Collection of articles, PHFL, 1960.

## For Chapter 4

1. Ya. I. Levinson. Aerodynamics of high velocities, Oborongiz, 1950.
2. A. Ferri. Aerodynamics of supersonic velocities, Gostekhnizdat, 1952.
3. R. Zauer. Flow of a compressible fluid, PHFL, 1954.
4. V. A. Andreyev, and S. Z. Bolen'kiy. Influence of condensation of water vapor

on supersonic flows, Trans. of Central Aero-Hydrodynamic Institute, No. 579, BNT, 1946.

5. F. W. Ross. The propagation in a compressible fluid of finite oblique disturbances with energy exchange and change of state, Journal of Applied Physics, 1951, v. 22, No. 12.

#### For Chapter 5

1. G. M. Bam-Zelikovich. Calculation of separation of boundary layer, News of Academy of Sciences of USSR, OTN, 1954, No. 12.

2. A. A. Gukhman, A. F. Gandel'sman, and N. V. Ilyukhin. Investigation of change of drag coefficient during flow of a gas with supersonic velocity, "Heat-power engineering," 1955, No. 1.

3. A. A. Gukhman, A. F. Gandel'sman, and L. N. Naurits, Concerning hydrodynamic drag in the transonic region of flow, "Heat-power engineering," 1957, No. 7.

4. M. Ye. Deych, and A. Ye. Zaryankin. Method of approximate calculation of the boundary layer at high subsonic velocities, "Heat-power engineering," 1958, No. 3.

5. M. Ye. Deych, and A. Ye. Zaryankin. Experimental investigation of a turbulent turbulent boundary layer at high velocities, Trans. MEI, No. XXX, 1958.

6. A. A. Dorodnitsyn. Boundary layer in a compressible gas, "Applied mathematics and mechanics", 1942, vol. VI, No. 6.

7. A. E. Zaryankin, Investigation of the boundary layer in turbine blade rows at high velocities, Dissertation, MEI, 1956.

8. L. M. Zysin-Moloshen. Concerning the character of transition from laminar to turbulent flow regime in a boundary layer, Journal of engineering physics, 1955, vol. XXV, No. 7.

9. L. Ye. Kalikhman. Gas-dynamic theory of heat transfer, "Applied mathematics and mechanics," 1956, Vol. X.

10. L. Ye. Kalikhman. Turbulent boundary layer on a flat plate with flow of gas around it, Oborongiz, 1954.

11. L. G. Loytsyanskiy. Aerodynamics of the boundary layer, Gostekhizdat, 1941.

12. E. M. Minskiy. Influence of turbulence of incident flow on transition, Proc. of Central Aero-Hydrodynamic Institute, No. 415, 1939.

13. A. P. Mel'nikov. Fundamentals of theoretical aerodynamics, Izd. LKVVIA, 1953.

14. B. S. Petukhov, A. S. Sukomel, and V. S. Protopopov, Investigation of the resistance of friction and temperature recovery factor of a wall during motion of gas in a round pipe with high subsonic velocity, "Heat-power engineering," 1957, No. 3.

15. G. Schlichting, Theory of the boundary layer, 1956.

16. H. Nippert. Über den Strömungsverlust in gekrümmten Kanälen, Forschungsarbeiten auf d. Geb. d. Ing. Wes, 1929, H. 320.

17. J. P. Hartnett, and E. R. Eckert. Experimental study of the velocity and temperature distribution in a high-velocity vortex-type flow, Transactions of the ASME, 1957, v. 79, No. 4.

18. A. P. Alekseyev, and V. S. Martynovskiy. Investigation of the effect of vortex temperature division of gases and vapors, News of Academy of Sciences USSR, OTN, 1956, v. 26, No. 10.

19. L. A. Vulis. On the Rank Effect, News of Academy of Sciences USSR, OTN, 1956, No. 10.

20. M. G. Dubinskiy. Concerning rotational flows of gas. News of Academy of Sciences of USSR, OTN, 1954, No. 8.

#### For Chapter 6

1. V. I. Astrov, Ye. A. Levin, L. D. Pavlov, and S. A. Khristianovich. On the design of Laval nozzles, "Applied mathematics and mechanics," No. 1, v. II, 1943.

2. A. V. Bolgarskiy, and V. K. Shchukin. Operating processes in liquid-jet engines, Oborongiz, 1958.

3. N. D. Dobrokhotoy. Gas-dynamic diagrams of outflow from a nozzle of a rocket motor at off-design pressure, 1947.

4. M. S. Kisenko. Comparative tests of several variants of nozzles, Trans. of Central Aero-Hydrodynamic Institute, No. 478, 1940.

5. J. E. Beckwith., and J. A. Mootel. An accurate and rapid method for the design of supersonic nozzles, NACA, TN, 1956, No. 3322.

6. A. Stodola. Dampf-und Gasturbinen, 1924.

#### For Chapter 7

1. Aerodynamics, Chief ed.: V. F. Dyurend, vol. III, Oborongiz, 1940.

2. L. P. Volkova, and M. Ya. Yudelovich. Shock losses in stepped tubes at supersonic ratios of pressure, Izv. AN USSR, OTN, 1958, No. 4.

3. I. D. Vinnik, M. P. Umanskiy, and V. A. Chernikov. Some results of aerodynamic investigation of the exhaust duct of a transport gas-turbine engine, "Power machine construction," No. 4, 1959.

4. A. Sh. Dorfman, M. M. Nazarchuk, N. I. Pol'skiy, and M. I. Saykorskiy. Aerodynamics of diffusers and exhaust ducts of turbomachines, Izd. AN Ukrainian SSR, 1960.

5. M. Ye. Deych, A. V. Robozhev, F. V. Stepanchuk, and A. A. Kokh. Investigation of the structure of flow in an ejector stage with isobaric initial section of mixing, "Heat-power engineering," 1954, No. 12.
6. M. Ye. Deych, A. V. Robozhev, and A. A. Kokh. Influence of certain geometric and gas-dynamic parameters of the ejector stage on the effectiveness of its operation, Trans. MEI, No. XXIII, 1955.
7. M. A. Dement'yev, and A. K. Chertkov. Hydromechanical investigation of variants of the exhaust duct of a steam turbine, "Boiler and turbine design," 1948, No. 1.
8. I. Ye. Idel'chik. Hydraulic resistances, State Power-Engineering Publishing House, 1954.
9. O. N. Ovchinnikov. Influence of the inlet velocity profile on the operation of a diffuser, "Herald of mechanical engineering," 1954, No. 6.
10. I. I. Orlov. Testing of models of the inlet duct of an axial compressor, "Herald of mechanical engineering," 1954, No. 6.
11. R. Penkkherst, and D. Kholler, Technique of experimentation in wind tunnels, PHFL, 1955.
12. Ye. Ya. Sokolov and N. M. Zinger, Jet apparatus, State Power-Engineering Publishing House, 1960.
13. L. P. Sokolovskiy. Investigation of aerodynamics of exhaust ducts of turbines and compressors, "Power machine construction," 1952, No. 9.
14. K. S. Stillard. Investigation of diffusers of wind tunnels of high velocities, Technical notes of Central Aero-Hydrodynamic Institute, No. 160, 1938.
15. G. A. Khanin, Several questions of aerodynamic investigation of auxiliary elements of the blading of turbomachines, "Heat-power engineering," 1955, No. 1.
16. B. N. Yur'ev. Experimental aerodynamics, Oborongiz, 1939.
17. F. Klauzer. Operation of diffusers of ramjet motors at supersonic velocities of flight, "Questions of rocket technology," 1954, No. 2; 1955, No. 1.
18. Ye. Neyman, and F. Lyustverk. Supersonic diffusers of high efficiency, "Questions of rocket technology," 1951, No. 6; 1953, No. 1.
19. S. A. Khristianovich, On the design of an ejector, "Industrial aerodynamics," 1944, No. 3.
20. S. A. Khristianovich, M. D. Millionshchikov, G. M. Ryabinkov, and F. A. Trebin. Application of ejectors in gas collecting networks, News of Academy of Sciences of USSR, OTN, 1946, No. 3.
21. M. Hibs, Mezikruhove difuzory, Proudění v lopatkových strojích, Sborník ustavu pro výzkum stroju, 1958.
22. V. Kmonicek, Základy konstrukce difuzorů a kompresorů, Sborník strojního sborník, 1955, 13.



For Chapter 8

1. Ye. A. Gukasova. Investigation of tip losses in turbine blade rows, Transactions of the TsKTI, aerohydrodynamics, Book 27, 1954.
2. M. Ye. Deych. On the question of tip losses in guide channels of steam turbines, "Soviet boiler and turbine design," 1945, No. 6.
3. M. Ye. Deych and A. V. Gubarev. On the question of "cutoff" of the supply nozzle and working blade row in supersonic flow, "Heat-power engineering," 1960, No. 12.
4. M. Ye. Deych and A. V. Gubarev. Investigation of active working rows at high velocities, "Heat-power engineering," 1958, No. 12.
5. M. Ye. Deych, A. Ye. Zaryankin, G. A. Filippov and M. F. Zatsepin. Increase of the efficiency of turbine impulse cascades of small height, "Heat-power engineering," 1960, No. 9.
6. M. Ye. Deych and A. Ye. Zaryankin. Method of approximate calculation of tip losses, "Heat-power engineering," 1958, No. 9.
7. M. Ye. Deych and G. S. Samoylovich. Fundamentals of aerodynamics of axial turbomachines, Mashgiz, 1959.
8. M. Ye. Deych, V. V. Frolov, and A. V. Gubarev. Investigation of new foils of rows of control stages and pressure stages of turbines, "Heat-power engineering," 1956, No. 5.
9. M. Ye. Deych, K. A. Rozanov and V. V. Frolov. Investigation and improvement of foils of control stage, Trans. MEI, No. 23, 1955.
10. M. Ye. Deych and A. Ye. Zaryankin. Investigation and improvement of nozzle rows of control stage, "Heat-power engineering," 1955, No. 10.
11. M. I. Zhukovskiy. Calculation of flow around rows of foils of turbomachines, Mashgiz, 1960.
12. M. I. Zhukovskiy and N. A. Sknar'. On the question of application of thickened edges of guide blades, "Power machine construction," 1957, No. 2.
13. M. I. Zhukovskiy and N. A. Sknar'. New rows of turbine foils, "Heat-power engineering," 1955, No. 1.
14. V. I. Kirsanov. On the improvement of turbine reactive rows of foils on the basis of investigation of the character of flow around them during change of operating regime by number M and number Re, News of the Academy of Sciences of USSR OTN, 1954, No. 7.
15. G. S. Samoylovich. Calculation of potential flow in a curved channel, "Heat-power engineering," 1954, No. 7.
16. G. Yu. Stepanov. Hydrodynamic investigations of turbine rows "Survey bulletin aircraft motor design," 1949, No. 4 and 5.

17. G. Yu. Stepanov. Fundamentals of the theory of blade machines, combined and gas-turbine engines, Mashgiz, 1958.
18. N. M. Markov. Calculation of aerodynamic properties of blade apparatus of turbomachines, Mashgiz, 1955.
19. I. D. Lyakhovitskiy. Turbulence of flow in turbine stage and loss of active blades, "News VTI," 1950, No. 5.
20. N. G. Rodin. Tip losses of energy in rows of turbine blades, Labors LPI, 1951, No. 1.
21. O. N. Yemin. Secondary flow and loss during motion of a liquid on a turn, Trans. MAI, No. 68, 1956.
22. A. N. Shestyuk. The determination of losses in turbine rows with thickened exit edges, "Heat-power engineering," 1959, No. 6.
23. A. N. Sherstyuk. Method of approximate calculation of curved channels, "Heat-power engineering," 1955, No. 8.
24. G. Flyugel'. Steam turbines, GONTI, 1939.
25. L. Belik. Application of theoretical and experimental methods during design of turbine rows of the impulsotype, "Heat-power engineering," 1959, No. 8.
26. Ya. Bukovskiy, Methods of experimental investigation of flow in rows of foils of turbomachines at high velocities, "Heat-power engineering," 1958, No. 9.
27. A. D. Corter, and E. M. Cohen, Preliminary investigation into the three-dimensional flow through a cascade of aerofoils, ARC, 1946, No. 2339.
28. H. B. Squire, and K. G. Winter, The secondary flow in a cascade of aerofoils in a non-uniform stream, J. Aeron. Sc., 1951, v. 18, No. 4.
29. J. M. Stephenson. Secondary flow in cascades, J. Aeron. Sc., 1951, v. 18, No. 18.
30. R. N. Alekseyev I. D. Lyakhovitskiy, and Yu. V. Rzhiznikov. "Heat-power engineering," No. 6.

#### For Chapter 9

1. M. Ye. Deych. Experimental investigations and fundamentals of aerodynamic design of steam and gas turbine stages, Dissertation, 1956.
2. M. Ye. Deych, and G. S. Samoylovich. Fundamentals of aerodynamics of axial turbomachines, Mashgiz, 1959.
3. M. Ye. Deych, F. V. Kazintsev, L. Ye. Kiselev, and V. G. Fillipov. Investigation of variable regime of stages with long blades of constant profile, "Heat-power engineering," 1959, No. 6.
4. V. Ya. Yershov. On the problem of the design of the cascade of aerofoils.

mechanisms, No. 5, 1955.

5. G. S. Zhuritskiy. Aviation gas turbines, Oborongiz, 1950.
6. I. I. Kirillov. Method of design of blading of steam turbines with twisted blades, Collection of labors, BITM, No. 15, 1955.
7. I. I. Kirillov. Gas turbines and gas turbine installations, Mashgiz, 1956.
8. B. S. Stechkin, P. K. Kazandzhan, L. P. Alekseyev, A. N. Govorov, Yu. N. Nechayev, and R. M. Fyodorov. Theory of jet engines (blade machines), Oborongiz, 1956.
9. G. S. Samoylovich, B. M. Troyanovskiy. Variable operating regime of steam turbines, Gosenergoizdat, 1955.
10. V. G. Tyryshkin, On the question of rational design of blades of a turbine stage taking into account compressibility, "Boiler and turbine design," 1949, No. 3.
11. A. N. Shyerstyuk. Axial compressors (aerodynamic design), State Power Engineering Publishing House, 1955.
12. Ya. I. Shneye. Theory of gas turbines, Mashgiz, 1950.
13. A. V. Shcheglyayev. Steam turbines, State Power-Engineering Publishing House, 1955.
14. V. V. Uvarov. Profiling of long blades of gas and steam turbines, Oborongiz, 1945.
15. J. Bílek, J. Čamek, P. Veselý. Soustavný výzkum lopatkové účinnosti na modelových turbinách, Proudění v lopatkových strojiích, Sborník ústavu pro výzkum strojů, 1958.
16. Wu Chung-Hua. The aerodynamic problem of radially long blades in turbomachines, Chinese Journal of Mechanics, 1957, v. 1, No. 1.
17. A. Stodola, Die Dampf-und Gasturbinen, 1924.

#### For Chapter 10

1. M. Ye. Deych, F. V. Kazintsyev, and B. A. Golovin. Computer for determination of energy loss factor, "power machine construction," 1959, No. 3.
2. N. A. Zaks. Fundamentals of experimental aerodynamics, Oborongiz, 1953.
3. G. S. Samoylovich, Ye. V. Mayorskiy, I. Neruda, and A. V. Stekolsichikov. Quick-response tensometric probes for investigation of non-steady processes in turbomachines, "Heat-power engineering," 1959, No. 1.
4. I. L. Povkh. Aerodynamic experimentation in mechanical engineering, Mashgiz, 1959.
5. S. G. Popov. Several problems and methods of experimental aerodynamics, Gosizdat, 1952.

6. A. N. Prudilov. Piezoelectric indicator of pressure for investigation of frequency and character of pulsation of air in a turbomachine, "Power machine construction," 1956, No. 12.
7. R. Pekkerst and D. Kholder. Technique of experimentation in wind tunnels, PHFL, 1955.
8. V. P. Preobrazhenskiy. Thermotechnical changes and instruments, State Power-Engineering Publishing House, 1953.
9. A. I. Turigin and P. V. Novitskiy. Wire transducers and their technical applications, State Power-Engineering Publishing House, 1957.
10. A. M. Turichin. Electrical measurements of nonelectrical quantities, State Power-Engineering Publishing House, 1954.
11. M. M. Fyetsiov. Use of inductive transducers for change of non-steady-state pressures, Transactions of LPI, 1955, No. 17.
12. Physical measurements in gas dynamics and during combustion, PHFL, 1957. literature, 1957.
13. W. F. Hilton. Aerodynamics of high velocities, PHFL, 1955. 1955.
14. Electric measurements, Ed.: A. V. Frenke, State Power-Engineering Publishing House, 1954.
15. A. Worant and I. Haffner. Methods of processing of experimental data, PHFL, 1953.

# DISTRIBUTION LIST

DEPARTMENT OF DEFENSE	NR. COPIES	MAJOR AIR COMMANDS	NR. COPIES
		DDC	20
HEADQUARTERS USAF		AFSC	
		SCFDD	1
		TDBTL	5
		TDRDP	2
ARL (ARB)	1	TDQS	1
		TDEMT	10
		TDBXP	1
		TDT	2
		AFFTC (FTY)	2
		TDEPA	1
OTHER AGENCIES		AEDC (AEY)	1
CIA	5	SSD (SSFI)	2
DIA	4	ASD (ASFA)	2
AID	2	BSD (BSF)	1
NASA (ATSS-T)	1	AFWL (WLF)	1
OAR	1		
OTS	2		
NSA	6		
ARMY (FSTC)	3		
NAVY	3		
NAFEC	1		
AEC	2		
RAND	1		